UNIVERSITAT DE BARCELONA

Diseño de nuevas formulaciones farmacéuticas mucoadhesivas para la quimioterapia del cáncer de colon

Ana Casadó Mora

TESIS DOCTORAL

Diseño de nuevas formulaciones farmacéuticas mucoadhesivas para la quimioterapia del cáncer de colon

Ana Casadó Mora

2017

Grupo de aplicaciones biomédicas de sistemas coloidales

Departamento de Bioquímica y Biomedicina Molecular
Facultad de Biología

Programa de Doctorado de Biomedicina

Diseño de nuevas formulaciones farmacéuticas mucoadhesivas para la quimioterapia del cáncer de colon

Memoria presentada por

Ana Casadó Mora

para optar al grado de Doctor por la Universidad de Barcelona

Firma de las directoras

Dra. Margarita Mora Giménez
(Directora y tutora)

Dra. M. Lluïsa Sagristá Gratovil
(Co-Directora)

Barcelona, septiembre 2017

A mis padres,

a Jaime.

“Un científico en su laboratorio no es sólo un técnico: es también un niño colocado ante fenómenos naturales que le impresionan como un cuento de hadas”.

Marie Curie

Agradecimientos

El camino que me ha llevado a completar esta tesis ha sido largo y, por suerte, en cada etapa me he encontrado con grandes personas que me han enseñado, ayudado, apoyado o que simplemente han estado ahí cuando más falta me ha hecho. A ellas, a todas, dedico este primer apartado, que sin duda alguna, será el más leído.

Pero vayamos al principio, donde comenzó todo. Mi relación con la ciencia y con el Departamento de Bioquímica y Biología Molecular de la Universidad de Barcelona empezó mucho antes de que me tocara escoger carrera o decidir qué hacer una vez acabada. Empezó antes de que supiera lo que era una probeta y cuando las micropipetas me parecían artilugios de otra galaxia. Todo empezó en aquellas mañanas en las que mi madre (y directora de tesis, pero a eso ya llegaremos) me llevaba al laboratorio porque tenía que ir a hacer algo que no podía esperar. Ahí me sentaba en un ordenador que había en una poyata y yo me dedicaba a observarlo todo, maravillada. Frascos, botellas, cachivaches de vidrio, mil cosas que se quedaron grabadas en mi pequeño cerebro a la espera de que, algún día, tomara el camino que me devolviera a ese lugar. Es por este motivo que al escribir estos agradecimientos se mezclan muchos sentimientos, personas a las que otra sólo conocería por su faceta académica o científica, yo las conozco de toda la vida y son más, mucho más, que compañeros laboratorio o departamento.

En primer lugar quiero dar las gracias a Mª África de Madariaga, Blanca, la directora del grupo de Biomembranas, por abrirme las puertas del laboratorio y darme la oportunidad de empezar mi carrera como investigadora. Siempre has estado ahí y sin ti no seríamos la familia “UB” que somos.

A mis directoras de Tesis. Gracias por darme la oportunidad de participar en el proyecto que teníais entre manos cuando acabé la carrera. Teóricamente iba a ser sólo un año, pero conseguisteis que me “picara” y quisiera acabar lo que había empezado. A Margarita Mora, mi madre, que no es porque sea mi madre, pero tiene una de las mentes más brillantes que conozco. Gracias por tus consejos, tu ayuda y por guiarme a lo largo de este camino. A Maria Lluïsa Sagristá, a quien conozco desde antes de que tuviera uso de razón. Gràcies per fer-ho tot tan fàcil, per estar sempre disponible, per la teva paciència i per ajudar-me en tot moment.

A Juan Carlos y a Félix. Al primero también lo conozco desde que nací, al segundo lo adoptamos más tarde. Gràcies pels consells i per totes les estones que hem compartit. Què hauria estat del nostre dia a dia sense els cafès matutins?!

A todos mis compañeros de laboratorio. Han pasado muchos, desde los Fernandos hasta Ester. No me quiero dejar a ninguno. Todos, de un modo u otro, habéis participado en esta tesis: las chicas IQS, Ana Jiménez, María García y Ester Boix; mis sicilianas del alma, Dorotea Micieli y Chiara Giuffrida; todas las italianas que han pasado por el laboratorio para su Tesi di Laurea, Chiara Pelillo, Deborah Siracussa, Federica Furnari, Veronica Inferrera, Giusy Tripodo y Rossana Sidoti. Gracias también por los buenos ratos a mis compañeros de NBM, Laia (tu sortiràs més endavant), Aroa, Jose, Nuria, Teresa, Dani, Paulina, los Jorges… No sé si me dejo alguno, pero gracias!

A Bego, gracias por los buenos ratos (incluso durante la súper mudanza del laboratorio) y por estar siempre disponible para ayudarme con los aparatejos. ¡Sin ti los liposomas del Emulsiflex no habrían salido igual de bien!

A Patri. Tú eres la persona que me enseñó cómo trabajar con cultivos celulares, de forma meticulosa y con infinita paciencia. Si todo ha salido tan bien, en parte también es gracias a ti.

Ahora cambio de ciudad y me voy a Madrid. Antes que nada, gracias a Ángeles y a Magdalena por acogerme en su laboratorio. A Ángeles en especial, gracias por todos tus consejos y, aunque me daba mucho miedo que dijeras que habías estado pensando en la ducha, la verdad es que tus ideas han llevado a buen puerto una parte muy importante de esta tesis.

A Santi. Tú has sido mi compañero de laboratorio con mayúsculas. Gracias por ayudarme siempre y acogerme como a una más. Mi estancia en Madrid no habría sido la misma sin ti. Y gracias también a toooooooodos los compañeros del laboratorio de enfrente. A Paloma, Jose, Ana, Vero y Óscar, ¡qué ratos tan buenos pasamos!

Volvemos a Barcelona. Gràcies als meus compis de feina, que sempre em pregunten com porto la Tesi, pero sin atosigar. Als jefes, Xavier i Jordi. A l'altre jefe, el Dani. A la Laia, la Sílvia, la Maria, la Karla, el Guillem. Treballar a comunicació no seria el mateix sense vosaltres! I a la Míriam, la meva Mili, gràcies per tant, #testimo!

A las otras dos integrantes del "Trío Lalala", Laia y Nerea. Vosaltres sou les millors amigues que quasevol persona podria tenir. Gràcies per ser com sou i per haver estat sempre quan us he necessitat. Y a las del cole, Ainhoa, Emma, Pili, Lourdes y Nely. A algunas os conozco desde hace… ¡33 años! Gracias por estar siempre (y aquí va en sentido literal) ahí.

A mis "nenis", Cris, Carol y Vicky. Mis primas y amigas del alma. Siempre puedo contar con vosotras. Sin nuestras cenas de desahogo la vida no sería lo mismo.

A mis cuñados, Jose, Anna y Rebeca. Sois geniales, gracias por todos los buenos momentos, por los viajes que nos hemos pegado… ¡Y los que nos quedan! A mis suegros, Jose y Trini, los mejores del mundo, y no es peloteo.

A mi hermano, Javier. Eres el mejor hermano del mundo mundial. Así de claro. Siempre, siempre, siempre, estás ahí cuando te necesito. Gracias infinitas.

A mis padres. Estaría páginas y páginas escribiendo y no tendría suficiente espacio para expresar por todo por lo que os estoy agradecida. Gracias a vosotros soy como soy. Me habéis educado y guiado y sin vosotros no habría llegado a dónde estoy. Siempre habéis sido y seréis mi gran referente, en todos los aspectos.

A Jaime, mi otra mitad. Gracias por estar siempre a mi lado y soportarme con mis virtudes, que son algunas, y mis defectos, que son muchos. Infinita paciencia has tenido aguantando todos los años que me ha llevado acabar esta tesis. Tú me has dado lo mejor de mi vida, a mis peques, Dani y Martina. Gracias por estar siempre a mi lado. TE QUIERO.

Contenidos

Abreviaturas (orden alfabético)

ADN	Ácido desoxirribonucleico
AFM	Microscopía de fuerzas atómicas
AH	Ácido hialurónico
APC	7-ethyl-10-[4-N-(5-aminopentanoic acid)-1-piperidino] carbonyloxycamptothecin
ATCC	American Type Culture Collection
ATP	Adenosín trifosfato
Bak	Bcl-2 antagonist/killer
Bax	Bcl-2-associated X protein
Bcl-2	B-cell lymphoma 2
CF	5(6)-carboxifluoresceína
CRC	Cáncer colorrectal
CES	Carboxilesterasas
CHOL	Colesterol
CPT	Camptotecina natural
CPT-11	irinotecan (7-ethyl-10-[4-(1-piperidino)-1-piperidino] carbonyloxycamptothecin)
CPT-11lip	Irinotecan encapsulado en liposomas
CPT-11sol	Irinotecan en tampón lactato
CS	Quitosano
CSA	Condroitín sulfato
DMAE	Degeneración macular asociada a la edad
DMEM	Dulbecco´s Modified Eagle´s Medium
DMSO	Dimetilsulfóxido
DOPE	Dioleoil-fosfatidiletanolamina
DOPS	Dioleoil fosfatidilserina
DPPC	Dipalmitoil fosfatidilcolina

DSC	Calorimetría diferencial de barrido
DSPC	Diestearoil fosfatidilcolina
EGFR	Receptor del factor de crecimiento epidérmico
EPC	Fosfatidilcolina de huevo
EPR	Efecto de permeabilidad y retención aumentada
ErbB	Oncogén B de la eritroblastosis aviar
FCS	Suero fetal bovino
FDA	U.S. Food and Drug Administration
Feq	Fuga en el equilibrio
FITC	Isotiocianato de fluoresceína
5-FU	5-fluorouracilo
GAPDH	glyceraldehyde-3-phosphate dehydrogenase
GM1	Ganglósido
H-33258	Hoechst-33258
HPMA	N-(2-hidroxipropil) metilacrilamida
IgG	Inmunoglobulina G
IUVs	Vesículas unilamelares intermedias
LB	Técnicas de monocapas – Balanza de Langmuir
LDH	Lactatodeshidrogenasa
LUVs	Vesículas unilamelares grandes
MLVs	Vesículas multilamelares
MMP	Metaloproteinasa
MTT	3-[4,5-dimethylthiazol-2-yl] 2,5-diphenyltetrazolium bromide
N_2	Nitrógeno
NPC	7-ethyl-10-[4-(1-piperidino)-1-amino]-carbonyloxycamptothecin
PBS	Tampón fosfato salino
PC	Fosfatidilcolina
PCR	Reacción en cadena de la polimerasa

PCS	Espectroscopía de correlación fotónica
PE	Fosfatidiletanolamina
PG	Fosfatidilglicerol
PS	Fosfatidilserina
PEG	Polietilenglicol
PLA	Ácido poli-láctico
PLGA	Ácido poli-láctico-co-glicólido
RT-PCR	PCR en tiempo real
RNA	Ácido ribonucleico
SD	Desviación estándar
SN-38	7-ethyl-10-hydroxycamptothecin
SN-38G	Glucoronidato de SN38
SN-38lip	SN38 encapsulado en liposomas
SM	esfingomielina
SRE	Sistema retículoendotelial
SUVs	Vesículas unilamelares pequeñas
TEM	Microscopía electrónica de transmisión
TGI	Tracto gastrointestinal
Tm	Temperatura de transición
TNF	Factor de necrosis tumoral
Topo I	Topoisomerasa I
TRITC	Isotiocianato de tetrametilrodamina B
UFT	Tegafur con Uracilo
UGT1A	UDP-glucuronosiltransferasa
UP CL 213	Cloruro de quitosano ultrapuro
UP CL 113	Cloruro de quitosano ultrapuro
UV	Ultravioleta
VEGF	Factor de crecimiento vascular endotelial

1. Introducción

1.1. El cáncer colorrectal

El cáncer es, en la actualidad, una de las principales causas de muerte en el mundo. A pesar de los avances experimentados en cuanto a la comprensión de las bases moleculares de la enfermedad, su diagnóstico y tratamiento constituyen uno de los principales retos de la medicina actual. De entre los diferentes tipos de cáncer (Figura 1), el de colon representa alrededor del 10-12% de los casos diagnosticados y ocupa el segundo lugar en orden de prevalencia.

El cáncer colorrectal (CRC) es un tipo de cáncer muy heterogéneo, tanto por el estadio en el que se encuentra cuando se diagnostica, como por la localización del tumor primario o por las diferencias entre los factores genéticos y ambientales que participan en su desarrollo. Además, las metástasis se producen mediante vías diferentes, entre ellas la hemática, que extiende la enfermedad principalmente al hígado y al pulmón.

1.1.1. Epidemiología e incidencia

El cáncer colorrectal (CRC) es el tipo de cáncer más frecuente en España y en Europa y se ha estimado que aproximadamente un 5% de la población desarrollará un tumor de este tipo, cifra que está previsto que aumente al ser mayor la esperanza de vida de la población. En 2012 se diagnosticaron en todo el mundo 1,4 millones de casos y 693.900 personas murieron a causa de esta enfermedad (1, 2). Si se tienen en cuenta ambos sexos por separado, en nuestro país es la segunda neoplasia más frecuente en hombres y mujeres por detrás del cáncer de pulmón y de mama, respectivamente.

La incidencia varía de forma amplia entre países, en función del grado de desarrollo y de sus registros de cáncer, y cerca del 55% de los nuevos casos se diagnostican en los países desarrollados. Las tasas más altas se encuentran en Australia, Nueva Zelanda, Europa y Norte América, mientras que las tasas más bajas corresponden a ciertas regiones de África y Asia (2) (Figura 1).

1.1.2. Características generales

El CRC es un tipo de cáncer del tracto digestivo que se desarrolla a partir de dos tipos de pólipos: los hiperplásicos y los adenomatosos. Alrededor del 95% de los cánceres colorrectales son adenocarcinomas. Son numerosos los mecanismos genéticos y moleculares responsables de la transformación maligna de los pólipos (3, 4).Los pólipos adenomatosos, sobre todo, pero recientemente también un subtipo de pólipo hiperplásico, el serrado, están considerados como los precursores de lesiones malignas (5). En función de su incidencia se clasifican en tres grupos: familiar, hereditario y, la forma más común, el esporádico, que no está asociado a los factores anteriores.

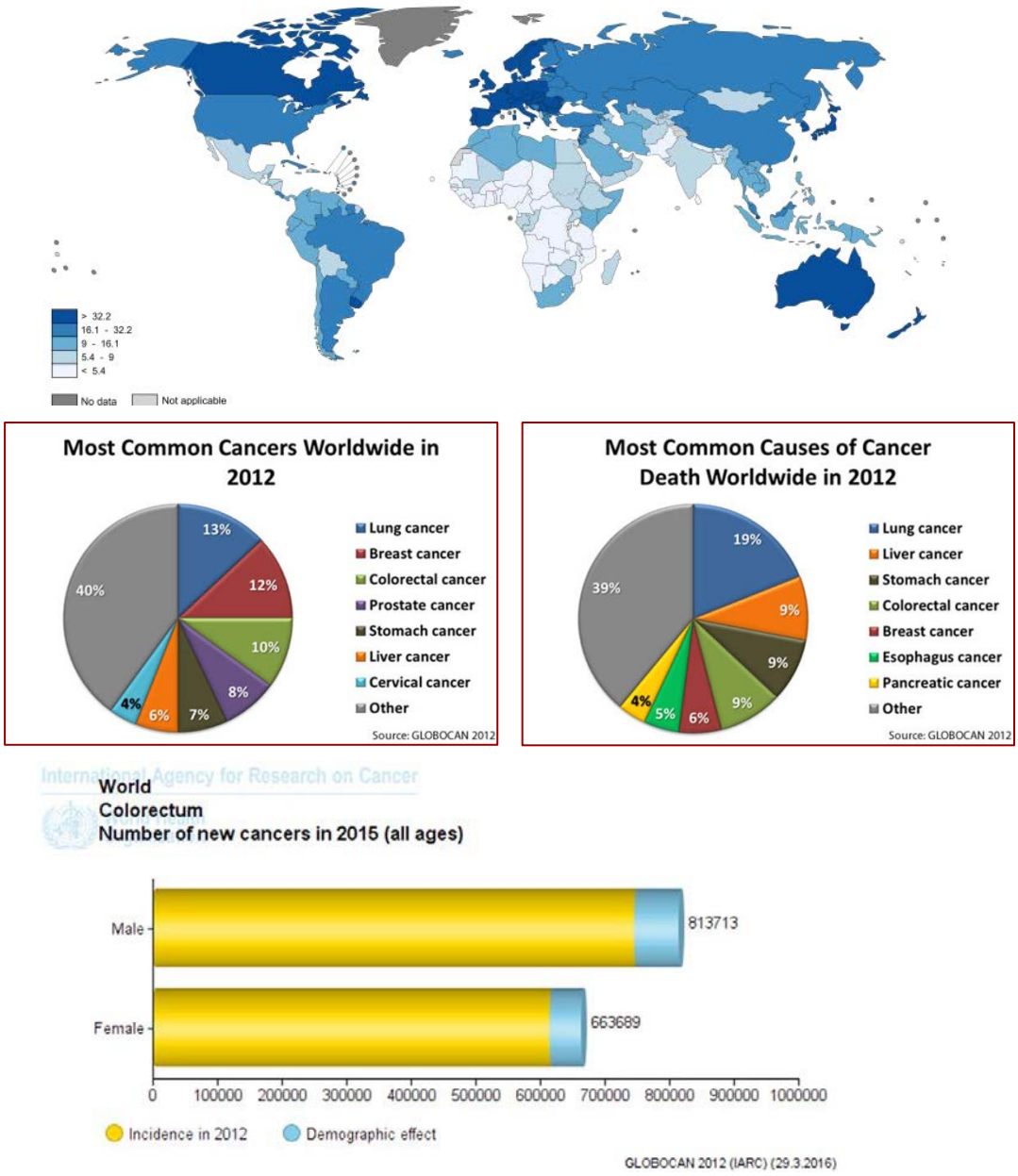

Figura 1. Mapa de la incidencia del cáncer a nivel mundial y por países (GLOBOCAN 2012, WHO 2015)

El CRC es un tipo de cáncer que no suele dar síntomas hasta que se encuentra en fases avanzadas, lo que condiciona que la mayoría de pacientes tengan tumores que ya han invadido toda la pared intestinal y/o afectado a los ganglios locorregionales (6). En el momento del diagnóstico, aproximadamente un 20% de los pacientes tienen la enfermedad en fase metastásica y entre un 30 y un 40% de los que tienen un tumor localizado acaban desarrollando metástasis. Este tipo de neoplasias aparece con mayor frecuencia a partir de los 50-70 años, aunque pueden darse casos por debajo de los 40 años, generalmente en el contexto de formas hereditarias de la enfermedad.

Los tumores se clasifican en función de la estructura a la que afectan y de su capacidad para diseminarse a los ganglios próximos o para dar lugar a metástasis (Tabla 1) (7).

Tabla 1. Definiciones de la clasificación TNM y estadiaje según esta clasificación del cáncer colorrectal. (Adaptada de Compton et al., 2004).

Clasificación TNM	Categoría	Descripción
Tumor primario (T)	T0	No hay evidencia de tumor primario
	Tis	Carcinoma in situ: intraepitelial o intramucoso
	T1	Tumor invade submucosa
	T2	Invasión de muscular propia
	T3	Invasión de la subserosa
	T4	Invasión órganos adyacentes y/o cavidad intraperitoneal
Afectación ganglionar (N)	N0	No hay afectación ganglionar
	N1	Metástasis en de 1 a 3 ganglios
	N2	Metástasis en más de 4 ganglios
Metástasis distantes (M)	M0	Ausencia de metástasis
	M1	Metástasis distantes

Clasificación TNM	Características		
Estadio 0	Tis	N0	M0
Estadio I	T1-T2	N0	M0
Estadio IIA	T3	N0	M0
Estadio IIB	T4	N0	M0
Estadio IIIA	T1-T2	N1	M0
Estadio IIIB	T3-T4	N1	M0
Estadio IIIC	Cualquier T	N2	M0
Estadio IV	Cualquier T	Cualquier N	M1

El estadio en el que se encuentra la enfermedad es el principal factor predictivo de la supervivencia de los pacientes, que varía desde un 90% de supervivencia a los 5 años para tumores detectados en la fase localizada (estadío I), hasta un 5-8% para aquellas personas a las que se les diagnostica un CRC metastásico (estadío IV) (8).

Como en otras enfermedades complejas, el CRC está causado por factores genéticos y ambientales. Diferentes estudios indican que la dieta y el estilo de vida occidental aumentan el riesgo de desarrollar este tipo de cáncer en los países industrializados. La contribución de estos factores al desarrollo de la enfermedad queda patente al comparar el aumento de la incidencia de este tipo de tumor en paralelo con el crecimiento económico y la adopción del estilo de vida occidental por parte de países en vías de desarrollo (9). Así, individuos con una predisposición genética adquirida o heredada y expuestos a estos factores ambientales tienen una mayor probabilidad de desarrollar un CRC (10).

1.1.3. Tratamiento del cáncer colorrectal

Para el tratamiento del CRC existen cuatro aproximaciones: cirugía, quimioterapia, radioterapia y las conocidas como terapias dirigidas. El pilar del tratamiento para este tipo de neoplasia es la cirugía. En los estadios iniciales de la enfermedad (0 y I), la escisión del tumor se puede llevar a cabo sin la necesidad de administrar otro tipo de tratamiento, ya que la tasa de recurrencia cuando los ganglios regionales no están afectados es muy baja. A medida que la enfermedad avanza, se requieren terapias adyuvantes para reducir el riesgo de reproducción del tumor. En este punto, el arsenal terapéutico incluye la quimioterapia, la radioterapia y las terapias dirigidas. La secuencia en la que los agentes terapéuticos se utilizan, solos o en combinación, es importante para conseguir el máximo periodo de control de la enfermedad con los mínimos efectos secundarios posibles. Se indican a continuación las características de algunos de los tratamientos terapéuticos más significativos.

1.1.3.1. Fluoropirimidinas

Hasta hace 20 años, el único fármaco disponible para el tratamiento del CCR era el 5-fluorouracilo (5-FU), una fluoropirimidina que inhibe la acción de la timidilato sintasa, una enzima clave en la síntesis de la timina, cuya carencia hace que el ADN no se pueda replicar impidiendo el crecimiento tumoral (11). Dada su corta vida media en el plasma, requiere de tiempos de perfusión prolongados con las molestias y complicaciones que puede ocasionar a los pacientes.

Para superar los problemas en la administración del 5-FU se desarrollaron la Capecitabina y el Tegafur con uracilo (UFT), dos fluoropirimidinas orales. La Capecitabina se absorbe intacta en el intestino donde se convierte, mediante una serie de reacciones enzimáticas, en el 5-FU. La timidina fosforilasa, enzima involucrada en la conversión final a 5-FU, se encuentra en niveles más altos en las células tumorales que en las sanas, con lo que este fármaco proporciona mayores dosis del agente quimioterapéutico al tumor a la vez que reduce la exposición sistémica al mismo (12). El Tegafur funciona de una forma similar aunque no se usa con tanta frecuencia.

1.1.2.1. Irinotecan y otras camptotecinas

Las camptotecinas son agentes citotóxicos con una actividad tumoral de amplio espectro y cuyo mecanismo de acción se basa en la inhibición de la topoisomerasa I sin afectar a la topoisomerasa II. La topoisomerasa I es una enzima que participa en procesos biológicos fundamentales que incluyen la replicación, la transcripción y la reparación del ADN. Actúa uniéndose al ADN durante la replicación celular y modificando su topología al provocar roturas transitorias que vuelve a sellar. Las

camptotecinas estabilizan un complejo ternario con el intermediario formado por el ADN y la enzima, impidiendo que siga realizando su función y provocando una muerte celular programada (13, 14).

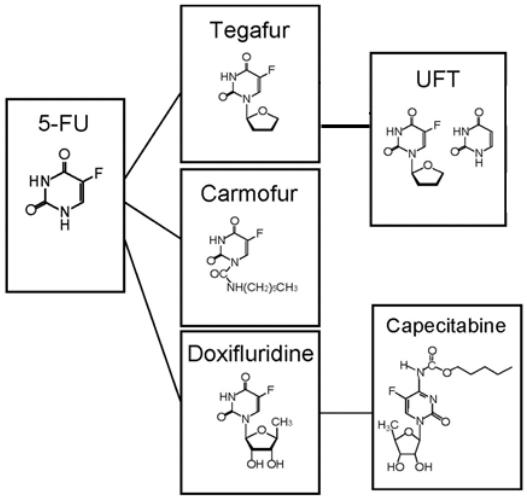

Figura 2. Evolución de las fluoropirimidinas. Estructura del 5-Fluorouracilo (5-FU) y sus derivados (Nakayama et al., 2010) (15).

La camptotecina natural (CPT), extraída del árbol *Camptotheca acuminata*, es insoluble en agua. Para facilitar la administración parenteral se sintetizaron y desarrollaron diferentes análogos solubles en agua: el irinotecan, CPT-11, (Figura 3), para CRC, y el topotecan, aprobado para el tratamiento de cáncer de ovario y el de pulmón de células pequeñas (16-18).

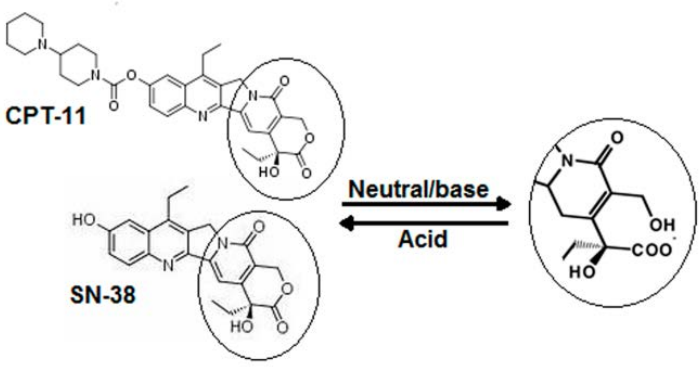

Figure 3. Estructura molecular de las camptotecinas. Equilibrio entre sus formas lactona y carboxylato (Casadó et al., BBA 2016) (19).

El irinotecan (7-ethyl-10-[4-(1-piperidino)-1-piperidino] carbonyloxycamptothecin, CPT-11) es un derivado semisintético de la camptotecina que inhibe la acción de la topoisomerasa I. Se convierte en SN-38 (7-ethyl-10-hydroxycamptothecin), su metabolito activo, por acción de una carboxilesterasa. Se trata de una enzima que

separa la cadena lateral de piperidina del CPT-11 mediante hidrólisis del enlace carbamato (20) y que se encuentra, principalmente, en hígado y sangre, así como en depósitos tumorales (Figura 4).

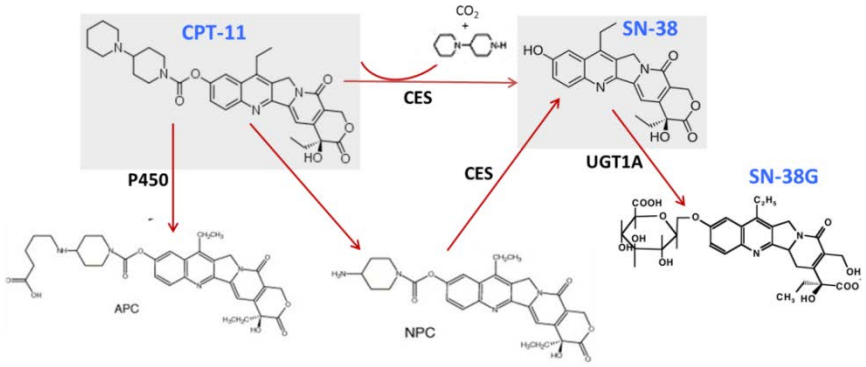

Figura 4. Metabolismo del Irinotecan. El CPT-11 es oxidado por una isoenzima del citocromo P450 (carboxilesterasa) y se transforma en 7-ethyl-10-[4-N-(5-aminopentanoic acid)-1-piperidino] carbonyloxycamptothecin (APC) y 7-ethyl-10-[4-(1-piperidino)-1-amino]-carbonyloxycamptothecin (NPC). Las carboxilesterasas (CES) metabolizan el CPT-11 a su metabolito activo SN-38. El SN-38 es inactivado por una isoforma de la UDP-glucuronosiltransferasa (UGT1A), que lo transforma en el derivado glucuronido (SN-38G).

Así pues, el CPT-11 se considera el pro-fármaco del SN-38, que se ha estimado que es entre 100 y 1000 veces más citotóxico que su progenitor (21). Actúan estabilizando el complejo ADN-topoisomerasa I frenando la replicación celular (Figura 5) (8, 14).

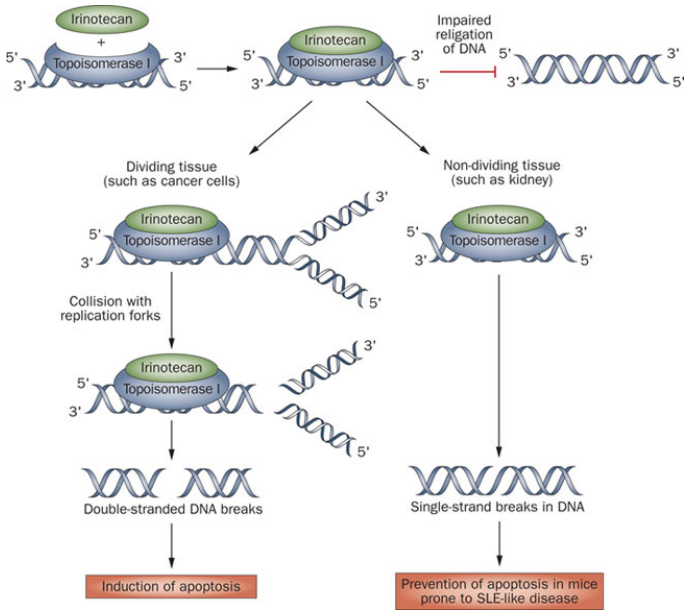

Figura 5. Mecanismo de actuación del Irinotecan sobre la toposiomerasa I. (Frese et al., 2011) (22).

El principal mecanismo de eliminación del SN-38 es a través del hígado, en donde se conjuga con el ácido glucorónico para dar el consiguiente glucoronidato (SN-38G). Se ha demostrado que la actividad de las β-glucoronidasas de la microflora intestinal rompe este complejo y libera el SN-38, lo que contribuye de forma sustancial a la toxicidad del irinotecan (23). La acumulación de SN-38 en el intestino provoca diarreas severas, el principal efecto secundario de su precursor.

Diferentes ensayos clínicos han demostrado la eficacia del irinotecan para el tratamiento del CRC (24, 25). La combinación de irinotecan con 5-FU muestra un incremento del 20% en la respuesta al tratamiento, aumenta la supervivencia global de los pacientes, y, aunque cuando se toma irinotecan las diarreas son más severas, esto no compromete la calidad de vida de los pacientes (26-28).

1.1.2.2. Oxaliplatino

El oxaliplatino es un compuesto de platino de tercera generación en el que el átomo de platino forma un complejo con el 1,2-diaminociclohexano y con un ligando oxalato (Figura 6). Su actividad citotóxica se basa en la formación de aductos con el ADN; en concreto, forma puentes cruzados al unirse de forma simultánea a dos bases nitrogenadas de la cadena. Esto inhibe la replicación y la reparación del ADN y provoca la muerte celular por apoptosis (29). En pacientes con CRC metastásico, el oxaliplatino en monoterapia tiene una eficacia limitada, pero sí que se han observado los beneficios de administrarlo en combinación con el 5-FU, doblando la eficacia de esta fluoropirimidina debido a que se ha propuesto que el compuesto de platino disminuye la expresión de la timidilato sintasa (30). El principal efecto secundario del oxaliplatino es la neuropatía, que se caracteriza por parestesias en manos y pies, y que puede persistir aun cuando se ha finalizado la pauta terapéutica.

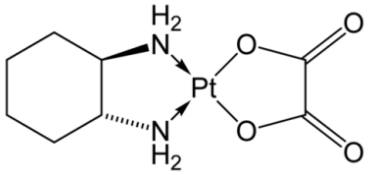

Figura 6. Estructura química del Oxaliplatino.

1.1.2.3. Terapias dirigidas

Los avances en la comprensión de los mecanismos moleculares asociados al desarrollo del CRC, han posibilitado la identificación de un gran número de potenciales dianas terapéuticas. Así, se han desarrollado diferentes anticuerpos monoclonales, algunos de los cuales ya han demostrado su eficacia en el tratamiento del CRC metastásico cuando se administran en combinación con la quimioterapia.

1.1.2.3.1. Inhibidores de la angiogénesis

Una estrategia para controlar la proliferación de las células tumorales y su diseminación consiste en la inhibición de la formación de nuevos vasos sanguíneos o neoangiogénesis. En la actualidad, la más eficaz se centra en bloquear el factor de crecimiento vascular endotelial (VEGF), una proteína que induce la creación de vasos sanguíneos y que tiene un papel crucial en el crecimiento del tumor al posibilitar la llegada de nutrientes y oxígeno. El Bevacizumab (Figura 7A) es un anticuerpo monoclonal humanizado dirigido contra el VEGF que ha demostrado su eficacia para el tratamiento de primera línea de pacientes con CRC metastásico cuando se administra con 5-FU o irinotecan y con un buen perfil de seguridad (31).

1.1.2.3.2. Inhibidores del receptor del factor de crecimiento epidérmico

El receptor del factor de crecimiento epidérmico (EGFR) es una glicoproteína transmembrana que interactúa con diversas rutas de señalización celular involucradas en el crecimiento celular, la proliferación y la muerte celular programada. Es un miembro de los receptores transmembrana tirosina quinasa (ErbB) y está sobreexpresado en tumores de origen epitelial, como es el caso del CRC. En la actualidad existen dos tipos de tratamientos anti-EGFR: anticuerpos monoclonales que se unen al antígeno EGFR bloqueándolo, como el cetuximab y el panitumumab e inhibidores de la tirosina quinasa del receptor del factor de crecimiento epidérmico humano tipo 1, entre los que se encuentran el erlotinib y el gefitinib, que impiden la fosforilación intracelular del EGFR, que se expresa en la superficie de células normales y cancerígenas (Figura 7B) (32).

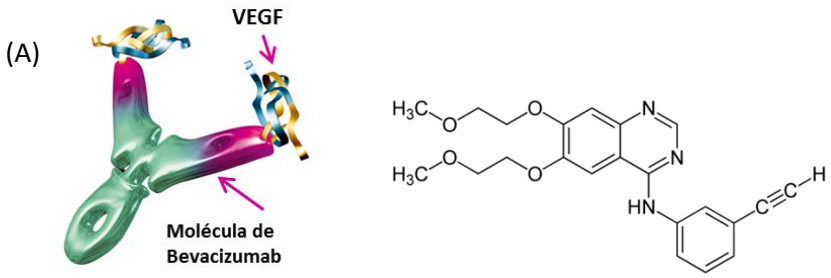

Figura 7. Estructura molecular del Bevacizumab (A) y del erlotinib (B).

1.2. Estrategias para el desarrollo de transportadores para el tratamiento del cáncer

Los compuestos de platino, las camptotecinas y muchos otros fármacos para el tratamiento o para el diagnóstico del cáncer tienen una solubilidad en disolventes acuosos y una biodisponibilidad bajas, así como numerosos efectos secundarios. Los nanotransportadores, como nanopartículas poliméricas o liposomas, proporcionan solución a estos problemas ya que encapsulan al fármaco en su interior y lo liberan en el lugar de actuación, con una especificidad mayor por las células tumorales y, por consiguiente, con menos efectos secundarios. Para su formulación y desarrollo deben tenerse en cuenta aspectos como el lugar al que se quiere llegar y la naturaleza del fármaco a encapsular para seleccionar el tipo de vehículo, su composición y la metodología más adecuada para su preparación. También, la forma de dirigir el fármaco hacia su diana terapéutica.

1.2.1. Barreras fisiológicas

Uno de los aspectos fundamentales en el desarrollo de un vehículo eficaz es la consideración de los impedimentos que se encontrará después de su administración *in vivo* y las dificultades que deberá superar para liberar el fármaco en el lugar de actuación: de ello dependerá la eficacia de cualquier tratamiento. Que el nanotransportador con su carga terapéutica alcance su destino, es decir, que llegue a las células del tumor, dependerá de una secuencia de procesos que incluye la distribución a través del espacio vascular, el transporte a través de las paredes de los vasos sanguíneos y la difusión hacia los espacios intersticiales en el tejido tumoral. Estos son procesos dinámicos que varían con el tiempo y las propiedades del tumor y que están influenciados por aspectos físico-químicos del fármaco y por factores biológicos del tumor.

Cuando la administración se realiza por vía intravenosa las primeras barreras son la membrana basal del tejido epitelial y el endotelio vascular. Si el fármaco se inyecta directamente en el tumor, su liberación en las células tumorales se producirá principalmente por difusión a través del espacio intersticial (Figura 8). La biodisponibilidad de los transportadores y su biodistribución, así como su paso a través del endotelio, dependerán del tamaño y de las características superficiales del vehículo. Para que el tiempo de residencia en el torrente sanguíneo sea mayor debe evitarse la opsonización y la posterior ingestión y eliminación por parte de los fagocitos. La siguiente barrera es la matriz extracelular, que debe atravesarse para poder llegar a las células diana dentro del tejido. Marcar la superficie del transportador con ligandos específicos para receptores de la membrana celular facilita la difusión del vehículo hacia estas células específicas. Una vez dentro de la célula, se deben cruzar

nuevas barreras si se quiere acceder al núcleo u otros orgánulos dentro del citoplasma (33).

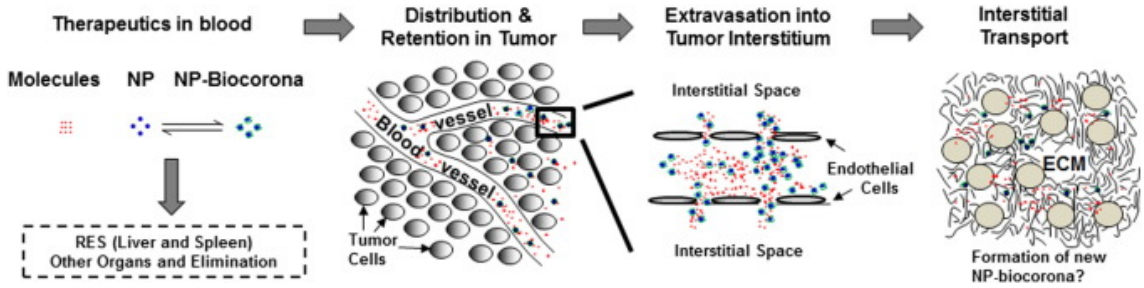

Figura 8. Proceso de transporte de un fármaco hacia el tejido tumoral (34).

Si se considera la administración oral (Figura 9A), la adhesión y la difusión de un fármaco sobre y a través de la mucosa del tracto gastrointestinal (TGI) constituye un serio inconveniente en lo que respecta a su biodisponibilidad y un reto en cuanto al diseño de formulaciones que deban superar esta barrera fisiológica (35). La fisiología propia del TGI es la responsable de estas limitaciones. Factores como la baja permeabilidad de la mucosa, junto con la posible degradación del fármaco antes de su absorción explicarían los pobres resultados obtenidos hasta el momento. Por otra parte, la eficacia de la vía oral se relaciona con el entorno químico, enzimático y físico del TGI. Apenas ingerido un fármaco, su estabilidad se ve comprometida por el pH ácido del estómago y por la acción de las enzimas digestivas secretadas a lo largo del TGI. Para salvar estas dificultades se están aplicando diferentes tipos de sistemas nanoparticulados. Debe tenerse en cuenta, no obstante, que el mucus que recubre las células del epitelio intestinal puede actuar como una barrera que dificulte la penetración de las nanopartículas (36). Este hidrogel biológico actúa como primera línea de defensa del organismo frente a patógenos y sus propiedades de permeabilidad selectiva desempeñan un papel crucial, tanto en estados de salud como de enfermedad (Figura 9B).

Tal y como sucede con los productos de deshecho, los sistemas tradicionales de vehiculización de fármacos como micro- y nanopartículas, son retenidos de forma eficaz por los componentes del mucus y eliminados rápidamente mediante diversos mecanismos, limitando, de esta manera, su eficacia. La existencia de esta capa de mucus ha permitido elaborar una interesante estrategia para aprovechar lo que en principio suponía un inconveniente: conseguir que el producto farmacéutico se adhiera a las membranas de la mucosa y posibilitar que el tiempo de retención en el lugar de absorción sea mayor, aumentando su biodisponibilidad. El diseño de transportadores dotados de superficies con características especiales ha permitido desarrollar sistemas

mucoadhesivos, eficaces en cuanto a su internalización celular y con posibilidades de ser vectorizados.

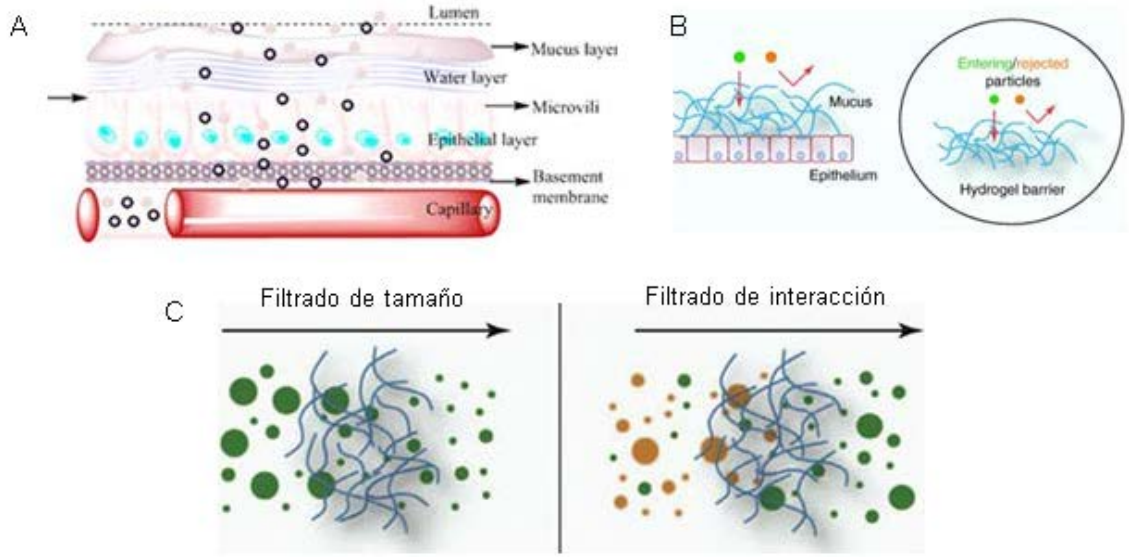

Figura 9. Transporte y absorción a través del TGI (A) (37); Polímeros de mucina que recubren el epitelio húmedo formando un hidrogel que actúa como un filtro selectivo (B); Propiedades de barrera estérica e interactiva del mucus (C) (38).

1.2.2. Vectorización pasiva y vectorización activa

Se han descrito diferentes aproximaciones para el diseño de nanotransportadores. La vehiculización pasiva o la vehiculización activa y la utilización de transportadores convencionales o de transportadores modificados en su superficie son criterios de selección para desarrollar formulaciones adecuadas para aplicaciones específicas. La vectorización pasiva hace referencia a la acumulación de fármacos o de transportadores en un lugar específico del organismo debido a factores fisicoquímicos o farmacológicos, mientras que la activa utiliza ligandos, polisacáridos o pequeñas moléculas de reconocimiento situados sobre la superficie del transportador para que las células de tejidos u órganos tumorales los reconozcan e incorporen de manera selectiva y específica (Figura 10).

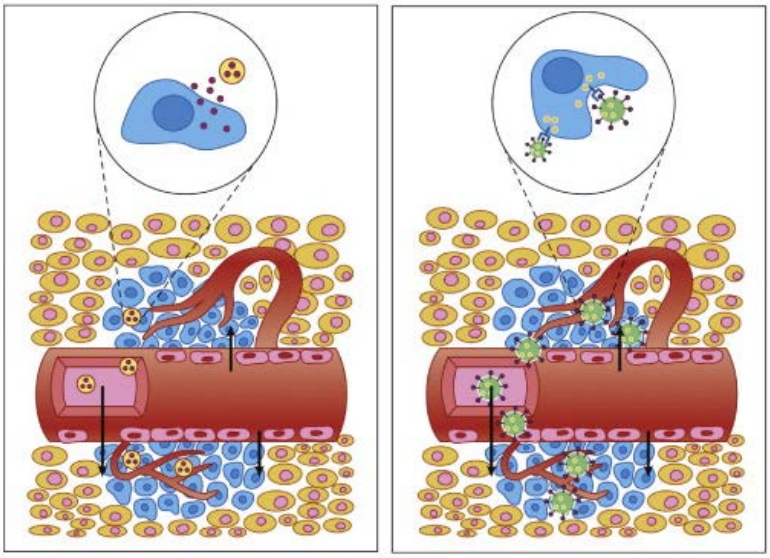

Figura 10. Vehiculización activa y pasiva. La vehiculización pasiva se basa en el efecto EPR y facilita la acumulación del transportador en la zona tumoral. En la vehiculización activa, ligandos de reconocimiento sobre la superficie del transportador median en la endocitosis e internalización celular (Xu et al., 2015) (39).

La aplicación de estrategias de transporte pasivo se basa en el efecto de permeabilidad y retención aumentada (EPR) (40). Los tejidos patológicos, inflamatorios o de tumores sólidos, se caracterizan por su mayor permeabilidad vascular debido a una angiogénesis rápida y defectuosa. En el caso de las células tumorales, su rápida proliferación hace necesaria la creación de nuevos vasos sanguíneos para cubrir las demandas de nutrientes y oxígeno (41).

Estos vasos tienen una arquitectura deficiente, con un endotelio discontinuo y grandes huecos entre células adyacentes que permiten el paso de moléculas de hasta 4.000 KDa o 500 nm, al espacio intersticial (33). Este hecho unido a que el drenaje linfático de los tumores no funciona correctamente, hace que la retención de los nanotransportadores en el tumor resulte incrementada. El diseño de un vehículo de vectorización pasiva implica la consideración de ciertos requisitos que determinen que el tiempo de circulación sea prolongado y pueda alcanzar la región del tumor. Dos factores influyen en este aspecto, el tamaño y la carga de superficie del transportador. Respecto al tamaño, se ha demostrado que valores de alrededor de 200 nm resultan adecuados para la vehiculización pasiva basada en el efecto EPR, mientras que valores superiores incrementan la captura por el sistema retículoendotelial (SRE). En cuanto a la carga de superficie, además de determinar la estabilidad física del transportador, facilitará su interacción con las células y su posterior internalización (42). La vectorización pasiva depende de las propiedades mecánicas y físicas del

transportador y, aunque permite la acumulación del fármaco en el lugar de acción, no asegura la especificidad del vehículo por la célula tumoral.

Las estrategias de vectorización activa implican la utilización de ligandos o anticuerpos específicos que, unidos a la superficie del tranportador, determinen su unión selectiva a aquellas células (dianas) que sobreexpresen el receptor adecuado. La vehiculización dirigida queda garantizada por la elevada especificidad de la interacción entre el ligando y su receptor de reconocimiento (43). De esta manera se asegura que el fármaco se libere sólo en un tipo determinado de célula o tejido. Para conseguir este propósito se han utilizado una gran variedad de moléculas de reconocimiento, algunas de pequeño tamaño como el ácido fólico o carbohidratos, mientras que otras son macromoléculas como péptidos, proteínas, anticuerpos y sus fragmentos, oligonucleótidos y ácidos nucleicos (aptámeros). El éxito de la vehiculización dirigida va a depender de la disponibilidad de la diana y del ligando, así como de la densidad de moléculas de reconocimiento sobre la superficie del transportador.

También es indispensable que los receptores diana se expresen de forma diferencial en las células tumorales y no en las células sanas y que lo hagan de forma homogénea para un mismo tipo celular. La internalización suele producirse por endocitosis (Figura 11A), como sucede, por ejemplo, cuando se usa folato como ligando para dirigir el transportador a células marcadas por el receptor, antígeno tumoral sobreexpresado en fases avanzadas del cáncer. En general, cuando el complejo transportador-ligando se une al receptor de la superficie celular, se produce una invaginación en la membrana que envuelve el complejo receptor-ligando y forma un endosoma. Este endosoma será transportado al orgánulo correspondiente posibilitando la liberación del fármaco en el interior de la célula (44) (Figura 11B).

Su internalización y el tránsito hacia el núcleo pueden tener lugar mediante diferentes mecanismos. Las moléculas pequeñas pueden atravesar la cubierta nuclear a través de canales acuosos mediante difusión pasiva, mientras que las moléculas de mayor tamaño o estructuras como los diferentes sistemas nanoparticulados pueden entrar en el núcleo durante la mitosis, mediante un mecanismo de transporte activo, dependiente de energía y con requerimientos específicos o, mediante la fusión de los endosomas, con su carga terapéutica, con la membrana nuclear (34).

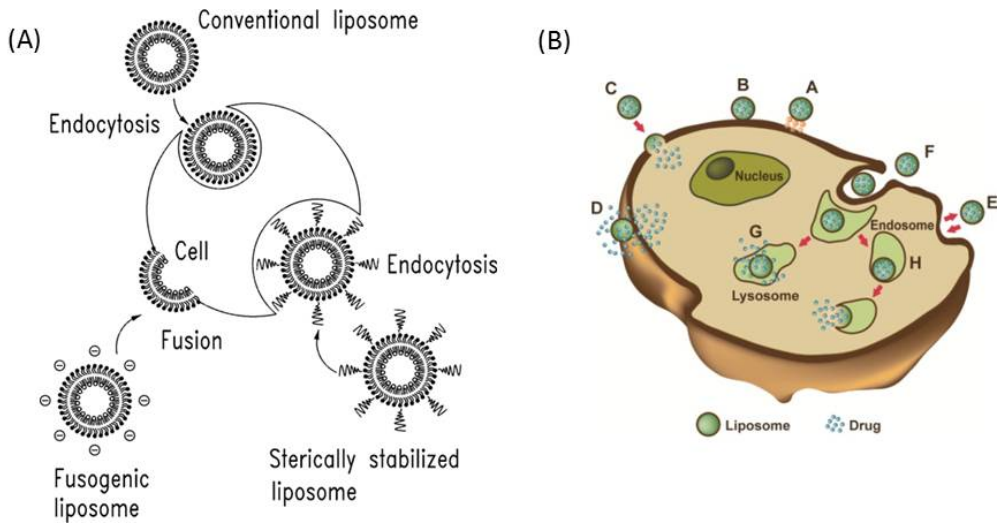

Figura 11. Mecanismos de internalización. (A) Formas de endocitosis y fusión de las membranas celular y liposomal (45). (B) Una vez internalizado, se forma un endosoma que desplazará al liposoma con su carga (46).

1.2.3. Plataformas nanotecnológicas en la terapia del cáncer

Una de las principales razones de las muertes causadas por el cáncer es la falta de selectividad en la actuación de los fármacos anticancerosos sobre los tejidos neoplásicos. La vehiculización dirigida y la liberación controlada de fármacos pueden proporcionar soluciones a los principales problemas subyacentes al tratamiento del cáncer y ha sido objeto de gran atención en los últimos años (Figura 12).

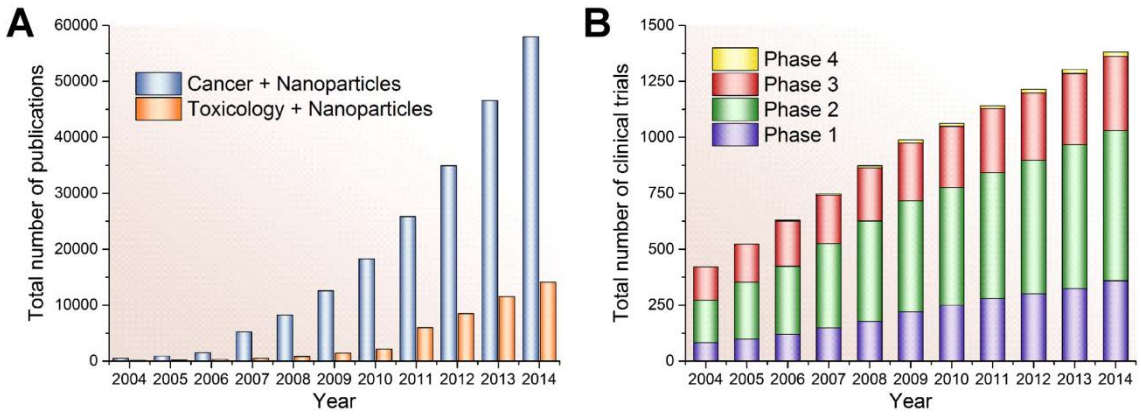

Figura 12. (A) Número total de publicaciones (Web of Science®) y (B) de ensayos clínicos, que utilizan nanomedicinas, en un período de tiempo de 10 años. El crecimiento de las publicaciones sobre la utilización de sistemas nanoparticulados en la terapia del cáncer ha sido exponencial (47).

Por otra parte, el auge de las nanotecnologías ha permitido desarrollar nanotransportadores versátiles y biocompatibles, que han representado progresos

significativos en la quimioterapia del cáncer, gracias al diseño de los sistemas apropiados. Estructuras particuladas, constituidas por lípidos y/o polímeros, son capaces de alterar la farmacocinética y biodistriobución de los fármacos, mejorando sus propiedades farmacológicas y proporcionando beneficios terapéuticos: liposomas, microesferas y nanopartículas lipídicas o poliméricas constituyen algunas de las mejores opciones. También se consideran las micelas, dendrímeros y nanotubos de carbono, entre otros (Figura 13).

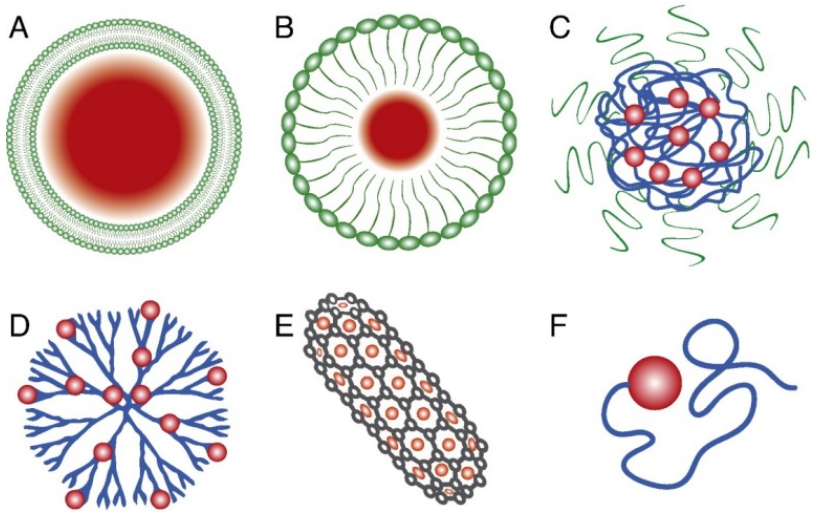

Figura 13. Tipos de transportadores: (A) liposomas, (B) micelas, (C) nanopartículas poiméricas, (D) dendrímeros, (E) Nanotubos de carbono y (F) Conjugados polímero-fármaco (48).

Existen argumentos sólidos que avalan el desarrollo de las terapias basadas en la administración de este tipo de medicinas. Por ejemplo, solucionan problemas relacionados con la solubilidad o la estabilidad química de los fármacos antitumorales y pueden mejorar su biodistribución mediante la aplicación del concepto de vehiculización dirigida. También se ha descrito que pueden disminuir la resistencia de los tumores a este tipo de compuestos (49). La utilización de las nanotecnologías ha permitido desarrollar terapias personalizadas que han mejorado el tratamiento de muchas enfermedades.

1.2.3.1. Nanopartículas y nanoconjugados poliméricos

Las nanopartículas preparadas mediante la utilización de polímeros transportan de forma efectiva fármacos y otras moléculas a los tejidos diana, con un tiempo de vida media prolongado y con baja toxicidad. Se han estudiado y desarrollado diferentes tipos de polímeros para el diseño de nanotransportadores. Los vehículos se pueden construir a partir de compuestos de síntesis, como el ácido poli-láctico (PLA) y el ácido poli-láctico-co-glicólido (PLGA) (50), o a partir de polímeros naturales como el quitosano (CS) y el colágeno (51). Estos polímeros también se utilizan para recubrir

otro tipo de sistemas de vectorización nanoparticulados. El polietilenglicol (PEG), por ejemplo, cuando se utiliza como recubrimiento, permite que las nanoparticulas no sean eliminadas por el SRE, lleguen al sistema nervioso central y puedan cruzar la barrera hematoencefálica (52).

Los nanoconjugados poliméricos son transportadores que llevan unidos de forma covalente distintas moléculas como péptidos o proteínas (53). Suelen prepararse con PEG, poliglutamato, dextrano y N-(2-hidroxipropil) metilacrilamida (HPMA) (54).

1.2.3.2. Nanotransportadores lipídicos

Los transportadores constituidos por lípidos son biocompatibles, biodegradables, permiten aislar a la molécula que transportan del entorno y pueden encapsular tanto compuestos hidrofílicos como hidrofóbicos. Los liposomas y las micelas son ejemplos de este tipo de nanotransportadores. Según su composición y la forma molecular de sus componentes, los constituyentes de las partículas lipídicas pueden adoptar diferentes estructuras cuando se dispersan en un medio acuoso y, así, se pueden formar liposomas o diferentes tipos de micelas.

La capacidad de las moléculas lipídicas para formar bicapas se ha explicado sobre la base de la denominada forma molecular y del parámetro de empaquetamiento (p) (55) (Figura 14). El concepto “forma” considera el tamaño de las regiones polar e hidrofóbica, la hidratación de la cabeza polar y su carga, la capacidad para establecer enlaces de hidrógeno y los efectos de contraiones. Así, los lípidos que forman bicapas, como la fosfatidilcolina (PC), fosfatidilserina (PS), esfingomielina y fosfatidilglicerol (PG), tienen una geometría cilíndrica compatible con este tipo de organización. Los lisofosfolípidos forman estructuras micelares, ya que su geometría corresponde a la de un cono invertido y los lípidos como la fosfatidiletanolamina (PE), cuya sección en la región hidrofóbica es mayor que en la cabeza polar, forman micelas invertidas y estructuras hexagonales HII. No obstante, debe tenerse en cuenta que cambios de temperatura o de pH pueden modificar el estado de agregación de mezclas de lípidos.

Los liposomas son estructuras esféricas formadas por una o varias bicapas lipídicas concéntricas que contienen espacios acuosos internos (56, 57). Son vehículos muy versátiles, dado el gran abanico de componentes que pueden utilizarse en su preparación y su diseño se puede adaptar a las características que requiera, tanto la molécula a transportar, como el lugar al que se quiere acceder. Los liposomas tienen dos entornos bien diferenciados lo que les permite transportar tanto sustancias hidrofílicas, ubicadas en el espacio acuoso interno, como moléculas hidrofóbicas, inmersas en la región hidrocarbonada de la bicapa (58, 59).

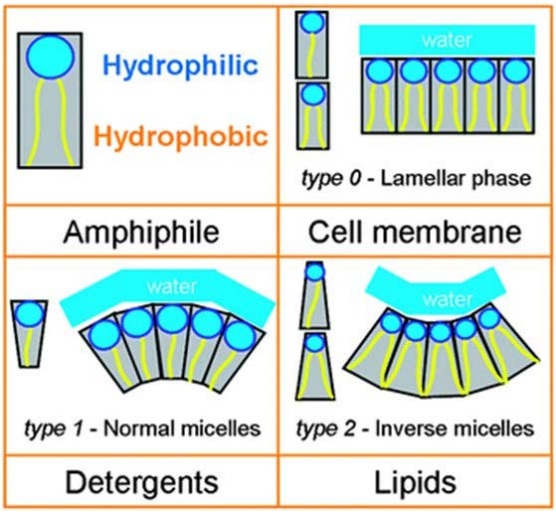

$$p = \frac{\upsilon}{a_0 \, l_0}$$

- p es el volumen molecular de la región hidrofóbica.
- a_0 es el área superficial óptima por molécula en la interfase lípido-agua.
- l_0 es el espesor medio crítico de la región hidrocarbonada.

Figura 14. Moléculas anfifílicas y formas de autoagregación (60).

Las micelas, en cambio, son agregados lipídicos con un núcleo hidrofóbico y una superficie polar o, por el contrario, con un núcleo polar y una cubierta lipofílica (micelas invertidas). Son estructuras esféricas formadas por una monocapa lipídica o polimérica. Las primeras son adecuadas para el transporte de moléculas insolubles en agua y su capa externa polar las hace estables en medios acuosos y apropiadas para su administración intravenosa (61). Su pequeño tamaño (inferior a 50 nm) y su cubierta hidrofílica las hace resistentes a la eliminación por el SRE, lo que incrementa el tiempo de circulación y la posibilidad de que el fármaco que incorporan alcance su diana terapéutica.

1.2.3.3. Dendrímeros

Los dendrímeros son macromoléculas sintéticas con una estructura similar a la de un árbol con diferentes ramas alrededor de un núcleo central, cuyo tamaño y forma se pueden modificar, lo que hace de este nanotransportador una herramienta muy versátil (62). Se han utilizado para transportar fármacos como el 5-FU o el metotrexato (51, 63), mejorando su eficacia y disminuyendo su toxicidad, o para sondas para el diagnóstico por la imagen (61).

1.2.3.4. Nanotubos de carbono

Los nanotubos de carbono son cilindros de carbono formados por anillos de benceno que se utilizan como sensores para detector ADN y proteínas, como herramientas de diagnóstico para discriminar proteínas en muestras de suero y como trasportadores para proteínas, vacunas o fármacos (64). Deben estar funcionalizados, pues son muy insolubles en cualquier disolvente, pero han demostrado *in vitro* su capacidad para internalizarse en las células (65).

1.3. Desarrollo de liposomas

Los liposomas son vesículas esféricas, de dimensiones coloidales, que contienen espacios acuosos delimitados por bicapas lipídicas o lamelas, análogas a las de las membranas biológicas. Su particular estructura les permite incorporar moléculas liposolubles, inmersas en su domino hidrofóbico, o alojar compuestos hidrosolubles en el entorno acuoso. Actúan como reservorios liberando el fármaco que transportan de forma lenta y controlada, prolongan su acción en el tiempo y disminuyen, por consiguiente, la frecuencia de las administraciones. Además, se pueden dirigir de forma selectiva a dianas específicas (uso de moléculas de reconocimiento, vehiculización activa) y se puede controlar la velocidad de liberación del producto incorporado (liberación inducida específicamente). Una combinación de algunas de las diferentes estrategias podría proporcionar formulaciones farmacéuticas muy útiles, con mejoras substanciales de los índices terapéuticos de los antitumorales.

Las propiedades de los liposomas dependen de su composición, que define las características mecánicas de la bicapa y de las propiedades de superficie, que condicionan los aspectos relacionados con las interacciones. Se formulan principalmente a partir de fosfolípidos, que pueden ser naturales de distinto origen o de síntesis. Algunos esfingolípidos y el colesterol son también constituyentes habituales de las bicapas liposomales. Desde que Bangham, hace más de 50 años, observara que las lamelas de fosfolípidos podían impedir la difusión de los iones que contienen (66, 67) y que formaban estructuras cerradas en forma de bicapas en medios acuosos, el estudio de las agregaciones organizadas de lípidos se ha utilizado como modelo de membrana celular en campos como la medicina, la bioquímica y la biología (68). El concepto de que los liposomas podían servir para encapsular fármacos y ser utilizados como sistemas para su transporte fue descrito por primera vez por Gregoriadis en 1976 (69, 70).

Los liposomas se forman espontáneamente cuando los fosfolípidos y otros lípidos anfipáticos se dispersan en agua, dando lugar a una población de vesículas cuyo tamaño puede oscilar desde 10 nm a 10 μm. La organización de estos sistemas se debe a la interacción hidrofílica de las cabezas polares con el agua y a la tendencia de la porción no polar de estas moléculas a situarse en un entorno de las mismas características. Los fosfolípidos tienen un grupo hidrófilo y dos cadenas hidrocarbonadas largas e hidrófobas que determinan su escasa o nula solubilidad en agua a menos que se estructuren conjuntamente en forma de bicapas. La formación de liposomas implica, pues, un proceso de autoagregación de las moléculas que los constituyen (Figura 15).

La minimización de la energía cuando la bicapa se cierra para formar una vesícula esférica tiene como contrapartida el coste energético asociado a la flexión de la bicapa hasta formar la esfera, que es proporcional a la inversa del cuadrado del radio de la misma. A medida que la bicapa se reorganiza y evoluciona desde la estructura de disco plano a la de esfera, la energía total del sistema aumenta, en primer lugar, debido a las contribuciones de la flexión de la bicapa; después, la energía total disminuye al desaparecer, cuando se unen, los extremos de la bicapa abierta. La autoagregación de las moléculas fosfolipídicas conduce a la formación de una serie de bicapas apiladas que, durante el proceso de hidratación darán lugar, cuando se unan los extremos, a liposomas multilamelares (MLVs), a partir de los cuales se podrán formar las estructuras unilamelares (71).

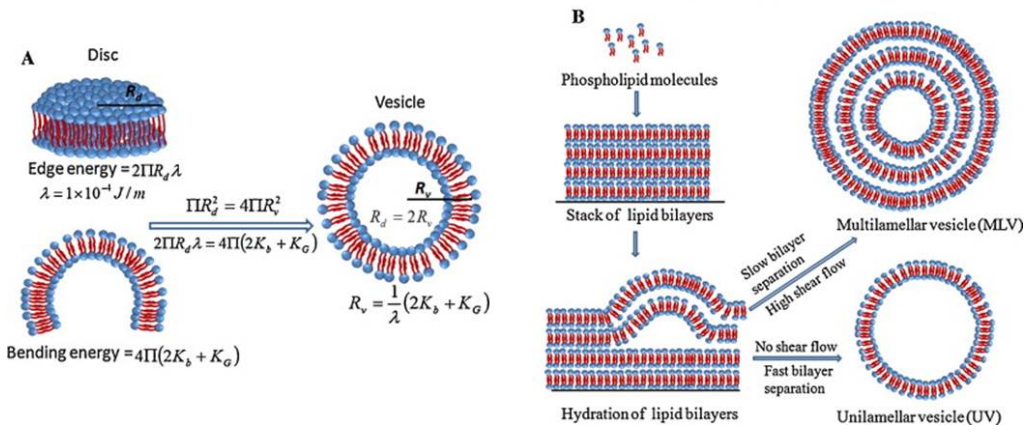

Figura 15. La figura muestra el proceso de autoagregación de las moléculas de fosfolípidos implicado en la formación de liposomas (71). La energía correspondiente a la bicapa abierta puede minimizarse eliminando los bordes si la bicapa se cierra formando una vesícula esférica (A). La cinética de plegamiento de la bicapa debido a fuerzas hidrodinámicas y la separación de las bicapas sometidas a las fuerzas de hidratación determinan el tamaño y la lamelaridad de las vesículas formadas (B).

La naturaleza anfifílica de estas vesículas constituye la clave para su utilización como sistemas para el transporte y la vehiculización de fármacos. Las aplicaciones de los liposomas en farmacología y medicina pueden clasificarse en terapéuticas y de diagnóstico, en función de que el producto incorporado sea un fármaco o un marcador (72, 73). Así, dentro del campo de la terapia, se han diseñado formulaciones liposomales para el tratamiento de enfermedades infecciosas y de procesos neoplásicos, para la administración de fármacos con actividad fungicida, para el tratamiento de determinadas infecciones víricas, la administración de vacunas y en terapia génica. En el campo del diagnóstico por la imagen, las preparaciones liposomales de agentes de contraste se están considerando en medicina experimental y clínica para su aplicación en todas las modalidades de imagen (tomografía computerizada, resonancia magnética, gammagrafía o ultrasonografía). En el campo

del inmunodiagnóstico, la incorporación o inmovilización de marcadores en la superficie liposomal se ha demostrado que permite disminuir de forma considerable el límite de detección y mejorar, en la mayoría de los casos, la sensibilidad de los inmunoensayos con liposomas.

Los liposomas se pueden formular como una suspensión, un polvo seco, un aerosol, como una crema o como una loción. Por ello se pueden utilizar para prácticamente cualquier ruta de administración. Hasta la fecha se han aprobado diferentes formulaciones liposomales para ser utilizadas en el tratamiento de distintas enfermedades o para el diagnóstico de las mismas (Tabla 2). Otras muchas están en diferentes fases de desarrollo clínico (74).

1.3.1. Composición y propiedades generales

Los liposomas se preparan, en general, a partir de material fosfolipídico, aunque también existen otros tipos de moléculas que pueden formar estructuras análogas como ciertos ésteres de colesterol ionizados. Por otra parte, no todos los fosfolípidos forman estructuras de bicapa. En el proceso de agregación se pueden formar micelas o fases hexagonales con propiedades totalmente distintas. La característica común de todos los compuestos que forman bicapas es su naturaleza anfifílica, es decir, tener regiones polares y no polares perfectamente definidas. La organización en bicapas es una de las posibilidades que existen como resultado del proceso de agregación de las moléculas lipídicas en contacto con una fase acuosa, pero no la única.

Los fosfolípidos pueden ser naturales o derivados sintéticos y las bicapas suelen estar formadas por dos o tres especies lipídicas diferentes. El fosfolípido más utilizado en las formulaciones farmacéuticas es la fosfatidilcolina (PC), con diferentes cadenas de ácido graso, de distintas longitudes y grado de insaturación. Otros fosfolípidos habituales son la esfingomielina (SM), la fosfatidiletanolamina (PE), la fosfatidilserina (PS) y el fosfatidilglicerol (PG) (Figura 16) (75). También suele añadirse colesterol (hasta un 30% del total) para modular la rigidez de la bicapa y mejorar la estabilidad de la membrana evitando la unión de proteínas del suero plasmático (Figura 17A). Su anillo rígido y plano interfiere con los movimientos de las cadenas de los ácidos grasos o actúa como un separador que facilita su movilidad.

Tabla 2. Aplicaciones de formulaciones liposomales aprobadas (arriba) y formulaciones liposomales en desarrollo clínico (abajo). (Adaptada de Pattni et al,. 2015).

Producto	Fármaco encapsulado	Aplicación
Myocet	Doxorubicina	Cáncer de mama metastásico
Doxil	Doxorubicina	Sarcoma de Kaposi, cáncer de mama y cáncer de ovario
Lipodox	Doxorubicina	Sarcoma de Kaposi, cáncer de mama y cáncer de ovario
DaunoXome	Daunorubicina	Sarcoma de Kaposi
Marqibo	Sulfato de vincristina	Leucemia linfoblástica aguda
Ambisome, Abelcet, Amphotec	Anfotericina B	Infecciones fúngicas
Depocyt	Citarabina	Meningitis neoplásica y meningitis linfomatosa
Visudyne	Verteporfina	Degeneración macular asociada a la edad (DMAE)
DepoDur	Sulfato de morfina	Dolor
Epaxal	Cepa RG-SB inactivada virus hepatitis A	Hepatitis A
Inflexal V	Hemaglutinina virus de la gripe inactivado (cepas A y B)	Gripe

Producto	Fármaco encapsulado	Indicación	Fase de ensayo
LEP-ETU	Paclitaxel	Cáncer de ovario, mama y pulmón	Fase I/II
EndoTAG-I	Paclitaxel	Cáncer de mama y de páncreas con propiedades antiangiogénicas	Fase II
ThermoDox	Doxorubicina	Carcinoma hepatocelular irresecable, cáncer de mama	Fase II, III
Inmunoliposomas Anti-EGFR	Doxorubicina	Tumores sólidos	Fase I
MM-398	Irinotecan	Tumores sólidos recurrentes, cáncer de mama, colon, páncreas y ovario	Fase I/III
Grb-2 liposomal	Oligonucleótido antisentido Grb-2	Leucemia mieloide aguda, leucemia mielogena crónica	Fase I
SPI-077	Cisplatino	Cáncer de pulmón y de cabeza y cuello	Fase I/II
Lipoplatin	Cisplatino	Cáncer de páncreas, mama, de pulmón de células grandes y de cabeza y cuello	Fase III
LEM-ETU	Mitoxantrona	Cáncer de mama, estómago, hígado y ovario. Leucemia	Fase I
Stimuvax	Lipopétido BLP25	Cáncer de pulmón de células grandes	Fase III
Liposome-annamycin	Anamicina	Cáncer de mama, leucemia linfocítica aguda	Fase I/II
INX-0076	Topotecan	Tumores sólidos avanzados	Fase I
INX-0125	Vinorelbina	Tumores sólidos avanzados	Fase I
2B3-101	Doxorubicina	Tumores sólidos, glioma maligno recurrente	Fase I
Pulmaquin/Lipoquin	Ciprofloxacino	Bronquiectasias no asociadas a fibrosis quística	Fase II/III
Arikace	Amikacina	Infección pulmonary	Fase III

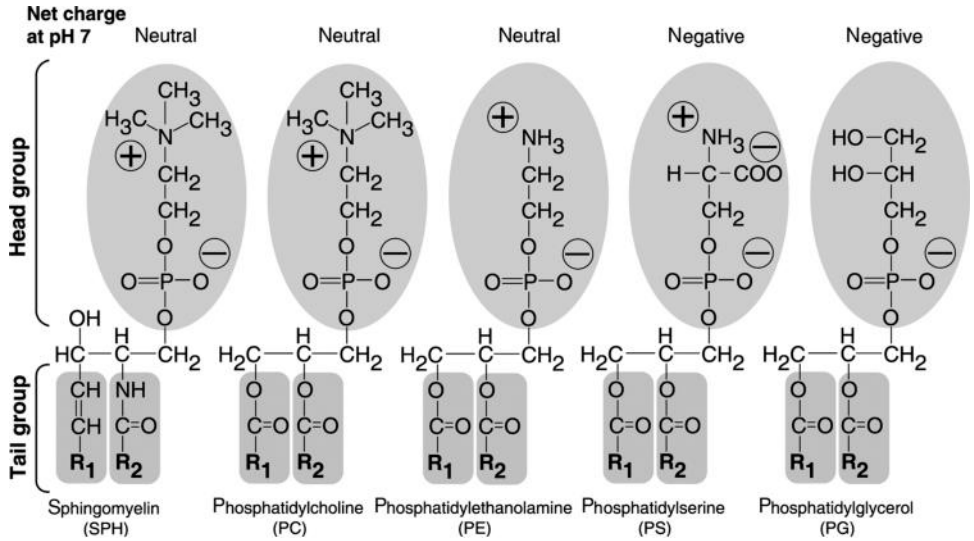

Figura 16. Representación esquemática de los fosfolípidos más utilizados para la formulación de liposomas. R1 y R2 son las colas hidrofóbicas de los fosfolípidos y tanto su longitud como su grado de saturación son variables. La cabeza hidrofílica es la que determina la carga del lípido y está indicada a pH 7 (75).

Los componentes que formen la bicapa determinarán su fluidez o rigidez, así como la carga de superficie. El uso de fosfolípidos insaturados, como especies de fosfatidilcolina de huevo o soja, determina la formación de bicapas menos estables y más permeables, mientras que los fosfolípidos saturados con cadenas largas de acilo, proporcionan estructuras rígidas y poco permeables (Figura 17B) (75, 76).

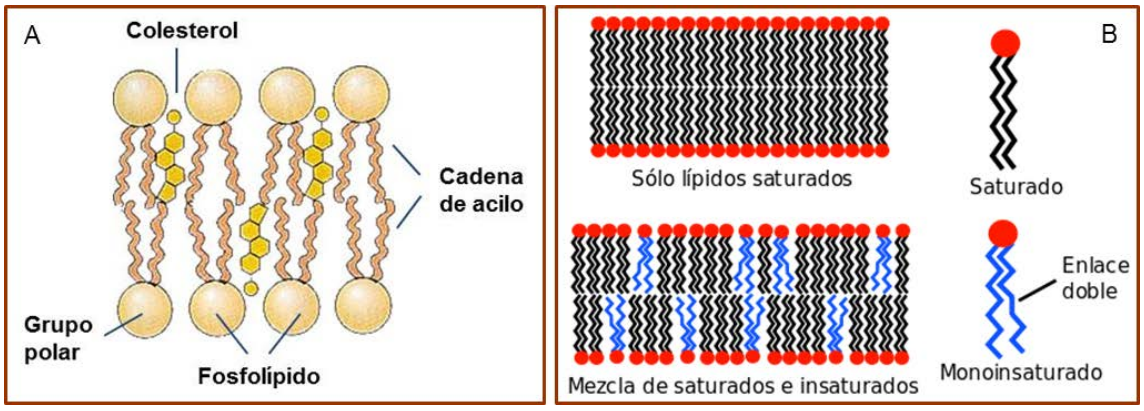

Figura 17. Organización de una bicapa lipídica en función de su composición.

El estudio de la permeabilidad de las membranas a las substancias de interés terapéutico es de relevancia para la aplicación de estos sistemas como transportadores de fármacos y para su liberación controlada. En cuanto a la carga de superficie, crea un campo eléctrico que afecta a la estructura de la bicapa, a su fluidez y al transporte de moléculas a través de la membrana (77, 78). Además la carga

superficial desempeña un papel trascendental en la estabilidad coloidal de los liposomas. Los procesos de agregación y fusión, por ejemplo, están controlados en gran parte por la repulsión o atracción de sus superficies lipídicas.

En función del número de bicapas concéntricas que tengan, los liposomas pueden clasificarse en multilamelares (MLVs), constituidos por varias bicapas y con un tamaño de entre 500 y 5000 nm o en unilamelares, formados por una única bicapa. Éstos últimos, a su vez, en función del tamaño se clasifican en vesículas unilamelares grandes (LUVs), cuando el rango de tamaño se sitúa entre 200 y 800 nm o unilamelares pequeñas (SUVs), con un tamaño de alrededor de 100 nm (79).

Las propiedades de los liposomas varían en función de la composición, el tamaño, la carga de superficie y el método de preparación. Entre las principales ventajas de estas nanoestructuras cabe destacar (79, 80):

- Son transportadores biocompatibles y biodegradables.
- Pueden encapsular tanto compuestos hidrofílicos, en su espacio acuoso interno, como hidrofóbicos, en la bicapa lipídica.
- Protegen a los fármacos encapsulados de ser degradados y optimizan su farmacocinética: aumenta la eficacia y disminuyen los efectos adversos.
- Mejoran la capacidad de penetración celular de los fármacos.
- Son muy versátiles: Propiedades como la carga, el tamaño o las características superficiales se pueden modificar fácilmente mediante la adición de distintos componentes a la mezcla de lípidos antes de la preparación de los liposomas y/o cambiando el método de preparación.
- Pueden encapsular varios fármacos a la vez, lo que permite preparar sistemas multifuncionales

Por otro lado, aunque tienen numerosas propiedades que los hacen atractivos para la encapsulación y el transporte de moléculas, existen diversas consideraciones que deben tenerse en cuenta a la hora de formularlos para que el transporte *in vivo* sea efectivo.

La capacidad de encapsulación y el porcentaje de liberación del fármaco encapsulado son dos aspectos importantes a tener en cuenta. Se deben seleccionar de forma cuidadosa los componentes ya que si una bicapa es demasiado fluida y permeable, la liberación del fármaco será alta antes de llegar al tejido o a la célula diana. La adición de, por ejemplo, esfingomielina o colesterol a una bicapa fluida aportará rigidez y reducirá la fuga de la molécula encapsulada.

La rápida eliminación de la circulación por parte del SRE es otro de los problemas que se deben superar. Modificar la superficie del liposoma para que no sea opsonizado por

las proteínas del suero (inmunoglobulinas, fibronectina y la proteína C-reactiva) aumenta el tiempo de circulación de los liposomas y su biodisponibilidad (81). En este sentido los liposomas estabilizados estéricamente, como los recubiertos con polietilenglicol (PEG), o liposomas en cuya composición se añaden glicolípidos como el fosfatidilinositol o el ganglósido (GM1), tienen una tendencia menor a ser eliminados por las células del SRE (82, 83). También la carga superficial del liposoma o su tamaño pueden modularse para conseguir tiempos de circulación mayores (58).

1.3.2. Tipos de liposomas

Existen diferentes tipos de liposomas que se clasifican en función de sus características superficiales, de sus propiedades fisicoquímicas o de los estímulos externos a los que responden (Figura 18).

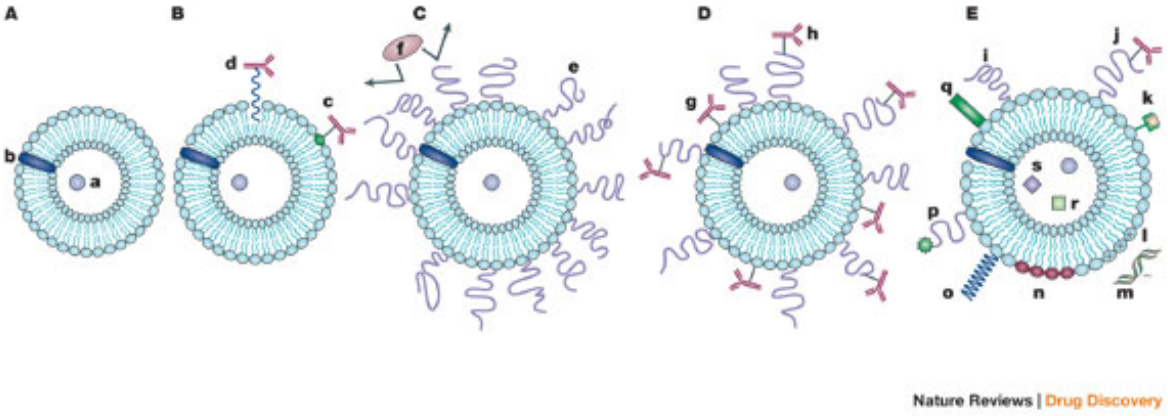

Figura 18. Evolución de los liposomas. (A) Liposomas convencionales para fármacos solubles (a) o insolubles (b); (B) Inmunoliposomas con el anticuerpo ligado de forma covalente a un fosfolípido (c) o anclado hidrofóbicamente a la membrana liposomal (d); (C) Liposomas furtivos recubiertos con un polímero protector; (D) Inmunoliposomas modificados estéricamente con el anticuerpo unido a la membrana del liposoma (g) o unido al extremo de la cadena polimeérica (h); (E) Liposomas de nueva generación con la superficie modificada mediante diferentes estrategias: (i) el anclaje de un polímero protector; (j) la unión de un polímero y un anticuerpo específico; (k) la unión de un molécula para marcaje diagnóstico; (l) incorporación de lípidos con carga positiva para permitir la complejación con DNA (m); incorporación de lípidos (n) o polímeros (o) sensibles a estímulos; unión de péptidos que faciliten la entrada en la célula (p). (Torchilin, 2005).

Los liposomas convencionales (Figura 18A) son aquellos que encapsulan el fármaco en su interior, si es soluble en disolventes acuosos, o en la bicapa, si se trata de una molécula hidrofóbica, protegiéndolo de su degradación, a la vez que minimizan sus efectos secundarios y su toxicidad asociada. El problema de estos liposomas es su baja especificidad por las células a tratar y la rapidez con la que el SRE los elimina del torrente sanguíneo. Se requieren diferentes estrategias para conseguir aumentar su selectividad y su tiempo de circulación.

Los inmunoliposomas (Figura 18B) son aquellos que tienen una mayor especificidad al llevar adheridos a su superficie ligandos que reconocen y se unen de forma específica a las células diana. Así se consigue aumentar la acumulación del fármaco en los tejidos u órganos de interés. Las inmunoglobulinas y en concreto las IgGs son las más ampliamente utilizadas ya que se pueden añadir a los liposomas sin que la integridad del vehículo o la especificidad del anticuerpo se vean afectados (80).

Por otra parte, los denominados liposomas furtivos (Figura 18C) consiguen tiempos de circulación mayores gracias a la estabilización estérica de su superficie. Para ello se modifica la superficie del liposoma con polímeros inertes, biocompatibles e hidrofílicos, como el PEG o determinantes sacáridos, gracias a los cuales se forma una barrera protectora a su alrededor que ralentiza la detección por parte de las opsoninas y su posterior eliminación (84) (Figura 19).

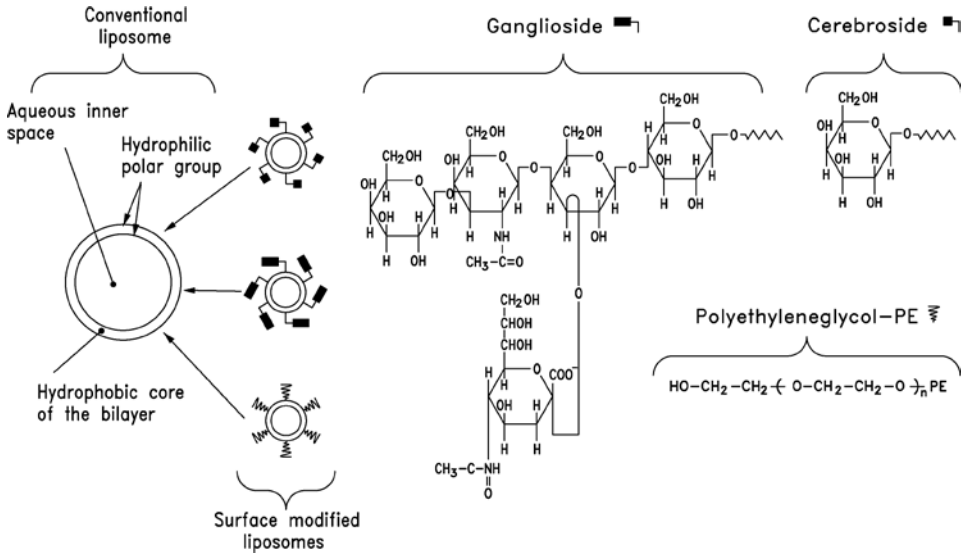

Figura 19. Modificaciones de la bicapa liposomal: creación de cubiertas hidrofílicas (45).

Ambos conceptos se pueden combinar en una misma vesícula. El diseño de inmunoliposomas estabilizados estéricamente (Figura 18D) ha supuesto un avance importante para superar las diferentes barreras fisiológicas. Estos liposomas están estabilizados con PEG para aumentar su tiempo de circulación y cuentan con un anticuerpo que es reconocido de forma específica por células determinadas de un tejido concreto. Así se consigue una mayor internalización del fármaco. Un aspecto clave a tener en cuenta en este tipo de formulaciones es que el polímero que estabilice el vehículo no enmascare a la molécula de reconocimiento utilizada para aumentar la especificidad. Para ello, suele unirse el anticuerpo al final de la cadena del polímero para que el anticuerpo quede en la parte externa de la cubierta protectora (85).

Además de utilizar anticuerpos, también se han formulado transportadores con otro tipo de moléculas de reconocimiento, como el folato, o con polisacáridos como el ácido hialurónico. La vectorización de liposomas modificados con folato es una estrategia que se basa en el hecho de que gran parte de las células tumorales sobreexpresan receptores de folato en su superficie (86, 87). Lo mismo sucede con el ácido hialurónico (AH) o el condroitín sulfato (88, 89), glicosaminoglicanos cuyos receptores están sobreexpresados en ciertos tipos de células tumorales, entre las que se encuentran las de cáncer colorrectal y de pulmón.

El AH natural (Figura 20) es un polímero hidrofílico, de peso molecular muy elevado, no inmunogénico, biocompatible y biodegradable, propiedades que permiten su incorporación a formulaciones farmacéuticas. Algunas referencias bibliográficas recientes destacan sus principales ventajas: interacciona específicamente con el receptor CD44 que es una glicoproteína transmembrana perteneciente a la familia de las moléculas de adhesión celular, prolonga el tiempo de circulación del fármaco (efecto similar al del PEG), incrementa los niveles de fármaco en las zonas tumorales (actúa como reservorio), disminuye las metástasis, inhibe el crecimiento tumoral (bloqueo de los receptores del AH por fragmentos de AH) y aumenta la supervivencia. Del AH podría decirse que proporciona una cubierta hidrofílica que confiere al nanotransportador algunas de las mejores propiedades atribuibles a la aplicación de otro tipo de recubrimientos o a la incorporación de otras moléculas de reconocimiento, como anticuerpos monoclonales (90, 91).

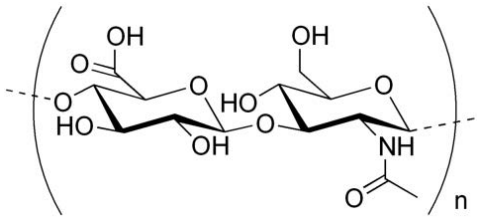

Figura 20. Unidad disacárida repetida en el ácido hialurónico. Está constituida por una molécula de ácido glucurónico y una de N-acetil-glucosamina.

La estabilidad e integridad de los liposomas en los medios biológicos es fundamental para garantizar que alcancen el lugar en donde deben ejercer su acción con su carga terapéutica, por lo que es uno de los principales aspectos a tener en cuenta en su diseño. Por otra parte, conseguir que el contenido se libere cuando el transportador ha alcanzado el tejido diana es otra de las características que deben considerarse cuando se formula el vehículo. La formulación ideal debe ser capaz de retener el fármaco durante su recorrido hacia el lugar de actuación y de liberarlo localmente en el tejido tumoral o en la vasculatura que lo rodea.

Existen diferentes estrategias para conseguir la liberación controlada de las moléculas encapsuladas: todas ellas se basan en la respuesta del vehículo a determinados

estímulos, externos o internos, como el calor, el pH o actuaciones enzimáticas y en el hecho de que, en ciertas patologías, el entorno biológico del tejido afectado es bastante diferente del de las zonas sanas. Este planteamiento ha conducido al desarrollo de los denominados sistemas de liberación inducida o liposomas sensibles a estímulos. La principal consideración para la liberación inducida es la desestructuración de la bicapa liposomal y cómo conseguir que esto suceda. Hay varias opciones entre las que podrían destacarse las siguientes:

- Los liposomas termosensibles son aquellos cuya bicapa presenta una temperatura de transición por encima de la temperatura fisiológica, lo que asegura su estabilidad en condiciones normales y permite que su contenido se libere en respuesta a una hipertermia suave. Esta hipertermia puede ser debida al propio lecho tumoral (89, 92) o bien inducida de forma remota como terapia adyuvante a la quimioterapia y radioterapia (48). En su diseño se utilizan lípidos o mezclas de lípidos con temperaturas de transición algo superiores a 40°C. La selección adecuada de los componentes de la bicapa, así como de sus proporciones en la mezcla, permitirá modular la transición de fase gel a cristal líquido y, por lo tanto, la permeabilidad de la membrana liposomal (Figura 21). De todas las alternativas, quizás esta sea la que ha proporcionado los sistemas que más han progresado y que se encuentran en fases más avanzadas de ensayos clínicos (93).

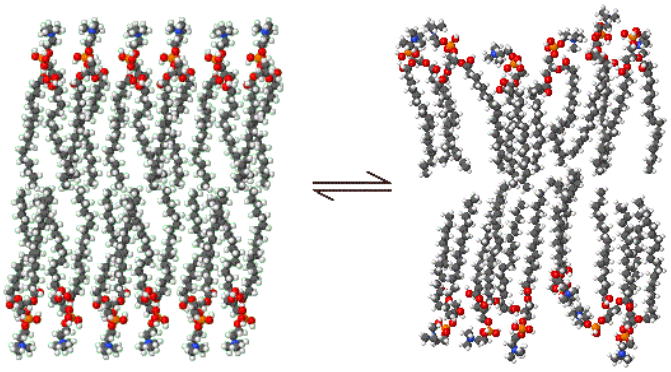

Figura 21. Transición de fase gel a cristal líquido en un agregado molecular de lípidos. La segunda fase, más desordenada, es más fluida y tiene una permeabilidad mayor.

- Los liposomas sensibles al pH se formulan a partir de componentes con grupos ionizables (amino o ácido carboxílico) cuyo estado de ionización dependa del pH del medio. Podrían ser, por ejemplo, lípidos insaturados como la dioleoil-fosfatidiletanolamina (DOPE), moléculas anfifílicas como el ácido oleico o el hemisuccinato de colesterol, o determinados polímeros. Estos liposomas están intactos a pH 7,4 pero cuando se internalizan por endocitosis, al ser el pH más

bajo en el endosoma (pH 5,5) se desestabiliza la bicapa y se libera su contenido en el citoplasma (75). El comportamiento *in vivo* de estos liposomas se basa en las características diferenciales del microentorno del tumor en cuanto a pH, oxigenación y contenido en nutrientes.

- Los sistemas de vehiculización sensibles a la acción enzimática se degradan debido a la actividad de ciertas enzimas locales cuya expresión es mayor en algunos tipos de cáncer. Así, se han demostrado incrementos en los niveles de fosfolipasa A2 en cáncer de próstata y de páncreas y que las metaloproteinasas de la matriz extracelular, especialmente MMP-2 y MMP-9, así como algunas proteasas, están relacionadas con el desarrollo de ciertos tumores. La importancia de estas consideraciones va más allá de su aplicación al diseño de sistemas de liberación controlada de fármacos; algunas de estas enzimas se utilizan actualmente como marcadores para el diagnóstico y pronóstico del cáncer (94).

En la figura 22 se representan las estrategias de liberación controlada basadas en la respuesta del transportador a estímulos específicos.

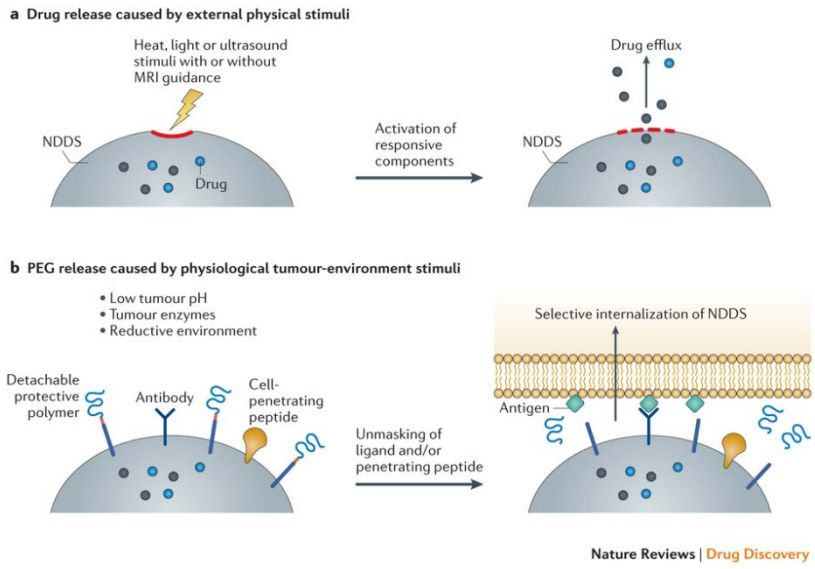

Figura 22. Estímulos externos (a) y estímulos locales asociados a características del entorno del tumor (b) que pueden utilizarse para facilitar la liberación intracelular de un fármaco (95).

1.3.3. Métodos de preparación de liposomas

En función del tipo de liposoma que se vaya a preparar y de la naturaleza de la molécula que se quiera encapsular se pueden considerar diferentes métodos de

preparación. Debe tenerse presente que la finalidad es obtener un sistema estable que incorpore el mayor porcentaje posible del fármaco en estudio. Esta eficacia depende de factores tales como la fuerza iónica del medio acuoso, el tiempo de hidratación y el método de preparación de la suspensión liposomal, entre otros. Existe mucha bibliografía al respecto y revisiones recientes en donde se analizan cuidadosamente las principales ventajas e inconvenientes de los diferentes procedimientos (71, 75, 96). Uno de los métodos más utilizados es el basado en la formación e hidratación de un film lipídico (Figura 23).

La preparación de los liposomas consta de cuatro etapas básicas: el secado de los lípidos a partir de un disolvente orgánico, su dispersión en un medio acuoso, la purificación de la suspensión resultante y el análisis del producto final.

La encapsulación de los fármacos en las vesículas lipídicas se puede llevar a cabo mediante técnicas de incorporación pasiva (durante la formación de las vesículas) o activa (después de la obtención de los liposomas). Las moléculas hidrofóbicas suelen incorporarse directamente durante su formación y tanto la cantidad encapsulada como la capacidad de retención del fármaco en los liposomas están gobernadas por las interacciones lípido-fármaco. Para los fármacos solubles en disolventes acuosos se suelen utilizar técnicas de incorporación activa y su encapsulación depende de la capacidad de los liposomas para atrapar el tampón acuoso que contiene disuelta la molécula durante la formación de la vesícula (96, 97).

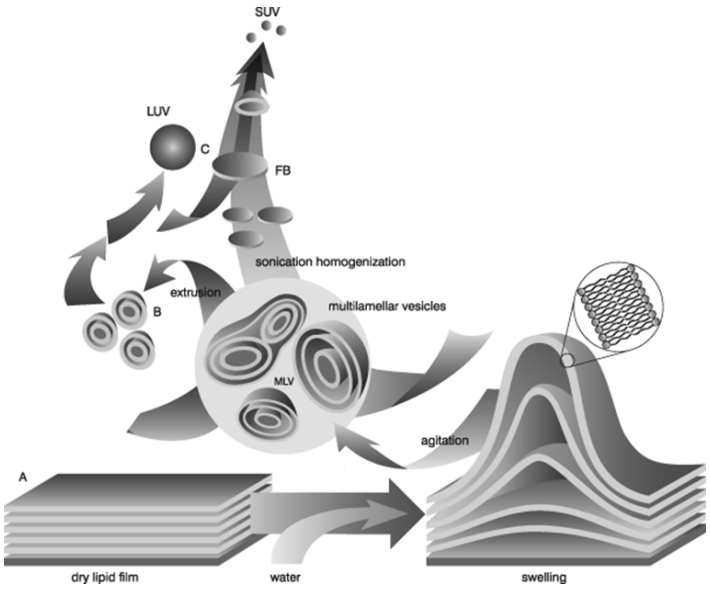

Figura 23. Procedimientos de preparación de liposomas basados en la hidratación de un film lipídico (Avanti Polar Lipids, Tech. Support Dept).

Además, es esencial tener en cuenta que cualquier preparación liposomal realizada a escala de laboratorio debe poder adaptarse a un proceso de fabricación a escala industrial y que el producto farmacéutico que se obtenga debe mantener las mismas características que el ensayado con la preparación de menor volumen. Existen diferentes metodologías para preparar liposomas que incorporen la molécula a encapsular de forma pasiva: los métodos de dispersión en un solvente y los métodos de dispersión mecánica. La tabla 3 resume las principales características de estos métodos.

1.3.3.1. Dispersión en un solvente

Entre los métodos de dispersión en un solvente se encuentran la evaporación en fase reversa y la inyección etanólica o en otro solvente orgánico (éter). La evaporación en fase reversa se basa en la formación de micelas invertidas. Consiste en la hidratación de los fosfolípidos disueltos en una fase orgánica mediante la adición una fase acuosa con agitación vigorosa. Se forma una emulsión y la eliminación lenta del disolvente orgánico proporciona una suspensión de liposomas formada por LUVs y MLVs (98).

Cuando un disolvente orgánico (etanol o éter) que contiene disueltos los fosfolípidos se inyecta en un tampón acuoso se forman, de manera espontánea, liposomas. Al utilizar éter, la formación de las vesículas tiene lugar al evaporarse el disolvente (99). Cuando la fase orgánica es el etanol, se requiere un gran exceso de tampón para que su concentración sea lo suficientemente baja como para forzar que los fosfolípidos se reestructuren y formen los MLVs en la fase acuosa (100). La desventaja de este método es que proporciona suspensiones liposomales muy heterogéneas.

1.3.3.2. Métodos de dispersión mecánica

Entre los métodos de dispersión mecánica se encuentran la hidratación por agitación de una película lipídica, la sonicación, la congelación y descongelación, la micro-emulsificación y la extrusión a través de membranas.

La hidratación de la película lipídica es un método que proporciona liposomas multilamelares grandes y con una gran polidispersidad. Para ello, se depositan los lípidos en las paredes de un vial a partir de una disolución de los mismos en un solvente orgánico que se evapora mediante una bomba de vacío o una corriente de N_2. Este *film* se hidrata con un tampón acuoso, generalmente mediante agitación mecánica y siempre a una temperatura superior a la de transición de los lípidos. Esta técnica, que proporciona suspensiones de MLVs grandes, suele ser el paso previo a la obtención de liposomas más pequeños, homogéneos y de lamelaridad más reducida.

Tabla 3. Métodos para la preparación de liposomas (adaptada de Kraft et al., 2014).

Método de preparación	Procedimiento básico	Ventajas para el escalado	Potencial de escalabilidad
Hidratación de un film lipídico	Evaporación disolvente e hidratación	Sencillo, aunque requiere reducción de tamaño	Adecuado para lotes pequeños o medianos
Evaporación en fase reversa	Formación emulsión con un disolvente no miscible en fase acuosa y eliminación del disolvente	Sencillo Proceso en varias etapas	Adecuado para lotes pequeños o medianos
Inyección en disolvente	Inyección en fase acuosa de disolvente miscible (habitualmente etanol)	Proceso en una sola etapa Proceso continuo Presencia disolventes	Muy bueno, pero no todos los componentes son solubles en etanol
Diálisis de detergente	Formación micelas mixtas con detergente y eliminación detergente	Sencillo, aunque presencia de detergente	Adecuado para proteínas y oligonucleótidos inestables
Reducción de tamaño	**Procedimiento básico**	**Ventajas para el escalado**	**Potencial de escalabilidad**
Sonicación	Ultrasonidos	Sencillo pero poca reproducibilidad	Adecuado únicamente para pequeños lotes
Filtración a alta presión	Colisiones mecánicas a alta velocidad	Población monodispersa, Reproducible, Proceso continuo	Muy bueno
Filtración a baja presión	Filtración a través de membrana de tamaño de poro definido	Población monodispersa, Reproducible, Proceso continuo	Bueno para lotes pequeños o medianos

La sonicación es el método más utilizado para la preparación de SUVs y se basa en la desestructuración de los MLVs mediante las ondas de ultrasonidos para proporcionar vesículas más pequeñas (101). Las dispersiones que se obtienen son heterogéneas y no demasiado estables, desde un punto de vista químico, ya que los ultrasonidos pueden degradar tanto los lípidos como el fármaco encapsulado, lo que ha limitado de forma considerable el uso de esta técnica. La sonicación puede llevarse a cabo con una sonda de titanio o en un baño sonicador. En el primer caso, la sonda se introduce directamente en la suspensión liposomal, mientras que en el segundo es el recipiente que contiene la suspensión de liposomas el que se introduce en el baño sonicador.

Con la técnica de congelación y descongelación se mejora la eficacia de encapsulación de los fármacos y se consigue reducir la lamelaridad de las vesículas. El procedimiento se basa en una congelación rápida de la suspensión en N_2 líquido, acompañada de una descongelación lenta en un baño termostatizado y con agitación mecánica (102). Los liposomas que se obtienen siguen siendo muy polidispersos.

Para conseguir suspensiones homogéneas de liposomas unilamelares las técnicas más utilizadas son la extrusión a través de membranas y la micro-emulsificación.

La extrusión consiste en hacer pasar, de forma repetida, la suspensión de liposomas obtenida mediante la hidratación de los lípidos a través de membranas de policarbonato con un tamaño de poro definido. La heterogeneidad de la preparación se reduce aumentando el número de ciclos de extrusión, es decir, el número de veces que se hacen pasar los liposomas a través de las membranas. El tamaño final de las vesículas viene determinado por el tamaño de poro de la membrana que se utiliza (103).

En el método de microemulsificación o microfluidificación, la dispersión de lípidos se hace circular a través de una cámara de interacción a alta presión (104, 105). Se generan dos corrientes que interaccionan a gran velocidad en microcanales donde se producen las colisiones. El dispositivo permite procesar volúmenes muy superiores a los de los otros procedimientos y trabaja de forma continua, recirculando la muestra el número de veces necesario y proporcionando vesículas multilamelares pequeñas o unilamelares. El tamaño, que se puede controlar de forma muy precisa, así como la homogeneidad de la suspensión obtenida, dependen del número de ciclos aplicados y de la presión de bombeo.

1.3.4. Caracterización de los liposomas

Las especiales e interesantes características de los liposomas han determinado que en la actualidad sean considerados como sistemas de transporte muy apropiados para la administración de un buen número de fármacos. Entre ellas, muy poca o prácticamente ninguna toxicidad e inmunogenicidad, biodegradabilidad y capacidad de transporte de sustancias hidro- y liposolubles. Las propiedades y el comportamiento *in vivo* de los liposomas están estrechamente relacionados con características estructurales y físicas como el tamaño, la carga superficial, el volumen capturado en su fase acuosa, la cantidad de fármaco encapsulado o la estabilidad de la suspensión. Así, el control y determinación de estos parámetros es de vital importancia durante el desarrollo de la formulación liposomal.

La determinación del tamaño de los liposomas puede realizarse mediante técnicas de microscopía, espectroscopia o cromatografía de exclusión molecular. La microscopía electrónica, además de proporcionar el tamaño de las partículas mediante el análisis de imagen correspondiente, permite visualizar su morfología y lamelaridad. No obstante, se trata de una técnica compleja y costosa por el equipamiento que requiere. También puede utilizarse la microscopía de fuerzas atómicas (AFM) que realiza un barrido rápido de la muestra, previamente depositada sobre una superficie de mica (71, 106) y proporciona el perfil de las vesículas. Una desventaja de esta técnica para la determinación de tamaños es que la absorción sobre la superficie de mica puede afectar a la forma del liposoma.

El uso de la espectroscopía de correlación fotónica (PCS) está mucho más extendido. Mediante esta técnica se puede determinar de forma rápida y precisa la distribución de tamaños de las suspensiones liposomales. Se basa en el análisis de las fluctuaciones en el tiempo de la intensidad de la luz dispersada por la muestra, debido al movimiento Browniano que presentan las partículas en suspensión. Estas fluctuaciones se relacionan con el tamaño de partícula.

La estabilidad coloidal de la suspensión liposomal depende en gran medida de la carga de superficie o potencial zeta de las vesículas. Este parámetro se puede controlar mediante la incorporación a la formulación de lípidos con carga o de lípidos unidos a polímeros. Este parámetro se puede evaluar de forma rápida y rutinaria a partir de la movilidad de las partículas sometidas a un campo eléctrico mediante Electroforesis Doppler con Láser (71, 77, 107).

Para conocer el volumen encapsulado y la permeabilidad de la bicapa se pueden utilizar sondas fluorescentes. La 5(6)-carboxifluoresceína (CF), por ejemplo, es un colorante cuya fluorescencia depende, entre otros factores, de la concentración: a concentraciones elevadas, superiores a 40 μM la molécula no es fluorescente debido al fenómeno de autoextinción de la fluorescencia (108). Esta propiedad ha permitido desarrollar un método sencillo y sensible para determinar la permeabilidad de las bicapas lipídicas liposomales. Cuando está encapsulada en el espacio acuoso intraliposomal, la CF no es fluorescente, pero cuando la sonda difunde desde el interior de las vesículas al medio externo la fluorescencia aumenta debido a su dilución (109). La fluorescencia de la CF liberada se determina mediante espectrofluorimetría fijando las longitudes de onda de excitación y emisión a 495 y 515 nm, respectivamente.

La cantidad de fármaco encapsulado es un parámetro fundamental ya que, además de indicar su concentración exacta en la muestra, informa sobre la idoneidad, tanto del vehículo como del método de preparación de la formulación en relación a la dosis terapéutica que requiera una determinada aplicación. La separación del material no encapsulado es un requisito previo a la determinación del fármaco incorporado. Para ello se utilizan técnicas de filtración, centrifugación o cromatografías en columnas de exclusión molecular. Después, para cuantificar el fármaco se utilizará el procedimiento analítico adecuado, en función de las propiedades químicas de la molécula que se va a valorar (espctroscopía UV-visible, espectroscopía de fluorescencia, etc).

Finalmente, además de la caracterización estándar basada en la determinación de parámetros físicos y estructurales de las vesículas, la consideración de las interacciones biofísicas entre los componentes de las bicapas y los fármacos proporciona una valiosa información acerca de los factores determinantes de la

estabilidad e integridad del sistema transportador-fármaco, esenciales para establecer la idoneidad de la formulación final (110). Estas consideraciones han determinado la aplicación, cada vez más frecuente, de este tipo de estudios al diseño y desarrollo de sistemas de vectorización y liberación controlada eficientes y selectivos (111). Los estudios con monocapas lipídicas y la aplicación de las técnicas de Langmuir y la calorimetría diferencial de barrido (DSC) con bicapas estructuradas, son especialmente útiles para estos propósitos.

1.4. Evaluación *in vitro* de preparaciones liposomales de citostáticos

El mecanismo de muerte celular desempeña un papel importante en muchas patologías, por lo que las estrategias dirigidas a modular las rutas relacionadas con este proceso se han aplicado con éxito al tratamiento de algunas enfermedades. En el caso del cáncer, los tratamientos están diseñados para inducir la muerte específica de las células tumorales sin comprometer la salud del paciente. Una primera aproximación de la eficacia de una formulación concreta la proporciona su evaluación *in vitro* en modelos de cultivos celulares. La concentración, las propiedades fisicoquímicas y la localización subcelular del fármaco, así como las características concretas de cada tipo celular determinan el alcance y el mecanismo por el que se produce la muerte (112). Mediante la consideración de criterios morfológicos se han podido establecer las diferencias entre ellos (113).

1.4.1. Mecanismos de muerte celular

Existen diferentes tipos de muerte celular, clasificados en base a aspectos morfológicos (que pueden ser apoptóticos, necróticos, autofágicos o asociados a la mitosis), a criterios enzimológicos (con o sin implicación de nucleasas o de distintas clases de proteasas, como caspasas, calpainas, catepsinas y transglutaminasas), aspectos funcionales (programada o accidental, fisiológica o patológica) o características inmunológicas (inmunogénica o no inmunogénica) (114). En la figura 24 se muestran algunas de las características de los estos procesos.

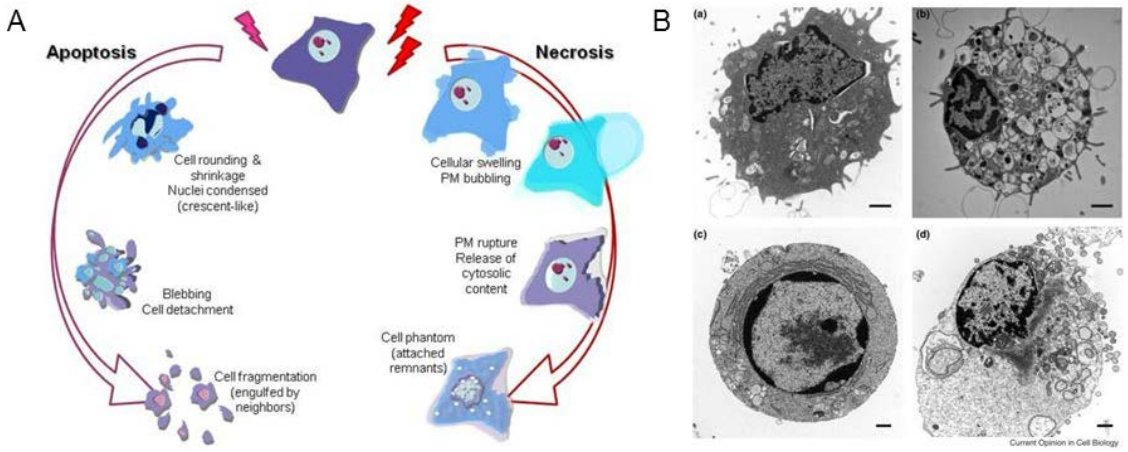

Figura 24. (A) Esquema que muestra las dos vías principales de muerte celular. La necrosis implica la eliminación celular por alteración de la homeostasis y lleva asociada una reacción inflamatoria. La apoptosis o muerte celular programada es un proceso más selectivo por el cual las células son eliminadas. En este caso los macrófagos de la zona fagocitan los restos celulares (cuerpos apoptóticos) (115). (B) Aspectos morfológicos característicos de (a) células normales, (b) autofágicas, (c) apoptóticas and (d) necróticas (112).

La muerte celular programada es un proceso de autodestrucción celular controlada que permite al organismo su correcta morfogénesis, así como su renovación y la eliminación de las células que amenacen su supervivencia. Esta muerte es de vital importancia, tanto durante el desarrollo embrionario como durante la vida adulta. Por otra parte, el mecanismo de muerte celular inducido por un fármaco o una formulación específica es un punto clave en el desarrollo de cualquier aproximación terapéutica. Permite interpretar los efectos secundarios provocados por el tratamiento, predecir cuándo éste puede fallar y ayudar a generar cohortes de pacientes basadas en su sensibilidad hacia un fármaco específico.

El principal tipo de muerte celular es la apoptosis (116, 117). Se trata de un mecanismo fisiológico altamente organizado, por el que la célula se autodestruye. Es un proceso que se produce de forma continua en condiciones fisiológicas y para el que casi todas las etapas están controladas de una manera muy precisa y segura para garantizar que produzcase inicie sólo cuando sea necesario. Se considera una forma regulada de suicidio celular que puede desencadenarse en respuesta a múltiples señales externas y a estímulos internos. El control se basa en la actuación de diferentes proteínas, entre las que debe destacarse el papel central de las pertenecientes a la familia Bcl-2, que determinan el inicio de la fase final de la apoptosis, ejecutado por una familia de proteasas denominadas caspasas. Estas enzimas son cisteína proteasas presentes como zimógenos inactivos en todas las células animales y su activación se puede producir después de la permeabilización de la membrana mitocondrial, de la activación de receptores con dominios de muerte

capaces de reclutar procaspasas y de la acumulación de ciertas proteínas en el retículo endoplásmico.

En cuanto a los cambios morfológicos, la apoptosis se caracteriza por una condensación de la cromatina y fragmentación del núcleo (picnosis) y del ADN, pliegues en la membrana plasmática, degradación del citoesqueleto y contracción celular. Estas características se pueden utilizar para estudiar y evaluar la muerte celular, ya que exiten técnicas que permiten obtener información y una visión global de este proceso. (115, 118). *In vitro*, las células apoptóticas se fragmentan en múltiples vesículas esféricas rodeadas de membrana. *In vivo*, estos cuerpos apoptóticos, que contienen material celular degradado, son eliminados por fagocitosis en un proceso controlado inmunológicamente, sin liberación del contenido citoplasmático y sin iniciar una respuesta inflamatoria.

Cuando se estudian los mecanismos de inducción de la apoptosis, se distinguen dos rutas: la extrínseca, mediada por la activación de receptores y la intrínseca o mitocondrial, desencadenada en respuesta a una amplia variedad de estímulos generados dentro de la célula. La primera está inducida por los receptores de muerte. Los ligandos de muerte, que son citokinas de la familia TNF (factor de necrosis tumoral), interaccionan con receptores transmenbrana y desencadenan una cascada que conduce a la activación de la caspasa-8, el principal mediador de esta ruta. En la ruta intrínseca, las proteínas fundamentales son de la familia Bcl-2; dentro de esta familia hay proteínas anti- o pro-apoptóticas (Bax y Bak), lo que hace que esta vía esté fuertemente regulada.

La necrosis, muerte celular accidental, se considera como un proceso no programado (112). Es una forma de degeneración violenta y rápida caracterizada por una expansión del citoplasma (la célula en su conjunto sufre un proceso de turgencia), destrucción de los orgánulos y disrupción de la membrana plasmática que conduce a la liberación del contenido intracelular y desencadena respuestas de tipo inflamatorio, que constituyen la manifestación más importante de este proceso. El aspecto de las células necróticas resulta de la desnaturalización de proteínas y de la digestión enzimática autolítica o heterolítica.

En la actualidad existen numerosas evidencias que demuestran que la necrosis puede ser inducida y que, al igual que la apoptosis, tiene lugar de una manera regulada. Golstein y Kroemer (119) revisaron y actualizaron el concepto de necrosis y plantearon que, en condiciones fisiológicas, este mecanismo no es una forma descontrolada de muerte, sin rutas de activación ni señalización claras, sino que puede ser desencadenado por ligandos específicos. Debido a su naturaleza, este mecanismo de

muerte necrótica ha sido denominado necroptosis y es la forma más importante y mejor estudiada de necrosis regulada, aunque sin la intervención de las caspasas (120, 121).Su conocimiento ha ilustrado dos principios básicos. En primer lugar, que la muerte celular regulada y programada no se limita a la apoptosis y, en segundo lugar, que las diferentes rutas de muerte celular pueden estar interconectadas. Se ha propuesto que existen rutas que, al ser activadas, desencadenan necrosis y no apoptosis y que estas rutas pueden ser impedidas mediante la inhibición de algún elemento clave de la misma. También se ha descrito la necrosis inducida por deficiencias de ATP en la isquemia y cuando hay alteraciones de las funciones dependientes de oxígeno y del ciclo de los ácidos tricarboxílicos.

La autofagia es un proceso homeostático, necesario para el reciclaje de componentes y nutrientes de la célula, que inicialmente afecta a orgánulos y compartimentos celulares. Aunque existen evidencias de que la autofagia puede constituir una forma de muerte celular, en determinadas circunstancias asociada a la apoptosis, generalmente actúa como un mecanismo de supervivencia. El estudio de la morfología asociada a la autofagia mediante microscopia electrónica de transmisión pone de manifiesto que no hay condensación de la cromatina y que, durante el proceso, algunas porciones del citoplasma quedan aisladas dentro de una vacuola de doble membrana y son digeridas por hidrolasas del lisosoma. Estas vacuolas autofágicas se diferencian perfectamente de otro tipo de vesículas como endosomas, lisosomas o burbujas apoptóticas (122). Se ha descrito que la autofagia transcurre por proteólisis asociada a la vía de la ubiqüitina y que el ADN no se fragmenta (123).

Otro suceso, también clasificado como una forma de muerte celular, es la catástrofe mitótica (115, 124). Es un proceso que puede conducir a la muerte celular, con características apoptóticas o necróticas o llevar a un estado de senescencia, pero que también puede representar un mecanismo de supervivencia (125). Se relaciona con una mitosis aberrante que produce la parada del ciclo celular, alteraciones en el huso mitótico y en la disposición de los cromosomas, aneuploidia y, finalmente, la muerte. La catástrofe mitótica y la ulterior aneuploidia están relacionadas con la inestabilidad del genoma, el crecimiento de tumores, el desarrollo de resistencias a fármacos, el envejecimiento y la senescencia.

1.4.2. Senescencia celular

La senescencia celular fue descrita por Hayflick en 1965 (126) como un proceso que limitaba la proliferación o crecimiento de las células humanas en cultivo (127). Las células senescentes son no quiescentes o células diferenciadas terminalmente, aunque la distinción no siempre es sencilla. No se han identificado marcadores de

senescencia totalmente específicos y, por otra parte, no todas las células senescentes expresan todos los marcadores posibles.

Las células senescentes son viables, dejan de sintetizar ADN, experimentan cambios morfológicos característicos, tienen un perfil de expresión génica diferente y pueden ser identificadas mediante un ensayo bioquímico que visualiza la mayor actividad de la β-galactosidasa asociada a la senescencia a pH ácido. La senescencia celular detiene la proliferación en respuesta a una determinada agresión o estímulo, en lo que podría considerarse un mecanismo de defensa (128).

1.4.3. Muerte celular y cáncer

La carcinogénesis o aparición de un cáncer es el resultado de dos procesos sucesivos: el aumento descontrolado de la proliferación de un grupo de células que da lugar a un tumor o neoplasia y la posterior adquisición de estas células de una capacidad invasiva que les permite diseminar y proliferar en otros tejidos u órganos desarrollando las metástasis. La desregulación de la muerte celular o el fallo en los mecanismos que controlan que células dañadas o que proliferan de forma descontrolada mueran, se ha postulado como una de las causas de desarrollo de tumores. Es imprescindible, por lo tanto, conocer en profundidad los mecanismos de muerte celular, tanto en células sanas como tumorales, para encontrar tratamientos contra el cáncer.

No está claro qué tipo de muerte resulta más beneficiosa para el tratamiento de un determinado tumor. La necrosis, al liberar el contenido celular, genera inflamación que parece facilitar la angiogénesis y el crecimiento del tumor. Esta inflamación, sin embargo, podría producir una activación del sistema inmunológico innato que resultaría beneficiosa. Por su parte, la apoptosis se considera inmunosupresora.

La mayoría de los agentes anticancerosos que se utilizan en la actualidad provocan alteraciones en la replicación del ADN y desencadenan la apoptosis. Pero alteraciones en este programa reducen la sensibilidad al tratamiento y, en el peor de los casos, pueden llegar a provocar la resistencia a la terapia. Se sabe que p53 está implicada en la activación de este proceso. Se trata de una proteína supresora de tumores, esencial, que induce apoptosis, parada del ciclo celular y senescencia en respuesta a situaciones de estrés para la célula. Es un factor de transcripción que regula la transcripción de un conjunto de genes clave en la generación de tumores por lo que la pérdida de función de p53 se asocia a la reducción de la apoptosis, a la supervivencia de células dañadas y al desarrollo del tumor (129).

p53, además de promover la apoptosis, controla la integridad del ADN e induce arresto del ciclo celular y senescencia. En un 50% de todos los cánceres existen mutaciones

en p53, por lo que se han desarrollado estrategias de terapia génica para suplementar las células cancerosas con este gen, mediante la transferencia *in vivo* del gen funcional. Por otra parte, algunos tratamientos de quimioterapia también tienen a p53 como diana para recuperar la estructura y funcionalidad de su forma natural y se han desarrollado fármacos para reactivar los mutantes de p53 (130).

1.5. Aproximaciones para el transporte específico de fármacos al colon

El conocimiento de las bases moleculares del cáncer ha permitido desarrollar nuevos e interesantes fármacos para combatir la enfermedad. Aun así, algunos de los agentes antitumorales habituales presentan ciertas limitaciones que plantean dudas sobre su eficacia: distribución sistémica inespecífica, dificultad para conseguir concentraciones terapéuticas en la diana tumoral, frecuentes y graves efectos secundarios sobre células y tejidos no tumorales o desarrollo de resistencias múltiples a los citostáticos. Existe una importante corriente de opinión que considera muy prometedoras las investigaciones dirigidas hacia la optimización de las propiedades farmacocinéticas de algunos de los fármacos convencionales mediante el desarrollo de nuevas formulaciones basadas en plataformas nanotecnológicas. . Estudios recientes permiten concluir que los nanotransportadores pueden tener un papel importante en el desarrollo futuro de nuevas líneas terapéuticas en el ámbito de la nanomedicina.

Estructuras particuladas, constituidas por lípidos y/o polímeros, son capaces de alterar la farmacocinética y biodistribución de los fármacos asociados y mejoran, así, sus propiedades farmacológicas: liposomas, microesferas y nanopartículas lipídicas o poliméricas son algunas de las mejores opciones. Todas ellas se han utilizado para liberar agentes citotóxicos de forma controlada y de todas se han descrito los beneficios terapéuticos que resultan de su utilización (131-133).

1.5.1. La vía oral

Las nuevas estrategias para la quimioterapia del cáncer se centran en la elección del mejor transportador, en buscar la ruta óptima para la administración del fármaco , en estudiar combinaciones de fármacos para explotar posibles sinergiaso la posibilidad de introducirlo directamente en la zona tumoral y la selección del principio en que se basa la vehiculización (pasiva o activa) y la liberación (difusión o específicamente inducida) del citostático. Si se combinan de forma adecuada los diferentes criterios será posible desarrollar los transportadores apropiados para aplicaciones específicas.

Respecto a la ruta de administración, la más utilizada tradicionalmente ha sido la intravenosa. A pesar de las ventajas que representa, también supone riesgos

evidentes para los tejidos sanos, produce efectos secundarios severos que reducen las dosis toleradas y requiere del uso de excipientes farmacéuticos específicos que contribuyen, en muchos casos, a la toxicidad de la formulación final. La quimioterapia oral emerge como una de las alternativas más prometedoras para el desarrollo de la oncología del futuro, ya que es la preferida por los pacientes , ya que es indolora, no-invasiva, no requiere de personal especializado y permite la autoadministración (134).

Aunque esta vía de administración puede cambiar los actuales regímenes de quimioterapia y aumentar de formanotable la calidad de vida del paciente, la baja solubilidad, estabilidad y biodisponibilidad de muchos citostáticos imponen severas restricciones para alcanzar niveles terapéuticos a través del TGI.

En la bibliografía se han descrito ampliamente las ventajas de utilizar sistemas de vehiculización para la administración de los fármacos por vía oral y su transporte específico al colon (35, 135, 136). Además de proporcionar un tratamiento eficaz para las enfermedades relacionadas con esta parte del TGI, como la enfermedad inflamatoria intestinal, la colitis ulcerosa o el cáncer colorrectal, tiene el potencial de permitir la llegada de péptidos y proteínas a la circulación sistémica a través de la absorción colónica (137). El transporte específico de un fármaco concreto al colon aumenta su concentración en el lugar de actuación, con lo que se requiere una dosis menor y se reducen los efectos secundarios (138).

Para que un nanotransportador pueda liberar el fármaco encapsulado intacto en el colon y que éste pueda absorberse en el lugar deseado, la formulación del vehículo debe desarrollarse teniendo en cuenta los diferentes obstáculos que presenta el tracto grastrointestinal y que, tanto la integridad del transportador, como la estabilidad química del fármaco, pueden verse seriamente comprometidas debido al ambiente agresivo de este entorno. Así, antes de llegar al colon, la formulación debe pasar a través del estómago, con un pH entre 1,5 y 3,5, el duodeno donde el pH es cercano a 6, el intestino con un pH entre 5,5 y 6,8, y el ciego, con pH entre 6,8 y 7,3 (139).

Existen alternativas diferentes para conseguir un transporte preciso y efectivo al colon: todas ellas se basan en la consideración de las características particulares de este órgano, como su pH, entre 6,4 en el colon ascendente, y 7,0, en el descendente, la existencia de una microflora anaerobia que produce unas enzimas hidrolíticas y reductoras específicas, el hecho de que represente un medio reductor, con un potencial redox medio de unos -200 mV y el elevado tiempo de tránsito (140).

La consideración y control del tiempo de tránsito se ha utilizado para formular vehículos en los que la liberación del fármaco se retrase el tiempo necesario para que el transportador llegue desde la cavidad bucal hasta la parte distal del intestino

delgado y se libere el fármaco en el colon (141, 142). El inconveniente de esta estrategia es que este parámetro varía de forma considerable entre individuos, sobre todo por diferencias en el tiempo de retención en el estómago, que depende de factores tales como la dieta, la motilidad gastrointestinal y la actividad física de las personas (143, 144).

Todas las estrategias se basan en la utilización de polímeros que confieren a la formulación propiedades específicas. Así se pueden utilizar polímeros sensibles al pH, que proporcionan una liberación retardada y protegen al fármaco del fluido gástrico. Tienen el inconveniente de tener que soportar también el pH ligeramente alcalino del intestino delgado, lo que podría provocar una liberación temprana del fármaco en el íleon (144, 145). También se pueden utilizar polímeros biodegradables sensibles a la acción hidrolítica de enzimas de la mucosa del colon. Finalmente, el uso de polímeros bioadhesivos permite prolongar el tiempo de residencia de la formulación en el lugar de actuación y confiere capacidad de interacción con células tumorales específicas. Algunos polímeros combinan estas dos últimas características por lo que son especialmente atractivos para este tipo de aplicaciones.

La bioadhesion es la situación en la que dos materiales, uno de los cuales, por lo menos, es de naturaleza biológica, entran en estrecho contacto y permanecen juntos durante el tiempo suficiente para establecer enlaces interfaciales. Si la superficie biológica es una mucosa, se habla de mucoadhesion. Existen diferentes materiales que pueden ser utilizados como mucoadhesivos, en la mayoría de los casos de naturaleza polimérica o macromolecular.

Las mucinas presentes en el mucus están implicadas de forma directa en el fenómeno de mucoadhesion. El mucus es un sistema viscoelástico no-newtoniano, altamente hidratado (>95% de agua) que está constituido por una red tridimensional de mucinas entrelazadas aleatoriamente dejando huecos de entre 50-1800 nm de ancho,. Las mucinas del mucus son glicoproteínas que difieren en el grado de glicosilación y en sus secuencias polipeptídicas. Son una familia heterogénea de moléculas que, en medio acuoso, se estructuran formando un sistema complejo y heterogéneo estabilizado por enlaces de hidrógeno intra- e intermoleculares, por interacciones electrostáticas y por puentes disulfuro entre cisteínas de las regiones no glicosiladas. Conocer las interacciones entre los materiales mucoadhesivos y el mucus es fundamental para el desarrollo de sistemas de vehiculización mucoadhesivos (Figura 25).

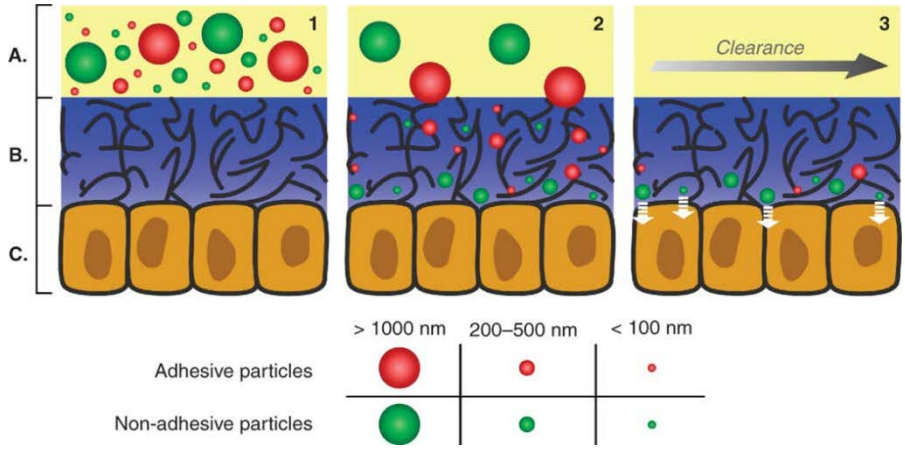

Figura 25. Representación esquemática de la interacción entre diferentes tipos de partículas y la capa de mucus (146).

En este sentido, en el diseño del trasnportador se deben tener en cuenta las propiedades físicas y de superficie más adecuadas para optimizar estas interacciones y potenciar la mucoadhesividad (Figura 26).

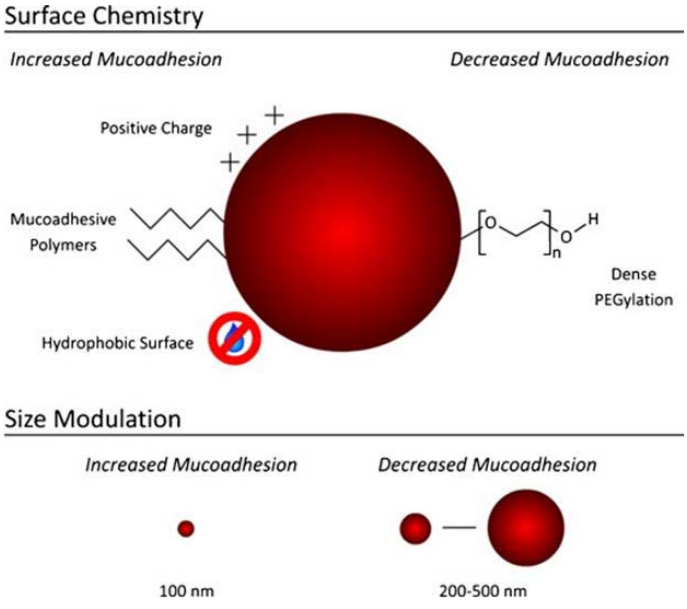

Figura 26. Estrategias para el diseño de nanotransportadores con comportamiento mucoadhesivo (146, 147).

1.5.2. Utilización de determinantes sacáridos para la vehiculización al colon

La microflora del colon se postula como el principal factor a tener en cuenta cuando se quiere desarrollar un sistema de transporte específico para este órgano. Está formada por más de 400 especies de bacterias anaerobias y su principal fuente de energía proviene de los polisacáridos presentes en los residuos de la dieta o en las propias secreciones. Estas bacterias producen un amplio espectro de enzimas, responsables

de la degradación de los polisacáridos, como la β-glucoronidasa, β-xilosidasa, β-galactosidasa, α- arabinosidasa, nitroreductasa, desaminasa o urea hidroxilasa, siendo los tres primeros los más activos (138, 144). La actividad hidrolizante o reductora de la microflora permite liberar el fármaco desde el transportador en el lugar de acción, sin que haya apenas pérdida del principio activo en el estómago o el intestino delgado.

Se han utilizado un gran número de polisacáridos por su potencial como sistemas para el transporte específico de fármacos al colon. Pueden ser de origen vegetal, como la pectina o la inulina, o animal, como el quitosano y el condroitín sulfato. La hidrólisis de los enlaces glicosídicos cuando el vehículo llega al colon permite que se libere el principio encapsulado.

1.5.2.1. Pectinas

Las pectinas son polisacáridos lineales no amiláceos que se extraen de las paredes celulares de las plantas. Están constituidas por ácido α-(1,4)-D-galacturónido y 1,2-D-ramnosa con cadenas laterales de D-galactosa y D-arabinosa y tienen un peso molecular de entre 50.000 y 150.000 kDa (Figura 27). Estos polisacáridos se mantienen intactos en el estómago y el intestino delgado pero las enzimas bacterianas del colon los degradan completamente.

La pectina es completamente soluble en agua con lo que si se usa sola, se hincha en contacto con los fluidos acuosos del tracto gastrointestinal y liberan el fármaco encapsulado por difusión. Así pues, el desarrollo de transportadores basados en pectinas se ha centrado en el uso de derivados menos solubles como las sales de calcio, cuyo contenido debe controlarse para asegurar un transporte óptimo, o en su combinación con polímeros hidrofóbicos como la etilcelulosa (140, 148).

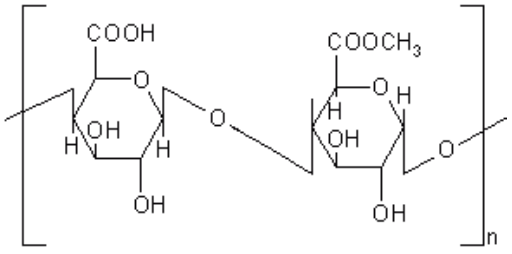

Figura 27. Estructura de la pectina

Otro aspecto a tener en cuenta cuando se usa este polímero es que su grado de metilación tiene una influencia directa sobre sus propiedades, sobretodo en su solubilidad. En función de si su grado de metilación está por encima o por debajo del 50% se clasifican en pectinas de alto o bajo metoxilo. Diversos estudios sugieren que las pectinas con un alto o bajo grado de metoxilación con una cantidad controlada de

calcio pueden proporcionar una especificidad enzimática máxima y una óptima protección del fármaco en su tránsito hasta el colon (149-151).

1.5.2.2. Condroitín Sulfato

El condroitín sulfato (CSA) es un polisacárido sulfatado constituido por una secuencia disacárida repetida de N-acetilgalactosamina y ácido glucurónico. La mayor parte de los residuos de N-acetilgalactosamina están sulfatados, variando la posición de sulfatación, según el tejido de que proceda, entre la 4 o la 6. El CSA es, pues, un polianión y esto le confiere algunas de sus propiedades más importantes. El condroitín sulfato es un mucopolisacárido soluble (Figura 28) degradado por bacterias anaerobias del intestino grueso (*Bacteroides* thetaiotaomicron y *B. ovatus*) (152, 153).

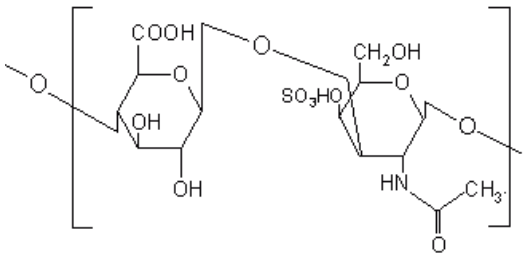

Figura 28. Estructura del condroitín sulfato.

Satoh et al. (154) demostraron que el condroitín sulfato puede unirse a la PC en condiciones fisiológicas. Los resultados descritos por estos autores pusieron de manifiesto que las cadenas de CSA de los proteoglicanos de membrana se doblan sobre su superficie y propusieron un modelo que dibuja a esta molécula sobre la membrana celular de manera similar a como se extienden las vides sobre la tierra.

Estudios realizados en nuestro laboratorio confirmaron la capacidad de interacción de esta macromolécula con los fosfolípidos constituyentes de una bicapa liposomal, sobre la que formaban una cubierta envolvente (Figura 29).

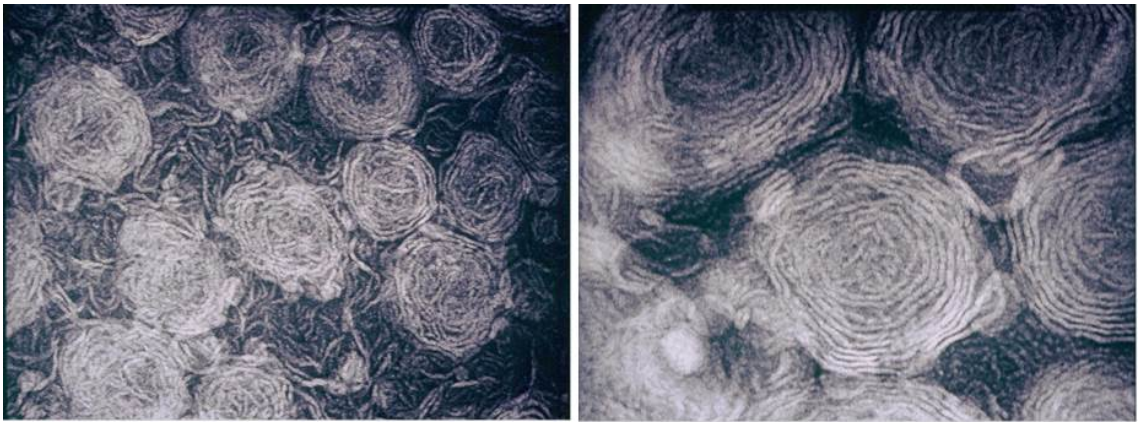

Figura 29. Moléculas de condroitín sulfato alrededor de una superficie liposomal. Imagen obtenida mediante microscopía electrónica de transmisión (TEM). Visualización del CSA con cloruro de cetilpiridinio. La preparación liposomal contenía 20 mg lípido/mL y un 0,5% de CSA respecto al lípido (155).

Las micrografías electrónicas muestran la disposición de las moléculas de CSA sobre la superficie de las vesículas, que constituyen una especie de red o entramado formado por sus cadenas polisacáridas e ilustran de la capacidad de organización de este glicosaminoglicano y del elevado grado de orden de los complejos resultantes.

Su utilización en formulaciones farmacéuticas se basa en su capacidad de resistir al entorno fisiológico del estómago y del intestino delgado aunque, siendo soluble en agua, podría no proteger de forma eficaz el material encapsulado. Si se entrecruza con otras moléculas, se puede superar este obstáculo. En diversos estudios se ha entrecruzado el condroitín sulfato con 1,2-diaminododecano para dar productos con una solubilidad baja en agua (156-158).

1.5.2.3. Quitosano

El quitosano es un polisacárido policatiónico de elevado peso molecular derivado de la quitina que se obtiene mediante desacetilación alcalina (148). Es un copolímero formado por unidades de 2-amino-2-desoxi-D-glucosa unidas por enlaces β-(1→4)-O-glicosídicos (Figura 30).

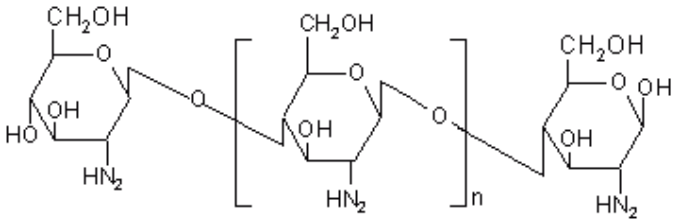

Figura 30. Estructura del quitosano.

Es el polisacárido natural más abundante junto con la celulosa y no es degradado por las enzimas digestivas del inicio del tracto gastrointestinal. Tiene propiedades biológicas interesantes ya que no es tóxico, es biocompatible y biodegradable y, además es mucoadhesivo (159). Debido a su solubilidad a pH ácido (precipita a pH superior a 6), es necesario protegerlo de la acidez del estómago. Esto se consigue con una cubierta entérica, que a pH ácido se mantiene íntegra para disolverse a medida que el pH aumenta (160).

Su carácter catiónico se ha explotado para diseñar algunas de sus principales aplicaciones. Gracias a sus propiedades mucoadhesivas tiene la ventaja, sobre otros polisacáridos, de interaccionar con la mucosa del colon para conseguir incrementar el tiempo de retención del fármaco en el lugar de actuación. Aunque sus propiedades adhesivas se justifican mediante diferentes mecanismos, su principal interacción con la mucosa es de tipo electrostático (Figura 31) y se da entre sus grupos amino primarios (con carga positiva) y los grupos sulfonato y residuos de ácido siálico de la capa de mucina (con carga negativa) (161-163).

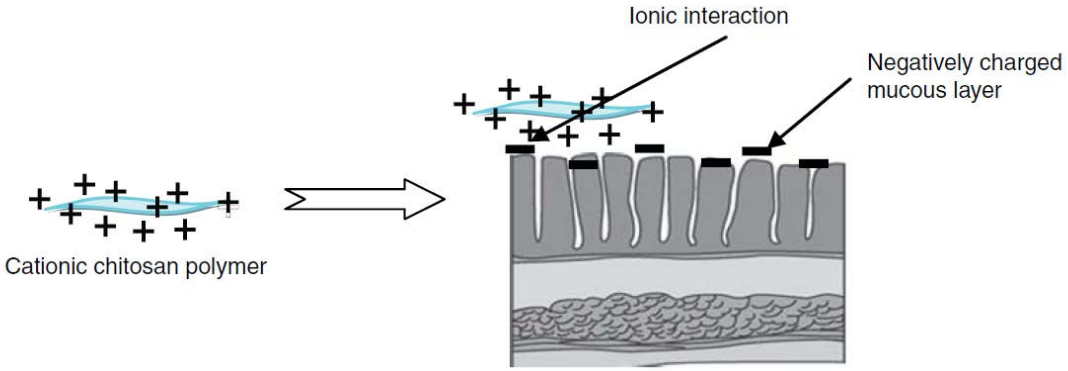

Figura 31. Esquema de la interacción entre el quitosano y la mucosa (159).

Diversos estudios han utilizado quitosano derivatizado o entrecruzado con otros polímeros o con calcio para desarrollar sistemas de transporte de fármacos al colon (164-170). Algunos de los más interesantes utilizan liposomas: si en su formulación se incluyen moléculas aniónicas, la bicapa resultante tendrá carga negativa y será posible crear una cubierta polisacárida, hidrófila, mucoadhesiva y estable entorno a la superficie liposomal. Las interacciones electrostáticas justificarían su estabilidad.

En el esquema de la figura 32 se muestra una disposición de las moléculas de quitosano alrededor de la superficie liposomal similar a la que presentan las vesículas rodeadas de moléculas de CSA en las micrografías electrónicas de transmisión de la figura 29. Una ventaja adicional es que los transportadores con quitosano se puedan formular como tabletas, micropartículas o microesferas, cápsulas, nanopartículas o hidrogeles (159).

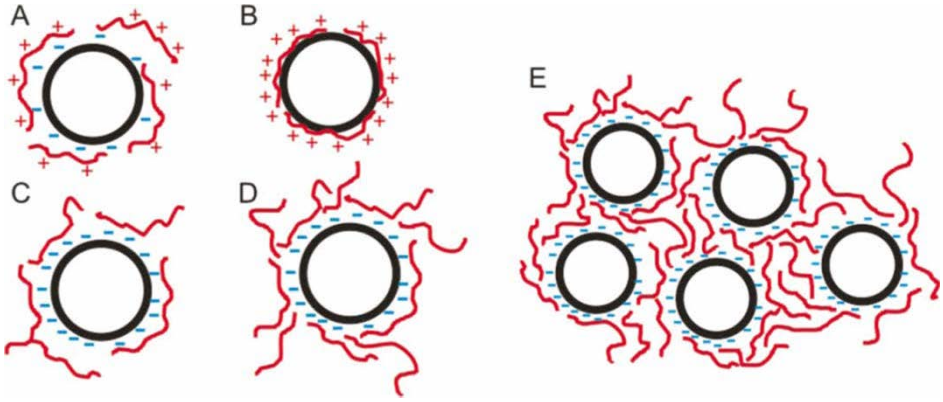

Figura. 32. Representación esquemática de la estructura de quitosomas: (A) Las cadenas positivas del quitosano son atraídas por las cargas negativas sobre la superficie liposomal; (B) and (C) Las cadenas del polímero recubren la monocapa externa de la bicapa de un liposoma neutro, ligeramente negativo o con una carga negativa más intensa, de manera que la carga externa de la partícula cambia a positiva; (D) A concentraciones más elevadas, las cadenas de quitosano llenan los espacios libres de la monocapa externa de un liposoma con una fuerte carga negativa; (E) Agregados de quitosomas que se forman por encima de una determinada concentración de polímero (171).

2. Hipótesis de trabajo y objetivos

Los recientes avances derivados de la intensa investigación oncológica realizada en los últimos años han proporcionado nuevos citostáticos y determinado nuevos planteamientos para la quimioterapia del cáncer. No obstante, la gran agresividad de los fármacos más eficaces impone consideraciones adicionales respecto a la formulación farmacéutica más adecuada o a la ruta de administración del producto. La finalidad última es reducir su toxicidad y los consiguientes efectos secundarios no deseados, manteniendo la actividad del/de los citostáticos, para evitar los graves daños que estos producen a las células normales. Con este planteamiento fundamental, el tema de la vehiculización controlada adquiere un especial protagonismo por cuanto que debe permitir dirigir el fármaco a una diana específica y ralentizar su liberación para que su efecto se prolongue en el tiempo. La obtención de productos farmacéuticos de estas características puede representar un avance notable en el tratamiento del cáncer, a la vez que permitir utilizar los actuales citostáticos de una manera más eficaz e inteligente, con un beneficio evidente para el paciente sometido a tratamiento.

La hipótesis de trabajo del presente Proyecto de Tesis se basa en estas consideraciones y puede resumirse en el esquema de la Figura 33.

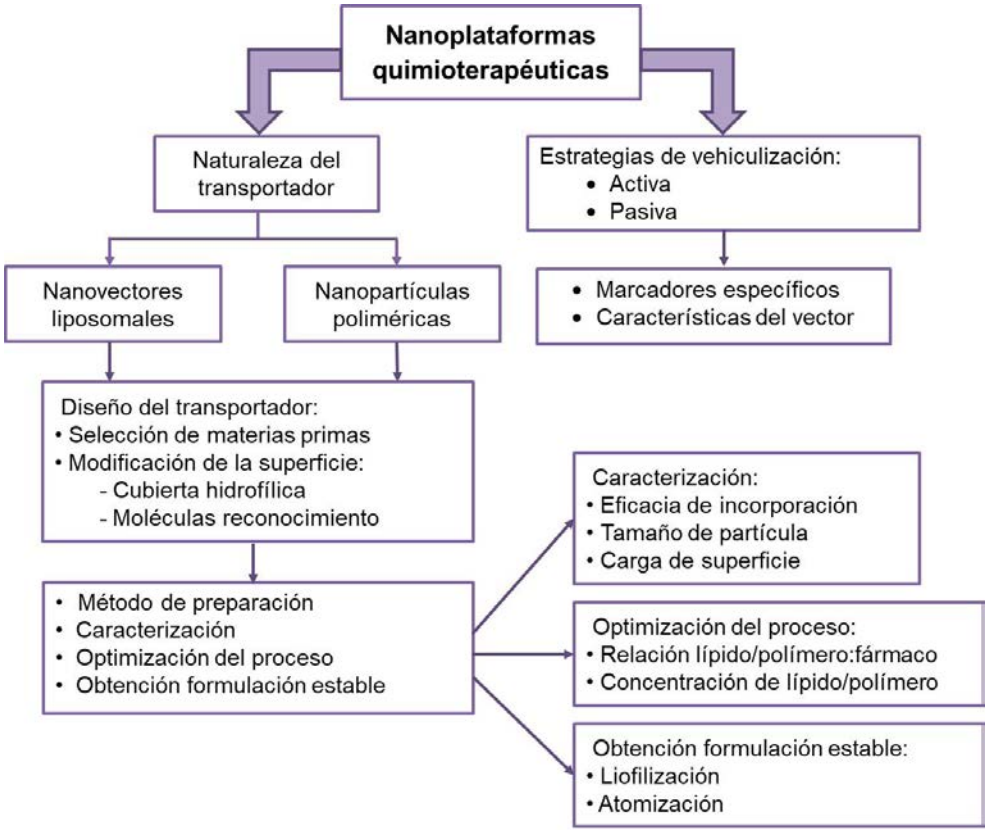

Figura 33. Esquema para las hipótesis de trabajo.

El trabajo plantea el desarrollo de formulaciones farmacéuticas, basadas en la utilización de nanovectores liposomales y constituye los primeros estudios para su aplicación a la quimioterapia oral del cáncer de colon. El transporte de fármacos a través de las diferentes barreras fisiológicas supone uno de los retos más importantes en relación al diseño de las nuevas formulaciones. Los beneficios de estos nuevos preparados deberán valorarse en relación a su efecto farmacológico.
Su objetivo general se centra en trasladar los avances recientes en el transporte y vectorización de fármacos al campo de la quimioterapia del cáncer para mejorar su selectividad y eficacia. Se contempla el desarrollo de nuevas formas de vehiculización y liberación selectiva de fármacos en tejidos y de sistemas alternativos de disposición para la administración de medicamentos. Para ello se han tenido en cuenta los siguientes aspectos:

- Aprovechar el potencial de los nanovectores liposomales como vehículos de administración de fármacos.
- Combinar estrategias de modificación de la superficie liposomal para obtener estructuras mecánicamente estables, bioadhesivas y con capacidad de interaccionar de forma específica con las células diana.
- Considerar formas de administración alternativas a la intravenosa para facilitar el tratamiento, incrementar los índices terapéuticos y reducir la toxicidad de los citostostáticos.
- Estudiar las interacciones biofísicas entre fármacos y sistemas modelo de membrana para dilucidar los mecanismos de transporte de fármacos y nanotransportadores a través de la membrana celular.

Con estos planteamientos y consideraciones generales, los objetivos específicos del presente trabajo se resumen en los siguientes puntos:

1. **Obtención y caracterización de formulaciones liposomales para las camptotecinas Irinotecan (CPT-11) y SN-38.** Desarrollo y estandarización de protocolos para la obtención de formulaciones liposomales de estos fármacos. Consideración de estrategias específicas para cada una de estas moléculas: sensibilidad a estímulos específicos y/o modulación de la fluidez de la bicapa. La utilización de liposomas sensibles a la temperatura debe permitir que, aun cuando el transportador presente una biodistribución más o menos amplia, se degrade solo en la zona afectada en respuesta a la hipertermia que caracteriza a las áreas neoplásicas. Los componentes lipídicos para su preparación se seleccionarán teniendo en cuenta esta premisa. Por su parte, la modulación de la fluidez de la

bicapa puede facilitar la incorporación de moléculas hidrofóbicas o ralentizar la liberación de fármacos hidrofílicos encapsulados en el interior acuoso y, en cualquier caso, evitar la opsonización del transportador por las proteínas del plasma, en caso de administración intravenosa. Validación de la técnica de liofilización para la obtención de las formulaciones liposomales en forma de polvo seco y caracterización de las preparaciones después del proceso de reconstitución.

2. **Funcionalización de la superficie liposomal mediante la creación de una cubierta bioahesiva y de reconocimiento con polímeros polisacáridos.** Se trata de incrementar la biodisponibilidad de fármacos que son mal absorbidos cuando se administran por vías diferentes de la intravenosa y de de potenciar la interacción con células cancerosas. Se trabajará, con polímeros hidrofílicos policatiónicos.

3. **Estudio de las interacciones moleculares entre citostáticos y membranas modelo.** Su conocimiento debe permitir dilucidar el papel que desempeñan los lípidos en el transporte de fármacos y de sistemas de liberación a través de las barreras biológicas, así como predecir la toxicidad asociada a estas moléculas o estructuras. Muchos de los antitumorales tienen dianas intracelulares, por lo que deben atravesar una o varias bicapas lipídicas para alcanzar su objetivo y obtener respuesta a su acción farmacológica. El estudio de las interacciones lípido-fármaco resulta, pues, fundamental para establecer los mecanismos de internalización celular y desarrollar nuevas moléculas o sistemas de vehiculización más eficaces.

4. **Evaluación del comportamiento y de la actividad *in vitro* de los nanovectores liposomales.** Selección de las líneas celulares apropiadas para el estudio de la acción citotóxica y antiproliferativa de las formulaciones desarrolladas y, por lo tanto, de su eficacia. Los ensayos de internalización de los fármacos en las células diana, de localización subcelular y de análisis del ciclo celular deben permitir realizar una valoración previa de la efectividad de los tratamientos sobre la base del establecimiento de los mecanismos moleculares de actuación.

5. **Identificación del mecanismo de muerte celular,** apoptosis y/o necrosis, por el que se inactiven las células después del tratamiento con la formulación liposomal de irinotecan o de su metabolito SN-38.

3. Informe de las directoras

Informe de las Directoras en relación a la tesis doctoral de Ana Casadó Mora: Publicaciones y papel de la doctoranda

Margarita Mora Giménez y M. Lluïsa Sagristá Gratovil, Profesoras Agregadas del Departamento de Bioquímica y Biomedicina Molecular de la Universidad de Barcelona, como directoras de la tesis titulada "Diseño de nuevas formulaciones farmacéuticas mucoadhesivas para la quimioterapia del cáncer de colon" que presenta Ana Casadó Mora, hacen constar que:

Esta Tesis Doctoral se presenta como "Compendio de Publicaciones", vertebrándose, su parte experimental, en 5 capítulos, de los cuales la doctoranda es primer autor.

Los resultados presentados en el primer artículo, **Formulation and in vitro Characterization of Thermosensitive Liposomes for the Delivery of Irinotecan,** han sido publicados en la revista "*Journal of Pharmaceutical Sciences*". El índice de impacto correspondiente al año de su publicación es de 2,590 (49/157, 1er Tercil, categoría Chemistry Multidisciplinary).

El segundo artículo, **Langmuir Monolayers and Differential Scanning Calorimetry for the Study of the Interactions between Camptothecin Drugs and Biomembrane Models,** se ha publicado en la revista "*Biochimica et Biophysica Acta-Biomembranes*", con un índice de impacto del año de su publicación de 3,687 (17/72, 1er Cuartil, categoría Biophysics).

El tercer artículo, **Improved Selectivity and Cytotoxic Effects of Irinotecan via Liposomal Delivery: a Comparative Study on Hs68 and HeLa Cells**, está publicado en la revista "*European Journal of Pharmaceutical Sciences",* con un índice de impacto del año 2016 de 3,756 (54/256, 1er Cuartil, categoría Pharmacology & Pharmacy).

El cuarto artículo, **Development and characterization of a novel SN-38 liposomal formulation and in vitro assessment of its cytotoxic effect on two tumor cell lines**, se acaba de enviar a la revista *"Journal of Drug Targeting",* con un índice de impacto del año 2016 de 3,068 (82/256, 1er Tercil, categoría Pharmacology & Pharmacy)

El quinto artículo, **Incorporation of the concept of mucoadhesiveness to the design of pharmaceutical formulations for the camptothecins CPT-11 and SN-38,** está en preparación, habiéndose finalizado su redacción.

Por lo que respecta a la contribución de la doctoranda a cada uno de los capítulos, Ana Casadó Mora ha sido la encargada de llevar a cabo el trabajo experimental de la investigación, desde la planificación y el desarrollo de los ensayos, hasta el análisis y discusión científica de los resultados, así como de la redacción de las publicaciones que se presentan.

Durante el período de realización de su Tesis Doctoral, Ana Casadó Mora participó en los proyectos CTQ2007-67763-C03-03 y CTQ2010-20870-C03-02 de los Ministerios de Educación y Ciencia y de Economía y Competitividad, respectivamente, supervisando el trabajo experimental de investigadores adscritos al mismo. Fruto de su participación en el desarrollo de los proyectos mencionados son las publicaciones y contribuciones a Congresos que se incluyen en el anexo de esta Memoria.

Esta Tesis Doctoral ha recibido el soporte económico del Ministerio de Educación y Ciencia, de la Universidad de Barcelona, de la Agencia de Gestión de Ayudas Universitarias y de Investigación (AGAUR) y de la Agencia de Valorización y Comercialización de los Resultados de la Investigación (AVCRI).

Dra. Margarita Mora Giménez

Profesora Agregada del Departamento
de Bioquímica y Biomedicina Molecular

Dra. M. LLuïsa Sagristá Gratovil

Profesora Agregada del Departamento
de Bioquímica y Biomedicina Molecular

4. Artículos

Primer artículo

Formulation and *in vitro* characterization of thermosensitive liposomes for the delivery of irinotecan.

Casadó A, Sagristá ML, Mora M.

J Pharm Sci. 2014 Oct;103(10):3127-38. doi: 10.1002/jps.24097

RESUMEN

Se ha investigado el efecto de la composición lipídica en las propiedades físico-químicas de un vehículo liposomal que contiene irinotecan, así como su actividad antitumoral *in vitro*. El presente trabajo describe la obtención de una nueva formulación para el irinotecan basada en la utilización de un transportador liposomal, fácil de preparar y con características termosensibles y demuestra su idoneidad como sistema de liberación sobre la base de su capacidad para incorporar el fármaco y de su eficacia para promover su internalización celular. Los datos de permeabilidad, determinados *in vitro* en un medio biológico simulado a diferentes temperaturas, han puesto de manifiesto que, tanto la naturaleza de los lípidos como la relación en la que han sido mezclados, desempeñan un papel clave en la liberación del producto encapsulado en el interior liposomal. A partir de una mezcla de DSPC/DOPS/CHOL, en relación molar 65:35:30, se han obtenido liposomas sensibles a la temperatura, que incorporan un porcentaje elevado de irinotecan (83-85%). La formulación se ha caracterizado mediante la determinación de parámetros físico-químicos específicos. Se ha realizado un estudio comparativo de la internalización celular y de la actividad citotóxica del irinotecan formulado en liposomas y administrado en tampón lactato (formulación comercial) con resultados prometedores. Se demuestra el efecto de la dosis y del tiempo de tratamiento en la actividad del fármaco y que esta es significativamente mayor cuando se utiliza la formulación liposomal. El perfil de internalización del CPT-11 justifica los resultados obtenidos. El análisis del ciclo celular y la evaluación de la unión de anexina muestran los cambios inducidos por el fármaco en la dinámica del ciclo y el efecto pro-apoptótico de la formulación liposomal.

ASPECTOS DESTACADOS DE LA INVESTIGACIÓN

- Se han formulado liposomas estables y sensibles a la temperatura a partir de la mezcla DSPC/DOPS/CHOL, 65:35:30
- Los liposomas cargados con Irinotecan se preparan fácilmente y son sistemas de liberación controlada de fármacos eficientes.
- Se ha comparado la citotoxicidad del irinotecan libre y encapsulado en liposomas con resultados prometedores.
- Se ha demostrado la idoneidad del tranportador liposomal en la promoción de la internalización del fármaco en la célula.
- El irinotecan liposomal induce cambios en la dinámica del cicle celular, así como una respuesta apoptótica.

RESUMEN GRÁFICO

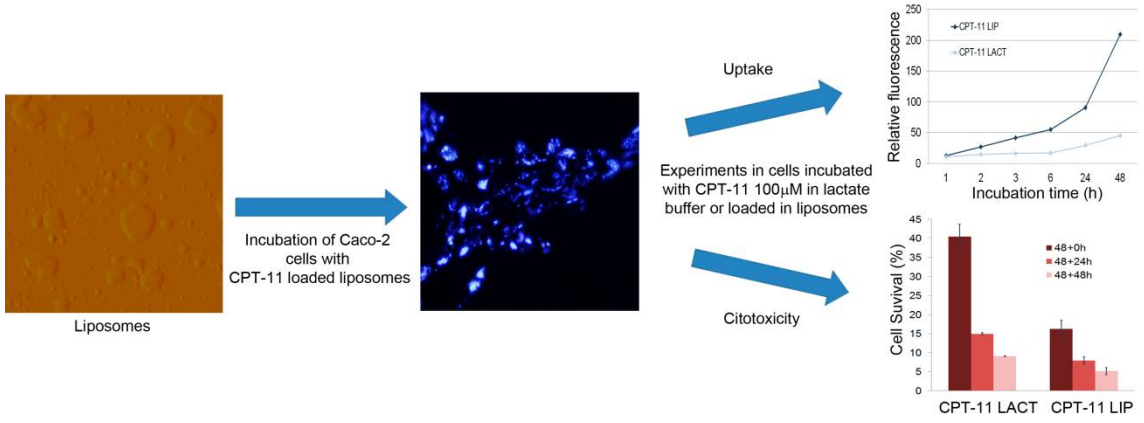

RESEARCH ARTICLE – *Pharmaceutics, Drug Delivery and Pharmaceutical Technology*

Formulation and *In Vitro* Characterization of Thermosensitive Liposomes for the Delivery of Irinotecan

ANA CASADÓ, MARIA LLUÏSA SAGRISTÁ, MARGARITA MORA

Departament de Bioquímica i Biologia Molecular, Facultat de Biologia, Universitat de Barcelona, Barcelona 08028, Spain

Received 16 January 2014; revised 6 June 2014; accepted 3 July 2014

Published online 4 August 2014 in Wiley Online Library (wileyonlinelibrary.com). DOI 10.1002/jps.24097

ABSTRACT: The effect of the lipid composition on the physicochemical properties of a liposomal carrier containing irinotecan (CPT-11) and its *in vitro* antitumoral activity on a colon cancer cell line has been investigated. The paper describes the procurement of a novel and easy-to-prepare temperature-sensitive carrier for CPT-11 and proves its suitability as delivery system on the basis of its ability to incorporate the drug and on its efficiency to promote drug internalization. Permeability data, studied *in vitro* in a simulated biological medium at different temperatures, showed that both the nature of the lipids and the ratio in which they have been mixed play a key role in the release of the encapsulated product. Stable temperature-sensitive liposomes with good drug incorporation efficiency were obtained and characterized. The cellular uptake and the cytotoxic activity of the CPT-11 liposomal formulation were compared with those corresponding to the free drug with promising results, being concentration and time dependent and significantly higher. Thus, it could be interpreted that the greatest cytotoxic effect of liposomal CPT-11 was because of the increased uptake provided by the liposomal carrier. Studies of cell cycle and annexin V binding showed drug-induced changes in cell cycle dynamics and the proapoptotic effect of liposomal CPT-11.

Keywords: Liposomes; Irinotecan; drug delivery; responsive delivery systems; controlled release; Caco-2 cells; drug uptake; cytotoxic activity

INTRODUCTION

Colorectal cancer represents 10%–12% of the whole of malignant diseases, is the second most prevalent cancer, and is one of the leading causes of cancer-related death worldwide.[1,2]

For years, fluoropyrimidines, such as 5-fluorouracil, have almost been the only chemotherapeutic option for colorectal cancer treatment, despite its limited efficacy.[3] Alternative drugs, formulations, and schedules for cancer treatment have been developed[4,5] and new therapeutic agents[6,7] such as irinotecan (CPT-11), a topoisomerase-I inhibitor metabolized to SN-38, and oxaliplatin, a third-generation platinum compound, have been introduced in first- and second-line studies with valuable benefits in survival.[8] Nevertheless, although camptothecins are undergoing extensive investigation in clinical trials, relative little information is available about their antitumor mechanism or about how chemotherapeutic schedules or drug formulation can affect them.

Chemotherapies are often limited by their toxicities and lack of specificity and, consequently, the effectiveness of many of the most useful cytostatics is dependent on bioavailability, specificity, and stability and limited by harmful side effects of the drugs. Because of this, the search for suitable formulations of antineoplastic drugs and the choice of the more appropriate route to supply them are, at present, one of the main goals in cancer chemotherapy. The challenge is to establish the best way of using cytostatics to exploit all of their potential for the benefit of patients.

In relation to the design of effective formulations, targeted drug delivery has gained special attention as it should direct the drug toward a specific target and sustain its release in the cancerous tissue. Among the approaches to satisfy these requirements, it can excel the use of particulate systems such as liposomes, solid microspheres, and nanoparticles. They have all been used to deliver cytotoxic agents in cancer chemotherapy, and for all of them, the therapeutic benefits and the improvement of the pharmacological drug properties have been reported.[9,10]

Liposomes are considered promising vectors for a wide variety of applications, including the delivery of enzymes, antibiotics, antivirals, cytostatics, vaccines, as well as for gene and photodynamic therapy.[11–13] Thus, several liposomal drug preparations are currently marketed (verteporfin, daunorubicin, doxorubicin, amphotericin B, or temoporfin); a variety of drugs have been studied in liposomal form, with promising pharmacokinetic results,[14–16] and many other liposome formulations (i.e., antioxidants) are in early phases of development.[17] Regarding the liposomal incorporation of camptothecins, the protection afforded by the carrier on their active lactone and the reduction of their serious side effects would result in a valuable drug formulation for the treatment of colorectal cancer.[18]

Liposomes constitute a suitable drug delivery system that can be designed by different approaches.[19] Passive versus

Abbreviations used: AFM, atomic force microscopyn; CF, 5(6)-carboxyfluorescein; CHOL, cholesterol; CPT-11, irinotecan; DMEM, Dulbecco's modified Eagle's medium; DMPG, L-α-dimiristoyl-phospathidylglycerol; DMSO, dimethyl sulphoxide; DOPS, L-α-dioleoyl-phospathidylserine; DPPC, L-α-dipalmitoyl-phospathidylcholine; DSPC, L-α-distearoyl-phospathidylcholine; IUV, intermediate unilamellar liposome; MLV, multilamellar unilamellar liposome; MTT, 3-[4,5-dimethylthiazol-2-yl] 2,5-diphenyltetrazolium bromide; PBS, sterile Dulbecco's phosphate-buffered saline; PCS, photon correlation spectroscopy; PI, propidium iodide; SM, sphyngomielin; SUV, small unilamellar liposome; TSL, temperature-sensitive liposomes.

Correspondence to: Margarita Mora (Telephone: +34-93-4021212; Fax: +34-93-4021559; E-mail: margarita.mora@ub.edu)

Journal of Pharmaceutical Sciences, Vol. 103, 3127–3138 (2014)

active targeting or conventional versus surface-modified vesicles are criterions of choice to develop the appropriate carrier for a specific application. For active targeting, specific ligands for epitope or receptor-positive tumor cells can be attached to the liposomal surface. Passive targeting is, however, governed by the carrier physical properties. Liposome size, surface charge, and bilayer fluidity, which can be modulated by handling properly bilayer lipid composition and by choosing suitable preparation conditions, determine the behavior of the vector both *in vitro* and *in vivo*.[20] The uptake of marked carriers, with recognition molecules, by tumor cells is not always higher[21] and increases the cost of the pharmaceutical formulation. On the contrary, the control of the physical parameters can give responsive drug carriers that offer different strategies to improve the efficacy of liposomal chemotherapies. Thus, liposomes with rigid bilayers are more stable *in vivo* because the penetration and adsorption of blood opsonins to their surface becomes hindered. Consequently, the use of rigid liposomes decreases their uptake by reticuloendothelial system, resulting in a decrease of their clearance from the bloodstream, solving the problem of the small circulation half-life of conventional liposomes.[22]

Triggered release through hyperthermia provides targeted bioavailability of encapsulated drugs. Temperature-sensitive liposomes (TSL), which can allow the release of drugs in anatomical regions subjected to local hyperthermia,[23] can be engineered from lipid mixtures with a phase transition above physiological temperature (40°C–44°C). The choice of the lipids and their molar ratio in the formulation of liposomes allow the control and modulation of their gel-to-liquid phase transition[24] and give structures stable enough at physiological temperature, but with an enhanced permeability in response to a mild hyperthermia.[25] This approach, first proposed by Yatvin et al.[26] and Weinstein et al.[27] was confirmed by several authors.[28] The use of TS nanovectors has important advantages, including their abilities to sustain the release of loaded drugs in the therapeutic region in response to specific stimuli. Moreover, it has been reported that the liposome–hyperthermia association displays a synergic cytotoxic action.[29]

This paper presents a formulation study focused on the procurement of a novel liposomal preparation for CPT-11 with temperature sensitivity and gives an *in vitro* evaluation of its potential for cancer chemotherapy. The *in vitro* uptake and the cytotoxic activity of liposomal CPT-11 have been analyzed and compared with those corresponding to the pharmaceutical product in lactate buffer by using the human intestinal cell line Caco-2, a well-established cell culture model for the study of intestinal drug transport across the small intestinal epithelium.[30]

MATERIALS AND METHODS

Materials

L-α-Dipalmitoyl-phospathidylcholine (DPPC), L-α-distearoyl-phospathidylcholine (DSPC), L-α-dioleoyl-phospathidylserine (DOPS), L-α-dimiristoyl-phospathidylglycerol (DMPG), sphyngomielin (SM), and cholesterol (CHOL) were obtained from Avanti Polar Lipids (Birmingham, Alaska). Polycarbonate membranes were obtained from Poretics Products, Osmonics, Inc. (Livermore, California). CPT-11, purchased from Afine Chemicals Limited (Hangzhou, China), was pure with a minimal grade of 99%. 5(6)-Carboxyfluorescein (CF) was obtained from Molecular Probes (Eugene, Oregon). Annexin V-DY-634 kit for apoptosis detection was obtained from Immunostep (Salamanca, Spain). 4′,6-Diamidino-2-phenylindole, dihydrochloride (DAPI) was a product from Molecular Probes. Sephadex G-50 medium was obtained from Pharmacia Biotech (Uppsala, Sweden) and Triton X-100 was obtained from Merck (Darmstadt, Germany). All the organic solvents (Panreac, Montcada i Reixac, Barcelona, Spain) were distilled before use. Milli-Q water system (EMD Millipore Corporation, Bedford, Massachusetts), resistivity of 18 MΩ cm, was used. All other chemicals were of analytical grade. Dulbecco's modified Eagle's medium (DMEM) with 4.5 g glucose/L, fetal calf serum, penicillin-streptomycin, nonessential amino acids, and L-glutamine solutions were obtained from Biological Industries (Kibbutz Beit Haemek, Galilee, Israel). Sterile Dulbecco's phosphate-buffered saline (PBS), dimethyl sulphoxide (DMSO), 3-[4,5-dimethylthiazol-2-yl] 2,5-diphenyltetrazolium bromide (MTT), and rat serum were obtained from Sigma–Aldrich Chemical Company (St. Louis, Missouri). Micro-BCA protein assay kit was obtained from Pierce Protein Research Products (Rockford, Illinois). Cell culture material was obtained from Techno Plastic Products (Trasadingen, Switzerland).

Preparation of Liposomes

Multilamellar, intermediate (100–200 nm), and small (up to 100 nm) unilamellar liposomes (MLVs, IUVs, and SUVs, respectively) were prepared following standard procedures.[31] DSPC, DPPC, DOPS, SM, CHOL, and DMPG chloroform solutions were mixed, in ternary combinations, at different molar ratios to prepare lipid films. MLVs were prepared by hydrating the dried films in 10 mM lactate (pH 4.4) or 10 mM phosphate, 0.82% NaCl (pH 7.4) (PBS) buffers to a final lipid concentration of 1–20 mg/mL. MLVs dispersions were frozen (liquid N_2) and thawed (water bath) five times above the phase transition temperature (T_m). For IUVs and SUVs preparation, MLVs were sonicated (sonicator bath; Branson 2510, Danbury, Connecticut) for 20 min above the T_m and extruded (Lipex Biomembranes Inc., Vancouver, Canada) through different pore-sized polycarbonate membranes (400–200 nm for IUVs and 400–100 nm for SUVs). Liposomes were stored in the dark at 4°C.

Characterization of Liposomes

Thermal Analysis

The thermal properties were analyzed by differential scanning calorimetry (Mettler DSC-30; Mettler-Toledo, Inc., Columbus, Ohio). The temperature scale was calibrated with indium, undecan, and water and the transitional enthalpies with indium. The T_m and the enthalpy (ΔH_{cal}) were determined with a Mettler TC10A TA processor. The cooperativity of the transition was evaluated from the widths at half-peak heights ($\Delta T_{1/2}$) of the main transition endotherms. MLVs suspensions (15 mg lipid mixtures in 100 μL of 10 mM lactate buffer, pH 4.4) were transferred to a 160-μL aluminum pan and several heating and cooling cycles were carried out before running the calorimetric scans. The heating rate was 2°C/min and only the heating scans were analyzed. The reference pan contained 100 μL of lactate buffer.

 DOI 10.1002/jps.24097

Determination of the Lipid Content

The lipid amount in liposome suspensions was measured following the Stewart's method.[32] Calibration curves for each lipid composition (0.01–0.2 mg lipid) were obtained. Chloroform and ammonium ferrothiocyanate (1:1, v/v) were added to each dried sample. The chloroformic phase, extracted after vortexing and centrifugation (2680xg, 10 min), was used to select the absorbance maximum. Measures were carried out in a Beckman DU40 spectrophotometer (Beckman Coulter, Inc., Fullerton, California). Lipid concentration in calorimetric samples was determined by phosphorus analysis.[33]

Vesicle Size and ζ-Potential

The size, size distribution, and ζ-potential of liposomes were determined by photon correlation spectroscopy (PCS), in a Malvern Zetasizer NANO-ZS device (Malvern Instruments Ltd., Malvern, UK) equipped with an optic unit containing a 5-mW He–Ne laser (Spectra Physics, Santa Clara, CA, USA) and an electrophoresis cell. The device was calibrated with standard carboxy-modified polystyrene latex samples. Measurements were performed at 25°C and $\lambda_{exc} = 633$ nm, using liposomal suspensions containing 0.2 mg lipid per milliliter of 10 mM, pH 4.4, lactate buffer.

Surface Morphology

Atomic force microscopy (AFM) images[34] were obtained in the Tapping Mode (Nanoscope III; Digital Instruments, Santa Barbara, California) under ambient conditions. Tapping Mode cantilevers, made of monocrystal silicon with spring constant of 38–74 N/m and typical resonance frequencies of 270–377 KHz (Point Probes; Nanosensors, Wetzlar-Blankenfeld, Germany), were used. Liposomes were deposited on a freshly cleaved mica substrate (20 μL, 0.05 mg lipid per milliliter buffer). Samples were maintained at room temperature for 45 min, in a closed vessel, and the mica surface was cleaned with the buffer.

Entrapment Efficiency and CPT-11 Liposomal Content

Irinotecan-containing IUVs (10–20 mg lipid per milliliter) were prepared as described before in lactate buffer. CPT-11 in chloroform–methanol (2:1, v/v) was added to the lipids before the film formation at 5:1, 7.5:1, or 10:1 lipid–CPT-11 molar ratio. CPT-11 loading was quantified spectrophotometrically after removing the nonencapsulated drug from the liposomal–CPT-11 suspension with Centricon YM-10 Filter Devices (EMD Millipore Corporation, Billerica, Massachusetts). Calibration curves for CPT-11 (0.005–0.02 mg/mL) were previously obtained both in lactate buffer and THF. Encapsulation percentage and drug concentration were obtained from the difference between total and nonentrapped CPT-11.

In Vitro Liposome Stability Assessment by Using a Fluorescent Marker

Determination of CF Content in Liposomes

The CF content was determined by measuring the fluorescence of an aliquot of SUVs, free of nonencapsulated CF, at 520 nm ($\lambda_{exc} = 492$ nm). CF-containing SUVs (1 mg lipid per milliliter) were prepared, as described above, in PBS containing 50 mM CF. Liposomes (178 μL) were applied to a Sephadex G-50 (medium) column, equilibrated with PBS isosmotic with the CF-containing buffer, and elution was carried out with the same buffer. A fraction of 1.6 mL of CF-loaded liposomes without free CF was collected. A sample of 80 μL was diluted in 2 mL of PBS and 150 μL of 10% Triton X-100. CF concentration was determined by fitting the 100% fluorescence emission with a standard CF solution. Lipid concentration of eluted liposomes was analyzed and found to be the same as that of the applied vesicles.[35] The amount of CF trapped inside liposomes was expressed as mmol CF/mmol lipid.

Release Kinetics of CF

The quenching behavior of the fluorescent marker CF[35] was used as a test to study *in vitro* the time-dependent and temperature-triggered CF release from liposomes.[36] Permeability experiments were carried out at physiological temperature (37°C) and in hyperthermia conditions (41°C and 45°C), in the absence and in the presence of rat serum. The efflux of the dye was monitored on a Kontron SFM25 spectrofluorimeter at $\lambda_{exc} = 492$ nm and $\lambda_{em} = 520$ nm. Small aliquots of CF-loaded liposomes were added to each cuvette to achieve a lipid concentration of 10 μg/mL and the fluorescence intensity at time zero (F_0) was measured. CF leakage was recorded continuously by measuring the increase of fluorescence intensity for 90 min (F_t). To determine the total entrapped CF, 150 μL of 10% Triton X-100 were added to each cuvette (F_T). CF efflux was expressed as the percentage of CF leakage from liposomes at each time and calculated from the following expression:

$$CF_{leakage}\,(\%) = \frac{F_t - F_0}{F_T - F_0} \times 100$$

Cell Culture

Human Caco-2 colon adenocarcinoma cells (ATCC HTB-37) were grown as monolayers in DMEM supplemented with 50 units/mL penicillin, 50 μg/mL streptomycin, 1% nonessential amino acids, and 10% (v/v) fetal bovine serum. Cell cultures were performed in a humidified sterile atmosphere of 95% air and 5% CO_2 at 37°C in a SteriCult 200 (Hucoa-Erloss S.A., Madrid, Spain) incubator. Caco-2 cells were seeded in 25 cm^2 flasks (90,000 cells), 24 multiwell plates (2500 cells) or in 35 mm Petri dishes (25,000 cells) with 22 mm square coverslips. Cells were grown for 72 h and treated when cultures were in exponential growth.

In Vitro Studies of Liposomal CPT-11 Cytotoxic Activity

Quantitative Evaluation

Caco-2 cells, seeded in 24-well plates, were incubated 48 h with variable CPT-11 concentrations (5–100 μM) in lactate buffer (10 mM, pH 4.4) or incorporated into liposomes. Cell survival was also evaluated after incubation with 100 μM CPT-11 for 3, 6, 24, and 48 h, at different postincubation times ($\Delta t = 0$, $\Delta t = 24$, and $\Delta t = 48$) by the MTT assay.[37] Briefly, 100 μL of a MTT stock solution (1 mg/mL PBS) were added to 2 mL of DMEM to reach a final concentration of 47.6 μg/mL. Five-hundred milliliters of this MTT solution was added to each well after removing culture media and washing the cells with PBS three times. Cells were incubated for 3 h and formazan precipitates were dissolved in 0.5 mL of DMSO. The absorbance was measured at 540 nm on a Synergy H1 microplate spectrofluorimeter (BioTek Instruments Inc., Winooski, Vermont).

Cell survival was expressed as the percentage of absorption of treated cells in relation to that of control cells (100% survival).

Microscopical Observation

Caco-2 cells, seeded on 22 mm square coverslips in 35 mm Petri dishes, were treated with liposomal CPT-11 at a concentration of 100 μM for 48 h, with postincubation times (Δt) of 0, 24, and 48 h. Control and treated cells were fixed in cold methanol and nuclei were stained using 0.5 mg Hoechst-33258 (H-33258; Sigma)/mL solution in distilled water. Observation was carried out using an Olympus BX61 epifluorescence microscope (Olympus America Inc., Melville, NY, USA) equipped with an HBO 100 W mercury lamp and an ultraviolet (UV; 365 nm) excitation filter. Photographs were obtained with an Olympus DP50 digital camera (Olympus America Inc.).

Cell Cycle Analysis

Cell cycle distribution was analyzed by flow cytometry after staining the cells with propidium iodide (PI).[38] Caco-2 cells were treated with 100 μM liposomal CPT-11, for 48 h, with postincubation times (Δt) of 0, 24, and 48 h. To evaluate cell cycle at $\Delta t = 24$ h and $\Delta t = 48$ h, cells, treated with liposomal CPT-11 for 48 h, were washed to remove the drug and detached cells before to be submitted to the postincubation times. Flasks were trypsinized (harvesting also the detached cells), centrifuged (380xg, 5 min) and fixed with cold (−20°C) 70% ethanol solution (15 min, on ice). The pellet was resuspended in 1 mL of fresh PBS with 50 μL of RNase solution (100 μg/mL) and incubated for 30 min at 37°C. DNA was stained by adding 25 μL of 1 mg/mL PI solution. Measurements were performed with an Epics XL flow cytometer (Beckman Coulter, Brea, California) with an argon laser line at 488 nm. Cell fractions in "sub-G0-G1," G0-G1, S, G2M and "super G2" phases were quantified in histograms with Summit software. The identification of apoptotic cells (sub-G0-G1 region) was achieved by determination of hypoploid cell populations. Polyploid cells were also identified in the "super G2" region. For each experiment, a minimum of 20,000 events were analyzed.

Annexin V Assay

An additional apoptosis assay was carried out to analyze the state of cells in the "sub-G0-G1" fraction. The annexin V kit, which detects apoptotic cells by binding phosphatidylserine, translocated to the outer leaflet of the membrane bilayer and exposed to the extracellular environment when apoptosis occurs, was used to perform this study. Caco-2 cells, cultured in 25 cm^2 flasks, were treated with 100 μM liposomal CPT-11 for 3, 24, and 48 h, without postincubation times ($\Delta t = 0$). Then, the cells were washed and stained with annexin V and DAPI as indicated by the manufacturer. Samples were analyzed using a Gallios multicolor flow cytometrer instrument (Beckman Coulter, Inc.) set up with the 3-lasers 10 colors standard configuration. Excitation was carried out using a blue (488 nm) laser for forward scatter and side scatter. A gate including both live and death cells was settled on this dot plot, to exclude only small debris. Red fluorescence for annexin V-APC was collected in a log scale (excitation = 635 nm, emission = 660 nm) and blue fluorescence was used for DAPI (excitation = 405 nm, emission = 450 nm). Apoptotic and dead cells were detected using a dot plot combining both fluorescences. The cursorposition was corrected according to the autofluorescence caused by the treatment, which was mainly detected in the blue channel.

CPT-11 Liposomal Uptake by Caco-2 Cells

Qualitative (fluorescence microscopy) and quantitative (fluorescence spectroscopy) studies were performed. Untreated and treated (24 h incubation with 100 μM liposomal CPT-11) Caco-2 cells were directly observed *in vivo* with UV excitation. Images were acquired as for microscopical observation. To quantify the CPT-11 uptake, Caco-2 cells were cultured in 96-well plates and treated with 100 μM CPT-11 (chosen after a screening of the best conditions), in liposomes or in lactate buffer, for 1, 2, 3, 6, 24, and 48 h. Then, the plates were washed three times with PBS and cells were incubated 1 h with 100 μL of 2% SDS under shaking. Fluorescence was measured at $\lambda_{exc} = 368$ nm and $\lambda_{em} = 429$ nm (Synergy H1 microplate spectrofluorimeter; BioTek Instruments Inc.). Fluorescence intensity values were normalized in relation to the protein content of each sample, determined by the BCA protein assay,[39] to correct for variations in the number of cells.

Statistical Analyses

All experiments were repeated at least three times. Data in Tables are presented as the mean ± SD from the separated samples analyzed. Figures show the mean values from the separated samples analyzed, being the coefficients of variation (CV) indicated in the legend.

RESULTS

Effect of Lipid Composition on the Thermotropic Properties of Liposomes

Calorimetric measurements were carried out with the purpose of procuring TSL. Single lipids and binary lipid mixtures had been previously assayed and the incorporation of either CHOL or SM and negatively charged lipids has also been considered. T_m values determined for individual lipids (results not shown) were close to those reported in the literature.[40,41] Table 1 gives the characteristic parameters for MLV suspensions prepared from selected ternary mixtures. The endothermic transition profiles showed a single endotherm, pointing out the complete miscibility of the components used. T_m values were always above physiological temperature, as required for bilayer thermosensitiveness. ΔH_{cal} and ΔS_{cal} values were dependent of the CHOL or SM content, being higher for SM-containing bilayers. The thermodynamic parameters of DOPS- or DMPG-containing negatively charged bilayers are quite similar, irrespective of the nature of the anionic lipid. The broadness of the single endotherms ($\Delta T_{1/2}$) could be related either to the complexity of the acyl chain mixture of the samples or to the presence of CHOL.

In Vitro Study of the Stability Properties of Liposome Formulations

5(6)-Carboxyfluorescein loading and time- and temperature-dependent release profiles of the dye were used to investigate *in vitro* the stability and release properties of formulated liposomes[36] and to establish their temperature sensitivity.[24]

The results of CF encapsulation in liposomes (Fig. 1, line) show that the amount of CF slightly increased when CHOL (Figs. 1A–1C) was replaced by SM (Figs. 1D–1G), and that the incorporation of DMPG (H) gives liposomes with the highest ratio.

 DOI 10.1002/jps.24097

Table 1. Thermodynamic Parameters of Bilayer Lipid Mixtures

Composition (Molar Ratio)	T_m[a] (°C)	ΔH_{cal}[b] (kJ/mol)	ΔS_{cal}[c] (J/Kmol)	$\Delta T_{1/2}$[d] (°C)
DSPC/DOPS/CHOL (65:35:30)	46.0 ± 1.3	11.0 ± 1.2	34.6 ± 3.7	11.9 ± 2.0
DSPC/DOPS/CHOL (80:20:30)	50.1 ± 1.4	12.8 ± 1.0	39.6 ± 3.5	10.9 ± 1.2
DSPC/DOPS/SM (65:35:30)	45.4 ± 1.2	22.0 ± 1.9	69.1 ± 5.9	8.1 ± 1.0
DSPC/DOPS/SM (80:20:30)	48.9 ± 1.0	25.9 ± 2.6	80.6 ± 8.4	7.5 ± 1.1
DSPC/DOPS/SM (70:20:40)	48.6 ± 1.1	24.2 ± 2.7	75.1 ± 6.7	8.2 ± 0.9
DPPC/DOPS/CHOL (80:20:30)	39.6 ± 0.8	9.6 ± 1.1	30.7 ± 2.8	16.4 ± 2.3
DPPC/DOPS/SM (80:20:30)	38.9 ± 0.9	25.9 ± 2.3	83.0 ± 8.6	9.1 ± 1.0
DPPC/DMPG/SM (80:20:30)	41.5 ± 1.0	28.0 ± 2.4	89.1 ± 8.8	6.4 ± 0.7

[a]Temperature corresponding to the maximum of the calorimetric peak.
[b]Calorimetric enthalpy calculated from the area under the peak.
[c]Calorimetric entropy calculated as $\Delta H_{cal}/T_m$.
[d]Width of the calorimetric peak at half-peak height.

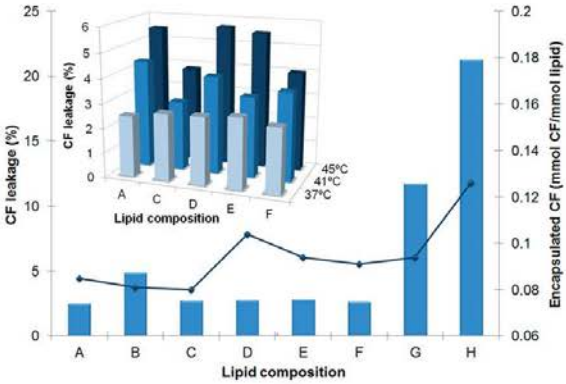

Figure 1. Influence of the lipid composition on liposomal CF content and CF leakage. Dye efflux (bars) was measured after 90 min at 37°C and was expressed as the percentage of initial trapped solute. CF content was expressed as μmol-encapsulated CF/μmol lipid. Lipid mixtures were: (A) DSPC/DOPS/CHOL (65:35:30); (B) DPPC/DOPS/CHOL (80:20:30); (C) DSPC/DOPS/CHOL (80:20:30); (D) DSPC/DOPS/SM (80:20:30); (E) DSPC/DOPS/SM (70:20:40); (F) DSPC/DOPS/SM (65:35:30); (G) DPPC/DOPS/SM (80:20:30); and (H) DPPC/DMPG/SM (80:20:30). Insert: CF leakage after 90 min at 37°C, 41°C and 45°C. Assay lipid concentration was 10 μg/mL. CV ranged from 4.5% to 20.5%.

Liposomes stability was evaluated *in vitro* by measuring the leakage, after 90 min (F_{90}) at 37°C, of CF encapsulated into vesicles.[36] It can be shown (Fig. 1, bars) that CF release depends on the bilayer composition and that it is near 3% for all the bilayers containing DSPC/DOPS/CHOL or DSPC/DOPS/SM, at different molar ratios. Moreover, when changing DSPC for DPPC, an increase in the permeability was observed, quite higher for the SM-containing mixture. It could be emphasized the increased CF release (up to 12%) from DPPC/DOPS/SM (80:20:30) liposomes with a T_m value near 39°C. Finally, CF efflux for liposomal bilayers containing DMPG (Fig. 1H) displays a great increase (~21%).

To assess the temperature effect on liposomes permeability, dye release was examined at temperatures ≥37°C. Results showed a gradual increase of F_{90} values when temperature was raised from 37°C to 45°C, irrespective of the bilayer lipid composition (graph insert in Fig. 1). Results also showed that DSPC/DOPS/CHOL (65:35:30)- and DSPC/DOPS/SM (80:20:30)-containing liposomes seemed to be more sensitive to temperature increases. This temperature study was carried out only with the DSPC-containing bilayers, having been rejected those containing DPPC or DMPG with permeability characteristics inappropriate for our purposes.

The destabilizing effect of serum was analyzed by following the time course and temperature-dependent CF release profile (Fig. 2) in PBS and in the presence of rat serum at 37°C and 41°C (mild hyperthermia conditions), at different lipid/serum ratios. SUVs of the two selected liposomal formulations, DSPC/DOPS/SM (80:20:30) and DSPC/DOPS/CHOL (65:35:30), containing 50 mM CF, were used. The efflux of CF at 37°C (Figs. 2a and 2b) increased in the presence of serum. Moreover, CF leakage from liposomes containing CHOL was always lower than 22% (Fig. 2b), whereas liposomes containing SM (Fig. 2a) were more permeable, as they lose up to 43.5% of CF at the highest serum content. The pattern for CF efflux at 41°C was similar to that observed at 37°C. The data corresponding to the temperature and serum content influence, on the release of the dye, after 90 min, in the presence of serum are given in Figures 2c and 2d.

Characterization of TSL

Empty liposome formulations, prepared from DSPC/DOPS/CHOL or DSPC/DOPS/SM mixtures, at different molar ratios, without CPT-11, were first characterized by size, size distribution, and ζ-potential and observed by AFM. Results (table insert in Fig. 3) show that vesicle sizes range from 117 to 202 nm, a fairly narrow size distribution (PI), and a negative surface charge according to DOPS content. The AFM micrographs in Figure 3 show tridimensional and bidimensional images of DSPC/DOPS/CHOL (65:35:30) liposomal formulation. The AFM images indicate that IUVs do not develop and shift on the mica surface easily, but are observed as tridimensional flattened structures. The analysis of the scan line of the liposomes surface gives additional information on liposomes size (156.9–164.0 nm) in agreement with those determined by PCS.

DSPC/DOPS/CHOL (65:35:30) and DSPC/DOPS/SM (80:20:30) lipid mixtures, which give similar-sized empty vesicles, were selected to prepare CPT-11-loaded liposomes. PCS analysis was carried out to determine the size and ζ-potential of the loaded vesicles and to prove the homogeneity of the liposomal suspensions (Table 2).

DOI 10.1002/jps.24097

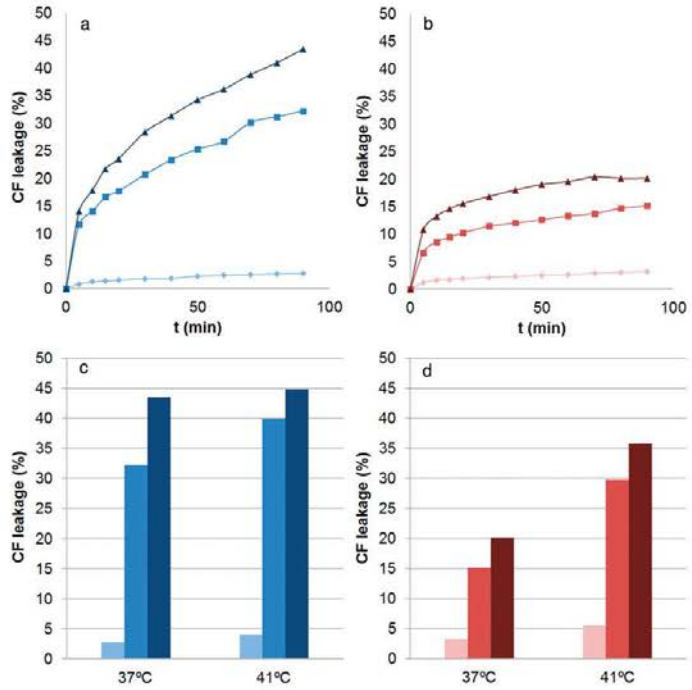

Figure 2. Influence of serum on CF leakage from liposomes. Lipid mixtures were DSPC/DOPS/SM (80:20:30; a and c) and DSPC/DOPS/CHOL (65:35:30; b and d). Efflux (a and b) was measured during 90 min in the absence (◆, ◆) and in the presence of rat serum, at 0.8 (■, ■) and 0.08 (▲, ▲)mg lipid per milliliter serum, at 37°C. c and d show the efflux of CF after 90 min, at 37°C and 41°C, in the absence (■, ■) and in the presence of rat serum, at 0.8 (■, ■) and 0.08 (■, ■) mg lipid per milliliter serum. Assay lipid concentration was 10 μg/mL. CV ranged between 4.1% and 18.2%.

Liposome Composition (Molar Ratio)	Size (nm)	PI	ζ (mv)
DSPC/DOPS/SM 80:20:30	139.4 ± 9.4	0.159 ± 0.020	− 25.50 ± 1.27
DSPC/DOPS/SM 65:35:30	117.8 ± 1.4	0.137 ± 0.008	− 36.60 ± 1.82
DSPC/DOPS/CHOL 80:20:30	202.5 ± 1.2	0.265 ± 0.012	−28.40 ± 1.60
DSPC/DOPS/CHOL 65:35:30	152.8 ± 12.9	0.109 ± 0.064	− 42.45 ± 2.70

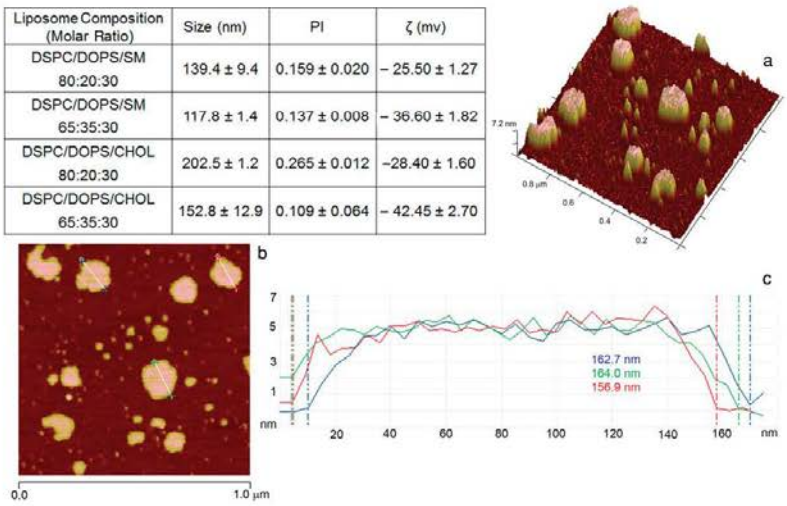

Figure 3. Physical and morphological characterization of thermosensitive liposomes. Tridimensional (a) and bidimensional (b) AFM images of DSPC/DOPS/CHOL (65:35:30) liposomes. (c) Scan line analysis of liposome surface revealing the peak height, diameter, and surface roughness of liposomes in AFM images. The diameters of the globular structures of marked liposomes were measured and indicated in the figure. The table insert gives the characteristic parameters of liposome formulations. Size (nm): Mean size (nm) of liposomes. PI: Polydispersity index. ζ: Zeta Potential values of liposomes.

DOI 10.1002/jps.24097

Table 2. Characterization of Different Temperature-Sensitive Liposomal Formulations Encapsulating CPT-11

Sample				Physical Parameters			Liposomal CPT-11	
Liposome composition (Molar Ratio)	$[L]_T$ [a]	$[D]_T$ [b]	L:D [c]	Size [d]	PI [e]	ζ [f]	$[Drug]_E$ [g]	EE [h]
DSPC/DOPS/CHOL (65:35:30)	10	0.95	10:1	140.0 ± 6.5	0.159 ± 0.021	−43.50 ± 3.68	0.69 ± 0.06	72.8
DSPC/DOPS/CHOL (65:35:30)	10	1.29	7.5:1	161.5 ± 2.1	0.114 ± 0.032	−46.8 ± 0.72	1.10 ± 0.08	85.2
DSPC/DOPS/CHOL (65:35:30)	10	1.93	5:1	172.0 ± 10.3	0.245 ± 0.066	−40.65 ± 0.92	1.14 ± 0.09	59.3
DSPC/DOPS/CHOL (65:35:30)	20	1.93	10:1	165.0 ± 4.6	0.183 ± 0.050	−49.8 ± 0.99	1.61 ± 0.10	83.2
DSPC/DOPS/CHOL (65:35:30)	20	3.86	5:1	182.0 ± 8.2	0.233 ± 0.059	−45.00 ± 1.99	2.28 ± 0.18	59.0
DSPC/DOPS/SM (80:20:30)	10	0.95	10:1	154.0 ± 7.7	0.191 ± 0.042	−25.65 ± 0.49	0.23 ± 0.08	24.1

The amount of lipid in the liposomal suspensions was always greater than 97%.
[a]Total concentration of the lipid added to the samples (mg/mL).
[b]Total concentration of CPT-11 added to the samples (mg/mL).
[c]Lipid:CPT-11 molar ratio in the organic solution, before film formation.
[d]Mean size (nm) of CPT-11-loaded liposomes.
[e]Polydispersity index.
[f]Zeta potential values of CPT-11-loaded liposomes.
[g]Concentration of CPT-11 in the liposomal suspensions (mg/mL) after removing the nonentrapped drug.
[h]Entrapment efficiency expressed as the percentage of total drug added to prepare liposomes.

The entrapment efficiency of CPT-11 in liposomes was evaluated at different lipid concentrations (10 or 20 mg/mL) and different lipid:CPT-11 molar ratios (Table 2). It can be shown that, at a fixed lipid composition and concentration, the greatest drug to lipid molar ratio, the greatest CPT-11 concentration in liposomal formulations (It can be shown that, for a given lipid composition and at a fixed lipid concentration, the encapsulation of CPT-11 in the liposomal formulations increased when rising the molar ratio of drug to lipid). It can be outlined that there is a limit for the CPT-11 amount to be encapsulated, as when working at a 5:1 lipid–drug ratio, the entrapment efficiency dramatically decreases and suspensions become unstable. The lipid composition also influences the entrapment efficiency, being the higher values (72%–85%) for CHOL-containing liposomes. SM-containing liposomes only incorporate a 24.1% of total CPT-11, and this value could not be raised, neither by increasing lipid concentration nor by modifying the lipid:drug ratio (results not shown). Moreover, the incorporation of CPT-11 does not significantly affect the physical parameters of liposomes (table insert in Fig. 3 and Table 2).

In Vitro Studies of Liposomal CPT-11 Cytotoxic Activity

The effectiveness of the DSPC/DOPS/CHOL (65:35:30) liposomal–CPT-11 was assessed and compared with that of the free drug by using the Caco-2 cell line. Cell survival, incubated for 48 h with a fixed CPT-11 molar concentration (100 μM), was also evaluated at different postincubation times ($\Delta t = 0$, $\Delta t = 24$, and $\Delta t = 48$). Additionally, Caco-2 cells were incubated with 100 μM CPT-11 and viability was determined immediately after 3, 6, 24, and 48 h of incubation. Results (Fig. 4) show that the cytotoxic effect is concentration dependent (left panel) and time dependent (middle panel), that, at a fixed CPT-11 concentration, is dependent on the postincubation time (right panel) and that liposomal CPT-11 action is stronger than that observed for the drug administered in lactate buffer at all of the assayed conditions. The cytotoxic effect was particularly higher after the 48-h treatment with the liposomal formulation (84% for liposomal CPT-11 vs. 60% for CPT-11 in lactate buffer). Fluorescence microscope images (Figs. 5a–5d) showed a time-dependent decrease in the number of cells and an increase in the size of the nuclei of untreated cells after the incubation with

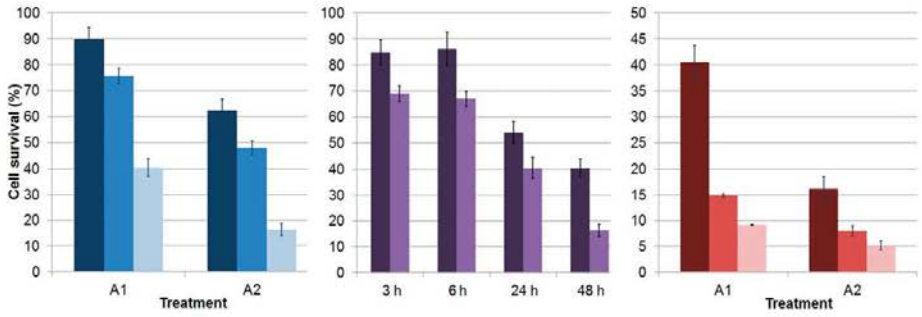

Figure 4. Surviving fraction of Caco-2 cells incubated with CPT-11. Left panel: Caco-2 cells incubated for 48 h with 5 (■), 10 (■), and 100 (■) μM lactate buffer-solubilized CPT-11 (A1) or liposomal CPT-11 (A2). Cell survival was determined immediately following drug exposure. Middle panel: Caco-2 cells incubated with 100 μM lactate buffer-solubilized CPT-11 (■) or liposomal CPT-11 (■). Cell survival was determined immediately following drug exposure after the incubation times indicated in the figure. Right panel: Caco-2 cells incubated for 48 h with 100 μM lactate buffer-solubilized CPT-11 (A1) or liposomal CPT-11 (A2). Cell survival was determined immediately (■, $\Delta t = 0$), 24 h (■, $\Delta t = 24$), and 48 h (■, $\Delta t = 48$) following drug exposure. CV ranged between 3.2% and 15.9%.

DOI 10.1002/jps.24097

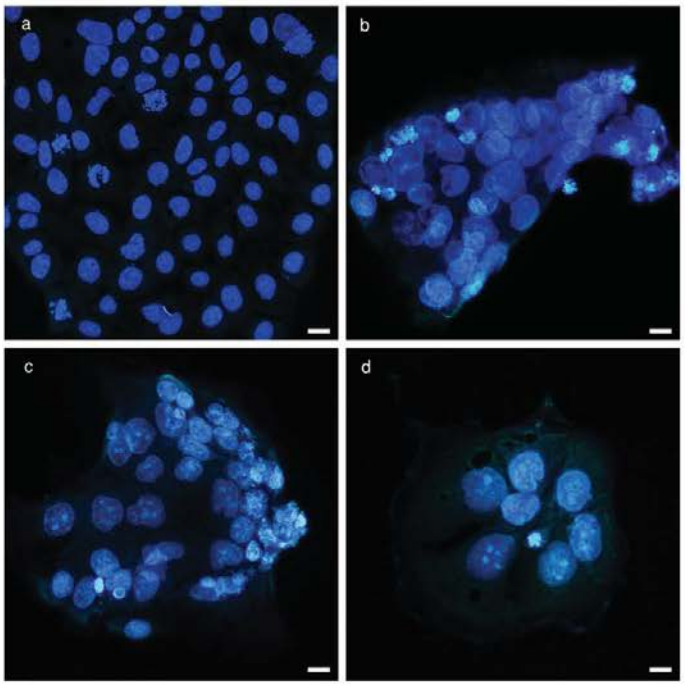

Figure 5. Hoechst 33258S-stained Caco-2 cancer cells treated with liposomal CPT-11. Control (untreated) cells stained with the probe (a). Cells treated with liposomal CPT-11 (100 μM for 48 h), stained with the same probe immediately (b, $\Delta t = 0$), 24 h (c, $\Delta t = 24$), and 48 h (d, $\Delta t = 48$) following drug exposure and observed under fluorescence microscopy. Scale bars: 10 μm.

the liposomal formulation of this drug. Hoescht-stained Caco-2 cells show some of the features corresponding to apoptotic cells,[42] although they are not very conclusive. Because of this, we have studied the effect of liposomal CPT-11 on Caco-2 cells cycle and analyzed the interaction of annexin V with treated cells to accurately assess the existence of apoptotic cells.

The effect of liposomal CPT-11 on cell cycle phase distribution after drug exposure was performed by flow cytometry. Figure 6a shows the diploid DNA histograms for untreated cells (control) and for those treated with 100 μM liposomal CPT-11 for 48 h, with postincubation times (Δt) ranging from 0 to 48 h. Cell cycle profiles of treated cells changed by suffering a movement toward the right with an increase of cells at the S and G2M peaks, in contrast with the DNA content of untreated cells. The table insert in Figure 6 shows the percentages of cells in each cell cycle phase, obtained from the analysis of the histograms. The analysis of the data shows a significant increase of cells placed in the polyploid sector (super G2 phase), a decrease in the G0-G1 phases, and a tendency of S and G2M phases to increase related to the increase of postincubation time for CPT-11-treated cells. Moreover, the percentage of cells in the sub-G0-G1 phase (Fig. 6b), which could correspond to apoptotic cells but also to cellular debris, was significantly increased for treated samples. It may be taken into account that the percentage of cells in the sub-G0-G1 phase at Δt 24 and 48 h corresponds to new cells appeared after removing those at $\Delta t = 0$.

The proapoptotic effect of the liposomal drug was investigated by the annexin V assay.[42,43] The results obtained for Caco-2 cells are shown in Figure 7. Treated cells with 100 μM liposomal CPT-11 for 3 h showed a little annexin V labeling of plasma membrane increase (annexin V +, DAPI − cells) with respect to control cells, and the annexin V labeling increases for 24- and 48-h treated cells. After 48 h, the percentage of viable cells (annexin V −, DAPI −) was 54.4%, being the 23.5% of cells in an early apoptotic stage with intact membranes (annexin V+, DAPI −), and the 17.5% of cells at the end stage of apoptosis and/or death (annexin V +, DAPI +), indicating the proapoptotc effect of CPT-11.

Evaluation of the Uptake of Liposomal CPT-11 by Caco-2 Cells

Cell uptake of drugs has been widely investigated in biomedical research in relation with their therapeutic effect. Fluorescence microscopy studies (Figs. 8a and 8b) showed that when Caco-2 cells are treated with the liposomal formulation, CPT-11 is homogeneously internalized and located in the cytoplasm of the cells (Figs. 8b).

The quantitative analysis of CPT-11 internalization in Caco-2 cells (Fig. 8c) shows the time and formulation dependence (liposomal vs. nonliposomal) of CPT-11 uptake, being always greater for the liposomal formulation.

DISCUSSION

Liposomes are versatile structures, abilities of which have been exploited in several disciplines. The goal of using liposome carriers in cancer nanomedicine is to achieve a product that

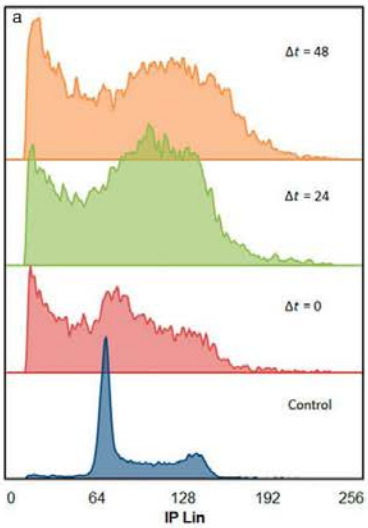

Treatment	Caco-2 Cell Cycle Phases			
	G0-G1	S	G2M	Super G2
Control	53.7	27.1	17.8	1.8
Δt = 0	31.7	45.2	17.7	5.9
Δt = 24	18.9	51.0	22.9	8.6
Δt = 48	16.2	42.4	23.6	17.3

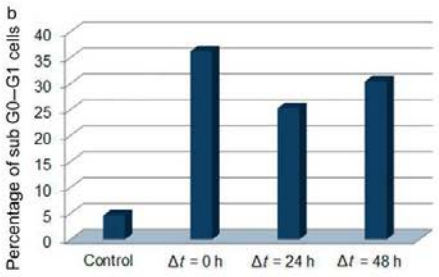

Figure 6. Flow cytometry analysis of DNA content (measured using PI). (a) DNA content profile of a control of Caco-2 population and of Caco-2 cells 0 ($\Delta t = 0$), 24 h ($\Delta t = 24$) and 48 h ($\Delta t = 48$) after 48 h incubation with 100 μM liposomal CPT-11. The peak pattern is clearly shifted toward G2M and polyploidy areas. The table insert shows the percentages of cells in each cell cycle phase, obtained from the analysis of the histograms. (b) Quantification of Caco-2 cells in the sub-G0-G1 phase for the different treatment groups.

combines traditional cytotoxic agents with targeted properties for optimum therapeutic effects and acceptable toxicity. Moreover, liposomes can be drawn to be multifunctional by choosing the appropriate components to control their properties. However, each drug has specific requirements to be efficiently encapsulated into liposomes, that is, the choice of the lipid species and the ratio in which they should be mixed, the optimum drug/lipid ratio, and the more suitable methodology to prepare the final formulation. Taking into account these premises, we have already developed a liposomal product for a photosensitizer and proved its usefulness as a drug carrier by an *in vivo* study.[44]

Different lipid combinations have been considered to endow liposome bilayers with temperature sensitiveness. Both the lipid nature and the amount of each lipid determine the thermodynamics of the resulting bilayers. The ternary mixtures proposed have appropriate T_m values (Table 1). The data showed significant differences, not only in T_m values, but also in the endothermic transition parameters, depending on the incorporation of CHOL or SM. The highest ΔH_{cal} and ΔS_{cal} values for bilayers containing SM indicate a greater degree order at the hydrophobic core, being in agreement with their smallest $T_{1/2}$ values regarding those of CHOL-containing mixtures.

To assess vesicle stability, the release kinetics of CF encapsulated in liposomes was examined at different temperatures and in the presence of rat serum (Fig. 2). Results revealed differences in function of both the nature of the lipids and the ratio in which they have been mixed. Thus, DSPC gives the less permeable bilayers at 37°C when mixed with DOPS and SM or CHOL. Nevertheless, CF release was higher when changing DSPC for DPPC, and the incorporation of DMPG- to DPPC-containing vesicles, instead DOPS, increases CF efflux significantly. The understanding of these results requires additional considerations, besides thermal behavior, such as bilayer lipids organization. Moreover, passive efflux of CF is inversely related to liposome size[45] and varies in acid environments.[46] In this way, the assay conditions and the interpretation of the results of liposomes stability study have been chosen taken into account these facts. The screening of a significant number of lipid combinations lead to the choice of DSPC/DOPS/CHOL (65:35:30) and DSPC/DOPS/SM (80:20:30) as the best mixtures to get liposomes with a sustained-release profile and stable enough at physiological temperature and in the presence of serum, to procure CPT-11 formulations. DSPC/DOPS/SM (80:20:30) was selected instead of DSPC/DOPS/SM (60:35:30) because its permeability properties seemed to be more sensitive to temperature increases. Although DMPG has often been used to provide negative liposomal surfaces, our DMPG-containing liposomes will not be good as drug carriers because of their higher permeability.

The physical parameters (size, size distribution, and ζ-potential) of empty liposomes were analyzed and AFM images were obtained, as a previous step to encapsulate CPT-11 (Fig. 3). The data confirm that DSPC/DOPS/CHOL (65:35:30) and DSPC/DOPS/SM (80:20:30) mixtures are the best to prepare CPT-11-loaded liposomes.

The efficiency of drug loading depends on its encapsulation in the aqueous core, its incorporation into the liposomal bilayer, or its partition between these two phases and is governed by such properties as liposome size, surface charge, and membrane fluidity. Our results showed that DSPC/DOPS/CHOL (65:35:30) is the more appropriate mixture to prepare a carrier for CPT-11 and that the 7.5:1 lipid to CPT-11 molar ratio (Table 2) represents the best option thinking about the formulation properties.

The efficiency of chemotherapeutic treatments depends on the cytotoxic activity of anticancer drugs which, in turn, depends on their uptake by tumor cells and on their subcellular localization. CPT-11 formulated into liposomes was

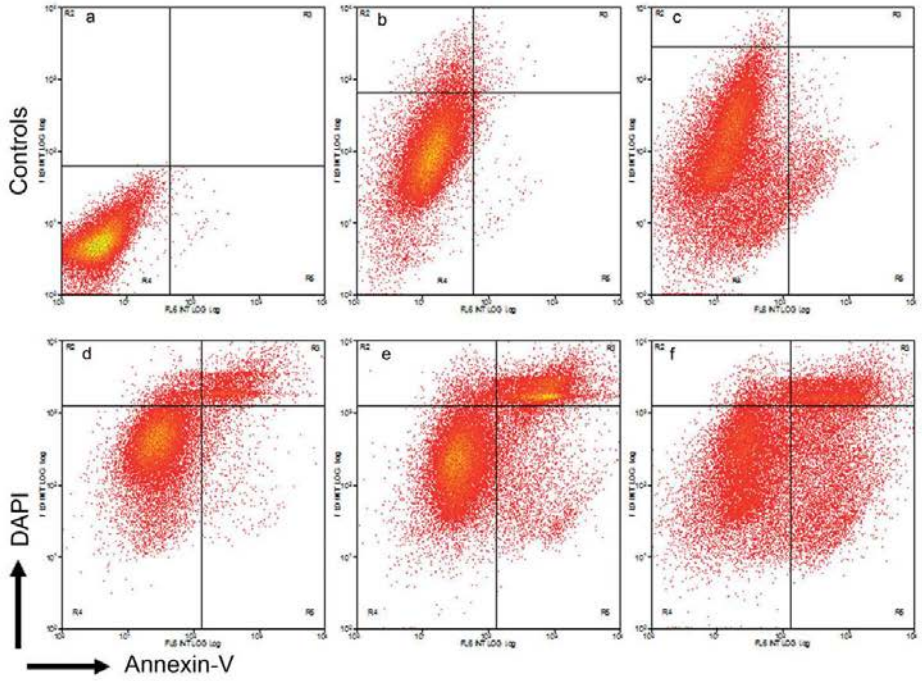

Cells	Liposomal CPT-11 Treatment			
	0 h	3 h	24 h	48 h
Annexin V –, DAPI –	93.3	75.2	61.8	54.4
Annexin V +, DAPI –	2.5	5.4	10.2	23.5
Annexin V –, DAPI +	3.5	4.5	4.0	4.5
Annexin V +, DAPI +	0.7	14.9	24.0	17.5

Figure 7. Contour diagram of annexin V–APC/DAPI flow cytometry of Caco-2 cells after liposomal CPT-11 treatment for different times. The lower left quadrants of each panels show the viable cells, which exclude DAPI and are negative for annexin V–APC binding. The upper right quadrants contain the nonviable cells, positive for annexin V–APC binding, and for DAPI uptake. The lower right quadrants represent the apoptotic cells, annexin V–APC positive, and DAPI negative. (a) Autofluorescence of untreated cells; (b and c) autofluorescence of liposomal CPT-11-treated cells for 24 and 48 h, respectively; (d, e, and f) fluorescence of annexin V–DAPI-containing CPT-11-treated cells for 3, 24, and 48 h. One representative experiment of three performed is shown. The table insert shows the percentage of cells in each quadrant, at different times, after treatment with 100 μM liposomal CPT-11.

significantly more cytotoxic to Caco-2 cells than CPT-11 solubilized in a buffered solution, as inferred from the decrease in cell viability after treatment (Fig. 4). This result agrees with the fact that when treated cells were observed under fluorescence microscopy (Fig. 5), a time-dependent decrease in the amount of cells was observed. Moreover, treated cells undergo an increase in the size of their nuclei and display some of the morphological features corresponding to apoptotic cells,[42] although the images are not very conclusive.

Cell cycle analysis showed that the treatment of Caco-2 cells with liposomal CPT-11 caused severe alterations (Fig. 6), being the characteristic diploid DNA histograms for untreated cells changed after drug treatment. A decrease of cells in the G0-G1 phase, increases of cells at S and G2M peaks, and a significant variation of cells placed in the polyploid sector (from 1.8% to 17.3% at $\Delta t = 48$) have been observed. These changes could indicate the progress of Caco-2 cells through G1 phase and the cycle arrest in S and G2M phases after liposomal CPT-11 treatment. Similar results have been reported in the literature for the effect of paclixactel or trastuzumab.[47] Moreover, a significant population, the percentage of which increases with time, arises in the sub-G0-G1 region. This population could be cells in apoptotic stage and/or cellular debris. The analysis of the content of the sub-G0-G1 region, as studied by the annexin V test and flow cytometry, confirms the existence of apoptotic cells (Fig. 7). The whole of the experimental data about the effect of CPT-11 on the colon cancer cell line model Caco-2 prove the progress of an increasing apoptosis process induced by this drug in its liposomal form. In the literature, there are only a few references about the analysis of the camptothecin-induced

 DOI 10.1002/jps.24097

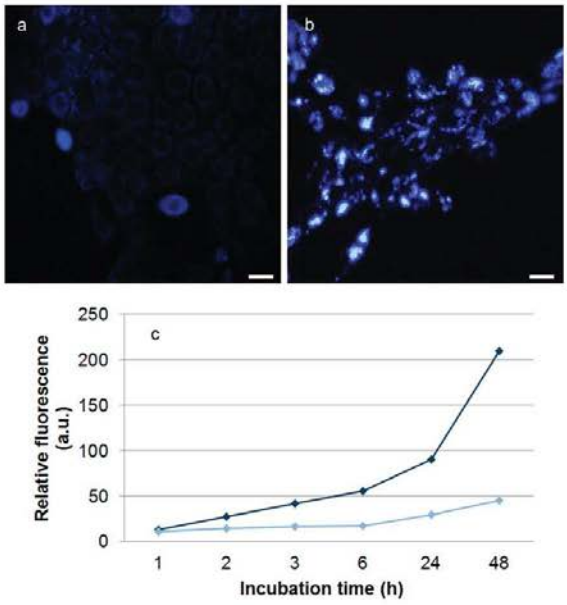

Figure 8. *In vitro* uptake of irinotecan by Caco-2 cells. Control (a) and treated cells with 100 μM liposomal CPT-11 for 24 h (b), observed by fluorescence microscopy. Scale bars: 10 μm. The graph (c) shows the quantitative analysis of the internalization of CPT-11 in Caco-2 cells carried out by fluorescence spectroscopy. Cells were incubated with 100 μM liposomal (♦) or buffer-solubilized CPT-11 (◦) for different periods of time and emission fluorescence at 429 nm (excitation 368 nm) was determined after lysing the cells. The fluorescence plotted is the ratio between the fluorescence emission and the protein content in each suspension. CV ranged from 8.1% to 11.4%.

cell cycle changes,[48] but neither of them considers the influence of selective delivery carriers in the effect of such drugs.

The internalization of liposomal CPT-11 into Caco-2 cells was first observed by fluorescence microscopy (Fig. 8). The analysis of the micrographs showed that nonfluorescent control cells became highly and homogeneously fluorescent after incubation with liposomal CPT-11. These results were in agreement with those of the quantitative evaluation of CPT-11 uptake by fluorescence spectroscopy. Drug internalization increased with the incubation time and the liposomal carrier promoted the entry of CPT-11 in comparison with that of the free drug in lactate. The results of uptake explain away the greatest cytotoxic activity of CPT-11 in its liposomal form.

The chance of improving the therapeutic safety and efficacy of anticancer drugs by means of the use of liposome carriers, revisited and documented in several exhaustive and actualized reviews, highlights the future opportunities of liposome and lipid nanoparticle therapeutics.[49]

CONCLUSIONS

A novel and easy-to-prepare liposome formulation for CPT-11 has been developed. The mixture DSPC/DOPS/CHOL (65:35:30) fulfills all the requirements raised in the purposes of this work and has been chosen to procure liposomes with a temperature-sensitive bilayer and the integrity of which in serum-containing media seems to be enough for therapeutic applications. The influence of the blend of lipid species on CPT-11 entrapment efficiency has been proved. The paper gives a rigorous and systematic analysis of the physicochemical properties of the liposomal system and analyzes their efficiency against a colorectal cancer cell line. Results show the potential interest of these liposomes for delivering CPT-11 and constitute a valid starting point for their use in preclinical *in vivo* tests directed to propose alternative strategies for colorectal cancer treatment.

ACKNOWLEDGMENTS

Funding for this project has been received from the Department d'Universitats, Recerca i Societat de l'Informació (DURSI) and Govern de la Generalitat de Cataluña (2009SGR-367). A. Casadó thanks to the University of Barcelona for a predoctoral fellowship. The authors are also grateful to Prof. M. L. García for the use of the Malvern Zetasizer NANO-ZS device and to Dr. J. Comas for his helpful technical support in the annexin V experiments.

REFERENCES

1. Edwards BK, Ward E, Kohler BA, Eheman C, Zauber AG, Anderson RN, Jemal A, Schymura MJ, Lansdorp-Vogelaar I, Seeff LC, van Ballegooijen M, Goede SL, Ries LAG. 2010. Annual report to the nation on the status of cancer, 1975–2006, featuring colorectal cancer trends and impact of interventions (risk factors, screening, and treatment) to reduce future rates. Cancer 116:544–573.
2. Jemal A, Siegel R, Ward E. 2008. Cancer statistics. CA Cancer J Clin 58:71–96.
3. Vanhoefer U, Harstrick A, Achterrath W, Cao S, Seeber S, Rustum YM. 2001. Irinotecan in the treatment of colorectal cancer: Clinical overview. J Clin Oncol 19:1501–1518.
4. Segal NH, Saltz LB. 2009. Evolving treatment of advanced colorectal cancer. Annu Rev Med 60:207–219.
5. Majer M, Akerley W, Kuwada SK. 2007. Oncologists' current opinion on the treatment of colon carcinoma. Anticancer Agents Med Chem 7:492–503.
6. Saltz LB. 2009. Looking ahead: What will change in colorectal cancer treatment? Gastrointest Cancer Res 3(suppl 1):S16–S18.
7. Wolpin BM, Mayer RJ. 2008. Systemic treatment of colorectal cancer. Gastroenterology 134:1296–1310.
8. Hind D, Tappenden P, Tumur I, Eggington E, Sutcliffe P, Ryan A. 2008. The use of irinotecan, oxaliplatin and raltitrexed for the treatment of advanced colorectal cancer: Systematic review and economic evaluation (review of NICE Guidance No. 33) . Health Technol Assess. 12(15).
9. Andresen TL, Jensen SS, Jørgensen K. 2005. Advanced strategies in liposomal cancer therapy: Problems and prospects of active tumour specific drug release. Prog Lipid Res 44:68–97.
10. Torchilin V. 2006. Nanoparticulates as drug carriers. London, UK: Imperial College Press.
11. Allen TM, Cullis PR. 2013. Liposomal drug delivery systems: From concept to clinical aplications. Adv Drug Deliv Rev 65:36–48.
12. Lasic DD, Papahadjopoulos D. 1998. Medical applications of liposomes. Amsterdam, The Netherlands: Elsevier Science B.V.
13. Sen K, Mandal M. 2013. Second generation liposomal cancer therapeutics: Transition from laboratory clinic. Int J Pharm 448:28–43.
14. Lanao JM, Briones E, Colino CI. 2007. Recent advances in delivery systems for anti-HIV1 therapy. J Drug Target 15:21–36.

15. Senge MO, Brandt JC. 2011. Temoporfin (Foscan®, 5,10,15,20-tetra(m-hydroxyphenyl) chlorin)-A second-generation photosensitizer. Photochem Photobiol 87:1240–1296.
16. Slingerland M, Guchelaar H-J, Gelderblom H. 2012. Liposomal drug formulations in cancer therapy: 15 years along the road. Drug Discov Today 17:160–166.
17. Habib L, Khreich N, Jraij A, Abbas S, Magdalou J, Charcosset C, Greige-Gerges H. 2013. Preparation and characterization of liposomes incorporating cucurbitacin E, a natural cytotoxic triterpene. Int J Pharm 448:313–319.
18. Hattori Y, Shi L, Ding W, Koga K, Kawano K, Hakoshima M, Maitani Y. 2009. Novel irinotecan-loaded liposome using phytic acid high therapeutic efficacy for colon tumors. J Control Release 136:30–37.
19. Mora M, Sagristá ML. 2009. Preclinical photodynamic therapy in Spain. 2: Liposome vectorization of photosensitizers. Different strategies, different outcomes. J Porphyrins Phthalocyanines 13:537–543.
20. Senior J. 1987. Fate and behavior of liposomes in vivo: A review of controlling factors. Crit Rev Ther Drug Carrier Syst 3:123–193.
21. García-Díaz M, Nonell S, Villanueva A, Stockert JC, Cañete M, Casadó A, Mora M, Sagristá ML. 2011. Do folate-receptor targeted liposomal photosensitizers enhance photodynamic therapy selectivity? Biochim Biophys Acta 1808:1063–1071.
22. Kong G, Dewhirst MW. 1999. Hyperthermia and liposomes. Int J Hyperthermia 15:345–370.
23. Li L, ten Hagen TLM, Schipper D, Wijnberg TM, van Rhoon GC, Eggermont AMM, Lindner LH, Koning GA. 2010. Triggered content release from optimized stealth thermosensitive liposomes using mild hyperthermia. J Control Release 143:274–279.
24. Mills JK, Needham D. 2004. The materials engineering of temperature-sensitive liposomes. Methods Enzymol 387:82–113.
25. Dicheva BM, ten Hagen TL, Li L, Schipper D, Seynhaeve ALB, van Rhoon GC, Eggermont AMM, Lindner, LH, Koning GA. 2013. Cationic thermosensitive liposomes: A novel dual targeted heat-triggered drug delivery approach for endothelial and tumor cells. Nano Lett 13:2324–2331.
26. Yatvin MB, Weinstein JN, Dennis WH, Blumenthal R. 1978. Design of liposomes for enhanced local release of drugs by hyperthermia. Science 202:1290–1293.
27. Weinstein JN, Magin RL, Cysyk RL, Zaharko DS. 1980. Treatment of solid L1210 murine tumors with local hyperthermia and temperature-sensitive liposomes containing methotrexate. Cancer Res 40:1388–1395.
28. Needham D, Dewhirst MW. 2001. The development and testing of a new temperature-sensitive drug delivery system for the treatment of solid tumors. Adv Drug Deliv Rev 53:285–305.
29. Arancia G, Calcabrini A, Matarrese P, Marcocci L, Pietrangeli P, Mondovì B. 1994. Effects of incubation with liposomes at different temperatures on cultured melanoma cells (M14). Int J Hyperthermia 10:101–114.
30. Artursson P, Palm K, Luthman K. 2001. Caco-2 monolayers in experimental and theoretical predictions of drug transport. Adv Drug Deliv Rev 46:27–43.
31. Mora M, Gutiérrez ME, García AF, De Madariaga MA, Sagristá ML, Casadó FJ. 2003. Interactions of tocopherols and phenolic compounds with membrane lipid components: Evaluation of their antioxidant activity in a liposomal model system. Life Sci 72:2337–2360.
32. Stewart JCM. 1980. Colorimetric determination of phospholipids with ammonium ferrothiocyanate. Anal Biochem 104:10–14.
33. Rouser G, Fleisher S, Yamamoto A. 1970. Two dimensional thin layer chromatographic separation of polar lipids and determination of phospholipids by phosphorus analysis of spots. Lipids 5:494–496.
34. Vermette P. 2009. Liposome characterization by quartz crystal microbalance measurements and atomic force microscopy. Methods Enzymol 465:43–73.
35. Weinstein JN, Ralston E, Leserman LD, Klausner RD, Dragsten P, Henkart P, Blumental R. 1984. Self-quenching of carboxyfluorescein fluorescence: Uses in studying lioposome stability and liposome–cell interaction. In Liposome technology; Gregoriadis G. Ed. Vol. III. Boca Raton, Florida: CRC Press, pp 183–204.
36. Volodkin D, Mohwald H, Voegel JC, Ball V. 2007. Coating of negatively charged liposomes by polylysine: Drug release study. J Control Release 117:111–120.
37. Mosmann T. 1983. Rapid calorimetric assay for cellular growth and survival: Application to proloferation and cytotoxicity assays. J Immunol Methods 65:55–63.
38. Fried J, Perez AG, Clarkson BD. 1976. Flow cytofluorometric analysis of cell cycle distributions using propidium iodide. Properties of the method and mathematical analysis of the data. J Cell Biol 71:172–181.
39. Smith PK, Krohn RI, Hermanson GT, Mallia AK, Gartner FH, Provenzano MD, Fujimoto EK, Goeke NM, Olson BJ, Klenk DC. 1985. Measurement of protein using bicinchoninic acid. Anal Biochem 150:76–85.
40. Cevc G. 1993. Phospholipid handbook. New York: Marcel Dekker Inc.
41. Degovics G, Latal A, Prenner E, Kriechbaum M, Lohner K. 1997. Structure and thermotropic behaviour of mixed choline phospholipids model membranes. J Appl Cryst 30:776–780.
42. Acedo P, Stocker JC, Cañete M, Villanueva A. 2014. Two combined photosensitizers: A goal for more effective photodynamic therapy of cancer. Cell Death Dis 5:e1122.
43. Cheng M-R, Li Q, Wan T, He B, Han J, Chen H-X, Yang F-X, Wang W, Xu H-Z, Ye T, Zha B-B. 2012. Galactosylated chitosan/5-fluorouracil nanopartícules inhibit mouse hepatic cancer growth and its side effects. World J Gastroenterol 18:6076–6087.
44. García-Díaz M, Kawakubo M, Mroz P, Sagristá ML, Mora M, Nonell S, Hamblin MR. 2012. Cellular and vascular effects of the photodynamic agent temocene are modulated by the delivery vehicle. J Control Release 162:355–363.
45. Hossann M, Wang T, Wiggenhorn M, Schmidt R, Zengerle A, Winter G, Eibl H, Peller M, Reiser M, Issels RD, Lindner LH. 2010. Size of thermosensitive liposomes influences content release. J Control Release 147:436–443.
46. Sulkowski WW, Pentak D, Nowak K, Sulkowska A. 2005. The influence of temperature, cholesterol content and pH on liposome stability. J Mol Struct 744–747:737–747.
47. Gabrielson M, Tina E. 2013. The mitochondrial transport protein SLC25A43 affects drug efficacy and drug-induced cell cycle arrest in breast cancer cell lines. Oncol Reports 29:1268–1274.
48. Wallin A, Svanvik J, Holmlund B, Ferreud L, Sun X-F. 2008. Anticancer effect of SN-38 on colon cancer cell lines with different metastatic potential. Oncol Reports 19:1493–1498.
49. Kraft JC, Freeling JP, Wang Z, Ho RJY. 2014. Emerging research and clinical development trends of liposome and lipid nanoparticle drug delivery systems. J Pharm Sci 103:29–52.

 DOI 10.1002/jps.24097

Segundo artículo

Langmuir monolayers and Differential Scanning Calorimetry for the study of the interactions between camptothecin drugs and biomembrane models.

Casadó A, Giuffrida MC, Sagristá ML, Castelli F, Pujol M, Alsina MA, Mora M.

Biochim Biophys Acta. 2016 Feb;1858(2):422-33. doi: 10.1016/j.bbamem.2015.12.007

RESUMEN

Las camptotecinas son fármacos de primera línea para el tratamiento de una gran variedad de enfermedades cancerosas. Pertenecen a la familia de inhibidores de la Topoisomerasa I y poseen una gran actividad antitumoral. Sin embargo, sus severos efectos secundarios y la inestabilidad química de su anillo de lactona, que se abre a pH fisiológico para dar un carboxilato inactivo, han cuestionado los protocolos y formas de administración de las actuales terapias y están centrando las investigaciones en el desarrollo de nuevas y más adecuadas formas farmacéuticas. El presente trabajo presenta un estudio biofísico de las interacciones interfaciales entre el CPT-11 y el SN-38, su metabolito, con sistemas modelo de membrana, constituidos por lípidos individuales o por mezclas complejas, mediante la utilización de técnicas de monocapas y de calorimetría diferencial de barrido. Su principal objetivo ha sido la obtención de datos que permitan profundizar en el conocimiento y comprensión de la mecánica de las bicapas lipídicas después de la incorporación de un fármaco. La información que se derive de estos estudios debe facilitar el diseño de sistemas de vehiculización de fármacos más eficientes. Debe destacarse, además, que las interacciones moleculares entre camptotecinas y fosfolípidos no se han investigado todavía en profundidad, a pesar de su evidente importancia en el contexto de la acción farmacológica. Los resultados obtenidos mediante calorimetría diferencial y monocapas de Langmuir muestran que ni el CPT-11 ni el SN-38 alteran la estructura de bicapas lipídicas complejas, a pesar de las especiales y diferentes propiedades de solubilidad de estas camptotecinas y de su diferente localización en los dos posibles entornos de la estructura liposomal, que el CPT-11, con carga positiva en su grupo piperidina, interacciona electrostáticamente con la DOPS, haciendo estable la incorporación de un elevado porcentaje de esta fármaco en liposomas y que el SN-38 establece interacciones de repulsión débiles con las moléculas lipídicas que, aunque modifican la compresibilidad de la bicapa, no afectan significativamente ni a la presión de colapso de los lípidos, ni al patrón de miscibilidad de las monocapas mixtas lípido-

fármaco. En su conjunto, todos estos datos han sido útiles para demostrar la idoneidad de una mezcla lipídica binaria, EPC/DOPS, y una ternaria, DSPC/DOPS/CHOL, para la obtención de SN-38 y CPT-11, respectivamente.

ASPECTOS DESTACADOS DE LA INVESTIGACIÓN

- El CPT-11 y el SN-38 interaccionan con sistemas modelo membrana sin perturbar su estructura.
- El CPT-11 y el SN-38 se localizan en dos entornos diferentes de la estructura liposomal.
- A pesar de su naturaleza similar, el CPT-11 muestra actividad superficial mientras que el SN-38 no.
- El CPT-11 interacciona electrostáticamente con la DOPS, haciendo estable su incorporación en liposomas.
- La incorporación del SN-38 proporciona una monocapa más fluida y compresible.

RESUMEN GRÁFICO

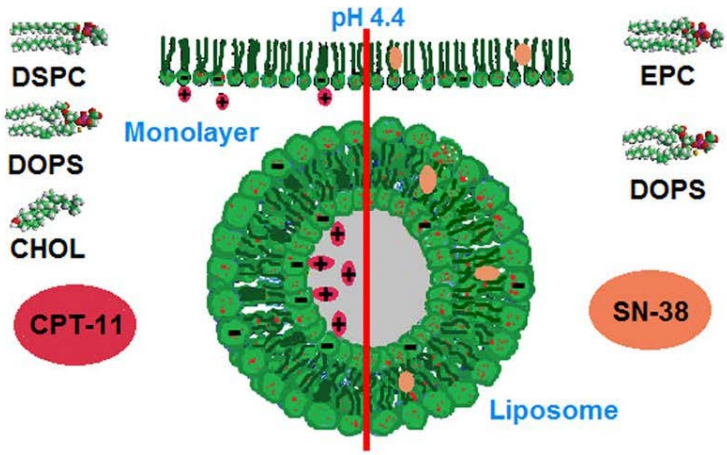

Biochimica et Biophysica Acta 1858 (2016) 422–433

Contents lists available at ScienceDirect

Biochimica et Biophysica Acta

journal homepage: www.elsevier.com/locate/bbamem

Langmuir monolayers and Differential Scanning Calorimetry for the study of the interactions between camptothecin drugs and biomembrane models

Ana Casadó [a], M. Chiara Giuffrida [a,c], M. Lluïsa Sagristá [a], Francesco Castelli [c], Montserrat Pujol [b], M. Asunción Alsina [b], Margarita Mora [a,*]

[a] Department of Biochemistry and Molecular Biology, Faculty of Biology, University of Barcelona, Av. Diagonal 643, 08028 Barcelona, Spain
[b] Department of Physical Chemistry, Faculty of Pharmacy, University of Barcelona, Av. Joan XXIII s/n, 08028 Barcelona, Spain
[c] Department of Drug Sciences, University of Catania, Viale A. Doria 6, 95125 Catania, Italy

ARTICLE INFO

Article history:
Received 8 September 2015
Received in revised form 20 November 2015
Accepted 3 December 2015
Available online 4 December 2015

Keywords:
Camptothecins
Biomembrane models
Langmuir monolayers
Bilayer systems
Liposomes
Membrane interactions

ABSTRACT

CPT-11 and SN-38 are camptothecins with strong antitumor activity. Nevertheless, their severe side effects and the chemical instability of their lactone ring have questioned the usual forms for its administration and have focused the current research on the development of new suitable pharmaceutical formulations. This work presents a biophysical study of the interfacial interactions of CPT-11 and SN-38 with membrane mimetic models by using monolayer techniques and Differential Scanning Calorimetry. The aim is to get new insights for the understanding of the bilayer mechanics after drug incorporation and to optimize the design of drug delivery systems based on the formation of stable bilayer structures. Moreover, from our knowledge, the molecular interactions between camptothecins and phospholipids have not been investigated in detail, despite their importance in the context of drug action. The results show that neither CPT-11 nor SN-38 disturbs the structure of the complex liposome bilayers, despite their different solubility, that CPT-11, positively charged in its piperidine group, interacts electrostatically with DOPS, making stable the incorporation of a high percentage of CPT-11 into liposomes and that SN-38 establishes weak repulsive interactions with lipid molecules that modify the compressibility of the bilayer without affecting significantly neither the lipid collapse pressure nor the miscibility pattern of drug–lipid mixed monolayers. The suitability of a binary and a ternary lipid mixture for encapsulating SN-38 and CPT-11, respectively, has been demonstrated.

1. Introduction

Irinotecan (camptothecin CPT-11; 7-ethyl-10-[4-(1-piperidino)-1-piperidino] carbonyloxycamptothecin) and SN-38; (irinotecan metabolite, ethyl-10-hydroxy-camptothecin) are antineoplastic agents belonging to the family of topoisomerase I inhibitors that arrest the synthesis of DNA and possess strong antitumor activity (Fig. 1) [1,2].

The sole catalytic mechanism for camptothecin action consists in the formation and stabilization of a reversible enzyme–drug–DNA ternary complex which prevents the ligation step of the nicking/sealing cycle performed by the topoisomerase enzyme. CPT-11 is converted to its metabolite SN-38, with a reported, at least, 100-fold biggest activity, by a human carboxylesterase (hCE), primarily in the liver [3], but also in tumors [4]. CPT-11 is a first-line drug approved for the treatment of a variety of human tumors, including colorectal, lung and gynecological cancers [5]. Both CPT-11 and SN-38 are currently in clinical trial in its liposomal form [6]. However, their severe side effects, such as myelosuppression and gastrointestinal disorders [7,8], impose some restrictions for camptothecin therapies and additional considerations to develop suitable pharmaceutical formulations for clinical purposes. Other drawbacks for their clinical applications are the chemical instability of the lactone ring, which opens to the inactive carboxylate form at physiological pH [9,10] and, in the case of SN-38, the great insolubility in almost all the solvents that could be used to formulate this drug. All of these considerations make evident the importance of protecting the drug from the external environment to maximize its pharmacological potential and the need of using solubilizers or membrane stabilizers [11]. Therefore, current investigations are focused on the development of new forms for camptothecin administration.

Abbreviations: CPT-11, irinotecan, 7-ethyl-10-[4-(1-piperidino)-1-piperidino] carbonyloxycamptothecin; SN-38, irinotecan metabolite, ethyl-10-hydroxy-camptothecin; DSC, Differential Scanning Calorimetry; P, partition coefficient; DSPC, L-α-Distearoyl-phospathidylcholine; DOPS, L-α-Dioleoyl-phospathidylserine; EPC, Egg Phosphathidylcholine; CHOL, Cholesterol; MLVs, Multilamellar liposomes.

* Corresponding author at: Department of Biochemistry and Molecular Biology, Faculty of Biology, University of Barcelona, Av. Diagonal 643, Prevosti Building, 1st floor, 08028 Barcelona, Spain.
E-mail addresses: ancasado@clinic.ub.es (A. Casadó), mcgiuffrida@gmail.com (M.C. Giuffrida), mlsagrista@ub.edu (M.L. Sagristá), fcastelli@unict.it (F. Castelli), mopujol@ub.edu (M. Pujol), aalsina@ub.edu (M.A. Alsina), margarita.mora@ub.edu (M. Mora).

http://dx.doi.org/10.1016/j.bbamem.2015.12.007
0005-2736/

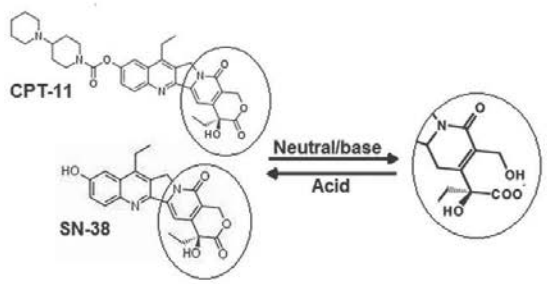

Fig. 1. Molecular structure of camptothecins. Equilibrium between their lactone and carboxylate forms.

The consideration of the pharmaceutical form of anticancer drugs and the procurement of stable formulations can overcome some of the main limitations for their use in clinical applications. Docetaxel, for example, is available in a formulation that contains a high concentration of Tween 80 [12] and Paclitaxel is often provided in Cremophor EL. Unfortunately, the use of both products has been associated with severe side effects related with hypersensitivity reactions [13], nephrotoxicity and neurotoxicity. In order to solve the problems derived from the use of such solubilizers or adjuvants, alternative dosage forms have been developed to improve its clinical administration. Among the potential drug delivery carriers, liposomes or lipid vesicles have endowed with interesting and useful characteristics that make them a pivotal biocompatible and biodegradable drug delivery and formulation platform [14].

Liposomes possess many interesting properties, such as the ability to entrap both hydrophilic and hydrophobic molecules without loss or alteration of their activity, which make them very suitable to create triggered release systems and to provide passive or active targeted strategies [15,16]. They may carry different surface charges, have different sizes and provide long systemic circulation times, depending on their lipid composition. Liposomes can act as sustained depots which release their cargo in a controlled form and in a specific target, giving a preferential accumulation in solid tumors [17]. Moreover, liposomal formulations can reduce the toxicity associated with free anticancer drugs in healthy tissues [18,19], which is severe in the case of CPT-11 and SN-38, and improve drug stability by protecting the compound from chemical degradation or transformation. Several lipid-based and liposomal nanomedicines have been approved in the last 20 years [20–22] and many others are undergoing clinical evaluation [23].

In the case of camptothecins, their encapsulation in liposomes would have the additional advantages of providing a suitable environment to maintain soluble the drug, either in the aqueous phase or in the lipid bilayer, and to afford protection for the lactone ring of the molecule, which is essential for its pharmacological activity, besides being an important structural requirement both for the passive diffusion of these drugs into cancer cells and for their successful interaction with the topoisomerase I enzyme [24,25]. Moreover, CTP-11 liposomalization increases its antitumor activity with an important reduction in the adverse reactions reported for this drug, being the use of carriers completely essential in the case of SN-38, because of its extreme insolubility, to make it a useful drug [26].

Liposomes can be engineered from a wide variety of lipid species, from natural or synthetic origin and can be endowed with special characteristics by adding to their formulation specific components. You can make liposomes sensitive to specific stimuli, stable as pharmaceutical products and in the biological media after administration and that can be vectorized to specific and targeted locations. To develop optimal drug formulations and efficient drug delivery systems it is essential to control the physicochemical parameters of the vehicle and, for this purpose, it is very useful to study how molecular interactions between the constituents of the carrier and the drugs can affect or modify its structure [27,28]. Moreover, the study of drug–lipid interactions can also be used to predict the pharmacokinetic properties of drugs, which are dependent on their chemical stability and, consequently, their bioavailability and efficacy.

When characterizing the interactions of drugs with membrane lipids, it is essential to consider the use of different techniques, each one with advantages or limitations regarding to their applications [29,30]. Among these, it could be outlined Differential Scanning Calorimetry (DSC) [31,32] and Langmuir monolayers [33,34].

DSC is a nonperturbative technique largely employed in pharmaceutical thermal analysis, because its ability to provide information about either the physical or energetic properties of substances. Moreover DSC is one of the more used methods to measure the enthalpy associated with physical processes [35]. As a thermoanalytical method, DSC has definite applications in nanosciences with important features for the development of nanostructured lipid carriers for drug delivery [36,37].

The Langmuir techniques, which use lipid monolayers at the air–water interface as the model for studying the two-dimensional arrangement, are very useful in the area of liposome formulation as they provide information on lipid packaging configuration and so, on liposome stability [34,38]. In addition, the knowledge of the partition coefficients (P) that can be determined in an n-octanol/aqueous medium [39] or by a reverse phase HPLC column [40], gives a good approach to predict the relative tendency of drugs to incorporate into biological membranes.

This work explores the physicochemical interactions of CPT-11 and SN-38 with pure and mixed lipid monolayers and bilayers and informs about the potential usefulness of the liposomal carriers designed for these drugs [41]. The long term stability is an essential parameter of the final formulation because it will control the sustained release of these camptothecins into the cell and because of the protection afforded to their cargos versus its biological degradation. The results will provide comprehensive insights about the possible effects of the molecular interactions of these drugs, on the liposomal formulation, either at the level of the hydrophobic domain of the lipid bilayer in which they can be inserted, or at the level of the polar region when encapsulated in their aqueous space, always in contact with the inner monolayer of the bilayer. It could also be emphasized that, from our knowledge, the molecular interactions between camptothecins and phospholipids have not been investigated in detail.

2. Experimental

2.1. Materials

L-α-Distearoyl-phospathidylcholine (DSPC), L-α-Dioleoyl-phospathidylserine (DOPS), Egg Phosphathidylcholine (EPC) and Cholesterol (CHOL) were purchased from Avanti Polar Lipids (Birmingham, AL, USA). CPT-11, purchased from Afine Chemicals Limited (Hangzhou, China), was pure with a minimal grade of 99%. SN-38 was from Tocris Bioscience (Bristol, United Kingdom). All the organic solvents (Panreac, Montcada i Reixac, Barcelona, Spain) have been distilled before use. Milli-Q water (Millipore Bedford, Massachusetts system, resistivity of 18 MΩ cm) was used. All other chemicals and solvents were of analytical grade.

2.2. Calorimetric studies

Differential scanning calorimetric (DSC) analysis was used to evaluate the thermodynamic aspects of the camptothecin/lipid interactions and was performed by using a Mettler DSC-30 device (Mettler-Toledo, Inc., Columbus, OH, USA) or a MicroCal VP-DSC (GE Healthcare LifeSciences, Uppsala, Sweden). The calorimetric systems were calibrated, in transition temperature and enthalpy changes, by

using indium and zinc or lysozyme (mol wt. 14.3 kDa) for the Mettler or MicroCal devices, respectively. Thermodynamic data were analyzed with Mettler-Toledo STARe or MicroCal-enabled Origin softwares.

2.2.1. Preparation of liposomes

Multilamellar liposomes (MLVs) were used for calorimetric studies and prepared as described previously [41]. DSPC, DOPS, CHOL and EPC were used, in ternary or binary combinations, to prepare lipid films. MLVs containing CPT-11 were prepared as follows: fifteen milligrams of the ternary lipid mixture (DSPC/DOPS/CHOL, 65:35:30) were dissolved in chloroform and mixed with the appropriate amounts of CPT-11 to produce exact molar fractions of the drug. Chloroform was evaporated under a nitrogen stream to get a thin lipid film, which was maintained overnight in a vacuum desiccator to remove all the traces of the solvent and the resulting film was hydrated with 1000 μL of 10 mM lactate buffer (pH 4.4). Finally, the MLV suspension was frozen (liquid N_2) and thawed (water bath above the phase transition temperature, T_m) five times. In the case of SN-38, MLVs were prepared by means of a different protocol: lipid (EPC/DOPS, 9:1, 50 mg)/drug mixtures, giving specific molar fractions of the drug, were hydrated with 1000 μL of 10 mM lactate buffer (pH 4.4), after weighting the appropriate amount of each component, with an Ultra-Turrax IKA T-25 (Staufen, Germany), at 20,000 rpm for 10 min.

Samples with transition temperatures below the freezing point of water (those containing EPC) had 50% ethyleneglycol included in the aqueous phase to prevent the freezing of the bulk solvent phase. It has been taken into account that ethyleneglycol can modify both Tm and ΔH [42,43].

2.2.2. DSC experiments

DSC-30 Mettler experiments for EPC/DOPS MLVs with SN-38 were carried out as follows. Aliquots of 120 μL of the different aqueous suspensions of MLVs were transferred to a 160 μL aluminum calorimetric pan, which was hermetically sealed. The samples were weighted and immediately submitted to DSC analysis, as follows: 1) a heating scan between −50 °C and 20 °C at 2 °C/min; 2) a cooling scan between 20 and −50 °C at 4 °C/min. This low heating scan rate was chosen in order to provide the higher peak resolution. Sharp peaks of a first order gel-to-liquid crystalline phase transition (L_α) in buffered aqueous solution require low scan rates, allowing also the resolution of the possible closely DSC peaks [44,45]. The reference pan contained 120 μL of a 1:1 ethyleneglycol/10 mM lactate buffer (pH 4.4) solution. The temperature of the maximum of the transition endotherm (T_m) and the enthalpy (ΔH_{cal}), calculated from the area under the peak, were determined with a Mettler TC15 TA controller. The cooperativity of the transition was evaluated, approximately, from the widths at half-peak heights (as °C) of the main transition endotherms ($\Delta T_{1/2}$). To carry out the experiments with the MicroCal device, 0.5181 mL of the DSPC/DOPS/CHOL MLV suspension, with and without CPT-11 at different molar fractions, was placed in the calorimetric cell and analyzed as follows: 1) a heating scan in the temperature range of 10–60 °C, at 0.5 °C/min; 2) a cooling scan from 60 to 10° at 1 °C/min. The reference cell contained 10 mM lactate buffer (pH 4.4). As a common procedure both the buffer and the samples were degassed for 10 min before being introduced into the MicroCal cell to avoid any signal artifacts due to air bubbles. In all the experiments, only the heating scans were analyzed. Each experiment was carried out in triplicate to check the result reproducibility. After the DSC analysis, aliquots of all samples were extracted from the calorimetric pan and used to determine the exact amount of lipids by the Stewart's method [46].

2.3. Partition coefficients in n-octanol/buffer solutions

The partition coefficients between n-octanol and buffer solutions (Po/w), at different pH values, were determined by a slight modification of the shake-flask method, earlier reported by Ross et al. [47] and described in the OECD guideline for the testing of chemicals [48]. Stock solutions in DMSO of CPT-11 and SN-38 10 mM were prepared and, prior to use, were diluted in n-octanol to a final concentration of 0.5 mM (1:20). The experiments were carried out as follows: 100 μL of the 0.5 mM camptothecin solutions was diluted with 4.9 mL of n-octanol and mixed with 5 mL of the appropriate buffer solution. The two phases were maintained under constant shaking for 1 h at 25 °C. The n-octanol phase was removed with a Pasteur pipette and both phases were analyzed spectrophotometrically for drug content. The partition coefficient (Po/w) was calculated as the ratio between the molar concentration in n-octanol (Co) and that in the aqueous phase (Cw). Calibration curves in n-octanol and in different buffer solutions were previously performed for both camptothecins at the experimental conditions previously determined (Table S1, Supplementary material).

2.4. Monolayer studies

The Langmuir technique measures the surface pressure as a function of the mean molecular area that occupies a molecule in a monolayer extended on an aqueous surface [49,50]. Experimental measurements were recorded with a Nima Langmuir balance equipped with a Wilhelmy platinum plate (Nima Technology, Coventry) and a Teflon trough that was rinsed with ethanol and distilled water before use. All experiments were performed at room temperature. The monolayer stability was verified by monitoring the change in surface pressure while the area was held constant.

2.4.1. Monolayer compression isotherms

The π–A isotherms were recorded with a Nima (U.K.) Langmuir Teflon trough of 595 cm^2 surface area and 297.5 cm^3 volume. Separate stock solutions of individual lipids or lipid mixtures (DSPC/DOPS/CHOL 65:35:30 or EPC/DOPS 9:1) were prepared in chloroform at 1 mg/mL. Required volumes of each of them were mixed with CPT-11 (1 mg/mL) or SN-38 (0.5 mg/mL) solutions to form the lipid–drug spreading solutions containing different drug molar fractions. Monolayers were formed by applying small drops of the spreading solutions on the 10 mM Lactate Buffer subphase (pH 4.4) with a microsyringe (Hamilton Co., Reno, NV, USA). After 15 min, monolayers of the desired composition were continuously compressed with an area reduction rate of 10 $cm^2\ min^{-1}$. The films were compressed to their collapse pressure. Each run was repeated three times and the reproducibility was ± 1 $Å^2\ molecule^{-1}$.

In order to study the effect of the adsorption of CPT-11 on the lipid isotherms and to establish a possible selective interaction with someone of the lipid components, another set of experiments was performed with monolayers made with the ternary mixture of lipids, DSPC/DOPS/CHOL 65:35:30 or with each one of the individual lipid constituents. CPT-11 was injected in the lactate buffer subphase at different molar concentrations, ranging from 5 to 30 μM. The procedure was the same described above.

2.4.2. Surface activity of CPT-11

The surface activity of CPT-11 was studied in order to determine the equilibrium spreading pressure. Using a cylindrical PTFE trough (surface area 19.6 cm^2, volume 27.2 cm^3), that was rinsed with ethanol and distilled water before use, increasing volumes of a 1 mg/mL (1.48 mM) CPT-11 solution in Milli-Q water (18 MΩ cm) were injected below the 10 mM lactate buffer subphase (pH 4.4) through a lateral hole and the adsorption of the drug in the air/water interface was monitored by following the increase in surface pressure as a function of time under continuous stirring of the subphase. All experiments were performed at room temperature.

2.4.3. Insertion of CPT-11 into monolayers

The kinetics of insertion of CPT-11 into monolayers of DSPC/DOPS/CHOL 65:35:30 were measured using the same trough as for the surface

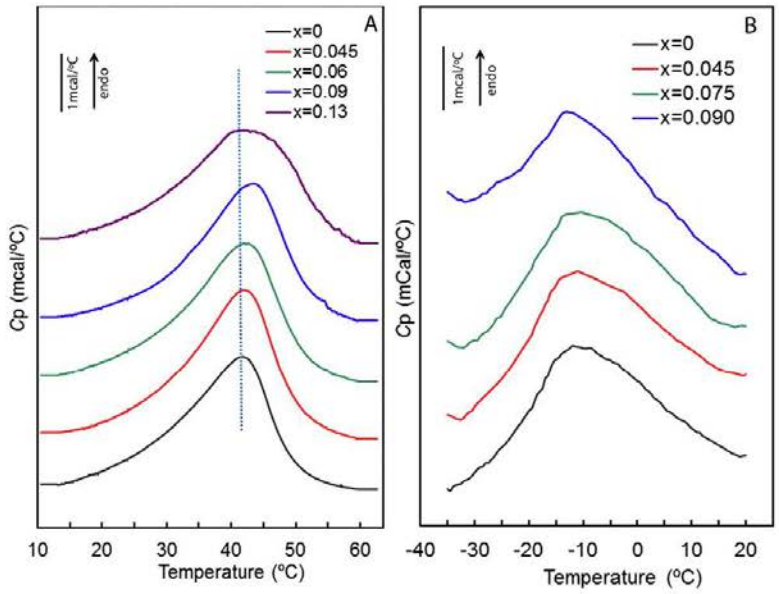

Fig. 2. Endothermic calorimetric curves in heating mode of DSPC/DOPS/CHOL-MLVs (A) and EPC/DOPS-MLVs (B) prepared in the absence and in the presence of increasing molar fractions of CPT-11(A) and SN-38 (B). x are the molar fractions of either CPT-11 (A) or SN-38 (B). Enthalpy values were calculated from the area under the peak by using Mettler STAR^e evaluation software. Dotted line in A shows the T_m shift.

activity, which was cleaned in the same way with ethanol and distilled water before use. For these experiments, a lipid stock solution was prepared and added drop wise on the subphase until the desired lipid pressure was achieved. After 10–20 min the equilibrium of the lipid monolayer was reached. Then, a 100 μL of the 1 mg/mL (1.48 mM) CPT-11 solution was injected into the subphase through the side hole of the trough. The subphase was magnetic stirred during the measurements and surface pressure changes were monitored as function of time until it remained constant.

2.4.4. Brewster angle microscopy

Brewster angle microscopy images were obtained in a KSV NIMA MicroBAM instrument (U.K.) mounted on a NIMA Langmuir balance trough. The instrument was equipped with a 30 mW laser emitting p-polarized light a 660 nm, which incises the air/water interface at 53.1° (Brewster angle). The shutter speed used was 1/50 s. All the images were taken at room temperature and under the same acquisition conditions for comparative purposes.

3. Results and discussion

3.1. Calorimetric analysis

Differential Scanning Calorimetry (DSC) was used as a first approach to determine the effect of the incorporation of CPT-11 and SN-38 on the physical state of the liposomal bilayers. Representative DSC thermograms obtained for DSPC/DOPS/CHOL/CPT-11 and EPC/DOPS/SN-38 multilamellar liposomes, acquired with the Mettler DSC-30 device, equipped with a subzero nitrogen-liquid system or with the MicroCal device, are shown in Fig. 2A and B, respectively. These lipid mixtures

Table 1
Thermodynamic parameters of mixed lipid bilayers containing CPT-11 or SN-38.

Sample	ΔHcal[2] (kJ/mol)	Tm[3] (°C)	Δ $T_{1/2}$[4] (°C)
DSPC/DOPS/Chol (x = 0)	11.24 ± 0.55	41.98 ± 1.98	13.28 ± 0.72
DSPC/DOPS/Chol/CPT-11 (x^1 = 0.045)	12.00 ± 0.58	42.19 ± 2.07	12.59 ± 0.61
DSPC/DOPS/Chol/CPT-11 (x = 0.060)	12.36 ± 0.61	42.58 ± 2.12	13.34 ± 0.69
DSPC/DOPS/Chol/CPT-11 (x = 0.090)	12.08 ± 0.57	43.81 ± 2.16	13.27 ± 0.59
DSPC/DOPS/Chol/CPT-11 (x = 0.130)	11.61 ± 0.56	43.76 ± 2.21	15.88 ± 0.81
EPC/DOPS (x = 0)	24.13 ± 1.18	− 11.89 ± 0.62	24.16 ± 1.31
EPC/DOPS/SN-38 (x = 0.045)	24.51 ± 1.19	− 10.91 ± 0.52	25.55 ± 1.17
EPC/DOPS/SN-38 (x = 0.075)	22.29 ± 1.11	− 10.40 ± 0.55	26.38 ± 1.35
EPC/DOPS/SN-38 (x = 0.090)	20.99 ± 1.03	− 11.84 ± 0.59	24.44 ± 1.22

Values reported are the mean ± SD of three independent experiments.
[1] x is the molar fraction of CPT-11 or SN-38.
[2] Calorimetric enthalpy calculated from the area under the peak.
[3] Temperature calculated from the maximum of the calorimetric peak.
[4] $\Delta T_{1/2}$ is the width of the calorimetric peak at the half height.

are those chosen, after an accurate selection in our laboratory, for achieving drug formulations [41]. The aim is to study how the molecular interactions between camptothecins and lipids can affect the stability of the liposomal formulations.

The endothermic transition profiles, obtained for the lipid dispersions, in the absence and in the presence of the CPT-11 and SN-38, at the indicated mole fractions of the drugs, showed, in all cases, a broad single endotherm, indicating that the incorporation of both camptothecins into MLVs does not significantly modify the organization of their respective bilayers. However, it could be noted that CPT-11 causes a slight shifting of the transition peak toward a higher temperature (as indicated by considering the dotted line in the Fig. 2A), with respect to the pure lipid mixture and a small broadening of the phase transition: these changes were clear at the highest molar fractions of the drug.

The case of SN-38 was rather different. It appears that SN-38 leaves the transition temperature of EPC/DOPS MLVs almost unchanged, being maintained the asymmetric shape of the peak corresponding to the phase transition observed in the absence of the drug. It should also be remarked that the broadness of the calorimetric peaks is that expected from the complex lipid and fatty acid composition of the bilayers analyzed. The thermodynamic parameters inferred from these thermograms are given in Table 1.

In addition to the aforementioned changes, it could stand out that SN-38 induces a gradual slight reduction of EPC/DOPS ΔH values. Despite the reported information about the changes induced, in both Tm and ΔH_{cal} values, by the presence of ethyleneglycol in the calorimetric pans [42,51], the calorimetric data for the SN-38 containing samples may be compared correctly since all of them include the same percentage of cryoprotectant. From the results of the calorimetric study, it could be underlined that neither the incorporation of CPT-11 nor that of SN-38 disturbs the structure of the complex composited liposome bilayers, despite the special and different solubility properties of these camptothecins.

3.2. Octanol–buffer partition coefficients

The hydrophilic–hydrophobic balance of any drug is generally measured by checking its distribution in a biphasic organic/aqueous system and can be quantitatively expressed as a partition coefficient. CPT-11 and SN-38 Po/w values were determined with an n-octanol/water system, at different pH buffered media (Table 2).

The results show the differences that exist between both camptothecins. At the conditions corresponding to the preparation of the pharmaceutical formulations of both CPT-11 [41] and SN-38 (acidic pH), CPT-11 is mainly in the aqueous media, although moves to the organic phase in neutral an alkaline environments, whereas SN-38 is already in the organic phase in a percentage of almost 93%. The structural characteristics of CPT-11 and SN-38 (Fig. 1) would account for the thermodynamic tendency to partition into the aqueous or organic phases of these drugs: the additional site for protonation of CPT-11 (piperidine group, pKa = 11.20) could influence its solubility in aqueous media [52] and its lactone form possesses more positive charge than the carboxylate form, fact that could be related with the different distribution of this molecule between n-octanol and water phases in function of pH.

Table 2
The octanol/aqueous solution experimental partition coefficients for CPT-11 and SN-38.

	$[Drug]_{oct}$ (μM)	$\%Drug_{oct}$	Po/w	logPo/w
CPT-11				
pH 4.4	1.88	17.15	0.207	−0.684
pH 7.4	10.13	92.43	12.20	1.087
pH 9.0	10.35	94.43	16.97	1.230
SN-38				
pH 4.4	9.23	92.86	13.00	1.11
pH 7.4	9.46	95.25	19.71	1.29
pH 9.0	9.57	96.30	25.86	1.41

The results are the mean values of three individual experiments. The variation coefficients (CV) range from 5.2 to 7.5%.

3.3. Surface studies of CPT-11 and SN-38 camptothecins

Langmuir monolayers of lipids or drugs and of mixed lipids and drugs of different molar compositions have been studied in terms of surface activity and compression isotherms. DSPC/DOPS/CHOL and EPC/DOPS were the lipid mixtures used to form the Langmuir monolayers, as indicated above.

3.3.1. Surface activity

Surface activity of CPT-11 was determined by injecting increasing volumes of a concentrated solution of the drug (1.48 mM) into the lactate buffer subphase of DSPC/DOPS/CHOL (65:35:30) monolayers and recording the surface pressures achieved, for each CPT-11 concentration, as a function of the time until saturation. The surface excess concentration (Γ), expressed in $mol \cdot cm^{-2}$, was calculated by applying the Gibbs equation (Eq. (1), Supplementary material) to the curves.

The value of the surface excess concentration, $\Gamma = 2.08 \times 10^{-10}$ $mol \cdot cm^{-2}$, allows us to calculate the area occupied per CPT-11 molecule at the saturated interface, A. The value obtained, 79.8 $Å^2$ $molecule^{-1}$ (Eq. (2), Supplementary material), correlates well with that expected from the structure and molecular weight (586.68 g/mol) of CPT-11, on the basis of some referenced data for other drugs such as docetaxel (MW = 807.88 g/mol) [12].

The attempts to analyze the surface activity of SN-38 failed because of the inability of this drug to form stable monolayers at the interface.

3.3.2. π–A compression isotherms

Representative compression isotherms of DPPC/DOPS/CHOL/CPT-11 and EPC/DOPS/SN-38, at several drug molar ratios, between zero (only lipids) and one (only drug) are illustrated in Fig. S1A and B (Supplementary material), respectively.

As can be seen, DPPC/DOPS/CHOL and EPC/DOPS form stable Langmuir monolayers at the air–water interface, CPT-11 forms a monolayer with low values of π (~12 mN/m) (Fig. S1A, Supplementary material, red line) and SN-38 does not forms monolayer at the conditions of the assay (Fig. S1B, Supplementary material, dark blue line), similarly to that observed for some resveratrol compounds [53] or for different coumarins [54]. In our case, however, the result should be explained on the basis of the high insolubility of SN-38 that prevents its spreading on the aqueous phase. Both DPPC/DOPS/CHOL and EPC/DOPS lipid mixtures form stable monolayers with CPT-11 and SN-38, respectively, at all the ratios studied (Fig. S1A and B, Supplementary material), being the π–A isotherms of the binary monolayers located between those of the pure components. Moreover, increases of the mole percentages of either CPT-11 or SN-38 caused the shift of the isotherms toward smaller areas per molecule.

The values for the collapse pressures of DPPC/DOPS/CHOL and EPC/DOPS monolayers were of about 46.4 and 45.6 mN/m, respectively, whereas the highest surface pressure that pure CPT-11 monolayer can reach on compression was <12 mN/m, probably because of the rigid carbon rings in their structure [55]. On the other hand, mixed DPPC/DOPS/CHOL/CPT-11 monolayers (Fig. S1A, Supplementary material) have collapse pressures similar to that of the lipid mixture for $x_{CPT\text{-}11} \leq 0.5$, slightly decreases when CPT-11 molar fraction was 0.6 (44.9 mN/m) and undergo a dramatic change when the mixed monolayer contained a 0.75 molar fraction of CPT-11; that is, the isotherm stopped at a surface pressure of 22.5 mN/m. Zhao et al. [27], by studying the behavior of DPPC/Paclitaxel mixed monolayers, observed similar results and suggested that they could be interpreted in terms of a squeezing out of paclitaxel from the lipid monolayer during compression. This explanation could also be applied to our results.

When mixed EPC/DOPS/SN-38 isotherms were analyzed (Fig. S1B, Supplementary material), similar considerations can be made. Besides the shifting of the area per molecule toward smaller values, probably because of the smaller area occupied by the SN-38 molecule in relation with that of the molecules of EPC and DOPS, SN-38 causes a slight decrease of the collapse pressure of the lipid mixture from 45.6 mN/m to the value corresponding to the 0.6 molar fraction of SN-38 (43.1 mN/m) and undergo a higher decrease when the molar fraction of the drug was 0.75 (36.4 mN/m). A similar behavior was observed by Jurak and Miñones [56] when studying the binary systems α-tocoferol/POPC and α-tocoferol/DOPC. The curves in Fig. S1 (A and B, Supplementary material), also give the mean molecular area values at the collapse for both lipid monolayers containing CPT-11 or SN-38, respectively.

The existence of a single collapse point in each of the individual drawn isotherms for the lipids/drug mixtures studied could be indicative of the miscibility of camptothecins and the corresponding lipid mixtures in the lipid/drug binary systems. However, if the components of the mixture were miscible, the collapse pressures of the binary mixtures would be, in some extent, dependent on the drug content of the lipid monolayers. Because of this, to discern between miscibility and immiscibility of lipids and drugs and to explore the existence of some kind of interactions between the components of the mixed monolayers in function of the film composition, the applicability of the additivity relationship for the binary systems was further examined and the results were analyzed together.

3.3.3. Isothermal compressibility of mixed monolayers

The isothermal data were also analyzed in terms of isothermal compressibility (C_s), giving additional information about the elasticity and compressibility of the bilayer (Eq. (3), Supplementary material) [57,58]. Its reciprocal, C_s^{-1}, the elastic modulus of area compressibility, is related to the packing degree and can be used to characterize the phase state of the monolayer [59], i.e. a larger C_s^{-1} value indicates a less compressible membrane and a higher degree of viscosity. For liquid expanded films it ranges from 12.5 to 50 mN m^{-1}, while for the liquid condensed phase it ranges from 100 to 250 mN m^{-1} [60].

Both C_s and C_s^{-1} can be calculated directly for DSPC/DOPS/CHOL/CPT-11 and EPC/DOPS/SN-38 mixed monolayers from the slope of their corresponding π–A isotherms. Our results show that the DOPC/DOPS/CHOL monolayer (Fig. 3A) has a value of the compressibility modulus around 83 mN/m at 30 mN/m, which is intermediate between those corresponding to the liquid expanded state and the liquid condensed phase.

The incorporation of CPT-11 increased significantly C_s^{-1}, changing the monolayer to the liquid condensed phase, with Cs^{-1} values higher than 100 mN/m for CPT-11 mole fractions from 0.045 to 0.13. Higher drug concentrations (mole fractions 0.5–0.75) returned the monolayer to the liquid expanded phase, with C_s^{-1} values significantly lower than those corresponding to the pure lipid monolayer. The highest C_s^{-1} values occur at surface pressures ranging between 25 and 40 mN/m, interval at which the compressibility curves display two peaks, the second of which fits with a well-defined shoulder in the lipid compressibility curve.

The plot of C_s^{-1} vs surface pressure for the EPC/DOPS monolayer is given in Fig. 3B. The EPC/DOPS monolayer is in the liquid condensed state (C_s^{-1} value slightly higher than 110 mN/m), with a maximum at a monolayer surface pressure of 30 mN/m. The incorporation of SN-38 into phospholipid monolayers causes a decrease of the C_s^{-1} at all the drug concentrations assayed, and changes gradually the monolayer state toward the liquid expanded phase, making it more compressible. Moreover, the surface pressure at which C_s^{-1} reaches the maximum value decreases down to 20 mN/m as the SN-38 mole ratio increases.

When analyzing together the effect of both camptothecins, the results obtained could be interpreted in terms of changes in the packing of the acyl chains of lipids induced by either CPT-11 or SN-38. The different location of CPT-11 and SN-38 within the liposome structure would account for the different effect of these drugs on the monolayer state.

3.4. Interaction of camptothecins with model lipid membranes

3.4.1. Miscibility analysis of mixed drug–lipid monolayers

The nature of the molecular interactions and also the miscibility of the components of the mixed monolayers, drug and lipids, can be examined by studying the deviations of the area per molecule in the mixed films with respect to the ideality in the context of the additivity rule, which relates the measured molecular area of the mixed drug–lipid film to the areas and mole fractions of the individual film components.

The plots of the average area per molecule of mixed drug–lipid films (DSPC/DOPS/CHOL/CPT-11 and EPC/DOPS/SN-38) versus the molar fraction of the drug, either CPT-11 or SN-38, at different surface pressures, can give information about the nature of the molecular interactions and, also, about the miscibility of the components in the film. A lineal dependence would indicate either ideal mixing of non-interacting molecules or complete immiscibility of two components [61], whereas, according to Costin and Barnes [62], a mixed monolayer would show non-ideal behavior, caused by significant molecular interactions, when its properties do not depend linearly on the monolayer composition. Thus, many authors have examined the area per molecule for a mixed monolayer as a function of its composition, at various surface pressures [63]. The mean molecular area of a monolayer with two components, in the case of an ideal mixture, can be calculated according to Eq. (4) of Supplementary material [64].

The experimental results are given in Fig. 4. The straight broken lines represent the ideal mixing behavior and the solid lines correspond to

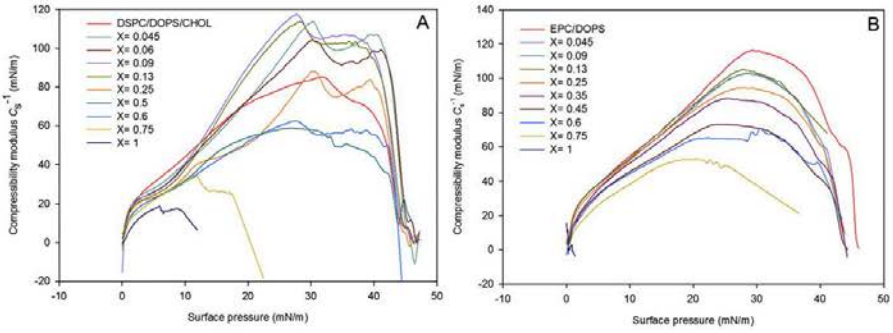

Fig. 3. The compression modulus (C_s^{-1}) of pure DSPC/DOPS/CHOL and mixed DSPC/DOPS/CHOL/CPT-11 (A) and pure EPC/DOPS and mixed EPC/DOPS/SN-38 (B) monolayers as a function of the surface pressure (π). x are the molar fractions of either CPT-11 (A) or SN-38 (B).

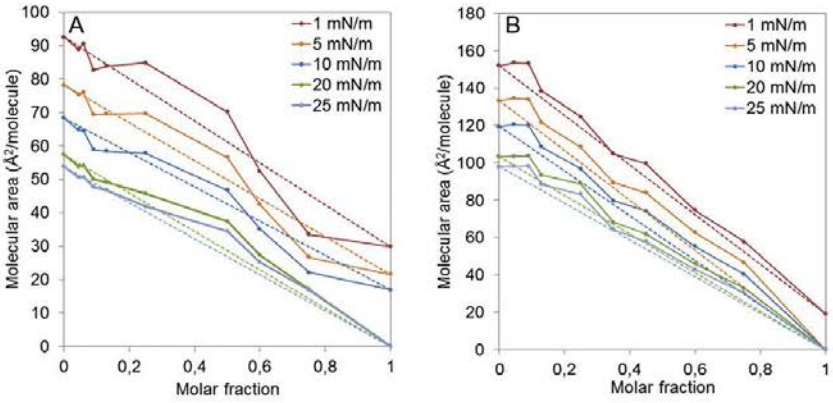

Fig. 4. Mean molecular areas for pure lipid and mixed lipid/drug monolayers as a function of camptothecin molar fractions at 25 °C and the indicated surface pressures. (A) Pure DSPC/DOPS/CHOL and mixed DSPC/DOPS/CHOL/CPT-11. (B) Pure EPC/DOPS and mixed EPC/DOPS/SN-38. The broken lines represent the ideal behavior and the solid lines correspond to the experimental values.

the experimental values and any deviation, positive or negative, from the ideal line would indicate some degree of molecular interactions between the drugs and lipids. In particular, positive deviations suggest that repulsive interactions occur with a perturbation of the regular packing of lipid molecules.

This would be the case of the effect of SN-38 on the monolayer of EPC/DOPS: the repulsive interactions between the drug and lipids would explain the decrease in the order degree of the acyl chains of lipids in a monolayer which becomes more compressible (compressibility analysis). On the contrary, negative deviations are indicative of the existence of increased attractive interactions between the two components in the mixed monolayers [65].

In the case of DSPC/DOPS/CHOL and CPT-11 mixtures, the data in Fig. 4A show the existence of positive and negative deviations from the ideality as a function of the drug molar fraction. It can be observed that the maximum positive deviation occurs at a mole fraction of CPT-11 of 0.5, that the maximum negative deviation is at 0.75, that the increases in the surface pressure up to 20 mN/m leads to lower deviations from the ideal line and that there are only positive deviations when surface pressures were ≥20 mN/m. These facts, together with the consideration of the collapse surface pressures, which do not change for mixtures with CPT-11 < 0.6, could be indicative of the immiscibility between the drug (CPT-11) and the lipid film components (DSPC/DOPS/CHOL) below this mole fraction, whereas for CTP-11 molar fractions higher than 0.6, the film formed would be stable. Moreover, in this range, the collapse pressures exhibit an intermediate value between those corresponding to the pure components individually. As indicated before, when surface pressure is higher than 20 mN/m, the system shifts to a more ideal behavior, being the positive deviations significantly decreased. This result could suggest that the high compression squeezes the CPT-11 molecules out of the lipid monolayer, with its consequent dissolution in the subphase, in agreement with the observations arising from the π–A compression isotherm experiments, and the loss of interaction with lipid molecules. If we also consider the values of the compressibility modulus (Fig. 3A) it would appear that the drug reaches its collapse pressure before and that the compression of lipids continues until their collapse. Thus, for the highest mole fraction of CPT-11 ($x_{CPT\text{-}11} = 0.75$, Fig. 3A) it can be observed a second inflection point at, approximately, 20 mN/m. The compressibility modulus values allow us to understand the miscibility behavior at low CPT-11 mole fractions ($x_{CPT\text{-}11} < 0.13$). In the range $0.045 < x_{CPT\text{-}11} < 0.13$ the system is ideal, with a very small negative deviation at 0.09–0.13 mole fractions, being Cs^{-1} values higher than those of the DSPC/DOPS/CHOL monolayer in this range. Probably CPT-11 and DSPC/DOPS/CHOL mixtures have a mixed miscibility pattern. They both mix well for $x_{CPT\text{-}11} \leq 0.13$ and $x_{CPT\text{-}11} \geq 0.6$, whereas become immiscible at any other mole fractions.

When EPC/DOPS and SN-38 mixtures are analyzed, it can be seen a greater alignment of the dashed lines and the solid lines and that the observed slight deviations are positive (Fig. 4B). This result suggests a mixed behavior close to the additivity rule predictions, unlike that observed for the CPT-11-containing system, indicating either ideal mixing or complete immiscibility of the mixture components. To distinguish between them it would be necessary to consider the isotherms at the collapse pressure. When analyzing together the collapse pressures and the compressibility moduli it can be observed that, despite its high hydrophobicity, the presence of SN-38 in the EPS/DOPS monolayer does not modify neither the shape of the isotherm nor its collapse pressure and, only at the highest mole fraction ($x = 0.75$), a slight change is produced. The fact that the collapse pressure of the lipid mixture does not change when adding SN-38 might be explained by considering that the molecules of SN-38, because of its apolar character, interact with the hydrophobic chains of lipids, the polar groups of which are in turn interacting with the subphase, and to the fact that it cannot be obtained a monolayer of SN-38. The high hydrophobicity of this drug prevents the spreading of the small drops within the air/water interface, avoiding the formation of the monolayer.

3.4.2. Stability of mixed monolayers

The interaction, either repulsive or attractive, between the two components of a mixed monolayer involves the generation of energy. This energy, known as excess Gibbs energy, G^E, represents the energy associated to the mixing process of the two pure components in the bidimensional phase and can be determined by means of Eq. (5) of Supplementary material [66,67]. The selected pressures (π) were 1, 2, 5 and 10 mN m^{-1}, which are values below the collapse of CPT-11.

The relevance of this study relies on the possibility of performing an analysis of the structural integrity of a system, which can incorporate certain drugs, through the quantitative assessment of the thermodynamic parameter G^E. If the system consists of lipids, and the drug is incorporated into a lipid monolayer, the assembly may be miscible and form a uniform mixed film or, conversely, be immiscible. This last situation would lead to the formation of a structure in which the drug and the lipids would be mixed heterogeneously, probably due to a selective interaction between the drug and some of the lipid constituents of the lipid monolayer [56]. These two situations will translate into different variations of G^E values: in the first case the excess Gibbs energy

should be negative, whereas, when immiscibility occurs, this parameter would have positive values [68].

The data in Fig. 5A show a complex behavior for DSPC/DOPS/CHOL/CPT-11 mixed monolayers, unlike a simple miscibility or immiscibility [69], although the energy values are in agreement with the partial miscibility deducted before from the analysis of Fig. 4A.

The minimal values observed below 0.13 and at 0.75 mole fractions of CPT-11 would account for the great thermodynamic stability of this drug and lipid combination. Additionally, the comparison of the absolute values of the excess Gibbs energy with RT (≈ 2500 J/mol), being R the ideal gas constant and T the experimental temperature, allows analyzing the relevance of such interactions, being significant for G^E values greater than 2500 J/mol [68,70]. A similar evaluation for SN-38-EPC/DOPS mixed monolayers (Fig. 5B), yielded absolute excess energy values very much lower than 2500 J/mol as it was expected according with the miscibility results.

3.5. Interaction studies with CPT-11 in the subphase

The dissolution of a drug in a subphase on which monolayers of lipids have been spread can help to determine the influence of these solutes on the compression isotherms of the lipids and give additional information about the drug–lipid affinity. In our study only the interaction between CPT-11 and lipids has been assessed by means this kind of experiment. The great insolubility of SN-38 has made impossible to introduce this drug in the subphase.

3.5.1. Penetration kinetics of CPT-11 at constant area

The ability of CPT-11 to penetrate into the DSPC/DOPS/CHOL monolayer at the air–water interface was investigated using a fixed 5.44 μM drug concentration in the lactate buffered subphase. The CPT-11 subphase concentration controls the penetration and can be previously determined from the adsorption isotherm profile for the drug. This value is a constant (K) that represents the drug concentration that achieves 1/2 π_{max}. In our case, the determination of the drug concentration to reach the equilibrium pressure and so, to determine the value of K, was not conclusive, probably because of the low surface activity of CPT-11 that hinders to monitor correctly the surface pressure changes with time. Because of this, we have chosen a CPT-11 concentration allowing the correct measurement of the changes in surface pressure in the penetration experiments.

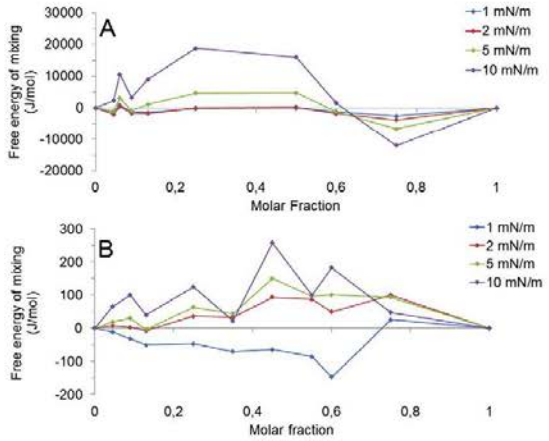

Fig. 5. The excess Gibbs energy (G^E) of DSPC/DOPS/CHOL/CPT-11 (A) and EPC/DOPS/SN-38 (B) mixed monolayers as a function of the monolayer composition, at different surface pressures.

The interaction between CPT-11 and mixed DSCP/DOPS/CHOL monolayers was recorded in terms of the increase of surface pressure for 30 min. It could be observed that CPT-11 insertion promoted an immediate increase in the surface pressure of the system, being remarkable the fact that the surface pressures attained the equilibrium values in no more than 10 min. A similar behavior has been reported for docetaxel insertion in DPPC monolayers [12]. The penetration curves obtained at various initial pressures are shown in Fig. 6.

As shown, these curves tend to an asymptote indicating the end of the penetration process. The graphical plot of the pressure increments vs the initial pressure, at a given drug concentration in the subphase (Fig. 6, upper image), is a straight line which intersection with the horizontal axis gives the critical pressure, above which there will be no penetration of CPT-11 into the lipid monolayer. This value was of ≈23–24 mN/m.

3.5.2. Compression isotherms with CPT-11 in the subphase

Compression isotherms of all the individual lipid components and, also, of the lipid mixture, were done in the absence and in the presence of CPT-11 in the subphase. This set of experiments was carried out in an attempt to go deeply into the potential selectivity of the interactions between the drug and each one of the constituents of the liposome bilayer. The results are plotted in Figs. 7 and S2 (Supplementary material).

When the phospholipid was DSPC, the isotherms recorded in the presence of CPT-11 were identical to that of the lipid alone at surface pressures higher than 25 mN/m, irrespective of the drug concentration, whereas at the lowest values of π (<20 mN/m), if any, a very tiny condensing effect could be observed (Fig. S2A, Supplementary material). In this case, it could be considered that CPT-11 does not modify the

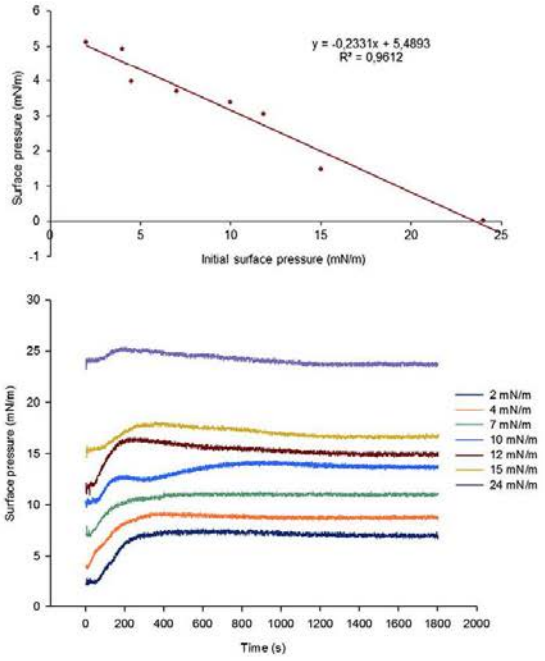

Fig. 6. Pressure increases promoted by CPT-11 when injected under DSPC/DOPS/CHOL monolayers spread at different initial pressures (lower image). The upper image is the linear plot of the increment in surface pressure after CPT-11 injection in the subphase as a function of the initial DSPC/DOPS/CHOL surface pressure and gives the critical surface pressure for CPT-11 penetration into the DSPC/DOPS/CHOL monolayer at the air–water interface.

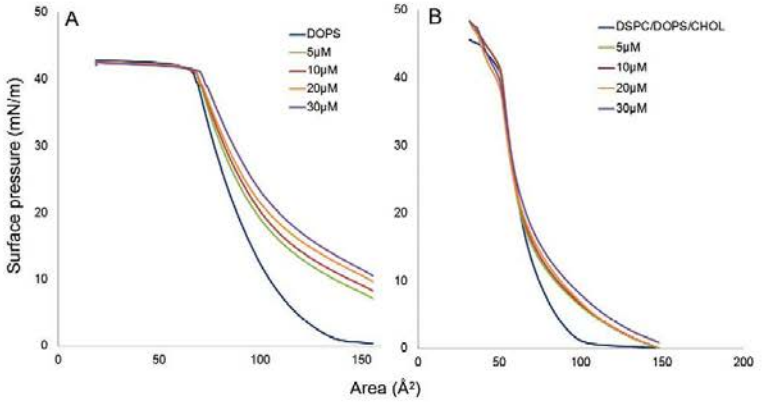

Fig. 7. Compression isotherms of (A) DOPS and (B) DSPC/DOPS/CHOL spread on a lactate buffered subphase alone or with increasing concentrations of CPT-11.

order of the lipid molecules nor establishes any specific interaction with DSPC. This fact was also observed in the case of CHOL (Fig. S2B, Supplementary material). Nevertheless, when the anionic phospholipid DOPS was considered (Fig. 7A), a completely different result was observed. DOPS isotherm was modified when CPT-11 was incorporated in the monolayer subphase, at all the concentrations assayed, and the changes were in the sense of producing an expanding effect within all the range of the surface pressures recorded, although more significant at low surface pressures: the result indicates the incorporation of the drug into the phospholipid monolayer. The interaction CPT-11-DOPS was confirmed by analyzing the effect of the incorporation of the drug in the subphase of a DSPC/DOPS/CHOL monolayer. The expanding effect of the drug was also manifest (Fig. 7B), but only at surface pressures lower than 20 mN/m, being the extent of the effect smaller than the measured in DOPS monolayers in accordance with the fact that the DSPC/DOPS/CHOL mixture only contains a 35% DOPS molar ratio. These results show that CPT-11 interacts specifically with the DOPS constituent of the lipid mixture.

The positive charge of CPT-11 at pH 4.4 and the negative charge of DOPS would account for the observed changes in the compression isotherms, on the basis of an electrostatic interaction. Taking into account the asymmetric distribution of the different lipids between the two leaflets of the bilayers [71] and the fact that the anionic PS is preferentially located in the inner monolayer [72], this result would explain the high percentage of CPT-11 encapsulated into liposomes. The drug encapsulated in their aqueous space, in contact with the inner monolayer, where PS is, will remain electrostatically anchored solving, somehow, the problems associated with the formulation and procurement of carriers for drug soluble molecules.

3.6. BAM images of the mixed CPT-11/lipid films

To get additional information about the influence of CPT-11 on the morphology of the investigated ternary mixed lipid monolayers, a series of BAM images, recorded at different stages of film compression, were analyzed [12,73]. Fig. 8 shows the images obtained at different surface pressures.

In the case of the DSPC/DOPS/CHOL film, the compression of the monolayer induces, according to its π–A isotherm, the formation of a LE phase which reflects in an uniform texture of images until 30 mN/m, when the monolayer becomes less compressible and a bright condensed phase that coexists at 40 mN/m near its collapse pressure. BAM images for CTP-11 demonstrate the ability of the drug to aggregate at the air/water interface at low pressures ($\pi = 3,7$ mN/m).

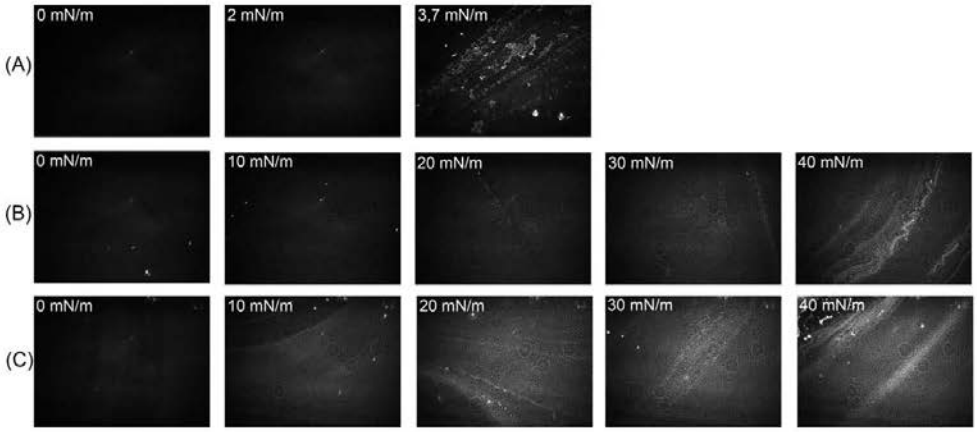

Fig. 8. BAM images of CPT-11 (A), DSPC/DOPS/CHOL (B) and mixed DSPC/DOPS/CHOL/CPT-11 (0.13 drug mole fraction) (C) Langmuir monolayers at the indicated surface pressures and composition. All the images were acquired at the same magnification for comparative purposes.

In the case of the mixtures of DSPC/DOPS/CHOL and CPT-11 (0.13 CPT-11 mole fraction), it can be observed the separation of two phases and the visualization of small nucleation points at a surface pressure of 10 mN/m (Fig. 8C) probably because of the drug, in agreement with the fact that the highest surface pressure that pure CPT-11 monolayer can reach on compression is <12 mN/m. Moreover, bright condensed phases when increasing the compression within the range of 20–40 mN/m (Fig. 8C) were observed, accordingly to the collapse region of the lipid/drug mixture. These phases appear much more marked than for DSPC/DOPS/CHOL monolayers, fact which could indicate that the molecules forming the film are packed more densely when the mole fraction of CPT-11 is 0.13. This result is the expected from the values of the excess area per molecule given in Fig. 4A. Bearing in mind that the properties of the lipid monolayers correlate with the properties of lipid bilayers at higher surface pressures (25 mN m^{-1}–35 mN m^{-1}) [74] it is worth stressing that, for this composition and at these pressures, the little condensation of the area per molecule and the squeezing out of CPT-11 from the lipid monolayer during compression correlate with the incorporation of CPT-11 into liposomes through the above mentioned electrostatic interactions between the drug and the anionic component of the bilayer.

4. Conclusions

The overall results have shown the ability of CPT-11 and SN-38 to interact with and/or to insert among phospholipid molecules in membrane mimetic models: CPT-11 is able to bind effectively to lipid bilayers through electrostatic interactions, whereas SN-38, because of its high lipophilicity, is inserted within the hydrophobic core of the bilayer.

The calorimetric study highlights that neither the incorporation of CPT-11 nor that of SN-38 disturbs the structure of the complex composited liposome bilayers, despite their different solubility properties and their different location within the two possible environments of the liposome structure.

CPT-11 shows surface activity and penetrates the DSPC/DOPS/CHOL monolayer whereas SN-38 does not. The high partition coefficient of SN-38, according with its great hydrophobicity, would explain that SN-38 neither adsorb at the air–water interface, nor form compressible monolayers. Similar results have been reported for some resveratrol and coumarin compounds [53,54].

CPT-11 and SN-38 cause a large contraction effect of the DSPC/DOPS/CHOL and EPC/DOPS Langmuir monolayers, respectively, as can be deduced from the values of the mean molecular area. This result could be explained by a high affinity of both camptothecins for monolayer lipids and would account for increased monolayer stability. On the other hand, the miscibility studies have shown that CPT-11 and DSPC/DOPS/CHOL mixtures mix well in a relatively narrow range of concentrations and that the EPC/DOPS/SN-38 combination exhibit a mixed behavior close to the additivity rule predictions.

The shape of the compression isotherms with CPT-11 in the subphase shows that the interaction between DSPC/DOPS/CHOL and CPT-11, with positive charge at pH 4.4, takes place mainly through the negative charge of DOPS and the miscibility pattern indicates that these interactions are possible at $x_{CPT\text{-}11} \leq 0.13$ and $x_{CPT\text{-}11} \geq 0.6$. This range, thermodynamically favored because their high excess Gibbs free energy values, includes the mole fractions used for the CPT-11 liposomal formulation ($x_{CPT\text{-}11} < 0.13$). Moreover, the existence of such electrostatic interactions would account for the high percentage of CPT-11 encapsulated into liposomes [41] in spite of its water-soluble character and its low n-octanol-water partition coefficient at pH 4.4. There are references in the literature in which CPT-11 is also efficiently encapsulated in liposomes, although neither the method nor the liposome lipid composition is the same [75].

Instead, SN-38 establishes repulsive interactions with the lipid molecules that, although weak, modify the compressibility of the bilayer without affecting significantly neither the collapse pressure of the lipid mixture nor the miscibility pattern of drug–lipid mixed monolayers with an ideal behavior. The decrease of the compressibility modulus and the consequent formation of a more fluid monolayer in the presence of SN-38 suggest the interaction between the drug and the binary EPC/DOPS system; the fact that SN-38 does not induce significant changes in the melting temperature of the EPC/DOPS bilayers, could suggest its localization in the outer hydrophobic zone of the bilayer, as it does paclitaxel when incorporated into DPPC bilayers [27].

Our results provide interesting remarks about the suitability of liposomes as devices for the delivery of camptothecins on the basis of stability criteria, highlight the usefulness of the ternary lipid composition for the delivery of CPT-11, reported previously [41] and supports the choice of the binary EPC/DOPS phospholipid mixture to get a stable formulation for SN-38. The preparation, characterization and evaluation of the efficacy in vitro of a liposomal formulation for SN-38 have already been carried out in our laboratory and the results will be published soon. The characterization of the interactions that occur between drugs and lipids is important when designing liposomal nanocarriers for the delivery of soluble molecules [76].

Transparency document

The Transparency document associated with this article can be found, in online version.

Acknowledgement

This study was funded by the Ministerio de Economía y Competitividad (CTQ2013-48767-C3-3-R) Spain and by the Department d'Universitats, Recerca i Societat de l'Informació (DURSI), Govern de la Generalitat de Cataluña (2009SGR-367). A. Casadó thanks to the University of Barcelona for a predoctoral fellowship.

Appendix A. Supplementary data

Supplementary data to this article can be found online at http://dx.doi.org/10.1016/j.bbamem.2015.12.007.

References

[1] C.J. Gerrits, M.J. De Jonge, J.H. Schellens, G. Stoter, J. Verweij, Topoisomerase I inhibitors: the relevance of prolonged exposure for present clinical development, Br. J. Cancer 76 (1997) 952–962.
[2] Y. Pommier, DNA topoisomerase I inhibitors: chemistry, biology and interfacial inhibition, Chem Rev. 109 (2009) 2894–2902, http://dx.doi.org/10.1021/cr900097c.
[3] M.H. Wu, B. Yan, R. Humerickhouse, M.E. Dolan, Irinotecan activation by human carboxylesterases in colorectal adenocarcinoma cells, Clin. Cancer Res. 8 (2002) 2696–2700.
[4] P. Tobin, S. Clarke, J.P. Seale, S. Lee, M. Solomon, S. Aulds, M. Crawford, J. Gallagher, T. Eyers, L. Rivory, The in vitro metabolism of irinotecan (CPT-11) by carboxylesterase and β-glucuronidase in human colorectal tumours, Br. J. Clin. Pharmacol. 62 (2006) 122–129, http://dx.doi.org/10.1111/j.1365-2125.2005.02477.x.
[5] S.T. Liew, L.Y. Yang, Design, synthesis and development of novel camptothecin drugs, Curr. Pharm. Des. 14 (2008) 1078–1097, http://dx.doi.org/10.2174/138161208784246180.
[6] V.P. Torchilin, Multifunctional, stimuli-sensitive nanoparticulate systems for drug delivery, Nat. Rev. Drug Discov. 13 (2014) 813–827, http://dx.doi.org/10.1038/nrd4333.
[7] R. García-Carbonero, J.G. Supko, Current perspectives on the clinical experience pharmacology, and continued development of the camptothecins, Clin. Cancer Res. 8 (2002) 641–661.
[8] A. Alimonti, A. Gelibter, I. Pavese, F. Satta, F. Cognetti, G. Feretti, D. Rasio, A. Vecchione, M. Di Palma, New approaches to prevent intestinal toxicity of irinotecan-based regimens, Cancer Treat. Rev. 30 (2004) 555–562, http://dx.doi.org/10.1016/j.ctrv.2004.05.002.
[9] S. Kruszewski, M. Cyrankiewicz, B. Ziomkowska, Biophysical properties of 10-hydroxy-camptothecin determined by fluorescence anisotropy measurements, Pol. J. Environ. Stud. 15 (2006) 69–71.

[10] A. Lansiaux, S. Léonce, L. Kraus-Berthier, C. Bal-Mahieu, R. Mazinghien, S. Didier, M.-H. David-Cordonnier, P. Hautefaye, G. Lavielle, C. Bailly, J.A. Hickman, A. Pierre, Novel stable camptothecin derivatives replacing the E-ring lactone by a ketone function are potent inhibitors of topoisomerase I and promising antitumor drugs, Mol. Pharmacol. 72 (2007) 311–319, http://dx.doi.org/10.1124/mol.107.034637.
[11] M.H. Ali, D.J. Kirby, A.R. Mohammed, Y. Perrie, Solubilisation of drugs within liposomal bilayers: alternatives to colesterol as a membrane stabilising agent, J. Pharm. Pharmacol. 62 (2010) 1646–1655, http://dx.doi.org/10.1111/j.2042-7158.2010.01090.x.
[12] A. Fernández-Botello, F. Comelles, M.A. Alsina, P. Cea, F. Reig, A monolayer study on interactions of docetaxel with model lipid membranes, J. Phys. Chem. 112 (2008) 13834–13841, http://dx.doi.org/10.1021/jp806423k.
[13] A.A. Argyriou, M. Koltzenburg, P. Polychronopoulos, S. Papapetropoulos, H.P. Kalofonos, Peripheral nerve damage associated with administration of taxones in patients with cancer, Critical Rev. Oncol./Hematol. 66 (2008) 218–228, http://dx.doi.org/10.1016/j.critrevonc.2008.01.008.
[14] J.C. Kraft, J.P. Freeling, Z. Wang, R.J.Y. Ho, Emerging research and clinical development trends of liposome and lipid nanoparticle drug delivery systems, J. Pharm. Sci. 103 (2014) 29–52, http://dx.doi.org/10.1002/jps.23773.
[15] S. Mura, J. Nicolas, P. Couvreur, Stimuli-responsive nanocarriers for drug delivery, Nat. Mater. 12 (2013) 991–1003, http://dx.doi.org/10.1038/nmat3776.
[16] K. Sen, M. Mandal, Second generation of liposomal cancer therapeutics: transition from laboratory to clinic, Int. J. Pharm. 448 (2013) 28–43, http://dx.doi.org/10.1016/j.ijpharm.2013.03.006.
[17] M. García-Díaz, M. Kawakubo, P. Mroz, M.L. Sagristá, M. Mora, S. Nonell, M.R. Hamblin, Cellular and vascular effects of the photodynamic agent temocene are modulated by the delivery vehicle, J. Control. Release 162 (2012) 355–363, http://dx.doi.org/10.1016/j.jconrel.2012.07.025.
[18] G. Gregoriadis, Overview of liposomes, J. Antimicrob. Chemother. Suppl. B (1991) 39–48, http://dx.doi.org/10.1093/jac/28.suppl_B.39.
[19] R. Langer, Drug delivery and targeting, Nature 392 (1998) 5–10.
[20] V.P. Torchilin, Recent advances with liposomes as pharmaceutical carriers, Nat. Rev. Drug Discov. 4 (2005) 145–160, http://dx.doi.org/10.1038/nrd1632.
[21] M. Slingerland, H.-J. Guchelaar, H. Gelderblom, Liposomal drug formulations in cancer therapy: 15 years along the road, Drug Discov. Today 17 (2012) 160–166, http://dx.doi.org/10.1016/j.drudis.2011.09.015.
[22] T.M. Allen, P.R. Cullis, Liposomal drug delivery systems: from concept to clinical applications, Adv. Drug Deliv. Rev. 65 (2013) 36–48, http://dx.doi.org/10.1016/j.addr.2012.09.037.
[23] Y. Fan, Q. Zhang, Development of liposomal formulations: from concept to clinical investigations, Asian J. Pharm. Sci. 8 (2013) 81–87, http://dx.doi.org/10.1016/j.ajps.2013.07.010.
[24] Y.H. Hsiang, R. Hertzberg, S. Hecht, L.F. Liu, Camptothecin induces protein-linked DNA breaks via mammalian DNA topoisomerase I, J. Biol. Chem. 260 (1985) 14873–14878.
[25] Z. Mi, T.G. Burke, Differential interactions of camptothecin lactone and carboxylate forms with human blood components, Biochemistry 33 (1994) 10325–10336, http://dx.doi.org/10.1021/bi00200a013.
[26] Y. Sadzuka, H. Takabe, T. Sonobe, Liposomalization of SN-38 as active metabolite of CPT-11, J. Control. Release 108 (2005) 453–459, http://dx.doi.org/10.1016/j.jconrel.2005.08.023.
[27] L. Zhao, S.-S. Feng, M.L. Go, Investigation of molecular interactions between Paclitaxel and DPPC by Langmuir Film Balance and Differential Scanning Calorimetry, J. Pharm. Sci. 93 (2004) 86–98, http://dx.doi.org/10.1002/jps.10523.
[28] C. Peetla, A. Stine, V. Labhasetwar, Biophysical interactions with model lipid membranes: applications in drug discovery and drug delivery, Mol. Pharm. 6 (2009) 1264–1276, http://dx.doi.org/10.1021/mp9000662.
[29] A.M. Seddon, D. Casey, R.V. Law, A. Gee, R.H. Templer, O. Ces, Drug interactions with lipid membranes, Chem. Soc. Rev. 38 (2009) 2509–2519, http://dx.doi.org/10.1039/b813853m.
[30] C. Nunes, G. Brezesinski, D. Lopes, J.L.F.C. Lima, S. Reis, M. Lúcio, Lipid–drug interaction: biophysical effects of tolmetin on membrane mimetic systems of different dimensionality, J. Phys. Chem. B 115 (2011) 12615–12623, http://dx.doi.org/10.1021/jp206013z.
[31] M.G. Sarpietro, A. Di Sotto, M.L. Accolla, F. Castelli, Interaction of β-caryophyllene and β-caryophyllene oxide with phospholipid bilayers: differential scanning calorimetry study, Termochimica Acta. 600 (2015) 28–34, http://dx.doi.org/10.1016/ltca.2014.11.029.
[32] S.-D. Clas, C.R. Dalton, B.C. Hancock, Differential scanning calorimetry: applications in drug development, Pharm. Sci. Technol. Today 2 (1999) 311–320.
[33] M.G. Sarpietro, M.L. Accolla, N. Santoro, F.M. Mansfeld, R. Pignatello, I. Toth, F. Castelli, Calorimetry and Langmuir–Blodgett studies on the interaction of a lipophilic prodrug of LHRH with biomembrane models, J. Colloid Interface Sci. 421 (2014) 122–131, http://dx.doi.org/10.1016/j.jcis.2014.01.040.
[34] B. Moghaddam, M.H. Ali, J. Wilkhu, D.J. Kirby, A.R. Mohammed, The application of monolayer studies in the understanding of liposomal formulations, Int. J. Pharm. 417 (2011) 235–244, http://dx.doi.org/10.1016/j.ijpharm.2011.01.020.
[35] P. Gill, T.T. Moghadam, B. Ranjbar, Differential scanning calorimetry techniques: applications in biology and nanoscience, J. Biomol. Tech. 21 (2010) 167–193.
[36] F. Castelli, M.G. Sarpietro, M. Ceruti, F. Rocco, L. Cattel, Characterization of lipophilic gemcitabine prodrug–liposomal membrane interactions by differential scanning calorimetry, Mol. Pharm. 3 (2006) 737–744, http://dx.doi.org/10.1021/mp060059y.
[37] F. Castelli, M.G. Sarpietro, F. Rocco, M. Ceruti, L. Cattel, Interaction of lipophilic gemcitabine prodrugs with biomembrane models studied by Langmuir–Blodgett technique, J. Colloid Interface Sci. 313 (2007) 363–368, http://dx.doi.org/10.1016/j.jcis.2007.04.018.
[38] M.C. Giuffrida, F. Dosio, F. Castelli, M.G. Sarpietro, Lipophilic prodrug of paclitaxel: interaction with a dimyristoylphosphatidylcholine monolayer, Int. J. Pharm. 475 (2014) 624–631, http://dx.doi.org/10.1016/j.ijpharm.2014.09.022.
[39] J.C. Dearden, G.M. Bresnen, The measurement of partition-coefficients, Quant. Struct.-Act. Relat. 7 (1988) 133–144, http://dx.doi.org/10.1002/qsar.19880070304.
[40] T. Braumann, Determination of hydrophobic parameters by reversed-phase liquid chromatography: theory, experimental techniques, and application in studies on quantitative structure-activity relationships, J. Chromatogr. 373 (1986) 191–225, http://dx.doi.org/10.1016/S0021-9673(00)80213-7.
[41] A. Casadó, M.L. Sagristá, M. Mora, Formulation and in vitro characterization of thermosensitive liposomes for the delivery of irinotecan, J. Pharm. Sci. 103 (2014) 3127–3138, http://dx.doi.org/10.1002/jps.24097.
[42] R.N.A.H. Lewis, B.D. Sykes, R.N. McElhaney, Thermotropic phase behavior of model membranes composed of phosphatidylcholines containing cis-monounsaturated acyl chain homologues of oleic acid: differential scanning calorimetric and 31P NMR spectroscopic studies, Biochemistry 27 (1988) 880–887, http://dx.doi.org/10.1021/bi00403a007.
[43] D. Bach, E. Wachtel, N. Borochov, G. Senisterra, R.M. Epand, Phase behaviour of heteroacid phosphatidylserines and cholesterol, Chem. Phys. Lipids 63 (1992) 105–113, http://dx.doi.org/10.1016/0009-3084(92)90027-M.
[44] M.H. Chiu, E.J. Prenner, Differential scanning calorimetry: an invaluable tool for a detailed thermodynamic characterization of macromolecules and their interactions, J Pharm. Bioallied Sci. 3 (2011) 39, http://dx.doi.org/10.4103/0975-7406.76463.
[45] W. Stillwell, An Introduction to Biological Membranes: From Lipid Bilayers to Lipid Rafts, Academic Press, San Diego (CA), 2013 117–129, http://dx.doi.org/10.1016/B978-0-444-52153-8.00008-8.
[46] J.C.M. Stewart, Colorimetric determination of phospholipids with ammonium ferrothiocyanate, Anal. Biochem. 104 (1980) 10–14, http://dx.doi.org/10.1016/0003-2697(80)90269-9.
[47] D.L. Ross, S.K. Elkinton, C.M. Riley, Physicochemical properties of the fluoroquinolone antimicrobials. III. 1-octanol/water partition coefficients and their relationships to structure, Int. J. Pharm. 88 (1992) 379–389, http://dx.doi.org/10.1016/0378-5173(92)90336-Z.
[48] OECD, Test No. 107: Partition Coefficient (n-octanol/water): Shake Flask Method, OECD Guidelines for the Testing of Chemicals, Section 1, OECD Publishing, Paris, 1995, http://dx.doi.org/10.1787/9789264069626-en.
[49] P. Dynarowicz-Latka, A. Dhanabalan, O.N.J. Oliveira, Modern physicochemical research on Langmuir monolayers, Adv. Colloid Interf. Sci. 91 (2001) 221–293, http://dx.doi.org/10.1016/S0001-8686(99)00034-3.
[50] M.J. Sánchez-Martín, I. Haro, M.A. Alsina, M.A. Busquets, M. Pujol, A Langmuir monolayer study of the interaction of E1(145–162) hepatitis G virus peptide with phospholipid membranes, J. Phys. Chem. B. 114 (2010) 448–456, http://dx.doi.org/10.1021/jp906900k.
[51] J.C. Domingo, M. Mora, M.A. De Madariaga, The influence of N-acyl chain length on the phase behavior of natural and synthetic N-acylethanolamine phospholipids, Chem. Phys. Lipids 75 (1995) 15–25, http://dx.doi.org/10.1016/0009-3084(94)02397-N.
[52] Y. Tang, P.R. Czuczman, S.T. Chung, A.L. Lewis, Preservation of the active lactone form of irinotecan using drug eluting beads for the treatment of colorectal cancer metastases, J. Control. Release 127 (2007) 70–78, http://dx.doi.org/10.1016/j.jconrel.2007.12.012.
[53] M.G. Sarpietro, C. Spatafora, M.L. Acolla, O. Cascio, C. Tringali, F. Castelli, Effect of resveratrol-related stilbenoids on biomembrane models, J. Nat. Prod. 76 (2013) 1424–1431, http://dx.doi.org/10.1021/np400188m.
[54] M.G. Sarpietro, M.C. Giuffrida, S. Ottimo, D. Micieli, F. Castelli, Evaluation of the interaction of coumarins with biomembrane models studied by differential scanning calorimetry and Langmuir–Blodgett techniques, J. Nat. Prod. 74 (2011) 295–-790, http://dx.doi.org/10.1021/np100850u.
[55] S.-S. Feng, K. Gong, J. Chew, Molecular interactions between a lipid and an antineoplastic drug Paclitaxel (Taxol) within the lipid monolayer at the air/water interface, Langmuir 18 (2002) 4061–4070, http://dx.doi.org/10.1021/la011545p.
[56] M. Jurak, J. Miñones Conde, Characterization of the binary mixed monolayers of α-tocopherol with phospholipids at the air–water interface, Biochim. Biophys. Acta 1828 (2013) 2410–2418, http://dx.doi.org/10.1016/j.bbamem.2013.07.005.
[57] J.B. Rosenholm, P. Ihalainen, J. Peltonen, Thermodynamic characterization of Langmuir monolayers of thiolipids: a conceptual analysis, Colloids Surf. A 228 (2003) 119–130, http://dx.doi.org/10.1016/S0927-7757(03)00301-7.
[58] B. Těrová, R. Heczko, J.P. Slotte, On the importance of the phosphocholine methyl groups for sphingomyelin/cholesterol interactions in membranes: a study with ceramide phosphoethanolamine, Biophys. J. 88 (2005) 2661–2669, http://dx.doi.org/10.1529/biophysj.104.058149.
[59] G.L. Gaines, Insoluble Monolayers at Liquid/gas Interfaces, Wiley-Interscience, New York, 1966.
[60] R. Maget-Dana, D. Lelièvre, Comparative interaction of α-Helical and β-Sheet amphiphilic isopeptides with phospholipid monolayers, Biopolymers 59 (2001) 1–10, http://dx.doi.org/10.1002/1097-0282(200107)59.
[61] D.K. Chattoraj, K.S. Birdi, Adsorption and the Gibbs Surface Excess, Plenum Press, New York, 1984 219–223.
[62] I.S. Costin, G.T. Barnes, 2-Component monolayers. 2. Surface pressure-area relations for octadecanol-docosyl sulfate system, J. Colloid Interface Sci. 51 (1975) 106–121, http://dx.doi.org/10.1016/0021-9797(75)90088-0.
[63] M. Pugelli, G. Gabrielli, Behavior of vinyl-polymers in mixed monolayers, J. Colloid Interface Sci. 6 (1977) 420–427, http://dx.doi.org/10.1016/0021-9797(77)90459-3.
[64] A.W. Adamson, Physical Chemistry of Surfaces, John Wiley and Sons, New York, 1990.

[65] M.J.G. Ruiz, M.A.C. Vilchez, A study of the miscibility of bile components in mixed monolayers at the air–liquid interface. 1. Cholesterol, lecithin and lithocholic acid, Colloid Polym. Sci. 269 (1991) 77–84, http://dx.doi.org/10.1007/BF00654662.
[66] R.E. Pagano, N.L. Gershfeld, Physical chemistry of lipid films at the air–water interface. II. Binary lipid mixtures. The principles governing miscibility of lipids in surfaces, J. Phys. Chem. 76 (1972) 1238–1243, http://dx.doi.org/10.1021/j100653a002.
[67] A. Villares, S. Martín, I. Giner, J. Díaz, D.P. Lydon, P.J. Low, P. Cea, The use of scanning polarization force microscopy to study the miscibility of a molecular wire candidate and an insulating fatty acid in mixed LB films, Soft Matter 4 (2008) 1508–1514, http://dx.doi.org/10.1039/b716798a.
[68] A. Eftaiha, M.F. Paige, The influence of salinity on surfactant miscibility in mixed dipalmitoylphosphatidylcholone–perfluorooctadecanoic acid monolayer films, J. Colloid Interface Sci. 353 (2011) 210–219, http://dx.doi.org/10.1016/j.jcis2010.09.045.
[69] F. Bordi, C. Cametti, F. De Luca, T. Gili, D. Gaudino, S. Sennato, Charged lipid monolayers at the air–solution interface: coupling to polyelectrolytes, Colloids Surf. B: Biointerfaces 29 (2003) 149–157, http://dx.doi.org/10.1016/S0927-7765(02)00185-6.
[70] S. Pérez-López, M. Nieto-Suárez, C. Mestres, M.A. Alsina, I. Haro, N. Vila-Romeu, Behaviour of a peptide sequence from the GB virus/hepatitis virus E2 protein in Langmuir monolayers: its interaction with phospholipid model membranes, Biophys. Chem. 141 (2009) 153–162, http://dx.doi.org/10.1016/j.bpc.209.01.007.
[71] A.J. Verkleij, R.F.A. Zwaal, B. Roelofsen, P. Comfurius, D. Kastelijn, L.L.M. van Deenen, The asymmetric distribution of phospholipids in the human red cell membrane. A combined study using phospholipases and freeze-etch electron microscopy, Biochim. Biophys. Acta 323 (1973) 178–193, http://dx.doi.org/10.1016/0005-2736(73)90143-0.
[72] A. Yamaji-Hasegawa, M. Tsujimoto, Asymmetric distribution of phospholipids in biomembranes, Biol. Pharm. Bull. 29 (2006) 1547–1553, http://dx.doi.org/10.1248/bpb.29.1547.
[73] A. Vila-Romeu, M. Nieto-Suárez, P. Dynarowicz-Latka, Miscibility of Gramicidin - ethyl nonadecanoate in Langmuir monolayers in the presence of salts dissolved in the subphase, J. Phys. Chem. B 109 (2005) 14965–14970, http://dx.doi.org/10.1021/jp014092.
[74] D. Marsh, Lateral pressure in membranes, Biochim. Biophys. Acta Rev. Biomembr. 1286 (1996) 183–223, http://dx.doi.org/10.1016/S0304-4157(96)00009-3.
[75] Liposomal irinotecan: formulation development and therapeutic assessment in murine xenograft models of colorectal cancer, Clin. Cancer Res. 10 (2004) 6638–6649, http://dx.doi.org/10.1158/1078-0432.CCR-04-0221.
[76] J. Oliveira Eloy, M. Claro de Souza, R. Petrilli, J.P. Abriata Barcelos, R.J. Lee, J. Maldonado Marchetti, Liposomes as carriers of hydrophilic small molecule drugs: strategies to enhance encapsulation and delivery, Colloids Surf. B: Biointerfaces 123 (2014) 345–363, http://dx.doi.org/10.1016/j.colsurfb.2014.09.029.

Supplementary Material

Langmuir Monolayers and Differential Scanning Calorimetry for the Study of the Interactions between Camptothecin Drugs and Biomembrane Models

Ana Casadó[§] M. Chiara Giuffrida[§†], M. Lluïsa Sagristá[§], Francesco Castelli[†], Montserrat Pujol[#], M. Asunción Alsina[#], and Margarita Mora[*, §]

[§] Department of Biochemistry and Molecular Biology, Faculty of Biology, University of Barcelona, Av. Diagonal 643, 08028-Barcelona, Spain.

[#] Department of Physical Chemistry, Faculty of Pharmacy, University of Barcelona, Av. Joan XXIII s/n, 08028-Barcelona, Spain.

[†]Department of Drug Sciences, University of Catania, Viale A. Doria 6, 95125, Catania, Italy.

*Corresponding author
Prof. Dr. Margarita Mora.
Tel: +34-93-402.12.12
Fax: +34-93-402.15.59
E-mail: margarita.mora@ub.edu

DATA ANALYSIS

Equation 1.

$$\Gamma = \frac{1}{RT}\frac{d\Delta\pi}{d\ \ln C}$$

Γ is the surface excess concentration and dΔπ/dlnC is the slope of the graph obtained by fitting the surface pressure *in* the asymptote to the ln [CPT-11].

Equation 2.

$$A = \frac{1}{\Gamma N_A}$$

Equation 3.

$$C_s = -\frac{1}{A}\left(\frac{d\,A}{d\,\pi}\right)$$

The two-dimensional compressibility C_s of a monolayer at a given molecular area or, equivalently, at a given surface pressure, is defined as the partial change of the area strain with respect to the surface pressure.

Equation 4.

$$A_{12} = A_1\,x_1 + A_2\,x_2$$

A_{12} is the area per molecule in the mixed film, at a given surface pressure, A_1 and A_2 are the areas per molecule at that surface pressure for the pure films, and x_1 and x_2 were the mole fractions of components 1 and 2 in the mixed film.

Equation 5.

$$G^{E} = \int_0^{\pi} A_{12}d\pi - x_1\int_0^{\pi} A_1 d\pi - x_2\int_0^{\pi} A_2 d\pi$$

G^E is the excess Gibbs energy and A_1, A_2, x_1 and x_2 have the same meaning as in equation 4; A_{12} is the area per molecule of a mixed monolayer consisting of components 1 and 2; π is the upper limit pressure at which the integrals have been calculated.

TABLES

Table S1. Experimental conditions for the evaluation of the CPT-11 and SN-38 partition coefficients

Drug	Solvent	λ (nm)	ε (μM^{-1} cm^{-1})
CPT-11	n-octanol	370	0.0269
	Lactate Buffer 10 mM pH 4.4	368	0.0265
	Citrate Buffer 10mM pH 7.4	379	0.0282
	Glycine Buffer 10 mM pH 9.0	373	0.0278
SN-38	n-octanol	397	0.0230

FIGURES

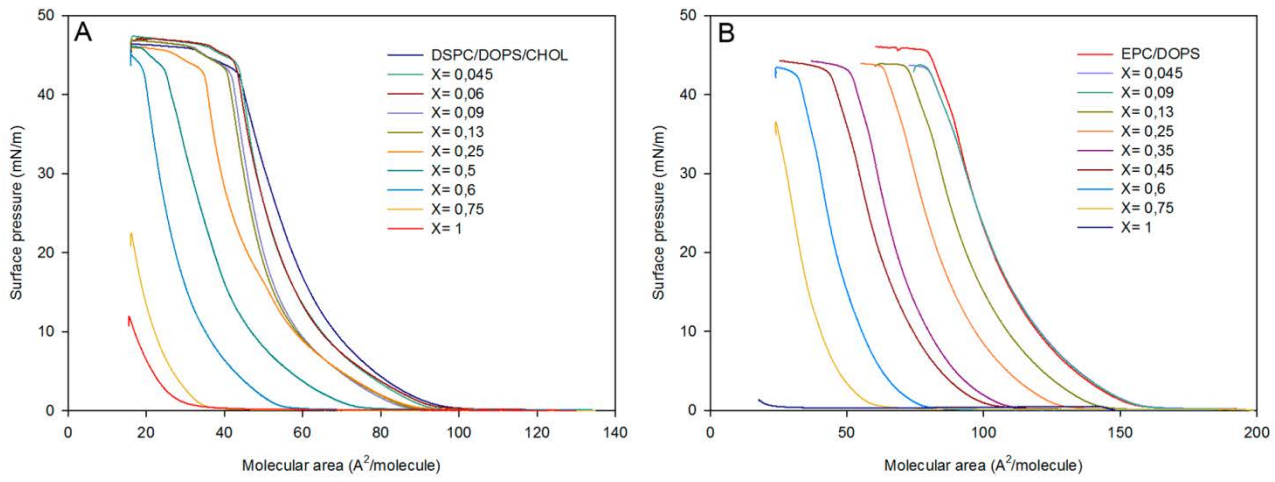

Figure S1. The surface pressure versus area per molecule of isotherms of pure lipid mixtures (DSPC/DOPS/CHOL, A or EPC/DOPS, B), pure drugs (CPT-11, A or SN-38, B) and mixed drug-lipids films (DSPC/DOPS/CHOL/CPT-11, A or EPC/DOPS/SN-38, B, at different molar ratios. *x* are the molar fractions of either CPT-11 (A) or SN-38 (B).

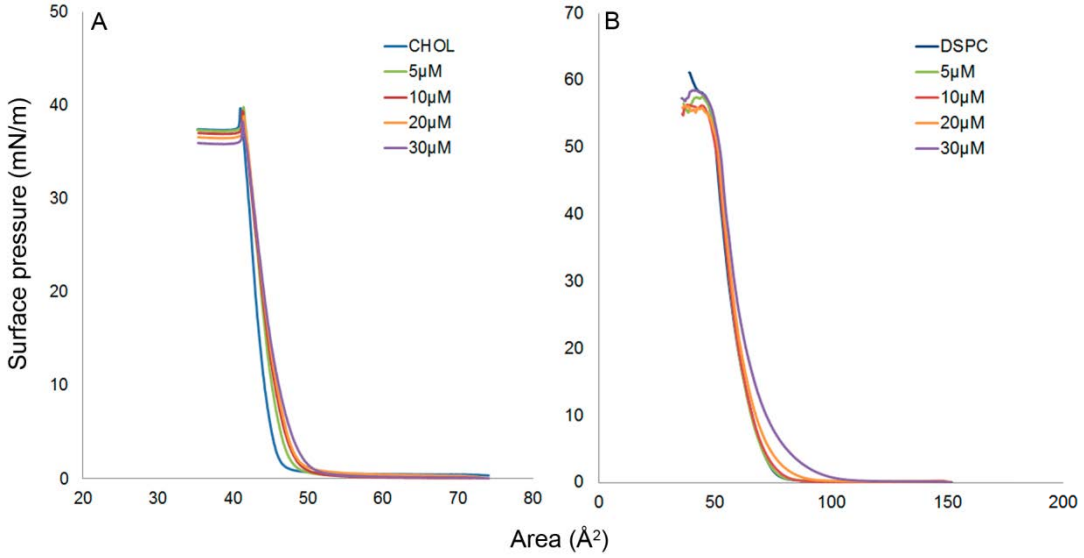

Figure S2. Compression isotherms of (A) DSPC and (B) CHOL spread on a lactate buffered subphase alone or with increasing concentrations of CPT-11.

Tercer artículo

Improved selectivity and cytotoxic effects of irinotecan via liposomal delivery: A comparative study on Hs68 and HeLa cells.

Casadó A, Mora M, Sagristá ML, Rello-Varona S, Acedo P, Stockert JC, Cañete M, Villanueva A.

Eur J Pharm Sci. 2017 Jul 19;109:65-77. doi: 10.1016/j.ejps.2017.07.024

RESUMEN

El Irinotecan (CPT-11) es un agente quimioterapéutico eficaz ampliamente utilizado para tratar diferentes tipos de cáncer. Por otra parte, se ha demostrado que la administración liposómica de agentes antitumorales es una estrategia quimioterapéutica prometedora. El objetivo de este estudio ha sido analizar el efecto de CPT-11 liposomal (CPT-11lip) en dos líneas celulares humanas (Hs68 y HeLa) para establecer la idoneidad del nanotransportador desarrollado. Hemos demostrado la mayor absorción de CPT-11lip en comparación con el de CPT-11sol, en tampón lactato, y que CPT-11lip fue internalizado en las células a través de un proceso de endocitosis mientras CPT-11sol lo hace por difusión pasiva. La formulación de CPT-11lip no fue citotóxica para los fibroblastos normales Hs68, pero indujo una apoptosis masiva acompañada de la senescencia celular en células HeLa. El tratamiento con CPT-11lip modificó la morfología de las células HeLa, indujo diferentes alteraciones del ciclo celular y se acumuló en lisosomas en ambas líneas celulares. En particular, el tratamiento con CPT-11lip mostró que las células HeLa supervivientes permanecieron en un estado de senescencia mientras que sólo se indujo una detención temporal del crecimiento en células Hs68. Los resultados de RT-PCR indicaron que las diferentes respuestas en células Hs68 (supervivencia) y HeLa (muerte apoptótica) parecían ser inducidas por un mecanismo dependiente e independiente de p53, respectivamente. El análisis del daño del ADN también determinó que el CPT-11 liberado de los liposomas era capaz de alcanzar el núcleo y ejercer un efecto genotóxico en ambas líneas celulares, que se reparó en Hs68 pero no en células HeLa. Todos los resultados indican que los liposomas formados por mezclas de fosfolípido y colesterol poseen propiedades óptimas para la vehiculización del CPT-11, siendo biocompatibles y selectivamente citotóxicos contra células tumorigénicas HeLa.

ASPECTOS DESTACADOS DE LA INVESTIGACIÓN

Los liposomas constituidos por mezclas de fosfolípidos y colesterol poseen excelentes propiedades para la vehiculización del CPT-11: inactivan células tumorales Hela, deficientes en p53, sin inducir la muerte de células no tumorales Hs68.

RESUMEN GRÁFICO

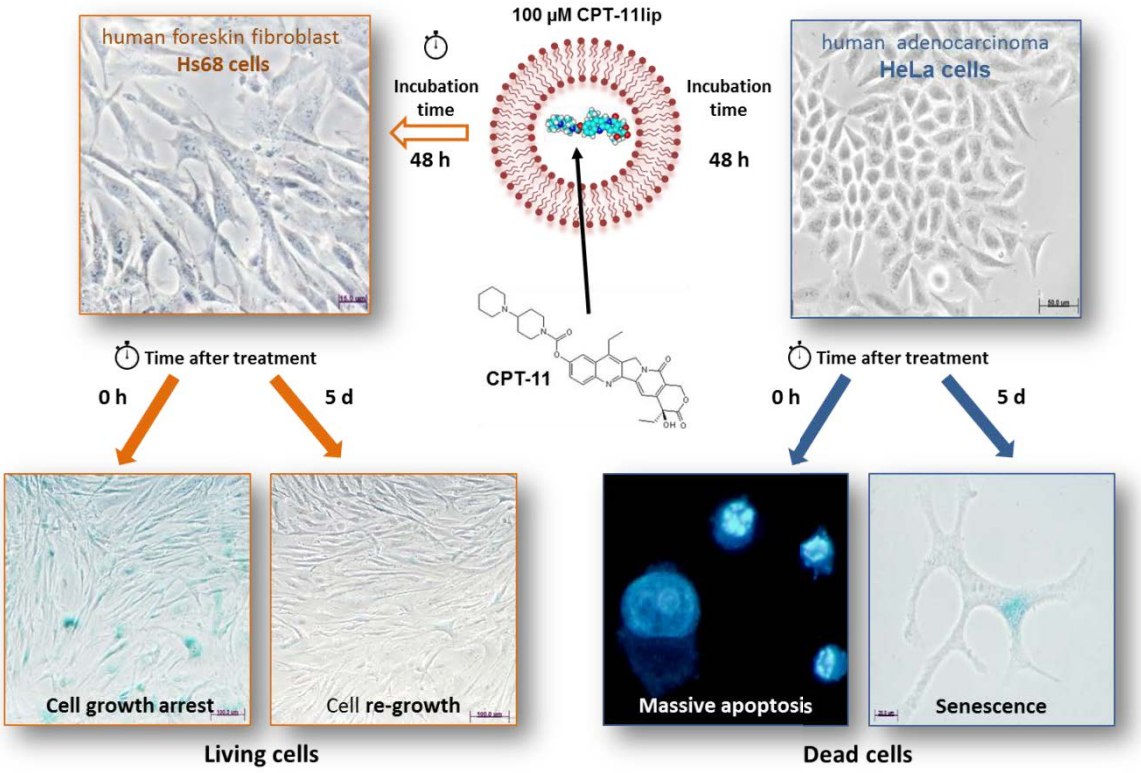

European Journal of Pharmaceutical Sciences 109 (2017) 65–77

Contents lists available at ScienceDirect

European Journal of Pharmaceutical Sciences

journal homepage: www.elsevier.com/locate/ejps

Improved selectivity and cytotoxic effects of irinotecan *via* liposomal delivery: A comparative study on Hs68 and HeLa cells

Ana Casadó[a,b,c], Margarita Mora[a], Maria Lluïsa Sagristá[a], Santi Rello-Varona[b,d], Pilar Acedo[b,e], Juan Carlos Stockert[b], Magdalena Cañete[b], Angeles Villanueva[b,f,*]

[a] Department of Biochemistry and Molecular Biomedicine, Facultat de Biologia, Universitat de Barcelona, Barcelona, Spain
[b] Departamento de Biología, Facultad de Ciencias, Universidad Autónoma de Madrid, Madrid, Spain
[c] Communication Department, Hospital Clinic of Barcelona, Barcelona, Spain.
[d] Sarcoma Research Group, Institut d'Investigació Biomèdica de Bellvitge-IDIBELL, L'Hospitalet de Llobregat, Barcelona 08908, Spain
[e] Division of Surgery and Interventional Science, University College London, London, United Kingdom
[f] Instituto Madrileño de Estudios Avanzados en Nanociencia (IMDEA Nanociencia), Madrid, Spain

ARTICLE INFO

Keywords:
Irinotecan
Liposomes
Cytotoxicity
Drug uptake
Apoptosis
Growth arrest
DNA double-strand breaks

ABSTRACT

Irinotecan (CPT-11) is an effective chemotherapeutic agent widely used to treat different cancers. Otherwise, the liposomal delivery of anti-tumor agents has been shown to be a promising strategy. The aim of this study has been to analyze the effect of liposomal CPT-11 (CPT-11lip) on two human cell lines (Hs68 and HeLa) to establish the suitability of this CPT-11 nanocarrier. We have demonstrated the highest uptake of CPT-11lip in comparison with that of CPT-11sol, in lactate buffer, and that CPT-11lip was internalized in the cells through an endocytic process whereas CPT-11sol does so by passive diffusion. CPT-11lip was not cytotoxic to normal fibroblast Hs68 cells, but induced a massive apoptosis accompanied by cell senescence in HeLa cells. CPT-11lip treatment modified the morphology of HeLa cells, induced different cell cycle alterations and accumulated into lysosomes in both cell lines. In particular, CPT-11lip treatment showed that surviving HeLa cells remained in a state of senescence whereas only a temporal growth arrest was induced in Hs68 cells. Results of RT-PCR indicated that the different responses in Hs68 (survival) and HeLa cells (apoptotic death), seemed to be induced by a p53- and p53- independent mechanism, respectively. An analysis of DNA damage also determined that released CPT-11 from liposomes was able to reach the nucleus and exert a genotoxic effect in both cell lines, which was repaired in Hs68 but not in HeLa cells. All results indicate that phospholipid-cholesterol liposomes possess optimum properties for CPT-11 delivery, being biocompatible and selectively cytotoxic against HeLa tumorigenic cells.

1. Introduction

Irinotecan (CPT-11; 7-ethyl-10-[4-(1-piperidino)-1-piperidino]-carbonyloxy-camptothecin) is one of the most widely used camptothecin (CPT) analogues that belongs to a novel class of antineoplastic agents, called topoisomerase I (Topo I) interactive compounds (Chen and Liu, 1994). CPT-11 is enzymatically converted *in vivo* by a carboxylesterase into its most active cytotoxic metabolite SN-38 (7-ethyl-10-hydroxy-camptothecin) (Wu et al., 2002). Both CPT-11 and SN-38 act by binding to Topo I, responsible for the relaxation of supercoiled duplex DNA during replication, inhibiting DNA synthesis (Hsiang et al., 1985; García-Carbonero and Supko, 2002).

CPT-11 has long been applied in the clinical treatment of various types of tumors (Liew and Yang, 2008). The whole of the published results established CPT-11 as one of the most active drugs in the first- and second-line chemotherapeutic treatment against colorectal cancer (CRC) due to its confirmed evidence of anti-tumor efficacy (Vanhoefer et al., 2001). Of special interest was the demonstration of considerable activity of this drug against 5-fluorouracil (5-FU)-refractory CRC (Diaz-Rubio, 2004). Moreover, camptothecins have also been successfully used to treat other types of cancers (Liu et al., 2016; Iyer et al., 2015). Nevertheless, camptothecin derivatives show some limitations, the principal related to the coexistence of a chemical equilibrium between an E ring-opened carboxylate form and a lactone form: the former has < 10% the potency of the lactone form as Topo I inhibitor and it is inactive in cell culture, perhaps due to inability to cross the cell membrane (Teicher, 2008).

The main adverse side effects associated to camptothecins therapies are neutropenia, thrombocytopenia, anemia and a number of non-hematological toxic effects after prolonged administration (Estanqueiro

* Corresponding author at: Departamento de Biología, Facultad de Ciencias, Universidad Autónoma de Madrid, C/Darwin 2, E-28049 Madrid, Spain.
E-mail address: angeles.villanueva@uam.es (A. Villanueva).

http://dx.doi.org/10.1016/j.ejps.2017.07.024
Received 9 May 2017; Received in revised form 14 July 2017; Accepted 18 July 2017
Available online 19 July 2017

et al., 2015). Numerous studies have reduced the incidence of the common complications of CPT-11 treatment, besides increasing its clinical effectiveness, in terms of overall survival, progressive-free survival and response rates (Hind et al., 2008). In an attempt to improve first- and second-line chemotherapy regimens, some investigators have combined novel biological agents with CPT-11 or oxaliplatin and 5-FU, whereas others have proposed the use of selective delivery carriers.

Some systemic and targeted therapies have recently been investigated and evaluated in metastatic CRC and the results have been discussed and reviewed by Hegde et al. (2008) and Köhne and Lenz (2009). Targeted agents have expanded the available treatment options for patients with metastatic CRC, prolonging survival when combined with the standard cytotoxic CPT-11-, oxaliplatin- and fluoropyrimidine-based regimens. Despite these gains, the overall impact of current targeted agents in the treatment of mCRC has been relatively modest, and while 2-year survival has improved, no gains have been, as of yet, in 5-years survival (Chu, 2012).

On the other hand, some innovations and developments in nanotechnology have revolutionised cancer therapeutics to solve one of the major drawbacks of cytostatics: most of the current agents do not differentiate cancerous from normal cells, giving systemic toxicity and a series of adverse effects that limit the maximum allowable dose of the drug. Drug carriers may increase the clinical utility of antineoplastic drugs by favoring their delivery to cancer cells Thus, in the last decade, numerous efforts are being made to investigate new drug delivery systems with a double aim: i) to promote tumor drug accumulation, and ii) to reduce doses needed for effective treatment, with the consequent decrease of the side effects (Deshpande et al., 2013). The design of vehicles to carry anti-tumor drugs has become a priority in the field of cancer chemotherapy. Therefore, one of the main challenges in human disease treatment is no longer the development of more efficient drugs, but the improvement of drug selectivity (Juillerat-Jeanneret and Schmitt, 2007).

In this sense, the use of liposomes has been proposed as a promising nanotherapeutic approach to increase the therapeutic index of a wide range of antineoplastic agents (De Jong and Borm, 2008; Sen and Mandal, 2013; Przybylo et al., 2016). Liposomes have been shown to improve the pharmacokinetics and tumor localization of encapsulated drugs, modify the toxicities associated with a particular drug, and ultimately enhance antitumor efficacy compared with the unencapsulated drug (Drummond et al., 2008). Numerous liposomal formulations bearing cancer therapeutics have been approved or are currently undergoing clinical trials (Bozzuto and Molinari, 2015). The consideration of the chemical properties of cytostatics is a pivotal aspect to get the appropriate formulation for any drug. Hydrophilic or hydrophobic molecules are differently incorporated into nanotechnological devices and, when considering liposomes, their solubility properties determine the greater or lesser encapsulation efficiency. The study of the molecular interactions between the constituents of the carrier and the drug is also important to predict the extent of drug encapsulation.

In vivo studies have shown that CPT-11 is an ideal candidate for encapsulation in different types of nanocarriers, liposomes included (Messerer et al., 2004; Ramsay et al., 2008). Liposome encapsulation can provide an internal aqueous environment of low pH that stabilizes the active, ring-closed, lactone form of the drug, easily hydrolysable at physiologic pH (Burke and Bom, 2000; Burke and Gao, 1994): the liposomal encapsulation of CPT-11 would thus provide a potent drug formulation for the treatment of different types of cancer. In October 2015, the U.S. Food and Drug Administration approved an encapsulated form of CPT-11 in liposomes (Onivyde, Merrimack Pharmaceuticals, Inc.), previously known as MM-398 (Chustecka, 2015), which use in combination with fluorouracil and leucovorin in patients with metastatic pancreatic cancer has been approved in several countries (Lamb and Scott, 2017).

This paper presents a study about the suitability of a liposomal formulation of CPT-11 (CPT-11lip) for cancer therapy protocols and a comparative analysis with a healthy and a malignant cell line has been performed to establish the possible specificity of a CPT-11lip-based chemotherapy. Different efficient and sophisticated methodologies, based on active loading procedures, have been reported in the literature to entrap the basic CPT-11 (pKapiperidino = 11.20) into liposomes. While effective in their ability to encapsulate the drug, they have some general disadvantages such as long manufacturing procedures, difficulties in removing some of the materials used to increase the encapsulation rate and high manufacturing costs.

Herein, we are reporting the characteristics and the efficiency of CPT-11 loaded temperature sensitive liposomes. Thermosensitive responsiveness had been incorporated as a criterion for the design of the liposomal formulation of this drug, being this property especially useful to ensure the integrity of the carrier when administered *in vivo*, besides allowing a controlled release of the drug in the therapeutic sites in response to temperature increases (Casadó et al., 2014). The feasibility as delivery vehicles and the potential of this nanomedicine have been determined by evaluating *in vitro* the cellular uptake, cytotoxic behavior and cell death mechanism.

2. Materials and methods

A more detailed version of the M & Ms. employed in this study can be found as Supplementary Material.

2.1. Preparation of liposomal CPT-11

Intermediate unilamellar liposomes (IUVs) were prepared by vortexing and extrusion as previously reported (Casadó et al., 2014). Briefly, lipids, DSPC, DOPS and CHOL (Avanti Polar Lipids, USA), were mixed in a molar ratio of 65:35:30 (Casadó et al., 2016) to prepare the lipid film and CPT-11 was added from a chloroform/methanol (2:1) solution at a 7.5:1 M ratio. Multilamellar vesicles (MLVs) were prepared by hydrating the dried lipid films in 10 mM lactate buffer (pH 4.4) to a final lipid concentration of 10 mg/mL. MLVs dispersions were frozen (liquid N_2) and thawed (55 °C water bath) above the phase transition temperature (Tm) for five times. For IUVs preparation, MLVs were extruded (Lipex Biomembranes, Canada) six times through 400 nm and twelve times through 200 nm polycarbonate membrane filters (Osmonics, USA). Control liposomes without CPT-11 were also prepared.

The ability of the IUVs to keep encapsulated their cargo was determined by carboxyfluorescein leakage experiments and the liposomes were visualized by transmission electron microscopy (TEM), characterized by size, polydispersity index and ζ-potential and by quantifying the amount of the drug inside vesicles. Total and entrapped CPT-11 was systematically quantified by absorbance spectroscopy as described previously (Casadó et al., 2014).

2.2. Cell cultures and treatments

Hs68 non-transformed fibroblasts and the tumor epithelial cell line HeLa (cervix adenocarcinoma), were purchased from American Type Culture Collection (USA). Cells were grown in DMEM supplemented with 50 U/mL penicillin, 50 μg streptomycin/mL and 10% FCS. Cells were maintained in a 5% CO_2 atmosphere at 37 °C. Cells were incubated with 100 μM CPT-11 entrapped in liposomes (CPT-11lip) or solubilized in 10 mM lactate buffer pH 4.4 (CPT-11sol), depending on the type of assay, at different times between 0 and 48 h to assess the cellular uptake of the drugs using flow cytometry and at 24 h to visualize subcellular localization by fluorescence microscopy. For cell survival studies, cell cycle analysis and morphological studies, a period of 48 h of incubation with post-incubation times up to 48 h, were used.

2.3. Measurement of CPT-11 uptake and internalization

Cells were treated with CPT-11lip or CPT-11sol up to 48 h. CPT-11 fluorescence was measured with a LSR II flow cytometer (BD Biosciences, USA) using excitation and emission wavelengths of 405 and 450 nm, respectively. Significance was assessed using a Student's paired *t*-test.

To analyze internalization mechanisms of CPT-11, cells were incubated with 100 μM of CPT-11lip or CPT-11sol for 3 h at 4 °C. Then, samples were washed three times with PBS and directly observed by fluorescence microscopy (under UV excitation) combined with phase contrast microscopy. Moreover, cells incubated for 24 h, were observed by confocal fluorescence microscopy combined with phase contrast microscopy under UV excitation. To analyze the possible participation of lysosomes in drug accumulation, cells were also incubated with 1 mL DMEM containing 50 nM LysoTracker Red DND-99 (Life Technologies, USA) for 30 min, washed three times with PBS and visualized by confocal microscopy.

2.4. Analysis of cell morphology

Morphological changes at different times (0, 24 and 48 h) after incubation with 100 μM CPT-11lip were assessed by toluidine blue staining using bright field microscopy.

2.5. Cell survival assessment

Thiazolyl blue (MTT; Sigma-Aldrich, USA) reduction and Trypan blue (Sigma-Aldrich) exclusion tests were used for the assessment of cell survival. Production of MTT formazan precipitates, dissolved in 100 μL DMSO per well, was measured as absorbance at 540 nm in a SpectraFluor spectrophotometer (Tecan, Switzerland). Cell survival was expressed as the percentage of absorption of treated cells in comparison with that of control cells. For Trypan blue exclusion test, treated and untreated cells were trypsinized (harvesting also the detached ones) and mixed with the same volume of a 0.2% Trypan blue solution in PBS. Cell counting of death (blue) or alive (white and bright) cells was performed using a Neubauer hemocytometer (Marienfeld, Germany). Data correspond to mean values ± standard deviation from at least eight different experiments for MTT assay and four different experiments for Trypan blue assay.

2.6. Cell death mechanisms

2.6.1. Necrosis analysis

Induction of necrosis was determined by measuring the activity of the enzyme LDH, released into the culture medium by necrotic cells following lethal membrane injury, by using a fluorimetric assay kit (CytoScan-Fluoro), following the manufacturer's instructions (G-Biosciences, USA). Fluorescence was measured with an excitation at 560 nm and emission at 590 nm after shaking the plates for 15 s in a SpectraFluor spectrophotometer. The percentage of cytotoxicity was calculated by using the average fluorescence values from experimental, maximum LDH release, and culture medium background.

2.6.2. Apoptosis identification

Apoptotic nuclear morphology of detached HeLa cells after incubation with CPT-11lip was visualized by H-33258 staining as previously described by us (Rello et al., 2005). Apoptosis was confirmed by immunofluorescence staining of pro-apoptotic Bax protein (monoclonal mouse anti-Bax sc-20067; Santa Cruz Biotechnology, USA).

2.7. Cell cycle analysis

Cell cycle phase distribution in both cell lines was analyzed by flow cytometry using Propidium iodide (PI) DNA staining. Measurements were performed with an Epics XL flow cytometer (Beckman Coulter, USA) with an argon laser line at 488 nm and complemented with the appropriate filters. Cell fractions in sub G1, G0/G1, S, G2/M and > 4C phases were quantified in histograms with Summit software. Identification of apoptotic cells (sub G1 region) was achieved by determination of hypoploid cell populations. Polyploid cells were also identified in the > 4C region.

2.8. Senescence-associated β-galactosidase staining

Senescence was assessed by measuring the β-galactosidase activity using the Senescence Cells Histochemical Staining Kit (Sigma-Aldrich). The percentage of senescent cells was calculated by the number of β-galactosidase-positive cells (blue cells) out of at least 500 cells from different microscope fields.

2.9. Quantitative real-time PCR

Cells were treated with CPT-11lip for 3 to 48 h, and the total RNA was extracted. Two microgram of total RNA from each sample was used for cDNA synthesis using the SuperScript™ III First-Strand Synthesis System for RT-PCR according to the manufacturer's instructions (Invitrogen, USA). Quantitative RT-PCR amplifications were performed with TaqMan Gene Expression Assays products in an ABI PRISM 7900 HT Sequence Detection System (Applied Biosystems). The following genes were analyzed: TP53 (Hs00153349_m1), Bax (Hs00180269_m1) and Bcl-2 (Hs00608023_m1). A sample without cDNA was used as negative control and glyceraldehyde-3-phosphate dehydrogenase (GAPDH) (Hs99999905_m1) was used as internal control. The expression level of the target gene in the treated cells was measured relative to the level observed in the untreated cells and was quantified using the formula $2^{-\Delta\Delta CT}$ (Livak and Schmittgen, 2001).

2.10. Cytoskeleton analysis

To get insight into the cytoskeleton disorganization after CPT-11lip treatment, adhesion to substrate was analyzed by fluorescent labelling against the focal contact proteins vinculin (monoclonal anti-vinculin clone hVIN-1, Sigma-Aldrich) and F-actin (phalloidin–tetramethylrhodamine B isothiocyanate, phalloidin-TRITC, Sigma-Aldrich).

2.11. DNA damage response by immunodetection of γ-H2AX

Hs68 and HeLa cells grown on glass coverslips and incubated with CPT-11lip for different times (3, 6 and 24 h) were immunostained for phosphorylated histone H2AX (monoclonal mouse anti-γ-H2AX antibody, Merck Millipore).

2.12. Live cell imaging studies

Untreated control cells as well as cells incubated with CPT-11lip or empty liposomes were visualized at different times under phase contrast inverted microscope.

2.13. Optical microscopy

Observations of samples processed for optical microscopy (bright field and fluorescence) were made with an Olympus BX61 epi-fluorescence microscope equipped with an Olympus DP50 digital camera (Olympus, USA), and processed using the Photoshop CS5 software (Adobe Systems, USA). In immunofluorescence determinations, cell nuclei were counterstained using H-33258 (5 μg/mL in distilled water, 5 min) and mounted with ProLong Gold antifade reagent (Thermo Fisher Scientific). Confocal microscopy was performed using a multispectral Leica TCS SP5 confocal microscope (Leica, Germany). In

addition, time-lapse images of living cells were captured with an inverted microscope Leica DMI 6000B equipped with a Leica DFC420 C digital camera (Leica) and images were processed with the same software.

3. Results and discussion

3.1. Characterization of CPT-11 loaded liposomes

Different methodologies have been reported in the literature to entrap CPT-11 into liposomes. All of these are based in active loading strategies: gradient loading-stabilization techniques, based in the formation of intraliposomal drug-polyanion complexes; other transmembrane gradient methods using ammonium sulfate, pH changes with or without the incorporation of ionophres and divalent cations to the liposome bilayers; or formulations with phosphorylated carbohydrates such as phytic acid (Ramsay et al., 2008; Hattori et al., 2009; Neijzen et al., 2015).

Besides the method, to procure optimal drug formulations and efficient drug delivery systems it is essential to control the physicochemical parameters of the vehicle (Peetla et al., 2009). By using different biophysical techniques we carried out a study of the molecular interactions between the constituents of the carrier and the drug and established the suitability of a ternary lipid mixture for encapsulating CPT-11 with high efficacy. We demonstrated that CPT-11, positively charged in its piperidine group at acidic pH, interacts electrostatically with the DOPS component of the DSPC/DOPS/CHOL bilayer, making stable the incorporation of a high percentage of the drug into liposomes (Casadó et al., 2016).

We have considered the different formulation strategies (passive or active drug loading) and the different options to enhance drug delivery reported in the literature (Eloy et al., 2014; Pattni et al., 2015). Finally, we choose passive drug loading and triggered delivery approaches to formulate CPT-11 in liposomes and developed an easy-to-perform, high-efficiency encapsulation method to prepare liposomes loaded with CPT-11(Casadó et al., 2014). Thus, the designed liposomes were endowed with the ability to control the release of the drug by means of responsiveness to temperature. The synthesis protocol was standardized and the liposomal suspension, procured from the DSPC/DOPS/CHOL (65:35:30) lipid mixture and a lipid/drug molar ratio of 7.5:1, was systematically and rigorously characterized by size, polydispersity index (0.114 ± 0.032) and ζ-potential and by quantifying the amount of the drug inside vesicles. In this regard, drug encapsulation efficiency (DEE% = 85.3 ± 6.2) and drug loading efficiency (DLE% = 11.8 ± 0.9) were calculated as the amount of drug inside liposomes with respect to the total amount of drug or lipids added in preparing formulation, respectively. The 5(6)-carboxyfluorescein aqueous marker was used to determine *in vitro* the drug retention ability and the trapped volume of the formulated liposomes. A new kinetic analysis of the *CF* release curves was carried out by fitting the data to an exponential curve by means the non-lineal regression program Graph Pad Prism (version 5.00) and the percent leakages at the equilibrium (Feq) have been evaluated at different temperatures and in the absence and in the presence of serum. All the characterization parameters corresponding to the budgets used in the experiments given in this paper are listed in Table 1 and are in good agreement with our previous published data (Casadó et al., 2014). TEM images showed the round shape of CPT-11lip (see Fig. S1B). On the other hand, the permeability analysis shows the effect of temperature on the *CF* release rate and that the efflux of *CF* increased in the presence of serum. Furthermore, at physiological temperature, the very small values of Feq highlight the high stability of the designed liposomal formulation.

3.2. Efficient cellular uptake of CPT-11lip by endocytosis

Uptake and accumulation of CPT-11 incorporated into liposomes (CPT-11lip) and dissolved in lactate buffer solution (CPT-11sol) into Hs68 and HeLa cells, was determined by flow cytometry measuring the intrinsic fluorescence properties of this camptothecin derivative under ultraviolet excitation. As shown in Fig. 1A, the amount of CPT-11 inside cells increases as a function of incubation time and in both cell lines was greater for CPT-11lip than CPT-11sol. Likewise, uptake kinetics depends on cell line, being the uptake at initial time faster and higher for normal fibroblast Hs68 cells. Taken together, these studies indicated that CPT-11 in this liposomal formulation was capable of an extensive cellular internalization into both cell lines.

Previously, we had shown that CPT-11lip displayed greater drug uptake compared with the non-liposomal CPT-11 formulation in human colon carcinoma Caco-2 cells (Casadó et al., 2014).

Internalization mechanism of CPT-11lip and CPT-11sol inside both cell types was analyzed after 3 h of incubation at different temperatures by fluorescence microscopy. At 4 °C, internalization of CPT-11lip was almost, completely suppressed; while uptake of CPT-11sol was not affected in the same experimental conditions (see Fig. 1B).

Together, these findings indicate that an endocytic process was involved in CPT-11lip internalization while free CPT-11 penetrates across plasma membrane by diffusion. It has been described that liposomes appear to enter cells *via* an energy-dependent vesicular transport (Torchilin, 2005).

3.3. Selective cytotoxicity against HeLa cells

The cytotoxic effectiveness liposomal-CPT-11 was also assessed and compared with that of the free drug. Cell proliferation was evaluated by the MTT colorimetric assay. Hs68 and HeLa cells were treated with CPT-11lip and CPT-11sol for 48 h and measures were carried out immediately (0), 24 and 48 h after drug removal.

Fig. 2 (A and B) shows reduced values obtained in the MTT assay for CPT-11 treated cells in relation to control cells depending on time elapsed after the end of treatment in both cell lines. Also, survival rates in both cell lines were lower for CPT-11lip in comparison with CPT-11sol at all post-incubation times analyzed. Results of MTT assay in Hs68 cells were different in those regarding to the percentage of cell survival. In the case of Hs68 cells the survival significantly decreases from 100 to 40% when incubated with CPT-11lip and after 48 h of drug removal.

On the contrary, HeLa cells survival decreased with time elapsed after the end of the CPT-11lip treatment from 100 to 3%, indicating the high cytotoxicity induced by CPT-11lip on this cell line. Furthermore, toxicity of liposomes without CPT-11 was assessed by MTT assay. Empty liposomes showed no toxicity in both Hs68 and HeLa cells. Surviving fractions of 92.5 ± 3.5% and 93.8 ± 3.1% were obtained in Hs68 and HeLa cells, respectively.

Trypan blue exclusion test was also employed in both cell lines to validate MTT results (Fig. 2 C and D). When the assay was carried out with Hs68 cells, the viability was > 97% after treatment for all elapsed times (no significant differences). Therefore, CPT-11 seems to induce an anti-proliferative activity without causing cell death on Hs68 fibroblasts. Interestingly, Fig. 2D shows that Trypan blue assay results on HeLa cells, were in total accordance with those of the MTT test, being the results of CPT-11lip and CPT-11sol significantly different (Fig. 2D).

For statistical calculations one-way ANOVA Tukey Kramer Multiple Comparisons test and the NCSS2007 software (NCSS 2007®; NCSS Statistical software, Kaysville, Utah) were used. P values < 0.05 (*), 0.005 (**), 0.001 (***), and 0.0001(****) were considered as statistical significant for the comparison between the effect of CPT-11lip and CPT-11sol at each time. In summary, Hs68 cells showed a large difference between data from MTT and Trypan blue assays. MTT results reflected a reduction of the proliferation of Hs68 cells due to the effect of CPT-11lip. However, Trypan blue exclusion test showed viability data higher than 97%.

These data emphasize the need of using different methods to

Table 1
Physicochemical (A) and permeability (B) parameters of DSPC/OOPS/CHOL (65:35:30) liposomes.

Sample composition	Vesicle size (nm)[a]	ζ-Potential (mV)[b]	[CPT-11] (mM)[c]	mg CPT-11/mmol phospholipid
DSPC/OOPS/CHOL 65:35:30	148.3 ± 8.5	− 42.5 ± 2.7	–	–
DSPC/OOPS/CHOL/CPT-11 65:35:30:17.3	157.0 ± 12.9	− 49.1 ± 4.8	1.74 ± 0.12[d]	107.7 ± 0.0

Trapped volume[d]	Feq (%)								
μLCF/μmol lipid	37 °C			41 °C			45 °C		
	0	25	250	0	25	250	0	25	250
1.6 ± 0.1	2.6 ± 0.4	12.6 ± 0.2	18.1 ± 1.9	5.7 ± 0.4	26.9 ± 3.5	32.2 ± 3.3	4.6 ± 0.9	10.8 ± 1.2	10.9 ± 1.5

[a] Particle size measured as Z average mean.
[b] ζ-potential determined by laser-Doppler anemometry.
[c] Bulk encapsulated drug concentration in the liposomes suspension (for CPT-11 loaded liposomes).
[d] Determined by carboxyfluorescein dye retention (for empty liposomes).

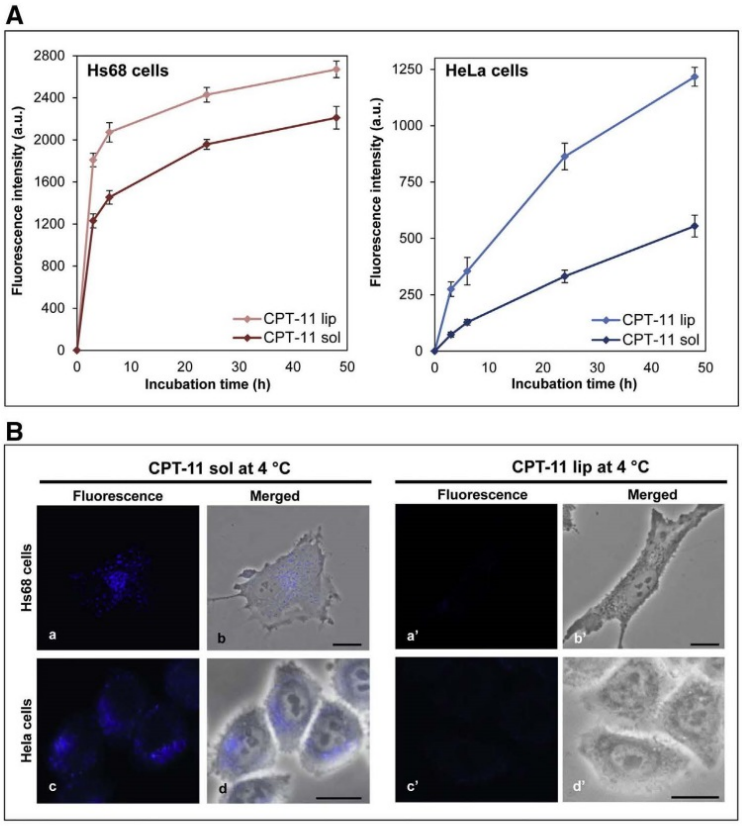

Fig. 1. Uptake and mechanisms of cell entry of CPT-11sol and CPT-11lip into Hs68 and HeLa cells. A) The graphs show the quantitative analysis of the internalization of CPT-11 in Hs68 (a) and HeLa (b) cells carried out by flow cytometry. Cells were incubated with 100 μM CPT-11lip (light symbols) or 100 μM CPT-11sol (dark symbols) for different periods of time, at 37 °C. Emission fluorescence at 450 nm was determined after excitation at 405 nm. Data are the means ± SD from three different experiments. Significance was assessed using a Student's paired *t*-test, being $P < 0.0014$ and $P < 0{,}018$ for Hs68 and HeLa cells, respectively. B) Incubations with CPT-11lip and CPT-11sol for 3 h at 4 °C visualized by fluorescence (UV excitation) and merged images with phase-contrast microscopy. (a, b) Hs68 cells incubated with CPT-11sol. (c, d) HeLa cells incubated with CPT-11sol. (a′, b′) Hs68 cells incubated with CPT-11lip. (c′, d′) HeLa cells incubated with CPT-11lip. Scale bar: 10 μm.

determine the effect of new agents or therapies on cell viability to avoid generating misleading results (Rello-Varona et al., 2015).

Wei et al. (2013) have also reported a study about the preparation and evaluation of two CPT-11 liposomal formulations, although the *in vitro* assessment of their cytotoxic effect on four different tumor cell lines gives quite different results from those described in our study. It should be noted, however, some significant differences that hinder the establishment of valid comparisons between the results of both studies. The different lipid composition used in the design of the carrier, the heterogeneous sized procured liposome populations and the experimental conditions and methodology used by Wei et al. (2013). Related to these comments, there are some interesting considerations made by Perche and Torchilin (2013). The authors emphasize on the influence of lipid composition on the release and internalization, endosomal escape strategies and mitochondria targeting when anticancer drugs where formulated in liposomal delivery carriers. In addition, it has also been demonstrated that the efficiency of cellular uptake and the subsequent intracellular processing of liposomes is influenced by both their size and

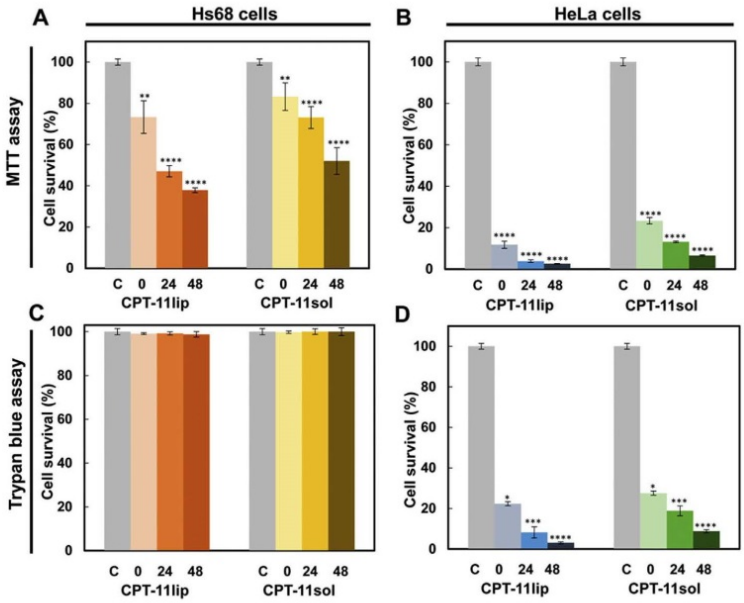

Fig. 2. Cell survival at different times (0, 24 and 48 h) after CPT-11 removal. (A, B) Surviving fraction of Hs68 and HeLa cells incubated 48 h with 100 μM CPT-11lip or CPT-11sol evaluated by MTT assay, respectively. (C, D) Surviving fraction of Hs68 and HeLa cells measured by Trypan blue assay, respectively. Data correspond to mean values ± standard deviation from at least eight different experiments for MTT assay and four different experiments for Trypan blue assay. (For interpretation of the references to colour in this figure legend, the reader is referred to the web version of this article.)

surface characteristics (Andar et al., 2014).

Finally, results of several assays performed in our study with empty liposomes (without CPT-11) evidenced their high degree of biocompatibility and have been incorporated in Supplementary Material (see Figs. S2 and S3).

3.4. Endosomal localization of CPT-11lip in HeLa and Hs68 cells

As can be observed in Fig. 3B, after 24 h incubation with CPT-11lip (100 μM), a similar localization pattern was detected in both cell lines. Blue fluorescence was mainly localized as a granular pattern dispersed in the cytoplasm near the nucleus in HeLa and Hs68 cells. Subcellular localization in the endosomal compartment was confirmed with LysoTracker Red DND-99 (Fig. 3B, c and g). The blue CPT-11 signal co-localizes with the red fluorescence of the labeled endosomes in both cell lines (Fig. 3B, d and h) indicating that endosomal acidic compartment was the main site of CPT-11lip accumulation. Subsequently, CPT-11 would be released from this site to reach the nucleus in order to exert

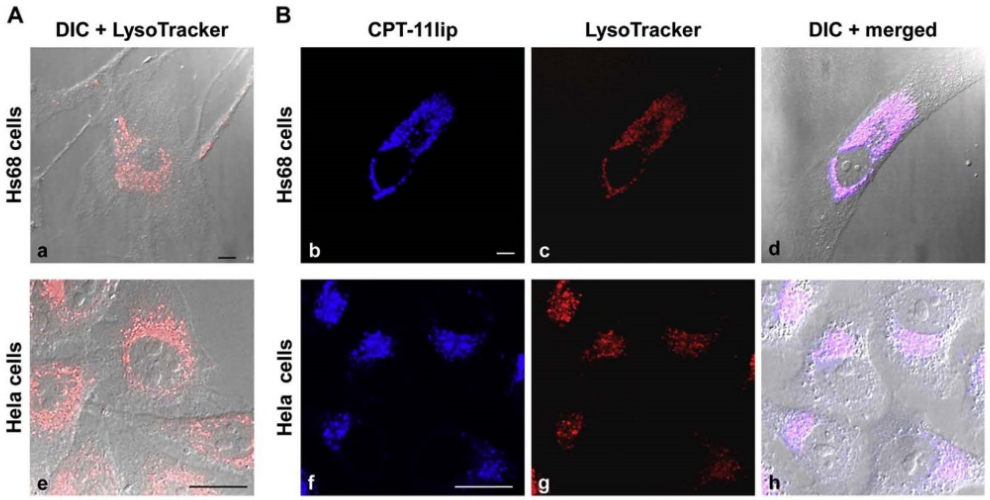

Fig. 3. Analysis of the CTP-11lip localization. A) (a,e) Confocal microscopy fluorescence images of LysoTracker® Green under blue exciting light, merged with differential interference contrast (DIC) microscopy of control Hs68 and HeLa cells, respectively. B) Cells were treated with CPT-11lip (100 μM) for 24 h and counterstained with LysoTracker® Red DND-99, before being observed by DIC and confocal microscopy. (b–d) Hs68 cells show blue fluorescent spots in the cytoplasm that almost completely co-localize with LysoTracker® Red. (f–h) HeLa cells show a similar subcellular distribution pattern. Scale bars: 10 μm. (For interpretation of the references to colour in this figure legend, the reader is referred to the web version of this article.)

their cytotoxic effect as Topo I poison.

There are relatively few studies related to the subcellular localization of CPT derivatives and the published results are somewhat heterogeneous. For instance, water-soluble topotecan has been mainly localized in mitochondria within HT-29 cells (Croce et al., 2004) and in nuclei in MCF-7 breast tumor cells line (Errington et al., 2005), whereas lipophilic gimatecan exhibited a lysosomal localization in HT-29 cells (Croce et al., 2004). These results indicate a quite different behavior of these CPT derivatives and suggest that subcellular distribution plays an important role in their cytotoxic potency. Localization in the endosomal-lysosomal compartment could contribute to the drug potency, because lysosomes represent a store allowing intracellular release of active drug (Croce et al., 2004). In a similar way, namitecan, a hydrophilic CPT derivative whose clinical development is currently ongoing, has been shown to accumulate in lysosomes of both A431 and A431/TPT (resistant to topotecan) cells (Zuco et al., 2010).

3.5. CPT-11lip induces morphological changes in HeLa cells but not in Hs68 cells

The next step was to analyze the time course (0, 24 and 48 h after CPT-11lip removal) of the morphological changes after treatment with 100 μM CPT-11lip, in both cell lines, by toluidine blue staining. As shown in Fig. 4A, Hs68 fibroblasts treated with CPT-11lip did not show any alteration in cell morphology, being the cells attached to the plates, although almost a complete absence of mitotic figures was detected. Starting from plates with the same number of seeded Hs68 cells, the cellular density after incubation with the drug did not increase as compared to non-treated control cells. Therefore, Hs68 fibroblasts seem to lose the ability to replicate during their treatment with CPT-11lip.

On the contrary, HeLa cells showed significant morphological changes, depending on time elapsed after the end of CPT-11lip treatment. As can be seen in Fig. 4B, after 0, 24 and 48 h of drug removal the cell density was considerably lower compared to control cultures and the great majority of cells (95%) became detached from the plates and appeared as floating cells in the culture medium, showing an altered cell shape with large and lateralized nucleus. Furthermore, 24 and 48 h after treatment, the few HeLa cells still attached to the plates were larger and flatter than control cells and had long cytoplasmic projections. Based on these morphological results, we hypothesized that in response to CPT-11lip treatment, apoptosis was triggered in detached HeLa cells, whilst attached cells showed long and thin cellular extensions.

To our knowledge similar studies have not been described previously for any CPT derivative. Several studies have shown that CPT-11 incorporated into liposomes is more effective than the free drug (Ramsay et al., 2008; Carnevale and Ko, 2016). Recent reviews have highlighted important advantages of liposomal formulations of chemotherapeutic agents, with an increased efficacy and reduced toxicity compared to un-entrapped drugs in cancer therapy (Perche and Torchilin, 2013; Allen and Cullis, 2013).

The different cell line sensitivity to CPT-11lip is in agreement with previous data in the literature. Rudolf et al. (2012) reported that CPT-11 induces apoptosis in normal colonic epithelial cells, whereas premature senescence was the prevalent response in normal colonic fibroblasts from mesenchymal origin. Also, the authors analyze the CPT-11 cytotoxic effects against HCT-116 cells (human colorectal carcinoma cell line). Comparing our results with those reported by the authors, liposomes appear to serve as an effective carrier system for CPT-11 delivery, since using equal exposure time (48 h), quarter-doses (100 μM *vs.* 250 μg/mL ≈ 370 μM) are required to kill a greater percentage of tumor cells (90% Hela cells *vs.* 73% HCT-116 cells).

3.6. CPT-11lip triggers massive apoptosis in Hela cells

LDH activity in the culture medium of CPT-11lip treated HeLa cells and Hs68 fibroblasts was the same as that present in the culture medium of controls (Fig. 5A), indicating that the cytosolic membrane of both cell lines conserves its integrity after drug exposure and allows to discard the involvement of necrotic processes (Chan et al., 2013).

Detached HeLa cells stained with H-33258 after 48 h of incubation with CPT-11lip, showed typical apoptotic features (Fig. 5B). Cells became rounded with chromatin condensed and fragmented, and packed into apoptotic bodies.

The involvement of mitochondrial apoptotic pathway as the main mechanism of HeLa cell death after treatment with CPT-11lip was supported by indirect immunofluorescence staining of diffuse green cytoplasmic fluorescence for Bax around the blue nuclear emission by H-33258 (Fig. 5C, a) (Rello-Varona et al., 2015). In contrast, immediately after treatment with CPT-11lip an increased intensity of the green signal for Bax, concentrated in structures corresponding to mitochondria, could be observed in the few attached HeLa cells (Fig. 5C, b and c). In addition to the relocation of the Bax protein, these cells showed nuclei with condensed and fragmented chromatin (H-33258 staining).

Furthermore, the analysis of images obtained under the inverted microscope and performed at different times of evaluation (before and after 48 h treatment), showed that the incubation with empty liposomes did not produce morphological alterations. On the contrary, after 48 h of CPT-11lip treatment, the few cells that were still attached to the culture substrate showed apoptotic characteristics (see Fig. S3).

3.7. Different responses of CPT-11lip in both cell lines related to cell cycle and senescence

Taking into account the different cytotoxic responses of Hs68 and HeLa cells to CPT-11lip, we proceeded to analyzed different physiological cellular parameters that might be involved in the different behavior of both cell types.

First, we analyzed the effects on cell cycle phase distribution on both cell lines, immediately, 24 and 48 h post-treatment after treatment with 100 μM CPT-11lip for 48 h. As can be seen in Fig. 6 A and B, we detected that CPT-11lip induced a marked G2/M arrest and polyploidization in HeLa cells, but not in Hs68 cells.

For Hs68 fibroblasts, the amount of cells in the sub G1 phase (apoptotic cell population), after CPT-11lip treatment, was negligible and aneuploidization-tetraploidization (> 4C) was only slightly and transiently promoted after CPT-11lip removal. 24 h after withdrawing the drug an increase in the percentage of cells in S and G2/M phases (29% and 20%, respectively) was detected in Hs68 cells. However, after 48 h, these values were reduced to 18% and 7%, respectively. Moreover, 24 h after drug removal, a significant decrease of the G0/G1 phase (42%) was observed but a new increase in the percentage of this cell cycle phase (62%) was obtained after 48 h post-treatment.

On the contrary, HeLa cells (Fig. 6B) cycle kinetics following CPT-11lip showed: i) a significant increase of the peak placed in the sector corresponding to apoptotic cells (sub G1); ii) a cell cycle arrest in G2/M, with a maximum value at 24 h, and iii) a progressive polyploidization of HeLa cells (42%) at 48 h after withdrawing CPT-11lip. It is important to note that results related to cell cycle changes in both cell lines were consistent with morphological, cytotoxic and apoptotic assays mentioned above.

In order to test if senescence was triggered in attached HeLa cells and in non-proliferating Hs68 cells after incubation with CPT-11lip, we carried out the β-galactosidase assay at different elapsed times (2 and 5 days) after drug removal. Senescent-associated β-galactosidase (SA-β-gal) cells can be visualized as a blue perinuclear staining under phase contrast microscopy. SA-β-gal positive cells were counted and their amount was referred to the total number of cells on the plate (Fig. 6C).

Hs68 cells appear to enter in a quiescent state only as a transient response and the percentage of positive SA-β-gal Hs68 cells was reduced from 72%, when the drug was removed, until 12% after five days

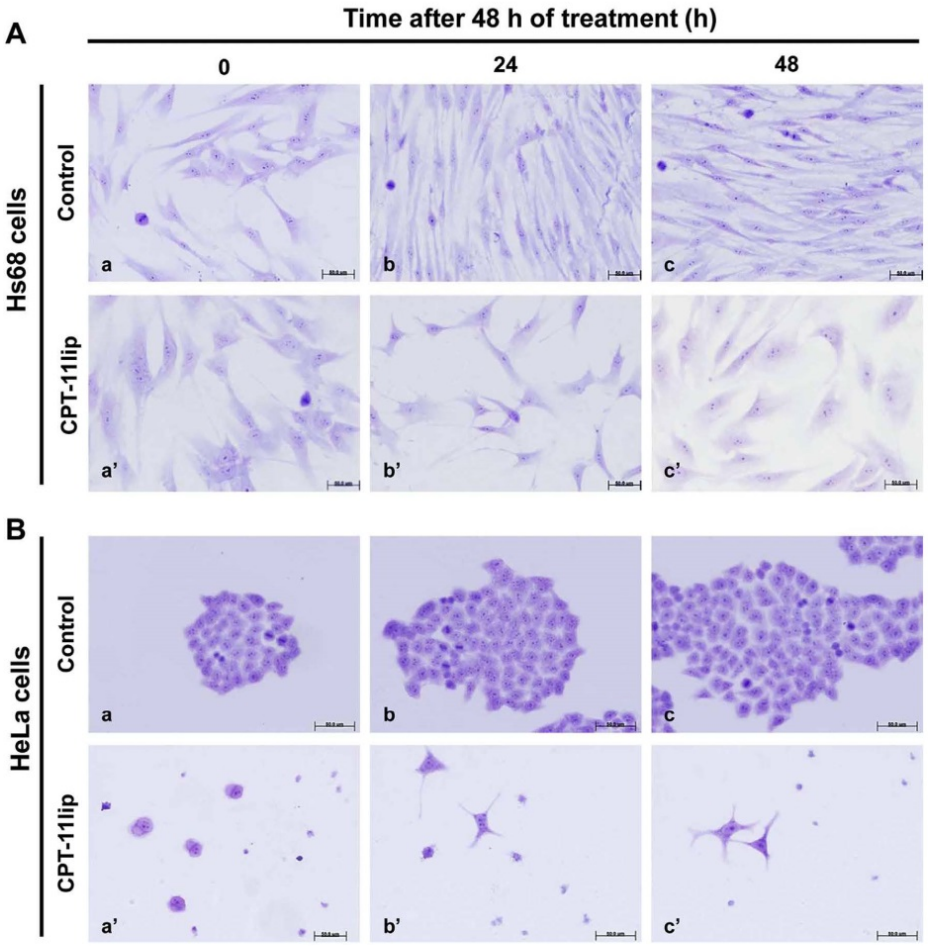

Fig. 4. Morphological changes after treatment. Cell morphology visualized by toluidine blue staining immediately, 24 and 48 h after CPT-11lip treatment. A) Analysis of Hs68 cells. (a–c) Untreated (control) Hs68 cells. (a′-c′) Treated Hs68 cells: CPT-11lip did not cause loss of cell adhesion or cell morphology changes in Hs68 cells at different times after incubation. B) Analysis of HeLa cells. (a–c) Control HeLa cells. (a′–c′) Treated HeLa cells: the vast majority of HeLa cells were detached from plastic after CPT-11lip incubation. Note that the few remaining adherent cells changed their shape and size. (For interpretation of the references to colour in this figure legend, the reader is referred to the web version of this article.)

of its removal, but without enlarged cell size (Fig. 6D).

By contrast, the surviving HeLa cells after treatment with CPT-11lip, though few and clearly recognizable as tetraploid cells because of its increased size, had higher records of senescent response than Hs68 fibroblasts. The quantitative results show that the percentage of senescent HeLa cells increased progressively with the time elapsed after the removal of the drug, being 92.6% within five days. In summary, our results indicate that some HeLa cells can survive after treatment with CPT-11lip, remaining in a state of senescence, whereas Hs68 fibroblasts temporarily enter a growth arrest but they become proliferative cells again after drug withdrawal.

Therefore, these results may reflect that Hs68 suffered a temporary and reversible entry in cell cycle arrest, different to senescence as proposed by Blagosklonny (2011). On the contrary, at the same time interval after drug removal, scarce HeLa cells can survive after treatment with CPT-11lip, remaining still attached to the substrate, being positive for SA-β-gal and showing a senescent phenotype. Our findings in HeLa cells are consistent with those of Haug et al. (2008) in human colon cancer cell lines: G2/M arrest, growth inhibition, polyploidization, cell death (96 h after treatment), and senescence phenotype in two cell lines, treated with CPT-11.

3.8. Effect of CPT-11lip on p53, Bax and Bcl-2 mRNA expression profiles

Finally, the expression levels of *TP53* (p53), *BAX* (Bax) and *BCL-2* (Bcl-2) mRNA at 3, 6, 24 and 48 h after incubation of Hs68 and HeLa cells with CPT-11lip were studied by real-time PCR. As shown in Fig. 7A, time-course experiments revealed that in Hs68 cells, p53 expression was slightly but significantly induced in treated cells compared with untreated control cells at 3 and 48 h after CPT-11lip incubation. Regarding the expression of Bax mRNA, no significant changes were detected at the different time intervals post-treatment analyzed. On the contrary, mRNA induction of Bcl-2 was significantly down-regulated after 6, 24 and 48 h of CPT-11lip treatment, compared to control Hs68 cells (without CPT-11lip treatment). In HeLa cells, p53 mRNA expression was also up-regulated from 3 until 24 h compared with control (Fig. 7B). Furthermore, our results of RT-PCR indicated that in the response of HeLa cells to CPT-11lip, a drastic decrease in expression level

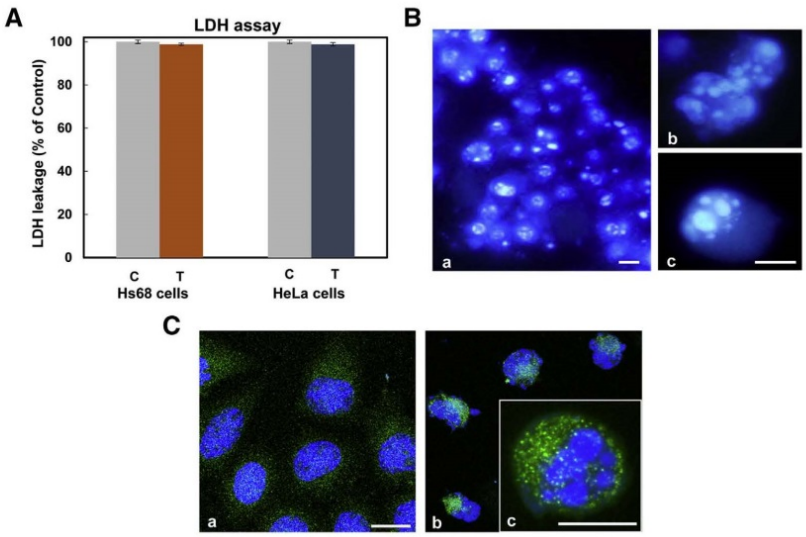

Fig. 5. Identification of apoptotic HeLa cells death induced by 100 μM CPT-11lip. A) LDH assay results. Statistical analysis showed that there was no significant difference between the control (C) and CPT-11lip treated (T) cells. B) Detached HeLa cells after 48 h of incubation with liposomal CPT-11 stained with H-33258. (a) Low magnification. (b, c) Images taken at a higher magnification. Scale bars 10 μm. C) Confocal fluorescence merged images of HeLa cells visualized by Bax immunofluorescence (green) and H-33258 counterstaining of nuclei (blue). (a) Control cells with diffuse Bax signal in the cytosol. (b) Images of translocation of Bax protein from the cytosol into mitochondria of HeLa cells. Scale bars: 10 μm. (c) Apoptotic cell at higher magnification. (For interpretation of the references to colour in this figure legend, the reader is referred to the web version of this article.)

of Bcl-2 was produced after 3 h of incubation with a slight but significant increase in Bax expression after 48 h of treatment. These results are consistent with massive apoptotic induction.

Our results related to mRNA levels of p53 in Hs68 cells indicated that the temporary cell arrest in Hs68 cells did not imply the continuous increase in p53 expression levels. In this sense, Michishita et al. (1998) have described that inhibitors of DNA topoisomerases induced arrest in cell division in human embryonic fibroblasts with SA-β-gal and without changes in p53 expression, but with cell growth upon inhibitors removal. Several publications have reported a p53-dependent senescence program in response to DNA damaging agents in different types of cells (Rudolf et al., 2012; Kim et al., 2015). On the other hand, CPT-11lip induced in HeLa cells a massive apoptotic response, which seems not being related to p53 status. It is well known that HeLa cells express wild-type p53, but the protein product is human papillomavirus inactivated and rapidly degraded (Kralj et al., 2003), so DNA damage in these cells could not be repaired, and a p53-independent apoptotic route was triggered by CPT-11lip on HeLa cells. These findings agree well with other published results (Shao et al., 2001; Rudolf et al., 2011), so CPT seems to trigger apoptosis through p53-dependent and -independent pathways.

3.9. Cytoskeleton organization of cells treated with CPT-11lip

To get additional insight into the global mechanism of inactivation of both cell lines underlying CPT-11lip cellular responses, the effects of incubation with CPT-11lip on the organization and distribution of F-actin microfilaments and on vinculin, a focal adhesion-associated

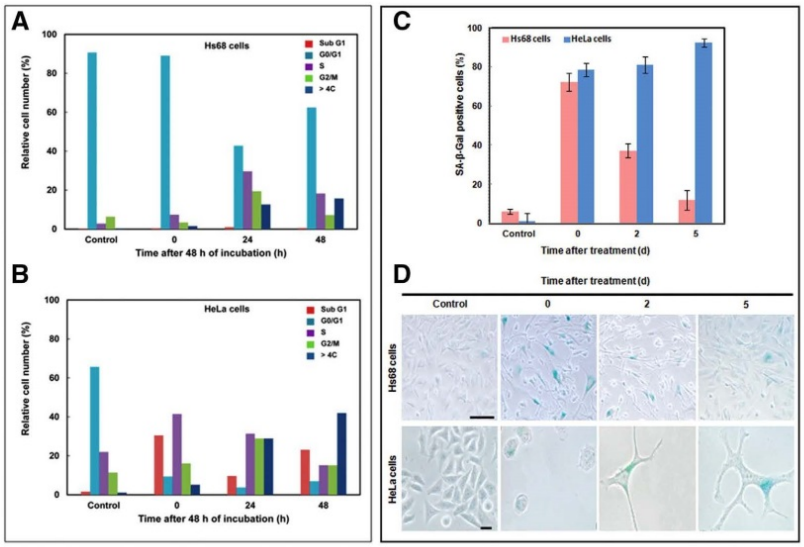

Fig. 6. Cell cycle analysis and senescence-associated β-galactosidase assay. (A, B) Effects of CPT-11lip on cell cycle phase distribution on Hs68 and HeLa cells, respectively. Results were obtained from two independent experiments. For each experiment, a minimum of 20,000 events were analyzed. (C) Cellular senescence-associated β-galactosidase activities at 0 (immediately), 2 and 5 days after incubation. Percentages of senescent cells referred to the total amount of cells on the plate. Results are the mean of three different experiments ± SD. (D) Images correspond to a representative assay. Scale bars: 10 μm.

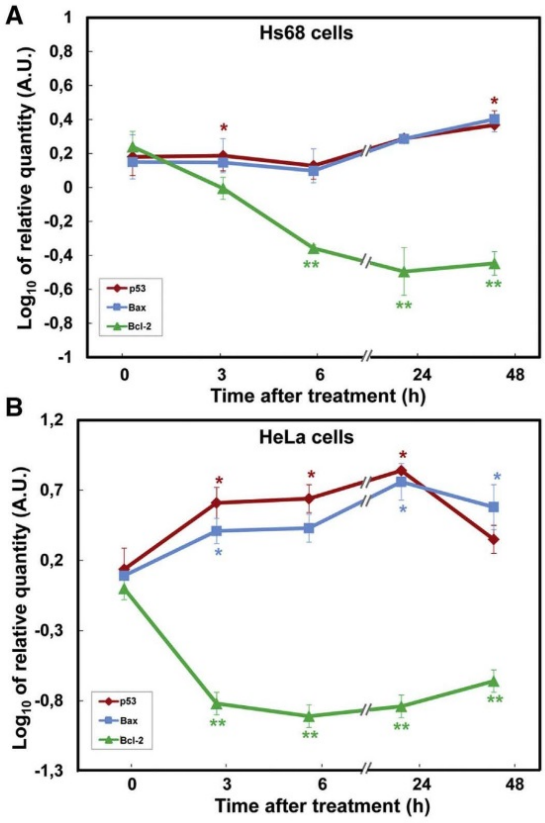

Fig. 7. Time-dependent effects of incubation with CPT-11lip on mRNA expression levels of p53, Bax and Bcl-2 by real-time PCR assay. A) RT-PCR in Hs68 cells. B) RT-PCR in HeLa cells. GAPDH mRNA was used as an internal control. Results are represented as the log10 of the relative quantity normalized to control cells. Data are means ± SD from at least three different experiments. Significance was assessed using Student's *t*-test: $*P < 0.05$, and $**P < 0.005$.

protein, at different post-incubation times (0, 24 and 48 h), were investigated.

Fig. 8 shows the sequence of events related to F-actin microfilaments and vinculin, leading to the death of HeLa cells by apoptosis and a reversible cell cycle arrest with temporary absence of proliferation of Hs68 cells. Confocal microscopy analysis of Hs68 samples revealed that CPT-11lip did not show, at all times selected, any alteration on F-actin and vinculin, which appeared at both ends of stress fibers as part of the focal adhesion, similar to control cells (see Fig. 8A).

On the contrary, attached HeLa cells at the end of treatment exhibited profound changes either in cell size and morphology, as well as in F-actin distribution, throughout the different time points studied (see Fig. 8B). Immediately after drug removal, attached HeLa cells presented a completely disorganized F-actin cytoskeleton with a dramatic increase in the vinculin signal and a partial cell rounding, which might represent an obstacle for the cell adhesion to substrate.

As time goes by, attached HeLa cells suffered other morphological changes and 24 h after drug removal, cells showed long extensions, like large filopodia, containing F-actin. These results directly correlate to the morphological changes observed on HeLa cells with toluidine blue staining (see Fig. 4). Likewise, 48 h after CPT-11lip treatment actin stress fibers and vinculin in focal adhesion were still found.

It is also important to note the general increase in size of cells, at the same time as the cell nucleus grows to almost 30 μm and its location in the cell is polarized.

These results were not surprising, since changes in size and cell morphology in attached HeLa cells must be due to cytoskeleton reorganisation. In this respect, cytoskeleton of senescent cells has been mainly studied using senescent and young skin fibroblasts. It has been reported that senescent cells developed a long and dense vimentin network, long and thin actin fibers, and numerous small focal contact sites (Nishio and Inoue, 2005).

3.10. Different cell line response to DNA damage

As part of our efforts to unravel CPT-11lip's mechanisms of action, we examined DNA double-strand breaks (DSBs) accumulation at different times (3, 6, and 24 h) after CPT-11lip incubation by immunodetection of the phosphorylated histone gamma-H2AX (Fig. 9). It is well known that the phosphorylation of histone H2AX at serine 139 (γ-H2AX) is the most sensitive molecular marker of DNA damage and repair in cells exposed to ionizing radiation or DNA-damaging chemotherapeutic drugs, given its specificity and sensitivity (Sharma et al., 2012).

As can be seen, an accumulation of DNA damage over time was detected in HeLa cells (Fig. 9B). On the contrary, the results obtained in Hs68 cells suggested that normal cells were able to repair CPT-11 induced DNA damage (Fig. 9A). These results are specific for CPT-11lip, as empty liposomes did not significantly induce DNA damage (see Fig. S2). The percentage of cells positive for γ-H2AX immunofluorescence revealed DNA damage of Hs68 cells at 3 h incubation with CPT-11lip. However, the positive cells were significantly reduced at 6 and 24 h of CPT-11lip administration. On the other hand, the percentage of positive HeLa cells was rapidly increased following exposure to CPT-11lip and virtually 100% of HeLa cells were positively labeled at 24 h of incubation. These results indicate that CPT-11 formulated in liposomes is capable of reach the cell nucleus after its release from carrier (liposomes), exerting a cytotoxic effect on HeLa cells but not in non-transformed Hs68 cells.

Similar to our findings, Tamura et al. (2012) evaluated the effect of three Topo I inhibitors (camptothecin, CPT-11 and SN-38) using cultures of 15 cell lines of human tumors and normal cells, and all Topo I poisons were shown to be more cytotoxic for tumor cell lines than for normal mesenchymal and epithelial cells.

Taken together, these results indicate that liposomes possess the following *in vitro* properties for the success of CPT-11 delivery: i) liposomes demonstrated both stability and high encapsulation efficiency, as well as biocompatibility (without CPT-11); ii) CPT-11lip were efficiently internalized by an endocytic process into both cell lines with a lysosomal subcellular accumulation; iii) CPT-11lip was not cytotoxic to normal fibroblast Hs68 cells, but induced a massive apoptosis, accompanied by cell senescence, in HeLa cells; iv) CPT-11 can be released from lysosomes and reach the cell nucleus; and v) DNA damage triggers different cellular responses: a p53-dependent Hs68 cell survival and a p53-independent apoptotic response in HeLa cells.

These remarkably different responses might constitute the basis for a promising approach to reduce the side effects associated to CPT-11 treatments. Anyhow, assessment of chemotherapeutic potential of new pharmaceutical formulations requires a detailed knowledge of its underlying mechanism of action, as a first step in the pharmacological study of the drug, by means of *in vitro* experiments with cell cultures before the *in vivo* assays (He et al., 2017). In addition, new studies to identify the different signaling pathways triggered by CPT-11lip in these and other cell types will be performed before long. If the results are as expected, experimental assays *in vivo* will be then carried out.

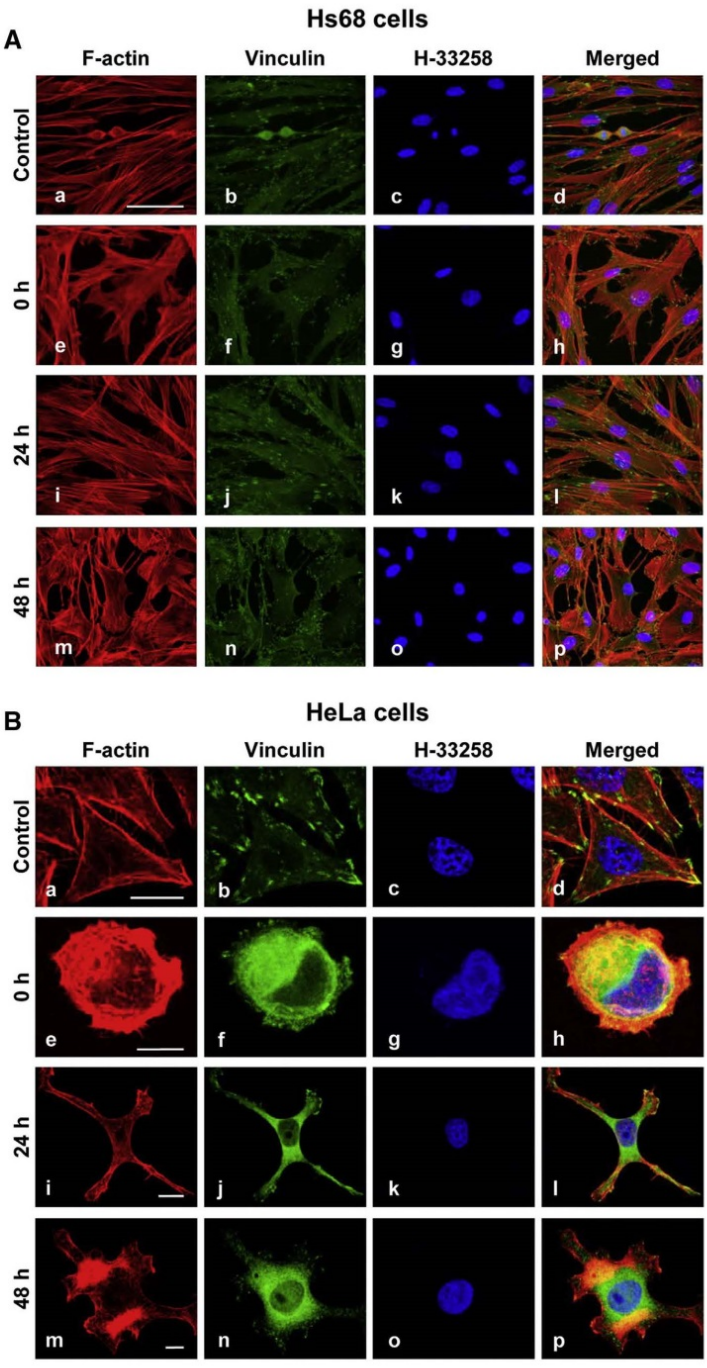

Fig. 8. F-actin and vinculin in Hs68 and HeLa cells after incubation with CPT-11lip. A) Cytoskeleton confocal images of Hs68 cells observed in control (a–d) and immediately, 24 or 48 h (e–p) after drug removal, respectively. B) The same analysis was performed in HeLa cells. F-actin structures are shown in red (stained with phalloidin-TRITC), green corresponds to immunolabelling of vinculin, the blue signal refers to chromatin (stained with H-33258), and last column to overlay images. The cells shown in each panel are representative of predominant morphologies observed in four separate experiments. Scale bars: 20 μm. (For interpretation of the references to colour in this figure legend, the reader is referred to the web version of this article.)

4. Conclusions

The development of new anticancer drug delivery systems has undergone a spectacular development over the last years, and a variety of nanocarriers, including liposomal devices, are being tested. Here, we present a comparative study of the cytotoxic effects induced by CPT-11 encapsulated into liposomes in two human cell lines: HeLa (cervix adenocarcinoma) and Hs68 (foreskin fibroblasts). Our findings indicate

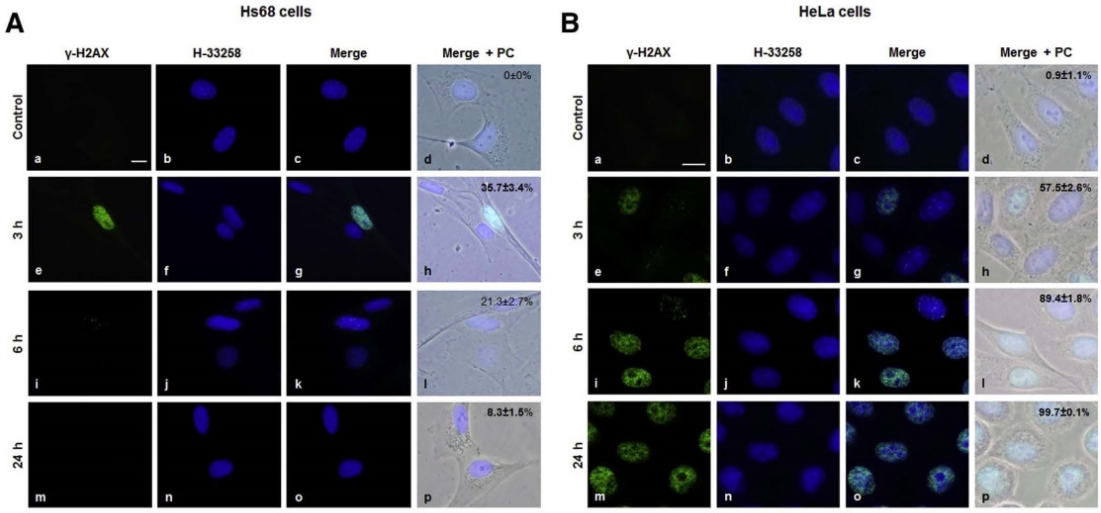

Fig. 9. Immunofluorescent analysis of γ-H2AX. A) Representative images of Hs68 cells immunostaining to H2AX γ-phosphorylated histone (green), counterstained with H-33258 (blue), merged images and overlay of fluorescence and phase-contrast microscopy (PC) at three different incubation times with CPT11-lip. (a–d) Control Hs68 cells. (e–h), (i–l), (m–p) Cells after 3, 6 and 24 h of incubation, respectively. B) Representative images of HeLa cells under the same experimental conditions. Scale bars: 10 μm. The percentage of cells positive for γ-H2AX immunofluorescence has been included in the images of the right column. Values represent means ± standard deviation of three independent experiments in which at least 200 cells were counted for each experimental condition. (For interpretation of the references to colour in this figure legend, the reader is referred to the web version of this article.)

that phospholipid-cholesterol liposomes possess optimum properties in order to be considered as suitable CPT-11 carriers. To our knowledge, it is the first time that a deep and multiparametric research (subcellular localization, cytotoxic effect and activation of signaling pathways) has been carried out using two cell lines with different gene profiles, justifying a chemotherapeutic drug (CPT-11) formulation in liposomes.

Acknowledgements

This work was supported by the Spanish Ministry of Economy and Competitiveness (grant numbers CTQ2013-48767-C3-1-R, CTQ2013-48767-C3-3-R), Comunidad de Madrid (S2013/MIT-2850) and Govern de la Generalitat de Catalunya (2009SGR-367). A. Casadó thanks to the University of Barcelona for a predoctoral fellowship and P. Acedo gratefully acknowledge postdoctoral fellowship support from the Ramón Areces Foundation. We recognise the valuable contribution of Sylvia Gutiérrez (Confocal Microscopy, Centro Nacional de Biotecnología, Madrid).

Appendix A. Supplementary data

Supplementary data to this article can be found online at http://dx.doi.org/10.1016/j.ejps.2017.07.024.

References

Allen, M.T., Cullis, P.R., 2013. Liposomal drug delivery systems: from concept to clinical applications. Adv. Drug Deliv. Rev. 65, 36–48. http://dx.doi.org/10.1016/j.addr.2012.09.037.

Andar, A.U., Hood, R.R., Vreeland, W.N., DeVoe, D.L., Swaan, P.W., 2014. Microfluidic preparation of liposomes to determine particle size influence on cellular uptake mechanisms. Pharm. Res. 31, 401–413. http://dx.doi.org/10.1007/s11095-013-1171-8.

Blagosklonny, M.V., 2011. Cell cycle arrest is not senescence. Aging 3, 94–101. http://dx.doi.org/10.18632/aging.100281.

Bozzuto, G., Molinari, A., 2015. Liposomes as nanomedical devices. Int. J. Nanomedicine 10, 975–999. http://dx.doi.org/10.2147/IJN.S68861.

Burke, T.G., Bom, D., 2000. Camptothecin design and delivery approaches for elevating anti-topoisomerase I activities in vivo. Ann. N. Y. Acad. Sci. 922, 36–45. http://dx.doi.org/10.1111/j.1749-6632.2000.tb07023.x.

Burke, T.G., Gao, X., 1994. Stabilization of topotecan in low pH liposomes composed of distearoylphosphatidylcholine. J. Pharm. Sci. 83, 967–969. http://dx.doi.org/10.1002/jps.2600830710.

Carnevale, J., Ko, A.H., 2016. MM-398 (nanoliposomal irinotecan): emergence of a novel therapy for the treatment of advanced pancreatic cancer. Future Oncol. 12, 453–464. http://dx.doi.org/10.2217/fon.15.333.

Casadó, A., Sagristá, M.L., Mora, M., 2014. Formulation and in vitro characterization of thermosensitive liposomes for the delivery of irinotecan. J. Pharm. Sci. 103, 3127–3138. http://dx.doi.org/10.1002/jps.24097.

Casadó, A., Giuffrida, M.C., Sagristá, M.L., Castelli, F., Pujol, M., Alsina, M.A., Mora, M., 2016. Langmuir monolayers and differential scanning calorimetry for the study of the interactions between camptothecin drugs and biomembrane models. Biochim. Biophys. Acta 1858, 422–433. http://dx.doi.org/10.1016/j.bbamem.2015.12.007.

Chan, F.K.-M., Moriwaki, K., De Rosa, M.J., 2013. Detection of necrosis by release of lactate dehydrogenase (LDH) activity. Methods Mol. Biol. 979, 65–70. http://dx.doi.org/10.1007/978-1-62703-290-2_7.

Chen, A.Y., Liu, L.F., 1994. DNA topoisomerases: essential enzymes and lethal targets. Annu. Rev. Pharmacol. Toxicol. 34, 191–218. http://dx.doi.org/10.1146/annurev.pa.34.040194.001203.

Chu, E., 2012. An update to the current and emerging targeted agents in metastatic colorectal cancer. Clin. Colorectal Cancer 11, 1–13. http://dx.doi.org/10.1016/j.clcc.2011.05.005 16.

Chustecka, Z., 2015. Liposomal Irinotecan (MM-398) Approved in Pancreatic Cancer. Medscape Oct 22. http://www.medscape.com/viewarticle/853072 accessed 15.10.22.

Croce, A.C., Bottiroli, G., Supino, R., Favini, E., Zuco, V., Zunino, F., 2004. Subcellular localization of the camptothecin analogues, topotecan and gimatecan. Biochem. Pharmacol. 67, 1035–1045. http://dx.doi.org/10.1016/j.bcp.2003.10.034.

De Jong, W.H., Borm, P.J., 2008. Drug delivery and nanoparticles: applications and hazards. Int. J. Nanomedicine 3, 133–149.

Deshpande, P.P., Biswas, S., Torchilin, V.P., 2013. Current trends in the use of liposomes for tumor targeting. Nanomedicine (London) 8, 1–32. http://dx.doi.org/10.2217/nnm.13.118.

Diaz-Rubio, E., 2004. New chemotherapeutic advances in pancreatic, colorectal and gastric cancers. Oncologist 9, 282–294. http://dx.doi.org/10.1634/theoncologist.9-3-282.

Drummond, D.C., Noble, C.O., Hayes, M.E., Park, J.W., Kirpotin, D.B., 2008. Pharmacokinetics and in vivo drug release rates in liposomal nanocarrier development. J. Pharm. Sci. 97, 4696–4740. http://dx.doi.org/10.1002/jps.21358.

Eloy, J.O., de Souza, M.C., Petrilli, R., Barcellos, J.P., Lee, R.J., Marchetti, J.M., 2014. Liposomes as carriers of hydrophilic small molecule drugs: strategies to enhance encapsulation and delivery. Colloids Surf. B: Biointerfaces 123, 345–363. http://dx.doi.org/10.1016/j.colsurfb.2014.09.029.

Errington, R.J., Ameer-Beg, S.M., Vojnovicb, B., Patterson, L.H., Zloh, M., Smith, P.J., 2005. Advanced microscopy solutions for monitoring the kinetics and dynamics of drug–DNA targeting in living cells. Adv. Drug Deliv. Rev. 57, 153–167. http://dx.doi.org/10.1016/j.addr.2004.05.005.

Estanqueiro, M., Amaral, M.H., Conceicão, J., Sousa Lobo, J.M., 2015. Nanotechnological carriers for cancer chemotherapy: the state of the art. Colloids Surf. B: Biointerfaces

126, 631–648. http://dx.doi.org/10.1016/j.colsurfb.2014.12.041.
García-Carbonero, R., Supko, J.G., 2002. Current perspectives on the clinical experience pharmacology, and continued development of the camptothecins. Clin. Cancer Res. 8, 641–661.
Hattori, Y., Shi, L., Ding, W., Koga, K., Kawano, K., Hakoshima, M., Maitani, Y., 2009. Novel irinotecan-loaded liposome using phytic acid with high therapeutic efficacy for colon tumors. J. Control. Release 136, 30–37. http://dx.doi.org/10.1016/j.jconrel.2009.01.013.
Haug, K., Kravik, K.L., De Angelis, P., 2008. Cellular response to irinotecan in colon cancer cell lines showing differential response to 5-fluorouracil. Anticancer Res. 28, 583–592. http://dx.doi.org/10.1158/0008-5472.CAN-14-0683.
He, R., Du, Y., Ling, L., Ismail, M., Hou, Y., Yao, C., Li, X., 2017. Nanoformulation of dual bexarotene-tailed phospholipid conjugate with high drug loading. Eur. J. Pharm. Sci. 100, 197–204. http://dx.doi.org/10.1016/j.ejps.2017.01.012.
Hegde, S.R., Manimaran, P., Mande, S.C., 2008. Systemic and targeted therapy for advanced colon cancer. Expert Rev. Gastroenterol. Hepatol. 2, 135–149. http://dx.doi.org/10.1586/17474124.2.1.135.
Hind, D., Tappenden, P., Tumur, I., Eggington, S., Sutcliffe, P., Ryan, A., 2008. The use of irinotecan, oxaliplatin and raltitrexed for the treatment of advanced colorectal cancer: systematic review and economic evaluation. Health Technol. Assess. 12. iii-ix, xi-162. http://dx.doi.org/10.3310/hta12150.
Hsiang, Y.H., Hertzberg, R., Hecht, S., Liu, L.F., 1985. Camptothecin induces protein-linked DNA breaks via mammalian DNA topoisomerase I. J. Biol. Chem. 260, 14873–14878.
Iyer, R., Croucher, J.L., Chorny, M., Mangino, J.L., Alferiev, I.S., Levy, R.J., Venkatadri, Kolla, Brodeur, G.M., 2015. Nanoparticle delivery of an SN38 conjugate is more effective than irinotecan in a mouse model of neuroblastoma. Cancer Lett. 360, 205–212. http://dx.doi.org/10.1016/j.canlet.2015.02.011.
Juillerat-Jeanneret, L., Schmitt, F., 2007. Chemical modification of therapeutic drugs or drug vector systems to achieve targeted therapy: looking for the grail. Med. Res. Rev. 27, 574–590. http://dx.doi.org/10.1002/med.20086.
Kim, R.H., Kang, M.K., Kim, T., Yang, P., Bae, S., Williams, D.W., Phung, S., Shin, K.H., Hong, C., Park, N.H., 2015. Regulation of p53 during senescence in normal human keratinocytes. Aging Cell 14, 838–846. http://dx.doi.org/10.1111/acel.12364.
Köhne, C.-H., Lenz, H.-J., 2009. Chemotherapy with targeted agents for the treatment of metastatic colorectal cancer. Oncologist 14, 478–488. http://dx.doi.org/10.1634/theoncologist.2008-0202.
Kralj, M., Husnjak, K., Körbler, T., Pavelić, J., 2003. Endogenous p21WAF1/CIP1 status predicts the response of human tumor cells to wild-type p53 and p21WAF1/CIP1 overexpression. Cancer Gene Ther. 10, 457–467. http://dx.doi.org/10.1038/sj.cgt.7700588.
Lamb, Y.N., Scott, L.J., 2017. Liposomal irinotecan: a review in metastatic pancreatic adenocarcinoma. Drugs 77, 785–792. http://dx.doi.org/10.1007/s40265-017-0741-1.
Liew, S.T., Yang, L.Y., 2008. Design, synthesis and development of novel camptothecin drugs. Curr. Pharm. Des. 14, 1078–1097. http://dx.doi.org/10.2174/138161208784246180.
Liu, X., Situ, A., Kang, Y., Villabroza, K.R., Liao, Y., Chang, C.H., Donahue, T., Nel, A.E., Meng, H., 2016. Irinotecan delivery by lipid-coated mesoporous silica nanoparticles shows improved efficacy and safety over liposomes for pancreatic cancer. ACS Nano 10, 2702–2715. http://dx.doi.org/10.1021/acsnano.5b07781.
Livak, K.J., Schmittgen, T.D., 2001. Analysis of relative gene expression data using real-time quantitative pcr and the 2-ΔΔCT method. Methods 25, 402–408. http://dx.doi.org/10.1006/meth.2001.1262.
Messerer, C.L., Ramsay, E.C., Waterhouse, D., Ng, R., Simms, E.M., Harasym, N., Tardi, P., Mayer, L.D., Bally, Marcel B., 2004. Liposomal Irinotecan: formulation development and therapeutic assessment in murine xenograft models of colorectal cancer. Clin. Cancer Res. 10, 6638–6649. http://dx.doi.org/10.1158/1078-0432.CCR-04-0221.
Michishita, E., Nakabayashi, K., Ogino, H., Suzuki, T., Fujii, M., Ayusawa, D., 1998. DNA topoisomerase inhibitors induce reversible senescence in normal human fibroblasts. Biochem. Biophys. Res. Commun. 253, 667–671. http://dx.doi.org/10.1006/bbrc.1998.9832.
Neijzen, R., Wong, M.Q., Gill, N., Wang, H., Karim, T., Anantha, M., Strutt, D., Waterhouse, D., Bally, M.B., Tai, I.T., Ng, Sylvia S.W., Yapp, D.T., 2015. Irinophore C™, a lipid nanoparticulate formulation of irinotecan, improves vascular function, increases the delivery of sequentially administered 5-FU in HT-29 tumors, and controls tumor growth in patient derived xenografts of colon cancer. J. Control. Release 199, 72–83. http://dx.doi.org/10.1016/j.jconrel.2014.11.031.
Nishio, K., Inoue, A., 2005. Senescence-associated alterations of cytoskeleton: extraordinary production of vimentin that anchors cytoplasmic p53 in senescent human fibroblasts. Histochem. Cell Biol. 123, 263–273. http://dx.doi.org/10.1007/s00418-005-0766-5.
Pattni, B.S., Chupin, V.V., Torchilin, V.P., 2015. New developments in liposomal drug delivery. Chem. Rev. 115, 10938–10966. http://dx.doi.org/10.1021/acs.chemrev.5b00046.
Peetla, C., Stine, A., Labhasetwar, V., 2009. Biophysical interactions with model lipid membranes: applications in drug discovery and drug delivery. Mol. Pharm. 6, 1264–1276. http://dx.doi.org/10.1021/mp9000662.
Perche, F., Torchilin, V.P., 2013. Recent trends in multifunctional liposomal nanocarriers for enhanced tumor targeting. J. Drug Delivery 2013, 705265. 32 pages. http://dx.doi.org/10.1155/2013/705265.
Przybylo, M., Glogocka, D., Dobrucki, J.W., Fraczkowska, K., Podbielska, H., Kopaczynska, M., Borowik, T., Langner, M., 2016. The cellular internalization of liposome encapsulated protoporphyrin IX by HeLa cells. Eur. J. Pharm. Sci. 85, 39–46. http://dx.doi.org/10.1016/j.ejps.2016.01.028.
Ramsay, E., Almajiim, J., Anantha, M., Zastre, J., Yan, H., Webb, M., Waterhouse, D., Bally, M., 2008. A novel liposomal irinotecan formulation with significant anti-tumour activity: use of the divalent cation ionophore A23187 and copper-containing liposomes to improve drug retention. Eur. J. Pharm. Biopharm. 68, 607–617. http://dx.doi.org/10.1016/j.ejpb.2007.08.011.
Rello, S., Stockert, J.C., Moreno, V., Gámez, A., Pacheco, M., Juarranz, A., Cañete, M., Villanueva, A., 2005. Morphological criteria to distinguish cell death induced by apoptotic and necrotic treatments. Apoptosis 10, 201–208. http://dx.doi.org/10.1007/s10495-005-6075-6.
Rello-Varona, S., Herrero-Martín, D., Lopez-Alemany, R., Munoz-Pinedo, C., Tirado, O.M., 2015. "(Not) all (dead) things share the same breath": identification of cell death mechanisms in anticancer therapy. Cancer Res. 75, 913–917. http://dx.doi.org/10.1158/0008-5472.CAN-14-3494.
Rudolf, E., Rudolf, K., Cervinka, M., 2011. Camptothecin induces p53-dependent and –independent apoptogenic signaling in melanoma cells. Apoptosis 16, 1165–1176. http://dx.doi.org/10.1007/s10495-011-0635-8.
Rudolf, E., John, S., Cervinka, M., 2012. Irinotecan induces senescence and apoptosis in colonic cells in vitro. Toxicol. Lett. 214, 1–8. http://dx.doi.org/10.1016/j.toxlet.2012.08.004.
Sen, K., Mandal, M., 2013. Second generation liposomal cancer therapeutics: transition from laboratory to clinic. Int. J. Pharm. 448, 28–43. http://dx.doi.org/10.1016/j.ijpharm.2013.03.006.
Shao, R.-G., Cao, C.-X., Nieves-Neira, W., Dimanche-Boitrel, M.-T., Solary, E., Pommier, Y., 2001. Activation of the Fas pathway independently of Fas ligand during apoptosis induced by camptothecin in p53 mutant human colon carcinoma cells. Oncogene 20, 1852–1859. http://dx.doi.org/10.1038/sj.onc.1204264.
Sharma, A., Singh, K., Almasan, A., 2012. Histone H2AX phosphorylation: a marker for DNA damage. Methods Mol. Biol. 920, 613–626. http://dx.doi.org/10.1007/978-1-61779-998-3_40.
Tamura, N., Hirano, K., Kishino, K., Hashimoto, K., Amano, O., Shimada, J., Sakagami, H., 2012. Analysis of type of cell death induced by topoisomerase inhibitor SN-38 in human oral squamous cell carcinoma cell lines. Anticancer Res. 32, 4823–4832.
Teicher, B.A., 2008. Next generation topoisomerase I inhibitors: rationale and biomarker strategies. Biochem. Pharmacol. 75, 1262–1271. http://dx.doi.org/10.1016/j.bcp.2007.10.016.
Torchilin, V.P., 2005. Recent advances with liposomes as pharmaceutical carriers. Nat. Rev. Drug Discov. 4, 145–160. http://dx.doi.org/10.1038/nrd1632.
Vanhoefer, U., Harstrick, A., Achterrath, W., Cao, S., Seeber, S., Rustum, Y.M., 2001. Irinotecan in the treatment of colorectal cancer: clinical overview. J. Clin. Oncol. 19, 1501–1518.
Wei, H., Song, J., Li, H., Li, Y., Zhu, S., Zhou, X., Zhanga, X., Yanga, L., 2013. Active loading liposomal irinotecan hydrochloride: preparation, in vitro and in vivo evaluation. Asian J. Pharm. Sci. 8, 303–311. http://dx.doi.org/10.1016/j.ajps.2013.10.006.
Wu, M.H., Yan, B., Humerickhouse, R., Dolan, M.E., 2002. Irinotecan activation by human carboxylesterases in colorectal adenocarcinoma cells. Clin. Cancer Res. 8, 2696–2700.
Zuco, V., Supino, R., Favini, E., Tortoreto, M., Cincinelli, R., Croce, A.C., Bucci, F., Pisano, C., Zunino, F., 2010. Efficacy of ST1968 (namitecan) on a topotecan-resistant squamous cell carcinoma. Biochem Pharmacol. 79, 535–541. http://dx.doi.org/10.1016/j.bcp.2009.09.012.

Supplementary Material to

Improved Selectivity and Cytotoxic Effects of Irinotecan via Liposomal Delivery: a Comparative Study on Hs68 and HeLa Cells

Ana Casadó et al.

1. Supplementary Materials and Methods

Preparation of liposomal CPT-11

L-α-distearoyl-phosphatidylcholine (DSPC), L-α-dioleoyl-phosphatidylserine (DOPS) and cholesterol (CHOL) were purchased from Avanti Polar Lipids (Birmingham, USA). Polycarbonate membranes were from Poretics Products (Osmonics, Inc., USA). Irinotecan (CPT-11), purchased from Afine Chemicals Limited (China), was pure with a minimal grade of 99%. All the organic solvents (Panreac, Montcada i Reixac, Spain) have been distilled before use. Milli-Q water (Millipore Bedford, Massachusetts system, resistivity of 18 MΩ.cm) was used. All other chemicals and solvents were of analytical grade. Dulbecco´s Modified Eagle´s Medium with 4.5 g glucose/L (DMEM), fetal calf serum (FCS), L-glutamine and penicillin-streptomycin solutions were provided by Gibco-Life Technologies (UK). Sterile Dulbecco´s Phosphate Buffered Saline (PBS), dimethyl sulphoxide (DMSO), 3-[4,5-dimethylthiazol-2-yl] 2,5-diphenyltetrazolium bromide (MTT), Trypan blue, toluidine blue and Hoechst-33258 (H-33258) were purchased from Sigma-Aldrich Chemical Co. (USA). CytoScan-Fluoro Assay Kit was purchased from G-Biosciences (USA).

Intermediate unilamellar liposomes (IUVs) were prepared by vortexing and extrusion following a procedure previously reported (Casadó *et al.*, 2014). Briefly, lipids, DSPC, DOPS and CHOL, were mixed in a molar ratio of 65:35:30 to prepare the lipid film and CPT-11 was added from a chloroform/methanol (2:1) solution, before the film formation, at a 7.5:1 molar ratio. The film was kept in a desiccator overnight to ensure complete solvent removal. Multilamellar vesicles (MLVs) were prepared by hydrating the dried lipid films in 10 mM lactate buffer (pH 4.4) to a final lipid concentration of 10 mg/mL. MLVs dispersions were frozen (liquid N_2) and thawed (55 °C water bath), above the phase transition temperature (Tm), for five times. For IUVs preparation, MLVs at 55 °C were extruded, using an extrusion device (Lipex Biomembranes, Canada), six times through 400 nm and twelve times through 200 nm polycarbonate membrane filters (Osmonics, USA), to afford a homogeneously sized liposome suspension. Control liposomes without CPT-11 were also prepared.

The designed liposomes were endowed with temperature sensitiveness. Thus, the lipid composition had been carefully chosen, taken into account this characteristic, after an accurate study of the molecular interactions between the constituents of the carrier and the drug by using different biophysical techniques (Casadó *et al.*, 2016). It was demonstrated that CPT-11, positively charged in its piperidine group at acidic pH, interacts electrostatically with the DOPS component of the bilayer making stable the incorporation of a high percentage of the drug into liposomes. The drug, mainly encapsulated in their aqueous space, and in contact with phosphatidylserine species, will remain anchored to the carrier solving the problems associated with the formulation and procurement of liposomal deliveries for drug soluble molecules. The liposomal suspension was characterized by size, polydispersity index and ζ-potential and by quantifying the amount of the drug inside vesicles. Liposomes were visualized by transmission electron microscopy (TEM). Uranyl acetate (1.5%) was used as a negative staining method to visualize the liposomes. Liposomal dispersion was placed on a carbon-Formvar coated copper grid for 1 min, after which 10 μL of negative stain was used for 30 s and excess sample and stain was blotted with filter paper.

Afterwards, the copper grid was air-dried for imaging using a JEOL JEM 1200 EXII electron microscope (JEOL Ltd., Tokyo, Japan). The size, size distribution, and ζ-potential of liposomes were determined by photon correlation spectroscopy (PCS), in a Malvern Zetasizer NANO-ZS device (Malvern Instruments Ltd., Malvern, UK) equipped with an optic unit containing a 5-mW He–Ne laser (Spectra Physics, Santa Clara, CA, USA) and an electrophoresis cell. Total and entrapped CPT-11 was systematically quantified by absorbance spectroscopy as described previously (Casadó *et al.*, 2014). Calibration curves for CPT-11 (0.005–0.02 mg/mL) had been obtained both in 10 mM lactate buffer (pH 4.4) or THF. Liposomal-CPT-11 suspension was centrifuged using Centricon YM-10 Filter Devices (Millipore, USA) to obtain a filtrate containing the non-entrapped drug, without liposomes. The concentration of non-entrapped CPT-11 was determined by comparison with the calibration curve obtained in the same conditions.

Encapsulation percentage and drug concentration inside liposomes were obtained from the difference between total (CPT-11 used to prepare the film) and non-encapsulated amount of drug. Drug encapsulation efficiency and drug loading efficiency were calculated as the amount of drug inside liposomes with respect to the total amount of drug or lipids added in preparing formulation, respectively. The inner aqueous volume of liposomes and the permeability of the liposome bilayers, assessed *in vitro* in a simulated biological medium at different temperatures, were determined by using the fluorescent marker 5(6)-carboxyfluorescein (CF) (Weinstein et al., 1984). The kinetic

data were analyzed from the CF release curves by means the non-lineal regression program Graph Pad Prism (version 5.00).

Cell cultures

Hs68 non-transformed fibroblasts (ATCC® CRL-1635™) and the tumor epithelial cell line HeLa (originated from a cervix adenocarcinoma) (ATCC® CCL-2™), were purchased from American Type Culture Collection (USA). Cells were grown in DMEM supplemented with 50 U/mL penicillin, 50 µg streptomycin/mL and 10% FCS. Cell cultures were performed in a 5% CO_2 atmosphere at 37 °C. Cells were grown for 72 h and treated when cultures were in exponential growth. All sterile plastics were from Corning (USA). Depending on the type of experiment, Hs68 or HeLa cells were seeded in 25 cm^2 flasks, in 24-well plates or in 35 mm Petri dishes with or without a 22 mm square coverslip.

Treatments

Cells were incubated with 100 µM CPT-11 entrapped in liposomes (CPT-11lip) or solubilized in 10 mM lactate buffer pH 4.4 (CPT-11sol), depending on the type of assay, at different times between 0 and 48 h to assess the cellular uptake of the drugs using flow cytometry and at 24 h to visualize subcellular localization by fluorescence microscopy. For cell survival studies, cell cycle analysis and morphological studies, a period of 48 h of incubation with post-incubation times up to 48 h, were used.

Measurement of CPT-11 uptake by flow cytometry

HeLa and Hs68 cells, cultured on 25 cm^2 flasks, were treated with CPT-11lip or CPT-11sol up to 48 h. After incubation, cells were washed twice with PBS, trypsinized and centrifuged at 1200 rpm before final resuspension in 1 mL PBS. CPT-11 fluorescence was measured with a LSR II flow cytometer (BD Biosciences, USA) using excitation and emission wavelengths of 405 and 450 nm, respectively. Three separate experiments were carried out with each cell line and, for each experiment, a minimum of 20,000 cells were analyzed. Significance was assessed using a Student's paired t-test.

Cellular internalization mechanisms of CPT-11

In order to analyze internalization mechanisms of CPT-11, Hs68 and HeLa grown on coverslips were incubated with 100 µM of CPT-11lip or CPT-11sol for 3 h at 4 °C. Then, culture medium was removed, samples were washed three times with PBS and directly observed by fluorescence microscopy (under UV excitation) combined with phase contrast microscopy.

CPT-11lip subcellular localization

Cells grown on coverslips were incubated with 100 µM CPT-11lip for 24 h, washed twice with PBS and directly observed by confocal fluorescence microscopy combined with phase contrast microscopy under UV excitation. After CPT-11 treatment, and to analyze the possible participation of lysosomes in drug accumulation, cells were incubated with 1 mL DMEM containing 50 nM LysoTracker Red DND-99 (Life Technologies) for 30 min, washed three times with PBS and visualized by confocal microscopy.

Analysis of cell morphology

Morphological changes at different times (0, 24 and 48 h) after incubation with 100 µM CPT-11lip were assessed by toluidine blue staining using light microscopy. Control and treated cells grown in coverslips were fixed with methanol at -20 °C for 5 min, air-dried and stained with toluidine blue (0.5% in distilled water, 2 min). After washing with distilled water, samples were air-dried before mounting in DePeX (Serva, Germany) for observation.

Cell survival assessment

Thiazolyl blue (MTT, Sigma-Aldrich) reduction and Trypan blue (Sigma-Aldrich) exclusion tests were used for the assessment of cell survival. Briefly, a MTT stock solution in PBS (1 mg/mL) was prepared immediately prior to use and diluted in complete medium to achieve a final concentration of 50 µg/mL. Cells were incubated for 2 h to allow reduction to formazan precipitates, which were dissolved in 100 µL DMSO per well and the absorbance was measured at 540 nm in a SpectraFluor spectrophotometer (Tecan, Switzerland). Cell survival was expressed as the percentage of absorption of treated cells in comparison with that of control cells. For Trypan blue exclusion test, treated and untreated cells were trypsinized (harvesting also the detached ones) and mixed with the same volume of a 0.2 % Trypan blue solution in PBS. Cell counting of death (blue) or alive (white and bright) cells was performed using a Neubauer hemocytometer (Marienfeld GmbH, Germany).

Cell death mechanisms

Necrosis analysis

Necrosis was determined by measuring the activity of the enzyme LDH, released into the culture medium of necrotic cells following lethal membrane injury, by using a fluorimetric assay kit (CytoScan-Fluoro), following the manufacturer's instructions (G-Biosciences, USA). Briefly, cells were seeded in black 96-well plates and treated for 48 h with 100 µM CPT-11lip. Plates were removed from the incubator and equilibrated to

room temperature for 20-30 min. 100 µL of the reaction buffer, containing the LDH substrates were added to each well, mixed with the medium and incubated for 10 min at room temperature prior the addition of 50 µL of the stop solution. Fluorescence was measured with an excitation at 560 nm and emission at 590 nm after shaking the plates for 15 s in a SpectraFluor spectrophotometer. The percentage of cytotoxicity was calculated by using the average fluorescence values from experimental, maximum LDH release, and culture medium background.

Apoptosis identification

Apoptotic nuclear morphology of detached HeLa cells after incubation with CPT-11lip was visualized by H-33258 staining. Cells were collected by centrifugation (1200 rpm, 5 min) and the pellet was fixed in cold methanol at -20 °C for 5 min before staining with H-33258 (5 µg/mL in distilled water, 5 min). Apoptotic nuclei morphology (chromatin condensation and/or fragmentation) was observed by fluorescence microscopy as previously described by us (*Rello et al.*, 2005).

Apoptosis was confirmed by immunofluorescence detection of pro-apoptotic Bax protein. HeLa cells were fixed in a formaldehyde-PBS (1:10) solution for 20 min at 4 °C, washed three times with PBS (5 min each), and permeabilized with 0.5% Triton X-100 (Sigma). After 5 min, cells were incubated in blocking solution (5% bovine serum albumin, 5% FCS, 0.5% Triton X-100 in PBS) for 30 min at room temperature. Once removed from blocking solution, 25 µl of a 1:100 solution of primary antibody (monoclonal mouse anti-Bax (sc-20067); Santa Cruz Biotechnology, USA) were added to each sample and incubated at 37 °C for 1 h. Three 5-min washings with PBS were then carried out before addition of Triton X-100 for 5 min. Incubation of secondary antibody (Fab specific goat anti-mouse FITC-IgG; Sigma-Aldrich) was carried out in the same conditions. Cells were counterstained using H-33258 (5 µg/mL in distilled water, 5 min) and mounted with ProLong Gold antifade reagent (Thermo Fisher Scientific, USA).

Cell cycle analysis

Cell cycle phase distribution in both cell lines was analyzed by flow cytometry using Propidium iodide (PI) DNA staining. Control and CPT-11lip treated cells were tripsinized (harvesting also detached cells) and centrifuged at 1200 rpm for 5 min to collect the pellet prior fixing with cold 70% ethanol solution (15 min). After centrifugation, the pellet was resuspended in 1 mL of fresh PBS with 50 µL of a 100 µg/mL solution of RNase and incubated for 30 min at 37 °C. Immediately prior to measurement, DNA was stained by adding 25 µL of 1 mg/mL PI solution. All reagents were from Sigma-Aldrich. Measurements were performed with an Epics XL flow

cytometer (Beckman Coulter, USA) with an argon laser line at 488 nm and complemented with the appropriate filters. Cell fractions in sub G1, G0/G1, S, G2/M and > 4C phases were quantified in histograms with Summit software. Identification of apoptotic cells (sub G1 region) was achieved by determination of hypoploid cell populations. Polyploid cells were also identified in the > 4C region. For each experiment, a minimum of 20,000 events were analyzed.

Senescence-associated β-galactosidase staining

Senescence was assessed by measuring the β-galactosidase activity using the Senescence Cells Histochemical Staining Kit (Sigma-Aldrich). HeLa cells and Hs68 fibroblasts were treated with CPT-11lip for 48 h with post-incubation periods up to 5 days. After removing the growth media and washing the cells twice with PBS, cells were incubated with the fixation buffer for 6 min at room temperature. Cells were washed three times with PBS and then 0.5 mL/well of the staining mixture were added. Then, cells were cultured at 37 °C without CO_2 overnight and mounted with ProLong Gold antifade reagent. The percentage of senescent cells was calculated by the number of β-galactosidase-positive cells (blue cells) out of at least 500 cells from different microscope fields.

Quantitative real-time PCR

Cells were treated with CPT-11lip for 3 to 48 h, and the total RNA was extracted. Two μg of total RNA from each sample was used for cDNA synthesis using the SuperScriptTM III First-Strand Synthesis System for RT-PCR according to the manufacturer's instructions (Invitrogen, USA). Quantitative RT-PCR amplifications were performed with TaqMan Gene Expression Assays products in an ABI PRISM 7900 HT Sequence Detection System (Applied Biosystems). The reactions were carried out using the TaqMan Low Density Arrays (TLDAs, Applied Biosystems) containing 50 mL TaqMan Universal PCR Master Mix (Applied Biosystems) and 50 mL of a cDNA template corresponding to 100 ng total RNA per channel of the microfluidic card. The following genes were analyzed using TaqMan Gene Expression assays, TP53 (Hs00153349_m1), Bax (Hs00180269_m1) and Bcl-2 (Hs00608023_m1). A sample without cDNA was used as negative control and glyceraldehyde-3-phosphate dehydrogenase (GAPDH) (Hs99999905_m1) was used as internal control. The expression level of the target gene in the treated cells was measured relative to the level observed in the untreated cells and was quantified using the formula $2^{-\Delta\Delta CT}$ (Livak and Schmittgen, 2001). Data are means ± SD from at least three different experiments. Significance was assessed using Student's t test: *P<0.05 and **P<0.005.

Cytoskeleton analysis

To get insight into the cytoskeleton disorganization after CPT-11lip treatment, adhesion to substrate was analyzed by fluorescent labelling against the focal contact proteins vinculin and F-actin. For vinculin immunostaining, cells grown on coverslips were fixed (1:10 formaldehyde in PBS, 20 min at 4 °C), washed three times for 5 min with PBS, incubated in blocking solution (5% bovine serum albumin, 5% FBS, 0.5% Triton X-100 in PBS) for 30 min at room temperature, and then incubated with a 1:50 solution of the primary antibody mouse monoclonal anti-vinculin (clone hVIN-1, Sigma-Aldrich). Primary binding was detected using the secondary antibody Fab specific goat anti-mouse FITC-IgG (Sigma-Aldrich). F-actin was visualized in the same samples by incubation with phalloidin–tetramethylrhodamine B isothiocyanate (phalloidin-TRITC, Sigma-Aldrich) solution (1:200) at 37 °C in a wet chamber for 25 min. For a complete study, cells were washed three times with PBS, counterstained with H-33258 for 5 min, washed with distilled water and mounted with ProLong Gold antifade reagent before imaging, as described above.

DNA damage response by immunodetection of γ-H2AX

Hs68 and HeLa cells grown on glass coverslips and incubated with CPT-11lip for different times (3, 6 and 24 h), were immunostained for phosphorylated histone H2AX (γ-H2AX). Cells were fixed with formaldehyde in PBS (1:10 v/v) for 20 min, washed three times for 5 min with PBS, and permeabilized with 0.5 % Triton X-100 in PBS for 5 min. After incubation with a blocking solution (5% bovine serum albumin, 5% FBS, 0.02% Triton X-100 in PBS) at room temperature for 30 min, cells were washed again three times with PBS. Then, cells were incubated with primary monoclonal mouse anti-γ-H2AX antibody (Merck Millipore) diluted 1:100 at 37 °C in a wet chamber for 1 h. After three washes with PBS, incubation with a secondary antibody (Alexa Fluor® 488 goat anti-mouse, Life Technologies) was identical to that of the first one and so were final washings. Finally, DNA was counterstained by addition of H-33258 (0.05 mg/mL in distilled water) for 5 min, and samples were mounted with ProLong Gold antifade reagent.

Live cell imaging studies

Untreated control cells as well as cells incubated with CPT-11lip or empty liposomes were visualized at different times under phase contrast inverted microscope.

Optical microscopy

Observations of samples processed for optical microscopy (bright field and fluorescence) were made with an Olympus BX61 epifluorescence microscope

equipped with an Olympus DP50 digital camera (Olympus, USA), and processed using the Photoshop CS5 software (Adobe Systems, USA). The UV (365–390 nm) filter was used in order to visualize H-33258 fluorescence signal and to analyze cellular internalization mechanisms of CPT-11. Moreover, analysis of CPT-11lip subcellular localization, pro-apoptotic protein Bax and cytoskeletal components was performed using a multispectral Leica TCS SP5 confocal microscope (Leica, Germany), operating with 405 nm (argon–UV), 488 nm (argon), and 561 nm (DPSS) laser lines. γ-H2AX samples (bright field and fluorescence) were visualized with an Olympus BX61 epifluorescence microscope equipped with an Olympus DP50 digital camera (Olympus, USA), and processed using the Photoshop CS5 software (Adobe Systems). The following filters were used in order to visualize the fluorescence signal: UV (365–390 nm) for H-33258 and blue (460–490 nm) for Alexa Fluor® 488. In addition, time-lapse images of living cells were captured with an inverted microscope Leica DMI 6000B equipped with a Leica DFC420 C digital camera (Leica Microsystems, Switzerland) and images were processed with the same software.

References

Casadó, A., Sagristá, M.L., Mora, M., 2014. Formulation and *in vitro* characterization of thermosensitive liposomes for the delivery of irinotecan. J. Pharm. Sci. 103, 3127-3138. doi: 10.1002/jps.24097

Casadó, A., Giuffrida, M.C., Sagristá, M.L., Castelli, F., Pujol, M., Alsina, M.A., Mora, M., 2016. Langmuir monolayers and Differential Scanning Calorimetry for the study of the interactions between camptothecin drugs and biomembrane models. Biochim. Biophys. Acta 1858, 422-433. doi: 10.1016/j.bbamem.2015.12.007

Livak, K.J., Schmittgen, T.D., 2001. Analysis of relative gene expression data using real-time quantitative pcr and the 2-ΔΔCT method. Methods 25, 402-408. doi: 10.1006/meth.2001.1262

Rello, S., Stockert, J.C., Moreno, V., Gámez, A., Pacheco, M., Juarranz, A., Cañete, M., Villanueva, A., 2005. Morphological criteria to distinguish cell death induced by apoptotic and necrotic treatments. Apoptosis 10, 201-208. doi: 10.1007/s10495-005-6075-6

Weinstein JN, Ralston E, Leserman LD, Klausner RD, Dragsten P, Henkart P, Blumental R. 1984. Self-quenching of carboxyfluorescein fluorescence: Uses in studying lioposome stability and liposome–cell interaction. In Liposome technology; Gregoriadis G. Ed. Vol. III. Boca Raton, Florida: CRC Press, pp 183–204.

2. Supplementary Results

Figure S1. Transmission electron microscopy images of CPT-11 loaded liposomes. TEM shows the round-shape of liposomes.

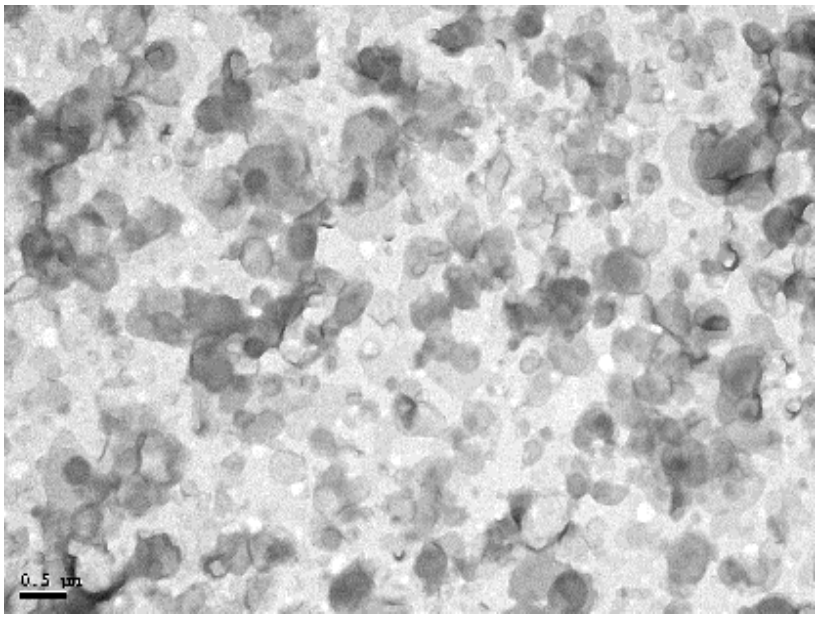

Figure S2. Bicompatibility of empty liposomes. Representative images of cells incubated 48 h with liposomes without CPT-11lip following different experimental techniques employed in this work. No significant changes were observed relative to untreated control cells.

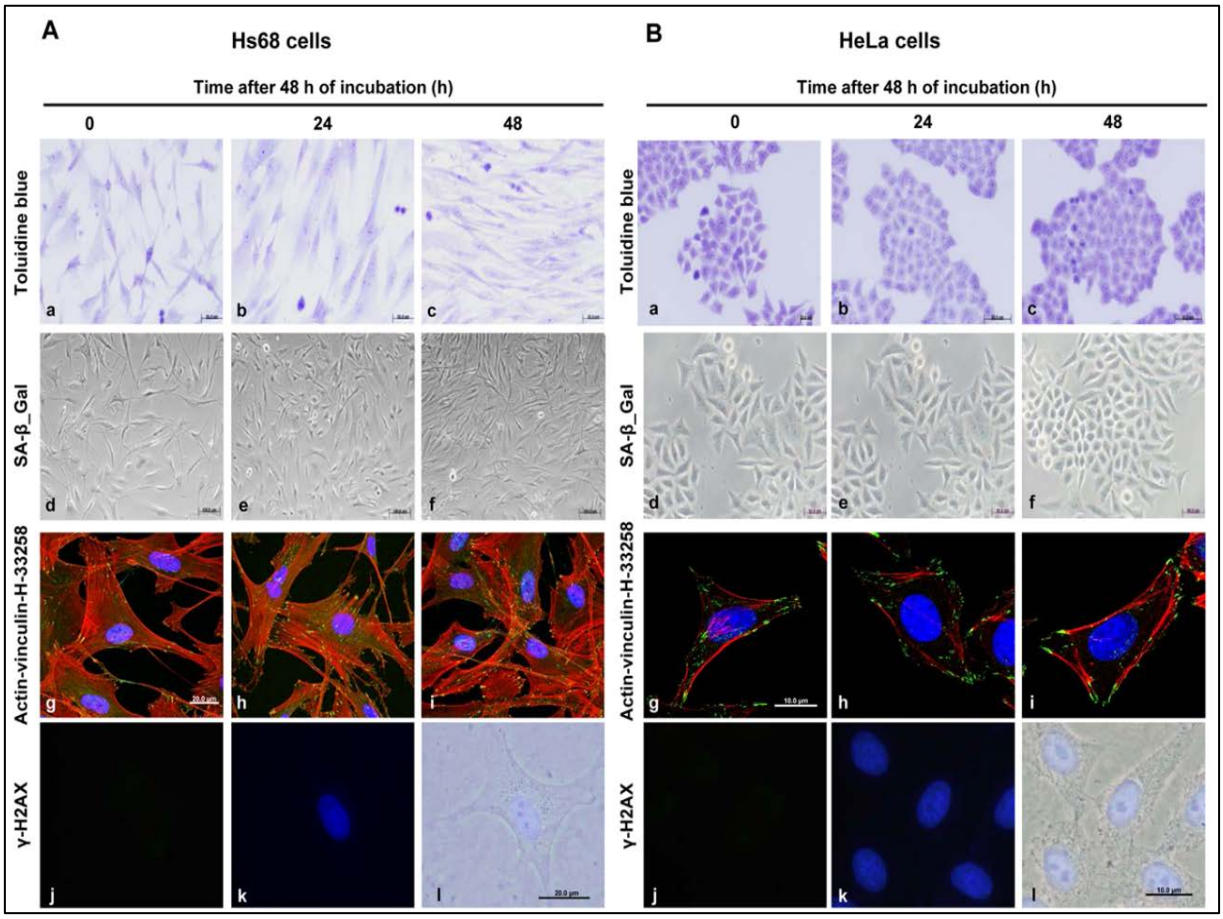

Images corresponding to controls of Hs68 and HeLa cells treated with empty liposomes (without CPT-11) for several assays performed in our study. It was evidenced the high degree of biocompatibility of the liposomal carrier.

Figure S3. Live-cell microscopy images before and after incubation with empty liposomes or CPT-11lip compared with untreated (control) cells. A) Hs68 cells. (a-c) Cell morphology of control cells and cells incubated with empty liposomes or CPT-11lip for 48 h, respectively. (d) Morphology of control cells at 48 h. (e,f) Normal cell without morphological alterations 48 h after empty liposomes administration. B) Representative images of HeLa cells under the same experimental conditions. (a) Control cells. (b, c) Cells exposed to empty liposomes or to CPT-11lip. (f) Remarkable cell detachment from plates was detected after 48 h incubation with CPT-11lip. Most of adhered cells showed typical morphological features of apoptosis, with cell rounding, shrinkage, and severe blebbing of plasma membrane (arrows). Scale bar: 10 μm.

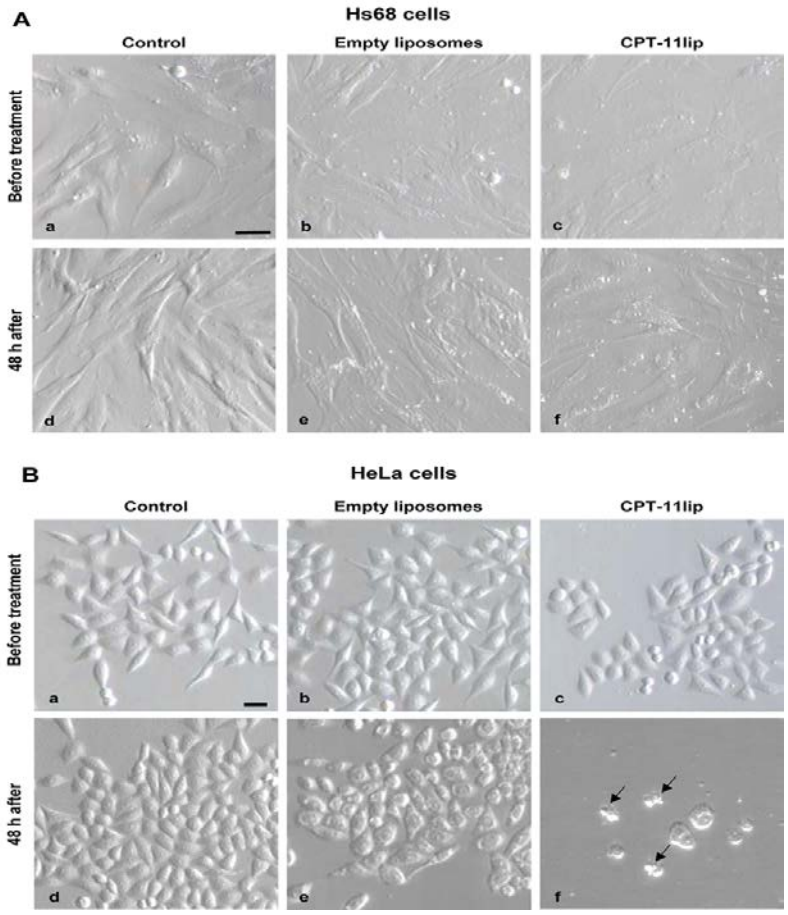

The images show that the incubation with empty liposomes did not produce morphological alterations. On the contrary, after 48 h of CPT-11lip treatment, the few cells that were still attached to the culture substrate showed apoptotic characteristics.

Cuarto artículo

Development and characterization of a novel SN-38 liposomal formulation and *in vitro* assessment of its cytotoxic effect on two tumor cell lines.

Casadó A, Sagristá ML, Mora M.

Enviado al Journal of Drug Targeting

RESUMEN

Las camptotecinas son compuestos derivados de alcaloides que interaccionan con la Topoisomerasa I. Entre ellos se encuentran el irinotecan (CPT-11) y el SN-38, metabolito más activo producido a partir del CPT-11 mediante la acción hidrolítica de una carboxilesterasa. El desarrollo de sistemas de liberación controlada, como liposomas, ha sido considerado una estrategia de incuestionable interés médico para resolver los problemas asociados, principalmente, a la inestabilidad del anillo de lactona de estas moléculas a pH fisiológico y a la extrema insolubilidad del SN-38. Este trabajo se centra en el diseño de un protocolo alternativo a los procedimientos clásicos de preparación de suspensiones liposomales, basados en la hidratación de un film lipídoco, para obtener una formulación farmacéutica prometedora para el SN-38. Además de la metodología más adecuada, la selección de la composición lipídica, la relación en la cual deben mezclarse las especies lipídicas y relación óptima lípido/fármaco, son factores decisivos para el éxito de la formulación final. El método utilizado, basado en la aplicación de las técnicas de microemulsificación, ha demostrado ser útil para obtener poblaciones de liposomas estables, de tamaño controlado y con carga negativa y ha permitido incorporar eficazmente el SN-38 en vesículas preparadas a partir de la mezcla EPC/DOPS (9:1) (SN-38lip). La formulación SN-38lip también se ha obtenido en forma de un polvo blanco liofilizado, que se reconstituye fácilmente conservando sus propiedades fisicoquímicas prácticamente invariables. También se describe la evaluación de la eficacia in vitro de SN-38lip sobre dos líneas celulares tumorales (HeLa y Caco-2) y se compara con la del fármaco solubilizado en DMSO (SN-38sol). Mediante citometría de flujo y el ensayo del MTT se ha demostrado la concordancia entre la mayor internalización y el mayor efecto citotóxico del fármaco formulado en liposomas (SN-38lip), en comparación con el solubilizado en DMSO (SN-38sol). Se muestran, además, las diferentes alteraciones inducidas por la formulación liposomal en el ciclo celular de ambas líneas celulares.

Development and characterization of a novel SN-38 liposomal formulation and in vitro assessment of its cytotoxic effect on two tumor cell lines

Ana Casadó[1], M. Lluïsa Sagristá and Margarita Mora[1]

[1]Department of Biochemistry and Molecular Biomedicine, Facultat de Biologia, Universitat de Barcelona, Barcelona, Spain.

Corresponding Author:

Prof. Dr. M. Margarita Mora.
Department of Biochemistry and Molecular Biomedicine, Facultat de Biologia, Universitat de Barcelona.
Av. Diagonal 643, Edifici Prevosti, -1. 08028-Barcelona, Spain.
Tel: +34-93-402.12.12
Fax: +34-93-402.15.59
E-mail: margarita.mora@ub.edu

Abstract

Camptothecins are alkaloid-derived Topoisomerase I interactive compounds. Among these, irinotecan (CPT-11) and SN-38, its more active metabolite produced from CPT-11 by carboxylesterase catalyzed hydrolysis. To solve the problems mainly associated to the instability of their lactone ring at physiological pH and with the extreme insolubility of SN-38, the development of controlled delivery carriers such as liposomes has been considered a subject of unquestionable medical interest. This paper focuses in the design of an alternative protocol to the classical lipid-film hydration procedures for obtaining a promising pharmaceutical formulation for SN-38. Besides the more suitable methodology, the choice of the lipid composition, the ratio in which lipid species should be mixed and the optimum drug/lipid ratio, are decisive factors for the success of the final formulation. The method used, based on the application of microfluidic techniques, has proved useful to procure stable and controlled sized negatively charged liposome populations and has allowed SN-38 being efficiently incorporated into EPC/DOPS (9:1) vesicles (SN-38lip). A lyophilized powder of SN-38lip, easily reconstitutable keeping their physicochemical parameters practically unchanged, has been obtained. The assessment of the efficacy in vitro of SN-38lip on two tumor cell lines (HeLa and Caco-2) is also reported and compared with that of the solubilized drug in DMSO (SN-38sol). Using flow cytometry and the MTT assay we have demonstrated the accordance of the highest uptake and cytotoxicity of SN-38lip in comparison with that of SN-38sol. In addition, the different cell cycle alterations induced in both cell lines by the liposomal formulation are shown.

Keywords: SN-38; liposomes; cytotoxicity, drug delivery, drug uptake, cell cycle analysis, HeLa cells, Caco-2 cells

Introduction

Camptothecins are efficient antineoplastic alkaloid-derived compounds that belong to the family of the so-called Topoisomerase I (Topo I) interactive compounds (Chen and Liu 1994, Li and Liu 2001). They are natural molecules or semisynthetic analogues which their different substituted five-ring backbone structure determines their solubility properties and their antitumor activity (Teicher 2008). Camptothecins cause cell death because of their ability to bind to DNA and Topo I and to the stabilization of the complex they both form during replication (Pommier 2006, Lacombe *et al.* 2014).

Topotecan and irinotecan (CPT-11) are two camptothecin derivatives already approved by the US Food and Drug Administration (FDA). Topotecan was approved in 1996 for the treatment of recurrent ovarian cancer, in 1998 for the second-line treatment of small cell lung cancer and in 2006 for the treatment of advanced, recurrent and metastatic cervical cancer (Randall-Whitis and Monk 2007). CPT-11, in turn, is a first-line drug approved for the treatment of a variety of human tumors, including colorectal, lung and gynecological cancers (Liew and Yang 2008). It has been administered in combination with 5-FU and as salvage treatment in 5-FU refractory disease. CPT-11 is a water-soluble molecule that can be converted, by a carboxylesterase catalyzed hydrolysis, to its metabolite SN-38, with a reported, at least, 100-fold biggest activity (Slatter *et al.* 1997, Wu *et al.* 2002). There are, however, certain clinical limitations for the use of all of these drugs. These include: 1) spontaneous inactivation to a carboxylate form in blood, 2) rapid reversal of the trapped cleavable complex after drug removal, requiring prolonged infusions, 3) resistance of cancer cells overexpressing membrane transporters, and 4) dose-limiting side effects of diarrhea, myelosuppresion, neutropenia and acute cholinergic-like syndrome (Garcia-Carbonero and Supko 2002). In the case of SN-38, another important drawback is its great insolubility in almost all the solvents that could be used to properly formulate this drug for clinical purposes.

To solve these problems and to optimize the therapeutic effectiveness of these cytostatic molecules several strategies have been examined. Among these, the development of controlled delivery carriers such as liposomes, polymeric nanoparticles or microspheres is providing promising alternative tools in the field of cancer therapy (Dawidczyk *et al.* 2014, Estanqueiro *et al.* 2015, Pérez-Herrero and Fernández-Medarde 2015, Zylberberg and Matosevic 2016).

The liposome platform has been extensively studied as a tool to encapsulate drugs and is considered a subject of unquestionable medical interest (Allen and Cullis 2013, Perche and Torchilin 2013, Sen and Mandal 2013, Kraft *et al,* 2014, Torchilin 2014, Bozzuto and Molinari 2015). Liposomal devices, which have emerged as one of the most studied and useful novel drug delivery systems in the last two decades, provide suitable strategies to improve the therapeutic index of chemotherapeutics in cancer

treatment. Liposomes can modify the pharmacokinetics of the encapsulated drugs, promote their intracellular uptake and allow the selective delivery to diseased cells. Moreover, it has been reported that liposomal encapsulation results in a decrease in some of the undesirable side effects associated with chemotherapy and in the consequent increase in the maximum tolerated dose, allowing the administration of a higher cumulative dose of the encapsulated drug (Dawidczyk *et al.* 2014). The US FDA has already approved various liposome formulations for clinical use and many others have been tested in clinical trials (Madni *et al.* 2014, Wicki *et al.* 2015, Panahi *et al.* 2017).

Liposomes offer a wide variety of possibilities to formulate chemically different molecules because of the two well-separate environments of their structure. Moreover, they are biodegradable and biocompatible and provide a galenic form endowed with drug sustained release abilities. The pharmacological efficacy of any liposomal formulation is dependent on such factors as physical structure (lamellarity, vesicle size and vesicle surface charge), physical stability and bilayer dynamics (fluidity and permeability). All of these factors can be controlled by such parameters of liposome formulation as lipid composition, method of preparation and specific labeling with recognizing molecules. In addition, the partition coefficients of the drug molecules in a biphasic organic/aqueous system and the interactions that they can establish with the lipid components of the liposomal bilayer influence the delivery of the encapsulated drugs and the stability of the liposomal formulation (Casadó *et al.* 2016).

The recent innovations and developments in nanotechnologies have encouraged new research programs to engineer nanotechnology products for therapeutic applications, has enabled the development and marketing of new bioactive macromolecules that require a precise intracellular location for its biological activity and have revolutionized the form to administered medicines (Farokhzad and Langer 2009, Wicki *et al.* 2015).

The development of sustained release nanodevices, with encapsulated products, is especially useful in the case of camptothecins (Emerson 2000, Hatefi and Amsden 2002). Two main advantages of using liposomes for the delivery of these drugs are the protection of the liposomal form from the hydrolysis of the lactone to the inactive carboxylate form and the possibility of solubilizing such insoluble molecules as SN-38, much more active than its pro-drug CPT-11, but with limited uses because of its great hydrophobicity. Until recently, CPT-11, as acidic solution (Camptosar®, Pfizer, USA), represented the only form approved for administering indirectly SN-38, but in October 2015, the U.S. Food and Drug Administration approved an encapsulated form of CPT-11, the pro-drug of SN-38, in liposomes (Onivyde, Merrimack Pharmaceuticals, Inc), previously known as MM-398 (Chustecka, 2015).. Although it was demonstrated, by in vitro experiments, that CPT-11 could be converted into SN-38 in intact liposomes after

their incubation with carboxylesterase (Sadzuka *et al.* 1999), it was also established that only a small fraction of the pro-drug generates the active metabolite (Bala *et al.* 2013). At present, both CPT-11 and SN-38 are in clinical trial in its liposomal form (Torchilin 2014).

Sadzuka *et al.* (2005) reported a comparative study of the application of different procedures to incorporate SN-38 into liposomes. The classic form to obtain liposomes, the Bangham method (Bangham *et al.* 1965), showed only an encapsulation efficiency of 5.6%, which could be increased up to 20.3% by means of the application of a modified remote loading method and up to 53.0% by using a novel developed film loading method. The poor solubility of SN-38 would explain the very low encapsulation efficiency achieved when the conventional methods, involving a hydration step of a lipid film to prepare liposomes, were used. Bala *et al.* (2013) also published a review in which some interesting considerations regarding to the preparation of nanomedicines for the delivery of SN-38 were made. Nevertheless, all the approaches to incorporate this drug in liposomes are variations on the classic procedure based on the hydration of a lipid film.

Improving the formulation of SN-38 is interesting from a biomedical point of view, given its great antitumor activity, although it presents a series of difficulties because of the special chemical characteristics of the molecule. The present paper describes the development of a new liposomal formulation for this camptothecin that constitutes a simpler alternative as well as effective in drug loading than that provided by other published methods. Data are also provided on its characterization and on the assessment of its cytotoxic activity *in vitro*.

Materials and Methods

Materials

L-α-Distearoyl-phospathidylcholine (DSPC), Egg yolk phosphatidylcholine (EPC), Soy bean lipid extract (SLE), L-α-Dioleoyl-phospathidylserine (DOPS) and Cholesterol (CHOL) were purchased from Avanti Polar Lipids (Birmingham, AL, USA). SN-38 was purchased from Tocris Bioscience (Bristol, United Kingdom). All the organic solvents (Panreac, Montcada I Reixac, Barcelona, Spain) have been distilled before use. Milli-Q water (Millipore Bedford, Massachusetts system, resistivity of 18 MΩ•cm) was used. All other chemicals and solvents were of analytical grade. Dulbecco´s Modified Eagle´s Medium with 4.5 g glucose/L (DMEM), fetal calf serum, L-glutamine and penicillin-streptomycin solutions were provided by Biological Industries (Crowell, CT, USA). Sterile Dulbecco´s Phosphate Buffered Saline (PBS), dimethyl sulphoxide (DMSO), 3-[4,5-dimethylthiazol-2-yl] 2,5-diphenyltetrazolium bromide (MTT), Trypan blue, Toluidine blue and Hoechst-33258 (H-33258) were purchased from Sigma-Aldrich Chemical Co. (St. Louis, MO, USA). CytoScan-Fluoro Assay Kit was purchased from

G-Biosciences (St Louis, USA) Sterilized plastic material was purchased from Corning (Corning, USA).

Preparation of SN-38 loaded liposomes

A suspension of multilamellar liposomes (MLVs) was first prepared by direct hydration of lipids and SN-38. DSPC, DPPC, DOPS, CHOL, SLE and EPC were used and mixed in binary and ternary combinations, at different molar ratios, without preparation of the standard lipid films. The appropriate amounts of lipids and SN-38 were weighted together and MLVs were formed by hydrating the dry powder lipids/SN-38 mixtures with 10 mM lactate (pH 4.4) buffer to a final lipid concentration of 10–20 mg lipid/mL. The hydration was performed with a T 25 digital ULTRA-TURRAX® dispersing device (IKA, Staufen, Germany). MLV dispersions were sonicated for 10 min in an ultrasonic bath (Branson, Danbury, USA) above the phase transition temperature (Tm) and processed by a high pressure Microfluidizer homogenizer (Avestin M-110EH-30 Microfluidizer® Processor or Emulsiflex C3). The Emulsiflex C3 processor is a high pressure homogenizer designed for lab scale production by continuous high shear fluid processing, easily scalable up to pilot and/or production volumes with guarantee of repeatability. Liposomes size can be controlled by adjusting the fluid flow rates in the microfluidic network. Liposomes were stored in the dark at 4°C.

Lyophilization process

To enhance stability during storage, liposomes were lyophilized using 5% trehalose as cryoprotectant agent. The protocol was established as follows: 2 mL of liposomal suspension were placed in 4 mL glass vials and frozen at -80°C (liquid nitrogen) during 3-5 hours. Vials were subsequently dried during 24 h at -55°C and 0.04 mbar (Freeze Dryer Alpha 1-2/LD, Martin Christ GmbH, Germany). Lyophilized liposomes were rehydrated immediately before the experiments by adding 2 mL of 10 mM lactate (pH 4.4) buffer. The resulted suspension was prewarmed at 45°C during 15 min and vortexed for 30 min (alternating 30 s periods of heating/vortexing).

Characterization of Liposomes

Determination of the Lipid Content

The lipid amount in liposome suspensions was measured following the Stewart's method (1980). Calibration curves for each lipid composition (0.01–0.2 mg lipid) were obtained. Chloroform and ammonium ferrothiocyanate (1:1, v/v) were added to each dried sample. The chloroformic phase, extracted after vortexing and centrifugation (2680xg, 10 min), was used to select the absorbance maximum. Measures were carried out in a Specord 205 UV/VIS spectrophotometer (Analytical Jena AG, Jena, Germany).

Vesicle Size and ζ -Potential

The average particle size, particle size distribution and ζ-potential of unilamellar liposomes were determined by photon correlation spectroscopy (PCS) and laser Doppler micro-electrophoresis in a Malvern Zetasizer NANO-ZS device (Malvern Instruments Ltd, Malvern, UK) equipped with an optic unit containing a 5 mW He-Ne laser (Spectra Physics) and an electrophoresis cell. The device was calibrated with standard carboxy-modified polystyrene latex samples. Measurements were performed at 25°C and λexc= 633 nm, using liposomal suspensions containing 0.2 mg lipid/mL of 10 mM, pH 4.4, lactate buffer. Data were collected with a Malvern data channel correlator and the mean hydrodynamic diameter was calculated from a cumulative analysis of the intensity autocorrelation function.

Transmission Electron Microscopy

A direct observation of liposomes was carried out by transmission electron microscopy (TEM). Ammonium molybdate (2.0%) was used for negative staining to visualize vesicles. Liposomal dispersion was placed on a carbon-Formvar coated copper grid for 1 min, after which 10 µL of negative stain was used for 30 s and excess sample and stain was blotted with filter paper. Afterwards, the copper grid was air-dried for imaging using an electron microscope JEOL JEM 1010 100 kv, with CCD Megaview 1kx1k (JEOL Ltd., Tokyo, Japan).

Entrapment Efficiency and SN-38 Liposomal Content

Total and entrapped SN-38 was systematically quantified by UV-visible absorption spectroscopy. A calibration curve for SN-38 (1–30 µM) was previously obtained in DMSO at λ_{max} (390 nm). Liposome-entrapped SN-38 was quantified as the difference between the total SN-38 used to prepare the film and the amount of non-encapsulated drug. An aliquot of the liposomal-SN-38 suspension was centrifuged using Centricon YM-10 Filter Devices (Millipore Corporation, Billerica, USA) to obtain a filtrate containing the non-entrapped drug, without liposomes. The concentration of non-entrapped SN-38 was determined by comparison with the calibration curve obtained in the same conditions. Drug Encapsulation Efficiency (DEE %) was calculated as the percentage of the drug amount in liposomes referred to the amount of added drug for their preparation.

Liposomes stability

To control the stability of the formulations, both before and after the lyophilization process, the drug and lipid content in liposomes, as well as the average size and polydispersity of the vesicles, were determined. The turbidity of all samples was

determined by diluting the suspension in 10 mM, pH 4.4, lactate buffer and measuring the absorbance of the sample at 400 nm in a Specord 205 UV/VIS spectrophotometer (Analytical Jena AG, Jena, Germany).

Cell cultures

Experiments were performed on the tumor epithelial cell line HeLa (originated from a cervix adenocarcinoma, ATCC CCL-2) and the human Caco-2 colon adenocarcinoma cells (ATCC HTB-37). Both cell lines were grown in Dulbecco's modified Eagle's medium (DMEM) supplemented with 50 U/mL penicillin, 50 µg/mL streptomycin, 1% nonessential amino acids and fetal bovine serum (FBS) at a final concentration of 10%. Cell cultures were performed in a humidified sterile atmosphere of 95% air and 5% CO2, at 37°C, in a Nuaire NU-4750 incubator (Plymouth, MN, USA). Cells were grown for 72 hours and treated when cultures were in exponential growth.

In Vitro Studies of Liposomal SN-38 Cytotoxic Activity

Cells were incubated with different concentrations of SN38, either entrapped in liposomes (SN-38lip) or solubilized in DMSO (SN-38sol), at different times between 0 and 48 h to assess the cellular uptake of the drugs using flow cytometry. For cell survival studies and cell cycle analysis a period of 24 h and a period of 48h of incubation with post-incubation times up to 48 h, were used.

SN-38 uptake by flow cytometry

Flow cytometry was used to quantify the uptake of SN-38 by HeLa and Caco-2 cells. Cells cultured on 25 cm2 flasks were treated with 10 µM of SN-38sol or SN-38lip up to 48 hours. After incubation, cells were washed twice with PBS, in order to remove the drug outside the cells, and cells were tripsinized and centrifuged at 1200 rpm before final resuspension in 1 mL PBS. SN-38 fluorescence was quickly measured within the cell population (after debris exclusion). The analysis was carried out using a Gallios multi-color flow cytometrer instrument (Beckman Coulter, Inc, Fullerton, CA) set up with the 3-lasers 10 colors standard configuration. Excitation was done using a blue (488nm) laser for Forward scatter (FS) and side scatter (SS). A gate on cells was settled on this dot plot, in order to exclude small debris and aggregates. Red fluorescence from Propidium Iodide (PI) (2-4 µg/ml) was collected in a log scale (λ_{exc}=488nm, λ_{em}=620nm). Permeabilized (death) cells incorporating PI were excluded. Uptake was measured according to the blue fluorescence (λ_{exc}=405nm, λ_{em}=450nm). Results were projected on a 1024-channel histogram, where percentage of positive cells was measured.

Cell survival

HeLa and Caco-2 cells were incubated with concentrations of SN-38lip or SN-38sol ranging from 1 to 50 μM for 3, 24 and 48 h. Thyazolyl blue (MTT, Sigma) reduction (Mossman 1983) was used for the assessment of cell survival. Briefly, a MTT stock solution in PBS (1 mg/mL) was prepared immediately prior to use and diluted in complete medium to achieve a final concentration of 50 μg/mL (100 μL of MTT stock solution to each 2 mL of medium). Cells were incubated for 2 h to allow formazan crystals to precipitate. Formazan precipitates were dissolved in 100 μL DMSO per plate and the absorbance was measured at 540 nm in a Synergy H1 microplate spectrofluorimeter (BioTek Instruments, Inc., Vermont, USA). Cell survival was expressed as the percentage of absorption of treated cells in comparison with that of control cells (100% survival). The results presented were the mean value and standard deviation from at least six independent experiments. Another set of experiments with the 10 μM concentration of SN-38 was performed with incubation times of 24 h or 48 h and post-incubations times up to 48 h.

Cell cycle analysis

HeLa and Caco-2 cell cycle distribution was analyzed by flow cytometry after staining the cells, to label cellular DNA content, with propidium iodide (PI) (Fried *et al.* 1976). Flasks of controls and 10 μM SN-38lip treated cells were tripsinized (harvesting also detached cells) and centrifuged at 1200 rpm for 5 min for pelleting prior fixing with cold 70 % ethanol solution (15 min). After centrifugation, the pellet was resuspended in 1 mL of fresh PBS with 50 μL of a 100 μg/mL solution of RNase and incubated for 30 min at 37°C. Immediately prior to measurement, DNA was stained by adding 25 μL of 1 mg/mL PI solution. All reagents were from Sigma. Measurements were performed with an Epics XL flow cytometer (Beckman Coulter, Brea, USA) with an argon laser line at 488 nm and complemented with the appropriate filters. Cell fractions in sub G1, G0-G1, S, G2/M and > 4C phases were quantified in histograms with Summit software. Identification of apoptotic cells (sub G1 region) was achieved by determination of hypoploid cell populations. Polyploid cells were also identified in the > 4C region. For each experiment, a minimum of 20.000 events were analyzed.

Necrosis analysis

To study the possible contribution of necrosis to the general death, we performed a test to measure the activity of the enzyme LDH, which is released into the culture medium of necrotic cells following rupture of the plasma membrane (Chan et al. 2013). For this purpose a fluorometric kit (CytoScan-Fluoro Assay Kit) for measure LDH release was employed following the manufacturer's instructions (G-Biosciences, St Louis, USA)

(Wolterbeek and van deer Meer 2005). Cells were seeded in black 96-well plates and treated for 24 h or 48 h with 100µL of culture medium containing concentrations ranging from 1 µM to 50 µM of SN-38 either as SN-38lip or SN-38sol. Plates were removed from the incubator and equilibrated to room temperature for 20-30 min. 100 µL of the reaction buffer, containing the LDH substrates were added to each well, mixed with the medium and incubated for 10 min at room temperature prior the addition of 50 µL of the stop solution. Fluorescence was measured with an excitation at 560 nm and emission at 590 after shaking the plates for 15 seconds in a Synergy H1 microplate spectrofluorimeter (BioTek Instruments, Inc., Vermont, USA). The percentage of citotoxicity was calculated by using the average fluorescence values from experimental, maximum LDH release, and culture medium background.

Statistical Analysis

All data are presented as the mean ± SD from the separated samples analyzed. The statistical significance of differences was evaluated by using a Student's paired t-test, where necessary. Data with $p<0.05$ was considered significant (significance levels are indicated in the figure legends).

Results and discussion

Formulation and characterization of SN-38-loaded liposomes

Liposome formulations were prepared from DSPC/DOPS/CHOL (DOC) and EPC/DOPS mixtures, at the appropriate molar ratios, and from the natural extracts SLE and EPC. The great hydrophobicity of SN-38 imposes substantial restrictions for using the standard lipid films hydration based procedures: the solubility characteristics of this molecule, as inferred by its partition between two different polar/apolar environments (Casado *et al.* 2016), must be considered when designing a liposomal carrier for its delivery because their influence on the mechanic properties of lipid bilayers. On the other hand, the dynamic properties of a bilayer could greatly hinder or facilitate the incorporation of such hydrophobic molecules as SN-38. Albeit carriers with rigid bilayers have evident advantages such as low permeability and stability in vivo (Kong and Dewhirst 1999), they suffer from considerable restrictions in terms of achieving useful pharmaceutical formulations with drug concentrations according to therapeutic doses. On the contrary, fluid bilayers accommodate more easily hydrophobic molecules inside their hydrophobic core. The design of the liposomal formulation for SN-38 has taken into account the above considerations.

It had previously described a lipid mixture to encapsulate CPT-11 in a drug delivery system (Casadó *et al.* 2014). The procured liposomes had the proper characteristics to be considered suitable to formulate CPT-11 in a liposomal carrier for therapeutic applications. However, each drug has specific requirements to be efficiently

encapsulated into liposomes, that is, not only the choice of the lipid species but also the ratio in which they should be mixed, the optimum drug/lipid ratio, and the more suitable methodology to prepare the final formulation are decisive factors for the success of the final formulation. Moreover, the efficiency of drug loading will depend on its encapsulation in the aqueous core, its incorporation into the liposomal bilayer, or its partition between these two phases and is governed by such properties as liposome size, surface charge, and membrane fluidity. In this way, SN-38, because of its high lipophilicity, can be inserted within the hydrophobic core of a mixed lipid bilayer, without disturbing its structure or affecting the stability of the formulated liposomes (Casadó *et al.* 2016).

SN-38 loaded liposomes were first prepared from a natural soy bean lipid extract (SLE). The lipid concentration of the liposomal suspensions was fixed at 10 mg/mL and different lipid/SN-38 molar ratios were used. After, we considered if the DSPC/DOPS/CHOL lipid mixture, which gives rigid bilayers, used to encapsulate the prodrug CPT-11 could be able to incorporate efficiently the CPT-11 metabolite SN-38. Alternatively, other compositions were assessed: the criterion to select them was to get liposomes with more fluid bilayers than that given by the DSPC/DOPS/CHOL mixture and the results of the studies on the molecular interactions between this camptothecin and phospholipids above mentioned. Thus, an EPC extract and the binary composition EPC/DOPS were also assayed.

To solve the problems associated with the insolubility of SN-38 and thinking about the design of an alternative protocol to obtain an improved formulation for this drug, a profound amendment of the methods described to date for the preparation of SN-38 loaded liposomes has been made. After discarding those based on a first step of preparation and hydration of a lipid film, assayed with very poor results, other alternative procedures were considered. In this sense, we have taken into account microfluidic techniques that have proved useful to procure controlled sized liposome populations (Jahn *et al.* 2007, Yu *et al.* 2009). In a recent review, Garg et al. (2016) have also underlined the advantages of applying microfluidic procedures to liposome production as they allow for improved drug loading efficiencies, reproducible manufacturing and uniform scaling.

Lipids and SN-38 were weighted in the same glass recipient, at the appropriate molar ratios, and the proper volume of 10 mM lactate buffer, pH 4.4, to get a lipid concentration of 10 mg/mL was added. The hydration of each lipid/drug combination was achieved by shaking vigorously the powder mixture with a high-performance dispersing IKA Ultra-Turrax® (T25 Digital, IKA-Werke GmbH & Co. KG). After a brief bath sonication, the lipid/SN-38 suspension was injected into the central channel of the Microfluidizer device and processed by circulating it 10 times through the circuit at a pressure of 150 kPa and a flow rate of 50 mL/min. Liposomes, procured under the

optimized preparation methodology, were systematically and rigorously characterized by size, polydispersity index and ζ-potential and by quantifying the amount of the drug The data are listed in Table 1.

Physicochemical parameters were determined by PCS and SN-38 loading was quantified spectrophotometrically after removing the non-encapsulated drug from the liposomal–SN-38 suspension with Centricon YM-10 Filter Devices (EMD Millipore Corporation, Billerica, Massachusetts). Calibration curves for SN-38 (1-30 μM) were previously obtained in DMSO. Encapsulation efficiency (DEE) and bulk drug concentration were obtained from the difference between total and non-entrapped SN-38. The values determined for DEE of SN-38 into liposomes were always in the range of 95-100%.

Table 1. Physicochemical characteristics of SN-38 loaded liposomes and SN-38 entrapment inside vesicles.

Sample		**Physical parameters**			**Liposomal SN-38**	
Liposome composition	Lipid/SN-38 (molar ratio)	Particle size[a] (nm)	PDI[b]	ζ-Potential[c] (mV)	[SN-38][e] (μM)	mg SN-38/ mmol lipid
SLE	(7.5:1)	355.3±13.2	0.472±0.011	-47.7±8.8	1770.0±10.2	52.2±0.3
	(10:1)	332.8±19.6	0.525±0.058	-54.3±10.3	1329.0±11.3	39.2±0.3
	(20:1)	196.2±9.4	0.415±0.033	-45.3±16.3	652.6±7.6	19.3±2.2
	(40:1)	119.1±1.9	0.398±0.081	-36.1±8.7	331.3±8.2	9.8±0.2
DSPC/DOPS/CHOL (65:35:30)	(20:1)	248.3±9.5	0.368±0.016	-32.1±17.5	713.6±6.2	19.7±1.7
EPC	(20:1)	146.3±14.2	0.401±0.120	-12.6±1.5	637.5±8.9	19.1±2.6
EPC/DOPS (9:1)	(20:1)	147.2±7.9	0.345±0.072	-31.4±7.4	670.2±5.7	20.3±1.6

[a]Particle size measured as Z-average mean. [b]Polydispersity index. [c]Zeta potential. [d]Drug Loading Efficiency, expressed as percentage of SN-38 relative to lipid (w/w). eBulk SN-38 concentration in the liposomes suspension. Lipid concentration in all the samples was 10 mg/mL. Three independent batches were processed and analyzed for physic-chemical characterization. The data are the mean ± SD values corresponding to three independent preparations.

It was observed that the size of the vesicles was strongly influenced by the lipid/drug molar ratio and that the lipid composition of the sample did not affect the entrapment efficiency, being the amount of SN-38 within the vesicles determined by the lipid/drug molar ratio. By considering the size, the molar ratio selected at first as the most suitable for liposome formulation was 20:1. The data indicate that the incorporation efficiency of SN-38 into liposomes was always higher than 95%, for fresh preparations, resulting in a final concentration ranging from $3.31x10^{-4}$ to $17.7x10^{-4}$ M in the liposomal/buffer suspension. With regard to the best lipid composition, the consideration of the stability of the liposomes suspension for all the assayed lipid combinations (see below) and the results of previously published biophysical data on

interfacial interactions of CPT-11 and SN-38 with membrane mimetic models using monolayer techniques and Differential Scanning Calorimetry (Casadó *et al.,* 2016) argue in favor of the choice of the binary EPC / DOPS phospholipid mixture To obtain the most suitable formulation for SN-38.

Physical stability of SN-38 liposome suspensions

During storage SN-38lip vesicles could aggregate and precipitate, with the consequent changes in their mean size and optical density (OD). These changes can be used to monitor their physical stability. Samples were kept at 4°C in the dark during the successive measurements. Firstly, the analysis was carried out during 168 h by measuring the OD of the different liposome suspensions at 400 nm. The data (Figure 1A) show that their turbidity did not undergo significant changes during storage. Accordingly with this fact, the vesicles size increases were never higher than 10%.

To enhance the stability during storage, liposomes suspensions were lyophilized using 5% trehalose as cryoprotectant agent. Samples were rehydrated immediately, 24 h and 168 h after their lyophilization and physicochemical parameters, particle size and polydispersity, ς-Potential and turbidity, were measured. As shown in Figure 1B, and in comparison with the data in Table 1, there were no significant differences in the particle size before and after the lyophilization process, what makes this methodology suitable to achieve long-term stability of the procured liposomal suspensions. ς-Potential and turbidity values were almost identical before and after the lyophilization process.

As a measure of stability, it was also assessed the ability of the different liposomal formulations to keep the drug inside the vesicles, in terms of the evolution of this parameter during the time of storage. The results show that EPC/SN-38 and EPC/DOPS/SN-38 liposomes exhibit a retention rate of about 95% over the time analyzed period (see Figure 1C).

Lyophilized liposomes were also visualized by Transmission Electron Microscopy (TEM) by using the technique of negative contrast with ammonium molybdate. The images (Figure 2) showed rounded vesicles in a somewhat heterogeneous preparation, as could also be deduced from the consideration of the polydispersity index (table 1).

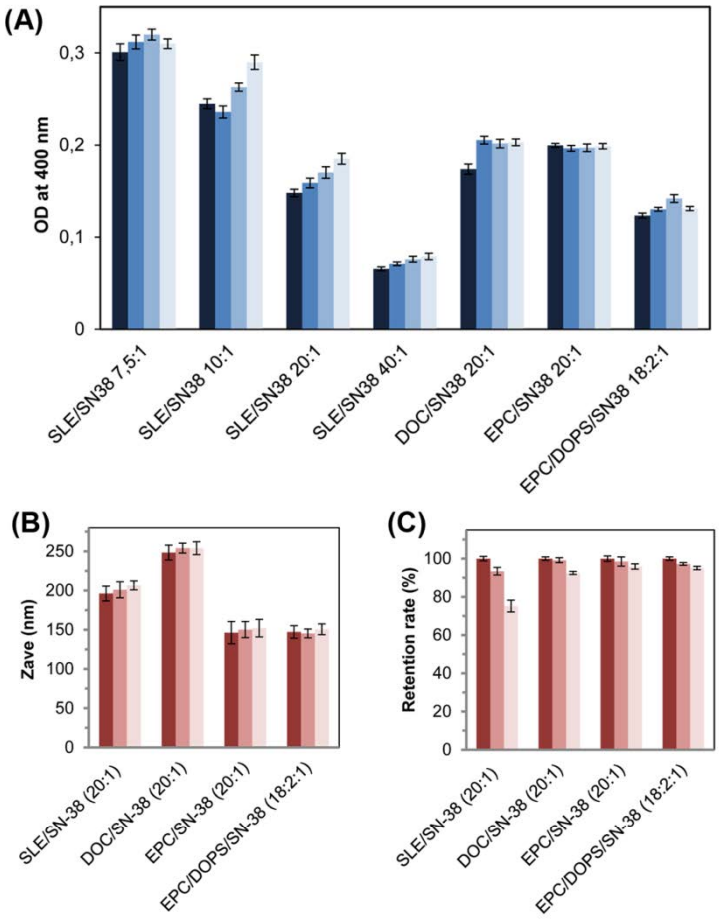

Figure 1. Physical stability of SN-38 liposome preparations. (A) Optical density measurements of SN-38 liposome suspensions. The measurements were performed, from left to right, immediately after preparation, and 24h, 72 h and 168 h after preparation. Samples were stored at 4°C in the dark. (B) Size and (C) SN-38 retention rate during storage of lyophilized SN-38 loaded liposomes. The measurements were performed, from left to right, after rehydratation of freshly lyophilized samples and 24, and 168 h after storage. Data correspond to mean values±SD of, at least, three different experiments.

Taken together, all the physicochemical data have allowed selecting the best lipid/drug ratio (20:1) and bilayer composition (EPC/DOPS, 9:1) to develop the final formulation for SN-38. This option would be supported by previous biophysical studies on lipids/camptothecins interactions (Casadó et al. 2016).

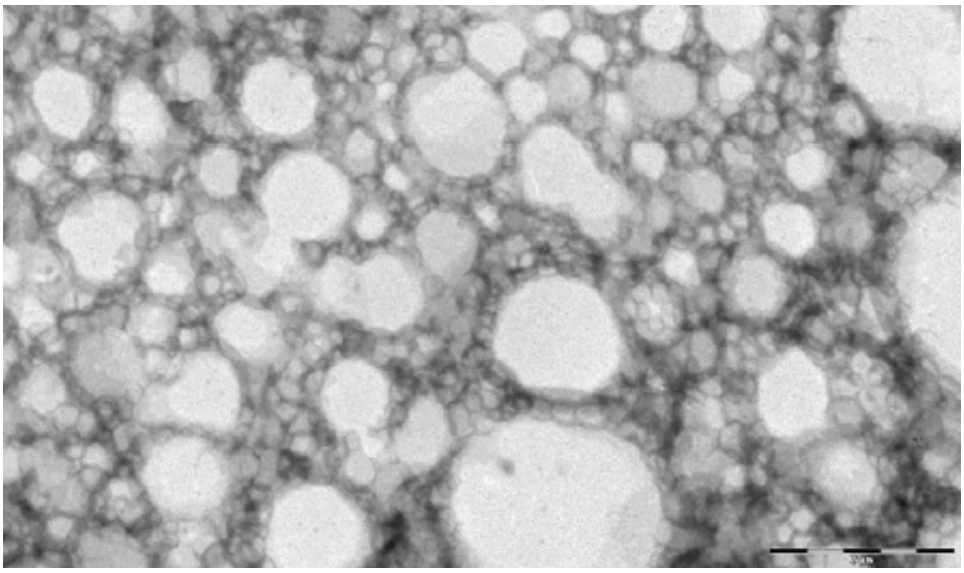

Figure 2. Transmission electron microscopy images of a white powder lyophilized preparation of SN-38 loaded EPC/DOPS liposomes. The bar is equivalent to 750 nm.

In Vitro assessment of Liposomal SN-38 Cytotoxic Activity

The quantification of cell cytotoxicity is regularly used to assess the efficacy of new drugs and new pharmaceutical formulations. The MTT assay was performed to determine the effect of liposomal-SN-38 (SN-38lip), in comparison with that of the free drug (SN-38sol), on the survival and growth of two tumor cell lines, HeLa and Caco-2.

A first series of experiments were carried out with HeLa cells to establish the importance of the liposome bilayer composition on the cytotoxic effect of the drug. The results are shown in Figure 3A and B. It can be observed that the cytotoxic effectiveness of the SN-38lip formulations was, in general, higher than that of the drug solubilized in DMSO. The possible toxicity of dimethyl sulfoxide (DMSO) on HeLa and Caco-2 cells was taken into consideration before analyzing comparatively the results of the MTT assay. DMSO is widely used to solubilize poorly soluble drugs in permeation assays because of its well-known effect as chemical penetration enhancer to deliver active molecules through the skin and into the cells (Kligman 1965). However, the maximal usable concentration of DMSO in cell cultures has not been perfectly established, although the toxicity of this amphiphilic solvent has already been evaluated in model membranes (De Menorval et al. 2012) and with different cell culture lines (Malinin and Perry 1967, Da Violante et al. 2002). The general consensus is that concentrations of DMSO safer for cells in culture are below or equals to 1% and that 1% DMSO doesn't cause any toxicity to cells.

At this stage, it is important to underline that, despite the effect of DMSO as permeation enhancer, the SN-38lip formulation was more effective both in increasing the uptake of SN-38 by cells (see below) and to improve its cytotoxic activity. All of

these considerations still further highlight the importance of using delivery systems for drug administration.

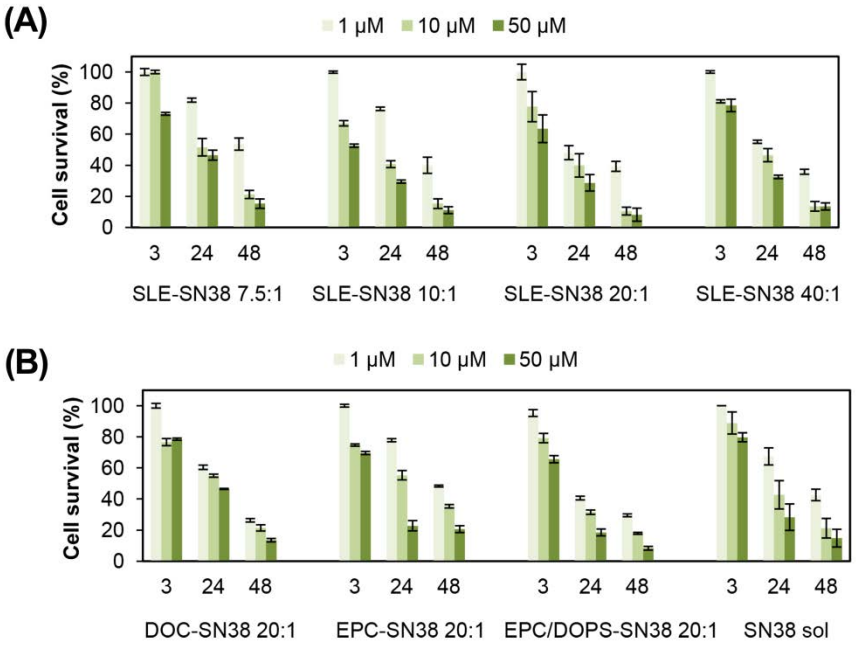

Figure 3. Cytotoxic effect of SN-38 solubilized in DMSO and encapsulated in liposomes (A) Survival (%) of HeLa cells after treatment with SN-38 encapsulated in SLE liposomes at different molar ratios. (B) Survival (%) of HeLa cells after treatment with SN-38 encapsulated in liposomes with the compositions indicated, at the same lipid/drug molar ratio (20:1) and in DMSO solution. For (A) and (B), cells were incubated for 24 h with the drug and survival was evaluated 3, 24 and 48 h after drug removal by the MTT assay. Data correspond to mean values ± SD of, at least, three different experiments.

Taken into account the results of the characterization of all the liposomal formulations (data in table 1), together with those of MTT assays to evaluate its potential as SN-38 carriers (data in Figure 3A and 3B), we have performed a second series of MTT experiments, both with HeLa and Caco-2 cells, with the SN-38lip formulation chosen as the more appropriate in terms of stability and cytotoxic activity. EPC/DOPS (9:1 molar ratio) liposomes were loaded with SN-38 at a 20:1 molar ratio and used in these series. Cells were incubated with a 10 μM SN-38 concentration, both in its liposomal form and solubilized in DMSO, for 24 and 48 hours, and measures were carried out immediately (0), 24 and 48 h after drug removal. The results are given in Figure 4.

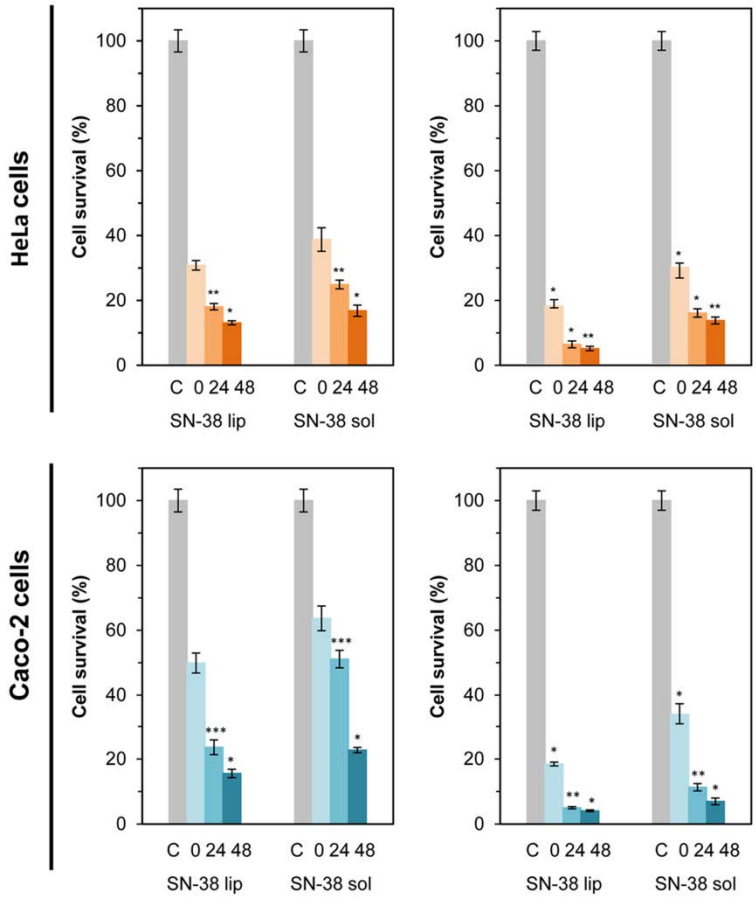

Figure 4. Assessment of survival of HeLa and Caco-2 cells incubated with 10 μM SN-38, both in liposomal form and in DMSO solution, for 24 (left panels) and 48 h (right panels). The surviving fraction was evaluated 0, 24 and 48 h after drug removal by the MTT assay. Data correspond to mean values ± SD of, at least, six different experiments. P values <0.03(*), 0.008 (**) and 0.0001(***) were as statistical significant.

To select the 10 μM SN-38 concentration it was considered the IC50 value that could be approximately estimated from the data showed in Figure 2B for the chosen liposome formulation (1 μM for incubation times of about 20 h) and the criterion of choosing a drug concentration high enough to induce a large cytotoxic effect.

The results show the acute cytotoxicity induced by SN-38 on both HeLa and Caco-2 cell lines: a dramatic decrease in cell survival for SN-38 treated cells in relation to control cells was observed, being the cytotoxicity of the drug increased with the incubation time and dependent on the time elapsed after the end of treatment in both cell lines. Moreover, the liposomal SN-38 action was always stronger than that observed when the drug was administered in DMSO, at all of the assayed conditions. The cytotoxic effect was particularly high after 48 h of treatment with the liposomal formulation (never reached a 20% survival) and the most pronounced differences between the action of the liposomal formulation and that of the molecule solubilized in DMSO were observed in the case of Caco-2 cells.

Evaluation of the Uptake of Liposomal SN-38 by HeLa and Caco-2 Cells

The study of the ability of a cell to internalize a drug provides useful information in relation with its possible therapeutic effect and has been widely investigated in biomedical research when designing products for pharmaceutical applications. The quantitative analysis of the uptake of SN-38, both free and in the liposomal form, by HeLa and Caco-2 cells, was carried out by flow cytometry, measuring the intrinsic fluorescence of this camptothecin derivative under ultraviolet excitation. Cells were incubated with a 10 µM SN-38 incorporated into liposomes (SN-38lip) or solubilized in DMSO (SN-38sol) and the results are plotted in Figure 5.

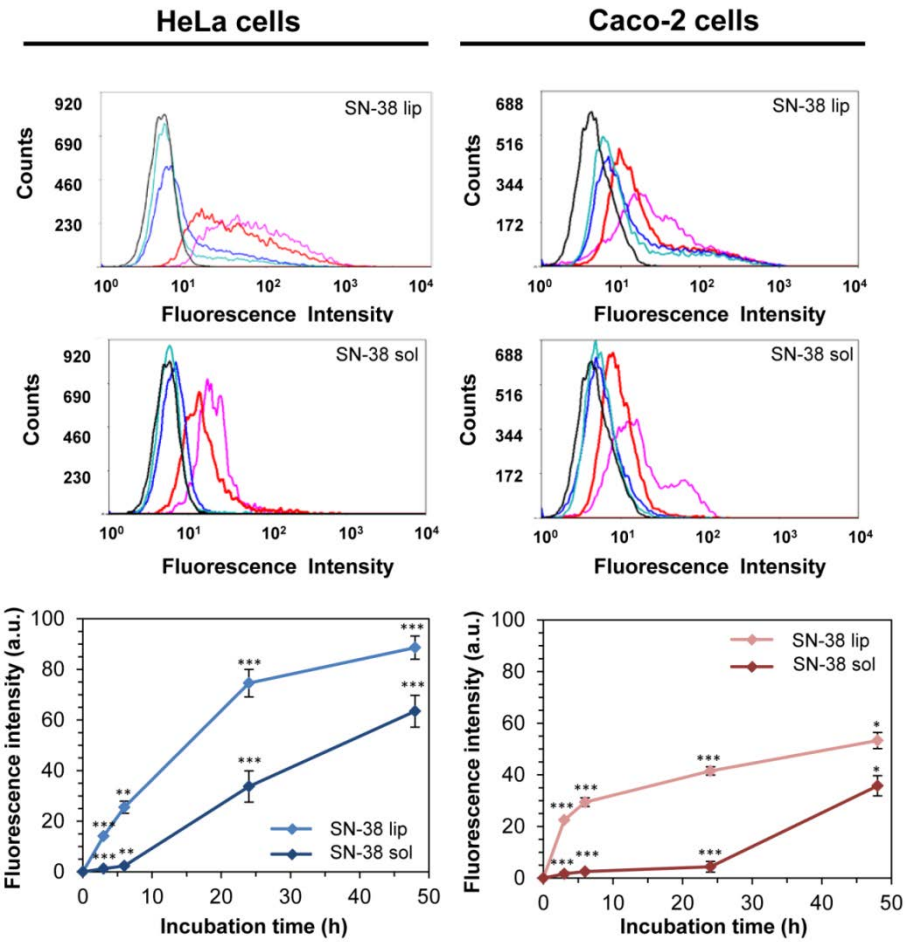

Figure 5. Uptake of SN-38 by HeLa and Caco-2 cells. The internalization of the drug was quantified by flow cytometry. Emission fluorescence at 450 nm was determined after excitation at 405 nm. Data are the means ± SD from three independent experiments. Significance was assessed using a Student's paired t-test, being P values <0.02 (*), <0.06 (**) and <0,003 (***). Fluorescence profiles are representative of the three experiments analyzed.

The data show that the amount of SN-38 within cells was dependent on the incubation time and that, in both cell lines, the uptake was higher for SN-38lip than for

SN-38sol. After 48 h of incubation, HeLa cells internalize 28.4% more SN-38 in their liposomal form than when solubilized in DMSO, whereas for Caco-2 this difference increases slightly to 32.9%. However, the greatest difference was observed after 24 h of incubation (54.8 and 89.4 %, respectively). Otherwise, the uptake kinetics was somewhat different for HeLa than for Caco-2 cells, being besides possible to observe that, at a given time, HeLa cells internalize a greater amount of drug than Caco2 cells, irrespective of the SN-38 formulation used, liposomal or solubilized. These results agree with those of the MTT analysis and account for the highest cytotoxicity of the liposomal form.

Cell cycle distribution

The effect of liposomal SN-38 on cell cycle phase distribution, after drug exposure, was performed by flow cytometry. HeLa and Caco-2 cells were treated with the EPC/DOPS/SN-38 (18:2:1 molar ratio) liposomal formulation for 24 and 48 h and, in each case, cell cycle profiles were acquired immediately (0 h) and 24 h after drug, and detached cells removal, and compared with those obtained for untreated controls. In all cases the SN-38lip concentration was 10 μM. The images are given in Figure 6A.

Figure 6B shows the different response of HeLa and Caco-2 cells to the SN-38 action, the marked influence of introducing post-incubation periods after drug treatment and before recording the cycle profile and the dramatic changes that occur in HeLa cells after SN-38lip treatment. In this case, the most significant changes were the huge increase in the number of cells in the Sub G1 phase and the large decrease in the percentage of cells at the G0/G1 sector in the two assayed conditions (without and with post-incubation times) (Figure 6B, left panel).

The effect of the post-incubation time on the cell cycle profile showed notable differences with regard to the changes observed when it was acquired immediately after drug incubation. In this case, the number of cells in the G0/G1 phase decreased dramatically again, but the increase of Sub G1 percentage was much more moderate. The changes in the sectors S, G2/M and >4c were also rather different: cells in the S phase showed sustained levels whereas the G2/M and polyploid cells (>4C) showed progressive increases. It should be considered that the percentage of cells in all cycle phases after a post-incubation period of 24 h correspond to the evolution of the cells remaining after removal those detached immediately after incubation (0 h). The visualization of the histograms shows the profound changes that SN-38lip induced in HeLa cells. Studies of the effect of CPT-11, the SN-38 pro-drug form, on different cell lines have shown some contradictory results, from cell cycle arrest at S and G2/M phases to apoptotic responses (Kaku *et al.,* 2015, Morandi *et al.*, 2008).

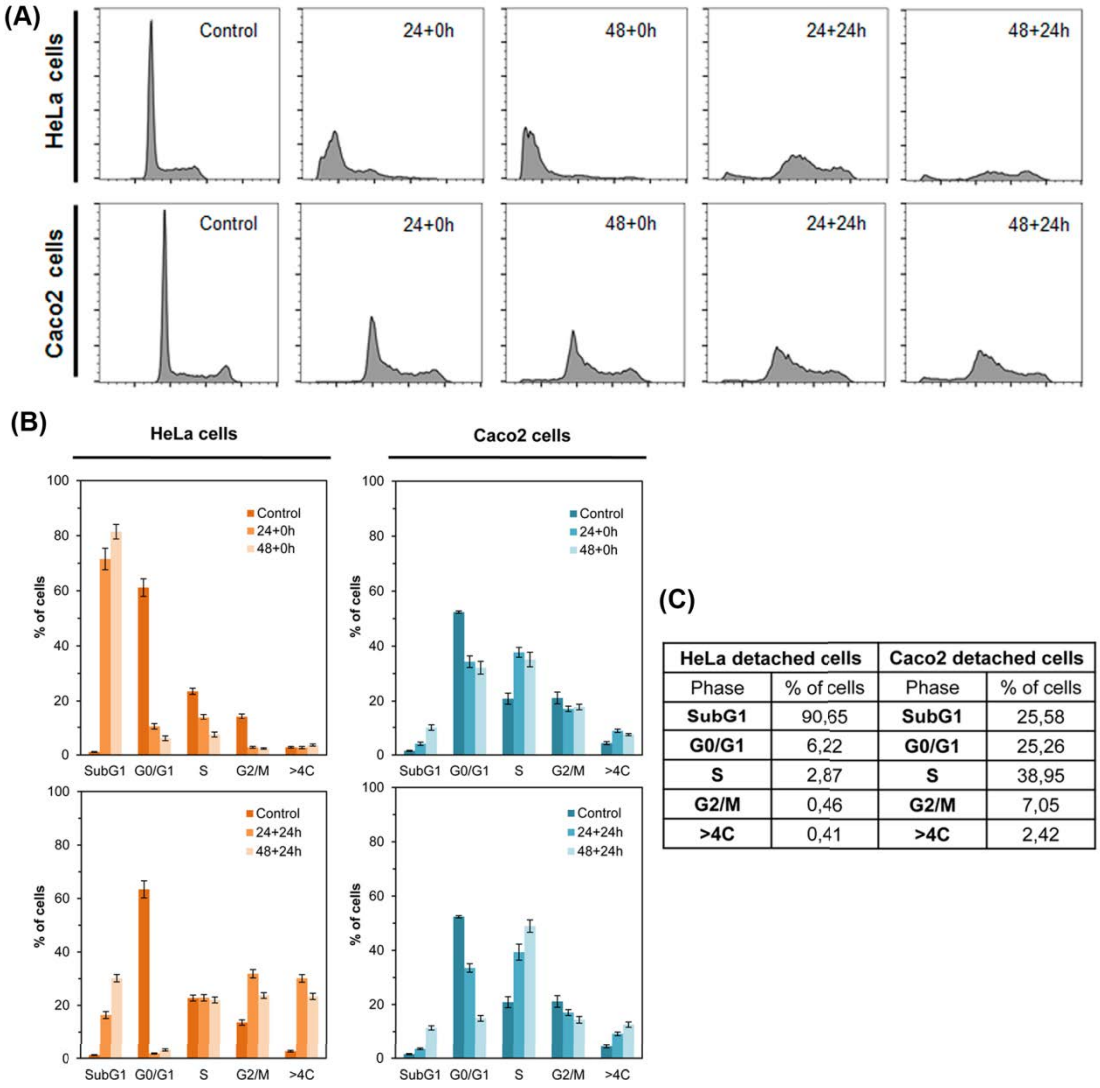

(C)

HeLa detached cells		Caco2 detached cells	
Phase	% of cells	Phase	% of cells
SubG1	90,65	**SubG1**	25,58
G0/G1	6,22	**G0/G1**	25,26
S	2,87	**S**	38,95
G2/M	0,46	**G2/M**	7,05
>4C	0,41	**>4C**	2,42

Fig 38lip (10 μM) for 24 and 48 h. (A) HeLa (upper panels) and Caco-2 (lower panels) cells. Cell cycle profiles were acquired for non-treated cells (control) and immediately (24+0h, 48+0h) after treatment and 24 h after drug removal (24+24h, 48+24h). For comparative purposes typical profiles, acquired maintaining the same scale for total counts (y axis) and DNA content (x axis), are shown. (B) Percentage of cells in each cell cycle phase calculated from the histograms. (C) Percentages of detached cells in each phase. For each experiment, a minimum of 20 000 events were analyzed.

The response of Caco-2 cells to SN-38lip treatment was quite different (Figure 6B, right panel). It could be observed the following features: i) a decrease in the proportion of cells at the G0/G1 sector, although more moderate than for HeLa cells, was quantified (from 52.7% for control cells, down to around 32.1% for treated cells for the longest incubation time, without post-incubation); ii) a cell cycle arrest at the S phase, which peak increased from 19.5% in control cells up to 35.2% in 48 h treated cells; iii) an almost sustained percentage of G2/M cells, irrespective of the incubation time, but slightly decreased when post-incubation time was applied and iv) a lesser percentage of cells that evolve both towards the Sub G1 sector and towards the

polyploid section. In this case, the influence of the post-incubation period in the cycle profile was also manifest. 24 h after removing SN-38 and detached cells, the remaining cells, which have also internalized the drug, evolve in a similar way as before. A significant difference, however, is the important decrease in the G0/G1 population (falls by up to 15%) and the largest increase in the number of cells in the S phase (up to 49%).

Previously, we have reported the cytotoxic activity of a liposomal Irinotecan (CPT-11) formulation, developed in our laboratory, on Caco-2 cells (Casadó *et al.* 2014), as well as an in deep study about the mechanism of the death induced by this camptothecin considered as the pro-drug of SN-38, on HeLa and Hs68 cells (Casadó et al., 2017). However, SN-38 is considered the active metabolite of CPT-11, and diverse references point out the convenience of using it, instead its pro-drug, because of the limited metabolic transformation of the latter *in vivo* (Rivory *et al.* 1996). The CPT-11lip formulation produced severe alterations in the characteristic diploid DNA histogram of untreated Caco-2 cells: as suggested, the changes were consistent with the progress of an increasing apoptotic process induced by this drug in its liposomal form. On the contrary, the response of Caco-2 cells to SN-38lip is quite different to that of CPT-11lip in terms of cell death mechanism, as commented before. Without analyzing in depth the features associated to apoptotic or necrotic processes, what is clear is that the profile of the cycle undergoes different changes than those observed after the incubation with CPT-11lip. From this result it could be interpreted that the cell cycle is arrested at the S phase when incubated with SN-38lip, without significant changes in the subG1 region (apoptotic population).

The response of colon cancer cells to irinotecan, in a solubilized form, has also been reported in the literature (Kaku *et al.* 2015, Haug *et al.* 2008). In general, arrests of cell cycling at G2/M phase (and at S, sometimes) together with decreases of the G1 population are the most common effects observed. However, it should be noted that there are discrepancies in some aspects of the entire cell cycle profiles presented in the most relevant bibliographic references consulted.

The results presented here showed similarities and differences with those reported previously (Casado et al., 2017). Thus, the effect of SN-38lip on HeLa cells is somewhat similar to that induced by CPT-11lip: substantial increases of the sub G1 peak, much higher that induced by SN-38lip, HeLa cells respond to treatment with CPT-11lip mainly with increases of the sub G1, G2/M and >4c peaks, allowing suggesting an arrest of cell cycle at G2/M, besides the existence of apoptotic cells after incubation with CPT-11lip. The response of HeLa cells to SN-38lip treatment was a strong increase of the peak placed in the sector sub G1 together with decreases, from dramatic to more moderates.

With regard to the results of the analysis of the Caco-2 cycle profile, the comparison, under the same treatment conditions, of cell percentages in the different phases of the cell cycle after CPT-11lip and SN-38lip treatments shows noticeable similarities, but also significant differences. As in the previous article, it could be interpreted that the cell cycle is arrested at the S phase when incubated with SN-38lip, but unlike those results, changes in the sub G1 region are considerably lower than those observed after treatment with CPT-11lip.

Lactate dehydrogenase leakage assay

Cell death, induced by the cytotoxic action of a drug, can be the result of chemical or physical cytoplasmic membrane damage associated to a necrotic membrane disruption or to an apoptotic-mediated membrane blebbing. There are several assays to study these processes. The MTT test and the LDH assay are two experimental methods used together for measuring the levels and the possible causes of cellular cytotoxicity and for obtaining reliable information about the death mechanism (Kim et al., 2009).

The measure of the release of intracellular enzymes, such as LDH, through permeabilized plasma membranes has proven to be a method useful to evaluate cellular membrane damage and to verify the results of the viability assay (MTT). Moreover, LDH is stable, quickly released by cells into the culture medium and its activity is easily quantified by a very sensitive spectrophotometric assay.

The results, plotted in Figure 7, show that the effect of SN-38, either in liposomal suspension or in DMSO solution, depends on both the drug concentration and the incubation time, being slightly more pronounced that caused by the liposomal formulation and the differences between survival of HeLa and Caco-2 cells after treatment were very small. Cell survival decreased around 40%, for the highest SN-38lip concentration and the longest incubation time and around 30% when the SN-38sol formulation was used, with the same conditions. The consideration of the statistical significance of the differences shows its validity for the highest SN-38 concentrations.

Both MTT and LDH assays showed the cytotoxic effect of SN-38 in its liposomal form and in DMSO solution. However, the degree of survival after pharmacological treatment is extremely different depending on the method used to evaluate it. Only a 17.9% of Caco-2 and a 20.6% of HeLa cells survive after 48 h incubation with 10 μM SN-38lip, as measured by the MTT test, while survival values of 77.7% and 64.6% were determined under the same conditions for Caco-2 and HeLa cells, respectively, by the LDH assay. This disagreement could indicate that membrane damage not seems to be the main factor involved in the decrease of cell viability.

The results described herein are not sufficient to propose a mechanism to justify the pathway by which SN-38 exerts its cytotoxic action. It should be noted that LDH

release is considered an early event in necrosis, but a late event in apoptosis and that late apoptosis may show, in some respects, the same signs as necrosis in long term assays measuring late events. In line with this comment would be the fact that if the incubation time is reduced to 24 h, the survival of Caco-2 and HeLa cells (LDH release assay) increases up to values of 91 and 96.2%, respectively, and that the SN- 38sol is practically non-cytotoxic in these concentration and time conditions. Therefore, more research is needed to draw conclusions about the mechanism of the cytotoxic effect of SN-38 and studies are currently underway to establish more precisely the action mode of SN-38 in its liposomal form.

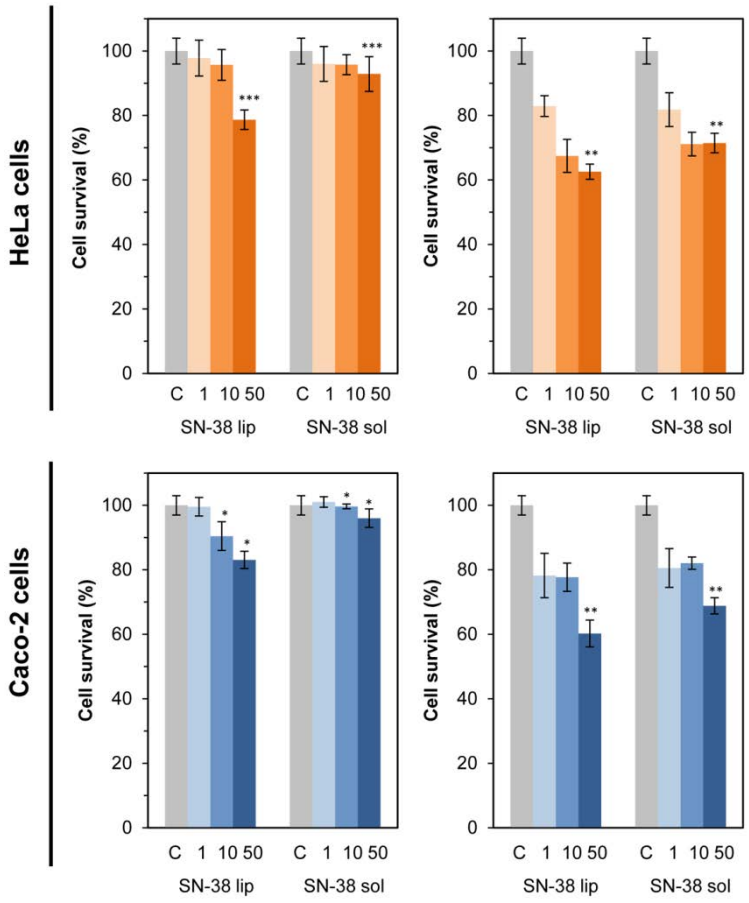

Figure 7. LDH assay after treatment of HeLa and Caco-2 cells with SN-38lip and SN-38sol formulations. The numbers in the x axis indicate the SN-38 concentration; 1, 10 and 50 μM. LDH release was measured at 24 (left panels) and 48 h (right panels). The columns represent the mean levels of LDH release and the error bars (±SD) from three independent experiments. Significance was assessed using a Student's paired t-test, being P values <0.05 (*) and <0.02 (**). The data of LDH activity in the culture medium was normalized with the total protein content.

Conclusions

The development of controlled delivery-sustained release nanodevices, such as liposomes, is providing promising alternative tools in the field of cancer therapy and is especially useful in the case of camptothecins because of their chemical characteristics. The present paper reports on the preparation of a new liposomal formulation for SN-38, designed by carefully selecting the liposomal lipid components and the optimal drug lipid ratio and taking into account our previous drug-lipid interaction studies, and determines *in vitro* its potential for cancer chemotherapy, as a first and necessary step before *in vivo* assays (He *et al.,* 2017).

SN-38 loaded liposomes were characterized and their cytotoxic activity was assessed. The analysis of the data has allowed establishing the following considerations: i) SN-38 loaded liposomes has been successfully formulated and obtained by a standardized protocol which gives stable and well-characterized vesicle suspensions. The SN-38lip formulation has been lyophilized to provide a readily reconstitutable white liposomal powder which maintains practically unchanged its physicochemical properties and drug retention ability after resuspension; ii) SN-38 was better internalized by HeLa and Caco-2 cells when formulated in liposomal devices than when solubilized in DMSO, despite the effect of this solvent as permeation enhancer; iii) The cytotoxicity of SN-38, both in liposomal and solubilized form, has been demonstrated by means two complementary experimental methods, the MTT reduction assay and the LDH release test. The improved cytotoxic effect of SN-38 when liposomes were used as delivery carriers could be directly related with the greater internalization of the liposomal form of the drug. Furthermore, regardless of the mechanism of action, SN-38 produces an acute cytotoxicity in both tumor cell lines, when survival and growth are evaluated by the MTT test; iv) The cellular response to SN-38 of HeLa and Caco-2 cells showed noticeable differences, being the more significant the huge increase in the number of HeLa cells in the sub G1 phase, that could be related to an apoptotic cell death process, and an arrest of the Caco-2 cell cycle in the S phase which may lead to the suppression of cell proliferation. In any case, it has been proposed that both actions could constitute a barrier for cancer development.

The results obtained highlight the potential of the developed formulation, but underline the need for more research to draw conclusions about the exact mechanism by which SN-38 exerts its cytotoxic action and studies to elucidate it are currently underway.

Acknowledgements

This work was supported by the Spanish Ministry of Economy and Competitiveness (grant number CTQ2013-48767-C3-1-R) and by the Govern de la Generalitat de

Catalunya (2009SGR-367). A. Casadó thanks to the University of Barcelona for a predoctoral fellowship. The authors are also grateful to Prof. M.L. Garcia (Faculty of Pharmacy, University of Barcelona) for the use of the Malvern Zetasizer NANO-ZS device and tanks and recognize the helpful technical support and the valuable contribution of Dr. Jaume Coma (Centres Científics i Tecnològics, University of Barcelona).

References

Allen, T.M., and Cullis, P.R., 2013. Liposomal drug delivery systems: From concept to clinical applications. *Adv Drug Deliv Rev*, 65, 36-48.

Bala V., *et al.*, 2013. Prodrug and nanomedicine approaches for the delivery of the camptothecin analogue SN-38. *J Control Release,* 172, 48-61.

Bangham, A.D., Standish, M.M., and Watkins, J.C., 1965. Diffusion of univalent ions across the lamellae of swollen phospholipids. *J Mol Biol*, 13, 238–252.

Bozzuto, G., and Molinari, A., 2015. Liposomes as nanomedical devices. *Int J Nanomedicine,* 10, 975-999.

Casadó, A., Sagristá, M.L., and Mora, M., 2014. Formulation and In Vitro Characterization of Thermosensitive Liposomes for the Delivery of Irinotecan. *J Pharm Sci.,* 103, 3127-3138.

Casadó, A., *et al.*, 2016. Langmuir monolayers and Differential Scanning Calorimetry for the study of the interactions between camptothecin drugs and biomembrane models. *Biochimica et Biophysica Acta,* 1858, 422–433.

Casadó, A., Mora, M., Sagristá, M.L., Rello-Varonab, S., Acedo, P., Stockert, J.C., Cañete, M., Villanueva, A., 2017. Improved selectivity and cytotoxic effects of irinotecan via liposomal delivery: A comparative study on Hs68 and HeLa cells. Eur. J. Pharm. Sci. 109, 65–77

Chan, F.K-M., Moriwaki, K., De Rosa, M.J., 2013. Detection of necrosis by release of lactate dehydrogenase (LDH) activity. Methods Mol Biol, 979, 65-70.

Chen, A.Y. and Liu, L.F., 1994. DNA topoisomerases: Essential enzymes and lethal targets. *Annu Rev Pharmacol Toxicol*, 34, 191-218.

Chustecka, Z., 2015. Liposomal Irinotecan (MM-398) Approved in Pancreatic Cancer. Medscape Oct 22. Available from: http://www.medscape.com/viewarticle/853072 [Accessed 22 October 2015].

Da Violante, G., *et al.*, 2002. Evaluation of the Cytotoxicity Effect of Dimethyl Sulfoxide (DMSO) on Caco2/TC7 Colon Tumor Cell Cultures. *Biol Pharm Bull*, 25, 1600-1603.

Dawidczyk, C.M., *et al.*, 2014. State-of-the-art in design rules for drug delivery platforms: lessons learned from FDA-approved nanomedicines. *J Control Release*, 187, 133-144.

De Menorval, M-A., *et al.*, 2012. Effects of Dimethyl Sulfoxide in Cholesterol-Containing Lipid Membranes: A Comparative Study of Experiments In Silico and with Cells. PLoS ONE [online], 7(7), e41733. https://doi.org/10.1371/journal.pone.0041733/

Emerson, D.L., 2000. Liposomal delivery of camptothecins. *Pharmaceutical Science & Technology Today,* 3, 205–209.

Estanqueiro, M., *et al.*, 2015. Nanotechnological carriers for cancer chemotherapy: The state of the art. *Colloids and Surfaces B: Biointerfaces*, 126, 631-648.

Farokhzad, O.C., and Langer, R., 2009. Impact of nanotechnology on drug delivery. *ACS Nano,* 3, 16-20.

Fried, J., Perez, A.G., and Clarkson, B.D., 1976. Flow cytofluorometric analysis of cell cycle distributions using propidium iodide. Properties of the method and mathematical analysis of the data. *J Cell Biol*, 71, 172–181.

García-Carbonero, R., and Supko, J.G., 2002. Current perspectives on the clinical, experience pharmacology, and continued development of the camptothecins, *Clin Cancer Res,* 8, 641-661.

Garg, S., Heuck, S., Ip, S., and Ramsay, E., 2016. Microfluidics: a transformational tool for nanomedicine development and production, *Journal of Drug Targeting*, 24, 821-835, DOI: 10.1080/1061186X.2016.1198354

Hatefi, A., and Amsden, B., 2002. Camptothecin Delivery Methods. *Pharm Res,* 19, 1389-1399.

Haug, K., Kravik, K.L., and De Angelis, P., 2008. Cellular response to irinotecan in colon cancer cell lines showing differential response to 5-fluorouracil. *Anticancer Res*, 28, 583-592.

He, R., *et al.*, 2017. Nanoformulation of dual bexarotene-tailed phospholipid conjugate with high drug loading. *Eur J Pharm Sci,* 100, 197–204.

Jahn, A., *et al.,* 2007. Microfluidic directed formation of liposomes of controlled size. *Langmuir*, 23, 6289–6293.

Kaku, Y., *et al.*, 2015. Irinotecan Induces cell cycle arrest, but not apoptosis or necrosis, in Caco-2 and CW2 colorectal cancer cell lines. *Pharmacology*, 95, 154-159.

Kim, H., *et al.*, 2009. Discriminative cytotoxicity assessment based on various cellular damages. *Toxicol Lett*, 184, 13–17.

Kligman, A.M., 1965. Topical pharmacology and toxicology of dimethylsulfoxide. *J Am Med Assoc*, 193, 796–804.

Kong, G., and Dewhirst, M.W., 1999. Hyperthermia and liposomes. *Int J Hyperthermia*, 15, 345–370.

Kraft, J.C., *et al.*, 2014. Emerging research and clinical development trends of liposome and lipid nanoparticle drug delivery systems. *J Pharm Sci*, 103, 29-52.

Lacombe, O.K., *et al.*, 2014. Effects of camptothecin derivatives and topoisomerase dual inhibitors on Trypanosoma cruzi growth and ultrastructure. *Journal of Negative Results in BioMedicine*, 13:11.

Li, T., and Liu, L., 2001. Tumor cell death induced by topoisomerase-targeting drugs. *Annu Rev Pharmacol Toxicol* 41, 53–77.

Liew, S.T., and Yang, L.Y., 2008. Design, synthesis and development of novel camptothecin drugs. *Curr Pharm Des,* 14, 1078-1097.

Madni, A., *et al.*, 2014. Liposomal drug delivery: a versatile platform for challenging clinical applications. *J Pharm Pharm Sci,* 17, 401-426.

Malinin, T.I., and Perry, V.P., 1967. Toxicity of dimethyl sulfoxide on HeLa cells. *Cryobiology,* 4, 90-96.

Morandi, E., et al., 2008. Gene expression time-series analysis of Camptothecin effects in U87-MG and DBTRG-05 glioblastoma cell lines. *Mol. Cancer* 7, 1-16.

Mosmann T. 1983. Rapid calorimetric assay for cellular growth and survival: application to proloferation and cytotoxicity assays. *J Immunol Methods*, 65, 55-63.

Panahi, Y., *et al.*, 2017. Recent advances on liposomal nanoparticles: synthesis, characterization and biomedical applications. *Artificial Cells, Nanomedicine, and Biotechnology,* 45, 788-799.

Perche, F., and Torchilin, V.P., 2013. Recent trends in multifunctional liposomal nanocarriers for enhanced tumor targeting. *Journal of Drug Delivery* [online], Article ID 705265, Available from: http://dx.doi.org/10.1155/2013/705265 [Accessed 6 February 2013].

Pérez-Herrero, E., and Fernández-Medarde, A., 2015. Advanced targeted therapies in cancer: Drug nanocarriers, the future of chemotherapy. *Eur J Pharm Biopharm,* 93, 52-79.

Pommier, Y., 2006. Topoisomerase I inhibitors: camptothecins and beyond. *Nat Rev Cancer*, 6, 789-802.

Randall-Whitis, L.M., and Monk, B.J., 2007. Topotecan in the management of cervical cancer, *Expert Opinion on Pharmacotherapy,* 8, 227-236.

Rivory, L.P., 1996. Conversion of irinotecan (CPT-11) to its active metabolite, 7-ethyl-10-hydroxycamptothecin (SN-38), by human liver carboxylesterase. *Biochem Pharmacol*, 52, 1103–1111.

Sadzuka, Y., Hirotsu, S., and Hirota, S., 1999. Effective Irinotecan (CPT-11)-containing liposomes: Intraliposomal conversion to the active metabolite SN-38. *Jpn J Cancer Res*, 90, 226-232.

Sadzuka, Y., Takabe, H., and Sonobe, T., 2005. Liposomalization of SN-38 as active metabolite of CPT-11. *J Control Release*, 108, 453–459.

Sen K., and Mandal, M., 2013. Second generation liposomal cancer therapeutics: Transition from laboratory to clinic. *Int J Pharm*, 448, 28-43.

Slatter J. G., *et al.*, 1997. Bioactivation of the anticancer agent CPT-11 to SN-38 by human hepatic microsomal carboxylesterases and the in vitro assessment of potential drug interactions. *Drug Metab Dispos,* 25, 1157-1164,

Stewart, J.C.M., 1980. Colorimetric determination of phospholipids with ammonium ferrothiocyanate. *Anal Biochem*, 104, 10–14.

Teicher, B.A., 2008. Next generation topoisomerase I inhibitors: rationale and biomarker strategies. *Biochem Pharmacol*, 75, 1262-1271.

Torchilin, V.P., 2014. Multifunctional, stimuli-sensitive nanoparticulate systems for drug delivery. *Nature Reviews Drug Discovery*, 13, 813-827.

Wicki, A., *et al.*, (2015) Nanomedicine in cancer therapy: Challenges, opportunities and clinical applications. *J. Control. Release,* 200, 138-157.

Wolterbeek, H.T., and van deer Meer, A.J.G.M., 2005. Optimization, application, and interpretation of lactate dehydrogenase measurements in microwell determination of cell number and toxicity. Assay Drug Dev Techno. 3, 675-682.

Wu, M.H., *et al.*, 2002. Irinotecan activation by human carboxylesterases in colorectal adenocarcinoma cells. *Clin Cancer Res*, 8, 2696-2700.

Yu, B., Lee, R.J., and Lee, L.J., 2009. Microfluidic Methods for Production of Liposomes. *Methods Enzymol*, 465, 129–141.

Zylberberg, C., and Matosevic, S., 2016. Pharmaceutical liposomal drug delivery: a review of new delivery systems and a look at the regulatory landscape. *Drug Delivery,* 23:9, 3319-3329.

Quinto artículo

Incorporation of the concept of mucoadhesiveness to the design of pharmaceutical formulations for the camptothecins CPT-11 and SN-38

Casadó A, Sagristá ML*, Mora M.

Pendiente de envío

RESUMEN

Objetivo La vehiculización dirigida mediante sistemas partículados, como los liposomas, y la liberación controlada de fármacos antitumorales, son de especial relevancia en el tratamiento del cáncer. Este artículo está dirigido a la obtención de liposomas mucoadhesivos para la administración oral de CPT-11 y SN-38 para el tratamiento del cáncer de colon.

Métodos Se han considerado liposomas unilamelares intermedios (IUVs) con carga superficial negativa, preparados siguiendo procedimientos estándar y tecnologías de recubrimiento para mejorar la biodisponibilidad de fármacos. Se han determinado las propiedades mucoadhesivas de los liposomas recubiertos con quitosano midiendo la adsorción de la mucina, utilizando un ensayo colorimétrico para glicoproteínas. El tamaño, la distribución de tamaños y el potencial ζ de los IUVs, no recubiertos y recubiertos con quitosano, se han determinado mediante espectroscopia de correlación fotónica. La nanoestructura de los liposomas recubiertos con quitosano se observó mediante microscopía de fuerzas atómicas.

Resultados El tamaño y el índice de polidispersidad de liposomas recubiertos aumentan a medida que se incrementa la concentración de quitosano hasta el 0,05%, independientemente de la composición de los liposomas. Sin embargo, a una concentración de 0,1% de quitosano, se observó un aumento de tamaño en función de la composición de los liposomas. En general, los liposomas recubiertos con quitosano, que posees el mayor potencial ζ y el diámetro más pequeño, son aquellos que presentan más mucoadhesividad. Las vesículas preparadas a partir de EPC/DOPS (90:10) y DSPC/DOPS/CHOL (65:35:30) que contienen, respectivamente, SN-38 y CPT-11 encapsulados y que se recubrieron utilizando una disolución de quitosano UPCl113 al 0,05% resultaron ser las dotadas de las mejores propiedades estructurales y mucoadhesivas.

Conclusiones La interacción electrostática del polímero catiónico quitosano con las superficies de las bicapas negativas, preparadas a partir de EPC/DOPS y

DSPC/DOPS/CHOL, proporciona la base para la formación de una cubierta estable alrededor de los liposomas. El diseño de nuevos productos farmacéuticos para administración oral, basado en la utilización de cápsulas entéricas rellenas con liposomas recubiertos con quitosano y que contienen SN-38 o CPT-11 encapsulados, representará un paso adelante en el tratamiento del cáncer.

RESUMEN GRÁFICO

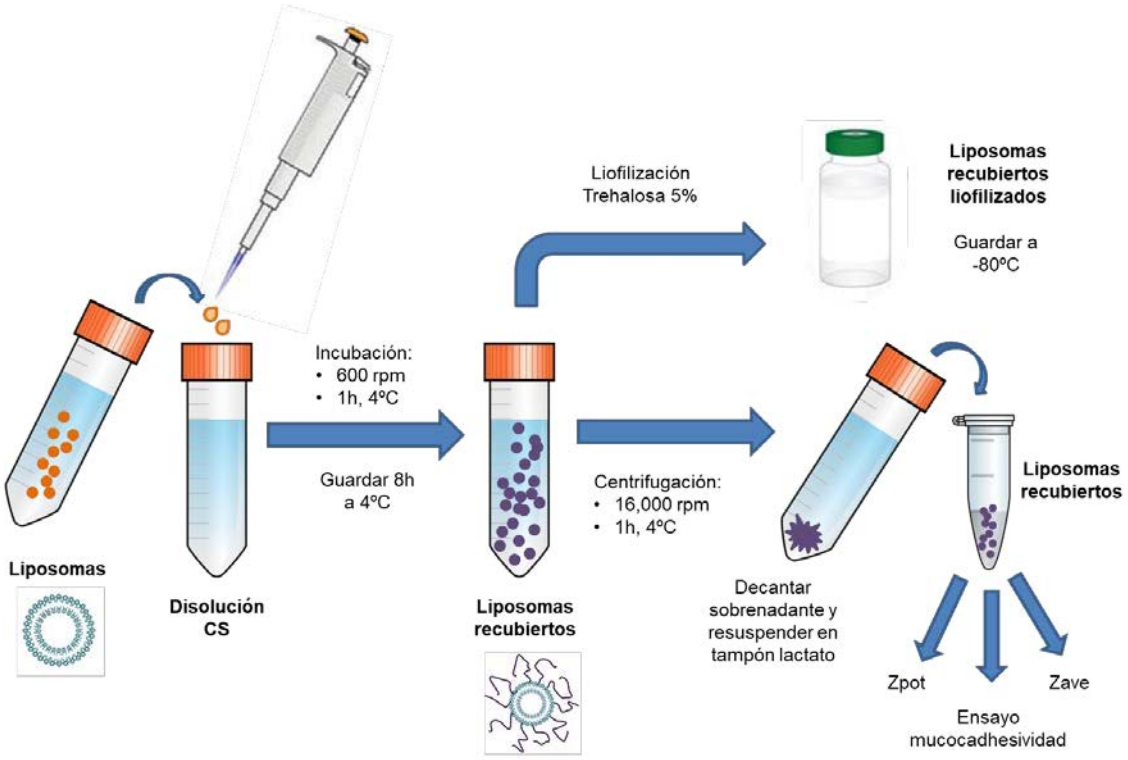

Incorporation of the concept of mucoadhesiveness to the design of pharmaceutical formulations for the camptothecins CPT-11 and SN-38

Ana Casadó, M. Lluïsa Sagristá*, Margarita Mora

[(1)]Departamento de Bioquímica y Biomedicina Molecular, Facultad de Biología, Universidad de Barcelona, Avenida Diagonal 643, 08028-Barcelona, España.

Corresponding Author:

Prof. Dr. M. Lluïsa Sagristá
Department of Biochemistry and Molecular Biology, Faculty of Biology, University of Barcelona, Av. Diagonal 643, Annex Building, 08028-Barcelona, Spain.
Tel: 0034-93-4021212, Fax: 0034-93-4021259, E-mail: mlsagrista@ub.edu

Running head: Mucoadhesive liposomal camptothecins

ABSTRACT

Purpose Drug targeting by using particulate systems, like liposomes, and controlled release of antitumor drugs are of special relevance in cancer treatment. The present paper is directed to the procurement of mucoadhesive liposomes for the oral delivery of CPT-11 and SN-38 to the colon.

Methods Intermediate unilamellar liposomes (IUVs) with negative surface charge, prepared following standard procedures and coating technologies to improve drug bioavailability, have been considered. Mucoadhesive properties of chitosan-coated liposomes were determined measuring the adsorption of mucin by using a colorimetric assay for glycoproteins. The size, size distribution and ζ potentials of un-coated and chitosan-coated IUVs were determined by photon correlation spectroscopy. The nanostructure of chitosan-coated liposomes was observed by atomic force microscopy.

Results The size and the polydispersity index of coated liposomes increases when raising chitosan concentration up to 0.05%, irrespective of liposome composition. Nevertheless, at a concentration of 0.1% chitosan, an increase in size as a function of the liposomes composition was observed. In general, chitosan-coated liposomes, with the highest ζ potential and the smallest diameter, are those with more mucoadhesiveness. EPC/DOPS (90:10) and DSPC/DOPS/CHOL (65:35:30) vesicles loaded with SN-38 and CPT-11, respectively, and coated with 0.05% UP Cl 113 chitosan were endowed with the best structural and mucoadhesive properties.

Conclusions The electrostatic interaction of the cationic polymer chitosan with the negative EPC/DOPS and DSPC/DOPS/CHOL bilayer surfaces establishes the basis for the formation of a stable coverage around liposomes. The design of new pharmaceutical products for oral administration, based on enteric capsules filled with chitosan-coated SN-38 or CPT-11 loaded liposomes will represent a step forward in cancer treatment.

KEY WORDS: anionic liposomes, CPT-11, SN-38, drug delivery, chitosan-surface coating, triggered release.

ABBREVIATIONS

AFM: Atomic Force Microscopy / BBE: Bovine Brain Extract / CHOL: Cholesterol / CPT-11: Irinotecan / DMSO: Dimethyl Sulphoxide / DSPC: L-α-Distearoyl-phospathidylcholine / IUV: Intermediate Unilamellar Liposome / MLV: multilamellar liposome / DOPS: L-α-Dioleoyl-phospathidylserine / PCS: Photon Correlation Spectroscopy /LE: Soy Lipid Extract / SM: Sphyngomielin / SN-38: CPT-11 metabolite / SUV: Small Unilamellar Liposome

INTRODUCTION

Cancer is currently one of the leading causes of death worldwide. Among the different types of cancer, colon cancer accounts for about 10% of diagnosed cases, is the third most common cancer in men and the second in women and almost 55% of the cases occur in the more developed regions. Moreover, colorectal cancer (CRC) causes the death of up to 50% of patients who, having potentially overcome the disease by surgery, experience a relapse due to metastatic processes (Edwards *et al.*, 2010; Ferlay *et al.*, 2015).

Different strategies have been developed in order to eliminate the growth of neoplastic tissues and to solve some of the main problems underlying cancer treatment. For the treatment of CRC, there are four approaches: i) surgery is the main treatment in the early stages of the disease, in which tumor excision can be carried out without the need to administer another treatment, since the rate of recurrence when regional nodes are not involved is very low; ii) chemotherapy is used for neoadjuvant therapy in order to shrink the tumor before surgery, facilitating the procedure, and it can be used after surgery to attack any cancer cells that might remain and reduce the risk of tumor reproduction; iii) radiation is the option used to shrink tumors before surgery or to destroy any remaining cancer cells after chemotherapy; iv) the treatments known as targeted therapies, which target the cancer's specific genes, proteins, or the tissue environment that contributes to cancer growth and survival. The sequence, in which the therapeutic agents are used, alone or in combination, is important for maximum control of the disease with minimal side effects (Cancer.Net, 2016).

Irinotecan (CPT-11, Camptosar), in soluble form, is among the first-line approved chemotherapeutic agents by the U.S FDA for the treatment of a variety of human tumors, including CRC (Liew and Yang, 2008). Only 2-8 % of irinotecan is converted to its active form SN38 in liver and cancer cells, but the clinical use of SN38 is limited by its poor aqueous solubility (< 5 μg/mL). The camptothecins, irinotecan and SN38 are antineoplastic agents belonging to the family of topoisomerase I inhibitors that arrest the synthesis of DNA and possess strong antitumor activity (Gerrits *et al.*, 1997; Pommier, 2009). However, the use of CPT-11 and SN38 is limited by the conversion of the pharmacologically active lactone ring to the inactive carboxylate form at pH > 6, which has less than 10% the potency of the lactone form as a topoisomerase I inhibitor (Kohn and Pommier, 2000; Teicher, 2008). Other drawbacks for their clinical applications are their severe systemic side effects, such as myelosuppression and gastrointestinal disorders with acute delayed diarrheas, with or without neutropenia (Garcia-Carbonero *et al.*, 2002; Alimonti *et al.*, 2004), due to the fact that most anticancer agents in soluble form are unable to differentiate between cancer cells and normal cells (Sinha *et al.*, 2006). Everything discussed so far, imposes some restrictions on the use of these camptothecins in their soluble form in cancer therapy

and makes necessary the search of appropriate formulations for these antineoplastic drugs.

Several research programs have focused on the design of effective formulations for anticancer drugs. In this sense, targeted drug delivery systems (DDSs) have received special attention because they can detect cancer in its premalignant stage, locate cancerous tissue in the body, direct the drug to a specific target and sustain their release in cancer tissue (Sinha *et al.*, 2006). Thus, the use of DDSs can overcome some of the problems associated with traditional drugs, such as poor aqueous solubility, low bioavailability, toxicity and nonspecific distribution in the body. The types of nanocarriers to be used are diverse and among of them we can consider: liposomes; polymeric nanoparticles; polymeric micelles; silica, gold, silver and other metal nanoparticles; carbon nanotubes; solid lipid nanoparticles; niosomes; and dendrimers (Torchilin, 2014). The majority of preclinical research with DDSs relates to the delivery of cytotoxic agents in cancer chemotherapy and, in all cases, the therapeutic benefits and the improvement of the pharmacological drug properties have been reported (Torchilin, 2006; Thassu *et al.*, 2007). Moreover, CPT-11 and SN38 encapsulated in liposomal DDSs, one of the most popular pharmaceutical nanocarriers, are now at different stages of development (Torchilin, 2014; Bozzuto and Molinari, 2015) and recently the FDA approved a novel liposomal encapsulated form of CPT-11 for pancreatic cancer therapy (Carnevale and Ko, 2016).

In the case of CRC, as well as in a variety of severe conditions of gastrointestinal diseases, the direct targeting of the drugs to the colon offers significant advantages over other therapeutic strategies (Yang *et al.*, 2002; Chourasia and Jain, 2003). Besides specific characteristics, in general, ideal liposome formulations should be stable in the bloodstream when systemically administered, have controlled circulation lifetimes, be localized at the site of disease and bind and deliver the drug specifically to the target cell. On the other hand, when thinking about the direct targeting to the colon and with the possibility to develop oral formulations, coating materials, such as biodegradable polymers, can be extremely useful. In this way, polysaccharides should be seriously considered as they can afford, besides protection, other additional and interesting properties to the carrier (Jain *et al.*, 2007). Natural polysaccharide polymers are highly stable, safe and non-toxic, have been approved as pharmaceutical excipients and have biodegradable and biocompatible characteristics. Because of this, a great number of polysaccharides have already been used as coating materials to get colon-specific drug carrier systems, such as inulin and pectins of vegetal origin, or chitosan, chondroitin sulphate and hyaluronic acid from animals (Sinha and Kumria, 2001; Patel *et al.*, 2007). In addition, liposomal particles with some polysaccharide coatings are endowed with mucoadhesive properties through a mechanism based on chemical and physical mucous-polymer interactions (Artursson et al., 2001). When

mucoadhesive polymers are used, the residence time of dosage forms on the mucosa can be significantly prolonged, allowing a sustained drug release at the target site. This is of particular relevance when the target for a pharmaceutical drug is the colon. All of these considerations and a few more not referenced here invite to use natural polymers in the design of colon-specific and sustained drug release systems.

Mucus is often the first barrier found by drugs in the body. Mucus is ubiquitous in many areas of the body, including lungs, gastrointestinal tract, vagina, eyes and nasal area. For this reason, the design of new DDSs able to diffuse through the mucus to achieve their pharmacological targets is needed (Groo and Lagarce, 2014). There are various models of mucus described in the literature, from the simplest ex vivo model (He *et al.*, 2012; Petit *et al.*, 2012) to the closest in vivo models (Behrens *et al.*, 2002; Jin et al., 2012), and from simple mucin (Larhed *et al.*, 1997; Khanvilkar *et al.*, 2001; Hosseinzadeh *et al.*, 2012) and artificial mucus (McGill and Smyth, 2010), to natural mucus (Li *et al.*, 2011). Different studies confirm the relation between the size of DDSs and mucoadhesion and conclude that smaller particles move faster in mucus (McGill and Smyth, 2010; He *et al.*, 2012), being the limited ability of particles > 0.5 μm to diffuse through mucus the result of a steric obstruction of mucin mesh spacing. Moreover, significant differences were showed between anionic and cationic particle mucus-penetrating capacities (Crater and Carrier, 2010).

The oral targeting of pharmaceutical drugs to the colon makes possible to achieve local or systemic delivery of drugs to this place. To deliver drugs to the lower part of the gastrointestinal tract without being degraded, DDSs must first pass through the stomach and the upper intestine without being altered, to reach the colon, where using their inherent characteristics, degradation occurs to specifically release the drugs to this part of the digestive tract (Jain *et al.*, 2007). The colonic microflora is formed by a large number of anaerobic bacteria that produce a broad spectrum of polysaccharidases, whose function is to degrade polysaccharides to obtain its main source of energy (Yang *et al.*, 2002; Krishnaiah and Khan, 2012). The hydrolysis of the glycosidic linkages of polysaccharides when the vehicle reaches the colon, allows the release of the DDSs with the encapsulated drug at the site of action, without there being barely any loss of the active ingredient in the stomach or small intestine.

Chitosan is a polycationic polysaccharide, with high molecular weight, obtained by alkaline deacetylation of chitin (Sinha and Kumria, 2001). Chitosan is the most abundant natural polysaccharide along with cellulose and is not degraded by digestive enzymes of the principle of the gastrointestinal tract. It is not toxic, biocompatible and biodegradable and also is mucoadhesive (Gulbake and Jain, 2012). Because of its solubility at acidic pH (it precipitates at pH above 6), chitosan must be protected from stomach acidity. This is achieved with an enteric coating, that remains intact at acidic pH and dissolves as the pH increases (Felt *et al.*, 1998). Thanks to its mucoadhesive

properties has the advantage over other polysaccharides, to interact with the colonic mucosa and get a longer retention time. Its interaction with the mucosa is of electrostatic type and takes place between its primary amino groups, positively charged, and the groups sulfonate and sialicate of the mucin layer, negatively charged (Gulbake and Jain, 2012; Bernkop-Schnurch, 2005; Vasir *et al.*, 2003). Several studies have used chitosan derivatized or crosslinked with other polymers or with calcium to develop drug delivery systems to the colon (Tozaki *et al.*, 2002; Lorenzo-Lamosa *et al.*, 1998; Zhang *et al.*, 2002; Zhang and Neau, 2002; Jain *et al.*, 2008; Jain *et al.*, 2010). If liposomes are used as the basic units of DDSs and in its formulation are included anionic lipids, the resulting bilayer will have negative charge and will be possible to create a coverage of chitosan hydrophilic, mucoadhesive and stable around the liposomal surface through electrostatic interactions. Moreover, it is interesting to note that the carriers with chitosan can be formulated as tablets, microparticles or microspheres, capsules, nanoparticles or hydrogels (Gulbake and Jain, 2012), which contituye an additional advantage.

This paper presents a preliminary study about the coverage of liposomal surface with cationic mucoadhesive polymers thinking in the oral delivery of CPT-11 or SN-38 to the colon. The adsorption of mucin over chitosan-coated liposomes was measured to prove the mucoadhesive properties of the obtained drug delivery systems.

MATERIALS AND METHODS

Materials

L-α-Distearoyl-phospathidylcholine (DSPC), L-α-Dioleoyl-phospathidylserine (DOPS), Sphyngomielin (SM), Cholesterol (CHOL), Egg phosphatidylcholine (EPC) and soy lipid extract (SLE) were purchased from Avanti Polar Lipids (Birmingham, AL, USA). Bovine brain extract (BBE) was kindly provided by Bioiberica S.A. (Palafolls, Spain). Polycarbonate membranes were from Poretics Products (Osmonics, Inc., Livermore, CA, USA). Chitosans (UP Cl 113, UP Cl 213, UP G 113, UP G 213) were obtained from Novamatrix (FMC Biopolymer AS, Drammen, Norway). Type III mucin and the Schiff reagent were from Sigma-Aldrich Chemical Co. (St. Louis, MO, USA). CPT-11, purchased from Afine Chemicals Limited (Hangzhou, China), was pure with a minimal grade of 99%. SN-38 was purchased from Tocris Bioscience (Bristol, United Kingdom). Centricon YM-10 Filter Devices were form EMD Millipore Corporation,(Billerica, MA, USA). All the organic solvents (Panreac, Montcada I Reixac, Barcelona, Spain) have been distilled before use. Milli-Q water (Millipore Bedford, Massachusetts system, resistivity of 18 MΩ·cm) was used. All other chemicals and solvents were of analytical grade. Dimethyl sulphoxide (DMSO) and was purchased from Sigma-Aldrich Chemical Co. (St. Louis, MO, USA).

Liposome preparation

Intermediate unilamellar liposomes (IUVs) were prepared following standard procedures (Mora *et al.*, 2003). DSPC, DPPC, DOPS and SM chloroform solutions were mixed in ternary combinations, at the appropriate molar ratios, to prepare the lipid films. Alternatively, liposomes were prepared using a bovine brain extract (BBE) or a soy lipid extract (SLE). Multilamellar liposomes (MLVs) were first prepared by hydrating the dried lipid films with 10 mM lactate buffer (pH 4.4) to a final lipid concentration from 1 to 20 mg/mL, unless otherwise was stated. MLVs dispersions were frozen -liquid N_2- and thawed -water bath- above the phase transition temperature (T_m)- five times. For IUVs preparation, MLVs suspension was sonicated in a bath sonicator (Branson 2510, Danbury, CT, USA) for 20 min above the T_m and extruded (Lipex Biomembranes Inc., Vancouver, Canadá) through different pore-sized polycarbonate membranes (Osmonics Inc., Livermore, CA, USA). The pore size of polycarbonate membrane filters ranged from 400 to 200 nm. Liposomes were stored in the dark at 4 ºC. Empty liposomes were prepared for the previous assays and CPT-11 and SN-38 loaded liposomes were procured, as summarized below, by the protocols standardized before (Casadó et al., 2014; Casadó et al., unpublished results)

Phospholipids quantization assay

The lipid amount in the liposome suspensions was measured following the Stewart's method (Stewart, 1980). Calibration curves for each lipid composition (from 0.01 to 0.2 mg lipid) were obtained to quantify the total lipid amount. Each sample was maintained under a nitrogen stream for chloroform evaporation and 2 mL of chloroform and 2 mL of ammonium ferrothiocyanate were added. Samples were vortexed and centrifuged (4000 rpm, 10 min) to extract the chloroformic phase and the absorption spectra were obtained to select the absorbance maximum. Absorbance measures were carried out in a Beckman DU40 spectrophotometer (Beckman Coulter, Inc., Fullerton, CA USA).

Coating of liposomes by chitosan

Coating of IUVs with chitosan was carried out following the Filipovic-Grcic method (38), by mixing the liposomal suspension with different chitosan solutions at 1:1 and 1:4 (v/v) ratios. Chitosan solutions were also prepared in 10 mM lactate buffer (pH 4.4) at a concentration range from 0.001% to 0.1 % (w/v). The liposomal suspension (10 mg lipid/mL) was added dropwise into the respective chitosan solution, at the appropriate volume ratio, under stirring for 1h, at 600 rpm and 20ºC (Thermomixer comfort,

Eppendorf). The suspension was kept overnight at 4 °C and chitosan-coated liposomes were harvested by centrifugation at 16,000 rpm at 4°C for 60 min (JA-25.50 rotor, Beckman Coulter) and dispersed in the appropriate buffer. The efficacy of the coating was expressed as the amount of chitosan adhered per mg of lipid. The lipid content in the coated liposomal suspensions was measured following the Stewart's method (Stewart, 1980).

Mucoadhesive assay of chitosan-coated liposomes

The adsorption of mucin on chitosan-coated liposomes was determined by using the colorimetric assay for glycoproteins described by He et al. (2012). Briefly, an aliquot of chitosan-coated liposomes, containing 1.4 mg of lipid, was diluted with lactate buffer to a final volume of 0.5 mL and mixed with 0.5 mL of an aqueous solution of mucin (0.5 mg/mL). The mixtures were shacked at 20ºC for 60 min and centrifuged at 12000 rpm for 10 min and supernatants were used to determine free mucin. Total amount of free mucin in solution was quantified by using a standard calibration curve prepared from standard solutions of mucine (0.005 to 0.1 mg mucin/mL). A volume of 0.1 mL of the periodic acid reagent, obtained by mixing 10 µL of 50% periodic acid and 7 mL of 7% acetic acid, was added to 1 mL of each mucin solution and the samples were incubated at 37°C for 2h. After cooling at room temperature, 0.1 mL of the Schiff reagent were added. Thirty minutes later, the absorbance was measured at 555 nm. The calibration curve used was obtained from the mean absorbance values calculated, for each mucine concentration, from eleven independent experiments:

$$A_{555} = 7{,}7166\ [\text{mucine}] - 0{,}0096, \quad R^2 = 1$$

where [mucine] was expressed as mg mucin/mL standard solution. To quantify free mucin, 0.2 mL of each supernatant were diluted with 0.8 mL of lactate buffer and the samples were subjected to the same procedure than that used for the standard calibration curve. The mucin adsorbed on the surface of the chitosan-coated liposomes was calculated from the difference between total and free mucin.

Vesicle size and ζ potential determination

The size, size distribution and ζ potentials of unilamellar vesicles were determined by photon correlation spectroscopy (PCS), in a Malvern Zetasizer NANO-ZS device (Malvern Instruments Ltd, Malvern, UK) equipped with an optic unit containing a 5 mW He-Ne laser (Spectra Physics) and an electrophoresis cell. Size measurements were performed at excitation wavelength of 633 nm and 25°C, from liposomal suspensions containing 0.2 mg lipid/mL. Data were collected with a Malvern data channel correlator and the mean hydrodynamic diameter was calculated from a cumulant analysis of the intensity autocorrelation function. ζ potential was also measured at 25 °C and 0.2 mg

lipid lipid/mL liposomal suspensions. The Malvern device was calibrated with carboxy-modified polystyrene latex samples of known ζ potential.

Atomic force microscopy

The possible structural changes induced by the chitosan coating of liposomes were analyzed by Atomic Force Microscopy (AFM). Imaging was performed in the Tapping Mode using a Nanoscope III (Digital Instruments, Santa Barbara, CA, USA) under ambient conditions. Tapping Mode cantilevers, made of monocrystal silicon with spring constant of 38-74 N/m and typical resonance frequencies of 270-377 KHz (Point Probes, Nanosensors, Wetzlar-Blankenfeld, Germany), were used. Liposomes were developed on a freshly cleaved mica substrate by depositing a drop (20 µL) of 0.05 mg lipid/mL buffered liposome suspension. The samples were maintained at room temperature for 45 minutes, in a closed vessel and the mica surface was cleaned with the buffer used for liposomes preparation.

Irinotecan entrapment in chitosan coated-liposomes

CPT-11-containing IUVs (10 mg lipid/mL) were prepared as described before, in lactate buffer 10 mM pH 4.4. CPT-11 in chloroform/methanol (2:1, v/v) was added to the lipids before the film formation at 7.5:1 lipid/CPT-11 molar ratio. Unilamelar liposomes were prepared by extrusion through polycarbonate membranes up to 200 nm pores size indicated previously (Casadó *et al*., 2014; Casadó *et al*., 2017). Liposomes coating by chitosan was carried out as indicated in the first section of methods by mixing the liposomal suspension with two different chitosan solutions (0.005 and 0.1%) at 1:4 (v/v) ratios. To quantify the total drug and the drug entrapped into coated liposomes a calibration curve for CPT-11 (from 0.005 to 0.02 mg/mL) was obtained. Absorbance measures were determined at 368.8 nm. To quantify entrapped CPT-11, the Liposomal-CPT-11 suspension was removed from the extraliposomal non-encapsulated drug by using Centricon YM-10 Filter Devices (EMD Millipore Corporation, Billerica, MA, USA) and the entrapped amount of CPT-11 was obtained from the total CPT-11 in the film and the non-entrapped quantified drug amount.

SN-38 entrapment in chitosan coated-liposomes

A suspension of multilamellar liposomes (MLVs) was first prepared by direct hydration of lipids and SN-38. EPC, DOPS and SN-38 were mixed in a 90:10:5 molar ratio and the dry powder mixture was hydrated with 10 mM lactate (pH 4.4) buffer to a final lipid concentration of 10 mg lipid/mL. The hydration was performed with a T 25 digital ULTRA-TURRAX® dispersing device (IKA, Staufen, Germany). MLV dispersions were then sonicated for 10 min in an ultrasonic bath (Branson, Danbury, USA) above the

phase transition temperature (Tm) and processed by a high pressure Microfluidizer homogenizer (Avestin M-110EH-30 Microfluidizer® Processor or Emulsiflex C3). Liposomes size can be controlled by adjusting the fluid flow rates in the microfluidic network. Liposomes were stored in the dark at 4°C. Liposomes coating by chitosan was carried out as indicated in the first section of methods by mixing the liposomal suspension with two different chitosan solutions (0,005 and 0,1%) at 1:4 (v/v) ratios. To calculate total SN-38 and SN-38 entraped into chitosan coated liposomes a calibration curve for SN-38 (from 1 to 30 μM) was previously obtained in DMSO at λ_{max} (390 nm). Liposome-entrapped SN-38 was quantified as the difference between the total SN-38 and the amount of non-encapsulated drug. An aliquot of the liposomal-SN-38 suspension was centrifuged using Centricon YM-10 Filter Devices (Millipore Corporation, Billerica, USA) to obtain a filtrate containing the non-entrapped drug, without liposomes.

RESULTS

Mucoadhesive test of chitosan coated liposomes

The coverage of negatively charged liposomes with the cationic polymer chitosan establishes the basis for the formation of a stable mucoadhesive carrier with the ultimate purpose of developing a product for oral administration. This strategy leads to the procurement of microflora-activated systems, sensitive to the special physiological conditions of the colon, by means a triggered mechanism in which bacterial polysaccharidases are involved (Guarner and Malagelada, 2003).

The phenomenon of bioadhesion was introduced by Park and Robinson (Park and Robinson, 1984) and studied extensively in the last years. Thus, a great number of polysaccharides, such as chitosan, pectins, chondroitin sulphate or hyaluronic acid, have already been used as coating materials to get colon-specific drug carrier systems (Jain *et al*., 2007). Among these, chitosan is one of the most used polymers, being underlined the benefits of chitosan coatings to improve drug absorption in oral, intraoral, sublingual and intestinal formulations. Thus, the protocol to get chitosan-coated liposomes has been established (see methods section).

The solution used to hydrate the lipid mixture and to dissolve chitosan was 10 mM lactate buffer pH 4.4, after studying the influence of the pH and the buffer nature on the coating process. Neither buffered solutions with pH values higher than 6.0 nor acidic buffers different to lactate, such as citrate or succinate, allowed a chitosan distribution over liposome surface in a flat manner, giving heterogeneous sized and unstable suspensions (Claesson and Ninham, 1992).

The mucoadhesive behavior of chitosan-coated and uncoated liposomes, used as controls, was assessed with a mucin aqueous solution at room temperature (Hea *et al.*,

1998). The free mucin concentration was measured after 1 h incubation of chitosan-coated liposomes with mucin, as indicated in Methods.

An initial experiment was performed to establish the mucoadhesive properties of DSPC/DOPS/CHOL liposomes coated with different chitosan molecules to choose the best option to continue with the study. This liposomal formulation was chosen after our data published in a previous paper (Casadó *et al*., 2014), corresponding to CF release measurements and CPT-11 entrapment efficiency using liposomes of different composition. Results showed that the DSPC/DOPS/CHOL (65:35:30, molar ratio) lipid mixture was the better composition to procure temperature-sensitive liposomes with a high entrapment efficiency for CPT-11. Thus, the effect of chitosan MW (50,000 to 400,000 g/mol) and the nature of the counter-ion (chloride or glutamate) of chitosans on the mucoadhesiveness of chitosan-coated liposomes were assessed (Fig. 1).

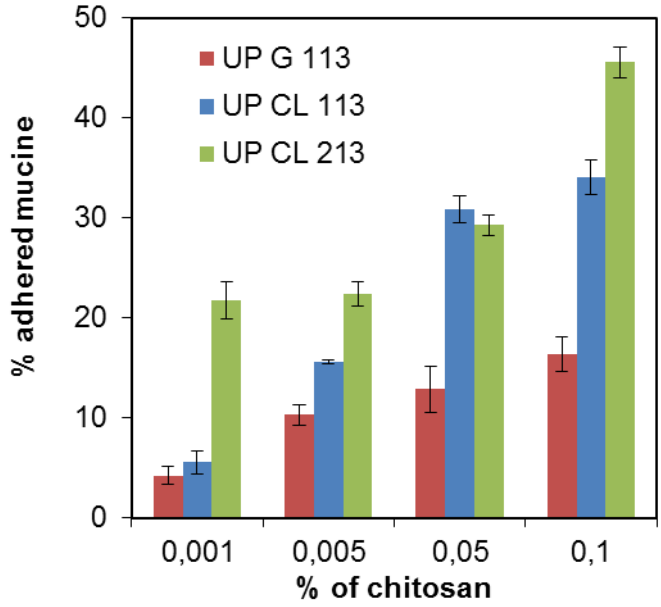

Fig. 1. Influence of chitosan nature on mucoadhesivity of DSPC/DOPS/CHOL (65:35:30) coated liposomes. To determine the effect of chitosan nature, liposomal suspensions and chitosans UP CL 113, UP CL 213 or UP G 113 solutions of different concentrations were mixed at 1:4 (v/v) ratios. Mucin assay was used to quantify mucoadhesivity. Uncoated liposomes were used as controls. Results are the means of individual experiments performed in triplicate. CV ranged from 5.5 to 20.7%.

The results show that, at the same MW, chitosan containing glutamate (UP G 113) gave less mucoadhesive chitosan-coated liposomes than those obtained with chitosan chloride (UP CL 113) for all the polysaccharide concentrations assayed. Moreover, the mucoadhesivity of chitosan-coated liposomes obtained with the high MW chitosan chloride (UP CL 213) was always higher than that obtained with the small MW chitosan chloride (UP CL 113). Nevertheles, chitosan UP CL 213 coating gives liposomes higher sized than those coated with chitosan UP CL 113 (Table I).

The results of Figure 1 and Table I indicate that the chitosan chloride UP CL 113 provides chitosan-coated DSPC/DOPS/CHOL liposomes with the best relationship between size and adhered mucine. Figure 2 shows the nanostructure of chitosan-coated and uncoated liposomes, as observed by AFM: the image in Fig 2B displays the association of coated liposomes through a net of chitosan chains.

Table I. Average size and polydispersity index of UP Cl 113 and UP Cl 213 chitosan-coated liposomes. Liposomes were obtained from a DSPC/DOPS/CHOL (65:35:30) mixture and coated with UP CL 113 and UP CL 213 chitosan solutions of different concentration.

[Chitosan]	UP CL 113 chitosan		UP CL 213 chitosan	
	Zave[1]	Poly[2]	Zave[1]	Poly[1]
0.001%	201.5 ± 23.6	0.158	210.1 ± 14.5	0.139
0.005%	307.6 ± 31.7	0.337	377.0 ± 33.2	0.730
0.05%	512.4 ± 17.8	0.435	893.2 ± 20.9	0.427
0.1%	637.9 ± 58.8	0.540	1210.3 ± 48.2	0.510

[1] Z average mean calculated from photon correlation spectroscopy data. Data are the mean values ± S.D. of three independent experiments. [2] Polydispersity index which measures of the homogeneity of the liposomal suspensions.

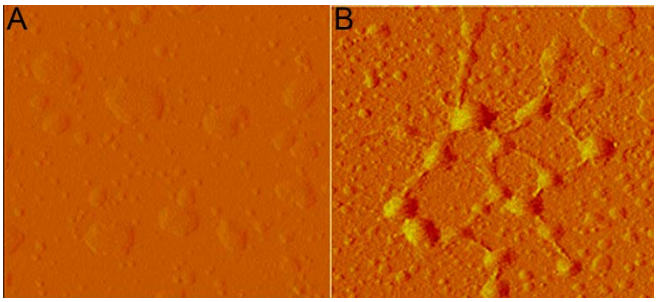

Fig. 2. AFM images of uncoated- and chitosan-coated liposomes. Uncoated DSPC/DOPS/CHOL (65:35:30) intermediate unilamellar liposomes (A) and chitosan-coated DSPC/DOPS/CHOL liposomes (B), prepared by mixing 1 volume of the liposomal suspension and 4 volumes of a 0.001% chitosan solution.

Mertind and Dimova (2011), characterized the binding and the organization of chitosan on the membrane of DOPC/DOPG small liposomes by thermodynamic studies. They showed that the polymer covers the outer monolayer with neutral charge, slightly or strong negative of the liposomal bilayer. However, they noted that the increase of the negative charge of the vesicles leads to an increase of chitosan absorption and to a weaker organization of the polymer chains. They also proposed that by saturating the negatively charged liposomes with chitosan, the free spaces left on the outer monolayer were filled and the aggregation of liposomes occurred.

The effect of the relative concentrations of liposomes and chitosan in incubates on the mucoadhesive properties of chitosan-coated liposomes was also studied by mixing the DSPC/DOPS/CHOL (65:35:30, molar ratio) and the EPC/DOPS (90:10, molar ratio) liposomal suspensions with chitosan UP Cl 113 solutions at 1:1 and 1:4 v/v ratio. For this experiment, the new lipid EPC/DOPS mixture was also considered after an accurate selection in our laboratory to establish the best lipid mixture to encapsulate SN-38 with high efficiency (Casadó *et al.,* 2017 submitted). Moreover, parallel studies related to the interactions between the camptothecin drugs CPT-11 and SN-38 and the biomembrane models obtained with DSPC/DOPS/CHOL and EPC/DOPS mixtures, respectively, carried out using Langmuir monolayers and differential scanning calorimetry techniques, showed the suitability of these ternary and binary lipid mixtures for encapsulating CPT-11 and its metabolite SN-38, respectively (Casadó *et al.*, 2016). The results obtained in this study are showed in Figure 3.

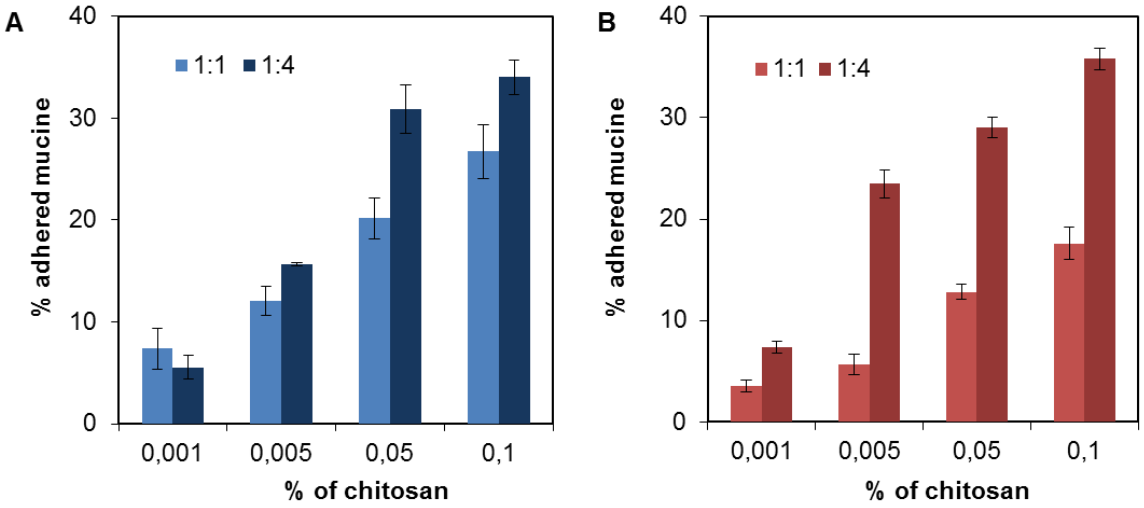

Fig. 3. Influence of the relative concentrations of liposomes and chitosan on the mucoadhesivity of coated liposomes. To study the influence of concentration, liposomal suspensions of (A) DSPC/DOPS/CHOL (65:35:30) and (B) EPC/DOPS (90:10), obtained at a lipid concentration of 10 mg lipid/mL, and chitosan UP CL 113 solutions of different concentrations were mixed at 1:1 and 1:4 (v/v) ratios. Mucin assay was used to quantify mucoadhesivity. Uncoated liposomes were used as controls. Results are the means of individual experiments performed in triplicate. CV ranged from 0.2 to 11.7%.

The plotted results show that the amount of mucin adsorbed is higher when liposomal suspensions and chitosan solutions are mixed at the 1:4 v/v ratios, irrespective of the chitosan concentration and the lipid mixture used. Moreover, the differences in the % of adhered mucin for the two ratios (1:1 and 1:4 v/v ratios) were higher for the chitosan coated liposomes prepared with the EPC/DOPS (90:10) mixture, but the % of adhered mucin was similar for both liposomal samples when the % of chitosan was 0.05 or 0.1 and the ratio 1:4 (v/v) for liposomal suspension and chitosan solution were used. This result can be explained by the higher content of

chitosan per mg lipid in the 1:4 mixtures. Thus, in the next set of experiments, liposomes were mixed with chitosan at 1:4 liposome suspension/chitosan solutions (v/v) ratio.

Characterization of chitosan-coated liposomes with different lipid composition

Liposomes with a negatively charged surface were used to study chitosan coating. To carry out this study, three more lipid mixtures were used, in addition to the ones used in the previous section, to prepare liposomes. The lipid mixture DSPC/DOPS/SM (80:20:30, molar ratio) was used because in our previous paper we showed that, although it incorporates only 24.1% of the total CPT-11, give similar-sized empty vesicles to that obtained with the lipid mixture DSPC/DOPS/CHOL (65:35:30, molar ratio) (Casadó *et al.*, 2014). A soybean lipid extract (SLE) and a bovine brain extract (BBE), which provide liposomes with a negative charge, were also used because being natural lipid extracts allow obtaining cheaper liposomal suspensions than if lipid molecular species synthesized in the laboratory were used.

Liposomal suspensions were prepared and the negative charged liposomes were covered with chitosan as indicated in Methods. The size and the surface potential of the liposomal vesicles after chitosan coating have been systematically determined to characterize the liposomal preparations and the effect of the polymer concentration on these parameters have been analyzed by PCS as indicated in Methods (Fig. 4).

The results summarized in Fig. 4A show that the size and the polydispersity index of coated liposomes increases when raising chitosan concentration, irrespective of liposome composition. The mean diameter (Zave) of uncoated liposomes ranged between 116 and 156 nm and the Zave for all chitosan coated liposomes increases as the concentration of chitosan increases in the dissolution used to make the coating. The mean diameter of DSPC/DOPS/CHOL, DSPC/DOPS/SM and BBE chitosan coated liposomes was similar, for all chitosan concentrations assayed up to 0.05%.

Nevertheless, at a concentration of 0.1% chitosan, an increase in size as a function of the liposomes composition was observed, increasing the size of chitosan coated liposomes in the order EPC/DOPS < DSPC/DOPS/CHOL < DSPC/DOPS/SM < BBE < SLE. On the other hand, the size of EPC liposomes coated with chitosan was the smallest and that of SLE liposomes was the higher for almost all chitosan concentrations assayed. ζ potential values (Fig. 4B) show the effect of the coating process in the surface charge of liposomes. Thus, the negative charge of uncoated EPC/DOPS (90:10), DSPC/DOPS/CHOL (65:35:30), DSPC/DOPS/SM (80:20:30), BBE (Mora et al., 2003) and SLE liposomes (mean values ranging from -25.5 and -496) shifted to the opposite charge as a .consequence of the electrostatic interaction between the anionic lipids and the cationic polysaccharide. The changes in surface charge were dependent on the lipid composition of the vesicles. Thus, EPC/DOPS,

DSPC/DOPS/CHOL, FPA and BBE and liposomes maintain almost its initial high negative charge even at 0.005% chitosan, with a sudden increase to positive values at 0.05% chitosan, whereas the modification of the charge of DSPC/DOPS/SM liposomes was more gradual. However, the Zeta Potential of all coated liposomes using 0.05 or 0.1 % chitosan solutions were positive and similar ranging the mean values between +26.9 and +31.2 or +30.6 and +41.0, respectively

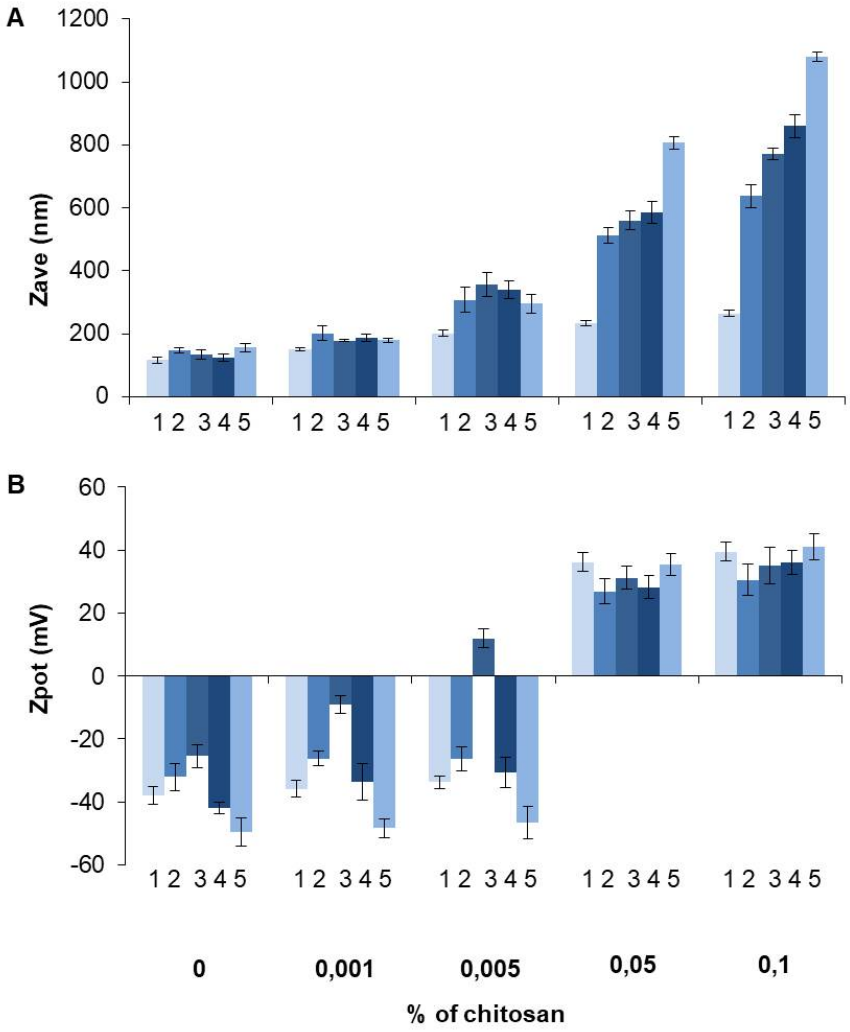

Fig. 4. Influence of chitosan coating on liposomes size and ζ potential. Liposomes uncoated (0% chitosan) and coated with 0.001, 0.005, 0.05 and 0.1% chitosan UP Cl 113 were analysed by size (A) and ζ potencial (B). (1) EPC/DOPS (90:10), (2) DSPC/DOPS/CHOL (65:35:30), (3) DSPC/DOPS/SM (80:20:30), (4) BBE and (5) SLE liposomes were prepared at a concentration of 10 mg lipid/mL with 10 mM lactate buffer pH 4.4. Results are means of individual experiments performed in triplicate. CV ranged from 2.3 to 16.25%.

Assessment of mucoadhesive behaviour of different chitosan coated liposomes

The mucoadhesive behavior of the different chitosan-coated and uncoated liposomes (used as controls) was assessed with mucin aqueous solutions at room temperature (Hea *et al.,* 1998), as indicated for the mucoadhesive test. The experiment to study the

effect of the lipids, used to procure the liposomes, in the mucoadhesive properties of chitosan coated liposomes, was performed using chitosan UP CL 113 and a 1:4 v/v ratio for liposomal suspensions and the chitosan solutions. The results, indicated in Figure 5, show that the percentage of adhered mucin to BBE- and SLE-coated liposomes is very small compared to that adhered to EPC/DOPS-, DSPC/DOPS/CHOL- and DSPC/DOPS/SM-coated liposomes, indicating that these latest formulations of liposomes coated with chitosan have higher mucoadhesive properties.

From the experimental data of Figures 4 and 5 it can be established that: i) at 0.001% chitosan DSPC/DOPS/SM-coated liposomes, with the highest ζ potential (-9.11) and a diameter of 178 nm (see Figure 4) are the most mucoadhesive, ii) the percentages of adhered mucin, using 0.05 and 0.1% chitosan, to DSPC/DOPS/CHOL-coated liposomes are a bit higher than that obtained for DSPC/DOPS/SM-coated liposomes, although their size and ζ potential follow an inverse order, iii) EPC/DOPS-coated liposomes with the little size at 0.05 and 0.1% chitosan concentrations and a ζ potential a bit higher than DSPC/DOPS/CHOL-coated liposomes shows a similar percentage of adhered mucin, iv) no adhered mucin was observed to BBE and SLE-coated liposomes at chitosan concentrations of 0.001 and 0.005%, iv) at 0.1 % chitosan the percentage of adhered mucin to BBE- and SLE-coated liposomes is not in accordance with its ζ potential value; this result and the larger size of these coated liposomes could indicate an irregular binding of chitosan to liposomes.

From the experimental data of Figures 4 and 5 it can be established that: i) at 0.001% chitosan DSPC/DOPS/SM-coated liposomes, with the highest ζ potential (-9.11) and a diameter of 178 nm (see Figure 4) are the most mucoadhesive, ii) the percentages of adhered mucin, using 0.05 and 0.1% chitosan, to DSPC/DOPS/CHOL-coated liposomes are a bit higher than that obtained for DSPC/DOPS/SM-coated liposomes, although their size and ζ potential follow an inverse order, iii) EPC/DOPS-coated liposomes with the little size at 0.05 and 0.1% chitosan concentrations and a ζ potential a bit higher than DSPC/DOPS/CHOL-coated liposomes shows a similar percentage of adhered mucin, iv) no adhered mucin was observed to BBE and SLE-coated liposomes at chitosan concentrations of 0.001 and 0.005%, iv) at 0.1 % chitosan the percentage of adhered mucin to BBE- and SLE-coated liposomes is not in accordance with its ζ potential value; this result and the larger size of these coated liposomes could indicate an irregular binding of chitosan to liposomes.

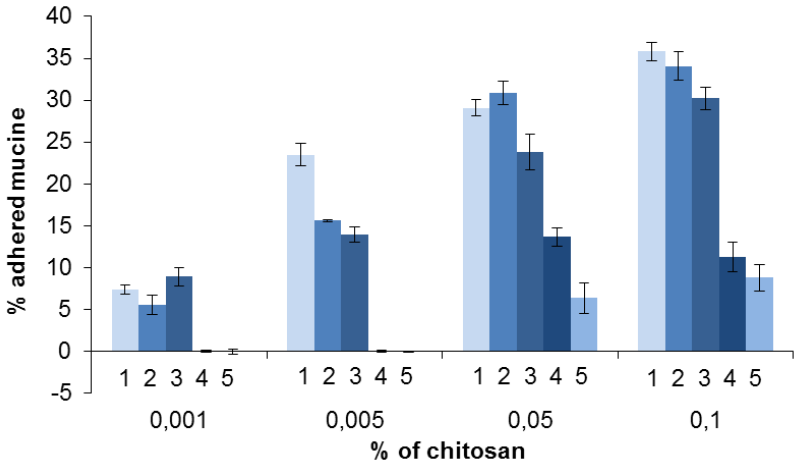

Fig. 5. Influence of chitosan UP CL 113 concentration on mucoadhesivity of chitosan coated liposomes. From left to right: EPC/DOPS (90:10), DSPC/DOPS/CHOL (65:35:30), DSPC/DOPS/SM (80:20:30), BBE and SLE coated liposomes. Liposomal suspensions and chitosan UP CL 113 solutions of different concentrations (0.001, 0.005, 0.050 and 0.100 %) were mixed at 1:4 (v/v) ratios. Mucin assay was used to quantify mucoadhesivity. Uncoated liposomes were used as controls. Results are means of individual experiments performed in triplicate. CV ranged from 0.2 to 11.7%.

From the above results we decided to use DSPC/DOPS/CHOL (65:35:30, molar ratio) and EPC/DOPS (90:10, molar ratio) liposomes to study the effect of the lipid bilayer composition on the mucoadhesive properties of chitosan-coated liposomes in a greater detail, since these liposomes showed a high incorporation efficiency for CPT-11 and SN-38, respectively (Casadó *et al*., 2014; Casadó *et al*., 2017 submitted), and the highest mucoadhesive behaviour. The results, summarized in table II, show that the amount of mucin adhered on EPC/DOPS coated-liposomes, at the same chitosan concentration used, is a bit higher than that adhered on DSPC/DOPS/CHOL coated-liposomes, in accordance with their slightly smaller positive charge.

We choose two chitosan concentrations (0.001 and 0.005%) leading to chitosan-coated DSPC/DOPS/CHOL and EPC/DOPS liposomes with negative ζ potential and another two (0.05% and 0.1%) yielding liposomes with positive ζ potential.

Our results (Table II) indicate that, while control liposomes showed no significant mucin adhesion (0.34 and 0.94%), the chitosan-coated liposomes with a net negative potential adhered a significant amount of mucin and that the percentage of adhered mucin increased with the concentration of chitosan used to coat the liposomes. The adhered mucin to chitosan-coated liposomes with a net positive potential was significantly higher and increased with the charge.

Taking together the results obtained with the two liposomal preparations, it can be deduced that binding of mucin to liposomes with net positive charge increases with increasing their charge. However, the percentage of the mucin bound to negatively charged liposomes, at low chitosan concentrations, could be explained by the interaction of mucin with chitosan molecules partially bound to liposomes.

Table II. Influence of lipid composition and chitosan concentration on the Z potential and mucoadhesive properties of chitosan-coated liposomes. Liposomes were obtained from a DSPC/DOPS/CHOL (65:35:30) or a EPC/DOPS (90:10) mixture and were coated with UP CL 113 chitosan solutions of different concentration.

[Chitosan]	DSPC/DOPS/CHOL (65:35:30)		EPC/DOPS (90:10)	
	Z potential (mV)	Adhered mucine (%)	Z potential (mV)	Adhered mucine (%)
0%	-32.12 ± 4.30	0.32 ± 0.02	-38.00 ± 2.90	0.94 ± 0.08
0.001%	-26.27 ± 2.30	5.55 ± 1.15	-35.90 ± 2.66	7.37 ± 0.56
0.005%	-26.37 ± 3.92	15.62 ± 0.15	-33.80 ± 1.89	23.50 ± 1.36
0.05%	26.91 ± 3.80	30.86 ± 2.40	36.20 ± 2.84	29.08 ± 1.01
0.1%	30.56 ± 4.9	34.05 ± 1.70	39.50 ± 3.10	35.80 ± 1.08

To procure chitosan-coated liposomes, liposomal suspensions and chitosan solutions of different concentrations were mixed at a 1:4 (v/v) ratio. Chitosan-coated liposomes were suspended in a mucin aqueous solution and the free mucin concentration was measured before and after 1 h incubation. Uncoated liposomes, used as controls, showed no significant mucin adhesion.

Characterization of mucoadhesive properties of CPT-11 and SN-38 loaded liposomes

Once it has been established that the liposomal formulations with high entrapment efficiency for the drugs CPT-11 and SN-38 are the most mucoadhesive, chitosan-coated liposomes containing the encapsulated drugs have been prepared and their mucosdhesive properties have been characterized. For this assay two concentrations of chitosan were used (0.005 and 0.1%) and un-coated liposomes (0% chitosan) were used as controls. The results are shown in table III.

It can be observed that the size of DSPC/DOPS/CHOL and EPC/DOPS un-coated liposomes containing CPT-11 and SN-38, respectively, was higher of that obtained for empty liposomes (see Fir. 4A) as usual (Casadó et al., 2017; Casadó et al., 2017 submitted). Moreover, the size of chitosan-coated liposomes and the percentage of adhered mucin increases as the percentage of chitosan is raised. The results in table III also shows that the incorporation of the drugs in the liposomes do not change the mocoadhesive properties of bot liposomes.

If we consider the lipid recovery, the results in the table III show that almost a 100 % recovery of the lipid was achieved. Nevertheless, the lipid recovery decreases to near 50% or 40% for CPT-11 and SN-38 chitosan-coated liposomes, respectively. This loss of lipid can be due to the introduction of an additional centrifugation step to recover chitosan-coated liposomes.

When determining drug recovery, a 100 % recovery of both drugs was obtained for both un-coated liposomes, in a same way as observed for lipids. However, in this

case, although recovery of SN-38 for the coated liposomes was similar to that of lipid recovery (about 40%), the recovery of CPT-11 (about 26%) became the half of the lipid recovery (about 50%). This result indicates that in the additional centrifugation step to recover chitosan-coated liposomes, some CPT-11 present in the initial un-coated liposomes was lost.

Table III. Characterization of camptothecine-loaded liposomes coated with chitosan and evaluation of their mocoadhesive properties. To prepare DSPC/DOPS/CHOL (63:35:30) liposomes containing CPT-11, a lipid/CPT-11 molar ratio of 7.5:1 was used. To prepare EPC/DOPS (90:10) liposomes containing SN-38, a lipid/SN-38 molar ratio of 20:1 was used.

[Chitosan]	DSPC/DOPS/ CHOL (65:35:30)					
	Zave (nm)	Adhered mucine (%)	Lipid rec[1] (Rate[2])	CPT-11 rec[3] (Rate[2])	CPT-11 entrap[4] (Rate[3])	Drug-Lipid ratio[5]
0%	157.00 ± 9.02	0.28 ± 0.03	9.85 ± 0.52 (98.5%)	1.28 ± 0.05 (99.22%)	1.11 ± 0.15 (86.05%)	79.29 ± 17.71
0.005%	335.00 ± 7.90	24.17 ± 1.87	5.24 ± 1.32 (52.4%)	0.32 ± 0.15 (25.06%)	0.25 ± 0.03 (78.17%)	34.14 ± 4.05
0.1%	555.30 ± 8.05	32.85 ± 2.09	5.62 ± 0.87 (56.2%)	0.36 ± 0.09 (27.57%)	0.29 ± 0.12 (80.85%)	36.41 ± 15.19
[Chitosan]	EPC/DOPS (90:10)					
	Zave (nm)	Adhered mucine (%)	Lipid rec[1] (Rate[2])	SN-38 rec[3] (Rate[2])	SN-38 entrap[3] (Rate[2])	Drug-Lipid ratio[5]
0%	147.20 ± 7.85	1.02 ± 0.21	9.65 ± 0.92 (96.5%)	0.256 ± 0.002 (99.53%)	0.256 ± 0.001 (99.73%)	20.48 ± 0,08
0.005%	245.30 ± 5.32	28.65 ± 2.01	3.93 ± 1.20 (39.3%)	0.100 ± 0.001 (38.93%)	0.098 ± 0.001 (97.65%)	19.21 ± 0.19
0.1%	301.20 ± 6.47	34.22 ± 1.56	4.01 ± 0.86 (40.1%)	0.102 ± 0.002 (39.58%)	0.102 ± 0.002 (99.80%)	19.61 ± 0.38

[1]Lipid recovery: mg/mL, [2] Percentage of lipid or drug recovery in relation to the initial drug amount added for liposome procurement, [3] Percentage of drug entrapped in relation to the total drug recovered in the same sample, [4] Total CPT-11 or SN-38 recovery: mg/mL, [5] Drug entrapped: mg/mL, [6] mg drug/mmol lipid.

The evaluation of the amount of both drugs entrapped into liposomes show that the recovery of CPT-11 and SN-38 was of 86 and 99%, respectively, for both un-coated liposomes. The concentration of both drugs, indicated as mg drug/mL liposomal suspension, decreases for chitosan coated liposomes, but the rate of entrapped drugs was similar than that obtained for un-coated liposomes. It should be taken into account

that to determine the rate of entrapped drugs in chitosan un-coated and coated liposomes the data used were the amount of drug entrapped and the amount of total drug expressed in mg/mL in each liposomal suspension. This result indicates that the cover process by chitosan for liposomes leads to the same loss of CPT-11 entrapped and total in each liposomal sample.

Finally, the ratio between CPT-11 and total lipid, expressed as mg drug/mmol lipid, decreases from 79 for un-coated liposomes to 35 for chitosan-coated liposomes, indicating that the loss of CPT-11 during the coating process is higher than the loss of lipid. On the contrary, for SN-38 containing liposomes the ratio of mg drug/mmol lipid has been the same (almost 20) for un-coated and chitosan-coated liposomes, showing that the coating process lead to liposomes with the same composition than those un-coated ones.

DISCUSSION

Cancer nanotechnology is an upcoming field that has received considerable attention in recent years. Their tools include liposomes, very versatile structures, which abilities have been exploited in biology, biochemistry and medicine. At present, several liposomal anticancer drugs are available in the clinic or are in advanced stages of clinical development (Bozzuto and Molinari, 2015; Torchilin, 2014). The principles of liposomal drug delivery arise from their improved pharmacokinetics and drug release, their enhanced cellular penetration and their possibilities for selective targeting of anticancer drugs.

When considering the route of administration of a drug it is observed that the intravenous route has been the most traditionally used. Although it presents some interesting advantages produces serious side effects that reduce the doses tolerated. Oral chemotherapy emerges as a promising alternative in oncology of the future and can radically change current regimens and dramatically increase patient quality of life. This option is especially interesting in the case of colon cancer, since the direct transport of the drugs to the treatment areas offers significant advantages over other therapeutic strategies (Chourasia and Jain, 2003). When a delivery system to the colon is used, it must be taken into account that in order for the transporter to reach its destination intact and to be absorbed by releasing the encapsulated drug, it must overcome some obstacles that present the gastrointestinal tract and consider that the mucosa covering it constitutes a real physiological barrier that the vehicle must pass through (Groo and Lagarce, 2014).

To this end, the surface of the carrier may be functionalized so that it acquires the ability to interact with specific tumor cells and exhibits a longer retention at the site of action. All the strategies developed to date are based on the use of pH-sensitive

polymers or polysaccharide polymers with bioadhesive properties (Jain *et al*., 2007). Among the latter, chitosans are interesting for its biodegradability and cationic character and will facilitate the interaction of the carrier with cell membranes and mucous membranes. When chitosan coated carriers are delivered to the colon, the hydrolysis of the glycosidic bonds of chitosan by the polysaccharidases (Krishnaiah *et al*., 2012) that produce the anaerobic bacteria of the microflora of this tissue, will allow the release of the encapsulated drug.

Recently, we published a paper which describes the procurement of a novel and easy-to-prepare temperature-sensitive carrier for CPT-11 (Casadó *et al.,* 2014). Our results, obtained from an *in vitro* study using the colon cancer Caco-2 cell line, showed that the cellular uptake and the cytotoxicity, through a proapoptotic mechanism, of the CPT-11 liposomal formulation were significantly higher than those corresponding to the free drug. We have also studied, in a previous work, the incorporation of SN-38, the active metabolite of CPT-11, in liposomes following a different formulation strategy because of the high insolubility of the compound (Casadó *et al.,* 2017 submitted). In the study, we have shown *in vitro* the higher efficacy of SN-38lip on two tumor cell lines (HeLa and Caco-2) and the different cell cycle alterations induced in both cell lines by this liposomal formulation. The work presented in this paper represents a step forward and focuses on the results obtained in the design of chitosan-coated liposomes, thinking in the oral delivery of C-PT-11 for the treatment of colon cancer. The need of liposomal bilayers with negative charge to prepare liposomes with a positively charged polysaccharide coating had led us to consider only liposomes with lipid compositions containing negatively charged lipids to proceed with the study. For this, we have chosen the anionic liposomes procured with the pure lipid mixtures EPC/DOPS (90:10), DSPC/DOPS/CHOL (65:35:30) and DSPC/DOPS/SM (80:20:30), well characterized in our previous papers, and liposomes procured with two natural lipid extracts, a soy lipid extract (SLE) and a bovine brain extract (BBE), which contain negative charged lipids.

After showing the effectiveness of liposomes containing CPT-11 or SN-38, an alternative formulation has been developed. Bearing in mind the possibility of an oral administration of this drug, instead its systemic application by which the already described formulation seems to be useful, liposomal carriers were endowed with mucoadhesive characteristics by means the coating of its bilayer surface with a polysaccharide matrix. The anionic liposomes procured with the five lipid mixtures indicated in the first paragraph were used to study chitosan coating and to test its mucoadhesive properties. Our results show changes in the size, the polydispersity index and the surface charge of the vesicles as a consequence of the coating (Fig. 4). The size and the polydispersity index increased when raising chitosan concentration, irrespective of liposome composition, but surface charge changes in a lipid composition-dependent manner. Although at 0.05% chitosan the positive charge of all

the coated liposomes was very similar, we choose the EPC/DOPS (90:10) and the DSPC/DOPS/CHOL (65:35:30) mixtures to prepare liposomes to pursue with the study because its higher efficiency to encapsulate SN-38 and CPT-11, respectively. AFM images of DSPC/ DOPS/CHOL (65:35:30) liposomes coated with chitosan (Fig. 2) showed the association of coated liposomes through a net of chitosan chains.

The mucoadhesive behavior of chitosan-coated liposomes was proved by measuring the adsorption of mucin by coated-liposomes. The most outstanding features of the chitosan liposomes coating studies could be summarized as follows: i) a higher average particle size and polydispersity indices of UP CL 213 with regard to those for UP CL 113 chitosan-coated liposomes (Fig. 1); ii) the same positive ζ potential values of UP CL 113 chitosan-coated liposomes obtained with a 0.05 and 0.1% chitosan solution together with the low size and heterogeneity of coated liposomes when the 0.05% chitosan solution was used (Fig. 1); iii) the similar mucoadhesivity of UP CL 113 and UP CL 213 coated liposomes at 0.05% chitosan solution (Fig. 1). With these premises (our previous results related to drugs entrapping (Casadó *et al*., 2014; Casadó *et al*., 2017 submitted) and the result showed in table III) it could be suggested that EPC/DOPS (90:10) and DSPC/DOPS/CHOL (65:35:30) liposomes and the coating with 0.05% UP CL 113 chitosan, at the 1:4 (v/v) ratio, gave liposomes with the best structural and mucoadhesive properties to entrap SN-38 and CPT-11, respectively. The chitosan layer on the surface of liposomes is responsible for mucoadhesion, since non-coated liposomes showed unremarkable adhesion.

CONCLUSION

Liposomal drugs are promising formulations in cancer therapy. Nevertheless, formulation parameters should be carefully selected because they strongly determine the behavior of the carrier *in vivo* and, consequently, the efficiency of the chemotherapeutic treatments. This paper describes a preliminary study about the coverage of liposomal surface with cationic mucoadhesive polymers thinking in the oral delivery of CPT-11 and its metabolite SN-38 to the colon.

The coverage of negatively charged liposomes with the cationic polymer chitosan establishes the basis for the formation of a stable mucoadhesive carrier with the ultimate purpose of developing a product for oral administration. The conditions and protocol for obtaining chitosan-coated liposomes, with entrapped CPT-11 or SN-38, have been established and it has been confirmed that the polymer layer on the liposomal surface is responsible for mucoadhesion.

Studies are currently being carried out to determine the stability of the developed liposomal systems, incorporated into enteric capsules, into different fluids that allow the emulation of the conditions in the stomach and in the different fragments of the

gastrointestinal tract. The purpose of the study is to demonstrate that the liposomes arrive intact to the colon, adhere to the mucin of the mucus and reach the tumor cells to release the drug.

ACKNOWLEDGEMENTS

Founding for this project has been received from the Department d'Universitats, Recerca i Societat de l'Informació (DURSI), Govern de la Generalitat de Cataluña (2009SGR-367). A. Casadó thanks to the University of Barcelona for a predoctoral fellowship. The authors are also grateful to Prof. M. Luisa Garcia for the use of the Malvern Zetasizer NANO-ZS device

REFERENCES

Alimonti, A., Gelibter, A., Pavese, I., Satta, F., Cognetti, F., Feretti, G., Rasio, D., Vecchione, A. and Di Palma M. New approaches to prevent intestinal toxicity of irinotecan-based regimens, Cancer Treat. Rev. 2004, 30555-30562. DOI: 10.1016/j.ctrv.2004.05.002

Artursson, P., Palm, K. and Luthman K. Caco-2 monolayers in experimental and theoretical predictions of drug transport. Adv. Drug Del. Rev. 2001, 46:27-43. DOI: 10.1016/S0169-409X(00)00128-9

Behrens, I., Vila Pena, A.I., Alonso, M.J. and Kissel. T. Comparative Uptake Studies of Bioadhesive and Non-Bioadhesive Nanoparticles in Human Intestinal Cell Lines and Rats: The Effect of Mucus on Particle Adsorption and Transport. Pharm. Res. 2002, 19:1185-1193.

Bernkop-Schnurch, A. Mucoadhesive systems in oral drug delivery. Drug Discov Today Technol. 2005, 2:83-7. DOI: 10.1016/j.ddtec.2005.05.001

Bozzuto, G. and Molinari, A. Liposomes as nanomedical devices. Int. J. Nanomedicine 2015, 10:975-999. DOI: 10.2147/IJN.S68861

Cancer.Net Editorial Board. Colorectal Cancer - Treatment Options. PDF generated on 2017 from http://www.cancer.net/cancer-types/colorectal-cancer/treatment-options

Carnevale, J. and Ko, A.H. MM-398 (nanoliposomal irinotecan): emergence of a novel therapy for the treatment of advanced pancreatic cancer. Future Oncology 2016, 12:453-464. DOI : 10.2217/fon.15.333

Casadó, A., Sagristá, M.L. and Mora, M. Formulation and in vitro characterization of thermosensitive liposomes for the delivery of irinotecan. J. Pharm. Sci. 2014, 103:3127-3138. DOI: 10.1002/jps.24097

Casadó, A., Giuffrida, M.C., Sagristá, M.L., Castelli, F., Pujol, M., Alsina, M.A. and Mora, M. Langmuir monolayers and Differential Scanning Calorimetry for the study of the interactions between camptothecin drugs and biomembrane models. Biochim. Biophys. Acta, 2016, 1858:422-433. DOI: 10.1016/j.bbamem.2015.12.007

Casadó, A., Mora, M., Sagristá, M.L., Rello-Varona, S., Acedo, P., Stockert, J.C., Cañete, M. and Vllanueva, A. Improved selectivity and cytotoxic effects of irinotecan via liposomal delivery: A comparative study on Hs68 and HeLa cells. Eur. J. Pharm. Sci. 2017, 109:64-77. DOI: 10.1016/j.ejps.2017.07.024

Chourasia, M.K. and Jain, S.K. Pharmaceutical approaches to colon targeted drug delivery systems. J. Pharm. Pharmaceut. Sci. 2003, 6:33-66.

Claesson, M. and Ninham, B.W. pH-Dependent interactions between adsorbed chitosan layers. Langmuir. 1992, 8:1406-1412. DOI: 10.1021/la00041a027

Crater, J.S. and Carrier. R. L. Barrier Properties of Gastrointestinal Mucus to Nanoparticle Transport. Macromol. Biosci. 2010, 10:1473-1483. DOI: 10.1002/mabi.201000137

Edwards, B.K., Ward, E,, Kohler, B.A., Eheman, C., Zauber, A.G., Anderson, R.N., Jemal, A., Schymura, M.J., Lansdorp-Vogelaar, I., Seeff, L.C., van Ballegooijen, M., Goede, S.L. and Ries, L.A.G. Annual Report to the Nation on the Status of Cancer, 1975-2006, Featuring Colorectal Cancer Trends and Impact of Interventions (Risk Factors, Screening, and Treatment) to Reduce Future Rates. Cancer 2010, 116:544-73. DOI: 10.1002/cncr.24760

Felt, O., Buri, P. and Gurny, R. Chitosan: a unique polysaccharide for drug delivery. Drug Dev Ind Pharm. 1998, 24:979-93. DOI: 10.3109/03639049809089942

Ferlay. J., Soerjomataram, I., Dikshit, R., Eser, S., Mathers, C., Rebelo, M., Parkin, D.M., Forman, D. and Bray, F. Cancer incidence and mortality worldwide: Sources, methods and major patterns in GLOBOCAN 2012. Int. J. of Cancer 2015, 136(5):E359-E386. DOI: 10.1002/ijc.29210

García-Carbonero, R. and Supko, J.G. Current perspectives on the clinical experience pharmacology, and continued development of the camptothecins. Clin. Cancer Res. 2002, 8:641-661.

Gerrits, C.J., De Jonge, M.J., Schellens, J.H., Stoter, G.and Verweij, J. Topoisomerase I inhibitors: the relevance of prolonged exposure for present clinical development. Br. J. Cancer 1997, 76:952-962. DOI: 10.1038/bjc.1997.491

Groo, A-C. and Lagarce, F. Mucus models to evaluate nanomedicines for difusion. Drug Discovery Today 2014, 19:1097-1108. DOI: 10.1016/j.drudis.2014.01.011

Guarner, F. and Malagelada, J.R. Gut flora in health and disease. Lancet 2003, 361:512-519. DOI: 10.1016/S0140-6736(03)12489-0

Gulbake, A. and Jain S.K. Chitosan: a potential polymer for colon-specific drug delivery system. Expert Opin Drug Deliv. 2012, 9:713-29. DOI: 10.1517/17425247.2012.682148

He, C., Yin, L., Tang, C. and Yin C. Size-dependent absorption mechanism of polymeric nanoparticles for oral delivery of protein drugs. Biomaterials 2012, 33:8569-8578. DOI: 10.1016/j.biomaterials.2012.07.063

Hea, P., Davis, S.S. and Illum, L. In vitro evaluation of the mucoadhesive properties of chitosan microspheres. Int. J. Pharm. 1998, 166:75-88. doi.org/10.1016/S0378-5173(98)00027-1

Hosseinzadeh, H., Atyabi1, F., Dinarvand, R., Ostad, S.N. Chitosan–Pluronic nanoparticles as oral delivery of anticancer gemcitabine: preparation and in vitro study. Int. J. Nanomedicine 2012, 7:1851-1863. DOI: 10.2147/IJN.S26365

Jain, A., Gupta, Y. and Jain, S.K. Perspectives of biodegradable natural polysaccharides for site-specific drug delivery to the colon. J. Pharm. Pharmaceut. Sci. 2007, 10:86-128.

Jain, S.K, Jain, A., Gupta, Y., Jain, A., Khare, P. and Kannandasan, M. Targeted delivery of 5-ASA to colon using chitosan hydrogel microspheres. J. Drug Del. Sci. Technol. 2008, 18:315-21. DOI: 10.1016/S1773-2247(08)50062-1

Jain, A., Jain, S.K., Ganesh, N., Barve, J. and Beg, A.M. Design and development of ligand-appended polysaccharidic nanoparticles for the delivery of oxaliplatin in colorectal cancer. Nanomedicine: Nanotechnology, Biology and Medicine 2010, 6:179-90. DOI: 10.1016/j.nano.2009.03.002

Jin, Y., Song, Y., Zhu, X., Zhou, D., Chen, C., Zhang, Z. and Huang. Y. Goblet cell-targeting nanoparticles for oral insulin delivery and the influence of mucus on insulin transport. Biomaterials 2012, 33:1573-1582. DOI: 10.1016/j.biomaterials.2011.10.075

Khanvilkar, K., Donovan, M.D. and Flanagan. D.R. Drug transfer through mucus. Adv. Drug Deliv. Rev. 2001, 48:173-193. DOI: 10.1016/S0169-409X(01)00115-6

Kohn K.W. and Pommier, Y. Molecular and biological determinants of the cytotoxic actions of camptothecins. Ann. N. Y. Acad. Sci. 2000, 922:11-26. DOI: 10.1111/j.1749-6632.2000.tb07021.x

Krishnaiah, Y.S.R. and Khan, M.A. Strategies of targeting oral drug delivery systems to the colon and their potential use for the treatment of colorectal cancer. Pharmaceutical Development and Technology. 2012, 17:521-40. DOI: 10.3109/10837450.2012.696268

Larhed, A.W., Artursson, P., Gråsjö, J. and Björk. E. Diffusion of Drugs in Native and Purified Gastrointestinal Mucus. J. Pharm. Sci. 1997, 86:660-665. DOI: 10.1021/js960503w

Li, X., Chen, D. Le, C., Zhu, C., Gan, Y., Hovgaard, L. and Yang. M. Novel mucus-penetrating liposomes as a potential oral drug delivery system: preparation, in vitro characterization, and enhanced cellular uptake. Int. J. Nanomedicine 2011, 6:3151-3162. DOI: 10.2147/IJN.S25741

Liew, S.T. and Yang, L.Y. Design, synthesis and development of novel camptothecin drugs. Curr. Pharm. Des. 2008, 14:1078-1097. DOI: 10.2174/138161208784246180

Lorenzo-Lamosa, M.L., Remunan-Lopez, C., Vila-Jato, J.L. and Alonso, M.J. Design of microencapsulated chitosan microspheres for colonic drug delivery. J Control Release. 1998, 52:109-18. DOI: 10.1016/S0168-3659(97)00203-4

McGill, S.L. and Smyth, H.D.C. Disruption of the mucus barrier by topically applied exogenous particles. Mol. Pharm. 2010, 7:2280-2288. DOI: 10.1021/mp100242r

Mertins, O. and Dimova, R. Binding of Chitosan to Phospholipid Vesicles Studied with Isothermal Titration Calorimetry. Langmuir 2011, 27:5506-5515. DOI: 10.1021/la200553t.

Mora, M., Gutiérrez, M.E., García, A.F., De Madariaga, M.A., Sagristá, M.L. and Casadó, F.J. Interactions of tocopherols and phenolic compounds with membrane lipid components: Evaluation of their antioxidant activity in a liposomal model system. Life Sci. 2003, 72:2337-2360. DOI: 10.1016/S0024-3205(03)00120-6

Park, K. and Robinson, J.R. Bioadhesive polymers as platforms for oral controlled drug delivery: method to study bioadhesion. Int. J. Pharm. 1984, 198:107-127. DOI: 10.1016/0378-5173(84)90154-6

Patel, M., Shah, T. and Amin, A. Therapeutic opportunities in colon-specific drug delivery systems. Crit. Rev. Ther. Drug Carrier Syst. 2007, 24:147-202. DOI: 10.1615/CritRevTherDrugCarrierSyst.v24.i2.20

Petit, B., Bouchemal, K., Vauthier, C., Djabourov, M. and Ponchel. G. The Counterbalanced Effect of Size and Surface Properties of Chitosan-Coated poly(isobutylcyanoacrylate) Nanoparticles on Mucoadhesion Due to Pluronic F68 Addition. Pharm. Res. 2012, 29:943-952. DOI: 10.1007/s11095-011-0634-z

Pommier, Y. DNA topoisomerase I inhibitors: chemistry, biology and interfacial inhibition, Chem Rev. 2009, 109:2894-2902. DOI: 10.1021/cr900097c

Sinha, V.R. and Kumria, R. Polysaccharides in colon-specific drug delivery. Int. J. Pharm. 2001, 224:19-38. DOI: 10.1016/S0378-5173(01)00720-7

Sinha, R., Kim, G.J., Nie, S. and Shin, D.M. Nanotechnology in cancer therapeutics: bioconjugated nanoparticles for drug delivery. Mol. Cancer Ther., 2006, 5:1909-1917. DOI: 10.1158/1535-7163.MCT-06-0141.

Stewart, J.C.M. Colorimetric determination of phospholipids with ammonium ferrothiocyanate. Anal. Biochem. 1980, 104:10-14. DOI: 10.1016/0003-2697(80)90269-9

Teicher, B.A. Next generation topoisomerase I inhibitors: Rationale and biomarker strategies. Biochem Pharmacol. 2008, 75:1262-1271. DOI: 10.1016/j.bcp.2007.10.016

Thassu, D., Deleers, M. and Pathak. Y. Nanoparticulate Drug Delivery Systems. CRC Press, 2007.

Torchilin, V.P. Nanoparticulates as drug carriers. London, UK: Imperial College Press, 2006.

Torchilin, V.P. Multifunctional, stimuli-sensitive nanoparticulate systems for drug delivery, Nat. Rev. Drug Discov. 2014, 13:813-827. DOI: 10.1038/nrd4333

Tozaki, H., Odoriba, T., Okada, N., Fujita, T., Terabe, A., Suzuki, T., Okabe, S., Muranishi, S. and Yamamoto A. Chitosan capsules for colon-specific drug delivery: enhanced localization of 5-aminosalicylic acid in the large intestine accelerates healing of TNBS-induced colitis in rats. J Control Release. 2002, 82:51-61. DOI: 10.1016/S0168-3659(02)00084-6

Vasir, J.K., Tambwekar, K. and Garg, S. Bioadhesive microspheres as a controlled drug delivery system. Int J Pharm. 2003, 255:13-32. DOI:10.1016/S0378-5173(03)00087-5

Yang, L., Chu, J.S. and Fix JA. Colon-specific drug delivery: new approaches and in vitro/in vivo evaluation. Int. J. Pharm. 2002, 235:1-15. DOI: 10.1016/S0378-5173(02)00004-2

Zhang, H., Alsarra, I.A. and Neau, S.H. An in vitro evaluation of a chitosan-containing multiparticulate system for macromolecule delivery to the colon. Int. J. Pharm. 2002, 239:197-205. DOI: 10.1016/S0378-5173(02)00112-6

Zhang, H. and Neau S.H. In vitro degradation of chitosan by bacterial enzymes from rat cecal and colonic contents. Biomaterials. 2002, 23:2761-2766. DOI: 10.1016/S0142-9612(02)00011-X

4. Discusión

La terapia del cáncer se centra en tres tipos de estrategias, quimioterapia, radioterapia y cirugía. Respecto a la quimioterapia, algunos de sus principales problemas son la distribución sistémica inespecífica de los agentes antitumorales, las dificultades para conseguir las concentraciones terapéuticas en la diana tumoral, los frecuentes y graves efectos secundarios sobre células y tejidos no tumorales y el desarrollo de resistencias múltiples. Una alternativa atractiva para solucionar estas limitaciones la es la utilización de sistemas de transporte, capaces de concentrar, de una manera selectiva, dosis citotóxicas de los fármacos en los centros tumorales con la finalidad de destruir células cancerosas y minimizar el daño sobre células normales. La búsqueda de soluciones para estos problemas ha reconducido parte de las investigaciones sobre el tratamiento del cáncer hacia aspectos farmacéuticos y farmacológicos. La formulación y la ruta de administración se han convertido en algo fundamental para la terapia de las neoplasias. El reto consiste en establecer la mejor forma de utilizar los citostáticos para explotar todo su potencial terapéutico en beneficio del paciente.

En relación con el desarrollo de formulaciones farmacéuticas eficaces, la vehiculización dirigida y la liberación controlada de fármacos han proporcionado soluciones han sido objeto de atención en los últimos años. Por otra parte, el auge de las nanotecnologías ha proporcionado nanotransportadores versátiles y biocompatibles, que han permitido progresar en la quimioterapia del cáncer. Liposomas, microesferas y nanopartículas lipídicas o poliméricas constituyen algunas de las mejores opciones. De entre las diferentes nanoplataformas analizadas, la importancia de los liposomas en el campo biomédico es, actualmente, incuestionable (46, 75, 81, 89, 95, 172). Así, varios antitumorales convencionales se han reformulado en liposomas y han sido ya aprobados por los organismos reguladores competentes.

Los liposomas son estructuras versátiles cuyas capacidades han sido utilizadas en distintas disciplinas. En nanomedicina, su aplicación como sistemas transportadores de agentes citotóxicos pretende conseguir formulaciones con actividades terapéuticas optimizadas y toxicidades reducidas. Los liposomas ofrecen enormes posibilidades para formular moléculas químicamente diferentes debido a los dos entornos perfectamente separados de su estructura, además de ser biodegradables y biocompatibles. Los liposomas pueden, además, diseñarse para ser multifuncionales escogiendo los componentes apropiados para controlar sus propiedades.

Sin embargo, aunque las propiedades de las bicapas liposomales dependan de la naturaleza de las moléculas que las constituyen, para obtener una formulación final estable y eficaz se deben tener en cuenta las características del fármaco a encapsular. Cada molécula tiene unos requerimientos específicos para su óptima encapsulación y debe considerarse qué especies lipídicas formarán la bicapa, en qué proporción se

mezclarán, la relación molar lípido-fármaco en la formulación final y qué metodología será la más apropiada para la preparación.

Las camptotecinas son agentes antineoplásicos muy eficaces que actúan mediante un mecanismo basado en su interacción con la Topoisomerasa I (Topo I), impidiendo la replicación del ADN. Existen, sin embargo, algunas limitaciones para la utilización clínica de estos fármacos entre las que destacan: i) su espontánea inactivación por apertura del anillo de lactona a la forma carboxilato en sangre; ii) la rápida reversibilidad del complejo ternario que forman con el ADN y la Topo I después de su eliminación, lo que hace necesario tiempos de infusión prolongados y iii) los efectos secundarios que limitan las dosis aplicables (16, 173). En el caso del SN-38, un inconveniente adicional lo constituye su gran insolubilidad, lo que dificulta el desarrollo de una formulación farmacéutica adecuada para su aplicación en clínica.

Para resolver estos problemas y optimizar la eficacia de estos y de otros citostáticos se han considerado estrategias terapéuticas basadas en el desarrollo de sistemas de vehiculización y liberación controlada, como liposomas, nanopartículas poliméricas, micelas o microesferas (174-177). De entre las diferentes nanoplataformas analizadas, la importancia de los liposomas en el campo biomédico es, actualmente, incuestionable (46, 75, 81, 89, 95, 172) y la FDA ya ha aprobado varias formulaciones liposomales para uso clínico y muchas otras están en diferentes fases de ensayos clínicos (47, 178).

El objetivo global de la tesis ha sido conseguir una formulación liposomal estable para dos camptotecinas, irinotecan (CPT-11) y SN-38, su metabolito activo, utilizadas para el tratamiento de distintos tipos de cáncer, ente ellos el de colon. En el diseño del transportador se tuvo en cuenta, además, que debía ser susceptible de ser modificado en su superficie mediante recubrimiento con algún polímero catiónico para su transporte y absorción específica a través de la mucosa del colon.

5.1. Diseño de dos formulaciones liposomales para las camptotecinas Irinotecan y SN-38

El artículo publicado en el *Journal of Pharmaceutical Sciences* (179) se centra en la obtención de una formulación liposomal óptima para el CPT-11, una camptotecina con un perfil de solubilidad particular, pues es parcialmente soluble tanto en solventes acuosos como en disolventes apolares. Se consideraron las diferentes estrategias de formulación y las opciones para controlar la liberación del fármaco encapsulado en el momento y lugar adecuados y, para su desarrollo, se escogió un procedimiento de incorporación pasiva y un mecanismo de liberación activado en situaciones determinadas. Se tuvo en cuenta que la formulación de liposomas sensibles a estímulos específicos, como temperatura, pH o actividades enzimáticas, constituía una

estrategia muy válida para el diseño de nanosistemas de liberación controlada de fármacos.

El objetivo final de este trabajo era conseguir un vehículo con una carga de superficie negativa, estable a temperatura fisiológica y con capacidad de liberar el contenido encapsulado en condiciones de hipertermia. La sensibilidad a la temperatura es una característica especialmente útil ya que garantiza la integridad del transportador a temperatura fisiológica y permitir, en cambio, la liberación controlada de su contenido en el lugar terapéutico, en respuesta al estímulo producido por un suave incremento de la temperatura. Por otra parte, se ha descrito el efecto citotóxico sinérgico que produce la asociación liposomas-hipertermia (180).

Se consideraron diferentes combinaciones de lípidos, mezclados en distintas relaciones molares, para conseguir estructuras estables, con capacidad de encapsulamiento elevada y con propiedades de termosensibilidad. El estudio se basó en una determinación sistemática y rigurosa de los parámetros termodinámicos de las combinaciones lipídicas analizadas mediante calorimetría diferencial de Barrido (DSC), en la determinación de la eficacia de incorporación del fármaco por los diferentes sistemas desarrollados y en la evaluación de la capacidad de retención del productos encapsulados en el espacio acuoso interior mediante un análisis de la cinética de liberación de la 5,6-carbofluoresceína, una sonda cuya fluorescencia depende de la concentración y que permite determinar las propiedades de permeabilidad de las bicapas al diluirse en el espacio extraliposomal. Los estudios de permeabilidad realizados mostraron el efecto de la temperatura en la liberación del fluoróforo utilizado y que su velocidad de salida se incrementaba en presencia de suero. Además, a temperatura fisiológica los muy bajos valores del porcentaje de fuga en el equilibrio (Feq), incluso en presencia de suero, destacaban la gran estabilidad de algunas de las formulaciones diseñadas.

Después de analizar las opciones ensayadas, dos de las mezclas ternarias propuestas se postularon como las más adecuadas para la encapsulación de CPT-11: DSPC/DOPS/CHOL (65:35:30) y DSPC/DOPS/SM (80:20:30). Ambas proporcionaban bicapas rígidas, con una temperatura de transición elevada y, por lo tanto, con las características apropiadas para el encapsulamiento efectivo de una molécula de las propiedades de solubilidad de este fármaco. La determinación de la eficacia de encapsulamiento de esta camptotecina en los liposomas seleccionados puso de manifiesto que la primera de las dos mezclas proporcionaba valores superiores, por encima del 85%, por lo que, en principio, fue la elegida para continuar con la investigación.

La formulación del SN-38 requirió consideraciones adicionales debido a la extrema insolubilidad de esta molécula en la mayor parte de los disolventes habituales, tanto

hidrófilicos como hidrofóbicos. Su marcado carácter apolar determina que la integración de este fármaco en el sistema liposomal se realice en su entorno hidrofóbico, es decir, en la bicapa lipídica, por lo que la rigidez de la bicapa de la formulación utilizada para encapsular CPT-11 debía constituir un inconveniente para la incorporación eficaz del SN-38. Las bicapas más fluidas tienen la ventaja de acomodar más fácilmente moléculas insolubles en su región hidrofóbica.

Por otra parte, las características del SN-38 no eran adecuadas para la utilización del procedimiento clásico de preparación de formulaciones liposomales, basado en la hidratación de un film lipídico, como el aplicado para la encapsulación del CPT-11, puesto que no era posible preparar un film con la mezcla de lípidos y fármaco para su posterior hidratación con la solución tamponada. El método tradicional propuesto por Bangham (66) aunque ensayado con diferentes modificaciones, solo proporcionaba eficacias de incorporación moderadas. Bajo estas premisas, se seleccionaron nuevos lípidos para la formación del vehículo, siempre teniendo en cuenta las propiedades deseadas para el transpor tador final, y se desarrolló un método alternativo de preparación, basado en la utilización de las técnicas de microemulsificación (104, 105). En el artículo sometido a revisión en *Journal of Drug Targeting* (181) se describe el desarrollo de una nueva formulación liposomal para el SN-38 que constituye una alternativa sencilla, además de eficaz, en lo que respecta a su capacidad para incorporar el fármaco, en comparación con los resultados que proporcionan otros métodos publicados.

Las formulaciones con SN-38 se prepararon a partir de un extracto de lípidos de soja, de la mezcla DSPC/DOPS/CHOL, utilizada para encapsular CPT-11 y de un extracto lipídico de huevo y de la mezcla de este con el fosfolípido aniónico DOPS. En todos los casos, el procedimiento utilizado para la preparación de la formulación fue la microemulsificación. Esta técnica tiene la ventaja adicional de que permite procesar, en continuo, volúmenes mayores de suspensiones lípido-fármaco, aspecto importante para procesos de fabricación a escala industrial. Las eficacias de incorporación fueron, en todos los casos, superiores al 95%, por lo que la selección de la composición más adecuada se decidió después de llevar a cabo la caracterización de las formulaciones obtenidas.

5.2. Caracterización de las formulaciones CPT-11lip y SN-38lip

Además del método de preparación y de la selección de los constituyentes de la formulación, para determinar la idoneidad de un nanotransportador es imprescindible analizar sus parámetros físico-químicos (111). Se determinaron, de forma sistemática, los tamaños de las vesículas y su carga superficial, así como la turbidez de las suspensiones liposomales obtenidas. Además se tuvieron en cuenta las interacciones

moleculares entre los componentes de las bicapas y los fármacos para determinar la estabilidad e integridad del transportador final. El conocimiento de estas interacciones también permite predecir las propiedades farmacocinéticas de los fármacos.

La caracterización de las formulaciones CPT-11lip y SN-38lip {Casadó, #596}{Casadó A, 2017 #624} se llevó a cabo mediante espectroscopia de correlación fotónica (PCS), para la determinación de tamaños, índices de polidispersidad y valores de potencial zeta, calorimetría diferencial de barrido (DSC), para el estudio del comportamiento termotrópico de las bicapas lipídicas, y técnicas de monocapas (LB) para el estudio de las interacciones interfaciales lípido/fármaco.

Se analizaron, en primer lugar, las características de liposomas vacíos como una etapa previa a la incorporación de los fármacos. Los datos de los parámetros físicos y termodinámicos obtenidos mediante PCS y DSC, respectivamente, confirmaron que las mezclas DSPC/DOPS/CHOL (65:35:30) y DSPC/DOPS/SM (80:20:30) proporcionaban bicapas termosensibles y estaban dotadas de las características más adecuadas para preparar liposomas con CPT-11 encapsulado. Posteriormente se realizó la valoración de los porcentajes de incorporación considerando, como variable adicional, la relación lípido/fármaco. Los resultados determinaron que se seleccionara la mezcla DSPC/DOPS/CHOL y la relación molar DSPC/DOPS/CHOL (65:35:30)/CPT-11, 7.5:1 para obtener la formulación liposomal del CPT-11.

En cuanto al SN-38, un estudio físico-químico análogo puso de manifiesto la enorme importancia de la relación lípido/fármaco en el tamaño de las vesículas obtenidas y que la eficacia de incorporación del fármaco, muy elevada en todos los casos, no dependía significativamente de la composición lipídica de la bicapa. El conjunto de los datos obtenidos y los estudios de estabilidad realizados determinaron que se seleccionara la mezcla EPC/DOPS (9:1) y la relación molar lípido/SN-38 20:1 para desarrollar la formulación final de este fármaco.

Además de la caracterización estándar, los estudios con monocapas de Langmuir han demostrado ser una herramienta muy útil para el desarrollo de sistemas de transporte y liberación de fármacos, ya que proporcionan información sobre aspectos tales como la mecánica de las bicapas o la estabilidad del transportador, esenciales para el diseño de una formulación final idónea (110).

En el artículo publicado en *Biochimica et Biophysica Acta* (19) se describen los estudios sobre las interacciones moleculares entre los constituyentes lipídicos del liposoma y las camptotecinas en estudio, mediante diferentes técnicas biofísicas, para determinar en qué medida y como estas pueden afectar o modificar la estructura del transportador y a la estabilidad de la formulación. El conjunto de los resultados

obtenidos puso de manifiesto la capacidad del CPT-11 y del SN-38 de interaccionar y/o insertarse entre las moléculas de fosfolípidos de las membranas.

Mediante calorimetría diferencial de barrido (DSC) se determinó, en primer lugar, el efecto de la incorporación del irinotecan o del SN-38 en el estado físico de las bicapas liposomales. La aparición de una única endoterma de transición en los termogramas indicaba que la incorporación de ambas camptotecinas en liposomas multilamelares (MLVs) no modificaba de forma significativa la organización de las respectivas bicapas, a pesar de sus diferentes propiedades de solubilidad y de su diferente ubicación en los dos entornos posibles de la estructura liposomal.

Se prepararon monocapas de Langmuir de los lípidos, de los fármacos y de las mezclas lípido-fármaco, a diferentes relaciones molares y se analizaron en términos de actividad superficial y de isotermas de compresión. Las mezclas DSPC/DOPS/CHOL (65:35:30) y EPC/DOPS (9:1) fueron las seleccionadas para realizar el estudio, al ser previamente consideradas las más adecuadas para incorporar CPT-11 y SN-38, respectivamente. También se estudiaron los coeficientes de reparto de las camptotecinas entre n-octanol y soluciones tamponadas a diferentes pH.

El CPT-11 presentaba actividad superficial y penetraba en la monocapa de DSPC/DOPS/CHOL, lo que permitió determinar el área ocupada por esta molécula en la interfase saturada. No se pudo analizar, en cambio, la actividad superficial del SN-38: el alto coeficiente de partición del SN-38, en consonancia con su gran hidofobicidad, era el responsable de la incapacidad de esta molécula de formar monocapas o de adsorberse en la interfase aire-agua.

El estudio de las isotermas de compresión puso de manifiesto que las mezclas DPPC/DOPS/CHOL and EPC/DOPS formaban monocapas de Langmuir estables en la interfase aire-agua, que el CPT-11 formaba monocapas con valores bastante inferiores de presión superficial y que el SN-38 no formaba monocapas en las condiciones del ensayo. Además, las dos mezclas, DPPC/DOPS/CHOL y EPC/DOPS formanban monocapas estables con CPT-11 y con SN-38, respectivamente, a todas las relaciones molares estudiadas. La existencia de un único punto de colapso en cada una de las isotermas de las mezclas estudiadas, era indicativa de la miscibilidad de las camptotecinas con su correspondiente mezcla de lípidos en el sistema binario lípido/fármaco. Los dos fármacos tenían un gran efecto de contracción sobre las mezclas de lípidos respectivas, lo que se explicaría por la gran afinidad de las dos camptotecinas por los lípidos de la monocapa y comportaría una mayor estabilidad de la misma.

El análisis de módulo de compresibilidad de las monocapas, que aporta información adicional sobre su elasticidad, permitió establecer que las dos camptotecinas inducían

cambios en el grado de empaquetamiento de las cadenas de acilo de los lípidos. La diferente ubicación de los fármacos en la estructura del liposoma era la responsable del distinto efecto que provocaban en el estado de la monocapa. Así, la monocapa de DSPC/DOPS/CHOL tenía un valor del módulo de compresibilidad de 83 mN/m a 30mN/m, que indicaba que es encontraba en un estado intermedio entre las fases de líquido condensado y líquido expandido. La incorporación del CPT-11 disminuía el valor del módulo de compresibilidad, provocando que la monocapa estuviera en un estado de líquido condensado. Al aumentar la concentración de fármaco, la monocapa volvía a la fase de líquido expandido. Por el contrario, la monocapa EPC/DOPS estaba en una fase de líquido condensado (valor del Cs-1 ligeramente superior a 110 mN/m a 30 mN/m) y, al incorporar el SN-38, disminuía el valor del Cs-1 a todas las concentraciones ensayadas y el estado de la monocapa cambiaba de forma gradual al de líquido expandido, con lo que era más compresible.

La naturaleza de las interacciones moleculares y la miscibilidad de los componentes de monocapas mixtas pueden examinarse determinando las desviaciones del área por molécula con respecto a la idealidad, en el contexto de la regla de aditividad. Este estudio puso de manifiesto que, mientras el CPT-11 se mezcla bien con los lípidos DSPC/DOPS/CHOL en un estrecho rango de concentraciones ($x_{CPT-11} \leq 0.13$ and $x_{CPT-11} \geq 0.6$), la combinación de EPC/DOOPS y SN-38 muestra un comportamiento mixto cercano a las predicciones de la regla de aditividad.

En el caso del CPT-11, se realizaron isotermas de compresión con el fármaco disuelto en la subfase con el objetivo de determinar con qué compuesto de la bicapa se establecía la interacción. Los resultados demostraron la interacción de este fármaco con el componente DOPS de la bicapa y el patrón de miscibilidad indicó que estas interacciones eran posibles a fracciones molares entre 0.13 y 0.6.

La solubilidad del CPT-11 en medios polares determina que se sitúe en el interior acuoso del liposoma. Pero además se deben tener en cuenta distintos aspectos: su grupo piperidinio tiene carga positiva al pH al que se preparan las vesículas; la bicapa de los liposomas tiene carga negativa debido al componente DOPS (una fostatidilserina) de la mezcla DSPC/DOPS/CHOL; se ha descrito la distribución asimétrica de los constituyentes de les bicapas de las membranas biológicas, propiedad que parece extensible a las bicapas liposomales, y que las fosfatidilserinas se localizan en una proporción mayor en su monocapa interna . Todo esto sugiere que se puede establecer una interacción electrostática entre CPT-11 y DOPS que desplazará al fármaco y lo situarápróximo a este componente de la bicapa. Así, el CPT-11 encapsulado en el espacio acuoso liposomal permarecerá anclado electrostáticamente a la monocapa interna de la bicapa, con lo que se resuelven, en

parte, los problemas asociados a la formulación y preparación de transportadores para moléculas solubles.

En el caso del SN-38, se observó que establecía interacciones repulsivas con las moléculas de lípido que, aunque débiles, modificaban la compresibilidad de la bicapa. Estas interacciones no afectaban de forma significativa ni a la presión de colapso ni al patrón de miscibilidad de las monocapas. La disminución del Cs-1, que indica la formación de una monocapa más fluidas en presencia de SN-38, sugería la interacción entre el fármaco y la mezcla binaria EPC/DOPS. El hecho de que el SN-38 no modificara la temperatura de fusión de las bicapas de EPC/DOPS, evidenciaba su localización en la zona hidrofóbica externa de la bicapa, al igual que lo hace el paclitaxel cuando se incorpora en bicapas de DPPC (182).

El conjunto de los resultados comentados en este apartado confirmó la idoneidad de los liposomas para la vehiculización de camptotecinas en base a criterios de estabilidad, destaca la conveniencia de utilizar la mezcla ternaria de lípidos DSPC/DOPS/CHOL para la formulación liposomal de CPT-11 y permite proponer la mezcla EPC/DOPS para la preparación de una formulación adecuada para el SN-38.

5.3. Internalización celular y actividad citotóxica de las formulaciones liposomales de CPT-11 y de SN-38

La eficacia de la quimioterapia depende de la actividad citotóxica del fármaco que, a su vez, es consecuencia de su posible internalización y acumulación en las células tumorales y de su localización subcelular. Los estudios *in vitro* en modelos de cultivos celulares constituyen una primera y necesaria aproximación, antes de los ensayos *in vivo*, para determinar el mecanismo de actuación del fármaco en la nueva formulación y para establecer la eficacia del mismo.

El potencial terapéutico de las formulaciones liposomales de CPT-11 (CPT-11lip) y de SN-38 (SN-38lip) se analizó utilizando dos líneas celulares tumorales, HeLa (ATCC CCL-2) y CaCo-2 (ATCC HTB-37). Tanto la primera, de adenocarcinoma de cérvix, como la segunda, de cáncer colorrectal, se han utilizado ampliamente como líneas tumorales modelo para realizar este tipo de estudios y, además, en el caso de Caco-2, para predecir la absorción de fármacos de administración oral a través de la mucosa del intestino. Con la formulación de CPT-11 también se ensayó el efecto sobre una línea celular sana, fibroblastos de piel humana Hs68 (ATCC CRL-1635), para comprobar si existía alguna acción diferencial inducida por el fármaco en este tipo de células respecto a las tumorales.

Antes de realizar los estudios de citoxicidad, se cuantificó la cantidad de fármaco captado por las células. Los ensayos con las distintas líneas celulares mostraron que

los liposomas, tanto con CPT-11 como con SN-38, se internalizaban de forma generalizada en las células y que la cantidad de fármaco localizada en el interior celular era superior cuando se administraba encapsulado en el nanotransportador que cuando se solubilizaba en el medio adecuado (tampón de lactato para el CPT-11 o DMSO para el SN-38). También se observó que la cinética de penetración era dependiente de la línea celular utilizada. Así, en el caso del CPT-11 la internalización en Hs68 era más rápida que en Caco2 o en HeLa.

El análisis detallado de la localización subcelular del CPT-11 en células HeLa y Hs68, mediante microscopia confocal y microscopía de contrate de fases, determinó que el patrón de acumulación en las dos líneas celulares era similar y que coincidía con el compartimento acídico de los lisosomas, desde donde se liberaría para llegar al núcleo y ejercer su efecto citotóxico inhibiendo la acción de la Topoisomerasa I. En Caco2 se observó un patrón similar mediante microscopía de fluorescencia. El interés de estos ensayos radica en la relación entre localización y actividad citotóxica. A pesar de ello no se han publicado demasiados estudios respecto a la localización subcelular de fármacos de la familia de las camptotecinas y, en cualquier caso, los resultados son bastante heterogéneos.

El estudio de la citotoxicidad inducida por las formulaciones desarrolladas, permitió observar diferencias interesantes entre células sanas y tumorales. Mediante el ensayo del MTT se observó que la formulación liposomal de CPT-11 inducía una gran disminución de la supervivencia celular tanto en HeLa - desde el 100% hasta el 3%-, como en Caco-2 – del 100% hasta el 5%-. Sin embargo, el tratamiento de fibroblastos Hs68 mostró resultados muy distintos: en las mismas condiciones de concentración y tiempo, la viabilidad celular disminuyó solo hasta el 40%. Además, la supervivencia siempre fue menor al tratar los distintos tipos celulares con la formulación CPT-11lip que con la formulación CPT-11sol. Para validar los resultados obtenidos, se realizó el ensayo de exclusión del Tripan Blue con dos de las líneas celulares, Hela y Hs68. Mientras que los resultados con HeLa eran concordantes, los datos obtenidos en el estudio con fibroblastos mostraron que la viabilidad fue siempre superior al 97%, para todos los tiempos ensayados, sin diferencias significativas. Así, puede sugerirse que el CPT-11 ejerce una acción antiproliferativa, sin inducir la muerte de las células Hs68. La mayor acumulación intracelular CPT-11lip, en comparación con CTP-11sol, justificaría su mayor actividad citotóxica sobre células HeLa y Caco-2.

El estudio morfológico, mediante tinción con azul de toluidina, de las células HeLa y Hs68 sometidas al tratamiento con la formulación CPT-11lip proporcionó también información interesante. Se demostró que CPT-11lip inducía cambios morfológicos importantes en células HeLa, pero no en Hs68. Los fibroblastos tratados con CPT-11lip no mostraban alteraciones, ni de tamaño ni de morfología, aunque en las

imágenes apenas se observaban células mitóticas. La respuesta de las células HeLa, era muy diferente. La visualización, realizada a diferentes tiempos después del tratamiento y eliminación del fármaco, mostró células de mayor tamaño y más planas, con largas proyecciones citoplasmáticas.

Mediante diferentes ensayos se estableció el mecanismo de muerte celular en HeLa. La determinación de la actividad LDH en el medio de cultivo de células HeLa y Hs68, después del tratamiento con CPT-11lip, permitió descartar la implicación de procesos de necrosis en la muerte celular, ya que la integridad de las membranas se conservaba después de la exposición al fármaco. En el caso de células HeLa, la tinción con Hoechst-33258 y el estudio de la relocalización de Bax mediante inmunofluorescencia permitieron identificar la ruta apoptótica mitocondrial como principal mecanismo de muerte de HeLa después del tratamiento con CPT-11lip (las células mostraban, además, núcleos con la cromatina condensada y fragmentada en la tinción con Hoechst-33258). En el caso de la línea celular Caco-2, los resultados obtenidos mediante la tinción con Hoechst-33258, que mostraban que las células adoptaban características morfológicas típicas de la apoptosis, se confirmaron con el test de la Anexina V, que permite cuantificar la cantidad de células que se encuentran en este estado. Se observó que el número de Caco-2 apoptóticas aumentaba al aumentar el tiempo de incubación y que la viabilidad de las células disminuía, en concordancia con los datos observados mediante otros ensayos.

El análisis del ciclo celular enfatizó la diferente respuesta de Hs68 y de Hela o Caco2 al CPT-11 en su formulación liposomal. En los histogramas de ADN de células HeLa, obtenidos a diferentes tiempos después del tratamiento, se observó un aumento significativo del pico situado en la zona correspondiente a células apoptóticas, una parada del ciclo en la fase G2/M y un aumento progresivo de células poliploides. En los perfiles de los fibroblastos Hs68, sin embargo, la cantidad de células apoptóticas era despreciable y sólo aumentaba de forma ligera y transitoria el número de células poliploides tras la eliminación del fármaco. En Caco-2 el perfil del ciclo era similar al de Hela, con un incremento del porcentaje de células en fase subG0, correspondiente a las apotóticas, un aumento significativo del número de células poliploides y una parada en las fases S y G2/M.

Existen resultados contradictorios en la literatura respecto a la capacidad del CPT-11 para inducir una parada del ciclo celular en G2/M y en ellos se hace referencia al diferente comportamiento de las células en función del estado de la proteína p53, que está mutada en más del 50% de los tumores humanos (183). Por este motivo se analizaron en profundidad los cambios inducidos por el CPT-11, en su formulación liposomal, en el perfil de expresión de p53 y de las proteínas Bax y Bcl-2. Se estudiaron los niveles de expresión mediante RT-PCR de las tres proteínas en HeLa y

Hs68 después de la incubación con CPT-11lip a diferentes tiempos. En Hs68, la expresión de p53 aumentaba de forma ligera pero significativa en las células tratadas, la de Bcl2 disminuía de forma significativa y no se observaron cambios respecto a la proteína proapoptótica Bax. En cambio en HeLa, había una sobre-expresión de p53 entre las 3h y 24h de incubación, la expresión de Bax también aumentaba mientras que, por el contrario, los niveles de la proteína anti-apoptótica Bcl-2 disminuían de forma drástica.

En el caso de Hela, el CPT-11 induce una respuesta apoptótica masiva, que no parece estar relacionada con el estatus de p53. Las células Hela expresan p53 en su forma natural, aunque es inactivada y degradada rápidamente por el virus del papiloma humano. Esto hace que el daño en el ADN de las células no pueda ser reparado, con lo que el CPT-11 induce una ruta apoptótica independiente de p53. El hecho de que los niveles de Bcl-2 disminuyeran drásticamente y los de Bax aumentaran, refuerzan el hecho de que el CPT-11 provoca una respuesta apotótica masiva.

En cuanto a los fibroblastos, la parada en el crecimiento en este tipo de celular no implicó un aumento continuado de los niveles de p53. En este sentido se ha descrito que los inhibidores de las topoisomerasas inducen una parada de las células en división sin cambios en la expresión de p53, pero que las células vuelven a crecer después de retirar el efecto inhibidor. En otro estudio se ha demostrado que un fármaco quimioterapéutico alcalino puede inducir de forma selectiva senescencia y no apoptosis a través de un mecanismo independiente de p53. Por otro lado, algunas publicaciones indican la existencia de un tipo de senescencia dependiente de p53 en respuesta a agentes dañinos para el ADN.

Para determinar si el tratamiento con CPT-11lip desencadenaba senescencia en las células HeLa viables después de la incubación y en los fibroblastos Hs68 que no proliferaban, se llevó a cabo el ensayo de la β-galactosidasa a diferentes tiempos después de retirar el fármaco. Una vez más, se observó un patrón de comportamiento distinto en ambas líneas celulares. Las células HeLa supervivientes, claramente identificadas como tretaploides por el aumento del tamaño de su núcleo, tenían una tasa de senescencia superior a la de los fibroblastos (mayor porcentaje de células β-galactosidasa positivas). Al cabo de 5 días, cerca del 93% de las células supervivientes eran sensecentes.

Los fibroblastos, por el contrario, parecían entrar en un estado de quiescencia, como respuesta transitoria al tratamiento, y el porcentaje de células Hs68 β-galactosidasa positivas disminuyó del 72%, justo después de eliminar el CPT-11lip del medio, hasta el 12%, después de 5 días, demostrándose que, además de temporal, el cambio era reversible. El conjunto de los resultados obtenidos puso de manifiesto que las células HeLa que sobreviven al tratamiento con CPT-11lip permanecen en un estado de

senescencia, mientras que los fibroblastos Hs68 experimentan una parada del crecimiento, que es temporal, convirtiéndose de nuevo en células proliferativas después de la retirada del fármaco. Se puede proponer, pues, que el tratamiento con la formulación liposomal de CPT-11 no produce efecto citotóxico (solo temporalmente cistostático) para las células normales Hs68, pero que induce una respuesta apoptótica masiva en células HeLa acompañada de sensecencia como mecanismo alternativo de muerte celular.

El análisis de la organización del citoesqueleto de las células Hs68 y HeLa tratadas con CPT-11lip permitió profundizar en el estudio del mecanismo global de inactivación de ambas líneas celulares. La observación, mediante microscopía Confocal, de las muestras de Hs68 puso de manifiesto que, con independencia del tiempo, no aparecía ninguna alteración de los microfilamentos de F-actina ni de la vinculina, los cuales eran similares a los de las células control. Las células HeLa, por el contrario, presentaban profundos cambios de tamaño y morfología, así como en la distribución de la F-actina, a los diferentes tiempos seleccionados. Inmediatamente después del tratamiento, HeLa mostraba un citoesqueleto de F-actina completamente desorganizado y un incremento espectacular de la señal de vinculina. Los resultados observados están de acuerdo con los cambios morfológicos observados mediante la tinción con azul de Toluidina. Se ha descrito que las células senescentes desarrollan una larga y densa red de vimentina, largas y delgadas fibras de actina y numerosos pequeños sitios de contacto focal.

También se examinó el efecto inducido por la formulación CPT-11lip sobre el ADN y la respuesta de dos de las líneas celulares en estudio, Hs68 y HeLa al tratamiento. Se estudió la inmunofluorescencia de γ-H2AX, para determinar el daño producido en el ADN, mediante microscopía de fluorescencia y de contraste de fases. Los resultados pusieron de manifiesto que las células HeLa mostraban alteraciones en su ADN, que aumentaban con el tiempo, mientras que los fibroblastos Hs68 eran capaces de reparar el daño que inicialmente, a tiempos cortos, producía la incubación con el fármaco. Se demuestra, pues, que el CPT-11 formulado en liposomas es capaz de alcanzar el núcleo celular después de ser liberado del vehículo (liposoma) y que ejerce un efecto citotóxico sobre células HeLa, pero no sobre fibroblastos Hs68. Por otra parte, el efecto nocivo producido por CPT-11lip sobre el ADN desencadena diferentes respuestas celulares: la supervivencia de las células Hs68 dependiente de p53 y la respuesta apoptótica, indepenciente de p53, de células HeLa. De manera análoga a nuestros resultados, un estudio en el que se ensayó el efecto de tres inhibidores de la Topoisomerasa I (sin utilizar sistemas de vehiculización y liberación controlada) sobre varias líneas celulares, puso de manifiesto que los fármacos eran más citotóxicos para las líneas tumorales que para las células sanas (184).

Esta respuesta notablemente diferente de líneas celulares tumorales y sanas podría constituir la base para el diseño de propuestas alternativas para reducir los efectos secundarios asociados a la quimioterapia con CPT-11

El SN-38 es el metabolito activo del CPT-11. La hidrólisis enzimática del CPT-11, catalizada por una carboxilesterasa, produce SN-38, producto con una actividad entre 100 y 1.000 veces superior a la del CPT-11. No obstante, se ha demostrado que solo una pequeña fracción del pro-fármaco genera la molécula activa. Así pues, siendo el potencial terapéutico del SN-38 superior, sería de gran interés disponer de una formulación farmacéutica más eficaz para esta camptotecina.

Mediante ensayos *in vitro* con dos líneas celulares tumorales se puso de manifiesto la gran eficacia de la formulación liposomal de SN-38. Se demostró que el fármaco era internalizado en mayor proporción por las células HeLa que por las Caco-2, que la cinética del proceso era sensiblemente diferente y que ambos tipos celulares internalizan mejor el SN-38 en su forma liposomal que cuando el fármaco está solubilizado en DMSO, a todos los tiempos ensayados, a pesar del efecto permeabilizante de este disolvente en las membranas celulares. Este hecho pone de relieve la importancia de utilizar nanotransportadores para la administración de fármacos.

El estudio de la citotoxicidad inducida por el SN-38, tanto en su forma liposomal, como solubilizado en DMSO, se utilizó para evaluar la eficacia de la nueva formulación farmacéutica de este fármaco. Los resultados del ensayo de reducción del MTT permitieron establecer, de forma cuantitativa, la mayor actividad citotóxica del SN-38 cuando se utilizan liposomas como sistema de vehiculización, y están de acuerdo con la mayor internalización de la formulación liposomal de esta molécula. Por otra parte, las células HeLa parecen más sensibles al efecto del fármaco cuando el tiempo de incubación es menor.

Un estudio del ciclo celular puso de manifiesto diferencias notables en la respuesta de las células HeLa y Caco-2 al tratamiento con SN-38lip.

En el caso de HeLa, los cambios más significativos fueron el enorme aumento en el número de células en la fase subG1, cuya presencia se relaciona con procesos de muerte celular por apoptosis, y la gran disminución en el porcentaje de células en el sector G0/G1, en las dos condiciones ensayadas (sin y con períodos de post-incubación). También deben considerarse los cambios en los sectores S, G2/M y >4c: el porcentaje de células en la fase S experimentó muy poca variación mientras que las células G2/M y poliploides (> 4 c) mostraron aumentos progresivos

La respuesta de Caco-2 al tratamiento con SN-38lip fue bastante diferente. Podrían destacarse los siguientes hechos: i) una disminución en la proporción de células en la

fase G0/G1, aunque algo más moderada que la observada en el perfil de HeLa; ii) una parada del ciclo en la fase S, cuyo pico aumenta de forma considerable en el perfil de las células tratadas correspondiente al tiempo de incubación superior; iii) el porcentaje de células G2/M solo experimenta un ligero descenso cuando se aplican tiempos de post-incubación y iv) cambios muy pequeños en el porcentaje de células que evolucionan hacia el sector Sub G1 o hacia la región poliploide. Pasadas 24 h después de eliminar el SN-38 y las células despegadas (condiciones de post-incubación), las células restantes, que también han internalizado el fármaco, evolucionan de una manera similar a como lo hacían en ausencia de post-incubación. Sin embargo, una diferencia significativa es la importante disminución de la población G0/G1 y el gran incremento en el número de células en la fase S. Esta parada del ciclo de Caco-2 en la fase S, puede conducir a la supresión de la proliferación celular.

El conjunto de los resultados comentados en este apartado también pone de manifiesto la diferente sensibilidad de las células Caco-2 al tratamiento con SN-38lip o con CPT-11lip, en términos de mecanismo de muerte celular. Sin analizar en profundidad las características asociadas a los procesos apoptóticos o necróticos, se puede observar que el perfil del ciclo de Caco-2 experimenta diferentes cambios a los observados después de la incubación con CPT-11lip. A partir de este resultado se podría interpretar que el ciclo celular se detiene en la fase S cuando la incubación se realiza con SN-38lip, sin cambios significativos en la región sub G1, mientras que el tratamiento con CPT-11lip produce alteraciones severas del histograma de ADN diploide característico de células Caco-2 no tratadas (179): como se sugirió entonces, los cambios observados eran consistentes con el progreso de un proceso de apoptosis creciente inducido por este fármaco en su forma liposomal. Ambas acciones podrían constituir una barrera para el desarrollo del cáncer.

En la bibliografía se describe la respuesta de algunas líneas celulares de cáncer de colon al tratamiento con CPT-11, en su forma solubilizada (185, 186). En general, paradas del ciclo celular en la fase G2/M (y, algunas veces, en la fase S), junto con descensos de la población en G1, son los efectos más observados. Sin embargo, cabe señalar que existen discrepancias en algunos aspectos de los perfiles completos del ciclo celular presentados en las referencias bibliográficas más relevantes consultadas.

La muerte celular inducida por la acción citotóxica de un fármaco puede ser el resultado de una disrupción de la membrana citoplasmática asociada a un proceso de necrosis o ser debida a la aparición de burbujas en la membrana como consecuencia de un proceso de apoptosis. Existen varios ensayos discernir entre ambas posibilidades. El test del MTT y el ensayo de la LDH son dos métodos experimentales que, utilizados conjuntamente, proporcionan información fidedigna acerca de las

posibles causas de la citotoxicidad celular y sobre el mecanismo de muerte que de este efecto se puede derivar (187).

Los resultados obtenidos mediante los ensayos de la LDH y del MTT demostraron el efecto citotóxico del SN-38, tanto en su forma liposomal, como solubilizado en DMSO. Sin embargo, desde un punto de vista cuantitativo, el grado de supervivencia después del tratamiento farmacológico de los dos tipos celulares, HeLa y Caco-2, fue muy diferente según el método utilizado para evaluarlo. Esta discrepancia podría indicar que la alteración o perturbación de la membrana no sería el principal factor implicado en la disminución de la viabilidad celular inducida por SN-38. Este comportamiento es bastante distinto al observado después del tratamiento de las células HeLa y Hs68 con CPT-11lip. En aquel caso se pudo descartar la implicación de procesos de necrosis en la muerte celular, ya que la integridad de las membranas se conservaba después de la exposición al fármaco. En el caso actual, los resultados obtenidos no son suficientes para proponer el mecanismo mediante el cual el SN-38 ejerce su acción citotóxica. Debe tenerse en cuenta que la liberación de LDH se considera un episodio inicial en la necrosis pero, también, un acontecimiento tardío en la apoptosis por lo que, en ensayos a tiempos largos, ambos procesos podrían mostrar señales similares.

El conjunto de los resultados discutidos en estos apartados destaca el potencial de los liposomas desarrollados para la vehiculización de las dos camptotecinas en estudio sobre la base de criterios de estabilidad, eficacia de incorporación de los fármacos y mayor actividad citotóxica que las formulaciones de los fármacos solubilizados. Son biocompatibles i selectivamente citotóxicos para células tumorales. Se confirma, además, la utilidad de las mezclas lipídicas ternaria DSPC/DOPS/CHOL y binaria EPC/DOPS para las formulaciones liposomales del CPT-11 y del SN-38, respectivamente.

5.4. Recubrimiento polimérico mucoadhesivo de las formulaciones CPT-11lip y SN-38lip

Cuando se considera la ruta de administración de un fármaco se observa que la más utilizada tradicionalmente ha sido la intravenosa. A pesar de que presenta algunas ventajas interesantes, supone riesgos evidentes para los tejidos sanos y produce graves efectos secundarios que reducen las dosis toleradas. La quimioterapia oral emerge como una alternativa prometedora en la oncología del futuro y puede cambiar radicalmente los actuales regímenes e incrementar de manera notable la calidad de vida del paciente. Esta opción es especialmente interesante en el caso del cáncer de colon, así como de otras enfermedades gastrointestinales severas, en donde la vehiculización directa de los fármacos a las zonas de tratamiento ofrece ventajas

significativas sobre otras estrategias terapéuticas (137). Cuando se utiliza un sistema de vehiculización para el colon, debe tenerse en cuenta que para que el transportador pueda alcanzar su destino en forma intacta y absorberse liberando el fármaco encapsulado, deberá superar algunos obstáculos que presenta el tracto gastrointestinaly que la mucosa que lo recubre constituye una barrera fisiológica real que deberá atravesar el vehículo (188).

Con esta finalidad, se puede funcionalizar la superficie del transportador para que adquiera propiedades especiales, como mayor resistencia en entornos agresivos, capacidad de interacción con células tumorales específicas y retención más prolongada en el lugar de actuación. Todas las estrategias hasta el momento desarrolladas se basan en la utilización de polímeros que dotan a la formulación de propiedades específicas: se pueden utilizar polímeros sensibles al pH o polímeros bioadhesivos de naturaleza polisacárida (140). Entre estos últimos destacan los quitosanos, interesantes por su biodegradabilidad y su carácter catiónico, que facilitará la interacción del transportador con membranas celulares y mucosas. Cuando se vehiculiza al colon, la hidrólisis de sus enlaces glicosídicos por acción de las polisacaridasas (138) que producen las bacterias anaerobias de la microflora de este tejido, permitirá la liberación del fármaco encapsulado.

Se ha considerado, pues, la aplicación de tecnologías bioadhesivas y de recubrimiento al mismo transportador para incrementar la absorción y biodisponibilidad de fármacos y para potenciar, por consiguiente, su capacidad como sistema de vehiculización.

Así, se han desarrollado formulaciones liposomales mucoadhesivas a partir de las composiciones establecidas para la incorporación de las camptotecinas CPT-11 y SN-38. Con esta finalidad se ensayaron recubrimientos con diferentes quitosanos, de distinto tamaño y contraión, y los resultados se analizaron a partir de la caracterización física y de la evaluación del comportamiento mucoadhesivo de los sistemas obtenidos.

Los aspectos más destacados de estos estudios pueden resumirse en los siguientes puntos: i) el tamaño de partícula y el índice de polidispersidad eran mayores cuando se utilizaba un quitosano de mayor peso molecular (UP CL 213 frente a UP CL 113); ii) las variaciones de potencial ζ con la concentración de polímero demuestran la eficacia del proceso de recubrimiento; iii) la carga de superficie de las vesículas adquiere valores similares a partir de una determinada concentración de polímero (0.05%); iv) los valores de mucoadhesividad de los liposomas recubiertos con los quitosanos UP CL 113 y UP CL 213 son similares. Con estas premisas, si se considera el conjunto de los resultados obtenidos en los estudios de formulación y los datos de caracterización de las vesículas cargadas con CPT-11 o SN-38 y recubiertas con quitosano, se puede proponer que los liposomas preparados a partir de las mezclas lipídicas EPC/DOPS (90:10) y DSPC/DOPS/CHOL (65:35:30) y el recubrimiento con un 0,05% de quitosano

UP CL 113, a una relación 1:4 (v/v), proporcionan los sistemas con las mejores características estructurales y propiedades mucoadhesivas para formular SN-38 y CPT-11, respectivamente. Se ha demostrado que la capa de quitosano que rodea la superficie de los liposomas es la responsable de la mucoadhesión, ya que los liposomas no recubiertos no muestran ninguna adhesión destacable.

6. Conclusiones

Las conclusiones de la presente tesis son las siguientes:

1. Se han formulado liposomas estables y con las características adecuadas para su utilización como transportadores de dos citostáticos de la familia de las camptocecinas, el irinotecan (CPT-11) y el SN-38. La influencia de la composición lipídica en las propiedades de los liposomas unilamelares obtenidos se ha establecido realizando un estudio riguroso de aquellos parámetros fisicoquímicos que inciden y condicionan el comportamiento de las vesículas *in vivo*. El análisis de un total de once composiciones diferentes para el CPT-11 y de cinco para el SN-38, junto con la consideración del método de preparación más adecuado para cada formulación, han permitido seleccionar la mezcla lipídica más adecuada para cada citostático. Ambas formulaciones se han obtenido en forma liofilizada, totalmente estable y de fácil reconstitución, manteniendo prácticamente inalteradas las propiedades de las suspensiones iniciales.

2. La combinación de lípidos utilizada para obtener la formulación liposomal de CPT-11 confiere propiedades de termosensibilidad a las vesículas obtenidas. El método de preparación es sencillo, reproducible y se ha estandarizado. La interacción electrostática entre el fármaco y uno de los constituyentes lipídicos de la bicapa, situado de forma preferente en su monocapa interna, garantiza el mantenimiento del producto encapsulado a pesar de que sus propiedades de solubilidad determinen la localización en el espacio acuoso de las vesículas. La integridad de la bicapa del transportador a temperatura fisiológica, en un medio que contiene suero, ha puesto de manifiesto su potencial para aplicaciones terapéuticas.

3. La composición lipídica y el método de preparación para la formulación del SN38 son totalmente novedosos. Mediante el uso de técnicas de microemulsificación se obtiene una suspensión homogénea de vesículas y se incorpora entre el 95 y el 100% del fármaco. El protocolo está estandarizado y las vesículas caracterizadas.

4. Se ha demostrado la capacidad del CPT-11 y del SN-38 de interaccionar con los constituyentes lipídicos de sistemas modelo de membrana y/o de insertarse en la región hidrofóbica de sus bicapas, deduciéndose la diferente localización de ambos fármacos en los dos posibles entornos de la estructura liposomal. Ni el CPT-11, ni el SN-38 perturban la estructura de las bicapas complejas constituidas por las mezclas DSPC/DOPS/CHOL y EPC/DOPS, respectivamente, proporcionando sistemas estables. El CPT-11 interacciona electrostáticamente y de manera selectiva con el componente aniónico de su mezcla y el SN-38 establece interacciones repulsivas débiles que modifican la compresibilidad de la bicapa en la que se inserta, sin afectar de forma significativa ni a la presión de colapso, ni al patrón de miscibilidad de la mezcla lípido-fármaco.

5. El estudio del efecto de las formulaciones CPT-11lip y SN-38lip desarrolladas sobre diferentes líneas celulares tumorales (HeLa y Caco-2) y sanas (Hs68) ha puesto de manifiesto los siguientes hechos: i) CPT-11lip es eficazmente internalizado, y en mayor proporción que CPT-11sol, por células HeLa y Hs68 mediante un proceso de endocitosis, con una acumulación en los lisosomas; ii) CPT-11lip no es citotóxico para fibroblastos Hs68, pero induce una apoptosis masiva, acompañada de senescencia en la población de células HeLa que sobrevive al tratamiento; iii) una vez internalizado, el CPT-11 es capaz de alcanzar el núcleo y ejercer un efecto genotóxico, en ambas líneas celulares, que se repara en Hs68 pero no en HeLa; iv) el SN-38 es internalizado en mayor proporción por las células HeLa y Caco-2 cuando se formula en liposomas que cuando se solubiliza en DMSO; v) la respuesta de las células HeLa y Caco-2 al SN-38 muestra diferencias notorias, siendo las más significativas el proceso de apoptosis que induce el fármaco en HeLa y una parada del ciclo de Caco-2 en la fase S que puede conducir a supresión de la proliferación celular.

6. La interacción electrostática del polímero catiónico quitosano con la superficie negativa de las bicapas de DSPC/DOPS/CHOL y de EPC/DOPS establece la base para la formación de una cubierta polisacárida estable alrededor de los liposomas. Se han establecido las condiciones y el protocolo para la obtención de liposomas recubiertos de este polisacárido y se ha confirmado que la capa del polímero sobre la superficie liposomal es la responsable de la mucoadhesión. Teniendo en cuenta el tamaño del nanotransportador final y su carga de superficie, así como sus propiedades mucoadhesivas determinadas *in vitro*, se ha establecido que los mejores resultados, analizados en conjunto, se obtienen con el tipo de quitosano UP CL 113, a una concentración del 0,05% y con una relación volumen suspensión liposomal/volumen solución quitosano de 1:4.

7. Bibliografía

1. Torre LA, Bray F, Siegel RL, Ferlay J, Lortet-Tieulent J, Jemal A. Global cancer statistics, 2012. CA: A Cancer Journal for Clinicians. 2015;65(2):87-108.
2. Ferlay J, Soerjomataram I, Dikshit R, Eser S, Mathers C, Rebelo M, et al. Cancer incidence and mortality worldwide: Sources, methods and major patterns in GLOBOCAN 2012. International Journal of Cancer. 2015;136(5):E359-E86.
3. Fearon ER, Vogelstein B. A genetic model for colorectal tumorigenesis. Cell;61(5):759-67.
4. Manne U, Shanmugam C, Katkoori VR, Bumpers HL, Grizzle WE. Development and progression of colorectal neoplasia. Cancer biomarkers : section A of Disease markers. 2010;9(1-6):235-65.
5. Esteban-Jurado C, Garre P, Vila M, Lozano JJ, Pristoupilova A, Beltran S, et al. New genes emerging for colorectal cancer predisposition. World J Gastroenterol. 2014;20(8):1961-71.
6. P. Farreras CR. Medicina Interna. 14 ed. Madrid, Spain: Ediciones Harcourt, S.A.; 2000:267-72.
7. Compton CC, Greene FL. The Staging of Colorectal Cancer: 2004 and Beyond. CA: A Cancer Journal for Clinicians. 2004;54(6):295-308.
8. Wolpin BM, Mayer RJ. Systemic treatment of colorectal cancer. Gastroenterology. 2008;134(5):1296-310.
9. Gingras D, Béliveau R. Colorectal Cancer Prevention Through Dietary and Lifestyle Modifications. Cancer Microenvironment. 2011;4(2):133-9.
10. Watson AJM, Collins PD. Colon Cancer: A Civilization Disorder. Digestive Diseases. 2011;29(2):222-8.
11. Kelly C, Cassidy J. Chemotherapy in metastatic colorectal cancer. Surg Oncol. 2007;16(1):65-70.
12. Sharma S, Saltz LB. Oral chemotherapeutic agents for colorectal cancer. Oncologist. 2000;5(2):99-107.
13. Zunino F, Pratesi G. Camptothecins in clinical development. Expert Opin Investig Drugs. 2004;13(3):269-84.
14. Gill S, Thomas RR, Goldberg RM. Review article: colorectal cancer chemotherapy. Aliment Pharmacol Ther. 2003;18(7):683-92.
15. Nakayama T, Noguchi S. Therapeutic Usefulness of Postoperative Adjuvant Chemotherapy with Tegafur–Uracil (UFT) in Patients with Breast Cancer: Focus on the Results of Clinical Studies in Japan. The Oncologist. 2010;15(1):26-36.
16. Garcia-Carbonero R, Supko JG. Current perspectives on the clinical experience, pharmacology, and continued development of the camptothecins. Clin Cancer Res. 2002;8(3):641-61.
17. Pizzolato JF, Saltz LB. The camptothecins. Lancet. 2003;361(9376):2235-42.
18. Pommier Y. DNA topoisomerase I inhibitors: chemistry, biology, and interfacial inhibition. Chem Rev. 2009;109(7):2894-902.
19. Casadó A, Giuffrida MC, Sagristá ML, Castelli F, Pujol M, Alsina MA, et al. Langmuir monolayers and Differential Scanning Calorimetry for the study of the interactions between camptothecin drugs and biomembrane models. Biochimica et Biophysica Acta (BBA) - Biomembranes. 2016;1858(2):422-33.
20. Smith NF, Figg WD, Sparreboom A. Pharmacogenetics of irinotecan metabolism and transport: An update. Toxicology in Vitro. 2006;20(2):163-75.
21. Wu MH, Yan B, Humerickhouse R, Dolan ME. Irinotecan Activation by Human Carboxylesterases in Colorectal Adenocarcinoma Cells. Clinical Cancer Research. 2002;8(8):2696-700.
22. Frese S, Diamond B. Structural modification of DNA[mdash]a therapeutic option in SLE? Nat Rev Rheumatol. 2011;7(12):733-8.
23. Gupta E, Lestingi TM, Mick R, Ramirez J, Vokes EE, Ratain MJ. Metabolic fate of irinotecan in humans: correlation of glucuronidation with diarrhea. Cancer Res. 1994;54(14):3723-5.
24. Rougier P, Van Cutsem E, Bajetta E, Niederle N, Possinger K, Labianca R, et al. Randomised trial of irinotecan versus fluorouracil by continuous infusion after fluorouracil failure in patients with metastatic colorectal cancer. Lancet. 1998;352(9138):1407-12.
25. Saltz LB. The role of irinotecan in colorectal cancer. Curr Oncol Rep. 1999;1(2):155-60.

26. Saltz LB, Cox JV, Blanke C, Rosen LS, Fehrenbacher L, Moore MJ, et al. Irinotecan plus fluorouracil and leucovorin for metastatic colorectal cancer. Irinotecan Study Group. N Engl J Med. 2000;343(13):905-14.
27. Kohne CH, van Cutsem E, Wils J, Bokemeyer C, El-Serafi M, Lutz MP, et al. Phase III study of weekly high-dose infusional fluorouracil plus folinic acid with or without irinotecan in patients with metastatic colorectal cancer: European Organisation for Research and Treatment of Cancer Gastrointestinal Group Study 40986. J Clin Oncol. 2005;23(22):4856-65.
28. Fuchs CS, Marshall J, Mitchell E, Wierzbicki R, Ganju V, Jeffery M, et al. Randomized, controlled trial of irinotecan plus infusional, bolus, or oral fluoropyrimidines in first-line treatment of metastatic colorectal cancer: results from the BICC-C Study. J Clin Oncol. 2007;25(30):4779-86.
29. Mehmood RK**.** Review of Cisplatin and Oxaliplatin in Current Immunogenic and Monoclonal Antibody Treatments. Oncology Reviews. 2014;8(2):256.
30. Raymond E, Faivre S, Chaney S, Woynarowski J, Cvitkovic E**.** Cellular and Molecular Pharmacology of Oxaliplatin1. Mol Cancer Ther. 2002;1(3):227-35.
31. Saltz LB**.** Looking Ahead: What Will Change in Colorectal Cancer Treatment? Gastrointestinal Cancer Research : GCR. 2009;3(2 Suppl 1):S16-S8.
32. Hagan S, Orr MC, Doyle B**.** Targeted therapies in colorectal cancer-an integrative view by PPPM. EPMA J. 2013;4(1):3.
33. Vasir JK, Labhasetwar V**.** Targeted drug delivery in cancer therapy. Technol Cancer Res Treat. 2005;4(4):363-74.
34. Au JLS, Yeung BZ, Wientjes MG, Lu Z, Wientjes MG**.** Delivery of cancer therapeutics to extracellular and intracellular targets: Determinants, barriers, challenges and opportunities. Advanced Drug Delivery Reviews. 2016;97(Supplement C):280-301.
35. Ensign LM, Cone R, Hanes J**.** Oral drug delivery with polymeric nanoparticles: The gastrointestinal mucus barriers. Advanced Drug Delivery Reviews. 2012;64(6):557-70.
36. Boegh M, Nielsen HM**.** Mucus as a Barrier to Drug Delivery – Understanding and Mimicking the Barrier Properties. Basic & Clinical Pharmacology & Toxicology. 2015;116(3):179-86.
37. Yuan H, Chen C-Y, Chai G-h, Du Y-Z, Hu F-Q**.** Improved Transport and Absorption through Gastrointestinal Tract by PEGylated Solid Lipid Nanoparticles. Molecular Pharmaceutics. 2013;10(5):1865-73.
38. Lieleg O, Ribbeck K**.** Biological hydrogels as selective diffusion barriers. Trends in Cell Biology. 2011;21(9):543-51.
39. Xu X, Ho W, Zhang X, Bertrand N, Farokhzad O**.** Cancer nanomedicine: from targeted delivery to combination therapy. Trends in Molecular Medicine;21(4):223-32.
40. Matsumura Y, Maeda H**.** A new concept for macromolecular therapeutics in cancer chemotherapy: mechanism of tumoritropic accumulation of proteins and the antitumor agent smancs. Cancer Res. 1986;46(12 Pt 1):6387-92.
41. Carmeliet P, Jain RK**.** Angiogenesis in cancer and other diseases. Nature. 2000;407(6801):249-57.
42. Cho K, Wang X, Nie S, Chen Z, Shin DM**.** Therapeutic Nanoparticles for Drug Delivery in Cancer. Clinical Cancer Research. 2008;14(5):1310-6.
43. Alonso MJ**.** Nanomedicines for overcoming biological barriers. Biomed Pharmacother. 2004;58(3):168-72.
44. Leamon CP, Reddy JA**.** Folate-targeted chemotherapy. Adv Drug Deliv Rev. 2004;56(8):1127-41.
45. Mora M, Sagristá ML**.** Preclinical photodynamic therapy in Spain 2: Liposome vectorization of photosensitizers; Different strategies, different outcomes. Journal of Porphyrins and Phthalocyanines. 2009;13(04n05):537-43.
46. Bozzuto G, Molinari A**.** Liposomes as nanomedical devices. International Journal of Nanomedicine. 2015;10:975-99.
47. Wicki A, Witzigmann D, Balasubramanian V, Huwyler J**.** Nanomedicine in cancer therapy: Challenges, opportunities, and clinical applications. Journal of Controlled Release. 2015;200(Supplement C):138-57.
48. Ta T, Porter TM**.** Thermosensitive liposomes for localized delivery and triggered release of chemotherapy. J Control Release. 2013;169(1-2):112-25.
49. Che-Ming Jack H, Liangfang Z**.** Therapeutic Nanoparticles to Combat Cancer Drug Resistance. Current Drug Metabolism. 2009;10(8):836-41.

50. Boix-Garriga E, Acedo P, Casadó A, Villanueva A, Stockert JC, Cañete M, et al. Poly(D , L -lactide-co-glycolide) nanoparticles as delivery agents for photodynamic therapy: enhancing singlet oxygen release and phototototoxicity by surface PEG coating. Nanotechnology. 2015;26(36):365104.
51. Peer D, Karp JM, Hong S, Farokhzad OC, Margalit R, Langer R**.** Nanocarriers as an emerging platform for cancer therapy. Nat Nano. 2007;2(12):751-60.
52. Kateb B, Chiu K, Black KL, Yamamoto V, Khalsa B, Ljubimova JY, et al. Nanoplatforms for constructing new approaches to cancer treatment, imaging, and drug delivery: what should be the policy? Neuroimage. 2011;54 Suppl 1:S106-24.
53. Duncan R**.** Polymer conjugates as anticancer nanomedicines. Nat Rev Cancer. 2006;6(9):688-701.
54. Narang AS, Chang RK, Hussain MA**.** Pharmaceutical development and regulatory considerations for nanoparticles and nanoparticulate drug delivery systems. J Pharm Sci. 2013;102(11):3867-82.
55. Front Matter A2 - Israelachvili, Jacob N. Intermolecular and Surface Forces (Third Edition). San Diego: Academic Press; 2011:iii.
56. Bangham AD**.** Liposomes: the Babraham connection. Chemistry and Physics of Lipids. 1993;64(1):275-85.
57. H. H**.** Phospholipid vesicles. In: G. C, ed. Phospholipids Handbook New York: Marcel Dekker Inc.; 1993:603-34.
58. Lian T, Ho RJ**.** Trends and developments in liposome drug delivery systems. J Pharm Sci. 2001;90(6):667-80.
59. Kumar P, Gulbake A, Jain SK**.** Liposomes a vesicular nanocarrier: potential advancements in cancer chemotherapy. Crit Rev Ther Drug Carrier Syst. 2012;29(5):355-419.
60. Kulkarni CV**.** Lipid crystallization: from self-assembly to hierarchical and biological ordering. Nanoscale. 2012;4(19):5779-91.
61. Misra R, Acharya S, Sahoo SK**.** Cancer nanotechnology: application of nanotechnology in cancer therapy. Drug Discov Today. 2010;15(19-20):842-50.
62. Tekade RK, Kumar PV, Jain NK**.** Dendrimers in Oncology: An Expanding Horizon. Chem Rev. 2009;109(1):49-87.
63. Choi Y, Thomas T, Kotlyar A, Islam MT, Baker JR, Jr. Synthesis and functional evaluation of DNA-assembled polyamidoamine dendrimer clusters for cancer cell-specific targeting. Chem Biol. 2005;12(1):35-43.
64. Bianco A, Kostarelos K, Prato M**.** Applications of carbon nanotubes in drug delivery. Curr Opin Chem Biol. 2005;9(6):674-9.
65. Klumpp C, Kostarelos K, Prato M, Bianco A**.** Functionalized carbon nanotubes as emerging nanovectors for the delivery of therapeutics. Biochimica et Biophysica Acta (BBA) - Biomembranes. 2006;1758(3):404-12.
66. Bangham AD, Standish MM, Watkins JC**.** Diffusion of univalent ions across the lamellae of swollen phospholipids. J Mol Biol. 1965;13(1):238-52.
67. Bangham AD, Standish MM, Miller N**.** Cation permeability of phospholipid model membranes: effect of narcotics. Nature. 1965;208(5017):1295-7.
68. Janoff AS**.** *L*iposomes: Rational Design. New York: Marcel Dekker, Inc.; 1999.
69. Gregoriadis G**.** The carrier potential of liposomes in biology and medicine (second of two parts). N Engl J Med. 1976;295(14):765-70.
70. Gregoriadis G**.** The carrier potential of liposomes in biology and medicine (first of two parts). N Engl J Med. 1976;295(13):704-10.
71. Patil YP, Jadhav S**.** Novel methods for liposome preparation. Chemistry and Physics of Lipids. 2014;177:8-18.
72. Lasic D.D. PD**.** Medical applications of liposomes. Amsterdam, The Netherlands: Elsevier Science B.V.; 1998.
73. Chen G, Roy I, Yang C, Prasad PN**.** Nanochemistry and Nanomedicine for Nanoparticle-based Diagnostics and Therapy. Chemical Reviews. 2016;116(5):2826-85.
74. Pattni BS, Chupin VV, Torchilin VP**.** New Developments in Liposomal Drug Delivery. Chemical Reviews. 2015;115(19):10938-66.
75. Kraft JC, Freeling JP, Wang Z, Ho RJ**.** Emerging research and clinical development trends of liposome and lipid nanoparticle drug delivery systems. J Pharm Sci. 2014;103(1):29-52.

76. Allen TM. Liposomes. Opportunities in drug delivery. Drugs. 1997;54 Suppl 4:8-14.
77. Cevc G. Electrostatic characterization of liposomes. Chem Phys Lipids. 1993;64(1–3):163-86.
78. Cevc G. MD. *Phospholipid Bilayers: Physical Properties and Models*. New York: Wiley-Interscience; 1987.
79. Gregoriadis G. *Liposome Technology*. 3 ed: CRC Press 2006.
80. Torchilin VP. Recent advances with liposomes as pharmaceutical carriers. Nat Rev Drug Discov. 2005;4(2):145-60.
81. Sen K, Mandal M. Second generation liposomal cancer therapeutics: transition from laboratory to clinic. Int J Pharm. 2013;448(1):28-43.
82. Mora M, Sagrista ML, Trombetta D, Bonina FP, De Pasquale A, Saija A. Design and characterization of liposomes containing long-chain N-acylPEs for brain delivery: penetration of liposomes incorporating GM1 into the rat brain. Pharm Res. 2002;19(10):1430-8.
83. Allen TM, Cullis PR. Drug delivery systems: entering the mainstream. Science. 2004;303(5665):1818-22.
84. Klibanov AL, Maruyama K, Torchilin VP, Huang L. Amphipathic polyethyleneglycols effectively prolong the circulation time of liposomes. FEBS Lett. 1990;268(1):235-7.
85. Blume G, Cevc G, Crommelin MD, Bakker-Woudenberg IA, Kluft C, Storm G. Specific targeting with poly(ethylene glycol)-modified liposomes: coupling of homing devices to the ends of the polymeric chains combines effective target binding with long circulation times. Biochim Biophys Acta. 1993;1149(1):180-4.
86. Garcia-Diaz M, Kawakubo M, Mroz P, Sagrista ML, Mora M, Nonell S, et al. Cellular and vascular effects of the photodynamic agent temocene are modulated by the delivery vehicle. J Control Release. 2012;162(2):355-63.
87. Ledermann JA, Canevari S, Thigpen T. Targeting the folate receptor: diagnostic and therapeutic approaches to personalize cancer treatments. Annals of Oncology. 2015;26(10):2034-43.
88. Bagari R, Bansal D, Gulbake A, Jain A, Soni V, Jain SK. Chondroitin sulfate functionalized liposomes for solid tumor targeting. J Drug Target. 2011;19(4):251-7.
89. Perche F, Torchilin VP. Recent trends in multifunctional liposomal nanocarriers for enhanced tumor targeting. J Drug Deliv. 2013;2013:705265.
90. El-Dakdouki M, Zhu D, El-Boubbou K, Kamat M, Chen J, Li W, et al. Development of Multifunctional Hyaluronan-Coated Nanoparticles for Imaging and Drug Delivery to Cancer Cells; 2012.
91. Arpicco S, Lerda C, Dalla Pozza E, Costanzo C, Tsapis N, Stella B, et al. Hyaluronic acid-coated liposomes for active targeting of gemcitabine. European Journal of Pharmaceutics and Biopharmaceutics. 2013;85(3, Part A):373-80.
92. Yatvin MB, Weinstein JN, Dennis WH, Blumenthal R. Design of liposomes for enhanced local release of drugs by hyperthermia. Science. 1978;202(4374):1290-3.
93. Al-Ahmady Z, Kostarelos K. Chemical Components for the Design of Temperature-Responsive Vesicles as Cancer Therapeutics. Chemical Reviews. 2016;116(6):3883-918.
94. Bibi S, Lattmann E, Mohammed AR, Perrie Y. Trigger release liposome systems: local and remote controlled delivery? Journal of Microencapsulation. 2012;29(3):262-76.
95. Torchilin VP. Multifunctional, stimuli-sensitive nanoparticulate systems for drug delivery. Nature reviews. Drug discovery. 2014;13(11):813-27.
96. Akbarzadeh A, Rezaei-Sadabady R, Davaran S, Joo SW, Zarghami N, Hanifehpour Y, et al. Liposome: classification, preparation, and applications. Nanoscale Res Lett. 2013;8(1):102.
97. Mozafari MR. Liposomes: an overview of manufacturing techniques. Cell Mol Biol Lett. 2005;10(4):711-9.
98. Szoka F, Jr., Papahadjopoulos D. Procedure for preparation of liposomes with large internal aqueous space and high capture by reverse-phase evaporation. Proc Natl Acad Sci U S A. 1978;75(9):4194-8.
99. Deamer D, Bangham AD. Large volume liposomes by an ether vaporization method. Biochim Biophys Acta. 1976;443(3):629-34.
100. Lasic DD. Mechanisms of Liposome Formation. J Liposome Res. 1995;5(3):431-41.

101. Maulucci G, De Spirito M, Arcovito G, Boffi F, Castellano AC, Briganti G**.** Particle Size Distribution in DMPC Vesicles Solutions Undergoing Different Sonication Times. Biophysical Journal. 2005;88(5):3545-50.
102. Ohsawa T, Miura H, Harada K**.** Improvement of encapsulation efficiency of water-soluble drugs in liposomes formed by the freeze-thawing method. Chem Pharm Bull (Tokyo). 1985;33(9):3945-52.
103. Hope MJ, Bally MB, Webb G, Cullis PR**.** Production of large unilamellar vesicles by a rapid extrusion procedure: characterization of size distribution, trapped volume and ability to maintain a membrane potential. Biochim Biophys Acta. 1985;812(1):55-65.
104. Jahn A, Vreeland WN, DeVoe DL, Locascio LE, Gaitan M**.** Microfluidic Directed Formation of Liposomes of Controlled Size. Langmuir. 2007;23(11):6289-93.
105. Yu B, Lee RJ, Lee LJ**.** Microfluidic Methods for Production of Liposomes. Methods in enzymology. 2009;465:129-41.
106. Jass J, Tjärnhage T, Puu G**.** Atomic Force Microscopy Imaging of Liposomes. Methods Enzymol: Academic Press; 2003:199-213.
107. Patil YP, Jadhav S**.** Novel methods for liposome preparation. Chem Phys Lipids. 2014;177:8-18.
108. Weinstein JN RE, Leserman LD, Klausner RD, Dragsten P, Henkart P, Blumental R**.** Self-quenching of carboxyfluorescein fluorescence: Uses in studying lioposome stability and liposome–cell interaction. In: G G, ed. Liposome Technology. Florida: CRC Press; 1984:183-204.
109. Volodkin D, Mohwald H, Voegel J-C, Ball V**.** Coating of negatively charged liposomes by polylysine: Drug release study. Journal of Controlled Release. 2007;117(1):111-20.
110. Moghaddam B, Ali MH, Wilkhu J, Kirby DJ, Mohammed AR, Zheng Q, et al. The application of monolayer studies in the understanding of liposomal formulations. International Journal of Pharmaceutics. 2011;417(1):235-44.
111. Peetla C, Stine A, Labhasetwar V**.** Biophysical interactions with model lipid membranes: applications in drug discovery and drug delivery. Molecular Pharmaceutics. 2009;6(5):1264-76.
112. Edinger AL, Thompson CB**.** Death by design: apoptosis, necrosis and autophagy. Current Opinion in Cell Biology. 2004;16(6):663-9.
113. Rello S, Stockert JC, Moreno V, Gámez A, Pacheco M, Juarranz A, et al. Morphological criteria to distinguish cell death induced by apoptotic and necrotic treatments. Apoptosis. 2005;10(1):201-8.
114. Kroemer G, Galluzzi L, Vandenabeele P, Abrams J, Alnemri ES, Baehrecke EH, et al. Classification of cell death: recommendations of the Nomenclature Committee on Cell Death 2009. Cell death and differentiation. 2009;16(1):3-11.
115. Rello-Varona S, Herrero-Martín D, Lagares-Tena L, López-Alemany R, Mulet-Margalef N, Huertas-Martínez J, et al. The Importance of Being Dead: Cell Death Mechanisms Assessment in Anti-Sarcoma Therapy. Frontiers in Oncology. 2015;5(82).
116. Saikumar P, Dong Z, Mikhailov V, Denton M, Weinberg JM, Venkatachalam MA**.** Apoptosis: definition, mechanisms, and relevance to disease. The American Journal of Medicine;107(5):489-506.
117. Taylor RC, Cullen SP, Martin SJ**.** Apoptosis: controlled demolition at the cellular level. Nat Rev Mol Cell Biol. 2008;9(3):231-41.
118. Kepp O, Galluzzi L, Lipinski M, Yuan J, Kroemer G**.** Cell death assays for drug discovery. Nat Rev Drug Discov. 2011;10(3):221-37.
119. Golstein P, Kroemer G**.** Cell death by necrosis: towards a molecular definition. Trends in Biochemical Sciences;32(1):37-43.
120. Su Z, Yang Z, Xie L, DeWitt JP, Chen Y**.** Cancer therapy in the necroptosis era. Cell Death Differ. 2016;23(5):748-56.
121. Conrad M, Angeli JPF, Vandenabeele P, Stockwell BR**.** Regulated necrosis: disease relevance and therapeutic opportunities. Nat Rev Drug Discov. 2016;15(5):348-66.
122. Kroemer G, El-Deiry WS, Golstein P, Peter ME, Vaux D, Vandenabeele P, et al. Classification of cell death: recommendations of the Nomenclature Committee on Cell Death. Cell Death Differ. 0000;12(S2):1463-7.
123. Baehrecke EH**.** How death shapes life during development. Nat Rev Mol Cell Biol. 2002;3(10):779-87.

124. Roninson IB, Broude EV, Chang B-D**.** If not apoptosis, then what? Treatment-induced senescence and mitotic catastrophe in tumor cells. Drug Resistance Updates. 2001;4(5):303-13.
125. Erenpreisa J, Cragg MS**.** Mitotic death: a mechanism of survival? A review. Cancer Cell International. 2001;1:1-.
126. Hayflick L**.** The limited in vitro lifetime of human diploid cell strains. Experimental Cell Research. 1965;37(3):614-36.
127. Rodier F, Campisi J**.** Four faces of cellular senescence. The Journal of Cell Biology. 2011;192(4):547-56.
128. Schmitt CA**.** Cellular senescence and cancer treatment. Biochimica et Biophysica Acta (BBA) - Reviews on Cancer. 2007;1775(1):5-20.
129. Bieging KT, Attardi LD**.** Deconstructing p53 transcriptional networks in tumor suppression. Trends in Cell Biology. 2012;22(2):97-106.
130. Blanden AR, Yu X, Loh SN, Levine AJ, Carpizo DR**.** Reactivating mutant p53 using small molecules as zinc metallochaperones: awakening a sleeping giant in cancer. Drug Discovery Today. 2015;20(11):1391-7.
131. Philip AK, Philip B**.** Colon Targeted Drug Delivery Systems: A Review on Primary and Novel Approaches. Oman Medical Journal. 2010;25(2):79-87.
132. Prasanth V.V, R J, Mathew S**.** Colon Specific Drug Delivery Systems: A Review on Various Pharmaceutical Approaches; 2012.
133. Hua S, Marks E, Schneider JJ, Keely S**.** Advances in oral nano-delivery systems for colon targeted drug delivery in inflammatory bowel disease: Selective targeting to diseased versus healthy tissue. Nanomedicine: Nanotechnology, Biology and Medicine;11(5):1117-32.
134. Jin J, Sklar GE, Min Sen Oh V, Chuen Li S**.** Factors affecting therapeutic compliance: A review from the patient's perspective. Therapeutics and Clinical Risk Management. 2008;4(1):269-86.
135. Mei L, Zhang Z, Zhao L, Huang L, Yang X-L, Tang J, et al. Pharmaceutical nanotechnology for oral delivery of anticancer drugs. Advanced Drug Delivery Reviews. 2013;65(6):880-90.
136. Mazzaferro S, Bouchemal K, Ponchel G**.** Oral delivery of anticancer drugs I: general considerations. Drug Discovery Today. 2013;18(1):25-34.
137. Chourasia MK, Jain SK**.** Pharmaceutical approaches to colon targeted drug delivery systems. J Pharm Pharm Sci. 2003;6(1):33-66.
138. Krishnaiah YSR, Khan MA**.** Strategies of targeting oral drug delivery systems to the colon and their potential use for the treatment of colorectal cancer. Pharmaceutical Development and Technology. 2012;17(5):521-40.
139. Vandamme TF, Lenourry A, Charrueau C, Chaumeil JC**.** The use of polysaccharides to target drugs to the colon. Carbohydrate Polymers. 2002;48(3):219-31.
140. Jain A, Gupta Y, Jain SK**.** Perspectives of biodegradable natural polysaccharides for site-specific drug delivery to the colon. J Pharm Pharm Sci. 2007;10(1):86-128.
141. Gruber P, Longer MA, Robinson JR**.** Some biological issues in oral, controlled drug delivery. Adv Drug Deliv Rev. 1987;1(1):1-18.
142. Hardy JG, Wilson CG, Wood E**.** Drug delivery to the proximal colon. J Pharm Pharmacol. 1985;37(12):874-7.
143. Kenyon CJ, Cole ET, Wilding IR**.** The effect of food on the in vivo behaviour of enteric coated starch capsules. Int J Pharm. 1994;112(3):207-13.
144. Yang L, Chu JS, Fix JA**.** Colon-specific drug delivery: new approaches and in vitro/in vivo evaluation. Int J Pharm. 2002;235(1-2):1-15.
145. Evans DF, Pye G, Bramley R, Clark AG, Dyson TJ, Hardcastle JD**.** Measurement of gastrointestinal pH profiles in normal ambulant human subjects. Gut. 1988;29(8):1035-41.
146. das Neves J, Bahia MF, Amiji MM, Sarmento B**.** Mucoadhesive nanomedicines: characterization and modulation of mucoadhesion at the nanoscale. Expert Opinion on Drug Delivery. 2011;8(8):1085-104.
147. Sosnik A, Neves J, Sarmento B**.** Mucoadhesive polymers in the design of nano-drug delivery systems for administration by non-parenteral routes: A review; 2014.
148. Sinha VR, Kumria R**.** Polysaccharides in colon-specific drug delivery. Int J Pharm. 2001;224(1-2):19-38.

149. Ashford M, Fell J, Attwood D, Sharma H, Woodhead P**.** Studies on pectin formulations for colonic drug delivery. Journal of Controlled Release. 1994;30(3):225-32.
150. Ashford M, Fell J, Attwood D, Sharma H, Woodhead P**.** An evaluation of pectin as a carrier for drug targeting to the colon. Journal of Controlled Release. 1993;26(3):213-20.
151. Rubinstein A, Radai R, Ezra M, Pathak S, Rokem JS**.** In vitro evaluation of calcium pectinate: a potential colon-specific drug delivery carrier. Pharm Res. 1993;10(2):258-63.
152. Salyers AA**.** Energy sources of major intestinal fermentative anaerobes. Am J Clin Nutr. 1979;32(1):158-63.
153. Toledo OM, Dietrich CP**.** Tissue specific distribution of sulfated mucopolysaccharides in mammals. Biochim Biophys Acta. 1977;498(1):114-22.
154. Satoh A, Toida T, Yoshida K, Kojima K, Matsumoto I**.** New role of glycosaminoglycans on the plasma membrane proposed by their interaction with phosphatidylcholine. FEBS Letters. 2000;477(3):249-52.
155. Gutiérrez ME**.** Liposomas complejos, modelos alternativos para estudios biológicos y transportadores de moléculas bioactivas. Universidad de Barcelona; 2004.
156. Rubinstein A, Nakar D, Sintov A**.** Colonic drug delivery: enhanced release of indomethacin from cross-linked chondroitin matrix in rat cecal content. Pharm Res. 1992;9(2):276-8.
157. Sintov A, Di-Capua N, Rubinstein A**.** Cross-linked chondroitin sulphate: characterization for drug delivery purposes. Biomaterials. 1995;16(6):473-8.
158. Rubinstein A, Nakar D, Sintov A**.** Chondroitin sulfate: A potential biodegradable carrier for colon-specific drug delivery. Int J Pharm. 1992;84(2):141-50.
159. Gulbake A, Jain SK**.** Chitosan: a potential polymer for colon-specific drug delivery system. Expert Opin Drug Deliv. 2012;9(6):713-29.
160. Felt O, Buri P, Gurny R**.** Chitosan: a unique polysaccharide for drug delivery. Drug Dev Ind Pharm. 1998;24(11):979-93.
161. Bernkop-Schnurch A**.** Mucoadhesive polymers: strategies, achievements and future challenges. Adv Drug Deliv Rev. 2005;57(11):1553-5.
162. Bernkop-Schnurch A**.** Mucoadhesive systems in oral drug delivery. Drug Discov Today Technol. 2005;2(1):83-7.
163. Vasir JK, Tambwekar K, Garg S**.** Bioadhesive microspheres as a controlled drug delivery system. Int J Pharm. 2003;255(1-2):13-32.
164. Tozaki H, Komoike J, Tada C, Maruyama T, Terabe A, Suzuki T, et al. Chitosan capsules for colon-specific drug delivery: improvement of insulin absorption from the rat colon. J Pharm Sci. 1997;86(9):1016-21.
165. Tozaki H, Odoriba T, Okada N, Fujita T, Terabe A, Suzuki T, et al. Chitosan capsules for colon-specific drug delivery: enhanced localization of 5-aminosalicylic acid in the large intestine accelerates healing of TNBS-induced colitis in rats. J Control Release. 2002;82(1):51-61.
166. Lorenzo-Lamosa ML, Remunan-Lopez C, Vila-Jato JL, Alonso MJ**.** Design of microencapsulated chitosan microspheres for colonic drug delivery. J Control Release. 1998;52(1-2):109-18.
167. Zhang H, Alsarra IA, Neau SH**.** An in vitro evaluation of a chitosan-containing multiparticulate system for macromolecule delivery to the colon. Int J Pharm. 2002;239(1-2):197-205.
168. Zhang H, Neau SH**.** In vitro degradation of chitosan by bacterial enzymes from rat cecal and colonic contents. Biomaterials. 2002;23(13):2761-6.
169. Jain A, Jain SK, Ganesh N, Barve J, Beg AM**.** Design and development of ligand-appended polysaccharidic nanoparticles for the delivery of oxaliplatin in colorectal cancer. Nanomedicine: Nanotechnology, Biology and Medicine;6(1):179-90.
170. Jain SK, Jain A, Gupta Y, Khare P, Kannandasan M**.** Targeted delivery of 5-ASA to colon using chitosan hydrogel microspheres. Journal of Drug Delivery Science and Technology. 2008;18(5):315-21.
171. Mertins O, Dimova R**.** Binding of Chitosan to Phospholipid Vesicles Studied with Isothermal Titration Calorimetry. Langmuir. 2011;27(9):5506-15.
172. Allen TM, Cullis PR**.** Liposomal drug delivery systems: From concept to clinical applications. Advanced Drug Delivery Reviews. 2013;65(1):36-48.

173. Lansiaux A, Léonce S, Kraus-Berthier L, Bal-Mahieu C, Mazinghien R, Didier S, et al. Novel Stable Camptothecin Derivatives Replacing the E-Ring Lactone by a Ketone Function Are Potent Inhibitors of Topoisomerase I and Promising Antitumor Drugs. Molecular Pharmacology. 2007;72(2):311-9.
174. Dawidczyk CM, Kim C, Park JH, Russell LM, Lee KH, Pomper MG, et al. State-of-the-Art in Design Rules for Drug Delivery Platforms: Lessons from FDA-approved Nanomedicines. Journal of controlled release : official journal of the Controlled Release Society. 2014;187:133-44.
175. Estanqueiro M, Amaral MH, Conceição J, Sousa Lobo JM**.** Nanotechnological carriers for cancer chemotherapy: The state of the art. Colloids and Surfaces B: Biointerfaces. 2015;126(Supplement C):631-48.
176. Pérez-Herrero E, Fernández-Medarde A**.** Advanced targeted therapies in cancer: Drug nanocarriers, the future of chemotherapy. European Journal of Pharmaceutics and Biopharmaceutics. 2015;93(Supplement C):52-79.
177. Zylberberg C, Matosevic S**.** Pharmaceutical liposomal drug delivery: a review of new delivery systems and a look at the regulatory landscape. Drug Delivery. 2016;23(9):3319-29.
178. Panahi Y, Farshbaf M, Mohammadhosseini M, Mirahadi M, Khalilov R, Saghfi S, et al. Recent advances on liposomal nanoparticles: synthesis, characterization and biomedical applications. Artificial Cells, Nanomedicine, and Biotechnology. 2017;45(4):788-99.
179. Casadó A, Sagristá ML, Mora M**.** Formulation and *In Vitro* Characterization of Thermosensitive Liposomes for the Delivery of Irinotecan. Journal of Pharmaceutical Sciences;103(10):3127-38.
180. Arancia G, Calcabrini A, Matarrese P, Marcocci L, Pietrangeli P, Mondovi B**.** Effects of incubation with liposomes at different temperatures on cultured melanoma cells (M14). International Journal of Hyperthermia. 1994;10(1):101-14.
181. Casadó A SM, Mora M**.** Development and characterization of a novel SN-38 liposomal formulation and in vitro assessment of its cytotoxic effect on two tumor cell lines. Journal of Drug Targeting. 2017.
182. Zhao L, Feng S-S, Go ML**.** Investigation of molecular interactions between paclitaxel and DPPC by langmuir film balance and differential scanning calorimetry. Journal of Pharmaceutical Sciences. 2004;93(1):86-98.
183. Casadó A, Mora M, Sagristá ML, Rello-Varona S, Acedo P, Stockert JC, et al. Improved selectivity and cytotoxic effects of irinotecan via liposomal delivery: A comparative study on Hs68 and HeLa cells. European Journal of Pharmaceutical Sciences. 2017;109(Supplement C):65-77.
184. Tamura N, Hirano K, Kishino K, Hashimoto K, Amano O, Shimada J. Analysis of Type of Cell Death Induced by Topoisomerase Inhibitor SN-38 in Human Oral Squamous Cell Carcinoma Cell Lines. Anticancer Research. 2012;32(11):4823-32.
185. Kaku Y, Tsuchiya A, Kanno T, Nishizaki T**.** Irinotecan Induces Cell Cycle Arrest, but Not Apoptosis or Necrosis, in Caco-2 and CW2 Colorectal Cancer Cell Lines. Pharmacology. 2015;95(3-4):154-9.
186. Haug K, Kravik KL, De Angelis PM**.** Cellular Response to Irinotecan in Colon Cancer Cell Lines Showing Differential Response to 5-Fluorouracil. Anticancer Research. 2008;28(2A):583-92.
187. Kim H, Yoon SC, Lee TY, Jeong D**.** Discriminative cytotoxicity assessment based on various cellular damages. Toxicology Letters. 2009;184(1):13-7.
188. Groo A-C, Lagarce F**.** Mucus models to evaluate nanomedicines for diffusion. Drug Discovery Today. 2014;19(8):1097-108.

8. Anexos

Do folate-receptor targeted liposomal photosensitizers enhance photodynamic therapy selectivity?

García-Díaz M, Nonell S, Villanueva A, Stockert JC, Cañete M, Casadó A, Mora M, Sagristá ML.

Biochim Biophys Acta. 2011 Apr;1808(4):1063-71. doi: 10.1016/j.bbamem.2010.12.014

RESUMEN

Uno de los objetivos actuales en la investigación centrada en la terapia fotodinámica es mejorar su selectividad por las células tumorales con el fin de minimizar el riesgo y la extensión de los efectos secundarios no deseados causados por el daño en células normales. Se presta especial atención a los sistemas de administración mediados por receptores, en particular, a los dirigidos al receptor de folato. La incorporación de un fotosensibilizador modelo (ZnTPP) en una formulación liposomal dirigida a este receptor se ha demostrado que provoca una captación dos veces mayor que la formulación no derivatizada en células HeLa (células con receptor folato en la membrana). Como resultado, se mejoró la fotocitotoxicidad inducida por los liposomas derivatizados. Esta selectividad se inhibió completamente con un exceso de ácido fólico presente en el medio de cultivo celular. Además, las células A549 (células deficientes en receptores de folato) no han mostrado variaciones en la incorporación liposómica. Sin embargo, las diferencias observadas fueron menores de lo esperado. Tanto los liposomas con folato como los liposomas sin folato se localizan en los lisosomas, lo que confirma que la vía de adsorción no específica también está involucrada. Estos resultados son consistentes con la cinética de oxígeno singlete medida en células vivas tratadas con ambas formulaciones liposomales.

Biochimica et Biophysica Acta 1808 (2011) 1063–1071

Contents lists available at ScienceDirect

Biochimica et Biophysica Acta

journal homepage: www.elsevier.com/locate/bbamem

Do folate-receptor targeted liposomal photosensitizers enhance photodynamic therapy selectivity?

María García-Díaz [a], Santi Nonell [a], Ángeles Villanueva [b], Juan C. Stockert [b], Magdalena Cañete [b], Ana Casadó [c], Margarita Mora [c], M. Lluïsa Sagristá [c,*]

[a] Grup d'Enginyeria Molecular, Institut Químic de Sarrià, Universitat Ramon Llull, Via Augusta 390, 08017 Barcelona, Spain
[b] Departamento de Biología, Facultad de Ciencias, Universidad Autónoma de Madrid, Darwin 2, Cantoblanco, 28049 Madrid, Spain
[c] Departament de Bioquímica i Biologia Molecular, Facultat de Biologia, Universitat de Barcelona, Avinguda Diagonal 645, 08028 Barcelona, Spain

ARTICLE INFO

Article history:
Received 6 October 2010
Received in revised form 15 December 2010
Accepted 16 December 2010
Available online 6 January 2011

Keywords:
Photodynamic therapy
Folate receptor
Liposomes
Targeted drug delivery
Singlet oxygen

ABSTRACT

One of the current goals in photodynamic therapy research is to enhance the selective targeting of tumor cells in order to minimize the risk and the extension of unwanted side-effects caused by normal cell damage. Special attention is given to receptor mediated delivery systems, in particular, to those targeted to folate receptor. Incorporation of a model photosensitizer (ZnTPP) into a folate-targeted liposomal formulation has been shown to lead an uptake by HeLa cells (folate receptor positive cells) 2-fold higher than the non-targeted formulation. As a result, the photocytotoxicity induced by folate-targeted liposomes was improved. This selectivity was completely inhibited with an excess of folic acid present in the cell culture media. Moreover, A549 cells (folate receptor deficient cells) have not shown variations in the liposomal incorporation. Nevertheless, the differences observed were slighter than expected. Both folate-targeted and non-targeted liposomes localize in acidic lysosomes, which confirms that the non-specific adsorptive pathway is also involved. These results are consistent with the singlet oxygen kinetics measured in living cells treated with both liposomal formulations.

1. Introduction

Photodynamic therapy (PDT) is an emerging modality for the treatment of various ophthalmic, dermatologic, cardiovascular, and predominantly, oncologic diseases, that involves light, a photosensitizer (PS) and tissue oxygen, all innocuous for the cells by themselves [1–4]. The combined action of the triplet state of the PS and molecular oxygen results in the formation of singlet oxygen ($^1O_2$) a reactive oxygen species (ROS) which is thought to be the main responsible of photo-induced cell death, playing a key role in both apoptotic and necrotic pathways [5–7]. Once produced, $^1O_2$ may diffuse away from the site of production; oxidize biomolecules encountered along its path, or decay back to the ground state within its lifetime. The tiny fraction of $^1O_2$ which undergoes radiative decay emitting at 1280 nm is employed for optical $^1O_2$ detection. The time-resolved measurement of this emission is a very well-established method for monitoring $^1O_2$ production and determining its lifetime [8,9].

One of the most actively pursued goals in PDT research is to enhance the selective targeting of tumor cells in order to minimize the risk and extension of unwanted side-effects caused by damage to normal tissues [10]. Targeted drug delivery systems are one of the strategies proposed to solve the problems underlying traditional cancer treatments. Drug delivery systems are able to modify the pharmacokinetics and biodistribution of their associated drugs. In this way, liposomes possess many interesting properties such as the ability to entrap both hydrophilic and hydrophobic drug molecules without loss or alteration of their activity, long systemic circulation times, preferential accumulation in solid tumors, and controlled drug release [11–13]. In PDT, it has been shown that liposomes increase the photosensitizing efficiency of some PDT agents by maintaining their monomeric form, by modifying the uptake of the dye by malignant cells, or by influencing their subcellular accumulation [14,15].

One approach to improve the therapeutic efficacy of drug-carrying liposomes is the grafting of tumor-specific ligands to their lipid bilayer, which can be recognized by specific cell surface components [16], e.g., antibodies [17], growth factors [18], glycoproteins

Abbreviations: BCA, bicinchoninic acid; DMEM, Dulbecco's Modified Eagle's Medium; DMSO, dimethyl sulfoxide; D-PBS, deuterated phosphate-buffered saline; FA-PEG-DSPE, 2-distearoyl-*sn*-glycero-3-phosphoethanolamine-N-[folate(polyethylene glycol)-2000] (ammonium salt); FBS, fetal bovine serum; FD-DMEM, folate-deficient Dulbecco's Modified Eagle's Medium; MLV, multilamellar vesicle; MTT, 3-[4,5-dimethylthiazol-2-yl]-2,5-diphenyltetrazolium bromide; OOPS, 1,2-dioleoyl-*sn*-glycero-3-[phospho-*L*-serine] (sodium salt); PBS, phosphate-buffered saline; PDT, photodynamic therapy; POPC, 1-palmitoyl-2-oleoyl-*sn*-glycero-3-phosphocholine; PS, photosensitizer; SDS, sodium dodecyl sulfate; THF, tetrahydrofuran; ZnTPP, 5,10,15,20-tetraphenyl-21*H*,23*H*-porphine zinc

* Corresponding author. Tel.: +34 934 02 12 12; fax: +34 934 02 15 59.
E-mail address: mlsagrista@ub.edu (M.L. Sagristá).

0005-2736/$ – see front matter © 2010 Elsevier B.V. All rights reserved.
doi:10.1016/j.bbamem.2010.12.014

(transferrin) [19], or specific receptors [20]. The incorporation of ligand-targeted therapies not only facilitates targeting to the cell but also drug retention at the target site by preventing the rapid elimination from the system circulation. These ligands represent a minimal risk of inducing immune response, are widely available and often inexpensive. At present, special attention is given to folate receptor (FR)-mediated delivery systems [21]. Folic acid is an essential vitamin for the proliferation and maintenance of all cells. The lack of this nutrient in human serum makes malignant cells to up-regulate this receptor to compete more aggressively for the vitamin. The overexpression of folate receptor on a variety of epithelial cancer cells including cancers of ovary, lung, kidney, breast, brain and colon [22], and the extremely high affinity of folate for its receptor provide a novel approach to specifically deliver PSs encapsulated in folate-functionalized liposomes *in vitro* [23]. Improved uptake of PS-folate conjugates has been reported previously [24,25] and different systemic carrier platforms have been developed to achieve selective accumulation of PSs [26–30]. However, the details of such improved PS uptake are poorly understood. For instance, to what extent does receptor-mediated uptake affect the accumulation of PSs in the cells? Does receptor-mediated uptake affect the localization of the PSs in the cells? Are the photosensitization properties affected?

In order to address these questions, the model PS zinc-tetraphenylporphyrin (ZnTPP) was encapsulated in folate-targeted and non-targeted liposomes to assess the role of folate receptors in the active uptake of folate-targeted liposomes. ZnTPP was chosen as PS as it can be conveniently encapsulated in liposomes in high yield and in monomeric state [31,32]. Our results show that targeting HeLa cells (FR-overexpressing cervical carcinoma cell line) with folate-decorated liposomes indeed leads to an increased PS uptake. This enhancement induces higher photodynamic cell death compared to that caused by incubation with non-targeted liposomes. We subsequently describe a comparative study of accumulation and phototoxicity in FR-expressing HeLa tumor cells, and in A549 tumor cells which do not express FR. Subcellular localization patterns of both formulations were studied, as well as $^1O_2$ kinetics measured in living cells.

2. Materials and methods

2.1. Chemicals

1-Palmitoyl-2-oleoyl-*sn*-glycero-3-phosphocholine (POPC), 1,2-dioleoyl-*sn*-glycero-3-[phospho-*L*-serine] (sodium salt) (OOPS) and 1,2-distearoyl-*sn*-glycero-3-phosphoethanolamine-N-[folate(polyethylene glycol)-2000] (ammonium salt) (FA-PEG-DSPE) were purchased from Avanti Polar Lipids (Birmingham, AL, USA). Imidazole, folic acid and 5,10,15,20-tetraphenyl-21*H*,23*H*-porphine zinc (ZnTPP) were purchased from Sigma-Aldrich Chemical Co. (St. Louis, MO, USA). The porphyrin used had a minimal purity of 99% and was used as received. Deuterium oxide (99.9%) was purchased from Solvents Documentation Synthesis (SDS, Peypin, France). All other chemicals were commercially available reagents of at least analytical grade. Milli-Q water (Millipore Bedford, Massachusetts system, resistivity of 18 MΩ cm) was used.

Dulbecco's Modified Eagle's Medium (DMEM) with 4.5 g/L glucose, folate-deficient DMEM with 4.5 g/L glucose (FD-DMEM), fetal bovine serum (FBS), penicillin–streptomycin solution and *L*-glutamine solution for biological assays were purchased from Biological Industries (Kibbutz Beit Haemek, Israel). Sterile Dulbecco's phosphate-buffered saline (PBS) and 3-[4,5-dimethylthiazol-2-yl]-2,5-diphenyltetrazolium bromide (MTT) were purchased from Sigma-Aldrich. MicroBCA protein assay kit was purchased from Pierce Protein Research Products (Rockford, IL, USA) and used according to the product information sheet. The sterilized material was purchased from Techno Plastic Products (Trasadingen, Switzerland).

2.2. Cell cultures

Human HeLa cervical adenocarcinoma cell line (ATCC CCL-2) is one of the many tumor cell types that are known to over-express folate receptors [33]. Human lung adenocarcinoma A549 cells (ATCC CCL-185), known to be deficient in FR expression, were used as negative control. HeLa and A549 cells are adherent cells which grow up to form cellular monolayers toward confluence after seeding. These cells were cultured at 37 °C in a humidified sterile atmosphere of 95% air and 5% CO_2, using DMEM supplemented with fetal bovine serum (10% v/v), glucose (4.5 g/L), *L*-glutamine (292 mg/L), streptomycin sulfate (10 mg/L) and potassium penicillin (10,000 U/L). Before the experiments the cells were subcultured in folate-deficient DMEM (FD-DMEM) supplemented with the same components as DMEM for 2 weeks to establish a folate deficiency. Cell lines were maintained frozen in DMEM with 10% DMSO. 1.8 mL CryoTubes™ (Nunc, Nalge Nunc International, IL, USA) were filled with the cell suspension and placed in a cell Cryo 1 °C Freezing Container (Nalgene, Nalge Nunc International, IL, USA) to be slowly frozen up to −80 °C at a cooling rate of −1 °C/min for successful cell cryopreservation. Frozen cells were rapidly transferred to a liquid nitrogen container (−196 °C) and stored.

2.3. Preparation of liposomes

Folate-targeted and non-targeted liposomes for porphyrin incorporation were prepared by microemulsification following standard procedures [31,32]. Briefly, POPC/OOPS (90:10 molar ratio, non-targeted liposomes) and POPC/OOPS/FA-PEG-DSPE (90:10:0.1 molar ratio, FR-targeted liposomes) mixtures containing the photosensitizer ZnTPP at 100:1 lipid/porphyrin molar ratio were evaporated to dryness from a chloroform solution and kept in a vacuum desiccator for 12 h over P_2O_5 in order to remove the last traces of the solvent. Multilamellar vesicles (MLVs) were prepared by hydratation of the dried lipid films by vortexing for 30 min (alternating 30 s periods of heating and 30 s of vortexing) at a concentration of 20 mg lipid/mL of 50 mM imidazole–HCl buffer (pH 7.4) at 45 °C. The MLVs dispersion was frozen and thawed (five times), sonicated (bath sonicator, 15 min, 45 °C) and microemulsified (EmulsiFlex B3 device, Avestin, Ottawa, Canada). Microemulsification was carried out by pumping the fluid fifteen times through the interaction chamber (45 °C, 200 kPa). Control liposomes were prepared in the same way but without the PS. The liposomes were stored in the dark at 4 °C. Subsequent liposome handling procedures were all performed in the dark.

2.4. Liposome characterization

The PS and the lipid content in the liposomes were evaluated following standard procedures. Liposomes were disrupted by the addition of THF to an aliquot of the liposomal suspension, free of non-entrapped PS, obtained in imidazole–HCl buffer (THF/imidazole–HCl buffer, 24/1, v/v) and the absorbance was measured at λ_{max} of the Soret band. The PS concentration was determined by comparison with standard curves obtained in the same conditions. Lipid content was quantified by a colorimetric assay with ammonium ferrothiocyanate according to the method of Stewart [34]. The average size and polydispersity of unilamellar vesicles and the zeta potential were determined by photon correlation spectroscopy (PCS). A Zetasizer Nano-ZS (Malvern Instruments, UK) and a 4 mW He—Ne laser (Spectra Physics), at an excitation wavelength of 633 nm, were used. Before measuring, samples were appropriately diluted to avoid multiple scattering. To control the stability of the formulations, the PS and lipid content in liposomes as well as the average size and polydispersity of the vesicles were also determined after storage up to 7 days.

The stability of liposomes was also tested in the presence of 10% FBS following the procedure described in [35]. Liposomal suspensions

containing ZnTPP with a final concentration of 10 μM were incubated in imidazole–HCl buffer with 10% FBS at 37 °C with continuous stirring for different periods of time up to 48 h. After each incubation period, 200 μL of the mixtures were withdrawn and centrifuged at 4000 rpm to eliminate any non-encapsulated PS, appeared as a result of the disruption of the liposomes due to its interaction with serum components. Then, 1.5 mL of THF was added to 50 μL of each supernatant to disrupt the liposomes, liberating the porphyrin still encapsulated in the liposomes and precipitating the serum components. These samples were centrifuged at 4000 rpm to obtain a clear supernatant and the absorption spectra were recorded.

2.5. Dark toxicity and cell uptake

To select the ZnTPP concentration in cell cultures for uptake experiments, the PS dark toxicity was determined after incubation with 1–50 μM ZnTPP for up to 24 h. Cell viability was evaluated 24 h after treatment by the MTT colorimetric assay [36]. Briefly, after washing with PBS, DMEM containing 0.5 mg/mL MTT was added and incubated for 1 h at 37 °C. The medium was replaced by DMSO and the absorbance at 550 nm was read on a Bio-Rad Benchmark Plus microplate reader.

A concentration of 10 μM ZnTPP was chosen as a good compromise between cell viability and PS concentration in culture medium, with survival fractions higher than 85% for non-targeted and folate-targeted formulations, for both cell lines. The cellular uptake of ZnTPP was determined by fluorescence spectroscopy. HeLa and A549 cells were seeded in 25 cm^2 tissue culture flasks and grown toward 80–85% confluence in FD-DMEM. Cells were incubated in the dark with the appropriate volume of the folate-deficient medium containing 10 μM ZnTPP encapsulated in the two different liposomal formulations, for different times ranging from 30 min to 24 h. In free folate competition studies, 1 mM folic acid was added to the incubation medium. Afterwards, the medium was discarded and the cells were washed three times with PBS, scrapped and resuspended in 1 mL of 2% sodium dodecyl sulfate (SDS) in Milli-Q water. The resulting suspension was centrifuged at 10,000 rpm for 10 min (Sigma 2-16P centrifuge, angle rotor 24×1.5/2.2 mL). The extent of PS uptake was assessed by comparison between the fluorescence of this supernatant to that of standard solutions under the same conditions. The fluorescence intensity values obtained for each sample were normalized to the number of cells determined by the bicinchoninic acid (BCA) protein assay [37]. Each experiment was repeated twice.

In order to study the liposome cell internalization [38] and to distinguish surface bound to internalized liposomes, HeLa cells were incubated either at 4 °C (where folate-receptor-mediated endocytosis is blocked [23,39]) or 37 °C in the dark for 4 h with FD-DMEM containing 10 μM ZnTPP encapsulated in non-targeted and FR-targeted liposomes. Since folate rapidly dissociates from specific, high-affinity binding factors in acid pH [40], we used an acidic saline wash to remove surface-bound liposomes and distinguish the uptake due to surface binding than that due to internalization. After rising with PBS, cells were incubated for 10 min with acetate buffer pH 3.5 (130 mM NaCl, 20 mM NaAc). Cells were then scrapped and resuspended in 1 mL of 2% SDS. The extent of PS uptake was assessed by the same procedure described above.

2.6. Subcellular localization and quantitative analysis

Folate-deficient HeLa cells were grown on 22 mm square coverslips placed into 35 mm culture dishes. They were incubated at 37 °C for 24 or 48 h with FD-DMEM containing 1 or 10 μM ZnTPP encapsulated in folate-targeted or non-targeted liposomes. Cells were washed four times with PBS, mounted in DMEM and observed immediately. Microscopic observations and photography were performed with a Leica TCS SP2 confocal microscope (Wetzlar, Germany), operating with the 561 nm laser line. To confirm the intracellular localization of ZnTPP, the endocytic compartments of the HeLa cells were labeled with the fluoroprobe LysoTracker Red DND-99 (200 nM, Molecular Probes, Eugene, OR) or MitoTracker Deep Red (50 nM, Molecular Probes, Eugene, OR) in the culture medium at 37 °C for 30 min. After labeling, the coverslips were washed with PBS and observed in a microscope under green excitation filter to detect the emission of LysoTracker or MitoTracker. Microscopy and photography of control cells were performed using a BX61 epifluorescence microscope (Olympus, Tokyo, Japan). Photographs were processed using Adobe Photoshop CS2 software (Adobe Systems, San Jose, CA). Quantitative studies on HeLa cells subjected to 1 or 10 μM ZnTPP in liposomes with and without folate were carried out using image processing and analysis (IPA) from the public domain ImageJ 1.42 software (http://rsbweb.nih.gov/ij/index.html) [41]. The red ZnTPP signal was recorded for each cell, brightness values in arbitrary units corresponding to the following ratio: integrated density/area. Results were the mean values and standard deviations from a total of 70 images. In addition, the frequency of brightness values (red signal) was also evaluated for cells subjected to 24 h treatments with 1 or 10 μM ZnTPP in liposomes either with or without folate.

2.7. Photodynamic treatment in vitro

Folate-deficient cells were seeded in 96-well plates and cultured towards 80–85% confluence. They were then incubated in the dark at 37 °C with FD-DMEM containing 0.1–10 μM ZnTPP encapsulated in the two different liposomal formulations. After 24 h incubation, cells were washed three times with PBS and replenish with fresh FD-DMEM. Irradiation was carried out with a Sorisa Photocare LED source with a wavelength range of 520–550 nm. The light intensity at the irradiation site was 16 mW/cm^2, measured with a LaserStar Ophir power meter (Logan, UT, USA). Cells were irradiated for different times ranging from 2 min to 30 min and then incubated for 24 h before the MTT assay for cell viability. Experiments were performed in triplicate.

2.8. Spectroscopic measurements

Absorption spectra were recorded on a Varian Cary 4E spectrophotometer, equipped with a 110 mm-diameter integrating sphere for transmittance measurements. Fluorescence emission and excitation spectra were recorded in a Jobin-Ybon Specx Fluoromax-2 spectrofluorometer. The fluorescence quantum yields were determined by comparison of the areas under the emission curves for optically-matched suspension of liposomes and a reference, after correcting for the refractive index of the solvent. ZnTPP in toluene was used as reference with $\Phi_F = 0.033$ [42]. Fluorescence decays were recorded in a time-correlated single photon counting system (Fluotime 200, PicoQuant GmbH, Berlin, Germany) with a 596-nm excitation LED. The fluorescence decays were analyzed using the PicoQuant FluoFit 4.0 data analysis software.

$^1O_2$ phosphorescence was detected using a customized PicoQuant Fluotime 200 system described elsewhere [43,44]. Briefly, a diode-pumped pulsed Nd:YAG laser (FTSS355-Q, Crystal Laser, Berlin, Germany) working at 10 kHz repetition rate at 532 nm (12 mW, 1.2 μJ per pulse) was used for excitation. A 1064 nm rugate notch filter (Edmund Optics, UK) was placed at the exit port of the laser to remove any residual component of its fundamental emission in the near-IR region. The luminescence exiting from the side of the cuvette was filtered by a cold mirror (CVI Melles Griot, USA) to remove any scattered laser radiation. A TE-cooled Hamammatsu near IR photomultiplier (model H9170-45), sensitive from 950 to 1400 nm, was used to detect the $^1O_2$ phosphorescence. The detector was operated in photon counting mode and its output sent to a multichannel scaler PicoQuant Nanoharp 250.

Transient absorption spectra were measured by nanosecond laser flash photolysis using a Q-switched Nd-YAG laser (Surelite I-10, Continuum) with right-angle geometry and an analyzing beam produced by a Xe lamp (PTI, 75 W) in combination with a dual-grating monochromator (mod. 101, PTI) coupled to a photomultiplier (Hamamatsu R928). Kinetic analysis of the individual transients was achieved with the FitLW software developed in our laboratory.

For spectroscopic measurements in cell suspensions HeLa cells were incubated in the dark with 10 μM ZnTPP encapsulated in folate-targeted and non-targeted liposomes for 24 h. The medium was discarded and the cells were washed three times with PBS, scrapped and resuspended in 1.5 mL of PBS or D_2O-based PBS (D-PBS). The samples contained about 8 millions of cells in 1.5 mL of PBS and were continuously stirred during the measurements. The measurements were then carried out within the following 45 min.

All spectroscopic measurements were carried out in 1-cm quartz cuvettes (Hellma, Germany), at room temperature and under continuous stirring.

2.9. Statistical analysis

Unpaired Student's *t* test was used to test for the significance level between two sets of measurements. The level of significance was set to $p<0.05$.

3. Results and discussion

3.1. Characterization of liposomal formulations

FR-targeted and non-targeted liposomes containing ZnTPP at 100:1 lipid/porphyrin molar ratio were prepared by microemulsification. This particular combination of PS and lipids allows for a high encapsulation of this PS [31]. The PS encapsulation efficacy was close to 90% and was not affected by folate functionalization. Photon correlation spectroscopy (PCS) showed a dynamic diameter of 110 nm for non-targeted liposomes and 140 nm for FR-targeted liposomes with a polydispersity index of 0.3. The stability of the formulations was monitored by changes in the particle size and porphyrin and lipid retention over one week storage at 4 °C in the dark (Table 1). The liposomal formulations showed excellent colloidal stability and drug retention during this period. We thus conclude that the properties and stability of liposomal preparations are not affected by the presence of the folate marker.

The phase transition temperature of POPC/OOPS (90:10) liposomes was reported previously as -5.1 ± 0.7 °C and was not affected by the incorporation of 1% ZnTPP [31]. Thus, one can reasonably expect that it won't be affected either by the presence of 0.1 mol% FA-PEG-DSPE. The liposomes can therefore be safely assumed to be in the fluid state at 37 °C, temperature at which cell experiments were carried out. In order to ensure that ZnTPP does not escape from liposomes interacting with serum proteins, the stability of liposomes was tested also in the presence of 10% FBS at 37 °C. The remaining PS in both FR-targeted and non-targeted liposomal suspensions was always above 90%, indicating that serum proteins do not affect liposome stability and, especially, do not induce the release of the entrapped ZnTPP (Table 1).

Table 1
Stability of FR-targeted and non-targeted formulations as measured by lipid and PS content, particle size and zeta potential.

Sample	Time/h	L (%)[a]	P (%)[b]	Zave/nm[c]	ζ pot/mV[d]
Non-targeted	0	90±2	94±8	110±20	−38±5
	24	97±9	85±10	130±30	−31±3
	168	79±3	83±13	140±20	−30±3
FR-targeted	0	87±4	96±7	140±20	−36±2
	24	97±12	93±4	130±30	−34±2
	168	78±3	83±5	110±20	−35±4

Data are mean values ± SD of at least three independent experiments.
[a] L: Lipid content, expressed as the percentage of lipid in the sample with respect to the lipid present at the initial stage of liposome preparation.
[b] P: Porphyrin content, expressed as the percentage of porphyrin in the sample with respect to the porphyrin present at the initial stage of liposome preparation.
[c] Z average mean.
[d] Zeta potential.

The same holds true for the photophysical properties of the sensitizer: Fig. 1 shows the absorption and emission spectra of ZnTPP encapsulated in folate-targeted liposomes and their non-targeted counterparts. No spectral shifts can be observed between the two sets of data, ruling out any significant interaction of the porphyrin with the folate ligand. Likewise, the fluorescence quantum yield of ZnTPP, calculated by steady-state comparative method of optically-matched solutions, was 0.025 and 0.024 for folate-targeted liposomes and non-targeted liposomes, respectively ($\Phi_{F\ (ZnTPP,\ toluene)}=0.033$) [42]. Finally, the fluorescence decay kinetics, determined by time-correlated single photon counting, also confirmed that the photophysics of ZnTPP in the lipid bilayers are not affected by the presence of the FA-PEG-DSPE ligand. The fluorescence decay could be fitted in both systems by two exponential components with lifetimes 2.0 ± 0.1 and 1.3 ± 0.1 ns, respectively, reflecting different endoliposomal locations of ZnTPP in the phospholipid bilayer [45].

3.2. Cellular uptake of FR-targeted liposomes

After confirming that ZnTPP incorporation into the lipid bilayers is not affected by the presence of the FA-PEG-DSPE ligand, the effect of the folate marker on the cellular uptake of ZnTPP was determined. HeLa and A549 cells were incubated for different times with 10 μM ZnTPP encapsulated in folate-targeted and non-targeted liposomes. The extent of PS uptake was then determined by fluorescence spectroscopy after lysing the cells and then normalized to the protein content of each sample to correct for variations in the number of cells. As shown in Fig. 2A, a clear differential uptake between folate-targeted and non-targeted liposomes was observed. Thus, when FR-overexpressing HeLa cells were incubated for 24 h with folate-targeted liposomes, a 70% increase of lysate fluorescence is observed compared to the values for non-targeted liposomes. Moreover, FR-deficient A549 cells showed no differences in the liposomal incorporation (Fig. 2B). These results confirm that active uptake mediated by folate receptors is an effective approach to increase the uptake of PS encapsulated in folate-functionalized liposomes.

Additional evidence for the specific role of folate-receptor interactions in the differential uptake of ZnTPP was obtained from competitive binding assays. Thus, 1 mM folic acid was added to the incubation medium to saturate the receptors on the cell surface. Fig. 3

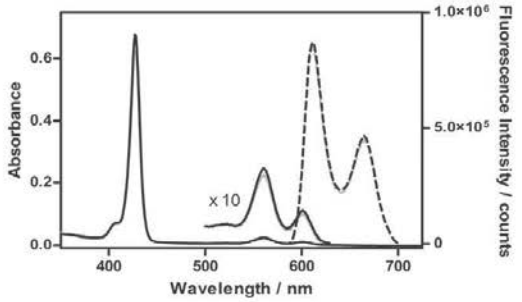

Fig. 1. Absorption (solid line) and emission (dashed line) spectra of ZnTPP incorporated in folate-targeted liposomes (black) and non-targeted liposomes (grey) in 50 mM imidazole–HCl buffer, pH 7.4. Note the factor ×10 in the 500–650 nm region of absorption spectra. The spectra were corrected relative to absorption at 550 nm.

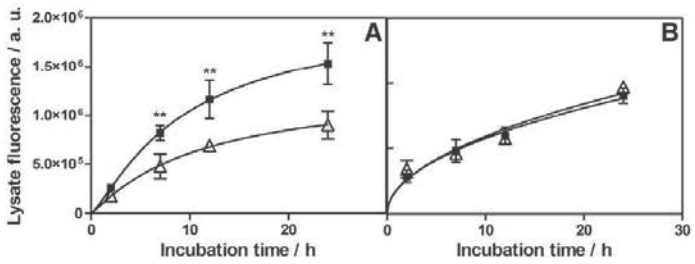

Fig. 2. Cellular uptake of ZnTPP encapsulated in folate-targeted liposomes (■) and non-targeted liposomes (△) by (A) HeLa and (B) A549 cells in folate-depleted DMEM media. The fluorescence change plotted is the ratio between the area under the fluorescence emission and the protein content in each suspension. Mean ± SD values from at least two different experiments are shown. $^{**}p<0.01$.

shows that 1 mM free folic acid significantly reduced the ZnTPP uptake in HeLa cells targeted with liposomes bearing folate ligands and no differences were observed between targeted and non-targeted liposomes uptake, indicating that the contribution of folate receptors to the uptake of ZnTPP was completely inhibited.

In a third series of experiments, the effect of FA-PEG-DSPE liposomal content on the uptake of ZnTPP was also assessed. HeLa cells were incubated for 24 h with different formulations containing 0–0.2 mol% of FA-PEG-DSPE and the fluorescence of the cell lysate was measured and normalized to the protein content of each sample. As expected, uptake of ZnTPP was found to be notably dependent on the amount of FA-PEG-DSPE present in the liposomes (Fig. 4). Increasing amounts of the folate ligand led to higher uptake of the PS although saturation effects were observed at the highest FA-PEG-DSPE concentration assayed. Since FR can bind only one molecule of folic acid [40], we chose to use 0.1 mol% FA-PEG-DSPE in all experiments, which also precludes the formation of folate dimers and trimers [46]. Thus, we can ensure an efficient interaction with folate receptors.

To check whether the incubation at 4 °C prevents ZnTPP uptake, the cell-surface binding capacity of folate-targeted and non-targeted liposomes was estimated from the differential uptake of ZnTPP by HeLa cells incubated at 4 °C or 37 °C (Fig. 5). In both cases, the extent of PS uptake was dramatically reduced when the incubation of ZnTTP-containing liposomes was performed at 4 °C, suggesting that endocytosis is the main cell internalization mechanism. Moreover, at this low temperature, almost a two-fold increase of cell-lysate fluorescence was observed for folate-targeted liposomes compared to non-targeted ones. This indicates that the differential uptake between folate-targeted and non-targeted liposomes is amplified due to enhanced surface binding of the former. Nevertheless, an acidic wash of the cells caused the release of surface-bound folate-targeted liposomes, showing that the uptake due to binding to the folate receptor was greatly diminished under such acidic conditions [23,39,40].

Taking all these results together, the preferential uptake of folate-targeted liposomes was demonstrated in HeLa cells. Nevertheless, the differences observed were smaller than expected [23,47,48]. Moreover, non-targeted liposomes are also internalized, revealing that non-specific endocytosis also contributes to the uptake. Qualls and Thompson [26] also observed non-specific liposomal uptake pathways when KB cells, also overexpressing folate receptors [24], were treated with $AlPcS_4^{4-}$ encapsulated in folate-displasmenylcholine liposomes.

3.3. Photosensitization experiments

Studies on the efficiency of the FR-targeted liposomes for PDT are summarized in Figs. 6 and 7. A549 and HeLa cells were incubated in the dark with different concentrations of ZnTPP entrapped in FR-targeted and non-targeted liposomes for 24 h prior to photosensitization. Afterwards, cells were exposed to green light using a LED source. Cell survival was assessed by MTT assay 24 h after treatment. Dark cytotoxicity experiments yielding survival cell fraction higher than 85% demonstrated that incubation with FR-targeted and non-targeted liposomes at the concentrations used did not induce significant cell death without irradiation. Fig. 6 shows the light and concentration dependence of the photodynamic response of HeLa cells for both types of ZnTPP-loaded liposomes. As expected, increasing the light dose and the concentration of the PS led to enhanced photocytotoxicity. Folate-decorated liposomes consistently

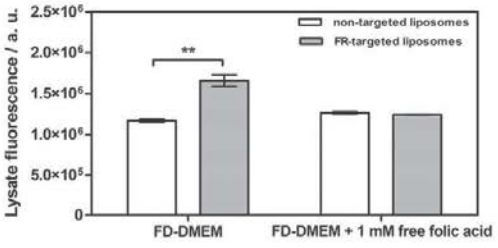

Fig. 3. Competitive binding assay in HeLa cells cultured with FR-targeted and non-targeted liposomes, with or without the addition of 1 mM free folic acid. The enhancement of the FR-targeted liposomes uptake was totally inhibited in the presence of 1 mM free folic acid. Fluorescence emission was normalized with protein content of each suspension. Mean ± SD values from at least two different experiments are shown. $^{**}p<0.01$.

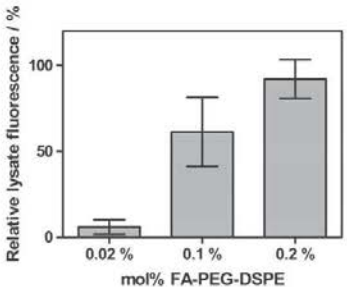

Fig. 4. Uptake of ZnTPP encapsulated in folate-targeted formulations with varying percentages of FA-PEG-DSPE by HeLa cells. Cells were incubated for 24 h with non-targeted liposomes (0 mol% FA-PEG-DSPE) or folate-targeted liposomes with the FA-PEG-DSPE mole percentage ranging from 0.02 to 0.2. Fluorescence emission was normalized with protein content of each suspension. The fluorescence emission plotted is relative to the lysate fluorescence of cells treated with non-targeted liposomes. The lysate fluorescence corresponding to 0 mol% FA-PEG-DSPE was normalized to 0 ± 12%. Mean ± SD values from at least three different experiments are shown.

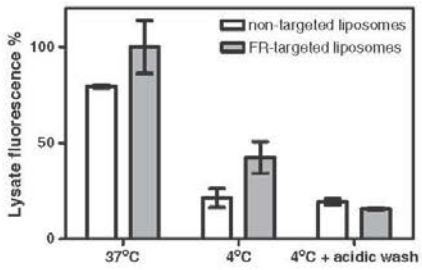

Fig. 5. Temperature-dependent uptake of ZnTPP encapsulated in folate-targeted and non-targeted liposomes. Cells were incubated for 4 h at 37 °C or 4 °C. The cells were then washed with cold PBS or with acidic saline buffer to remove unattached liposomes or either stripped of surface-bound liposomes. Fluorescence emission was normalized with protein content of each suspension. The fluorescence emission plotted is relative to the mean lysate fluorescence of cells treated with folate-targeted liposomes at 37 °C, normalized to 100 ± 14%. Mean ± SD values from at least three different experiments are shown.

led to higher photosensitivity of the cells. Irradiation of cell cultures alone or incubated with empty liposomes did not induce any toxicity.

A better appreciation of the folate-labeling effects can be gained by comparing the photodynamic effect under the same conditions. Thus, for 1 μM ZnTPP incubated for 24 h in A549 and HeLa cells and irradiated with 10 J cm^{-2} (Fig. 7), non-targeted liposomes caused 65 ± 5% cell death in both cell lines. The use of FR-targeted liposomes increased the cell mortality to 94 ± 5% for FR-positive HeLa cells, while it remained at 60 ± 5% for FR-negative A549 cells. Thus folate-targeted liposomes enhanced cell mortality by 50% in FR-positive HeLa cells.

3.4. Subcellular localization

Fluorescence and differential interference contrast images of HeLa cells after 24 or 48 h incubation with folate-targeted and non-targeted liposomes (10 μM ZnTPP bulk concentration) are shown in Fig. 8. The cells displayed a pattern of intense granular signal in the cytoplasm. The site of ZnTPP accumulation strongly resembled that of acidic organelles and therefore, lysosomes could be the main site of ZnTPP accumulation. Additionally, the intracellular localization of ZnTPP was compared with the distribution of fluorescent probes specific to lysosomes (LysoTracker Red) and to mitochondria (MitoTracker Red). LysoTracker and Mitotracker Red probes are commonly used in several research areas, including PDT studies [49–52]. As shown in Fig. 8A, the intracellular distribution of ZnTPP was clearly similar to LysoTracker Red, and clearly different from the mitochondrial network displayed with MitoTracker Red, under green excitation epifluorescence microscopy. We could not observe the co-localization of ZnTPP and LysoTracker probe because of the red emission of both dyes. The intensity of the punctate fluorescence was dependent on the porphyrin concentration, incubation time, as well as ZnTPP liposomal formulation. It is important to note that no morphological changes were detected in the cells under these conditions and no relocalization of the PS was observed when cells were exposed to prolonged exciting light. Non-specific adsorptive endocytosis pathway was confirmed by the fact that the intracellular localization of ZnTPP by non-targeted liposomes was identical to that of liposomes with folate.

Cells treated with 10 μM ZnTPP vehiculizated in liposomes with folate appeared with a higher fluorescence signal in relation to folate-free liposomes (see Fig. 8A). These results were confirmed by the quantitative analysis of fluorescence intensity using ImageJ 1.42 software (Fig. 8B and C), and results are consistent with the cellular uptake measured by cell lysate fluorescence.

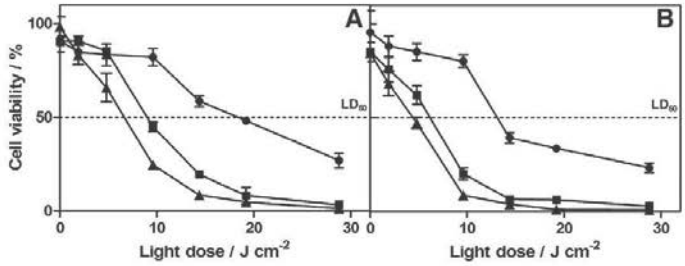

Fig. 6. Concentration and irradiation time dependence of photocytotoxicity of ZnTPP encapsulated in (A) non-targeted liposomes and (B) folate-targeted liposomes by HeLa cells. The concentrations represented are (●) 0.1 μM, (■) 1 μM and (▲) 10 μM. Mean ± SD from at least three different experiments are shown.

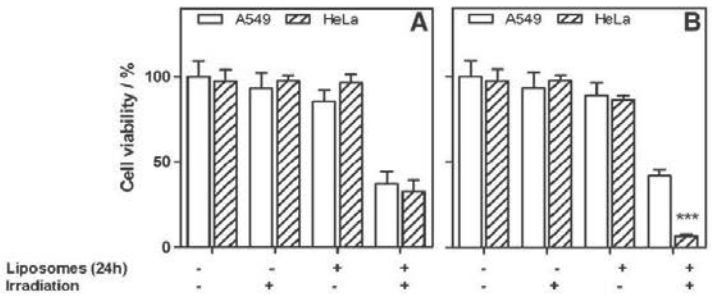

Fig. 7. Photodynamic induced cytotoxicity of ZnTPP encapsulated in (A) non-targeted liposomes and (B) folate-targeted liposomes (1 μM, 10 J/cm^2). Mean ± SD from at least three different experiments are shown. ***$p<0.001$.

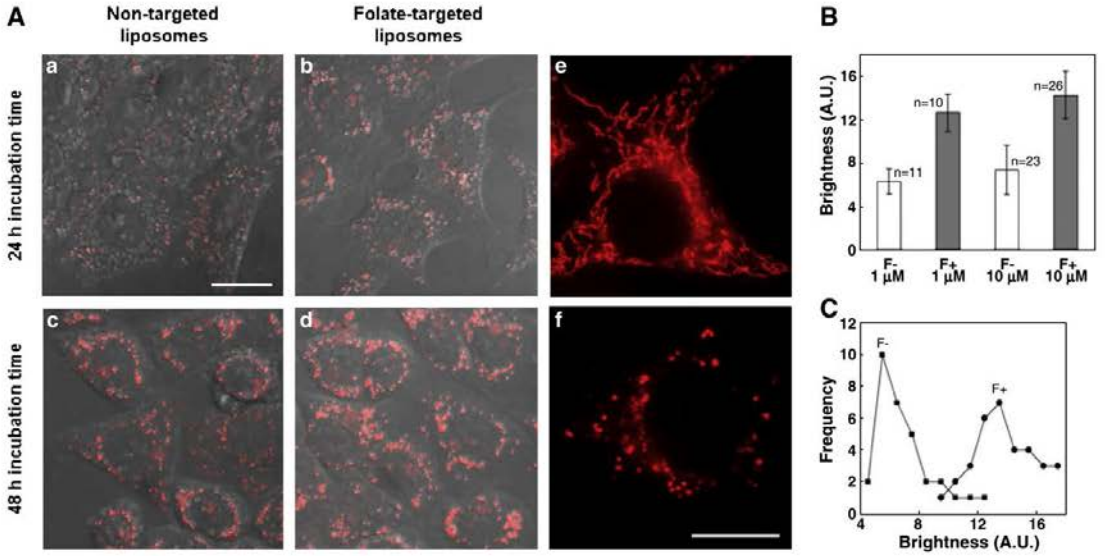

Fig. 8. (A) Confocal microscopy images of living HeLa cells incubated 24 or 48 h with different liposomal formulations of 10 μM ZnTPP. (a) and (b) Subcellular localization of ZnTPP in HeLa cells incubated 24 h in liposomes without and with folate, respectively. (c) and (d) Cells displaying the fluorescence pattern of ZnTPP 48 h after incubation in liposomes without and with folate, respectively. All images are the overlay of the fluorescence signal and differential interference contrast (DIC). Scale bar: 10 μm. (e) Localization of MitoTracker Red in HeLa control cells. (f) Localization of LysoTracker Red in HeLa control cells. (B) and (C) Microscopical evaluation of ZnTPP uptake. B: Mean brightness values (±SD) of the signal from HeLa cells treated for 24 h with 1 or 10 μM ZnTPP in liposomes with (F+) or without (F−) folate. C: Distribution of brightness values from HeLa cells subjected to 24 h treatments with both 1 and 10 μM ZnTPP in liposomes either with or without folate.

3.5. Time-resolved $^1O_2$ detection in HeLa cells incubated with ZnTPP encapsulated in FR-targeted and non-targeted liposomes

In a typical experiment, 1.5 mL-D_2O-based PBS (D-PBS) cell suspension containing ~8×10^6 cells incubated with ZnTPP encapsulated in FR-targeted and non-targeted liposomes was assayed for $^1O_2$ using pulsed laser excitation at 532 nm and observing the $^1O_2$ phosphorescence at 1280 nm. Indeed, the samples produced clear $^1O_2$ phosphorescence signals showing the expected rise-and-decay shape (Fig. 9). Kinetic analysis of the data in Fig. 9 yielded lifetimes $\tau_1 = 1.5 \pm 0.4$ μs for the rise and $\tau_2 = 6.0 \pm 0.5$ μs for the decay, the same results being obtained for both FR-targeted and non-targeted liposomes. Thus, the kinetics of $^1O_2$ production and decay in HeLa cells are not affected by the presence of folate ligands on the surface of the liposomes used for delivery of the ZnTPP, suggesting a similar final localization of the PS, in agreement with the confocal microscopy results.

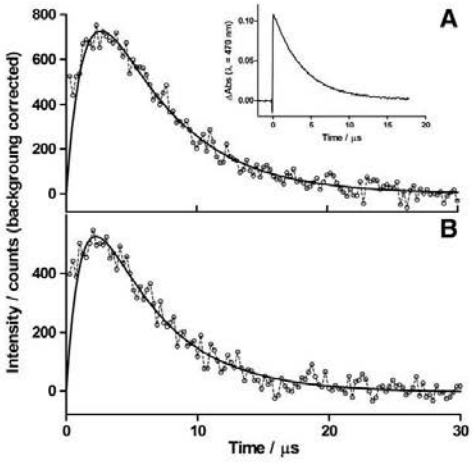

Fig. 9. Time-resolved luminescence decays of $^1O_2$ recorded at 1280 nm upon 532 nm excitation of a D-PBS HeLa cell suspension, previously incubated with 10 μM ZnTPP encapsulated in (a) non-targeted and (b) folate-targeted liposomes during 24 h in the dark. A: Fitted parameters: $\tau_1 = 1.5 \pm 0.4$ μs, $\tau_2 = 5.8 \pm 0.5$ μs; Inset A: ΔAbs signal recorded at 470 nm (triplet absorption), fitted parameters: $\tau_1 = 5 \pm 1$ μs; B: fitted parameters: $\tau_1 = 1.5 \pm 0.4$ μs, $\tau_2 = 6.1 \pm 0.5$ μs.

The inset in Fig. 9A shows the transient absorbance of ^{3}ZnTPP in the cell suspension. Kinetic analysis of this signal yields $\tau_T = 5 \pm 1$ μs, which means that $\tau_\Delta = 1.5 \pm 0.4$ μs in HeLa cells. This lifetime is much shorter than the typical value in D_2O (60–70 μs, [53]) indicating that $^1O_2$ is substantially quenched in these cells. Given diffusion coefficients of singlet oxygen in the $0.4–2\times10^{-5}$ $cm^2 s^{-1}$ range [54–56] and the typical size of the lysosomes (50–500 nm), it can be safely concluded that primary $^1O_2$ damage will be confined to this organelle, as found previously in human skin fibroblasts [44]. Indeed, we were not able to quench $^1O_2$ with standard quenchers such as sodium azide or bovine serum albumin.

4. Conclusions

A novel folate-targeted liposomal formulation of the model PS ZnTPP has been developed for its selective delivery to FR-overexpressing cancer cells. The stability of liposomal formulations and the photophysical properties of the PS are not affected by the presence of the folate ligand. This folate-targeted formulation shows enhanced ZnTPP internalization and phototoxicity by folate-receptor-positive cells, although non-specific pathways are also involved in cellular uptake. Confocal microscopy and $^1O_2$ kinetics measured in living cells indicate a lysosome localization of ZnTPP in HeLa cells, irrespective of the presence of folate on the liposome surface.

The prevention of liposome uptake at low temperature accounts for the involvement of endocytic pathways in the cellular internalization of

both targeted and non-targeted liposomes. Moreover, the reduction of ZnTPP fluorescence in the cells' lysates after an acidic wash confirms the interaction of the folate-targeted liposomes with the receptors. These observations are consistent with the lysosomal localization of ZnTPP.

Taken together, our results suggest that folate ligands enhance the cellular uptake in FR-positive cells mainly as a result of a sustained contact between the liposome and the cell surface, thereby increasing the liposomes' ability to internalize drugs. It will be interesting to see whether in cells with higher FR overexpression this folate-induced selectivity can be further increased. In addition, it will be interesting to study the efficacy of FR-targeted liposomes in preclinical models and their potential for future clinical application in photodynamic therapy.

Acknowledgements

This work was supported by a grant from the Spanish Ministerio de Ciencia e Innovación (CTQ2007-67763-C03/BQU). M.G-D. thanks the Comissionat per a Universitats i Recerca del Departament d'Innovació, Universitats i Empresa de la Generalitat de Catalunya i del Fons Social Europeu for a predoctoral fellowship. We thank Sorisa® (Dr. Albert Amat) for providing us with the Sorisa® Photocare LED source, Dr. Salvador Borrós and Dr. M. Luisa Grarcía for Zetasizer Nano-ZS measurements, and Xavier Ragàs for excellent technical assistance.

References

[1] B.C. Wilson, M.S. Patterson, The physics, biophysics and technology of photodynamic therapy, Phys. Med. Biol. 53 (2008) R61–R109.
[2] M. Ochsner, Photophysical and photobiological processes in the photodynamic therapy of tumours, J. Photochem. Photobiol. B 39 (1997) 1–18.
[3] S. Choudhary, K. Nouri, M.L. Elsaie, Photodynamic therapy in dermatology: a review, Lasers Med. Sci. 24 (2009) 971–980.
[4] G. Jori, C. Fabris, M. Soncin, S. Ferro, O. Coppellotti, D. Dei, L. Fantetti, G. Chiti, G. Roncucci, Photodynamic therapy in the treatment of microbial infections: basic principles and perspective applications, Lasers Surg. Med. 38 (2006) 468–481.
[5] T.J. Dougherty, C.J. Gomer, B.W. Henderson, G. Jori, D. Kessel, M. Korbelik, J. Moan, Q. Peng, Photodynamic therapy, J. Natl Cancer Inst. 90 (1998) 889–905.
[6] T.J. Dougherty, An update on photodynamic therapy applications, J. Clin. Laser Med. Surg. 20 (2002) 3–7.
[7] R.W. Redmond, I.E. Kochevar, Spatially resolved cellular responses to singlet oxygen, Photochem. Photobiol. 82 (2006) 1178–1186.
[8] S. Nonell, S.E. Braslavsky, Time-resolved singlet oxygen detection, Meth. Enzymol. 319 (2000) 37–49.
[9] C. Schweitzer, R. Schmidt, Physical mechanisms of generation and deactivation of singlet oxygen, Chem. Rev. 103 (2003) 1685–1757.
[10] W.M. Sharman, J.E. van Lier, C.M. Allen, Targeted photodynamic therapy via receptor mediated delivery systems, Adv. Drug Deliv. Rev. 56 (2004) 53–76.
[11] A.S. Derycke, P.A. de Witte, Liposomes for photodynamic therapy, Adv. Drug Deliv. Rev. 56 (2004) 17–30.
[12] T.L. Andresen, S.S. Jensen, K. Jorgensen, Advanced strategies in liposomal cancer therapy: problems and prospects of active and tumor specific drug release, Prog. Lipid Res. 44 (2005) 68–97.
[13] D.K. Chatterjee, L.S. Fong, Y. Zhang, Nanoparticles in photodynamic therapy: an emerging paradigm, Adv. Drug Deliv. Rev. 60 (2008) 1627–1637.
[14] X. Damoiseau, H.J. Schuitmaker, J.W. Lagerberg, M. Hoebeke, Increase of the photosensitizing efficiency of the Bacteriochlorin a by liposome-incorporation, J. Photochem. Photobiol. B 60 (2001) 50–60.
[15] M.C. Galanou, T.A. Theodossiou, D. Tsiourvas, Z. Sideratou, C.M. Paleos, Interactive transport, subcellular relocation and enhanced phototoxicity of hypericin encapsulated in guanidinylated liposomes via molecular recognition, Photochem. Photobiol. 84 (2008) 1073–1083.
[16] A.A. Gabizon, H. Shmeeda, S. Zalipsky, Pros and cons of the liposome platform in cancer drug targeting, J. Liposome Res. 16 (2006) 175–183.
[17] K. Maruyama, O. Ishida, T. Takizawa, K. Moribe, Possibility of active targeting to tumor tissues with liposomes, Adv. Drug Deliv. Rev. 40 (1999) 89–102.
[18] A. Gijsens, L. Missiaen, W. Merlevede, P. de Witte, Epidermal growth factor-mediated targeting of chlorin e6 selectively potentiates its photodynamic activity, Cancer Res. 60 (2000) 2197–2202.
[19] M. Singh, Transferrin as a targeting ligand for liposomes and anticancer drugs, Curr. Pharm. Des. 5 (1999) 443–451.
[20] P. Sapra, T.M. Allen, Ligand-targeted liposomal anticancer drugs, Prog. Lipid Res. 42 (2003) 439–462.
[21] W. Xia, P.S. Low, Folate-targeted therapies for cancer, J. Med. Chem. 53 (2010) 6811–6824.
[22] N. Parker, M.J. Turk, E. Westrick, J.D. Lewis, P.S. Low, C.P. Leamon, Folate receptor expression in carcinomas and normal tissues determined by a quantitative radioligand binding assay, Anal. Biochem. 338 (2005) 284–293.
[23] R.J. Lee, P.S. Low, Delivery of liposomes into cultured KB cells via folate receptor-mediated endocytosis, J. Biol. Chem. 269 (1994) 3198–3204.
[24] R. Schneider, F. Schmitt, C. Frochot, Y. Fort, N. Lourette, F. Guillemin, J.F. Muller, M. Barberi-Heyob, Design, synthesis, and biological evaluation of folic acid targeted tetraphenylporphyrin as novel photosensitizers for selective photodynamic therapy, Bioorg. Med. Chem. 13 (2005) 2799–2808.
[25] J. Gravier, R. Schneider, C. Frochot, T. Bastogne, F. Schmitt, J. Didelon, F. Guillemin, M. Barberi-Heyob, Improvement of meta-tetra(hydroxyphenyl)chlorin-like photosensitizer selectivity with folate-based targeted delivery. Synthesis and in vivo delivery studies, J. Med. Chem. 51 (2008) 3867–3877.
[26] M.M. Qualls, D.H. Thompson, Chloroaluminum phthalocyanine tetrasulfonate delivered via acid-labile diplasmenylcholine-folate liposomes: intracellular localization and synergistic phototoxicity, Int. J. Cancer 93 (2001) 384–392.
[27] R. Hudson, R.W. Boyle, Strategies for selective delivery of photodynamic sensitisers to biological targets, J. Porphyrins Phthalocyanines 8 (2004) 954–975.
[28] D. Bechet, P. Couleaud, C. Frochot, M.L. Viriot, F. Guillemin, M. Barberi-Heyob, Nanoparticles as vehicles for delivery of photodynamic therapy agents, Trends Biotechnol. 26 (2008) 612–621.
[29] K. Stefflova, H. Li, J. Chen, G. Zheng, Peptide-based pharmacomodulation of a cancer-targeted optical imaging and photodynamic therapy agent, Bioconjug. Chem. 18 (2007) 379–388.
[30] B.C. Bae, K. Na, Self-quenching polysaccharide-based nanogels of pullulan/folate-photosensitizer conjugates for photodynamic therapy, Biomaterials 31 (2010) 6325–6335.
[31] F. Postigo, M. Mora, M.A. De Madariaga, S. Nonell, M.L. Sagrista, Incorporation of hydrophobic porphyrins into liposomes: characterization and structural requirements, Int. J. Pharm. 278 (2004) 239–254.
[32] F. Postigo, M.L. Sagrista, M.A. De Madariaga, S. Nonell, M. Mora, Photosensitization of skin fibroblasts and HeLa cells by three chlorin derivatives: role of chemical structure and delivery vehicle, Biochim. Biophys. Acta 1758 (2006) 583–596.
[33] C.P. Leamon, P.S. Low, Membrane folate-binding proteins are responsible for folate–protein conjugate endocytosis into cultured cells, Biochem. J. 291 (Pt 3) (1993) 855–860.
[34] J.C. Stewart, Colorimetric determination of phospholipids with ammonium ferrothiocyanate, Anal. Biochem. 104 (1980) 10–14.
[35] M.L. Sagrista, F. Postigo, M.A. De Madariaga, R.M. Pinto, S. Caballero, A. Bosch, M.A. Valles, M. Mora, Photodynamic inactivation of viruses by immobilized chlorin-containing liposomes, J. Porphyrins Phthalocyanines 13 (2009) 578–588.
[36] T. Mosmann, Rapid colorimetric assay for cellular growth and survival — application to proliferation and cyto-toxicity assays, J. Immunol. Meth. 65 (1983) 55–63.
[37] P.K. Smith, R.I. Krohn, G.T. Hermanson, A.K. Mallia, F.H. Gartner, M.D. Provenzano, E.K. Fujimoto, N.M. Goeke, B.J. Olson, D.C. Klenk, Measurement of protein using bicinchoninic acid, Anal. Biochem. 150 (1985) 76–85.
[38] H. Hillaireau, P. Couvreur, Nanocarriers' entry into the cell: relevance to drug delivery, Cell. Mol. Life Sci. 66 (2009) 2873–2896.
[39] C.P. Leamon, P.S. Low, Delivery of macromolecules into living cells: a method that exploits folate receptor endocytosis, Proc. Natl Acad. Sci. USA 88 (1991) 5572–5576.
[40] B.A. Kamen, A. Capdevila, Receptor-mediated folate accumulation is regulated by the cellular folate content, Proc. Natl Acad. Sci. USA 83 (1986) 5983–5987.
[41] M. Alvarez, A. Villanueva, P. Acedo, M. Canete, J.C. Stockert, Cell death causes relocalization of photosensitizing fluorescent probes, Acta Histochem. 113 (2011) 363–368.
[42] J.P. Strachan, S. Gentemann, J. Seth, W.A. Kalsbeck, J.S. Lindsey, D. Holten, D.F. Bocian, Effects of orbital ordering on electronic communication in multiporphyrin arrays, J. Am. Chem. Soc. 119 (1997) 11191–11201.
[43] A. Jimenez-Banzo, X. Ragas, P. Kapusta, S. Nonell, Time-resolved methods in biophysics. 7. Photon counting vs. analog time-resolved singlet oxygen phosphorescence detection, Photochem. Photobiol. Sci. 7 (2008) 1003–1010.
[44] A. Jimenez-Banzo, M.L. Sagrista, M. Mora, S. Nonell, Kinetics of singlet oxygen photosensitization in human skin fibroblasts, Free Radic. Biol. Med. 44 (2008) 1926–1934.
[45] F. Ricchelli, G. Jori, Distribution of porphyrins in the various compartments of unilamellar liposomes of dipalmitoyl-phosphatidylcholine as probed by fluorescence spectroscopy, Photochem. Photobiol. 44 (1986) 151–157.
[46] F. Ciuchi, G. Dinicola, H. Franz, G. Gottarelli, P. Mariani, M.G.P. Bossi, G.P. Spada, Self-recognition and self-assembly of folic-acid salts — columnar liquid-crystalline polymorphism and the column growth-process, J. Am. Chem. Soc. 116 (1994) 7064–7071.
[47] J.M. Saul, A. Annapragada, J.V. Natarajan, R.V. Bellamkonda, Controlled targeting of liposomal doxorubicin via the folate receptor in vitro, J. Control. Release 92 (2003) 49–67.
[48] J. Wu, Q. Liu, R.J. Lee, A folate receptor-targeted liposomal formulation for paclitaxel, Int. J. Pharm. 316 (2006) 148–153.
[49] N.S. Trivedi, H.W. Wang, A.L. Nieminen, N.L. Oleinick, J.A. Izatt, Quantitative analysis of Pc 4 localization in mouse lymphoma (LY-R) cells via double-label confocal fluorescence microscopy, Photochem. Photobiol. 71 (2000) 634–639.
[50] J.A. Caruso, P.A. Mathieu, J.J. Reiners, Sphingomyelins suppress the targeted disruption of lysosomes/endosomes by the photosensitizer NPe6 during photodynamic therapy, Biochem. J. 392 (2005) 325–334.
[51] T.I. Peng, C.J. Chang, M.J. Guo, Y.H. Wang, J.S. Yu, H.Y. Wu, M.J. Jou, Mitochondrion-targeted photosensitizer enhances the photodynamic effect-induced mitochondrial dysfunction and apoptosis, Ann. N.Y. Acad. Sci 1042 (2005) 419–428.

[52] B.F.P. Tamietti, A.H.A. Machado, M. Maftoum-Costa, N.S. Da Silva, A.C. Tedesco, C. Pacheco-Soares, Analysis of mitochondrial activity related to cell death after PDT with AlPCS4, Photomed. Laser Surg. 25 (2007) 175–179.
[53] P.R. Ogilby, C.S. Foote, Chemistry of singlet oxygen. 42. Effect of solvent, solvent isotopic substitution and temperature on lifetime of singlet molecular oxygen ($^1\Sigma_g$), J. Am. Chem. Soc. 105 (1983) 3423–3430.
[54] J. Moan, On the diffusion length of singlet oxygen in cells and tissues, J. Photochem. Photobiol. B 6 (1990) 343–347.
[55] E. Skovsen, J.W. Snyder, J.D.C. Lambert, P.R. Ogilby, Lifetime and diffusion of singlet oxygen in a cell, J. Phys. Chem. B 109 (2005) 8570–8573.
[56] S. Hackbarth, J. Schlothauer, A. Preuss, B. Roder, New insights to primary photodynamic effects — singlet oxygen kinetics in living cells, J. Photochem. Photobiol. B 98 (2010) 173–179.

Poly(D,L-lactide-co-glycolide) nanoparticles as delivery agents for photodynamic therapy: enhancing singlet oxygen release and phototototoxicity by surface PEG coating.

Boix-Garriga E, Acedo P, Casadó A, Villanueva A, Stockert JC, Cañete M, Mora M, Sagristá ML, Nonell S.

Nanotechnology. 2015 Sep 11;26(36):365104. doi: 10.1088/0957-4484/26/36/365104.

RESUMEN

Las nanopartículas de ácido Poli(D,L-láctico-co-glicólido) (PLGA) están siendo consideradas como nanotransportadores para la terapia fotodinámica. Los aspectos físico-químicos y biológicos de su uso siguen siendo en gran parte desconocidos. En este artículo presentamos los resultados de un estudio con nanopartículas de PLGA para el transporte a células HeLa del fotosensibilizador modelo hidrófobo ZnTPP. Las nanopartículas de PLGA, con potenciales Z negativos y diámetros cercanos a los 110 nm, encapsularon la ZnTPP con una alta eficiencia. El revestimiento con polietilenglicol (PEG), utilizado para prevenir opsonización y eliminación por parte de los macrófagos, disminuyó el tamaño y el potencial zeta de las nanopartículas en aproximadamente un factor de dos y mejoró su estabilidad en presencia de proteínas séricas. Los estudios fotofísicos revelaron dos y tres poblaciones de ZnTPP y de oxígeno singlete en las nanopartículas no recubiertas y en las pegiladas, respectivamente. El oxígeno singlete está confinado dentro de las nanopartículas de PLGA mientras que se libera más fácilmente al medio externo después del revestimiento de PEG, que contribuye a una mayor fotocitotoxicidad *in vitro* en células HeLa. Las nanopartículas de PLGA se internalizan por endocitosis, liberan su carga a los lisosomas e inducen la muerte celular por apoptosis después de la exposición a la luz. En conclusión, las nanopartículas de PLGA recubiertas con PEG muestran un alto potencial como transportadores para aplicaciones fotodinámicas.

IOP Publishing Nanotechnology
Nanotechnology 26 (2015) 365104 (16pp) doi:10.1088/0957-4484/26/36/365104

Poly(*D*, *L*-lactide-co-glycolide) nanoparticles as delivery agents for photodynamic therapy: enhancing singlet oxygen release and phototoxicity by surface PEG coating

Ester Boix-Garriga[1], Pilar Acedo[2], Ana Casadó[3], Angeles Villanueva[2], Juan Carlos Stockert[2], Magdalena Cañete[2], Margarita Mora[3], Maria Lluïsa Sagristá[3] and Santi Nonell[1]

[1] Grup d'Enginyeria Molecular, Institut Químic de Sarrià, Universitat Ramon Llull, Via Augusta 390, 08017 Barcelona, Spain
[2] Departamento de Biología, Facultad de Ciencias, Universidad Autónoma de Madrid, Darwin 2, 28049 Cantoblanco-Madrid, Spain
[3] Departament de Bioquímica i Biologia Molecular, Facultat de Biologia, Universitat de Barcelona, Avinguda Diagonal 645, 08028 Barcelona, Spain

E-mail: santi.nonell@iqs.url.edu

Received 19 June 2015, revised 17 July 2015
Accepted for publication 23 July 2015
Published 21 August 2015

Abstract

Poly(D, L-lactide-co-glycolide) (PLGA) nanoparticles (NPs) are being considered as nanodelivery systems for photodynamic therapy. The physico-chemical and biological aspects of their use remain largely unknown. Herein we report the results of a study of PLGA NPs for the delivery of the model hydrophobic photosensitizer ZnTPP to HeLa cells. ZnTPP was encapsulated in PLGA with high efficiency and the NPs showed negative zeta potentials and diameters close to 110 nm. Poly(ethylene glycol) (PEG) coating, introduced to prevent opsonization and clearance by macrophages, decreased the size and zeta potential of the NPs by roughly a factor of two and improved their stability in the presence of serum proteins. Photophysical studies revealed two and three populations of ZnTPP and singlet oxygen in uncoated and PEGylated NPs, respectively. Singlet oxygen is confined within the NPs in bare PLGA while it is more easily released into the external medium after PEG coating, which contributes to a higher photocytotoxicity towards HeLa cells *in vitro*. PLGA NPs are internalized by endocytosis, deliver their cargo to lysosomes and induce cell death by apoptosis upon exposure to light. In conclusion, PLGA NPs coated with PEG show high potential as delivery systems for photodynamic applications.

Keywords: nanoparticle, photodynamic therapy, PLGA, polyethyleneglycol, photosensitizer, singlet oxygen

(Some figures may appear in colour only in the online journal)

1. Introduction

Photodynamic therapy (PDT) is a clinically approved, minimally invasive, therapeutic modality that can exert a selective cytotoxic activity for the treatment of malignant and non-malignant diseases. PDT can be curative in early stage tumors, can prolong survival of patients with inoperable cancers, and can significantly improve quality of life, with minimal normal tissue toxicity, negligible systemic effects, and lack of intrinsic or acquired resistance mechanisms (Agostinis *et al* 2011).

PDT involves the administration of a photosensitizing drug (or photosensitizer, PS), the application of visible light at

a specific wavelength matching the absorption band of the PS, and the generation of reactive oxygen species (ROS) by reaction of the photoexcited PS with molecular oxygen present in living tissues (Kiesslich *et al* 2013). Photoexcitation of the photosensitizer promotes it to its singlet electronic excited state ($^1PS^*$), which rapidly undergoes intersystem crossing to the longer-lived triplet excited state ($^3PS^*$). Subsequent energy transfer to molecular oxygen results in the production of singlet oxygen ($^1O_2$) that oxidizes a variety of biological molecules, ultimately leading to cell death (Agostinis *et al* 2011, Castano *et al* 2005, Dougherty *et al* 1998, Kiesslich *et al* 2013).

Subcellular localization of the PS plays an important role in the photodynamic efficacy, since $^1O_2$ has a very short lifetime and thus can only oxidize targets close to its site of generation. A large number of biochemical studies have demonstrated that most of the subcellular compartments, such as mitochondria, nucleus, lysosomes, outer cellular membrane, endoplasmic reticulum or Golgi apparatus, can become targets for PDT. The properties of the PS, such as electric charge, amphiphilicity and partition coefficient, as well as those of the vehicle used for its delivery, affect the main site of intracellular accumulation and therefore the efficiency and mechanism of cell death (Blazquez-Castro *et al* 2009, Dovigo *et al* 2009, Oliveira *et al* 2011, Tejedor-Estrada *et al* 2012).

Most PSs are highly hydrophobic, which hinders their solubility in physiological media and consequently, their systemic administration. The lack of aqueous solubility also produces their aggregation in this media, which leads to a loss of their chemical and especially their photophysical properties, for instance, a decrease in $^1O_2$ formation. Thus, research in PDT during the last few years has been focused on developing delivery systems such as liposomes, micelles or polymeric NPs to improve their water solubility and enhance their accumulation onto the target site (Paszko *et al* 2011). Biodegradable NPs have emerged as promising delivery systems for PDT due to their biocompatibility, their various drug release patterns depending on the characteristics of the carrier, and a large variety of available materials and manufacturing processes (Konan *et al* 2002).

Much attention has recently been given to poly(D,L-lactide-co-glycolide) (PLGA) NPs as delivery vehicles since this polymer is biodegradable, biocompatible, non-immunogenic, and it has been approved by the Food and Drug Administration (FDA) for therapeutic use (Panyam and Labhasetwar 2003). Hence, abundant literature has been published on the benefits of PS incorporation into PLGA nanodelivery systems (Allemann *et al* 2004, Gomes *et al* 2007, Konan *et al* 2003a, 2003b, Vargas *et al* 2004, 2008, 2009, Zeisser-Labouebe *et al* 2006). Moreover, it has been shown that coating the hydrophobic surfaces of PLGA NPs with hydrophilic polymers such as PEG is efficient in preventing their rapid uptake by macrophages, and hence in lengthening their circulation time in the body (Avgoustakis *et al* 2003, Betancourt *et al* 2009, Locatelli and Comes Franchini 2012). Although in all these studies the feasibility and suitability of the PEGylated PLGA nanosystems as vehicles for photodynamic therapy were demonstrated, the effects of the NPs on the photophysical properties of the encapsulated PSs, their ability to photosensitize $^1O_2$, and the influence of PEG on the photodynamic response were not determined in detail.

On the basis of these considerations, in this paper we report a comparative study of bare and PEG-coated PLGA NPs as delivery vehicles for the model hydrophobic PS Zn (II)-tetraphenylporphine (ZnTPP). Specifically, we have evaluated (i) the physicochemical characteristics of both types of ZnTPP-loaded NPs; (ii) their spectroscopic and photophysical properties; (iii) their ability to photosensitize $^1O_2$, (iv) their photodynamic activity; (v) their effect on the subcellular localization of ZnTPP in HeLa cells; and (vi) their effect on the cell death mechanism induced by PDT. Our results demonstrate that coating of the PLGA surface with PEG leads to a faster and superior photodynamic response in HeLa cells.

2. Materials and methods

2.1. Materials

Poly(ethylene glycol)-*block*-poly(D,L-lactide-co-glycolide) (PEG-PLGA), with PEG M_n 5000, 5 (RGP d 5055) or 15 (RGP d 50155) wt% PEG, and molar ratio D,L-lactide:glycolide 50:50, were purchased from Evonik Industries (Birmingham, AL, USA). Poly(D,L-lactide-co-glycolide) (PLGA) RESOMER® RG 752 H (molar ratio of D,L-lactide:glycolide 75:25, Mw 4000-15000 Da, acid terminated) and 5, 10, 15, 20-tetraphenyl-21H,23H-porphine zinc (ZnTPP) were purchased from Sigma-Aldrich Chemical Co. (St. Louis, MO, USA). The porphyrin used had a minimal purity of 99% and was used as received. Deuterium oxide (99.9%) was purchased from Solvents Documentation Synthesis (SDS, Peypin, France). All other chemicals were commercially available reagents of at least analytical grade. Milli-Q water (Millipore, Bedford, MA system, resistivity of 18 MΩ cm) was used.

Fetal bovine serum was purchased from Lonza Ibérica S. A.U. (Barcelona, Spain). Tripsyn (0.05% Tripsyn-EDTA (1x)) was purchased from Life Technologies S. A. (Madrid, Spain). L-Glutamine 200 mM was purchased from PAA GmbH (Pasching, Austria). Penicillin-Streptomycin Solution 100x was purchased from Biowest (Nuaillé; France). Plasmocin™ was purchased from Nucliber S.A. (Zaragoza, Spain). Dulbecco's Modified Eagle's Medium (DMEM) with 4.5 g/L glucose, sterile Dulbecco's phosphate-buffered saline (PBS 1x) and 3-[4, 5-dimethylthiazol-2-yl]-2, 5-diphenyltetrazolium bromide (MTT) were purchased from Sigma-Aldrich. The sterilized cell culture material was purchased from LabClinics S. A. (Barcelona, Spain).

2.2. Preparation of PLGA NPs

PLGA (without PEG) and PEG PLGA (with 5, 10% or 15% PEG) NPs (NPs) were prepared by a modified nanoprecipitation method (Barichello *et al* 1999, Yallapu *et al* 2010). Briefly, for bare PLGA NPs, PLGA 75:25 was dissolved in

acetone at a concentration of 9 mg mL^{-1}. For PEG-coated PLGA NPs (PEG-PLGA NPs) either the commercial polymers were used directly (5% or 15% PEG) or a mixture of 33% PLGA 75:25 and 67% PEG15%-PLGA 50:50 was used in order to obtain a mixture with a 10% of PEG, keeping in all cases the same final polymer concentration in acetone as for bare PLGA NPs. To obtain ZnTPP-loaded NPs, the porphyrin was added to the organic solution at a 0.8% (w/w) drug loading concentration with respect to PLGA. The acetone solution was then injected dropwise to ultrapure water (organic phase: aqueous phase 1:2 v/v) under continuous magnetic stirring at 800 rpm for 10 min. Subsequently, acetone was removed from the colloidal suspension under reduced pressure for at least 1 h. Larger aggregates, free PLGA polymer and non-encapsulated ZnTPP were removed by centrifugation at 5000 rpm on an Avanti J21 centrifuge (Beckman Coulter, Inc., Brea, CA, USA) and the suspension was stored at 4 °C.

2.3. Physicochemical characterization of NPs

Drug loading was estimated by UV-visible absorption spectroscopy. An aliquot of ZnTPP-loaded PLGA or PEG-PLGA NPs was dissolved in tetrahydrofuran (THF) (NPs suspension: THF 1:15, v/v) to disrupt NPs and extract the entrapped ZnTPP. This solution was stirred in a Rotamax 120 orbital shaker (Heidolph Instruments, Schwabach, Germany) for 40 min to ensure a complete dissolution of the polymer and the PS, and the absorption spectra were recorded on a Varian Cary 6000i UV–vis–NIR spectrophotometer (Agilent Technologies, Santa Clara, CA). ZnTPP concentration was determined by comparison with standard curves obtained at the same conditions.

Drug loading and entrapment efficiency were calculated as follows:

$$\text{Drug loading } \% = \frac{\text{PS mass}}{\text{PLGA mass}} \times 100 \quad (1)$$

$$\text{Entrapment efficiency } \% = \frac{\text{drug loading}}{\text{theoretical drug loading}} \times 100 \quad (2)$$

Size and polydispersity index of NPs were determined by dynamic light scattering (DLS) and zeta potential by laser Doppler micro-electrophoresis, using a Zetasizer Nano ZS (Malvern Instruments Ltd, Malvern, UK) at room temperature. To carry out the measures, NP suspensions were diluted (NP suspension:H_2O 1:6 v/v) to avoid multiple scattering. Size measurements were performed at excitation wavelength of 633 nm. To measure zeta potential, the Malvern device was calibrated with carboxy-modified polystyrene latex samples of known zeta potential.

2.4. Stability of ZnTPP formulations in cell culture medium

The stability of NPs was assessed in cell culture medium in the presence of 10% fetal bovine serum (FBS) (same concentration supplied to cultured cells). The NP suspension was diluted to a final ZnTPP concentration of 10 μM in DMEM containing 1% (v/v) L-Glu, 1% (v/v) Penicillin/Streptomycin, 0.02% (v/v) Plasmocin™ and 10% FBS. These suspensions were incubated for various times at 37 °C at 400 rpm in a Termomixer Comfort equipped with an exchangeable thermoblock for 15 mL falcon tubes (Eppendorf AG, Hamburg, Germany). After certain time, an aliquot of 700 μL was removed, put in ice to stop the reaction, and centrifuged at 6400 × g for 15 min at 4 °C. The pellet, containing NP aggregates, was discarded and an aliquot of the supernatant was diluted in dimethylsulfoxide (DMSO) (supernatant: DMSO 1:15, v/v) to disrupt the remaining NPs. Spectra were recorded in a Beckman DU40 UV–vis spectrophotometer (Beckman Coulter, Inc., Brea, CA, USA) and ZnTPP concentration was determined by comparison with standard curves obtained in the same conditions.

2.5. Spectroscopic and photophysical properties of NPs

ZnTPP-loaded NPs were appropriately diluted in water for all photophysical measurements. Absorbance spectra of diluted blank NPs were also recorded for scattering corrections for absorbance matching purposes. Absorption and fluorescence spectra of the ZnTPP-loaded NP aqueous suspensions were compared with NP suspensions diluted in THF. For time-resolved fluorescence measurements, reference kinetic parameters were those of the ZnTPP in toluene.

Absorption spectra were recorded on a Varian Cary 6000i UV–vis–NIR spectrophotometer (Agilent Technologies, Santa Clara, CA, USA). Fluorescence spectra were recorded in a Fluoromax 4 spectrofluorometer (Horiba Jobin Yvon, Edison, NJ, USA) exciting at 556 nm.

The fluorescence quantum yields (Φ_F) were determined by the comparative method (Brouwer 2011). Fluorescence emission spectra were collected for a set of samples and reference solutions of increasing absorbance values and the area under the spectrum (F) was plotted against the absorption factor ($1 - 10^{-A}$). According to equation (3), a linear plot should be obtained the slope of which is proportional to Φ_F:

$$F = \left[\frac{\kappa}{n_r^2} I_0 \Phi_F\right] \times \left(1 - 10^{-A}\right) \quad (3)$$

where κ is an instrumental factor, I_0 is the radiant power of the excitation beam, and n_r is the solvent's refractive index. Thus, Φ_F for the ZnTPP-loaded PLGA NPs was determined from the ratio of slopes measured for the NP suspensions and ZnTPP in toluene as reference with $\Phi_F = 0.033$ (Strachan *et al* 1997).

Time-resolved fluorescence decays were recorded at 650 nm using a time-correlated single-photon counting system (Fluotime 200, PicoQuant GmbH, Berlin, Germany) with a pulsed 596 nm LED source for excitation. Decays were analyzed using the PicoQuant FluoFit 4.5.3 data analysis software. Absorbance of the samples was kept below 0.1 at the excitation wavelength in all cases and the photon counting rate was kept below 1%.

Transient absorption experiments in the UV–visible (UV–vis) region were carried out using a home-built

nanosecond laser flash photolysis system. In this instrument, the second harmonic (532 nm) of a Continuum Surelite I-10 Nd:YAG laser (10 Hz, 5 ns pulsewidth, 0.05–1 mJ per pulse) was directed onto the sample. Changes in the sample absorbance were detected by a Hamamatsu R928 photomultiplier in order to monitor the intensity variations of an analyzing beam produced by a 75 W short arc Xe lamp (USHIO) and spectral discrimination was provided by a PTI 101 monochromator. The signal was fed to a Lecroy Wavesurfer 454 oscilloscope for digitizing (1 shot, typically) and finally transferred through a GPIB interface (National Instruments) to a PC computer for data storage and analysis. The TTL sync output of the laser was used to trigger the oscilloscope. The energy of the laser pulse was varied by controlling the Q-switch delay and measured with a pyroelectric energy meter (RJP 735 and RJ 7610) from Laser Precision Corp. The system was controlled by the in-house-developed LKS software (LabView, National Instruments).

$^1O_2$ phosphorescence was detected using a customized PicoQuant Fluotime 200 system described elsewhere (Jiménez-Banzo *et al* 2008). Briefly, a diode-pumped pulsed Nd:YAG laser (FTSS355-Q, Crystal Laser, Berlin, Germany) working at 1 kHz repetition rate at 532 nm (10 mW, 1 μJ per pulse) was used for excitation. A 1064 nm rugate notch filter (Edmund Optics, York, UK) was placed at the exit port of the laser to remove any residual component of its fundamental emission in the near-IR region. The luminescence exiting from the side of the cuvette was filtered by a cold mirror and a bandpass filter of the appropriate wavelength (Spectrogon AB, Täby, Sweden). A TE-cooled Hamamatsu near-IR photomultiplier (model H9170-45, Hamamatsu Photonics, Japan), sensitive from 950 to 1400 nm, was used to detect IR luminescence. The detector was operated in photon counting mode and its output sent to a multichannel scaler (PicoQuant Nanoharp 250). Photon histograms were analyzed using the PicoQuant FluoFit 4.5.3 data analysis software. For temperature-dependent measurements, an Ultraterm 6000383 (JP Selecta S.A., Abrera, Spain) thermostat was used in order to control the temperature.

2.6. $^1O_2$ Production in HeLa cells

HeLa cells were seeded in 175 cm^2 flasks and grown up to 70% confluence in complete growth medium, in the dark at 37 °C and 5% CO_2. Cells were then incubated with ZnTPP-loaded PLGA and PEG-PLGA NPs for different periods of time (2, 6 and 24 h). A bulk 5 μM concentration of ZnTPP was chosen as a good compromise between acceptable $^1O_2$ signals and avoiding particle aggregation. Cells incubated with the complete medium in the absence of nanoparticles were used as control. After incubation, the medium was discarded and cells were washed three times with cold PBS 1x, scraped and resuspended. Subsequently, the suspension was centrifuged at 1000 rpm for 5 min at 20 °C, the supernatant was discarded, and the pellet was resuspended in 1.5 mL d-PBS. $^1O_2$ phosphorescence of these final cellular suspensions was then detected using the customized equipment described in the previous section. Afterwards, a series of control experiments were carried out in order to ensure that the signal detected was due to $^1O_2$ inside the cells: (1) detection of luminescence at 1220 and 1325 nm, where $^1O_2$ does not emit, to ensure that the 1275 nm luminescence was due to $^1O_2$; (2) addition of NaN_3, a known $^1O_2$ quencher (Hall and Chignell 1987, Wilkinson and Brummer 1981), to further confirm the presence of $^1O_2$; (3) after the measurements, centrifugation of cell suspensions at 5000 rpm for 12 min at room temperature followed by analysis of the supernatant luminescence at 1275 nm to demonstrate that there was no significant leakage of the PS during the measurements.

2.7. Photosensitization of HeLa cells

HeLa cells were seeded in 12-well plates and grown up to 70% confluence. Cells were then incubated in the dark at 37 °C for 24 h with ZnTPP-loaded PLGA and ZnTPP-loaded PEG-PLGA NPs at ZnTPP concentrations of 1, 5 and 10 μM in complete culture medium for 24 h. Empty NPs at equivalent concentrations of the loaded ones were used as controls to ensure that photocytotoxicity was not caused by the delivery systems. Cells without any treatment were taken as controls. Subsequently, the medium was discarded, cells were washed three times with cold PBS 1x and fresh complete medium was added. Irradiation was carried out with a Sorisa Photocare LED source (Barcelona, Spain) with a wavelength range of 520–550 nm. The light intensity at the irradiation site was 13 mW cm^{-2} measured with a LaserStar Ophir power meter (Logan, UT, USA). Samples were irradiated at different times ranging from 6 min to 40 min to achieve the intended light fluence. Cells were again incubated for 24 h in the dark and reduction in cell viability was determined by means of the of 3-(4, 5-dimethylthiazol-2-yl)-2, 5-diphenyltetrazolium bromide (MTT) assay (Mosmann 1983). Briefly, the remaining HeLa cells were incubated with 0.05 mg ml^{-1} MTT in complete DMEM for 2–3 h, after MTT had been metabolized by viable cells to form purple crystals of formazan. The medium was discarded, crystals were solubilized with pure DMSO and formazan concentration was determined by absorption at λ_{ex} of 562 nm. Cell viability was determined by the ratio between the absorbance of treated cells and that of non-treated cells (control, 100% viability).

2.8. Subcellular localization of ZnTPP

To determine the intracellular localization of ZnTPP encapsulated in PLGA or PEG-PLGA NPs, endocytic compartments of HeLa cells were labeled with the fluoroprobe LysoTracker Green (50 nM, Molecular Probes, Eugene, OR, USA) in the culture medium at 37 °C for 30 min. Previously, cells were incubated with ZnTPP-loaded NPs at 5 μM for 24 h. After labeling, coverslips were washed with PBS and were observed in a multispectral Leica TCS SP5 confocal microscope (Wetzlar, Germany), operating with 405 nm (argon-UV) to detect the internalized ZnTPP NPs and 488 nm (argon) for emission of LysoTracker Green.

2.9. Characterization of cell death mechanisms

Morphological changes after different photodynamic treatments were assessed by visualizing control and treated cells under phase contrast and fluorescence microscopy. HeLa cells were fixed with methanol at −20 °C for 5 min, stained with Neutral red (NR; Panreac Química, Spain; 0.5% in distilled water, 2 min) for analysis of general morphology, or with Hoechst-33258 (H-33258; Sigma-Aldrich; 5 μg ml^{-1} in distilled water, 3 min) for visualization of DNA. After washing and air drying, preparations were mounted in DePeX (Serva, Heidelberg, Germany).

For indirect immunofluorescence detection of cytochrome c, cells on coverslips were fixed in formol-PBS (1:10) for 20 min at 4 °C, washed three times with PBS (5 min each), and permeabilized with 0.5% Triton X-100. After 5 min, Triton X-100 was removed and cells were incubated in blocking solution (5% bovine serum albumin, 5% FBS, 0.02% Triton X-100 in PBS) for 30 min at RT. Once removed from the blocking solution, 25 μl of a 1:25 solution of the primary antibody (monoclonal mouse anti-cytochrome c, Invitrogen) were added to each sample and incubated at 37 °C for 1 h. Three 5 min washings with PBS were then carried out before the addition of Triton X-100 for 5 min. Incubation with the secondary antibody was performed at 37 °C for 1 h (Fab specific goat anti-mouse FITC-IgG; Sigma-Aldrich). Cells were washed 3 times with PBS and counterstained using H-33258 and mounted in ProLong Gold antifade reagent.

3. Results

3.1. Physicochemical characterization of ZnTPP-loaded PLGA formulations

ZnTPP was encapsulated in bare or PEG-decorated PLGA NPs, following a modified nanoprecipitation method (Barichello *et al* 1999, Yallapu *et al* 2010). Table 1 summarizes the physicochemical properties of the formulations and the incorporation efficiency of ZnTPP in the NPs.

Coating of PLGA NPs with 5% or 10% PEG resulted in a reduction of their size, in agreement with previous observations (Gref *et al* 2000), a somewhat higher polydispersity, a less-negative zeta potential, and a slightly larger encapsulation efficiency. Nevertheless, the final ZnTPP loading and ZnTPP bulk concentration were comparable for both formulations. In the case of NPs containing 15% PEG, two different populations were obtained and were thus ruled out for further studies.

3.2. Stability of ZnTPP formulations in cell culture medium

PLGA NPs aggregate in the presence of serum albumin and other plasma proteins (Armstrong *et al* 1997, Chang *et al* 2012, Karmali and Simberg 2011). Thus, a study of NP stability in cell culture medium was carried out to analyze the formation of NP aggregates due to the FBS content of the medium, and to determine the influence of PEGylation on their stability. Aliquots of ZnTPP-loaded PLGA or ZnTPP-loaded PEG-PLGA suspensions, containing the same amount of ZnTPP, were added to the medium containing a 10% FBS and the remaining ZnTPP in suspension was determined after defined periods of time. Figure 1 shows that all ZnTPP entrapped in PEG-PLGA NPs containing 10% PEG remains in the suspension, even after 30 h of incubation, whereas 75% of the ZnTPP initially embedded in the bare NPs has already precipitated at 1 h. PEG-PLGA NPs containing 5% PEG showed intermediate results but since they were less stable than those containing 10% PEG we decided to rule them out at this stage. Hereafter the term PEG-PLGA NPs refers to nanoparticles containing 10% PEG. The elimination of ZnTPP can be attributed to the formation of large aggregates of PLGA NPs that precipitate as a consequence of their interaction with FBS proteins. This experiment also shows that PEGylation of the NPs protects them from FBS proteins and yields a stable formulation of the PS.

3.3. Spectroscopic and photophysical properties

3.3.1. Absorption, steady-state and time-resolved fluorescence. Absorption and emission spectra (figure 2) of aqueous suspensions of ZnTPP-loaded PLGA and ZnTPP-loaded PEG-PLGA NPs were recorded in water and in THF to compare the behavior of ZnTPP entrapped in the NPs or solubilized in the organic solvent. THF dissolves the PLGA polymer and causes the release of all the ZnTPP content into the organic solvent, where it is completely soluble. The spectra in the NPs were essentially identical to those in THF, which suggests that entrapped ZnTPP is largely in a monomeric state.

This was confirmed by fluorescence quantum yield measurements, which showed the same results in the NPs as in the toluene solutions (table 2). The fluorescence decay kinetics showed two components (table 2, figure 3) indicating two different populations of ZnTPP in the NPs. The main component had a time constant very similar to that in organic solvents, ~2.0 ns (Wilkinson and Brummer 1981).

3.3.2. Triplet lifetime and quenching by oxygen. Laser flash photolysis experiments were used to monitor the triplet state of ZnTPP (^{3}ZnTPP*) through its time-resolved absorption at 470 nm (figure 4). Data analysis revealed two and three populations of ZnTPP in bare and PEG-coated PLGA NPs, respectively. The triplet states could be quenched by oxygen with rate constants that varied for each population and for each type of NP (table 2).

3.3.3. $^1O_2$ production and kinetics. Quenching of ^{3}ZnTPP* by oxygen led to the production of the cytotoxic species $^1O_2$ as unequivocally demonstrated by the observation of the specific NIR phosphorescence of this species at 1275 nm. The temporal profile of the signals (S_t, figure 4) showed the

Table 1. Physico-chemical characteristics of PLGA NPs and ZnTPP entrapment. Values reported are the mean ± SD of at least three independent experiments.

Composition	Z-ave[a] (nm)	PI[b]	ζ pot[c] (mV)	Drug loading[d] (%)	E E[e] (%)	[ZnTPP][f] (μM)
PLGA	114 ± 5	0.10 ± 0.01	−45 ± 2	—	—	—
ZnTPP/PLGA (0.8% ZnTPP, w/w)	115 ± 4	0.10 ± 0.02	−44 ± 1	0.6 ± 0.1	73 ± 4	41 ± 2
5% PEG-PLGA	72 ± 1	0.13 ± 0.01	−32 ± 7	—	—	—
ZnTPP/5% PEG-PLGA (0.8% ZnTPP, w/w)	71 ± 1	0.10 ± 0.01	−27 ± 1	0.6 ± 0.1	68 ± 2	43 ± 2
10% PEG-PLGA	58 ± 18	0.19 ± 0.07	−23 ± 7	—	—	—
ZnTPP/10% PEG-PLGA (0.8% ZnTPP, w/w)	52 ± 6	0.26 ± 0.12	−19 ± 5	0.7 ± 0.1	81 ± 4	45 ± 2
15% PEG-PLGA	58 (65%) 500 (35%)	0.41 ± 0.02	−20 ± 0.3	—	—	—

[a] Particle size measured as Z-average mean.
[b] Polydispersity index.
[c] Zeta potential.
[d] Drug loading expressed as percentage of ZnTPP relative to PLGA (w/w).
[e] Encapsulation efficiency.
[f] Bulk ZnTPP concentration in the NPs suspension.

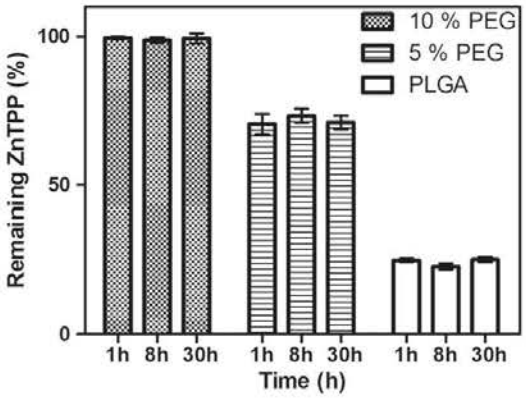

Figure 1. Stability of ZnTPP-loaded PLGA and PEG-PLGA NPs in cell culture medium. NP suspensions were diluted in supplemented cell culture medium (DMEM) at a concentration of 10 μM ZnTPP for various periods of time, at 37 °C. The stability was measured as the percentage of remaining ZnTPP in suspension in the incubation medium after each period of time. Results are the mean ± SD of two replicate values.

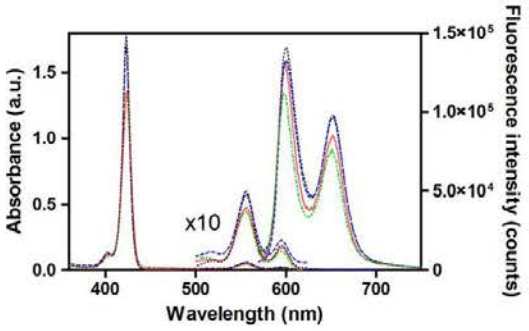

Figure 2. Absorption and emission spectra (λ_{ex}: 556 nm) of 2.6 μM ZnTPP in aqueous suspensions of ZnTTP-loaded PLGA (— · · ·) and 2.8 μM ZnTTP-loaded PEG-PLGA (——) NPs. Absorption and emission spectra of ZnTPP-loaded PLGA (– –) or ZnTTP-loaded PEG-PLGA (••••••) NPs dissolved in THF at the same concentrations are shown for comparison.

typical rise-and-decay function that characterizes $^1O_2$ kinetics:

$$S_t = \sum_i S_{0_i} \times \frac{\tau_{\Delta_i}}{\tau_{\Delta_i} - \tau_{T_i}} \times \left(e^{-t/\tau_{\Delta_i}} - e^{-t/\tau_{T_i}}\right) \quad (4)$$

The subscript i refers to the number of independent $^1O_2$ populations in the sample, S_0 is a quantity proportional to the concentration of $^1O_2$ created by the laser pulse and τ_Δ and τ_T are the lifetimes of $^1O_2$ and ^{3}ZnTPP*, respectively.

Data analysis (table 3) confirmed the presence of two and three populations of ^{3}ZnTPP* and $^1O_2$ in bare and PEG-coated PLGA NPs, respectively. The ^{3}ZnTPP* lifetimes derived from NIR phosphorescence matched those from the laser flash photolysis experiments. Sodium azide had no effect on the $^1O_2$ lifetime in bare PLGA but quenched one of the $^1O_2$ populations in the PEG-coated NPs (table 4).

3.3.4. Temperature and quenching effects. The results above prompted us to investigate the effect of temperature on the kinetics of $^1O_2$ production and decay since both processes appear to be constrained by the rigidity of the PLGA nanoparticle. The decay rate constants of both ^{3}ZnTPP* and $^1O_2$ increased at higher temperatures (figure 5(a), table 4). At the highest temperature studied (55 °C) the two $^1O_2$ populations previously observed in bare PLGA merged, and the $^1O_2$ lifetime was close to the value commonly observed in water (~3 μs). Addition of sodium azide reduced it further (figure 5(c), table 4). Similar observations were made in the PEG-coated NPs: increasing the temperature caused a general decrease of the ^{3}ZnTPP* and $^1O_2$ lifetimes and two of the three populations merged at the highest temperature (figure 5(b), table 4). Quenching by azide at this

Table 2. Fluorescence quantum yields, singlet state lifetimes and their relative amplitudes, and triplet state lifetimes and their quenching rate constants by oxygen of the individual components observed in ZnTPP-loaded PLGA and PEG-PLGA NPs in water suspensions. Results are the mean ± SD of at least three independent experiments.

Sample	Φ_F[a]	τ_{Si} (ns)	A_{Si} (%)	τ_{T1} (μs)	k_{qTi}^{O2} (M ^{1}s ^{1})
	0.036 ± 0.005	1.7 ± 0.2	67 ± 14	77 ± 10	(3.7 ± 0.3) × 10^7
ZnTPP-PLGA		3.1 ± 0.5	33 ± 14	209 ± 35	(1.2 ± 0.4) × 10^7
	0.034 ± 0.002	1.8 ± 0.2	78 ± 14	17 ± 3	(2.7 ± 0.6) × 10^8
ZnTPP-PEG-PLGA		3.4 ± 0.5	22 ± 14	105 ± 29	(1.2 ± 0.1) × 10^7
		—	—	286 ± 13	(4.9 ± 1.9) × 10^6
ZnTPP toluene	0.033	2.0 ± 0.2	100	—	—

[a] ZnTPP in toluene was used as a reference (Strachan *et al* 1997).

temperature caused an even more pronounced decrease of the $^1O_2$ lifetime than in the bare NPs.

3.3.5. $^1O_2$ in HeLa cells. Cells incubated with the PLGA NPs, either bare or coated with PEG, showed clear $^1O_2$ phosphorescence signals at 1275 nm (figure 6).

Control experiments confirmed that the signals were due to $^1O_2$ and that they originated in the cells since the luminescence showed a maximum at 1275 nm and no signal could be observed from the supernatant obtained by centrifugation of the suspensions. Analysis of the $^1O_2$ kinetics revealed important differences with respect to the aqueous suspension of the NPs. For bare PLGA, only one of the previously observed two $^1O_2$ populations could now be detected, and it showed similar kinetics as in the aqueous suspensions. Moreover it could not be quenched by 10 mM NaN_3 and the only effect of solvent deuteration was to slightly increase its intensity. In contrast, cells incubated with PEG-coated NPs failed to show the long emission tail and the short-lived decay component could be quenched by azide. In this case also, deuteration allowed the observation of a longer-lived emission (figure 6 right).

3.4. Photosensitization of HeLa cells

HeLa cells were incubated in the dark with various concentrations of ZnTPP-loaded PLGA and PEG-PLGA NPs for 24 h. Afterwards cells were exposed to various fluences of LED green light and cell viability was assessed 24 h after treatment. Cell death was observed in a concentration- and light fluence-dependent manner (figure 7(a)). ZnTPP delivered in PEGylated NPs was more phototoxic than in the bare PLGA, particularly at low light fluences. On the other hand, it also showed a slightly higher dark cytotoxicity. Light alone or in combination with empty NPs was devoid of any detectable cytotoxicity (figure 7(b)).

3.5. Subcellular localization

ZnTPP delivered in PLGA or PEG-PLGA NPs showed similar intracellular localization in lysosome-like structures (figure 8). Co-localization studies performed in non-fixed HeLa cells using LysoTracker Green, a marker for lysosomes, confirmed that ZnTPP entrapped in both types of NPs was specifically accumulated in the lysosomes.

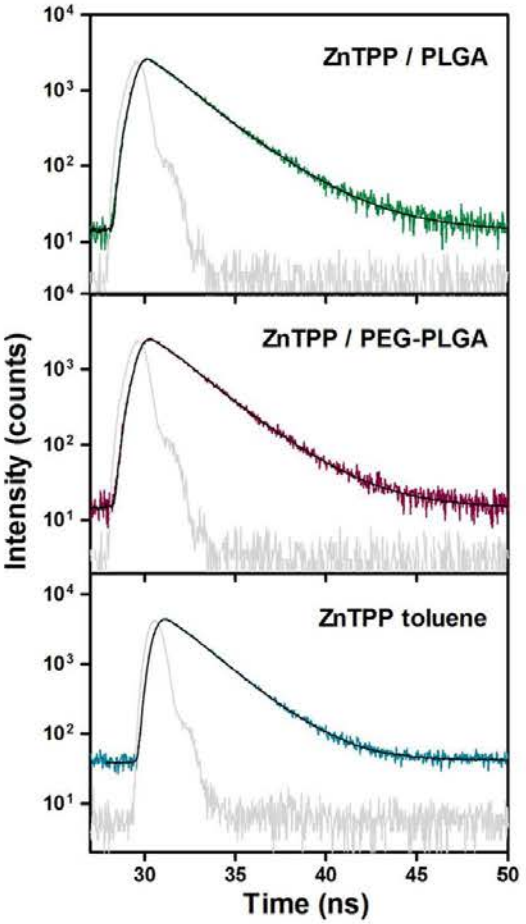

Figure 3. Time-resolved fluorescence decays of ZnTPP in PLGA, PEG-PLGA NPs and toluene. λ_{exc}: 596 nm. λ_{em}: 650 nm. Light grey line corresponds to instrumental response factor.

3.6. Mechanism of cell death

Apoptotic cell death induced by PDT treatments was confirmed by two methods: analysis of morphological alterations (Rello *et al* 2005) and cellular distribution of cytochrome c.

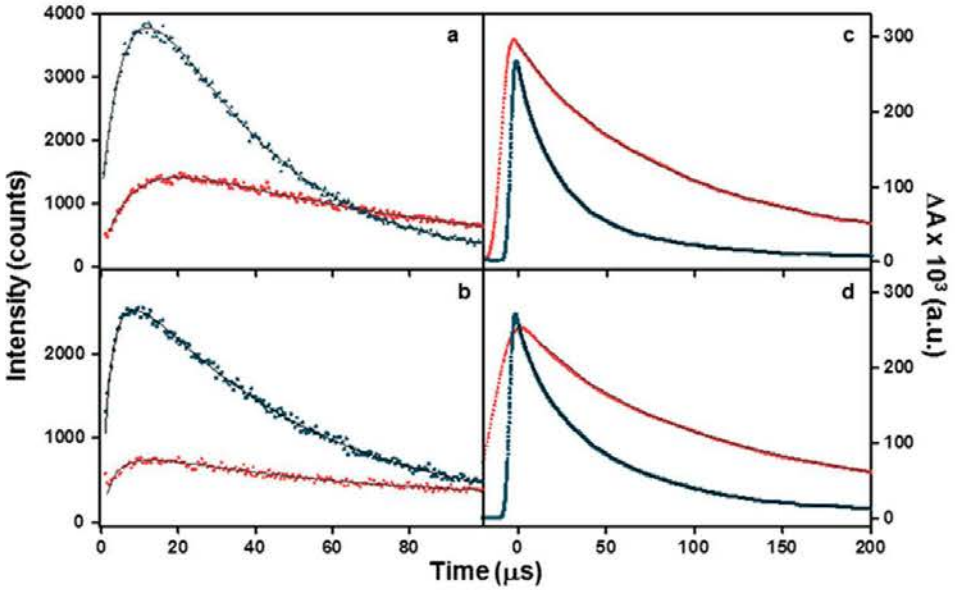

Figure 4. Left: time-resolved $^1O_2$ phosphorescence in air (grey; red online) and in O_2 (black; blue online) saturated aqueous suspensions of (a) PLGA or (b) PEG-PLGA NPs loaded with ZnTPP. ZnTPP was excited at 532 nm and $^1O_2$ phosphorescence was recorded at 1275 nm. Right: time-resolved triplet absorption transients at 470 nm of aqueous suspensions of ZnTPP-loaded PLGA NPs (c) and ZnTPP-loaded PEG-PLGA NPs (d), excited at 532 nm. Transients were acquired in air (grey; red online) and in O_2 (black; blue online) saturated suspensions.

Table 3. Time constants of $^1O_2$ luminescence of ZnTPP-loaded PLGA NPs or ZnTPP-loaded PEG-PLGA NPs under air and oxygen saturated solutions. Results are the mean ± SD of two independent experiments.

	ZnTPP-PLGA		ZnTPP-PEG-PLGA	
	air	O_2	air	O_2
$\tau_{\Delta 1}/\mu s$	5.0 ± 0.5	4.0 ± 0.1	1.6 ± 0.3	1.3 ± 0.2
$\tau_{T1}/\mu s$	92 ± 8	45 ± 3	18 ± 1	3.5 ± 0.3
$\tau_{\Delta 2}/\mu s$	14 ± 2	13 ± 2	5.0 ± 0.3	4.8 ± 0.3
$\tau_{T2}/\mu s$	219 ± 10	20 ± 1	79 ± 6	43 ± 2
$\tau_{\Delta 3}/\mu s$	—	—	12 ± 1	10 ± 1
$\tau_{T3}/\mu s$	—	—	307 ± 54	100 ± 10

3.6.1. Morphological changes. Photodynamic treatments on HeLa cells with ZnTPP-loaded PLGA or PEG-PLGA NPs at 5 μM ZnTPP and 4 J.cm^{-2} light fluence resulted in apoptotic pattern of cell death morphology, revealed by neutral red and Hoechst-33258 (H-33258) staining (figure 9). After photodynamic treatment with ZnTPP-loaded PLGA but especially with ZnTPP-loaded PEG-PLGA, cells showed significant morphological changes depending on the time elapsed after the end of treatment (6 and 24 h). As shown in figure 9, a significant number of cells have undergone apoptosis 6 h after ZnTPP-loaded PEG-PLGA photodynamic treatment, as deduced from the cell shrinkage, chromatin condensation, and nuclear fragmentation, which are typical apoptotic features. At 24 h most cells have undergone apoptosis and only a few cells remain alive. Cells treated with ZnTPP-loaded NPs but not irradiated, as well as cells irradiated without preincubation with NPs, presented a similar morphology to the control HeLa cells (data not shown).

3.6.2. Detection of cytosolic cytochrome c. Immunofluorescence techniques showed that cytochrome c was confined to mitochondria in control cells (figure 10). However, photoactivated ZnTPP-loaded PEG-PLGA triggered release of cytochrome c from the mitochondria to cytosol and the majority of cells displayed diffuse cytochrome c cytoplasmic staining and condensed and fragmented nuclei (figures 10(a″)–(d″)).

4. Discussion

In the present study, we investigate the photodynamic activity of the model photosensitizer ZnTPP delivered to cancer cells using bare or PEGylated PLGA NPs. The NPs, prepared by a modified nanoprecipitation method, had a diameter of around 100 nm and a pronounced negative zeta potential, consistent with the terminal carboxylic groups of the polymer. Coating their surface with 5% or 10% PEG chains led to a decrease in their size, as previously observed (Avgoustakis *et al* 2003, Gref *et al* 2000), and to a less negative zeta potential.

Table 4. Time constants of $^1O_2$ luminescence transients of ZnTPP-loaded PLGA and PEG-PLGA NPs at three different temperatures and in absence and presence of NaN_3, a typical $^1O_2$ quencher. Results are the mean ± SD of two independent experiments.

	$[NaN_3] = 0$			$[NaN_3] = 10$ mM		
ZnTPP-PLGA	20 °C	37 °C	55 °C	20 °C	37 °C	55 °C
$\tau_{\Delta1}/\mu s$	5.0 ± 0.5	4.4 ± 0.4	2.9 ± 0.5	6.0 ± 1.0	4.0 ± 0.1	1.4 ± 0.3
$\tau_{T1}/\mu s$	92 ± 8	36 ± 3	14 ± 1	110 ± 15	41 ± 5	15 ± 1
$\tau_{\Delta2}/\mu s$	14 ± 2	4.4 ± 0.4	—	16 ± 1	4.0 ± 0.1	—
$\tau_{T2}/\mu s$	219 ± 10	78 ± 7	—	265 ± 18	99 ± 18	—
	$[NaN_3] = 0$			$[NaN_3] = 10$ mM		
ZnTPP-PEG-PLGA	20 °C	37 °C	55 °C	20 °C	37 °C	55 °C
$\tau_{\Delta1}/\mu s$	1.6 ± 0.3	2.1 ± 0.4	2.7 ± 0.5	0.4 ± 0.3	0.2 ± 0.1	<0.2
$\tau_{T1}/\mu s$	18 ± 1	12 ± 1	10 ± 2	15 ± 1	8.1 ± 2.2	10 ± 2.2
$\tau_{\Delta2}/\mu s$	5.0 ± 0.3	4.4 ± 0.7	2.7 ± 0.5	4.0 ± 1	5.3 ± 0.6	<0.2
$\tau_{T2}/\mu s$	79 ± 6	37 ± 4	22 ± 4	91 ± 14	49 ± 4	22 ± 4
$\tau_{\Delta3}/\mu s$	12 ±± 1	4.4 ± 0.7	—	12 ± 1	5.3 ± 0.6	—
$\tau_{T3}/\mu s$	307 ± 54	97 ± 14	—	356 ± 50	116 ± 2	—

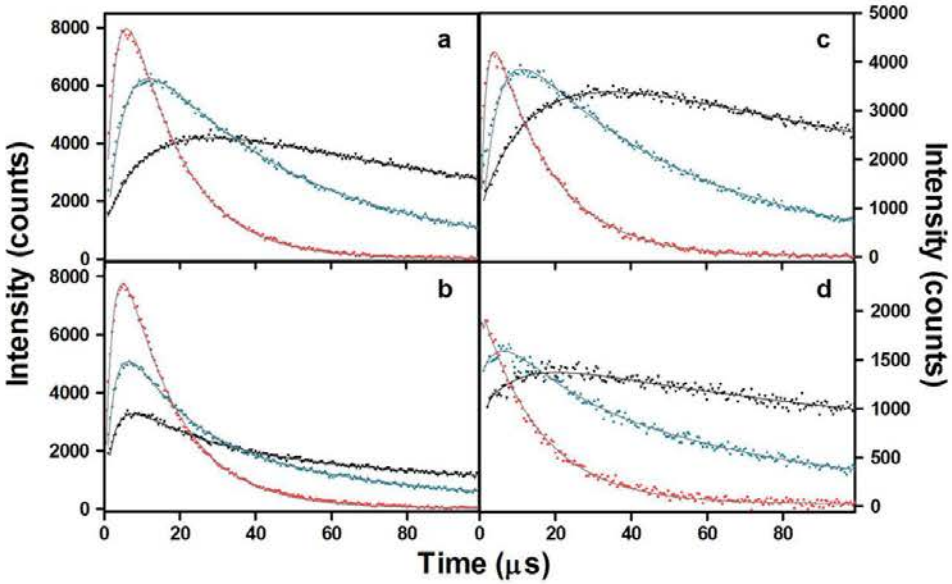

Figure 5. Time-resolved $^1O_2$ phosphorescence of aqueous suspensions of ZnTPP-loaded PLGA (a), (c) and PEG-PLGA (b), (d) NPs as a function of temperature: 20 °C (black), 37 °C (grey; blue online), 55 °C (light grey; red online) and of NaN_3 concentration: $[NaN_3] = 0$ mM (a), (b)) and $[NaN_3] = 10$ mM (c), (d). ZnTPP was excited at 532 nm and the luminescence was observed at 1275 nm.

However, increasing the PEG content to 15% produced highly heterogeneous NP populations (table 1).

Bare PLGA NPs aggregated and precipitated when added to the culture medium containing 10% FBS (Armstrong *et al* 1997, Avgoustakis *et al* 2003, Chang *et al* 2012, Karmali and Simberg 2011), whereas the 10% PEG coating conferred stability to the suspension (figure 1). These results rule out bare PLGA NPs as drug carriers for *in vivo* PDT.

Absorption and fluorescence spectra as well as fluorescence quantum yields of ZnTPP in both types of NPs were similar to those in THF or toluene solution (figure 2), indicating that ZnTPP is not appreciably aggregated in the core of the NPs. These results are in contrast to those for *meso*-tetrahydroxyphenyl porphyrin (m-THPP) in PLGA, which shows large red shifts and an important reduction of intensities (Vargas *et al* 2009). This indicates that the chemical properties of the PS exert a profound influence on its interaction with PLGA.

Time-resolved fluorescence and triplet–triplet absorption revealed different populations of ZnTPP in the NPs (table 2).

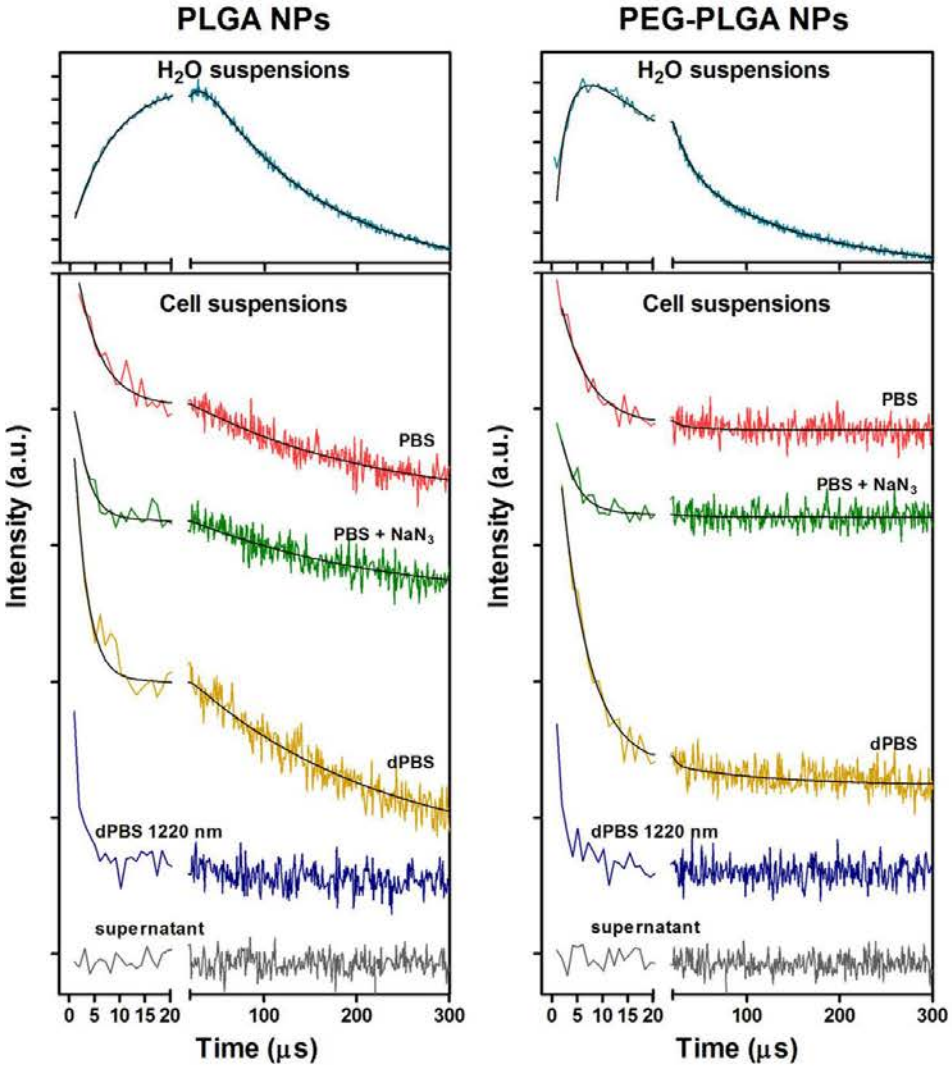

Figure 6. Time-resolved $^1O_2$ phosphorescence of ZnTPP-loaded PLGA (left) and PEG-PLGA (right) NPs in aqueous suspensions (TOP) and in HeLa cell suspensions (bottom) after 24 h incubation. ZnTPP was excited at 532 nm and $^1O_2$ phosphorescence was recorded at 1275 nm. The signal at 1220 nm, where $^1O_2$ shows almost no emission, was recorded to measure light scattering by cells. All measurements were taken at 20 °C; dPBS stands for D_2O-based PBS.

Thus, two different populations were identified in bare PLGA whereas in PEG-PLGA a third population could also be detected. The long triplet lifetimes observed in aerated suspensions indicate that ^{3}ZnTPP* is largely shielded from oxygen in the NPs. The rate constants for oxygen quenching (table 2) were 1–3 orders of magnitude lower than in aqueous solutions (Redmond and Gamlin 1999) depending on the specific ^{3}ZnTPP* population and type of NP. This would indicate that each population occupies a different region of the NPs.

Despite such shielding, ZnTPP is able to produce $^1O_2$ and we find different populations for this species as well, which is in agreement with a heterogeneous microenvironment within the NPs. The fact that sodium azide, a water-soluble $^1O_2$ quencher, is unable to reduce the $^1O_2$ lifetime in bare PLGA, indicates that $^1O_2$ is confined within these NPs. Although NaN_3 is a small anion that can readily enter the cell from the extracellular medium (Snyder *et al* 2006) our results indicate that it is not able to enter the NPs, probably due to electrostatic repulsion by their negative surface charge. The situation is slightly different for PEGylated NPs, in which the zeta potential is less negative and we see quenching of the third population. We therefore tentatively assign this

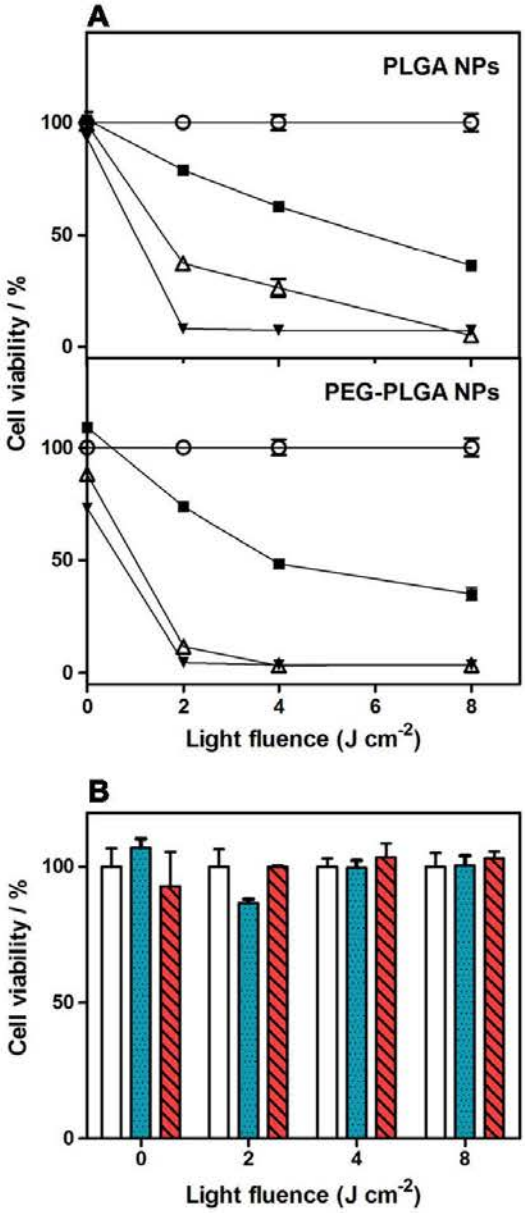

Figure 7. (a) HeLa cells viability (expressed in percentage) after incubation with ZnTPP-loaded PLGA or PEG-PLGA NPs at various concentrations and subsequent irradiation at various light fluences. ZnTPP concentrations are 1 μM (■), 5 μM (△) and 10 μM (▼). Plain circles (○) represent cell controls incubated only with complete growth medium. (b) HeLa cells viability as a function of light fluence after incubation with empty PLGA (blue dotted bars) or PEG-PLGA (red lined bars) NPs. In both cases, the concentration of NPs in incubates was equivalent to that delivered at 10 μM ZnTPP. White bars represent cell controls exposed to light without NPs.

population to $^1O_2$ molecules at the PLGA/PEG interface. Increasing the temperature reduced the differences between the different populations, which ultimately merged into a single one that decayed with the typical lifetime of aqueous solutions (~3 μs (Redmond and Gamlin 1999)) and that was amenable to azide quenching (table 4, figure 5). This likely reflects the decrease in PLGA rigidity at higher temperatures, which facilitates the diffusion of ZnTPP, O_2 and $^1O_2$. In films of poly(lactide) acid (PLA), one of the components of the PLGA polymer, an increase in oxygen permeability with temperature has also been observed (Auras *et al* 2004).

The kinetics of $^1O_2$ production and decay in HeLa cells yielded a number of striking findings (figure 6). Firstly, the decay of the phosphorescence signal was, in the case of bare PLGA, essentially as long as in aqueous suspensions, even after 24 h incubation. This suggests that a large fraction of $^1O_2$ molecules is still confined within the NP, implying that bare NPs hold their cargo, or at least a substantial fraction of it, even after 24 h. Since Chernenko *et al* (2009) demonstrated that PLGA NPs are completely digested by HeLa cells within 6 h, the most likely explanation for our observations is that it reflects cell uptake, which must be very slow, hence the most recently internalized NPs are still largely intact. In fact, the phosphorescence of $^1O_2$ in the cells is found to increase steadily over a period of 24 h incubation (data not shown). The uptake mechanism for PLGA is not fully understood yet. Many publications support the hypothesis of an endocytosis-mediated uptake (Cartiera *et al* 2009, Danhier *et al* 2009, Konan *et al* 2003a, Lei *et al* 2011, Reix *et al* 2012) while others advocate for delivery of the cargo via extracellular release or contact-based transfer (Chen *et al* 2008, Sunoqrot *et al* 2011, Xu *et al* 2009). It is beyond the scope of this study to elucidate the uptake mechanism; however, the observation that $^1O_2$ signals resemble so much those in aqueous suspensions of the NPs would favor the hypothesis of an endocytic mechanism. A substantial fraction of $^1O_2$ molecules is nevertheless outside the NP and leads to the fast decay component observed in the early part of the signal. This is demonstrated by the shortening of the early component in the presence of azide, the increase of the signal intensity upon solvent deuteration, and by the induction of cell mortality (figures 7 and 9). Notice that laser light scattered by the cells decays much faster (figure 6), as demonstrated by the signal at 1220 nm where $^1O_2$ has almost no emission.

The situation for PEGylated NPs is much different. The slow decay observed in aqueous suspensions is no longer detectable, which indicates the faster release of ZnTPP in this case, confirmed by the quenching effect of azide, the signal enhancement upon solvent deuteration (figure 6), and the faster appearance of dead cells after PDT treatments (figure 9). This finding is consistent with the observations reported by Avgoustakis *et al* (2002), who studied the *in vitro* degradation and drug release of a series of PLGA-mPEG polymers with various PLGA:PEG compositions and observed that both the rate of NP degradation and drug release at 37 °C increased with PEG content. In another work comparing free and encapsulated temoporfin in PLGA

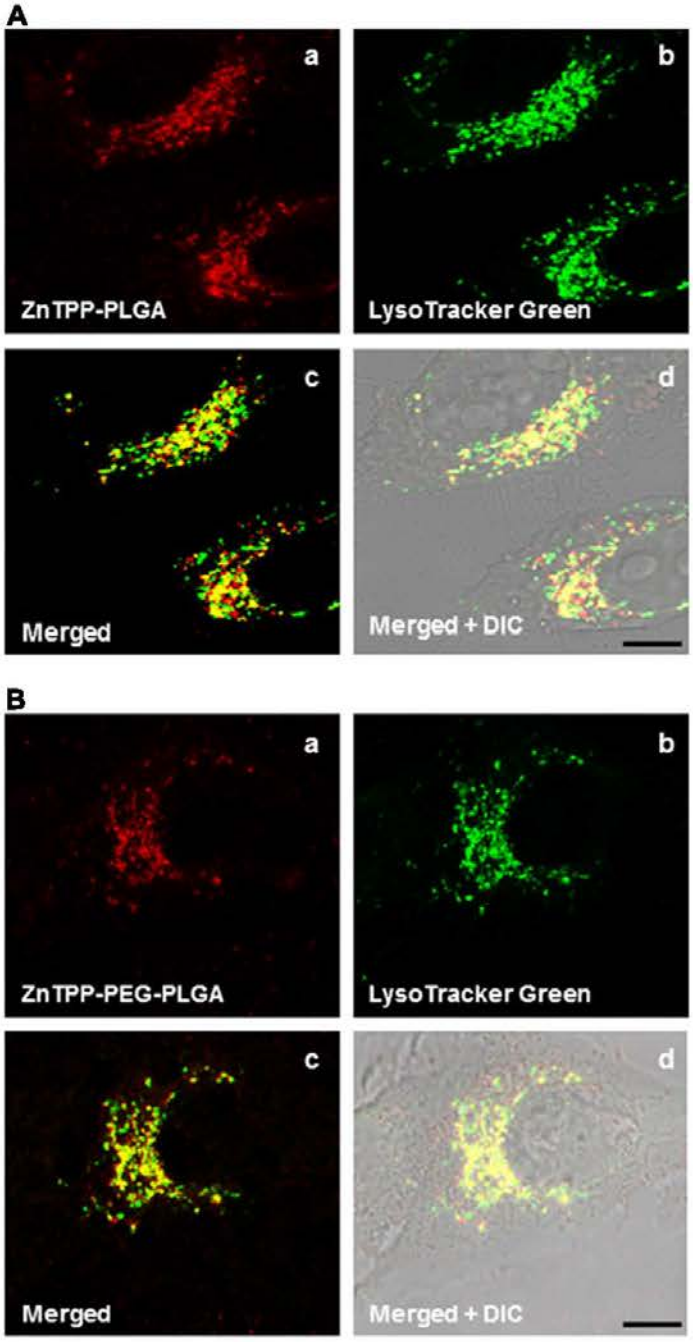

Figure 8. Panel A. (a) Live imaging HeLa cells showing the localization of ZnTPP-loaded PLGA, (b) lysosomes labeled with LysoTracker Green, (c) merged image. Yellow in the overlay images (a) and (b) appears where the red fluorescence of ZnTPP colocalizes with the green fluorescence of LysoTracker Green, (d) and overlap of UV and green channels with differential interference contrast (DIC) image of the same cells. Panel B. Same instrument settings were used to acquire images after incubation of the cells with ZnTPP-loaded PEG-PLGA by confocal microscopy. Scale bar = 10 μm.

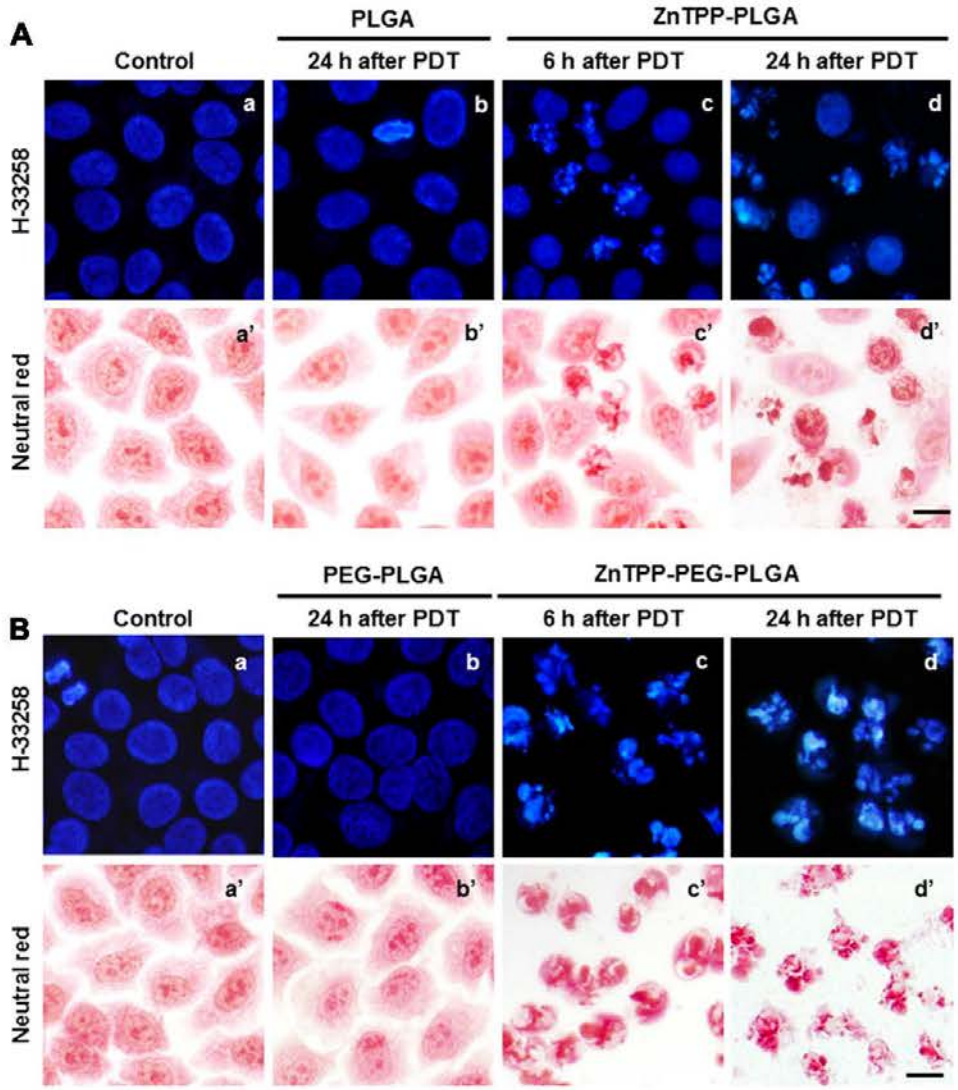

Figure 9. Morphology of cells treated with PDT by ZnTPP-loaded PLGA (panel A) and ZnTPP-loaded PEG-PLGA (panel B) NPs, after neutral red or H-33258 staining. (a)–(a′) HeLa control cells morphology. (b)–(b′) Cells incubated 24 h with empty PLGA or PEG-PLGA NPs followed by green light irradiation (4 J.cm ^{2}) and observed 24 h later. (c)–(d) and (c′)–(d′) Cells incubated 24 h with 5 μM ZnTPP entrapped in PLGA or PEG-PLGA NPs followed by green light irradiation (4 J.cm ^{2}) and observed 6 and 24 h later, respectively. Note that ZnTPP-loaded PEG-PLGA induced apoptotic cell death more effectively than ZnTPP-loaded PLGA. Most of the HeLa cells displayed the morphological features of apoptosis (cell shrinkage and chromatin fragmentation) after 24 h PDT-treatment. Scale bar = 10 μm.

or PEG-PLGA NPs, Rojnik *et al* (2012) also observed a faster temoporfin release for PEGylated NPs than for PLGA NPs.

The photodynamic activity of ZnTPP delivered by the PLGA NPs was evaluated *in vitro* against HeLa cells. ZnTPP was more effective when encapsulated into PEG-PLGA NPs, which is consistent with the results of $^{1}O_{2}$ production. The inactivation process led to a significant percentage of apoptotic morphology 24 h after irradiation, characterized by cell shrinkage, chromatin condensation and nuclear fragmentation with apoptotic body formation (figure 9).

The intracellular localization of ZnTPP was compared with the distribution of specific fluorescent probes commonly used in several research areas, including PDT studies (García-Díaz *et al* 2012, Tamietti *et al* 2007). ZnTPP was mainly located in the acidic endo-lysosomal compartment as evidenced by its co-localization with Lyso Tracker Green (figure 8). The same localization was previously observed

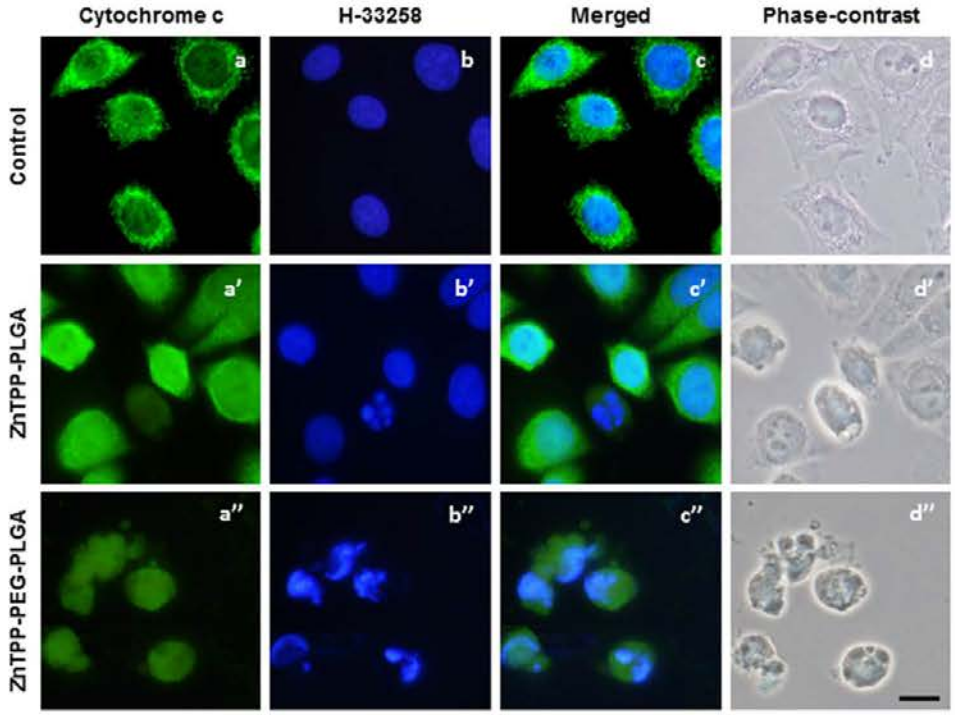

Figure 10. HeLa cells visualized by cytochrome c immunofluorescence (green) and DNA counterstaining with H-33258 (blue), overlap images and corresponding phase-contrast of HeLa cells. (a)–(d) Control cells showing mitochondrial cytochrome c. (a′)–(d±) Cells 24 h after PDT treatment with ZnTPP-loaded PLGA and green light irradiation (4 J cm ^{2}) show cytochrome c release to cytosol only in cells with condensed and fragmented chromatin. (a″)–(d″) The same PDT treatment with ZnTPP-loaded PEG-PLGA led to diffuse cytoplasmic cytochrome c staining with condensed and fragmented chromatin 24 h after irradiation. Scale bar = 10 μm.

when ZnTTP was delivered using liposomes (García-Díaz *et al* 2011). Lysosomes are the final destination for many macromolecules taken up by endocytosis from the extracellular space and from the cell surface (Bonifacino and Traub 2003), which, together with the results of the $^{1}O_{2}$ phosphorescence experiments above, would support the hypothesis of PLGA and PEG-PLGA NPs internalization by an endocytic mechanism.

After the photodynamic treatments, cytochrome c was released from the mitochondrial compartment to the cytosol in cells with condensed and fragmented chromatin (figure 10). This increase in mitochondrial membrane permeability must therefore be held responsible for the initiation of apoptotic cell death processes (Liu *et al* 2011, Moserova and Kralova 2012). All these results together indicate that treatment with 5 μM ZnTPP entrapped in NPs for 24 h followed by irradiation (4 J cm^{-2}) induced massive apoptotic cell death (>90%), thus PEG-PLGA NPs are a more effective vehicle than bare PLGA NPs.

5. Conclusions

In the present study, we investigated physico-chemical and biological aspects of the use of PLGA nanoparticles as delivery vehicles for the model hydrophobic photosensitizer ZnTPP in the photodynamic killing of HeLa cells. The 10% PEG coating confers higher stability to the PLGA NPs in the presence of serum proteins, thereby enabling its use *in vivo*. ZnTPP molecules are distributed between two and three different compartments within bare and PEG-coated NPs, respectively. As a result, $^{1}O_{2}$ is confined within the NP in the case of bare PLGA; however, coating with PEG facilitates its release to the external medium, as does raising the temperature. In agreement with these observations, ZnTPP delivered with PEG-coated PLGA NPs acts faster and more efficiently in inducing cell death upon exposure to light. Both types of PLGA NPs are internalized by endocytosis, deliver their cargo to lysosomes and kill cells mainly by apoptosis. Taken together, the reported results indicate that PEG-PLGA NPs show high potential as delivery agents for PDT.

Acknowledgments

The research described herein has been supported by the Spanish Ministerio de Economía y Competitividad through grant nos. CTQ2013-48767-C3-1-R and CTQ2013-48767-C3-3-R and by the predoctoral fellowship BES-2011-044125

(EB-G). We thank Sorisa® for lending us the LED source and Dr Salvador Borrós and Dr Carlos Semino at IQS for the Zetasizer Nano-ZS measurements and the cell culture laboratory facilities, respectively.

References

Agostinis P *et al* 2011 Photodynamic therapy of cancer: An update *CA: Cancer J. Clin.* **61** 250–81

Allemann E, Konan Y, Gurny R and Boch R E 2004 Compositions and methods for delivery of photosensitive drugs *US Patent Specification* 2004/0047913 A1

Armstrong T I, Davies M C and Illum L 1997 Human serum albumin as a probe for protein adsorption to nanoparticles: relevance to biodistribution *J. Drug Targeting* **4** 389–98

Auras R, Harte B and Selke S 2004 Effect of water on the oxygen barrier properties of poly (ethylene terephthalate) and polylactide films *J. Appl. Polym. Sci.* **92** 1790–803

Avgoustakis K, Beletsi A, Panagi Z, Klepetsanis P, Karydas A G and Ithakissios D S 2002 PLGA-mPEG nanoparticles of cisplatin: *In vitro* nanoparticle degradation, in vitro drug release and *in vivo* drug residence in blood properties *J. Control. Release* **79** 123–35

Avgoustakis K, Beletsi A, Panagi Z, Klepetsanis P, Livaniou E, Evangelatos G and Ithakissios D S 2003 Effect of copolymer composition on the physicochemical characteristics, *in vitro* stability, and biodistribution of PLGA–mPEG nanoparticles *Int. J. Pharm.* **259** 115–27

Barichello J M, Morishita M, Takayama K and Nagai T 1999 Encapsulation of hydrophilic and lipophilic drugs in PLGA nanoparticles by the nanoprecipitation method *Drug Dev. Ind. Pharm.* **25** 471–6

Betancourt T, Byrne J D, Sunaryo N, Crowder S W, Kadapakkam M, Patel S, Casciato S and Brannon-Peppas L 2009 PEGylation strategies for active targeting of PLA/PLGA nanoparticles *J. Biomed. Mater. Res.* A **91** 263–76

Blazquez-Castro A, Stockert J C, Sanz-Rodriguez F, Zamarron A and Juarranz A 2009 Differential photodynamic response of cultured cells to methylene blue and toluidine blue: role of dark redox processes *Photochem. Photobiol. Sci.* **8** 371–76

Bonifacino J S and Traub L M 2003 Signals for sorting of transmembrane proteins to endosomes and lysosomes *Annu. Rev. Biochem.* **72** 395–447

Brouwer A M 2011 Standards for photoluminescence quantum yield measurements in solution (IUPAC Technical Report) *Pure Appl. Chem.* **83** 2213–28

Cartiera M S, Johnson K M, Rajendran V, Caplan M J and Saltzman W M 2009 The uptake and intracellular fate of PLGA nanoparticles in epithelial cells *Biomaterials* **30** 2790–8

Castano A P, Demidova T N and Hamblin M R 2005 Mechanisms in photodynamic therapy: part two—cellular signaling, cell metabolism and modes of cell death *Photodiagn. Photodyn. Ther.* **2** 1–23

Chang J, Paillard A, Passirani C, Morille M, Benoit J-P, Betbeder D and Garcion E 2012 Transferrin adsorption onto PLGA nanoparticles governs their interaction with biological systems from blood circulation to brain cancer cells *Pharm. Res.* **29** 1495–505

Chen H, Kim S, Li L, Wang S, Park K and Cheng J 2008 Release of hydrophobic molecules from polymer micelles into cell membranes revealed by Förster resonance energy transfer imaging **105** 6596–601

Chernenko T, Matthäus C, Milane L, Quintero L, Amiji M and Diem M 2009 Label-free Raman spectral imaging of intracellular delivery and degradation of polymeric nanoparticle systems *ACS Nano* **3** 3552–9

Danhier F, Vroman B, Lecouturier N, Crokart N, Pourcelle V, Freichels H, Jérôme C, Marchand-Brynaert J, Feron O and Préat V 2009 Targeting of tumor endothelium by RGD-grafted PLGA-nanoparticles loaded with paclitaxel *J. Control. Release* **140** 166–73

Dougherty T J, Gomer C J, Henderson B W, Jori G, Kessel D, Korbelik M, Moan J and Peng Q 1998 Photodynamic therapy *J. Natl. Cancer Inst.* **90** 889–905

Dovigo L, Pavarina A, de Oliveira Mima E, Giampaolo E, Vergani C and Bagnato V 2009 Fungicidal effect of photodynamic therapy against fluconazole-resistant *Candida albicans and Candida glabrata Mycoses* **54** 123–30

García-Díaz M, Kawakubo M, Mroz P, Sagristà M L, Mora M, Nonell S and Hamblin M R 2012 Cellular and vascular effects of the photodynamic agent temocene are modulated by the delivery vehicle *J. Control. Release* **162** 355–63

García-Díaz M, Nonell S, Villanueva A, Stockert J C, Cañete M, Casadó A, Mora M and Sagristá M L 2011 Do folate-receptor targeted liposomal photosensitizers enhance photodynamic therapy selectivity? *Biochim. Biophys. Acta* **1808** 1063–71

Gomes A J, Lunardi C N and Tedesco A C 2007 Characterization of biodegradable poly(D, L-lactide-co-glycolide) nanoparticles loaded with bacteriochlorophyll-a for photodynamic therapy *Photomed. Laser Surg.* **25** 428–35

Gref R, Lück M, Quellec P, Marchand M, Dellacherie E, Harnisch S, Blunk T and Müller R 2000 'Stealth' corona-core nanoparticles surface modified by polyethylene glycol (PEG): Influences of the corona (PEG chain length and surface density) and of the core composition on phagocytic uptake and plasma protein adsorption *Colloids Surf.* B **18** 301–13

Hall R D and Chignell C F 1987 Steady-state near-infrared detection of singlet molecular oxygen: a Stern–Volmer quenching experiment with sodium azide *Photochem. Photobiol.* **45** 459–64

Jiménez-Banzo A, Ragàs X, Kapusta P and Nonell S 2008 Time-resolved methods in biophysics 7 photon counting versus. analog time-resolved singlet oxygen phosphorescence detection *Photochem. Photobiol. Sci.* **7** 1003–10

Karmali P P and Simberg D 2011 Interactions of nanoparticles with plasma proteins: Implication on clearance and toxicity of drug delivery systems *Expert Opin. Drug Deliv.* **8** 343–57

Kiesslich T, Tortik N, Pichler M, Neureiter D and Plaetzer K 2013 Apoptosis in cancer cells induced by photodynamic treatment —a methodological approach *J. Porphyrines Phthalocyanines* **17** 197–209

Konan Y N, Berton M, Gurny R and Allemann E 2003a Enhanced photodynamic activity of meso-tetra(4-hydroxyphenyl) porphyrin by incorporation into sub-200 nm nanoparticles *Eur. J. Pharm. Sci.* **18** 241–9

Konan Y N, Cerny R, Favet J, Berton M, Gurny R and Allémann E 2003b Preparation and characterization of sterile sub-200 nm meso-tetra(4-hydroxyphyenyl)poprhyrin-loaded nanoparticles for photodynamic therapy *Eur. J. Pharm. Biopharm.* **55** 115–24

Konan Y N, Gurny R and Allémann E 2002 State of the art in the delivery of photosensitizers for photodynamic therapy *J. Photochem. Photobiol.* B **66** 89–106

Lei T, Srinivasan S, Tang Y, Manchanda R, Nagesetti A, Fernandez-Fernandez A and McGoron A J 2011 Comparing cellular uptake and cytotoxicity of targeted drug carriers in cancer cell lines with different drug resistance mechanisms *Nanomedicine* **7** 324–32

Liu L, Zhang Z and Xing D 2011 Cell death via mitochondrial apoptotic pathway due to activation of Bax by lysosomal photodamage *Free Radical Biol. Med.* **51** 53–68

Locatelli E and Comes Franchini M 2012 Biodegradable PLGA-b-PEG polymeric nanoparticles: synthesis, properties, and

nanomedical applications as drug delivery system *J. Nanopart. Res.* **14** 1316

Moserova I and Kralova J 2012 Role of ER stress response in photodynamic therapy: ROS generated in different subcellular compartments trigger diverse cell death pathways *PLoS One* **7** e32972

Mosmann T 1983 Rapid colorimetric assay for cellular growth and survival - application to proliferation and cyto-toxicity assays *J. Immunol. Methods* **65** 55–63

Oliveira C S, Turchiello R, Kowaltowski A J, Indig G L and Baptista M S 2011 Major determinants of photoinduced cell death: Subcellular localization versus photosensitization efficiency *Free Radical Biol. Med.* **51** 824–33

Panyam J and Labhasetwar V 2003 Biodegradable nanoparticles for drug and gene delivery to cells and tissue *Adv. Drug Deliv. Rev.* **55** 329–47

Paszko E, Ehrhardt C, Senge M O, Kelleher D P and Reynolds J V 2011 Nanodrug applications in photodynamic therapy *Photodiagn. Photodyn. Ther.* **8** 14–29

Redmond R W and Gamlin J N 1999 A compilation of singlet oxygen yields from biologically relevant molecules *Photochem. Photobiol.* **70** 391–475

Reix N *et al* 2012 *In vitro* uptake evaluation in Caco-2 cells and in vivo results in diabetic rats of insulin-loaded PLGA nanoparticles *Int. J. Pharm.* **437** 213–20

Rello S, Stockert J C, Moreno V, Gamez A, Pacheco M, Juarranz A, Cañete M and Villanueva A 2005 Morphological criteria to distinguish cell death induced by apoptotic and necrotic treatments *Apoptosis* **10** 201–08

Rojnik M *et al* 2012 *In vitro* and *in vivo* characterization of temoporfin-loaded PEGylated PLGA nanoparticles for use in photodynamic therapy *Nanomedicine* **7** 663–77

Snyder J W, Skovsen E, Lambert J D C, Poulsen L and Ogilby P R 2006 Optical detection of singlet oxygen from single cells *Phys. Chem. Chem. Phys.* **8** 4280–93

Strachan J-P, Gentemann S, Seth J, Kalsbeck W A, Lindsey J S, Holten D and Bocian D F 1997 Effects of orbital ordering on electronic communication in multiporphyrin arrays *J. Am. Chem. Soc.* **119** 11191–201

Sunoqrot S, Bae J W, Jin S-E, Pearson R, Liu Y and Hong S 2011 Kinetically controlled cellular interactions of polymer-polymer and polymer-liposome nanohybrid systems *Bioconjugate Chem* **22** 466–74

Tamietti B F P, Machado A H A, Maftoum-Costa M, Da Silva N S, Tedesco A C and Pacheco-Soares C 2007 Analysis of mitochondrial activity related to cell death after PDT with AlPCS(4) *Photomed. Laser Surg.* **25** 175–9

Tejedor-Estrada R, Nonell S, Teixido J, Sagrista M L, Mora M, Villanueva A, Canete M and Stockert J C 2012 An artificial neural network model for predicting the subcellular localization of photosensitizers for photodynamic therapy of solid tumors *Curr. Med. Chem.* **19** 2472–82

Vargas A, Eid M, Fanchaouy M, Gurny R and Delie F 2008 *In vivo* photodynamic activity of photosensitizer-loaded nanoparticles: formulation properties, administration parameters and biological issues involved in PDT outcome *Eur. J. Pharm. Biopharm.* **69** 43–53

Vargas A, Lange N, Arvinte T, Cerny R, Gurny R and Delie F 2009 Toward the understanding of the photodynamic activity of m-THPP encapsulated in PLGA nanoparticles: correlation between nanoparticle properties and *in vivo* activity *J. Drug Targeting* **17** 599–609

Vargas A, Pegaz B, Debefve E, Konan-Kouakou Y, Lange N, Ballini J-P, van den Bergh H, Gurny R and Delie F 2004 Improved photodynamic activity of porphyrin loaded into nanoparticles: an *in vivo* evaluation using chick embryos *Int. J. Pharm.* **286** 131–45

Wilkinson F and Brummer J G 1981 Rate constants for the decay and reactions of the lowest electronically excited singlet state of molecular oxygen in solution *J. Phys. Chem. Ref. Data* **24** 809–999

Xu P, Gullotti E, Tong L, Highley C B, Errabelli D R, Hasan T, Cheng J-X, Kohane D S and Yeo Y 2009 Intracellular drug delivery by poly(lactic-co-glycolic acid) nanoparticles, revisited *Mol. Pharm.* **6** 190–201

Yallapu M M, Gupta B K, Jaggi M and Chauhan S C 2010 Fabrication of curcumin encapsulated PLGA nanoparticles for improved therapeutic effects in metastatic cancer cells *J. Colloid Interface Sci.* **351** 19–29

Zeisser-Labouebe M, Lange N, Gurny R and Delie F 2006 Hypericin-loaded nanoparticles for the photodynamic treatment of ovarian cancer *Int. J. Pharm.* **326** 174–81